

ADVANCES IN
QUANTUM CHEMISTRY

EDITED BY
PER-OLOV LÖWDIN

QUANTUM THEORY PROJECT
DEPARTMENTS OF CHEMISTRY AND PHYSICS
UNIVERSITY OF FLORIDA
GAINESVILLE, FLORIDA

VOLUME 18—1986



ACADEMIC PRESS, INC.
Harcourt Brace Jovanovich, Publishers
Orlando San Diego New York Austin
Boston London Sydney Tokyo Toronto

COPYRIGHT © 1986 BY ACADEMIC PRESS, INC.
ALL RIGHTS RESERVED.
NO PART OF THIS PUBLICATION MAY BE REPRODUCED OR
TRANSMITTED IN ANY FORM OR BY ANY MEANS, ELECTRONIC
OR MECHANICAL, INCLUDING PHOTOCOPY, RECORDING, OR
ANY INFORMATION STORAGE AND RETRIEVAL SYSTEM, WITHOUT
PERMISSION IN WRITING FROM THE PUBLISHER.

ACADEMIC PRESS, INC.
Orlando, Florida 32887

United Kingdom Edition published by
ACADEMIC PRESS INC. (LONDON) LTD.
24-28 Oval Road, London NW1 7DX

LIBRARY OF CONGRESS CATALOG CARD NUMBER: 64-8029

ISBN 0-12-034818-7

PRINTED IN THE UNITED STATES OF AMERICA

86 87 88 89

9 8 7 6 5 4 3 2 1

PREFACE

In investigating the highly different phenomena in nature, scientists have always tried to find some fundamental principles that can explain the variety from a basic unity. Today they have not only shown that all the various kinds of matter are built up from a rather limited number of atoms, but also that these atoms are constituted of a few basic elements of building blocks. It seems possible to understand the innermost structure of matter and its behavior in terms of a few elementary particles: electrons, protons, neutrons, photons, etc., and their interactions. Since these particles obey not the laws of classical physics but the rules of modern quantum theory of wave mechanics established in 1925, there has developed a new field of "quantum science" which deals with the explanation of nature on this ground.

Quantum chemistry deals particularly with the electronic structure of atoms, molecules, and crystalline matter and describes it in terms of electronic wave patterns. It uses physical and chemical insight, sophisticated mathematics, and high-speed computers to solve the wave equations and achieve its results. Its goals are great, but perhaps the new field can better boast of its conceptual framework than of its numerical accomplishments. It provides a unification of the natural sciences that was previously inconceivable, and the modern development of cellular biology shows that the life sciences are now, in turn, using the same basis. "Quantum biology" is a new field which describes the life processes and the functioning of the cell on a molecular and submolecular level.

Quantum chemistry is hence a rapidly developing field which falls between the historically established areas of mathematics, physics, chemistry, and biology. As a result there is a wide diversity of backgrounds among those interested in quantum chemistry. Since the results of the research are reported in periodicals of many different types, it has become increasingly difficult for both the expert and the nonexpert to follow the rapid development in this new borderline area.

The purpose of this serial publication is to try to present a survey of the current development of quantum chemistry as it is seen by a number of the internationally leading research workers in various countries. The authors have been invited to give their personal points of view of the

subject freely and without severe space limitations. No attempts have been made to avoid overlap—on the contrary, it has seemed desirable to have certain important research areas reviewed from different points of view. The response from the authors has been so encouraging that a nineteenth volume is now being prepared.

The Editor would like to thank the authors for their contributions, which give an interesting picture of the current status of selected parts of quantum chemistry. The topics in this volume range from studies of the Jahn–Teller effect, the quantum theory of tautomeric equilibria, over the dynamics of molecular crystals to coupled-cluster many-body perturbation theory.

It is our hope that the collection of surveys of various parts of quantum chemistry and its advances presented here will prove to be valuable and stimulating, not only to the active research workers but also to the scientists in neighboring fields of physics, chemistry, and biology who are turning to the elementary particles and their behavior to explain the details and innermost structure of their experimental phenomena.

PER-OLOV LÖWDIN

The Jahn—Teller Effect in Dipole (Multipole) Moments and Polarizabilities of Molecules

I. B. BERSUKER and I. Ya. OGURTSOV

*Department of Quantum Chemistry
Institute of Chemistry, Academy of Sciences
Moldavian SSR, 277028 Kishinev, USSR*

I.	Introduction	1
II.	Dipole Moments of Symmetric Molecular Systems	5
	A. Temperature Dependence of the Mean Dipole Moment	5
	B. Pure Rotational Absorption Spectra	12
	C. Dielectric Losses	23
III.	Anisotropy of Polarizability and Hyperpolarizabilities in Degenerate States	28
	A. Anomalous Birefringence in Gases of Spherical-Top Molecules: The Kerr and Cotton—Mouton Effects.	28
	B. Depolarization of Light in Rayleigh, Hyper-Rayleigh, and Pure Rotational Raman Scattering	45
	C. Temperature-Dependent Optical Activity of Symmetric Molecules in Magnetic Fields	59
IV.	Quadrupole Moments of Symmetric Systems and Their Manifestations in Intermolecular Interactions	68
	A. Birefringence in Inhomogeneous Electric Fields	69
	B. Spectroscopic Manifestations of the Anisotropy of Intermolecular Interactions Induced by Degeneracy	75
V.	Conclusions	81
	References	82

I. Introduction

The development of the theory of vibronic interactions in molecules and crystals is one of the important achievements of quantum chemistry in the past quarter of a century. The theory is based on a new approach to the problem of electronic structure and properties of poliatomic systems that goes beyond the framework of the full separation of the motions of the electrons and nuclei in the adiabatic approximation; the nonadiabacity being taken into account by means of mixings of the electronic states by nuclear displacements. This vibronic mixing is especially important in the presence of degenerate or close-in energy electronic states, resulting in

the so-called Jahn–Teller effect, which is a commonly used title for the works of this trend.

At present the new approach has reached widespread development and applications in the form of a new concept of molecular structure, the concept of vibronic interactions. The applications of this concept involve practically all the areas of investigation in physics and chemistry of molecules and crystals, including spectroscopy in the full range of electromagnetic waves (visible, UV, IR, Raman, ESR, NMR, NGR, NQR and radiospectroscopy, as well as ultrasonics), magnetic and electric properties, scattering of light and particles, crystal chemistry, and crystal physics (including structural phase transitions and ferroelectricity, chemical reactivity, activation and catalysis, and electron-conformational interactions in biology) (see the following monographs: Bersuker and Polinger, 1983; Bersuker, 1984; Englman, 1972; Abragam and Bleaney, 1970; Perlin and Tsukerblat, 1974; and the following articles: Ham, 1972; Bersuker, 1975; Bersuker *et al.* 1975; Ghering and Ghering, 1975; Bersuker and Vekhter, 1978; Bates, 1978; Ogurtsov and Kazantseva, 1979, 1981; Bersuker and Polinger, 1982; Reinen and Friebel, 1979, and others).

In the present review article 1985's results obtained in applications of the concept of vibronic interactions to the investigation of electric properties of molecules (dipole and multipole moments and polarizabilities) are presented. Molecular aspects of these topics are almost untouched in the publications listed in the preceding paragraph. The idea of dipole instability was used first as a basis of the so-called vibronic theory of ferroelectricity (Bersuker, 1966; Bersuker and Vekhter, 1978). Meanwhile, the manifestation of the electronic or vibronic degeneracy in the electric responses of molecules, being no less essential than other vibronic effects, has some special features.

The traditional description of individual properties of molecules is based on the assumption of a definite charge distribution in them determined by the symmetry of the nuclear framework. The light electrons, moving in the field of heavy nuclei, adjust (adiabatically) their space distribution to the nuclear configuration, which results from the self-consistent electrostatic interaction of the electrons and nuclei.

Usually in the study of the electric properties of molecules, it is assumed that the electron and nuclear dynamics cannot destroy the molecular symmetry, and hence the individual characteristics of molecules are conceptually determined by the symmetry of the nuclear framework only. This statement is based on the assumption that the charge distribution (either classical or quantic) is totally symmetric (with respect to the nuclear configuration); i.e., it transforms into itself under the operations of the point symmetry group of the molecule. In cases in which the elec-

tronic state of the molecule is nondegenerate, the preceding considerations are correct, and they remain the same in both the classical and quantum descriptions.

However, when distinguished from the former case, the quantum description also allows degenerate states of the molecule. In each of the states of the degenerate term or in their linear combinations, the charge distribution is not invariant with respect to all the operations of the assumed symmetry of the molecule. Therefore all the conclusions based on the assumption of a totally symmetric charge distribution in the case of degeneracy become invalid.

In addition, in the case of electronic degeneracy the nuclear configuration, following the Jahn–Teller theorem, is not appropriate to the minimum of the adiabatic potential, and hence the system is unstable with respect to nuclear displacements lowering the symmetry of the molecule. In these cases there are several (or an infinite number of) nuclear configurations equivalent in energy appropriate to the minima of the adiabatic potential, and for a correct description of the system the possibility of transitions between different equivalent minima has to be taken into account. This results in a complicated mixing of the electron and nuclear motions, and their full separation becomes impossible. These considerations become extremely important in evaluations of molecular electric properties determined by dipole and quadrupole moments and polarizabilities. Some symmetry considerations given in the following illustrate these statements.

Consider a molecule with an even number of electrons in a degenerate ground state belonging to the irreducible representation Γ of the point symmetry group of the molecule.* Denote the line of this representation by γ . In accordance with group theory the reduced matrix elements of tensor operators even with respect to time reversal in the basis of the function $|\Gamma\gamma\rangle$ are nonzero if their components belong to the representation $\bar{\Gamma}$ contained in the symmetric product $[\Gamma^2]$ (for other cases the rules are similar; see the following discussion). It follows directly from this rule that in the nondegenerate state the matrix elements are nonzero for totally symmetric components of the polarizability tensor and for that multipole moment 2^l , for which the decomposition of the full spherical group representation D^l into irreducible ones of the point symmetry group contains the totally symmetric representation. For instance, in the case of spheri-

* It is known from the theory of vibronic interactions that the vibronic states can be classified by the same representations of the point group appropriate to the high-symmetry nuclear configuration, for which the ground electronic term is degenerate, the ground vibronic level having the same degeneracy and belonging to the same representation as the initial electronic term (Bersuker and Polinger, 1983).

cal-top molecules in nondegenerate states, the scalar part of the polarizability is nonzero, and the totally symmetric representation is first met in the decomposition D^l for $l = 3$ in tetrahedral molecules and $l = 4$ in octahedral ones. This leads to the conclusion that in spherical-top molecules the polarizability is isotropic and the minimal multipole moment is an octupole one in the case of T_d symmetry and hexadecapole one in the case of O_h symmetry.

In degenerate states the situation is essentially changed. In these cases in the decomposition of the product $[\Gamma^2]$ into irreducible representations there are other representations in addition to the totally symmetric representation. As a result, there may be nonzero matrix elements for nontotally symmetric components of irreducible tensor operators of the polarizability and multipole moments. In particular, in the decomposition of $[\Gamma^2]$ there may be representations contained in D^l with an l value less than l_A , for which D^{l_A} contains the totally symmetric representation.

Let us illustrate this conclusion by the example of spherical-top molecules. In the degenerate states E , T_1 , T_2 , and $G_{3/2}$ there is the E representation in the decomposition of the appropriate symmetric product, and hence in these cases the matrix elements are nonzero for anisotropic components of the tensors of polarizability and quadrupole moment, since E is first met in the decomposition of the spherical representation D^2 . Moreover, in tetrahedral systems in states of the type T and $G_{3/2}$ the matrix elements of the dipole moment are nonzero, since $[T^2]$ and $\{G_{3/2}^2\}$ contain the representation T_2 .

Thus in degenerate states beside the totally symmetric components of the tensor of polarizability and multipole moments, the anisotropic components also have to be taken into account; i.e., the point symmetry of the charge distribution becomes lower than in nondegenerate states. Note that in nondegenerate states the diagonal matrix element of an operator coincides with the mean value of the appropriate magnitude (polarizability, multipole moments, etc.), whereas in the case of degeneracy there is no such direct relation between the matrix elements and observables since in the basis of the degenerate states each physical magnitude is appropriate to no matrix element but a matrix. Therefore the correlation between the matrix elements and the observables has to be carried out for each concrete experimental situation separately. Note also that concerning the manifestations in the observable properties, relatively close-in (but in fact far from being close) energy states may be the most similar to the case of exact degeneracy (see Bersuker *et al.*, 1984).

In work discussed in this paper some fundamental differences in dipole (multipole) moments and polarizabilities of molecules in degenerate

states, as compared with nondegenerate ones, are established, and the manifestations of these differences in electric properties of matter studied by physical methods are discussed.

II. Dipole Moments of Symmetric Molecular Systems

In accordance with the widespread knowledge introduced in manual books there are two classes of molecules that differ by their behavior in external electric fields: (1) rigid dipole molecules and (2) nondipolar (polarizable) ones. The first class contains molecular systems that, due to the internal symmetry, have a proper dipole moment, whereas the molecules of the second class, being high symmetrical ones, have no proper dipole moment, but acquire such a dipole moment under the influence of the external field due to charge displacements (polarization). However, as mentioned in the introduction, owing to the past 20 to 25 years' achievements in vibronic interaction theory (Bersuker, 1984; Bersuker and Polinger, 1982, 1983), this classification becomes incomplete and even incorrect. As will be shown in this section in more detail, highly symmetric molecules that have no proper dipole moment (from a symmetry consideration) may behave in the electric field as rigid dipole ones if they are in a degenerate electronic state. This possibility was first suggested by Child and Longuet-Higgins (1961). Moreover, owing to the Jahn–Teller effect such molecules may have both types of behavior in electric fields dependent on the temperature region (Bersuker, 1969; Bersuker *et al.*, 1973). The possibility of nonpolar molecules manifesting rigid dipole properties in the excited degenerate vibrational states was suggested even earlier (Mizushima and Venkateswarlu, 1953).

A. Temperature Dependence of the Mean Dipole Moment

The mean value of the electric dipole moment of a molecule in an external electric field \mathcal{E} directed along the Z axis of laboratory system of coordinates (LSC), if the intermolecular interaction and the quantization of the rotational degrees of freedom are neglected, is given by the relation

$$\bar{d} = \int_0^\beta d\lambda \int \frac{d\Omega}{8\pi^2} \frac{\text{Sp}\{e^{-\beta\hat{H}} \hat{d}_Z(\lambda) \hat{d}_Z\}}{\text{Sp}\{e^{-\beta\hat{H}}\}} \mathcal{E} \quad (1)$$

where \hat{H} is the Hamiltonian of the internal degrees of freedom of the molecule, \hat{d}_Z is the operator of the projection of its dipole moment on the Z axis of the LSC, $\beta = 1/(kT)$, k' is the Boltzmann constant, T is the temperature, $\hat{d}(\lambda) = \exp(\lambda\hat{H})\hat{d}\exp(-\lambda\hat{H})$, $\Omega = (\alpha, \beta, \gamma)$ is the set of Euler-

ian angles giving the orientation of the molecule in the space,

$$\int d\Omega \dots = \int_0^{2\pi} d\alpha \int_0^\pi \sin \beta d\beta \int_0^{2\pi} d\gamma \dots$$

and Sp is the operation of a spur. If we constrain ourselves with the contribution to Eq. (1) originating from the vibronic states of the ground electronic term only (i.e., if we neglect the population of the excited electronic states), then after the averaging over the orientations of the molecule the expression (1) can be reduced to the form

$$\bar{d} = [\alpha(T) + \alpha_0] \mathcal{E} \quad (2)$$

where α_0 is the polarization of the molecule due to the displacement of the electrons in the electric field,

$$\alpha(T) = \frac{1}{3} \int_0^\beta d\lambda \frac{\text{Sp}\{\exp[-(\beta - \lambda)\hat{H}_{\text{vibr}}] \hat{\mathbf{d}} \exp(-\lambda\hat{H}_{\text{vibr}}) \hat{\mathbf{d}}\}}{\text{Sp}\{\exp(-\beta\hat{H}_{\text{vibr}})\}} \quad (3)$$

is the temperature-dependent contribution to the dielectric constant, \hat{H}_{vibr} is the vibronic Hamiltonian of the ground electronic state, $\hat{\mathbf{d}}$ is the operator of the dipole moment in the molecular system of coordinates (MSC), and the spur operation (Sp) in Eq. (3) is taken over the states that belong to the ground electronic term only. Let us investigate the temperature dependence $\alpha(T)$ for several concrete cases.

1. Molecular Systems in Twofold Degenerate Electronic States of Dipolar Type

The twofold degeneracy of dipolar type can be realized, for instance, in molecules with D_{3h} symmetry. Consider first the $\alpha(T)$ dependence in the absence of vibronic interaction. In this case

$$\alpha(T) = \frac{d_e^2}{3kT} \quad (4)$$

where d_e is the reduced matrix element of the operator of the dipole moment calculated by electronic functions.

Taking into account the linear vibronic coupling in the Hamiltonian of the system (the linear $E \otimes e$ problem), we have

$$\hat{H}_{\text{vibr}} = \frac{\hbar\omega}{2} (\hat{\mathbf{p}}^2 + \hat{\mathbf{q}}^2) + \hbar\omega a(\hat{\sigma}\hat{\mathbf{q}}) \quad (5)$$

Here $\hat{\mathbf{q}}$ and $\hat{\mathbf{p}}$ are the vectors of dimensionless coordinates and impulses, respectively, ω is the frequency of the harmonic vibrations active in the Jahn–Teller effect; a is the vibronic constant related to the usual F (Ber-

suker, 1984) by the equation (m is reduced mass)

$$\sqrt{\hbar m \omega^3} a = F, \quad \hat{\sigma} = \{-\hat{\sigma}_z, \hat{\sigma}_x\}$$

$\hat{\sigma}_z$ and $\hat{\sigma}_x$ being the Pauli matrices. In the case under considerations, the vibrations in the direction \mathbf{q} are of dipolar type, and therefore the operator of the dipole moment can be written as

$$\hat{\mathbf{d}} = d_e \hat{\sigma} + d_n \hat{\mathbf{q}} \quad (6)$$

where d_n is the effective dipole moment formed by the nuclear displacements \mathbf{q} . It follows from Eq. (6) that

$$\hat{\mathbf{q}} + a \hat{\sigma} = \frac{1}{i\hbar\omega} [\hat{H}_{\text{vibr}}, \hat{\mathbf{p}}] \quad [\hat{A}, \hat{B}] = \hat{A}\hat{B} - \hat{B}\hat{A} \quad (7)$$

Using this relation and the Kubo identity

$$[\hat{A}, e^{-\beta\hat{H}}] = \int_0^\beta d\lambda e^{-(\beta-\lambda)\hat{H}} [\hat{H}, \hat{A}] e^{-\lambda\hat{H}} \quad (8)$$

we obtain*

$$\alpha(T) = \frac{(d_e - a d_n)^2}{3kT} \times \left[\frac{1}{\beta} \int_0^\beta d\lambda \frac{\text{Sp}\{\exp[-(\beta - \lambda)\hat{H}_{\text{vibr}}] \hat{\sigma} \exp(-\lambda\hat{H}_{\text{vibr}}) \hat{\sigma}\}}{\text{Sp}\{\exp(-\beta\hat{H}_{\text{vibr}})\}} \right] \quad (9)$$

In Eq. (9) the factor in brackets

$$Q_E(E, \beta) = \frac{1}{\beta} \int_0^\beta d\lambda \frac{\text{Sp}\{\exp[-(\beta - \lambda)\hat{H}_{\text{vibr}}] \hat{\sigma} \exp(-\lambda\hat{H}_{\text{vibr}}) \hat{\sigma}\}}{\text{Sp}\{\exp(-\beta\hat{H}_{\text{vibr}})\}} \quad (10)$$

as it can be shown is smaller than unity if $a \neq 0$, and therefore this term can be called the temperature reduction factor for the electronic contribution to the polarizability $\alpha(T)$. When compared with the usual linear in β temperature dependence, this parameter introduces additional more-complicated terms. The calculation requires a knowledge of the temperature density matrix, its exact expression being unknown for the problem under consideration. Nevertheless, some approximate analytical expressions for the $Q_E(E, \beta)$ function can be obtained for some particular and limited cases. In the case of low enough temperatures when the population of the

* Strictly speaking, an additional term $\frac{2}{3}(d_n^2/\hbar\omega)$ that represents the so-called atomic polarization (the polarization of a two-dimensional harmonic vibration of dipolar type) has to be present in Eqs. (4) and (9). In the preceding consideration this term is omitted due to its smallness as compared with the other contributions to $\alpha(T)$.

ground vibronic states is predominant, the vibronic reduction factor can be presented in the form

$$Q_E(E, \beta) \approx q_E^2 + \frac{2}{\beta} \sum_{n_0, n_e} \frac{\langle n_0 | \hat{\sigma} | n_e \rangle \langle n_e | \hat{\sigma} | n_0 \rangle}{E_{n_e} - E_{n_0}} \quad (11)$$

where q_E is the electronic reduction factor for operators of the type E in the ground vibronic state (Ham, 1965, 1968, 1972; Bersuker and Polinger, 1983) and E_n and $|n\rangle$ are the vibronic energy levels and wave functions, with the indices 0 and e indicating the ground and excited states, respectively. Substituting Eq. (11) into Eq. (9), we obtain for the $\alpha(T)$ dependence in the region of low temperatures

$$\alpha(T) \approx \frac{(d_e - ad_n)^2}{3kT} + \frac{2}{3} (d_e - ad_n)^2 \sum_{n_0, n_e} \frac{\langle n_0 | \hat{\sigma} | n_e \rangle \langle n_e | \hat{\sigma} | n_0 \rangle}{E_{n_e} - E_{n_0}} \quad (12)$$

The second term in Eq. (12) has the form characteristic for atomic polarization, the summation in this term being performed over the vibronic states of the ground electronic term. The occurrence of this term is due to the Jahn-Teller effect, since in the absence of the effect the matrix elements $\langle n_0 | \hat{\sigma} | n_e \rangle$ are identically equal to zero. Its contribution to the atomic polarization is determined by the magnitude of vibronic interaction and, generally speaking, it is not small. Visually, the vibronic contribution to the atomic polarization can be explained by the increase of the mobility and hence the polarizability of the vibrational system due to the Jahn-Teller effect.

For the calculation of the $Q_E(E, \beta)$ value in a more general case, one can use the following approximation for the density matrix in the coordinate representation (Ogurtsov and Kazantseva, 1982):

$$\langle \mathbf{q} | \exp(-\beta \hat{H}_{\text{vibr}}) | \mathbf{q}' \rangle \approx \frac{1}{2\pi \operatorname{sh}(2x)} \exp \left\{ -\frac{1}{2 \operatorname{sh}(2x)} [(\mathbf{q}^2 + \mathbf{q}'^2) - 2\mathbf{q}\mathbf{q}'] + 2a^2(x - \operatorname{th} x) \right\} \exp\{-a \operatorname{th} x(\mathbf{q}\hat{\sigma})\} \exp\{-a \operatorname{th} x(\mathbf{q}'\hat{\sigma})\} \quad (13)$$

where $x = \hbar\omega\beta/2$. It can be shown (Ogurtsov and Kazantseva, 1982) that the statistical sum and the mean-square amplitude $\langle \mathbf{q}^2 \rangle$ calculated by means of Eq. (13) in the limit case of high temperatures coincide with the appropriate analytical expressions obtained in the approximation of independent ordering of electronic and nuclear coordinates (Ogurtsov *et al.*, 1977; Ogurtsov and Kazantseva, 1979). In the opposite limit case of low temperatures, the expression in Eq. (13) transforms into an operator of projection on the states of the ground vibronic term, this operator being built up by means of analytical expressions obtained in the framework of

the so-called inverse adiabatic approximation (Englman, 1972). Numerical results obtained for a wide region of vibronic constant values and temperatures show that the approximation of independent ordering allows high accurate results for the temperature dependence $\langle q^2 \rangle$ to be obtained, while the inverse adiabatic approximations give good results for the mean values of different characteristics of the system in the ground vibronic state. Therefore one can hope that by means of Eq. (13) and based on the above two approximations adequate analytical expressions for the reduction parameters for arbitrary temperatures and vibronic constant values can be obtained.

At high temperatures when the number of populated vibronic states is large enough, one can neglect the nondiagonality of the density matrix (13) on nuclear coordinates. This results in

$$Q_E(E, \beta) \approx \frac{1}{2} \left[1 + \frac{1 - p(a\sqrt{x})}{2a^2x} \right] \quad (14)$$

where

$$p(y) = [1 + \sqrt{\pi} y e^{y^2} \Phi(y)]^{-1} \quad (15)$$

$\Phi(Y) = (2/\sqrt{\pi}) \int_0^Y \exp(-t^2) dt$ being the error function. In the case under consideration $Q_E(E, \beta)$ is a complicated function of the product $a\sqrt{x}$, and its values lay within the limits of $1(a\sqrt{x} = 0)$ and $\frac{1}{2}(a\sqrt{x} \rightarrow \infty)$. If $a\sqrt{x} \ll 1$, appropriate to the case of either a small vibronic constant a or high enough temperature with arbitrary values of a , $Q_E(E, \beta)$ can be presented by the first two terms of the expansion:

$$Q_E(E, \beta) \approx 1 - \frac{2}{3} a^2 x = 1 - \frac{2}{3} \beta E_{JT} \quad (16)$$

where E_{JT} is the Jahn-Teller stabilization energy. Substituting Eq. (16) into Eq. (9), we obtain for the temperature dependence of $\alpha(T)$

$$\alpha(T) \approx \frac{(d_e - ad_n)^2}{3kT} - \frac{2}{9} \frac{(d_e - ad_n)^2}{(kT)^2} E_{JT} \quad (17)$$

2. Dipolarly Unstable Molecules

We will consider now the temperature dependence $\alpha(T)$ for high-symmetry molecules that have no proper dipole moment owing to symmetry properties, but owing to vibronic interactions possess an adiabatic potential with a finite number of minima of dipolar type at which the molecule has a dipole moment. Such molecules can be called dipolarly unstable molecules (DUM). The initial ground electronic term of these molecules can be both degenerate or nondegenerate. In the latter case in

the absence of vibronic interactions, the system has to be classified as a nonpolar one. This means that in the absence of vibronic interaction the molecule has no temperature-dependent mean dipole moment of the type (4). The dipolar-type minima in the case of the nondegenerate electronic term are formed by the vibronic mixing of the latter with the excited one of appropriate symmetry by vibrations of dipolar type (pseudo-Jahn-Teller effect) (see Bersuker and Polinger, 1983).

Consider now several concrete cases (Bersuker *et al.*, 1973).

If the system has two minima of dipolar type equivalent in energy, as in the case of, e.g., the ammonia molecule, then instead of each vibrational state in the minimum, two stationary states divided by an energy interval 2Δ arise owing to tunneling (inversion splitting). We constrain ourselves to the consideration of $\alpha(T)$ for the lowest inversion states only. In this approximation

$$\hat{H}_{\text{vibr}} = \Delta \hat{\sigma}_z, \quad \hat{d}_0 = d \hat{\sigma}_x, \quad \hat{d}_{\pm 1} = 0 \quad (18)$$

where d is the value of the dipole moment at the minimum configuration and \hat{d}_m is the spherical component of the operator of the dipole moment in the MSC. Substituting Eq. (18) into Eqs. (3) and (10), we obtain

$$\alpha(T) = \frac{d^2}{3kT} \frac{\text{th}(\beta\Delta)}{\beta\Delta}, \quad Q(\beta) = \frac{\text{th}(\beta\Delta)}{\beta\Delta} \quad (19)$$

In other cases there may be three equivalent minima of dipolar type on the adiabatic potential, e.g., in the cases of molecules with D_{3h} symmetry. Such an adiabatic potential can be due to either the pseudo-Jahn-Teller effect or the Jahn-Teller effect in the case of twofold degenerate electronic terms with quadratic terms of the vibronic interactions included (the quadratic $E \otimes e$ problem). If the dipolar minima are deep enough and only the tunneling states are populated, then \hat{H}_{vibr} and the operator of dipole moment can be expressed by matrices of the dimension 3×3 :

$$\hat{H}_{\text{vibr}} = \Delta \begin{bmatrix} 1 & 0 & 0 \\ 0 & -1 & 0 \\ 0 & 0 & -1 \end{bmatrix},$$

$$\hat{d}_{\pm 1} = \frac{d}{2} \begin{bmatrix} 0 & \pm 1 & -i \\ \pm 1 & \pm \frac{1}{\sqrt{2}} & \frac{i}{\sqrt{2}} \\ -i & \frac{i}{\sqrt{2}} & \pm \frac{1}{\sqrt{2}} \end{bmatrix}, \quad \hat{d}_0 = 0 \quad (20)$$

Using these expressions and Eq. (3), we obtain the following formulas for $\alpha(T)$ and $Q(\beta)$ in the case under consideration:

$$\alpha(T) = \frac{d^2}{3kT} \frac{e^{\beta\Delta} + 2[\text{sh}(\beta\Delta)/\beta\Delta]}{e^{\beta\Delta} + 2 \text{ch}(\beta\Delta)}, \quad Q(\beta) = \frac{e^{\beta\Delta} + 2[\text{sh}(\beta\Delta)/\beta\Delta]}{e^{\beta\Delta} + 2 \text{ch}(\beta\Delta)} \quad (21)$$

In the more complicated case of a tetrahedral system with an adiabatic potential having four equivalent minima of dipolar type, \hat{H}_{vibr} and the operators of Cartesian components of the dipole moment are given by the following matrices of dimension 4×4 , provided that the overlap integrals of the vibronic functions in different minima are neglected:

$$\begin{aligned} \hat{H}_{\text{vibr}} &= -\Delta \begin{bmatrix} \hat{1} & \hat{0} \\ \hat{0} & \hat{\sigma}_z \end{bmatrix}, & \hat{d}_z &= \frac{d}{\sqrt{3}} \begin{bmatrix} \hat{0} & \hat{\sigma}_x \\ \hat{\sigma}_x & \hat{0} \end{bmatrix} \\ \hat{d}_x &= \frac{d}{\sqrt{3}} \begin{bmatrix} \hat{\sigma}_x & \hat{0} \\ \hat{0} & \hat{\sigma}_x \end{bmatrix}, & \hat{d}_y &= \frac{d}{\sqrt{3}} \begin{bmatrix} \hat{0} & \hat{1} \\ \hat{1} & \hat{0} \end{bmatrix} \end{aligned} \quad (22)$$

Here $\hat{1}$ and $\hat{0}$ are the unit and zero matrices of the second order, respectively. This situation is appropriate to the tunneling splitting of four states in the minima resulting in two levels, A_1 and T_2 . Substituting Eqs. (22) into Eqs. (3) and (10), we have (Bersuker *et al.*, 1973)

$$\alpha(T) = \frac{d^2}{3kT} \frac{e^{\beta\Delta} + [\text{sh}(\beta\Delta)/\beta\Delta]}{e^{\beta\Delta} + \text{ch}(\beta\Delta)}, \quad Q(\beta) = \frac{e^{\beta\Delta} + [\text{sh}(\beta\Delta)/\beta\Delta]}{e^{\beta\Delta} + \text{ch}(\beta\Delta)} \quad (23)$$

The analysis of the preceding results leads to several important conclusions about the electric properties of vibronic systems. First, in accordance with the results obtained in the preceding, nonpolar molecules may have both types of behavior of the mean dipole moment—that for rigid dipole molecules and that for nondipolar ones. Only in the cases of limit values of temperatures or vibronic coupling constants can they be related to either the former or the latter. This statement can be illustrated by the case of a molecule with two dipolar-type minima [Eq. (19)]. Consider the two limit cases: $\Delta \ll kT$ and $\Delta \gg kT$. In the former case the function $\alpha(T)$ transforms into the classical linear dependence on $1/kT$ inherent to rigid dipole molecules. In the limit case of low temperatures, $\alpha(T)$ is reduced to a constant value equal to the static polarizability of molecules that have no proper dipole moment.

Another conclusion is that the temperature dependence of the mean dipole moment for vibronic systems has a complicated form essentially dependent on several parameters of the system (the effective electronic d_e and nuclear d_n dipole moments and the vibronic constant a or the values of the dipole moments in the adiabatic potential minima configurations d and the tunneling splitting magnitude, etc.). Therefore the measurement

of the temperature dependence of the mean dipole moment in a wide range of temperatures can serve as a source of information about the energy spectrum of the vibronic systems, the charge distribution, vibronic constant values, nuclear dynamics, and so on. Note that the neglect of quantization of rotations in the calculation of the $\alpha(T)$ dependence is not a strong restricting approximation (Bersuker *et al.*, 1973).

B. Pure Rotational Absorption Spectra

The classical ideas about the presence or absence of a dipole moment of a molecule based on point symmetry considerations are also used in the solution of the problem of possible light absorption due to transitions between rotational states without changes of the energy of internal degrees of freedom, i.e., to pure rotational transitions. This resulted in the conclusion about the absence of pure rotational absorption spectra for high-symmetry nonpolar molecules, e.g., for molecules of D_{nh} symmetry and for spherical-top ones. The preceding results on the temperature dependence of the mean dipole moment of vibronic systems in constant electric fields indicate the necessity of also reconsidering their behavior in alternating fields.

The possibility of pure rotational absorption spectra of high-symmetry vibronic systems was suggested by Child and Longuet-Higgins (1961). It was shown in this work that in molecules of D_{3h} symmetry in a twofold degenerate electronic state the matrix elements of the spherical components of the internal angular momentum \hat{P}_0 and of the operator of the dipole moment $\hat{d}_{\pm 1}$ are nonzero. It follows from this statement that, first, the Coriolis interaction is effective in the first order of perturbation theory, and therefore the rotational structure of the vibronic levels is different from that expected for systems without electronic degeneracy. Within the accuracy up to terms independent of the rotational quantum numbers of the total angular momentum J and its projection K on the Z axis of the MSC, this rotational structure has the form*

$$BJ(J + 1) + (A - B)K^2 - 2A\zeta K \quad (24)$$

where B and A are the rotational constants of symmetric-top molecules and ζ is the effective Coriolis constant dependent on the vibronic quantum number.

* In several papers a more detailed consideration of the rotational structure of the energy levels for symmetric-top molecules with a ground E term is given. In particular, in the work of Child (1963) the I -type doubling resulting from JTE is revealed, while in the paper of Brown (1971) the spin-orbital interaction for the 2E term (beside the JTE) is taken into account. However, since the pure rotational spectrum is not considered in these works, they are not discussed here.

Second, due to the nonzero matrix elements of the operator of the dipole moment, transitions between the rotational sublevels of the same vibronic level with the change of the projection K by unity ($\Delta K = 1$) are possible. In the work of Child and Longuet-Higgins (1961) it is noted that the possible vibronic pure rotational absorption spectrum within the same vibronic level is somewhat similar to the pure rotational spectrum in the excited degenerate dipolar-type state of harmonic oscillators predicted by Mizushima and Venkatesvarlu (1953).

1. Rotational Spectra of Dipolarly Unstable Systems

The possibility of observing pure rotational spectra in tetrahedral molecules was discussed in the paper of Bersuker *et al.* (1974). In order to elucidate the origin and main features of this spectrum, a vibronic system with four equivalent deep enough minima of dipolar type arising owing to either the pseudo-Jahn–Teller dipole instability or the Jahn–Teller effect is chosen as an example. In this case the tunneling splitting of each four-fold degenerate (over the number of minima) electron-vibrational state results in two levels, a nondegenerate one A_1 and a threefold degenerate T_2 , with the energy gap between them equal to 2Δ . The tunneling states corresponding to this level may be described as follows:

$$|\Gamma\gamma\rangle = \frac{1}{2} \sum_{i=1}^4 a_{\Gamma\gamma i} \Psi_i, \quad \Gamma = A_1, T_2 \quad (25)$$

where Ψ_i is the electron-vibrational function in the i th minimum and the coefficients ($a_{\Gamma\gamma 1}$, $a_{\Gamma\gamma 2}$, $a_{\Gamma\gamma 3}$, $a_{\Gamma\gamma 4}$) form the sets (1, 1, 1, 1) and (1, 1, -1, -1), (1, -1, 1, -1), (1, -1, -1, 1) for the states A_1 and T_2 , respectively.

The full wave functions for the system can be presented in the form of a product of the functions (25) and the rotational functions JMK of a spherical top (provided that the vibronic–rotational interaction is neglected):

$$|\Gamma\gamma JMK\rangle = |\Gamma\gamma\rangle |JMK\rangle \quad (\Gamma = A_1, T_2; \quad K, M = 0, \pm 1, \dots, \pm J) \quad (26)$$

while the appropriate energy eigenvalues may be written in the form

$$E_{A_1 J} = BJ(J+1) + \Delta, \quad E_{T_2 J} = BJ(J+1) - \Delta \quad (27)$$

The representation of the full eigenfunction of the system in the form (26) is based on the assumption that the interatomic distances at the minima points of the adiabatic potential do not differ very much from that of the high-symmetry configuration, and the deviations of the rotational functions from the spherical-top ones may be neglected. If these small deviations are taken into account, a small splitting of the degenerate vibronic–

rotational levels and small corrections to the transition intensities obtained below have to be expected.

The absolute intensity of stimulated dipole transition $\Gamma J \rightarrow \Gamma' J'$ per unit of radiation density is given by the expression

$$\alpha_{\Gamma J \rightarrow \Gamma' J'} = \frac{8\pi^3}{3h^2c^2} \frac{N}{Z} (E_{\Gamma' J'} - E_{\Gamma J}) [\exp(-\beta E_{\Gamma J}) - \exp(-\beta E_{\Gamma' J'})] \times g_{\Gamma J}^{\downarrow} \sum_{r=X,Y,Z} \sum_{\gamma' M' K'} |\langle \Gamma \gamma J M K | \hat{d}_r | \Gamma' \gamma' J' M' K' \rangle|^2 \quad (28)$$

where

$$Z = \sum_{J=0}^{\infty} (2J+1)^2 [3g_{\Gamma 2J}^{\downarrow} \exp(\beta \Delta) + g_{\Gamma 1J}^{\downarrow} \exp(-\beta \Delta)] \exp[-BhcJ(J+1)]$$

is the statistical sum, N is the number of molecules per unit volume, $\hat{d}_{X,Y,Z}$ are the operators of projection of the vector of the dipole moment on the Cartesian axis of the LSC and $g_{\Gamma J}^{\downarrow}$ is the statistical gravity of the states of Eq. (26) dependent on the spin of the nuclei I (see Wilson, 1935). For instance, for a tetrahedral molecule containing nuclei with the spin $I = \frac{1}{2}$, $g_{\Gamma J}^{\downarrow}$ is determined by the formula

$$g_{\Gamma J}^{\downarrow} = \frac{5a_{\Gamma} + 2b_{\Gamma} + 3c_{\Gamma}}{[\Gamma](2J+1)} \quad (29)$$

in which $[\Gamma]$ is the dimensionality of the irreducible representation Γ ; a_{Γ} , b_{Γ} , and c_{Γ} are the coefficients in the expansion of the direct product $\mathcal{D}^J \otimes \Gamma$ (where \mathcal{D}^J is the representation of the full spherical group) with respect to the irreducible representations of the point group T_d :

$$\mathcal{D}^J \otimes \Gamma = a_{\Gamma} A + b_{\Gamma} E + c_{\Gamma} T, \quad a_{\Gamma} + 2b_{\Gamma} + 3c_{\Gamma} = [\Gamma](2J+1) \quad (30)$$

Passing in Eq. (28) from the components of the dipole moment in the LSC to the ones in the MSC presented in the case under consideration by the matrices (22) and performing integration over the rotational coordinates and summation over M , K , M' , K' , we obtain

$$\alpha_{\Gamma J \rightarrow \Gamma' J'} = \frac{8\pi^3}{9h^2c^2} \frac{N}{Z} (E_{\Gamma' J'} - E_{\Gamma J}) (e^{-\beta E_{\Gamma J}} - e^{-\beta E_{\Gamma' J'}}) g_{\Gamma J}^{\downarrow} d^2 (2J+1)(2J'+1) \quad (\Delta J = J' - J = 0, \pm 1) \quad (31)$$

The R transitions with $J' = J + 1$ are of three possible types: $T_2 J \rightarrow T_2(J+1)$ (R), $A_1 J \rightarrow T_2(J+1)$ (R'), $T_2 J \rightarrow A_1(J+1)$ (R''), whereas the Q transitions ($J' = J$) and P transitions ($J' = J - 1$) are allowed only as $T_2 J \rightarrow A_1 J$ (Q) and $T_2 J \rightarrow A_1(J-1)$ (P).

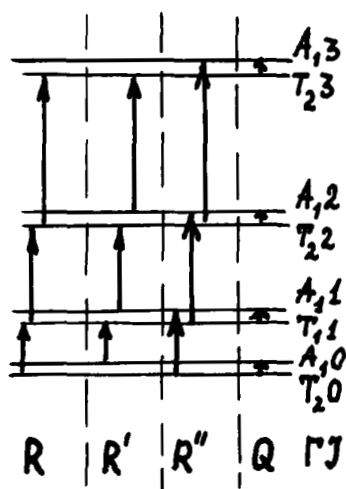


Fig. 1. Tunneling-rotational energy levels and allowed transitions for $\Delta < B$. The dashed lines divide the transitions of different branches.

Typical energy-level schemes for dipolarly unstable systems with indications of the allowed rotational, tunneling, and tunneling-rotational transitions in two limit cases, when the rotational frequency is larger than the tunneling one and when the inverse inequality takes place, are presented in Figs. 1 and 2. The expected pure rotational spectra for three concrete sets of parameter values are shown in Figs. 3 to 5. If $\Delta = 0$ (or

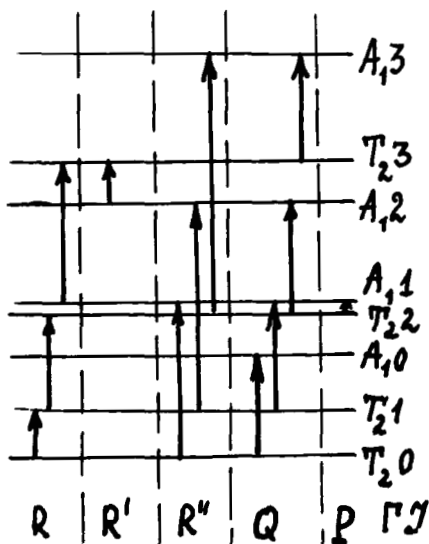


Fig. 2. The same as in Fig. 1 for $\Delta > B$.

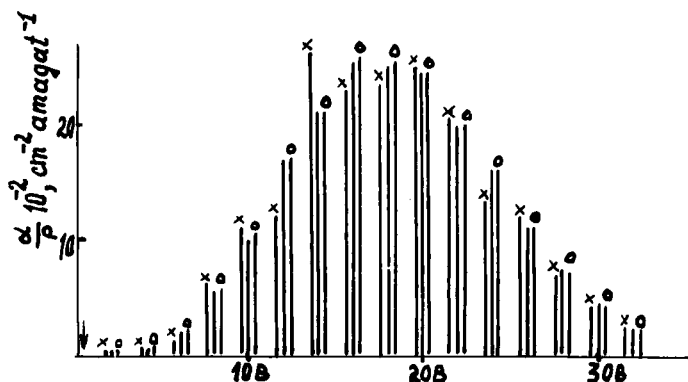


Fig. 3. Numerical calculated position and intensities of the pure rotational spectrum of dipolarly unstable tetrahedral systems for the following parameter values (in inverse centimeters): $\Delta = 0.5$, $B = 5.24$, $kT = 200$. Marked with crosses and circles and unmarked are the R' , R'' , and R branches, respectively, with the Q transition indicated by an arrow (p is the gas pressure in amagat units).

more correctly if $\Delta \ll B$, the transition frequencies of the three R -type bands (R' , R , R'') coincide, and the resulting spectrum consists of equidistant lines with a $2B$ spacing, the branches P and Q being absent. When Δ increases each of the lines of the type R splits into three lines, R' , R , and R'' , the frequencies of the R' and R'' ones being, respectively, smaller and larger than the frequency of the R transition. In addition, the line appropriate to the Q transition occurs at the frequency 2Δ .

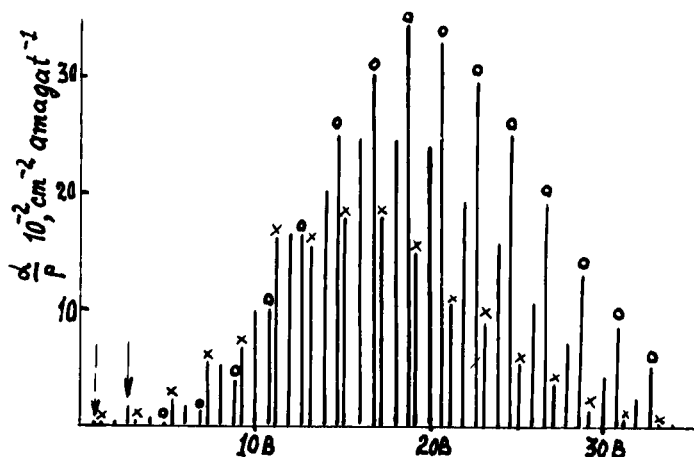


Fig. 4. The same as in Fig. 3 for $\Delta = 7.5$, $B = 5.24$, $kT = 200$. The dashed arrow indicates the P transition.

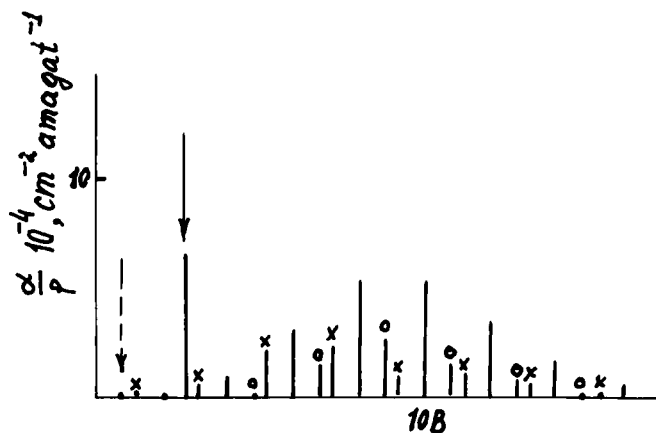


Fig. 5. The same as in Fig. 3 for $\Delta = 7.5$, $B = 5.24$, $kT = 50$ (note that the scale here is 100 times smaller than in Figs. 3 and 4).

In the case of $\Delta > B$ the picture of the spectrum changes drastically (Fig. 4). Besides the increase of the difference in the frequencies of the lines in the three branches R' , R , and R'' , their relative intensities also change, increasing in the R'' branch and decreasing in the R' one. Simultaneously, the Q transition becomes stronger and the P -type lines occur. The number and intensity of the latter increase with the strength of the inequality $\Delta > B$. Note that in the usual pure rotational spectra of molecules with proper dipole moments the R transitions only are observed, whereas all the branches R , P , and Q can be observed only in the rotational structure of the vibrational band. In the predicted vibronic spectrum all these branches occur simultaneously in the region of pure rotational transitions with three R -type branches instead of one in the usual spectrum and the branches P and Q emerging for large Δ values only.

Another feature of the pure rotational spectra under consideration is that the intensity of the Q transition increases as compared with the other lines by lowering the temperature, and hence beginning from some temperatures the Q line becomes distinguished from the background band (Fig. 5). This Q line, being appropriate to the transition without change of the rotational quantum number ($\Delta J = 0$), is by its manifestation (by shape and peculiarities of the temperature behavior) analogous to the zero-phonon line in optical spectra, and therefore it can be called the zero-rotation line. The absorption of microwaves appropriate to this transition (without taking into consideration the rotations) was considered by Bersuker and Vekhter (1965) and presumably was observed by Gyorgy *et al.* (1966).

The question of the intensity of the predicted pure rotational spectrum needs special consideration. It follows from Eq. (31) that the intensities of the lines are proportional to d^2 . Unfortunately, accurate calculations of the dipole moment d at the minima points of adiabatic potential are very difficult. However, it is known that the d value may vary within wide limits depending on the value of the constant of vibronic coupling. For instance, empirical estimation of d value for the PO_4^{3-} ion under the assumption that its dipole instability is responsible for the triggering of the spontaneous polarization of the crystal KH_2PO_4 results in the value $d \sim 0.1$ D.

2. Pure Rotational Transitions Induced

by the Jahn–Teller Effect and Spin–Orbital Interactions

Let us consider another example in which the unusual pure rotational spectrum in spherical-top molecules with the Jahn–Teller effect occurs (Ogurtsov, 1982, 1984). Consider a molecular system that in the high-symmetry configuration of T_d symmetry has a twofold degenerate electronic ground term with one unpaired electron (the term 2E). The vibronic energy levels in this case, if the interaction with e-type vibrations in the linear approximation (linear $E \otimes e$ problem) is taken into account, are twofold degenerate (Longuet-Higgins *et al.*, 1958; Bersuker and Polinger, 1983). The total vibronic–rotational Hamiltonian of this system is

$$\hat{H} = \hat{H}_{\text{vibr}} + B(\hat{\mathbf{J}} - \hat{\mathbf{I}} - \hat{\mathbf{s}})^2 + \lambda \hat{\mathbf{I}} \cdot \hat{\mathbf{s}} \quad (32)$$

where \hat{H}_{vibr} is the Hamiltonian of the internal degrees of freedom without taking into account the spin-orbital interaction; $\hat{\mathbf{s}}$, $\hat{\mathbf{I}}$, and $\hat{\mathbf{J}}$ are the operators of the spin, orbital, and total momentum, respectively; and λ is the constant of the spin-orbital interaction. Considering the operator

$$\hat{V} = (\lambda + 2B)\hat{\mathbf{I}} \cdot \hat{\mathbf{s}} - 2B\hat{\mathbf{J}} \cdot \hat{\mathbf{I}} \quad (33)$$

as a perturbation, its matrix elements in the basis of the vibronic function of $E \otimes e$ problem being zero, and neglecting the rotational structure of the vibronic levels of the excited electronic terms, we obtain instead of the Hamiltonian (32)

$$\hat{\hat{H}} = \hat{H}_{\text{vibr}} + B(\hat{\mathbf{J}}^2 + \hat{\mathbf{s}}^2) - 2(B - B^*)\hat{\mathbf{J}} \cdot \hat{\mathbf{s}} \quad (34)$$

where $B^* \sim \lambda B/\Delta E$ and ΔE is the energy gap between the ground electronic term 2E and the lowest excited term 2T . The eigenvalues and wave functions of the Hamiltonian (34) are determined by the relations

$$E_{neJR} = E_{ne} + BR(R + 1) + B^*[-R(R + 1) + J(J + 1) + \frac{3}{4}] \quad (35)$$

$$|neJRK_R M\rangle_0 = |ne\rangle \sqrt{\frac{2R+1}{8\pi^2}} \sum_{K_m} C_{RK_R 1/2m}^{JK} D_{MK}^{J*}(\Omega) \left| \frac{1}{2} m \right\rangle \quad (36)$$

in which E_{ne} is the energy of the vibronic state $|ne\rangle$ [here the notations used by Child and Longuet-Higgins (1961) are retained]; J and M , K are the values of the total momentum and projections on the Z axes of the LSC and MSC, respectively; $|\frac{1}{2}m\rangle$ are the spin functions; D_{MK}^J is the Wigner function; $C_{RK_R 1/2m}^{JK}$ are the Clebsh–Gordan coefficients for the full spherical group; R and K_R are the magnitudes of the pure rotational moment and its projection on the Z axis of the MSC.

The vibronic functions $|ne\rangle$ belong to the representation A_1 , A_2 , and E of the symmetry point group. Therefore in the group T_d the matrix elements of the operator of the dipole moment (belonging to the T_2 representation) calculated by the functions in (36) are identically equal zero. Hence the dipole transitions between the states (36) are forbidden as pure rotational or vibronic–rotational ones.

Consider now the change of the selection rules due to the mixing of the nondipolar states (36) with excited states of dipolar type by the interaction in Eq. (33). The wave functions in the first-order perturbation are

$$\begin{aligned} |neJRK_R M\rangle &= |neJRK_R M\rangle_0 \\ &+ \sum_{mTtJ''R''K_R''M''} \frac{\langle mTtJ''R''K_R''M'' | \hat{V} | neJRK_R M \rangle_0}{E_{neJR} - E_{mTtJ''R''}} \\ &\times |mTtJ''R''K_R''M''\rangle_0 \end{aligned} \quad (37)$$

where $|mTtJ''R''K_R''M''\rangle$ are the vibronic–rotational states arising from the vibronic state $|mTt\rangle$ of the $|mT\rangle$ electronic term of the type T (T_1 or T_2). If the dependence of the energy denominators in Eq. (37) on the rotational quantum number is neglected, then in the first order with respect to the spin-orbital interaction constant we obtain for the matrix elements of the r th circular component (in LSC) of the operator of the dipole moment the expression

$$\begin{aligned} &\langle n'e'J'R'K_R'M' | \hat{d}_r | neJRK_R M \rangle \\ &= -(-1)^r \frac{\sqrt{3(2R'+1)(2R+1)}}{2(2J+1)} C_{J'M'1-r}^{JM} \sum_{\sigma\sigma'Qq} \\ &\times A_{n'e',ne}^{\sigma'\sigma} C_{RK_R R'K_R}^{Qq} C_{1-\sigma 1-\sigma'}^{Qq} \begin{Bmatrix} \frac{1}{2} & 1 & 1 \\ J' & J & 1 \\ R' & R & Q \end{Bmatrix} \end{aligned} \quad (38)$$

where

$$A_{n'e',ne}^{\sigma'\sigma} = \lambda \sum_{mT} \left\langle n'e' \left| \hat{d}_\sigma \times \frac{1}{E_{mT} + \hat{H}_{mT} - E_{ne}} \hat{l}_{\sigma'} + \hat{l}_{\sigma'} \frac{1}{E_{mT} + \hat{H}_{mT} - E_{n'e'}} \hat{d}_\sigma \right| ne \right\rangle \quad (39)$$

\hat{d}_σ and $\hat{l}_{\sigma'}$ are circular components of the dipole and orbital momentum in the MSC, \hat{H}_{mT} is the vibronic Hamiltonian for the excited electronic state $|mT\rangle$ that lies at an energy interval E_{mT} above the ground on E , and the material within the braces is the $9j$ symbol (Varshalovich, *et al.*, 1975).

The expression (39) can be simplified by employing the Franck-Condon principle, which allows us to substitute \hat{H}_{mT} by the operator of vibronic interaction V_{mT} in the appropriate electronic term mT .^{*} Using this approximation and taking into account that the energy differences $|E_{ne} - E_{n'e'}|$ are small compared with the energy E_{mT} , we come to the expression

$$\begin{aligned} A_{n'e',ne}^{\sigma'\sigma} &\simeq \langle n'e' | \hat{A}_{\sigma'\sigma}(q) | ne \rangle \\ &= \lambda \left\langle n'e' \left| \sum_{mT} \left[\hat{d}_\sigma \frac{1}{E_{mT} + V_{mT}(q) - \bar{\epsilon}} \hat{l}_{\sigma'} + \hat{l}_{\sigma'} \frac{1}{E_{mT} + V_{mT}(q) - \bar{\epsilon}} \hat{d}_\sigma \right] \right| ne \right\rangle \end{aligned} \quad (40)$$

in which q denotes all the normal coordinates of the molecule and $\bar{\epsilon}$ is an averaged value over the $E_{n'e'}$ and E_{ne} magnitudes.

Now we expand the operator $\hat{A}_{\sigma'\sigma}(q)$ in power series with respect to q and constrain ourselves by the zero-order term only considering that the contributions of the higher-order terms to the $(E_{mT} - \bar{\epsilon})$ mean values are small. In this approximation $\hat{A}_{\sigma'\sigma}(0)$ are pure electronic operators transforming as $(\hat{d}_\sigma \hat{l}_{\sigma'} + \hat{l}_{\sigma'} \hat{d}_\sigma)$, e.g., they belong to the reducible representation $T_1 \times T_2$. Using the vibronic functions of the linear $E \otimes e$ problem and taking into account that the $\hat{l}_{\sigma'}$ operators are pure imaginary ones, we can show that the matrix elements are nonzero only for those components $\hat{A}_{\sigma'\sigma}(0)$, from which irreducible tensor operator belonging to the A_2 repre-

^{*} Similar approximations are traditionally used for estimations of matrix elements of the operator of polarizability that differ from that of Eq. (39) only by the substitution of the operator $\hat{l}_{\sigma'}$ by the appropriate component of the operator of the dipole moment \hat{d}_σ (Child and Longuet-Higgins, 1961).

sensation can be formed. For them we have

$$\langle n'e' | \hat{A}_{\sigma'\sigma}(0) | ne \rangle = \frac{(-1)^\sigma}{3} \delta_{\sigma-\sigma'} d_{n'e',ne} d_{\text{eff}} \quad (41)$$

where $\delta_{\sigma\sigma'}$ is the Kroneker delta symbol,

$$d_{n'e',ne} = \langle n'_+ | n_+ \rangle - \langle n'_- | n_- \rangle \quad (42)$$

is one of the so-called primitive vibronic parameters introduced in the work of Child and Longuet-Higgins (1961), and

$$d_{\text{eff}} = \lambda \sum_{mT} \frac{\langle E | \hat{d} | mT \rangle \langle mT | \hat{l} | E \rangle}{E_{mT} - \bar{E}} \quad (43)$$

is the effective value of the electronic dipole moment in the ground electronic state induced by the spin-orbital interaction, $\langle E | \hat{d} | mT \rangle$ and $\langle mT | \hat{l} | E \rangle$ being the reduced matrix elements of the operators of the dipole moment and orbital momentum calculated by the functions of the ground E and excited mT electronic terms.

The absolute intensity of the transition $neJR \rightarrow n'e'J'R'$ is determined by the magnitude of the expression

$$I_{n'e'J'R',neJR} = \sum_{rMM'K_RK_R'} | \langle n'e'J'R'K_R'M' | \hat{d}_r | neJRK_RM \rangle |^2 \quad (44)$$

which by means of Eqs. (38), (40), and (41) can be reduced to the form

$$I_{n'e'J'R',neJR} = \frac{3}{2} d_{\text{eff}}^2 d_{n'e',ne}^2 \delta_{RR'} (2R+1)(2J'+1)(2J+1) \begin{pmatrix} \frac{1}{2} & J' & R \\ \frac{1}{2} & J & R \\ 1 & 1 & 0 \end{pmatrix} \quad (45)$$

It follows from Eqs. (43) and (45) and the properties of the $9j$ symbols that for nonzero λ values vibronic–rotational transitions are allowed with selection rules $\Delta R = R' - R = 0$ and $\Delta J = J' - J = 0, \pm 1$, which correspond to pure rotational transitions, if $E_{n'e'} = E_{ne}$, and vibronic transitions, when $E_{n'e'} \neq E_{ne}$, provided that the coefficients $d_{n'e',ne}$ are nonzero. In the case of $E_{n'e'} \neq E_{ne}$ this is possible only in the presence of the vibronic interaction. Therefore the predicted vibronic–rotational spectrum can be observed only in systems in which the spin-orbital interaction is strong enough and there is the Jahn–Teller effect.

In some cases, not the line of pure rotational spectrum itself, but the spectrum envelop of the band shape is of primary interest (e.g., due to the low resolution of the measurement technique). In the conditions under consideration the line shape can be determined by the relation

$$\begin{aligned}
 F(\omega) = d_{\text{eff}}^2 \frac{\sum_{ne} d_{ne,ne}^2 \exp(-\beta E_{ne})}{2B^*Z} \\
 \times \sum_{R=0}^{\infty} \exp[-BR(R+1)] \left\{ \exp\left[b^* \left(R - \frac{1}{2}\right)\right] \right. \\
 \left. - \exp\left[-b^* \left(R - \frac{3}{2}\right)\right] \right\} R(R+1) \\
 \times \delta\left[R - \left(\frac{\hbar\omega}{2B^*} - \frac{1}{2}\right)\right]
 \end{aligned} \quad (46)$$

where Z is the partition function of the system, ω is the frequency of the incident light, $b = \beta B$, $b^* = \beta B^*$, and $\delta(x)$ is the Dirac delta function. The deduction of Eq. (46) was performed by using the explicit form of the $9j$ symbol for the appropriate absorption pure rotational transitions ($J = R - \frac{1}{2}, R \rightarrow (J' = R + \frac{1}{2}, R)$).^{*} Assuming that $B \ll kT$ and passing in Eq. (46) from summation over R to integration, we have

$$\begin{aligned}
 F(\omega) = d_{\text{eff}}^2 \frac{\sum_{ne} d_{ne,ne}^2 \exp(-\beta E_{ne})}{B^*Z} \exp\left[-\beta \left(\frac{\hbar\omega}{2B^*}\right)^2\right] \\
 \times \text{sh}\left(\frac{\hbar\omega\beta}{2}\right) \left[\left(\frac{\hbar\omega}{2B^*}\right)^2 - \frac{1}{4}\right]
 \end{aligned} \quad (47)$$

By way of example consider the possibility of observation of the predicted pure rotational spectrum in the case of the VCl_4 molecule, the ground state of which is twofold degenerate (Morino and Uehara, 1966; Truax *et al.*, 1974; and others). It can be shown by means of numerical calculation after Eq. (47) (assuming for the VCl_4 molecule $B \sim 0.04 \text{ cm}^{-1}$) that at room temperatures the band appropriate to the pure rotational spectrum has a maximum at $\omega \sim 0.3 \text{ cm}^{-1}$. When the temperature is raised, the maximum of this band shifts to a region of higher frequencies.

^{*} Note that in the 2E term of a spherical-top molecule with the spin-orbital interaction taken into account, dipole transitions are allowed between the vibronic states $|ne\rangle$ and $|n'e'\rangle$, which are nondipolar states since they originate from a nondipolar electronic term interacting with nonactive in the IR absorption E vibrations. The intensity of such transitions in accordance with Eq. (45) is proportional to $d_{\text{eff}}^2 d_{n'e',ne}^2$ (Ogurtsov, 1984).

In order to estimate the effective dipole moment of the pure rotational transitions under consideration we constrain ourselves in the calculation of the sum in Eq. (43) by the contribution of the lowest excited electronic term T_2 only. Then, using the experimental data $E_{T_2} \approx 9000 \text{ cm}^{-1}$ (Orgel, 1955; Blankenship and Belford, 1962), $\lambda \approx 270 \text{ cm}^{-1}$ (Clarck and Machin, 1963), $\langle E \| \hat{d} \| T_2 \rangle \approx 0.7 \text{ D}$ [from the value of the oscillator strength of the $E \rightarrow T_2$ transition (Blankenship and Belford, 1962)], we obtain for the effective dipole moment

$$d_{\text{eff}} \sim 10^{-2} \text{ D} \quad (48)$$

This value is smaller than that obtained from the estimation of the dipole moment value in the minima configurations of the dipolarly unstable systems. Nevertheless, even in this case the expected pure rotational absorption spectrum can be observed. Indeed, at the present time even very weak pure rotational lines induced by collisions and vibration–rotational centrifugal interactions, for which the effective dipole moment is estimated equal to 10^{-6} D , are observed experimentally and investigated (Rosenberg *et al.*, 1972; Ozier and Rosenberg, 1973). By comparison, one can see that the predicted vibronic pure rotational spectrum may be about 10^8 times more intensive than that experimentally observed in the works of Ozier *et al.*, provided that the $d_{ne,ne}$ coefficients are not very small. Using the numerical results of Child and Longuet-Higgins (1961), we can make sure that in the case of the VCl_4 molecule these coefficients lower the estimation of the intensity of the pure rotational spectrum by no more than one or two orders of magnitude (Ogurtsov, 1984).

C. Dielectric Losses

In this section the properties of dipolarly unstable molecules (DUMs) in a viscous nonpolar medium in the presence of a electromagnetic field are considered. We consider especially the microwave spectrum of absorption. It is not related to the resonance transitions between rotational levels (nonresonance spectrum of Debye type). We assume that there is a weak solution of the DUM in a dense nonpolar medium in the presence of a variable electric field $\mathcal{E}(t)$. The Hamiltonian of such a system has the form

$$\hat{H} = \hat{H}_{\text{mol}} + \hat{H}_{\text{diss}} + \hat{H}_{\text{mol-diss}} \quad (49)$$

where \hat{H}_{mol} , \hat{H}_{diss} , and $\hat{H}_{\text{mol-diss}}$ are the Hamiltonians, respectively, for the solute molecules, dissipative subsystem (the medium), and the interaction between them. In order to investigate the absorption spectrum of such a system, we assume that the dissipative medium is transparent in the region of field frequencies under consideration. Then, owing to the assumed

smallness of the concentration of the solution, the contribution to the spectrum from the molecules is additive and the Hamiltonian \hat{H}_{mol} is in fact the one of a separate molecule,

$$\hat{H}_{\text{mol}} = \hat{H}_{\text{vibr}} - \hat{d}_Z \mathcal{E}(t) \quad (50)$$

where it is assumed that the field $\mathcal{E}(t)$ is directed along the Z axis of the LSC and \hat{d}_Z is the operator of projection of the dipole moment on the same axis. The dynamic variables of the internal degrees of freedom and the operator \hat{H}_{vibr} are presented by the matrices in the basis of the most essential lowest vibronic states.

In accordance with the fluctuation-dissipation theory (see, e.g., Huber and Van Vleck, 1966; Zubarev, 1971) the imaginary part of the polarizability $\alpha''(\omega) = \text{Im } \alpha(\omega)$, which determines the absorption of the field energy, has the form

$$\alpha''(\omega) = 2N\hbar \left(\frac{\beta\omega}{2} \right) \int_0^\infty \varphi(t) \cos(\omega t) dt \quad (51)$$

where N is the concentration of DUMs, ω is the field frequency,

$$\varphi(t) = \frac{1}{2} \langle \hat{d}_Z \hat{d}_Z(t) + \hat{d}_Z(t) \hat{d}_Z \rangle \quad (52)$$

is the symmetrized quantum-mechanical correlation function, and $\hat{d}_Z(t)$ is the operator of the dipole moment in the Heisenberg representation. Hereafter the system of units is used in which $\hbar = 1$.

Suppose that the interaction of the molecule with the dissipative medium is realized through the rotational-only degrees of freedom of the molecule and does not affect the vibronic ones. Then, passing to the system of coordinates linked to the molecule by means of the Wigner functions D_{mm}^j and using the classical description for the rotational diffusion, we have

$$\varphi(t) = \frac{1}{2} \sum_{mm'} \langle \hat{d}_m \hat{d}_{m'}(t) + \hat{d}_{m'}(t) \hat{d}_m \rangle_{\text{vibr}} K_{mm'}(t) \quad (53)$$

where \hat{d}_m are the circular components of the operator of the dipole moment in the MSC, the material within angle brackets means statistical averaging with the equilibrium density matrix of the vibronic degrees of freedom, and $K_{mm'}(t) = \langle D_{m0}^1[\Omega(t)] D_{m'0}^1[\Omega(0)] \rangle$ is the orientational correlation function. If we assume that in the case under consideration the rotational motion is of the Brown origin, $K_{mm'}(t)$ can be presented in the form

$$K_{mm'}(t) = \frac{(-1)^m}{3} \delta_{m-m'} K(h_m, t) \quad (54)$$

where $K(h_m, t)$ is a complicated function of several variables including time, main values of the viscosity tensor ξ_i ($i = 1, 2, 3$) (or of the appropriate tensor of rotational diffusion $D_i = kT/\xi_i$), the tensor of the moment of inertia I_i and temperature, $h_m = 2D_1 + (D_3 - D_1)m^2$. The nature of the rotational relaxation is unknown in detail, and hence so are the functions $K(h_m, t)$. The latter have to be determined by comparison of the theoretical and experimental data. The interpretation of these functions is usually performed on the basis of the following approximation (Steele, 1963):

$$K(h_m, t) = \begin{cases} \exp(-h_m t), & \sqrt{\beta/I} \xi_i > 2 \\ \exp(-t^2/\beta I), & \frac{1}{2} < \sqrt{\beta/I} \xi_i < 2 \end{cases} \quad (55)$$

where I is the mean moment of inertia determined by the relationship $I^{-1} = \frac{1}{3}(I_1^{-1} + I_2^{-1} + I_3^{-1})$. In the case of spherical-top molecules the orientational correlation function of free rotations in the limit of high temperatures ($B \ll kT$) can be written in the form (Steele, 1963)

$$K(t) = \frac{1}{3} + \frac{2}{3} \left(1 - \frac{t^2}{\beta I}\right) \exp\left(-\frac{t^2}{2\beta I}\right) \quad (56)$$

With these ideas we consider now the spectra of the dielectric losses for systems with dipole instability. The DUM with two, three, and four minima of the adiabatic potentials are taken as examples. The matrices \hat{H}_{vibr} and \hat{d}_m needed for the calculation of microwave spectra are given by Eqs. (18), (20), and (22).

1. Dipolarly Unstable Molecules with Two Minima

Substituting Eq. (18) into Eq. (53) we obtain the following expressions for the correlation function $\varphi(t)$ and the imaginary part of polarizability

$$\varphi(t) = \frac{1}{3} d^2 K(h_0, t) \cos(2\Delta t) \quad (57)$$

and

$$\alpha''(\omega) = \frac{2Nd^2}{3} \text{th}\left(\frac{\beta\omega}{2}\right) [f(\omega - 2\Delta) + f(\omega + 2\Delta)] \quad (58)$$

where

$$f(\omega) = \begin{cases} \frac{D_1}{\omega^2 + 4D_1^2}, & \sqrt{\beta/I} \xi_1 > 2 \\ \frac{\sqrt{\pi\beta I}}{4} \exp\left(-\frac{\beta I}{4} \omega^2\right), & \frac{1}{2} < \sqrt{\beta/I} \xi_1 < 2 \end{cases} \quad (59)$$

2. Dipolarly Unstable Molecules with Three Minima

In the case of symmetric-top DUMs with three minima the functions $\varphi(t)$ and $\alpha''(\omega)$ by means of relations (20) and (53) may be presented in the form

$$\varphi(t) = \frac{1}{3} d^2 \frac{2 \cos(2\Delta t) \operatorname{ch}(\beta\Delta) + \exp(\beta\Delta)}{2 \operatorname{ch}(\beta\Delta) + \exp(\beta\Delta)} K(h_1, t) \quad (60)$$

$$\alpha''(\omega) = \frac{4Nd^2 \operatorname{th}(\beta\omega/2)}{3[2 \operatorname{ch}(\beta\Delta) + \exp(\beta\Delta)]} \times \{\exp(\beta\Delta)g(\omega) + \operatorname{ch}(\beta\Delta)[g(\omega - 2\Delta) + g(\omega + 2\Delta)]\} \quad (61)$$

where the function $g(\omega)$ either coincides with $f(\omega)$ if $\frac{1}{2} < \sqrt{\beta/I} \xi_i < 2$, or it can be obtained from $f(\omega)$ by substitution of D_1 by $(D_1 + D_3)$, if $\sqrt{\beta/I} \xi_{1,3} > 2$.

3. Dipolarly Unstable Molecules with Four Minima

In tetrahedral systems with an adiabatic potential having four dipolar type minima, the correlation function $\varphi(t)$ and $\alpha''(\omega)$ have the form

$$\varphi(t) = \frac{1}{3} d^2 \frac{\cos(2\Delta t) \operatorname{ch}(\beta\Delta) + \exp(\beta\Delta)}{\operatorname{ch}(\beta\Delta) + \exp(\beta\Delta)} K(h_0, t) \quad (62)$$

$$\alpha''(\omega) = \frac{2Nd^2 \operatorname{th}(\beta\omega/2)}{3[\operatorname{ch}(\beta\Delta) + \exp(\beta\Delta)]} \times \{2 \exp(\beta\Delta)f(\omega) + \operatorname{ch}(\beta\Delta)[f(\omega - 2\Delta) + f(\omega + 2\Delta)]\} \quad (63)$$

It is seen from Eq. (58) that the microwave absorption spectrum of DUMs with two minima can be described in the case of large viscosity by the Van Vleck-Weiskopf formula with the correlation time $\tau = 1/(2D_1)$. For intermediate values of the viscosity, the spectrum changes qualitatively, approaching to a Gaussian distribution. In the case of DUM with three or four minima of the adiabatic potential, the microwave spectra became essentially complicated. Their distinguished feature is the presence of two maxima on the absorption curve that are realized for a special relationship between the parameter values. One of these maxima is positioned near the frequency of the resonance transition $\omega \sim 2\Delta$, the other being at the frequency $\omega \sim 2D$. The occurrence of the additional maximum of nonresonance (Debye-type) absorption can be explained by the considerations given earlier owing to which the threefold degenerate states $T_{1,2}$ in tetrahedral systems and the twofold degenerate states in systems with D_{3h} symmetry are of dipolar type.

It is interesting to compare the results obtained in this section for the absorption spectrum in a viscous medium with the pure rotational spec-

trum of free-rotating molecules. In the case of DUMs with four minima in the absence of viscosity ($\xi = 0$) $K(t)$ is determined the relation (56) and

$$f(\omega) = \frac{\pi}{6} \delta(\omega) + \sqrt{\frac{\pi}{18}} (\beta I)^{3/2} \omega^2 \exp\left(-\frac{\beta I}{2} \omega^2\right) \quad (64)$$

Substituting the expression in Eq. (64) into Eq. (63) and comparing the expression obtained for $\alpha''(\omega)$ with the pure rotational spectrum, we can see that the term $[f(\omega - 2\Delta) + f(\omega + 2\Delta)]$ describes the Q transition [contribution proportional to $\delta(\omega - 2\Delta)$] and the envelope of the lines of the type R', R'', and P. Besides, in $\alpha''(\omega)$ there is a contribution $f(\omega)$ with the maximum at the frequency $\omega = \sqrt{3kT/(2I)}$ appropriate to pure rotational transitions with unchanged vibronic quantum numbers [of the type R: $T_2J \rightarrow T_2(J + 1)$]. The expression of the type (63) with the $f(\omega)$ function described by Eq. (64) can be obtained directly from Eq. (31) if in the limit case of high temperatures ($B \ll kT$) one substitutes the summation over J by integration [similar to the procedure used in the deduction of Eq. (47)].

The results of this section show also that in a viscous medium the DUMs preserve the peculiar electric properties and are manifest either as rigid dipole molecules (in the region of irradiation frequencies $\omega \sim 2D$) or as polarizable nondipolar ones (in the region of resonance $\omega \sim 2\Delta$). It follows that the interpretation of DUM spectra is essentially dependent on the ratio between the constant of rotational diffusion D and the tunneling splitting magnitude Δ . In particular, in the case of two minima of the adiabatic potential in the limit of weak diffusion, the frequency dependence of the spectral curve has a resonance character with a maximum at the frequency $\omega = 2\Delta$, while in the opposite limit case this frequency dependency coincides with the Debye curve. In a visual interpretation this result means that in the former case the frequency of reorienting collisions is much less than the frequency of tunneling transitions, and hence the absorption takes place at the tunneling energy levels. In the opposite limit case, there are many collision reorientations during the stay of the system in one of the minima configurations, and therefore the molecule is manifest as a rigid dipole one.

In the case of three or four minima on the adiabatic potential, beside the transition between the A , E or A_1 , T_2 energy levels broadened by the interaction with the medium, the transitions without change of the energy of internal degrees of freedom of the molecule also contribute to the spectrum. The broadening is due to the fact that there is a probability of transitions of the system from one of its minimum configurations to another equivalent one as the result of a diffusional reorientation, and not by tunneling. Consequently, in these systems there is always a Debye-type

contribution to the absorption, although the general form of the spectrum depends on the relation between the tunneling splitting and diffusion rotational transition frequencies.

In conclusion of this section we present some examples of molecular systems in which the Jahn–Teller or pseudo-Jahn–Teller effects result in configurations having dipole moments. The simplest ones seem to be CH_4^+ in the ground state (Gemmel *et al.*, 1980a,b) and CH_4 in the excited one, as well as any other systems of the type AX_4 , where $\text{A} = \text{C}, \text{Si}, \text{Sn}, \dots$, and $\text{X} = \text{H}, \text{F}, \text{Cl}, \text{Br}, \text{J}, \text{CH}_3, \dots$, in the ground ion or excited molecular states. Molecules of the type X_3 (O_3 , C_3H_3 , $\text{C}_6\text{H}_3\text{X}_3$, etc.) can also be DUMs. The condition for the possibility of investigation of the microwave absorption spectrum in the excited states is that the lifetime in the latter τ' must be larger than the time of rotational relaxation $\tau \sim (2D)^{-1}$. This condition is usually fulfilled, since by the order of the magnitude $\tau' \sim 10^{-8} - 10^{-9}$ sec and $\tau \sim 10^{-10} - 10^{-11}$ sec. Another possibility for studying dielectric losses in the excited states can be realized by means of laser excitation of the molecule to the degenerate state of dipolar type or to a state with dipole instability.

III. Anisotropy of Polarizability and Hyperpolarizabilities in Degenerate States

As mentioned in the preceding section, for degenerate states there may be nonzero matrix elements of anisotropic components of the tensor of polarizability that belong to the nontotally symmetric representation of the point group. It seems to be interesting to elucidate the possible manifestations of this fact in experiments traditionally used for the investigation of the anisotropic polarizabilities of molecular systems. The birefringence in constant and alternating fields and light scattering belong to such experiments.

A. Anomalous Birefringence in Gases of Spherical-Top Molecules:

The Kerr and Cotton–Mouton Effects

The birefringence in external electric and magnetic fields (the Kerr and Cotton–Mouton effects) can be explained by the anisotropy of the properties of the medium that is due to either the orientation of anisotropic molecules in the external field (the Langevin–Born mechanism) or the deformation of the electric or magnetic susceptibilities by this field, i.e., to hyperpolarizabilities (Voigt mechanism). The former mechanism is effective for molecules that are anisotropic in the absence of the field and

results in temperature-dependent birefringence. The contribution due to the second mechanism is usually small and independent of temperature. The usual statement is that in gases of spherical-top molecules the birefringence can arise only due to the Voight mechanism. This statement is implicitly based on the initial assumption of the isotropy of dynamic and static polarizabilities or magnetic susceptibility of spherical-top and other high-symmetry molecules. However, this assumption is incorrect when the preceding systems are in degenerate states. The degeneracy introduces some special anisotropy leading to appropriate anisotropic properties of the system as a whole.

1. General Theory of Birefringence in External Fields

Consider first the general theory of birefringence in gases of noninteracting molecules in an external constant and homogeneous electric or magnetic field \mathcal{F} (Ogurtsov *et al.*, 1982, 1983a,b). Neglecting the quantization of the rotation, we obtain for the difference in the indices of refraction of the light polarized along and perpendicular to the direction of the field \mathcal{F} (which is chosen as the Z axis of the LSC) the following relation:

$$\Delta n = n_Z^2 - n_X^2 = 2\pi N \{ \mathcal{F}^{-2} \text{Re}[\overline{\alpha_{ZZ}(\omega, \mathcal{F}, \Omega)} - \overline{\alpha_{XX}(\omega, \mathcal{F}, \Omega)}] \}_{\mathcal{F}=0} \quad (65)$$

in which $\alpha_{IK}(\omega, \mathcal{F}, \Omega)$ is the component of the tensor of dynamic molecular polarizability with respect to the LSC, the overbar denotes the procedure of averaging over the orientations of the molecule Ω , and ω is the frequency of the light propagating along the Y axis of the LSC. The real part of the components of the polarizability $\text{Re } \alpha_{IK}(\omega, \mathcal{F}, \Omega)$ can conveniently be presented by the correlation functions $J_{IK}(t) = \langle \hat{d}_I(t, \mathcal{F}) \hat{d}_K \rangle$. Following Zubarev (1971), we have

$$\text{Re } \alpha_{IK}(\omega, \mathcal{F}, \Omega) = \frac{1}{2\pi} \int_{-\infty}^{\infty} (1 - e^{\beta\omega'}) J_{IK}(\omega') \frac{\omega' d\omega'}{\omega^2 - \omega'^2} \quad (66)$$

where

$$J_{IK}(\omega') = \int_{-\infty}^{\infty} J_{IK}(t) e^{-i\omega' t} dt \quad (67)$$

is the Fourier transformation of the correlation function $J_{IK}(t)$,

$$\hat{d}_K(t, \mathcal{F}) = \exp[it\hat{H}(\mathcal{F})] \hat{d}_K \exp[-it\hat{H}(\mathcal{F})] \quad (68)$$

is the operator of the dipole moment in the Heisenberg representation, $\hat{H}(\mathcal{F}) = \hat{H} - \hat{\mu}_Z \mathcal{F}$ is the Hamiltonian of the molecule in the external field \mathcal{F} , $\hat{\mu}_Z$ is the projection of the operator of the dipole moment \hat{d}_Z , if \mathcal{F} is the electric field ($\mathcal{F} = \mathcal{E}$), and magnetic moment \hat{m}_Z , if \mathcal{F} is the magnetic field

($\mathcal{F} = \mathcal{H}$). The correlation function is defined by the expression

$$J_{IK}(t) = Z^{-1}(\mathcal{F}) \text{Sp}\{\exp[-\beta\hat{H}(\mathcal{F})]\hat{d}_K(t, \mathcal{F})\hat{d}_I\} \quad (69)$$

where Sp denotes the spur operation over the states of the internal degrees of freedom and $Z(\mathcal{F}) = \text{Sp}\{\exp[-\beta\hat{H}(\mathcal{F})]\}$ is the statistical sum of the system.

Assuming that the intensity of the external field \mathcal{F} is small enough (the criterion of smallness will be given later), we expand the correlation function (69) in a power series with respect to the field \mathcal{F} . This can be done in two steps. In the first step partial diagonalization of the Hamiltonian $\hat{H}(\mathcal{F})$ is performed by means of the unitary transformation \hat{U} . The latter excludes that part of the interaction with the field that couples the vibronic states of the ground electronic term $|0v\rangle$ with the excited ones $|Nv'\rangle$ ($N \neq 0$). Since the splitting of the vibronic levels in the field \mathcal{F} (the linear Stark or Zeeman effect) is small compared with the energy interval between the ground and excited electronic levels, their ratio is a small parameter. In the framework of the unitary transformation \hat{U} , the equation for the correlation function (69) can be written in the form

$$J_{IK}(t) = \text{SP}\{\exp[-\beta\hat{H}(\mathcal{F})]\widetilde{\hat{d}_K(t, \mathcal{F})}\widetilde{\hat{d}_I}\}/\text{Sp}\{\exp[-\beta\hat{H}(\mathcal{F})]\} \quad (\hat{\tilde{A}} = \hat{U}\hat{A}\hat{U}^{-1}) \quad (70)$$

Expanding the transformed operator $\hat{H}(\mathcal{F}) = \hat{U}\hat{H}(\mathcal{F})\hat{U}^{-1}$ in a power series with respect to the preceding small parameter and keeping the terms up to the second-order ones, one can obtain the following expression for the matrix elements of the operator $\hat{H}(\mathcal{F})$ in the basis of the vibronic states of the ground electronic term (Bir and Pikus, 1971):

$$\begin{aligned} \langle 0v''|\hat{H}(\mathcal{F})|0v'\rangle &= \langle 0v''|\hat{H}(\mathcal{F})|0v'\rangle \\ &- \frac{\mathcal{F}^2}{2} \sum_{N \neq 0, v} \langle 0v''|\hat{\mu}_Z|Nv\rangle[(E_{Nv} - E_{0v'})^{-1} \\ &+ (E_{Nv} - E_{0v''})^{-1}]\langle Nv|\hat{\mu}_Z|0v'\rangle \end{aligned} \quad (71)$$

Here E_{Nv} is the energy of the vibronic state $|Nv\rangle$ of the N th ($|N\rangle$) excited electronic term. Assuming that the energy of the vibrational excitations in the ground and excited electronic states is small compared with the energy gap between the electronic states, one can neglect in Eq. (71) the dependence of the energy denominators on vibrational quantum numbers v, v' , and v'' . Then, in the basis of the functions of the ground electronic term, the operator $\hat{H}(\mathcal{F})$ is given by the expression

$$\hat{H}(\mathcal{F}) = \hat{H}_{\text{vibr}} - \hat{\mu}_Z\mathcal{F} - \frac{1}{2}\kappa_{ZZ}\mathcal{F}^2 \quad (72)$$

in which $\hat{\kappa}_{ZZ} = 2\hat{\mu}_Z\hat{G}\hat{\mu}_Z$ is the ZZ component of the molecular susceptibility,

$$\hat{G} = \sum_{N \neq 0} \frac{|N\rangle\langle N|}{E_N} \quad (73)$$

is the electronic Green function, and E_N is the energy of the excited electronic state $|N\rangle$ read from the ground electronic term.

In the framework of the preceding approximation in the first order with respect to the introduced small parameter, we have

$$\widetilde{\hat{d}_K(t, \mathcal{F})\hat{d}_I} = \hat{d}_K(t, \mathcal{F})\hat{d}_I + \mathcal{F}[\hat{\mu}_Z\hat{G}\hat{d}_K(t, \mathcal{F})\hat{d}_I + \hat{d}_K(t, \mathcal{F})\hat{d}_I\hat{G}\hat{\mu}_Z] \quad (74)$$

If we restrict ourselves with the zero and first order terms only with respect to the field \mathcal{F} in Eq. (74), we obtain the following expression:

$$\widetilde{\hat{d}_K(t, \mathcal{F})\hat{d}_I} = \hat{d}_K(t)\hat{d}_I + \mathcal{F}\hat{\chi}_{Z,IK}(t) \quad (75)$$

in which

$$\begin{aligned} \hat{d}_K(t) &= \hat{d}_K(t, \mathcal{F} = 0) \\ \hat{\chi}_{Z,IK}(t) &= \hat{\mu}_Z\hat{G}\hat{d}_K(t)\hat{d}_I + \hat{d}_K(t)\hat{d}_I\hat{G}\hat{\mu}_Z \\ &\quad - i \int_0^t dt_1 [\hat{\mu}_Z(t_1), \hat{d}_K(t)]\hat{d}_I \end{aligned} \quad (76)$$

is the operator of hyperpolarizability in the time representation that describes the deformation of the molecule in the alternating electric and constant (\mathcal{F}) fields. In particular, when passing from time representation to the frequency one in the electric field ($\mathcal{F} = \mathcal{E}$), the mean value of $\hat{\chi}$ in nondegenerate states coincides with the hyperpolarizability introduced by Buckingham and Longuet-Higgins (1968).

Assuming that the excited electronic states are not populated and substituting Eqs. (70), (72), and (75) into Eqs. (66) and (67), we obtain

$$\text{Re } \alpha_{IK}(\omega, \mathcal{F}, \Omega) = \frac{\text{Sp}\{\exp[-\beta\widetilde{\hat{H}(\mathcal{F})}][\hat{\alpha}_{IK}(\omega, \Omega) + \mathcal{F}\hat{\chi}_{Z,IK}(\omega, \Omega)]\}}{\text{Sp}\{\exp[-\beta\widetilde{\hat{H}(\mathcal{F})}]\}} \quad (77)$$

where

$$\hat{\alpha}_{IK}(\omega, \Omega) = \hat{d}_K \frac{\hat{H}}{\hat{H}^2 - \omega^2} \hat{d}_I \quad (78)$$

is IK th component of the polarizability of the molecule in the ground electronic state in the absence of external field and

$$\hat{\chi}_{Z,IK}(\omega, \Omega) = \frac{1}{2\pi} \int_{-\infty}^{\infty} \frac{\omega' d\omega'}{\omega^2 - \omega'^2} \int_{-\infty}^{\infty} dt e^{-i\omega't} \hat{\chi}_{Z,IK}(t) \quad (79)$$

In the deduction of Eq. (77) all the hyperpolarizabilities of order higher than $\hat{\chi}_{Z,IK}$ were omitted. In particular, in Eq. (77) the term proportional to \mathcal{F}^2 responsible for the contribution to $\alpha(\omega, \mathcal{F}, \Omega)$ due to the Voight mechanism is absent. Thus, by means of the preceding approximations the contributions to the polarizability that in principle may lead the Langevin–Born mechanism of birefringence are separated.

Next we expand Eq. (77) in a power series with respect to field \mathcal{F} by assuming that this field is small and cannot result in an orientational saturation. Then, after averaging over the orientations of the molecule, we obtain for the Langevin–Born contribution to the birefringence the expression

$$\Delta n^{\text{or}} = 2\pi N \sum_{iklm} W^{iklm} J_{iklm}^{\text{or}}(\omega, \beta) \quad (80)$$

where

$$J_{iklm}^{\text{or}} = \int_0^\beta d\beta_1 \int_0^{\beta_1} d\beta_2 \langle \hat{\mu}_i(\beta_1) \hat{\mu}_k(\beta_2) \hat{\alpha}_{lm}(\omega) \rangle + \frac{1}{2} \int_0^\beta d\beta_1 \langle \hat{\kappa}_{ik}(\beta_1) \hat{\alpha}_{lm}(\omega) \rangle + \int_0^\beta d\beta_1 \langle \hat{\mu}_i(\beta_1) \hat{\chi}_{klm}(\omega) \rangle \quad (81)$$

$$\langle \hat{A} \rangle = \text{Sp}\{\exp(-\beta \hat{H}_{\text{vibr}}) \hat{A}\} / \text{Sp}\{\exp(-\beta \hat{H}_{\text{vibr}})\}$$

$$\hat{F}(\beta) = \exp(-\beta \hat{H}_{\text{vibr}}) \hat{F} \exp(-\beta \hat{H}_{\text{vibr}}) \quad (82)$$

$$W^{iklm} = \frac{1}{30} [3(\delta_{il}\delta_{km} + \delta_{im}\delta_{kl}) - 2\delta_{ik}\delta_{lm}]$$

i, k, l, m are the indices of the projections of the appropriate magnitudes on the Cartesian coordinates of the MSC. The coefficients W^{iklm} are symmetric with respect to the permutations of indices $i \rightleftharpoons k$ and $l \rightleftharpoons m$. Therefore in all the final results the Cartesian components of the tensors of polarizability, susceptibility, and hyperpolarizability are present in symmetric combinations only:

$$\begin{aligned} \hat{\alpha}_{lm}^{(s)} &= \frac{1}{2}(\hat{\alpha}_{lm} + \hat{\alpha}_{ml}) \\ \hat{\kappa}_{ik}^{(s)} &= \frac{1}{2}(\hat{\kappa}_{ik} + \hat{\kappa}_{ki}) \\ \hat{\chi}_{k,lm}^{(s)} &= \frac{1}{2}(\hat{\chi}_{k,lm} + \hat{\chi}_{k,ml}) \end{aligned} \quad (83)$$

Using the explicit expressions for W^{iklm} , we can present the final expression for the birefringence in the form of a sum of three terms:

$$\Delta n^{\text{or}} = \Delta n_1^{\text{or}} + \Delta n_2^{\text{or}} + \Delta n_3^{\text{or}} \quad (84)$$

where

$$\Delta n_1^{\text{or}} = \frac{2\pi N}{5} \sum_{\bar{\Gamma}\bar{\gamma}} b_{\bar{\Gamma}} \int_0^\beta d\beta_1 \int_0^{\beta_1} d\beta_2 \langle (\hat{\mu}(\beta_1) \otimes \hat{\mu}(\beta_2))_{\bar{\Gamma}\bar{\gamma}} \hat{\alpha}_{\bar{\Gamma}\bar{\gamma}}^{(s)}(\omega) \rangle \quad (85a)$$

$$\Delta n_2^{\text{or}} = \frac{\pi N}{5} \sum_{\bar{\Gamma}\bar{\gamma}} b_{\bar{\Gamma}} \int_0^\beta d\beta_1 \langle \hat{\kappa}_{\bar{\Gamma}\bar{\gamma}}(\beta_1) \hat{\alpha}_{\bar{\Gamma}\bar{\gamma}}(\omega) \rangle \quad (85b)$$

$$\Delta n_3^{\text{or}} = \frac{2\pi N}{15} \sum_{\nu=1,2,3; \Gamma_\mu \gamma_\mu} h_{\nu \Gamma_\mu} \int_0^\beta d\beta_1 \langle \hat{\mu}_{\Gamma_\mu \gamma_\mu}(\beta_1) \hat{\chi}_{\nu \Gamma_\mu \gamma_\mu}(\omega) \rangle \quad (85c)$$

Here the operators with the indicies $\bar{\Gamma}\bar{\gamma}$ belong to the line $\bar{\gamma}$ of representations $\bar{\Gamma}$; $\bar{\Gamma}$ and Γ_μ are representations of the tensor of polarizability and the moment $\hat{\mu}$, respectively; $b_{\bar{\Gamma}}$ and $h_{\nu \Gamma_\mu}$ are numerical coefficients dependent on the choice of the form of the irreducible tensor operators in the point group of each concrete molecule. The irreducible tensor operators $(\hat{\mu} \otimes \hat{\mu})_{\bar{\Gamma}\bar{\gamma}}$ are determined by the Clebsh–Gordan coefficients $U_{\gamma_1 \gamma_2 \bar{\gamma}}^{\Gamma_1 \Gamma_2 \bar{\Gamma}}$ of the point group of the molecule (Koster *et al.*, 1963) as follows:

$$(\hat{\mu} \otimes \hat{\mu})_{\bar{\Gamma}\bar{\gamma}} = \sum_{\gamma_1 \gamma_2} U_{\gamma_1 \gamma_2 \bar{\gamma}}^{\Gamma_\mu \Gamma_\mu \bar{\Gamma}} \hat{\mu}_{\Gamma_\mu \gamma_1} \hat{\mu}_{\Gamma_\mu \gamma_2} \quad (86)$$

The index ν in Eq. (85c) occurs because of the fact that in any point group there are three components of the hyperpolarizability that belong to the same representation Γ_μ as the components of the vector $\hat{\mu}$. In particular, for cubic groups these three sets are

$$\begin{aligned} \hat{\chi}_{1\Gamma_\mu} &= (\hat{\chi}_{x,xx}, \hat{\chi}_{y,yy}, \hat{\chi}_{z,zz}) \\ \hat{\chi}_{2\Gamma_\mu} &= (\hat{\chi}_{x,yy} + \hat{\chi}_{x,zz}, \hat{\chi}_{y,xx} + \hat{\chi}_{y,zz}, \hat{\chi}_{z,yy} + \hat{\chi}_{z,xx}) \\ \hat{\chi}_{3\Gamma_\mu} &= (\hat{\chi}_{y,xy}^{(s)} + \hat{\chi}_{x,xz}^{(s)}, \hat{\chi}_{x,xy}^{(s)} + \hat{\chi}_{z,yz}^{(s)}, \hat{\chi}_{x,xz}^{(s)} + \hat{\chi}_{y,yz}^{(s)}) \end{aligned}$$

Without constraint of generality, all the operators in Eqs. (85a)–(85c) may be considered pure electronic ones neglecting, thus the nuclear contributions to the moment, polarizability, magnetic susceptibility, and hyperpolarizability due to their smallness compared with the appropriate electronic contributions. In the framework of this consideration some general group-theoretical selection rules can be suggested that allow us to predict the possible nonzero contribution to the birefringence arising from the Langevin–Born mechanism.

In order to formulate these selection rules, consider the behavior of the operators in Eqs. (85a)–(85c) with respect to the operation of time

reversal $\hat{\Theta}$. Using the properties of the $\hat{\Theta}$ operator (see, e.g., Abragam and Bleaney, 1970), one can show that

$$\begin{aligned}\hat{\Theta}\hat{\mu}\hat{\Theta}^{-1} &= \pm\hat{\mu}, & \hat{\Theta}\hat{\chi}_\nu\hat{\Theta}^{-1} &= \pm\hat{\chi}_\nu \\ \hat{\Theta}\hat{\alpha}_{\Gamma\bar{\gamma}}^{(s)}\hat{\Theta}^{-1} &= \hat{\alpha}_{\Gamma\bar{\gamma}}^{(s)}, & \hat{\Theta}\hat{\kappa}_{\Gamma\bar{\gamma}}^{(s)}\hat{\Theta}^{-1} &= \hat{\kappa}_{\Gamma\bar{\gamma}}^{(s)}\end{aligned}\quad (88)$$

In these relations the upper sign has to be taken in the case of the external electric field (when $\hat{\mu}$ coincides with the operator of the dipole moment $\hat{\mathbf{d}}$, which is even with respect to the time reversal), and the lower one has to be taken if $\hat{\mu}$ is the operator of magnetic moment $\hat{\mathbf{m}}$.

Independent of the choice of the full set of electron-vibrational functions with which the average values in Eqs. (85a)–(85c) are calculated, owing to the preceding assumption the final results are always expressed by matrix elements of electronic operators $\hat{\mu}_{\Gamma\mu}$, $\hat{\alpha}_{\Gamma\bar{\gamma}}^{(s)}$, $\hat{\kappa}_{\Gamma\bar{\gamma}}^{(s)}$ and $\hat{\chi}_{\nu\Gamma\mu}$ calculated within the basis functions of the initial electronic term $\bar{\Gamma}$. Thus, following Eq. (87), the matrix elements of these operators are nonzero if in the case of the system with an even (odd) number of electrons the direct products $[\Gamma^2] \otimes \bar{\Gamma}$ and $\{\Gamma^2\} \otimes \Gamma_m$ or $[\Gamma^2] \otimes \Gamma_d$ ($\{\Gamma^2\} \otimes \bar{\Gamma}$ and $[\Gamma^2] \otimes \Gamma_m$ or $\{\Gamma^2\} \otimes \Gamma_d$) contain the totally symmetric representation. The brackets and braces in these expressions denote, respectively, symmetric and antisymmetric products of the representation Γ by itself.

It follows from these rules, in particular, that for gases of molecules with cubic symmetry that are in nondegenerate states A, Δn^{or} is identically equal to zero. Indeed, $[A^2] \otimes \bar{\Gamma} = \bar{\Gamma}$ ($\bar{\Gamma} = E, T_2$) and $\{A^2\} \otimes (\Gamma_m = T_1) = 0$, $[A^2] \otimes (\Gamma_d = T) = T$ do not contain the totally symmetric representation. In this case the traditional statement that in the case of spherical-top molecules the temperature-dependent birefringence is impossible is confirmed. However, this statement is not general, being correct only when there is no electron degeneracy of the electronic term. As one can easily see, in the case of E terms in cubic symmetry systems the product $[E^2] \otimes (\bar{\Gamma} = E)$ contains the totally symmetric representation, and therefore in any field (electric or magnetic) the contribution to the Δn_2^{or} value determined by the matrix elements of the anisotropic components of the tensor of polarizability is, generally speaking, nonzero.

In a similar way one can make sure that in degenerate states of the type T and $G_{3/2}$ one term or even all the three terms in Eq. (84) can be nonzero, depending on the point symmetry (T_d or O_h) and the kind of applied constant field (electric or magnetic).

The selection rules allow us to choose the systems in which the orientational mechanism of birefringence is effective. On the other hand, the explicit form of the temperature dependence $\Delta n^{\text{or}}(\beta)$ is of no less interest. Its general investigation for any external field and for arbitrary molecular

symmetries and state degeneracies is impossible for the following reasons. First, the selection rules in the electric and magnetic fields are different owing to the differences in the behavior of the operators of electric and magnetic dipole moments with respect to the operation of time reversal. Second, such investigations became even more difficult owing to the Jahn–Teller effect, which is always present when there is electronic degeneracy. In the next subsection, we consider some concrete cases of degeneracy manifestation in the Kerr and Cotton–Mouton effects separately.

2. Anomalous Kerr Effect

As a first example consider birefringence in an electric field by a gas of molecules with D_{3h} symmetry and a twofold degenerate ground electronic term belonging to representation E' . Using the explicit form of the matrices of the components of the operators of the dipole moment [Eq. (20)] and polarizability and by means of Eqs. (84) and (85a)–(85c), we obtain for the molecular constant in the Kerr effect in the E term case under consideration the expression

$$\begin{aligned} {}_mK_{E'}^{\text{or}} = & \frac{\pi N}{5} \left\{ \beta b_{A'} \alpha_{A'} \alpha_{A'}(\omega) \right. \\ & + \left[\frac{\beta^2}{2} b_{A'} d_{E'}^2 \alpha_{A'}(\omega) + \beta b_{E'} \alpha_{E'} \alpha_{E'}(\omega) \right. \\ & \left. \left. + \frac{2}{3} \beta \sum_{\nu} h_{\nu E'} \alpha_{E'} \chi_{\nu E'}(\omega) \right] Q_{E'}(E', \beta) \right\} \end{aligned} \quad (89)$$

where α_{Γ} , $\alpha_{\Gamma}(\omega)$, d_{Γ} , and $\chi_{\nu\Gamma}(\omega)$, are the reduced matrix elements of the operators $\hat{\alpha}_{\Gamma\bar{\gamma}}$, $\hat{\alpha}_{\Gamma\bar{\gamma}}(\omega)$, $\hat{d}_{\Gamma\bar{\gamma}}$, and $\hat{\chi}_{\nu\Gamma\bar{\gamma}}(\omega)$ calculated with the basis function of the initial electronic term Γ . Hereafter the wave function representation Γ is omitted and the denotation F_{Γ} instead of $\langle \Gamma | \hat{F}_{\Gamma} | \Gamma \rangle$ is used.

In the case of the linear $E \otimes e$ problem the nuclear dipole moment can be taken into account by means of the substitution of $d_{E'}$ by $(d_e - ad_n)$ [the proof of this statement is analogous to that given above when Eq. (9) was deduced].

The temperature dependence of the Kerr constant, obtained earlier, is essentially different from the classical relationship

$${}_mK_{A'}^{\text{or}} = \frac{\pi N}{5} \beta b_{A'} \alpha_{A'} \alpha_{A'}(\omega) \quad (90)$$

due to which the Kerr constant for nonpolar molecules is linear in β . At low temperatures when the population of the ground vibronic level is

predominant, Eq. (89) simplifies. Substituting $Q_{E'}(E', \beta)$ in the form of Eq. (11) into Eq. (89), we come to the following approximate relation:

$$\begin{aligned}
 {}_m K_{E'}^{\text{or}} \approx & \frac{\pi N}{5} \left\{ \beta b_{A'} \alpha_{A'} \alpha_{A'}(\omega) + \frac{\beta^2}{2} b_{A'} d_{E'}^2 \alpha_{A'}(\omega) q_{E'}^2 \right. \\
 & + \beta b_{A'} d_{E'}^2 \alpha_{A'}(\omega) \sum_{n_0, n_e} \frac{\langle n_0 | \hat{\sigma} | n_e \rangle \langle n_e | \hat{\sigma} | n_0 \rangle}{E_{n_e} - E_{n_0}} \\
 & + \beta \left[b_{E'} \alpha_{E'} \alpha_{E'}(\omega) + \frac{2}{3} \sum_{\nu} h_{\nu E'} d_{E'} \chi_{\nu E'}(\omega) \right] q_{E'}^2 \\
 & \left. + \left[b_{E'} \alpha_{E'} \alpha_{E'}(\omega) + \frac{2}{3} \sum_{\nu} h_{\nu E'} d_{E'} \chi_{\nu E'}(\omega) \right] \sum_{n_0, n_e} \frac{\langle n_0 | \hat{\sigma} | n_e \rangle \langle n_e | \hat{\sigma} | n_0 \rangle}{E_{n_e} - E_{n_0}} \right\} \quad (91)
 \end{aligned}$$

It follows from this formula that at low temperatures (in the sense given earlier) light refraction by molecules of D_{3h} symmetry in degenerate states E' is similar to that of rigid dipole molecules, ${}_m K^{\text{or}}$ being dependent on β quadratically. Note that in Eq. (91) the third and the last terms in braces are contributions due to the Jahn–Teller effect. The former term contributes to the atomic polarization of the vibronic type (it was discussed earlier when the static polarizability was investigated), whereas the latter one is related to the atomic hyperpolarizability of the Jahn–Teller type, i.e., to the Voigt mechanism within the vibronic states of the same electronic term. Thus Jahn–Teller molecules with a ground dipolar-type electronic term behave with respect to the light refraction in an electric field as rigid dipole molecules. In this case the vibronic coupling results in additional contributions to the birefringence that are due to the atomic polarizability and hyperpolarizability.

3. The Kerr Effect in Molecules with Ground Electronic $G_{3/2}$ Terms

Consider now the Kerr effect in a more interesting case of spherical-top molecules in which the temperature-dependent birefringence is conditioned exclusively by the degeneracy and vibronic coupling. By way of example we choose a cubic symmetry system with a fourfold degenerate ground electronic term $G_{3/2}$. This case is realized in a series of octahedral (ReF_6 , IrF_6) and tetrahedral (VCl_4 , VBr_4) molecules. In the latter case the electronic term $G_{3/2}$ arises from the orbital E by taking into account the spin-orbital interaction.

Assume now that in the cases of $G_{3/2}$ terms under consideration there is no linear Stark effect. This assumption is absolutely true in the case of

octahedral systems, but in the case of tetrahedral ones it implies that the reduced matrix element of the operator of the dipole moment calculated in the basis of the electronic functions $|G_{3/2}\gamma\rangle$ is negligibly small. Then, taking the matrices of the anisotropic components of the tensor of polarizability in the form

$$\hat{\alpha}_{\bar{\Gamma}\bar{\gamma}} = \alpha_{\bar{\Gamma}} \hat{\rho}_{\bar{\Gamma}\bar{\gamma}}, \quad \hat{\alpha}_{\bar{\Gamma}\bar{\gamma}}(\omega) = \alpha_{\bar{\Gamma}}(\omega) \hat{\rho}_{\bar{\Gamma}\bar{\gamma}} \quad (92)$$

where $\bar{\Gamma} = E, T_2$, and

$$\begin{aligned} \hat{\rho}_{Eu} &= \begin{bmatrix} \hat{\sigma}_z & \hat{0} \\ \hat{0} & -\hat{\sigma}_z \end{bmatrix}, & \hat{\rho}_{Ev} &= \begin{bmatrix} \hat{0} & \hat{1} \\ \hat{1} & \hat{0} \end{bmatrix} \\ \hat{\rho}_{T_2\xi} &= \begin{bmatrix} \hat{\sigma}_y & \hat{0} \\ \hat{0} & -\hat{\sigma}_y \end{bmatrix}, & \hat{\rho}_{T_2\eta} &= \begin{bmatrix} -\hat{\sigma}_x & \hat{0} \\ \hat{0} & \hat{\sigma}_x \end{bmatrix}, & \hat{\rho}_{T_2\zeta} &= \begin{bmatrix} \hat{0} & i\hat{1} \\ -i\hat{1} & \hat{0} \end{bmatrix} \end{aligned} \quad (93)$$

and substituting them into Eqs. (84) and (85b), we obtain for the Kerr constant

$${}_m K_{G_{3/2}}^{\text{or}} = \frac{\pi N \beta}{5} \{b_E \alpha_E \alpha_E(\omega) Q_{G_{3/2}}(E, \beta) + b_{T_2} \alpha_{T_2} \alpha_{T_2}(\omega) Q_{G_{3/2}}(T_2, \beta)\} \quad (94)$$

in which

$$Q_{G_{3/2}}(\bar{\Gamma}, \beta) = \frac{1}{\beta} \int_0^\beta d\lambda \langle \hat{\rho}_{\bar{\Gamma}}(\lambda) \hat{\rho}_{\bar{\Gamma}} \rangle \quad (95)$$

is analogous to the temperature-dependent vibronic reduction factor introduced in Eq. (10) of the electronic contribution to the birefringence, which is due to the anisotropic $\bar{\Gamma}$ components of the polarizability, and

$$\hat{\rho}_E = \{\hat{\rho}_{Eu}, \hat{\rho}_{Ev}\}, \quad \hat{\rho}_{T_2} = \{\hat{\rho}_{T_2\xi}, \hat{\rho}_{T_2\eta}, \hat{\rho}_{T_2\zeta}\}$$

Let us investigate the temperature dependence of the vibronic reduction factors $Q_{G_{3/2}}(\bar{\Gamma}, \beta)$ with the vibronic coupling with E and T_2 vibrations taken into account [$G_{3/2} \otimes (e + t_2)$ problem]. Within the basis set used for the construction of the $\hat{\rho}_{\bar{\Gamma}\bar{\gamma}}$ operators the density matrix for the linear $G_{3/2} \otimes (e + t_2)$ problem in the framework of the approximation, analogous to Eq. (13), is determined by the following relation (Ogurtsov and Kazantseva, 1983):

$$\begin{aligned} &\langle \mathbf{q}_E, \mathbf{q}_{T_2} | \exp(-\beta \hat{H}_{\text{vibr}}) | \mathbf{q}'_E, \mathbf{q}'_{T_2} \rangle \\ &\simeq \rho_0(\mathbf{q}_E, \mathbf{q}'_E, \beta) \rho_0(\mathbf{q}_{T_2}, \mathbf{q}'_{T_2}, \beta) \times \exp[-a_E \text{th } x_E(\hat{\rho}_E \mathbf{q}_E) \\ &- a_{T_2} \text{th } x_{T_2}(\hat{\rho}_{T_2} \mathbf{q}_{T_2})] \exp[-a_E \text{th } x_E(\hat{\rho}_E \mathbf{q}'_E) - a_{T_2} \text{th } x_{T_2}(\hat{\rho}_{T_2} \mathbf{q}'_{T_2})] \\ &\times \exp[2a_E^2(x_E - \text{th } x_E) + 3a_{T_2}^2(x_{T_2} - \text{th } x_{T_2})] \end{aligned} \quad (96)$$

where

$$\mathbf{q}_E = \{q_u, q_v\} \quad \text{and} \quad \mathbf{q}_{T_2} = \{q_\xi, q_\eta, q_\zeta\}$$

are the vectors of the dimensionless coordinates of the E and T_2 vibrations, respectively, $\rho_0(\mathbf{q}_E, \mathbf{q}_{T_2}, \beta)$ is the density matrix of harmonic vibrations of the type $\bar{\Gamma}$, not disturbed by the Jahn–Teller interaction, a_E and a_{T_2} are dimensionless constants of vibronic coupling to the E and T_2 vibrations, their frequencies being ω_E and ω_{T_2} , and

$$x_E = \hbar\omega_E\beta/2, \quad x_{T_2} = \hbar\omega_{T_2}\beta/2$$

The calculation of $Q_{G_{3/2}}(\bar{\Gamma}, \beta)$ as a function of temperature and vibronic coupling constants a_E and a_{T_2} in a general analytical form, even in the framework of the approximation of Eq. (96), seems to be impossible. Therefore we restrict ourselves to the consideration of the limit cases of low and high temperatures.

In the case of low temperatures when only the ground vibronic state is populated, the sought for parameters $Q_{G_{3/2}}(E, \beta)$ and $Q_{G_{3/2}}(T_2, \beta)$ are independent of temperature and equal to the squares of the appropriate vibronic reduction constants of electronic operators of E and T_2 type in the ground vibronic state $Q_{3/2}$:

$$\lim_{\beta \rightarrow \infty} Q_{G_{3/2}}(\bar{\Gamma}, \beta) = K_{G_{3/2}}^2(\bar{\Gamma}) \quad (97)$$

In the framework of approximation (96) the parameters $K_{G_{3/2}}(E)$ and $K_{G_{3/2}}(T_2)$ can be reduced to the following relations:

$$\begin{aligned} K_{G_{3/2}}(E) &= \frac{1}{2}\{1 + p(a_E, a_{T_2})[1 + s(a_E, a_{T_2})]\} \\ K_{G_{3/2}}(T_2) &= p(a_E, a_{T_2})[1 - \frac{1}{3}s(a_E, a_{T_2})] \end{aligned} \quad (98)$$

in which

$$\begin{aligned} p(x, y) &= \left\{ \frac{x^2}{x^2 - y^2} \left[e^{y^2} + \sqrt{\pi} x^2 e^{x^2} \frac{\Phi(\sqrt{x^2 - y^2})}{\sqrt{x^2 - y^2}} \right] \right. \\ &\quad \left. - \frac{y^2}{x^2 - y^2} (1 + 2y^2) e^{y^2} \right\}^{-1} \end{aligned} \quad (99a)$$

$$\begin{aligned} s(x, y) &= \frac{y^2}{x^2 - y^2} [(1 + 2y^2) e^{y^2} - 1] \\ &\quad + \frac{3x^2 y^2}{(x^2 - y^2)^2} \left[e^{y^2} - 1 + \frac{\sqrt{\pi} x^2}{\sqrt{x^2 - y^2}} \right. \\ &\quad \times \left. \int_0^1 dt e^{x^2 t^2} \Phi(t\sqrt{x^2 - y^2}) \right] \end{aligned} \quad (99b)$$

It follows from Eqs. (98), (99a), (99b), (14), and (15) that in the absence of vibronic coupling with T_2 vibrations $K_{G_{3/2}}(E)|_{a_{T_2}=0}$ coincides with the expression for the vibronic reduction constant of operators of E type in the $E \otimes e$ problem. The values of the parameter $K_{G_{3/2}}(T_2)|_{a_{T_2}=0}$ as a function of the coupling constant a_E lie within 0 and 1, $0 < K_{G_{3/2}}(T_2)|_{a_{T_2}=0} < 1$.

In the other particular case $a_E = 0$, $a_{T_2} \neq 0$ the parameter $K_{G_{3/2}}(T_2)$ as a function of a_{T_2} varies within the values 1 and $\frac{1}{3}$, and hence $Q_{G_{3/2}}(T_2)|_{a_E=0}$ lies within the values 1 ($a_{T_2} = 0$) and $\frac{1}{3}$ ($a_{T_2} \rightarrow \infty$).

If $a_E = a_{T_2} = a$, the following relationship takes place:

$$K_{G_{2/3}}(E) = K_{G_{2/3}}(T_2) = \frac{1}{5} + \frac{4}{5} \frac{\exp(-a^2)}{1 + 4a^2 + \frac{4}{3}a^4}$$

which can be obtained from Eqs. (98), (99a), and (99b) by means of the limit transition $a_E \rightarrow a_{T_2}$. Note that in Eqs. (99a) and (99b) for $|a_{T_2}| > |a_E|$

$$\Phi(ix) = \frac{2i}{\sqrt{\pi}} \int_0^x \exp(t^2) dt$$

It follows from the analyses given earlier of the vibronic reduction parameters that in the case under consideration the vibronic reduction due to the Jahn–Teller effect cannot result in the complete disappearance of the effects predicted without considering the vibronic coupling, although some of the contributions in Eq. (94) may be equal to zero. Even for the most unfavorable parameter relationship, the full electronic contribution to the birefringence is reduced no more than by one order of magnitude.

In the limit case of high temperatures the dependence of the $Q_{G_{3/2}}(\bar{\Gamma}, \beta)$ parameters on the temperature-dependent coupling constants $a_E^* = a_E \sqrt{x_E}$ and $a_{T_2}^* = a_{T_2} \sqrt{x_{T_2}}$ is determined by the equations

$$Q_{G_{3/2}}(E, \beta) = \frac{1}{2}[1 + p(a_E^*, a_{T_2}^*)][f(a_E^*, a_{T_2}^*) + g(a_E^*, a_{T_2}^*)]$$

$$Q_{G_{3/2}}(T_2, \beta) = p(a_E^*, a_{T_2}^*)[f(a_E^*, a_{T_2}^*) - \frac{1}{3}g(a_E^*, a_{T_2}^*)]$$

where $p(a_E^*, a_{T_2}^*)$ can be obtained from Eq. (99a) by the substitution of a_E and a_{T_2} by a_E^* and $a_{T_2}^*$, respectively,

$$f(x, y) = \frac{\sqrt{\pi}}{2} \frac{x^2 e^{x^2}}{x^2 - y^2} \frac{\Phi(\sqrt{x^2 - y^2})}{\sqrt{x^2 - y^2}} - \frac{y^2 e^{y^2}}{x^2 - y^2} \quad (101)$$

$$g(x, y) = \frac{y^2}{x^2 - y^2} [3f(x, y) - (3 + 2y^2)e^{y^2}]$$

The expressions for the reduction parameters [Eq. (100)] are complicated function of a_E^* and $a_{T_2}^*$, and we shall consider now some limiting cases. In the absence of interaction with T_2 vibrations $g(a_E^*, 0) = 0$, and

the reduction factors obey the following inequalities: $\frac{1}{2} < Q_{G_{3/2}}(E, \beta)|_{a_{T_2}=0} \leq 1$, $0 < Q_{G_{3/2}}(T_2, \beta)|_{a_E=0} \leq 1$. If $a_E = 0$, then $0 < Q_{G_{3/2}}(E, \beta)|_{a_E=0} \leq 1$, $\frac{1}{3} < Q_{G_{3/2}}(T_2, \beta)|_{a_E=0} \leq 1$. If the vibronic constant values coincides ($a_E^* = a_{T_2}^* = a^*$), we have

$$Q_{G_{3/2}}(E, \beta) = Q_{G_{3/2}}(T_2, \beta) = \frac{1 + \frac{4}{3}a^{*2} + \frac{4}{15}a^{*4}}{1 + 4a^{*2} + \frac{4}{3}a^{*4}}$$

Note that $a_{\bar{\Gamma}}^* = \beta E_{JT}(\bar{\Gamma})$, where $E_{JT}(\bar{\Gamma})$ is the Jahn–Teller stabilization energy for the coupling with $\bar{\Gamma}$ -type vibrations. If a_E^* , $a_{T_2}^* \ll 1$, appropriate to the case of either weak vibronic coupling, or high temperatures and arbitrary values of a_E and a_{T_2} , then the reduction parameters can be expanded in a series with respect to the small a_E^* and $a_{T_2}^*$ value, and with the accuracy up to the linear in $E_{JT}(\bar{\Gamma})$ terms they can be represented by the relations

$$\begin{aligned} Q_{G_{3/2}}(E, \beta) &\approx 1 - \frac{2}{3}\beta E_{JT}(E) - 2\beta E_{JT}(T_2) \\ Q_{G_{3/2}}(T_2, \beta) &\approx 1 - \frac{4}{3}\beta E_{JT}(E) - \frac{4}{3}\beta E_{JT}(T_2) \end{aligned} \quad (102)$$

It follows that in the case of $a_{\bar{\Gamma}}^* \ll 1$ under consideration the Kerr constant in accordance with Eq. (94) can be written in the form

$${}_m K^{\text{or}} \approx A\beta + B\beta^2 \quad (103)$$

in which, besides the linear in β contribution, there is the term proportional to β^2 . In accordance with the traditional theory of the electro-optic Kerr effect the β^2 term is characteristic for molecules having a proper dipole moment.

It follows from the preceding results that the electro-optical properties of molecules in degenerate electronic states should have unusual temperature dependence, which is absent in the case of nondegenerate states. Even for nondipolar degenerate electronic states (e.g., for states in which the reduced matrix elements of the dipole moment are zero) for certain relationships between the vibronic constant and the temperature, there may be a quadratic dependence of the Kerr effect on β , similar to that observed in the case of molecules that are simultaneously anisotropic polarizable and possess a proper dipole moment. The nonlinear dependence on β under consideration is due exclusively to the vibronic interaction that redetermines the vibronic spectrum and leads to different polarizability in different vibronic states. This dependence on β has to be distinguished from that which arises due to the nonzero value of the dipole moment in the initial ground electronic state (e.g., as in the case of the E' term in molecules with D_{3h} symmetry). The two sources of the

quadratic in β contribution to the birefringence, the vibronic coupling and the dipolarity of the states, can be distinguished, say, by means of the optical Kerr effect in which the contribution of the dipolar origin is absent.

In conclusion, let us estimate the experimental possibility of observing the predicted temperature dependence of the Kerr effect in gases of concrete spherical-top molecules. In the case of the VCl_4 molecule, if one neglects the spin-orbital interaction, $a_{T_2} = 0$ and $\alpha_{T_2} = 0$. In the calculation of the reduced matrix element of the polarizability α_E , one can take into account only the lowest [in the summation over N in Eq. (73)] excited electronic term T_2 appropriate to the experimentally observed optical transition with $\omega_{T_2} \sim 9000 \text{ cm}^{-1}$, and the dipole moment can be taken as $d \sim 1 \text{ D}$ (Blankenship and Belford, 1962; Clark and Machin, 1963). Using these data and the value of the Jahn–Teller stabilization energy $E_{JT} = 73 \text{ cm}^{-1}$ (Englman, 1972), we obtain for the vibronic reduction constant $Q_E(E, \beta) \approx 1 - \frac{2}{3}$ and the Kerr constant ${}_mK^{\text{or}} \sim 10^{-12} \text{ CGSE}$ for room temperatures ($kT \sim 210 \text{ cm}^{-1}$). This value of ${}_mK^{\text{or}}$ coincides in order of magnitude with the Kerr constant for anisotropic polarizable molecules. The reduction constant value $Q_E(E, \beta) \approx 1 - \frac{2}{3}\beta E_{JT}$ is different from its limit value equal to one by $\frac{2}{3}$; thus the quadratic in β contribution to the Kerr constant [see Eqs. (102) and (103)] for VCl_4 molecules at room temperatures can be about 20% of the pure electronic value.

Similar estimations can be carried out for octahedral molecules ReF_6 and IrF_6 . For them the data taken from the works of Meredith *et al.* (1977), Webb and Bernstein (1979), and Bernstein and Webb (1979) about the Jahn–Teller stabilization energies and appropriate values of the deviation of the reduction parameters from unity at room temperatures calculated by Eq. (100) are given in Table I. It can be seen from these data that the predicted corrections are between 10 and 40%. Note that by changing the temperature by several tens of degrees the change of these corrections may be essential.

TABLE I

Molecule	$\bar{\Gamma}$	$E_{JT}(\bar{\Gamma})$ (cm^{-1})	$1 - Q_{G_{3/2}}(\bar{\Gamma}, \beta)$ ($T \sim 300 \text{ K}$)
ReF_6	E	60.3	0.14
	T_2	103.5	0.70
IrF_6	E	19	0.38
	T_2	33	0.33

4. Cotton–Mouton Effect in Gases of Molecules in Electronic States $G_{3/2}$

The classical ideas about the isotropy of electrical properties of spherical-top molecules are usually extrapolated to the magnetic properties. This leads to the conclusion about the isotropy of the magnetic susceptibility in high-symmetry molecules and hence about the disappearance of the orientational contribution to the birefringence in magnetic fields (the Cotton–Mouton effect). In the case of degenerate electronic terms or in the pseudodegeneracy situation, these conclusions are incorrect and have to be reconsidered.

Magnetic properties of degenerate electronic systems so far were investigated mainly by the method of magnetic susceptibility and EPR (Abragam and Bleaney, 1970; Bersuker and Polinger, 1983). In this section we consider the features of birefringence by systems with the ground electronic term $G_{3/2}$. In this case the matrices of the components of the tensor of magnetic susceptibility $\hat{\kappa}_{T\bar{\gamma}}$ have the same form as $\hat{\alpha}_{T\bar{\gamma}}$ and differ from them by substitution of $\alpha_{T\bar{\gamma}}$ by the appropriate reduced matrix elements of magnetic susceptibility $\kappa_{T\bar{\gamma}}$. Since in the point groups T_d and O_h the symmetric quadrate $[G_{3/2}^2]$ contains the representation T_1 of the magnetic moment twice, the matrices of the operators $\hat{m}_{T_1\bar{\gamma}}$ can be determined by the formula

$$\hat{m}_{T_1\bar{\gamma}} = m_1 \hat{R}_{1\bar{\gamma}} + m_2 \hat{R}_{2\bar{\gamma}} \quad (104)$$

where m_1 and m_2 are the reduce matrix elements of the operator of the magnetic moment. The matrices $\hat{R}_{1\bar{\gamma}}$ and $\hat{R}_{2\bar{\gamma}}$ are related to the matrices $\hat{O}_1(T_1\bar{\gamma})$ and $\hat{O}_2(T_2\bar{\gamma})$ used by Ham *et al.* (1976) by the relations

$$\begin{aligned} \hat{R}_{1\bar{\gamma}} &= \frac{2}{3} \hat{O}_1(T_1\bar{\gamma}) + \frac{4}{3} \hat{O}_2(T_2\bar{\gamma}) \\ \hat{R}_{2\bar{\gamma}} &= -\frac{4}{3} \hat{O}_1(T_1\bar{\gamma}) + \frac{2}{3} \hat{O}_2(T_2\bar{\gamma}) \end{aligned} \quad (105)$$

and have the following explicit form

$$\begin{aligned} \hat{R}_{1x} &= \begin{bmatrix} \hat{0} & \hat{\sigma}_x \\ \hat{\sigma}_x & \hat{0} \end{bmatrix}, & \hat{R}_{1y} &= \begin{bmatrix} \hat{0} & \hat{\sigma}_y \\ \hat{\sigma}_y & \hat{0} \end{bmatrix}, & \hat{R}_{1z} &= \begin{bmatrix} -\hat{\sigma}_z & \hat{0} \\ \hat{0} & -\hat{\sigma}_z \end{bmatrix} \\ \hat{R}_{2x} &= \begin{bmatrix} -\frac{\sqrt{3}}{2} \hat{\sigma}_x & \frac{i}{2} \hat{\sigma}_y \\ -\frac{i}{2} \hat{\sigma}_y & -\frac{\sqrt{3}}{2} \hat{\sigma}_x \end{bmatrix}, & \hat{R}_{2y} &= \begin{bmatrix} \frac{\sqrt{3}}{2} \hat{\sigma}_y & -\frac{i}{2} \hat{\sigma}_x \\ \frac{i}{2} \hat{\sigma}_x & \frac{\sqrt{3}}{2} \hat{\sigma}_y \end{bmatrix}, \\ \hat{R}_{2z} &= \begin{bmatrix} \hat{1} & \hat{0} \\ \hat{0} & \hat{1} \end{bmatrix} \end{aligned} \quad (106)$$

As will be shown subsequently, this choice allows us to reduce the number of different vibronic reduction parameters in the electronic contribution to the birefringence. The components of the operators of hyperpolarizability in the magnetic field $\hat{\chi}_{\nu T_1 \bar{\gamma}}(\omega)$ are determined by relations of the type (104) in which m_1 and m_2 are substituted by the appropriate reduced matrix elements of hyperpolarizability $\chi_{\nu 1 T_1}(\omega)$ and $\chi_{\nu 2 T_2}(\omega)$.

By means of Eqs. (85a)–(85c), (92), (93), (104), and (106) for the three contributions to the molecular Cotton–Mouton constant arising from the orientational mechanism of birefringence in the magnetic field, we obtain

$${}_m C_1^{\text{or}} = \frac{\pi N \beta^2}{5} \left[-2m_1 m_2 \alpha_E(\omega) Q_{G_{3/2}}^{(12)}(E, \beta) + 3\sqrt{3} m_2^2 \alpha_{T_2}(\omega) Q_{G_{3/2}}^{(2)}(T_2, \beta) \right] \quad (107a)$$

$${}_m C_2^{\text{or}} = \frac{\pi N \beta}{5} \left[\kappa_E \alpha_E(\omega) Q_{G_{3/2}}(E, \beta) + 18 \kappa_{T_2} \alpha_{T_2}(\omega) Q_{G_{3/2}}(T_2, \beta) \right] \quad (107b)$$

$${}_m C_3^{\text{or}} = \frac{2\pi N \beta}{5} \sum_{i=1,2} m_i \left[2\chi_{1 T_1}(\omega) - \chi_{2 T_1}(\omega) + 3\chi_{3 T_1}(\omega) \right] Q_{G_{3/2}}^{(i)}(T_1, \beta) \quad (107c)$$

where besides the reduction parameters used earlier some new ones are introduced as determined by the relations

$$Q_{G_{3/2}}^{(i)}(T_1, \beta) = \frac{1}{\beta} \int_0^\beta d\beta_1 \langle \hat{\mathbf{R}}_{1 T_1}(\beta_1) \hat{\mathbf{R}}_{i T_1} \rangle \quad (108)$$

$$Q_{G_{3/2}}^{(12)}(E, \beta) = \frac{1}{\beta^2} \sum_{\bar{\gamma}} \int_0^\beta d\beta_1 \int_0^{\beta_1} d\beta_2 \langle (\hat{\mathbf{R}}_{1 T_1}(\beta_1) \otimes \hat{\mathbf{R}}_{2 T_1}(\beta_2))_{E \bar{\gamma}} \hat{\rho}_{E \bar{\gamma}} \rangle \quad (109)$$

$$Q_{G_{3/2}}^{(22)}(T_2, \beta) = \frac{1}{\beta^2} \sum_{\bar{\gamma}} \int_0^\beta d\beta_1 \int_0^{\beta_1} d\beta_2 \langle (\hat{\mathbf{R}}_{2 T_1}(\beta_1) \otimes \hat{\mathbf{R}}_{2 T_1}(\beta_2))_{T_2 \bar{\gamma}} \hat{\rho}_{T_2 \bar{\gamma}} \rangle \quad (110)$$

It can easily be seen that in the absence of the vibronic coupling all the parameters $Q_{G_{3/2}}(\bar{\Gamma}, \beta)$, $Q_{G_{3/2}}^{(i)}(T_1, \beta)$, and $Q_{G_{3/2}}^{(ii')}(\bar{\Gamma}, \beta)$ are equal to one, and the Cotton–Mouton constant in this approximation is a quadratic function of the inverse temperature, similar to that inherent to molecules with nonzero magnetic moments and with anisotropic polarizability and magnetic susceptibility. The vibronic interaction modifies the temperature dependence by means of the temperature-dependent reduction factors, a part of which was discussed in the investigation of the Kerr effect.

Consider now the parameters $Q_{G_{3/2}}^{(i)}(T_1, \beta)$, and $Q_{G_{3/2}}^{(ii')}(\bar{\Gamma}, \beta)$ at low and high temperatures. In the former case,

$$\begin{aligned}
Q_{G_{3/2}}^{(0)}(T_1, \beta) &\approx K_{iG_{3/2}}^2(T_1) \\
Q_{G_{3/2}}^{(12)}(E, \beta) &\approx K_{1G_{3/2}}(T_1)K_{2G_{3/2}}(T_1)K_{G_{3/2}}(E) \\
Q_{G_{3/2}}^{(22)}(T_2, \beta) &\approx K_{2G_{3/2}}^2(T_1)K_{G_{3/2}}(T_2)
\end{aligned} \tag{111}$$

where $K_{iG_{3/2}}(T_1)$ are the reduction parameters of the magnetic moment in the ground vibronic state $G_{3/2}$. Note that by means of the choice of the matrices $\hat{R}_{iT_1\bar{y}}$ we obtained only two reduction parameters for the operators of the type T_1 against four K_{ij} values in the work of Ham *et al.* (1976), for which $K_{12} = \frac{2}{3} K_{21} = \frac{4}{9} (K_{22} - K_{11})$. In the framework of the approximation (96)

$$\begin{aligned}
K_{1G_{3/2}}(T_1) &= 1 + \frac{2}{3}p(a_E, a_{T_2})s(a_E, a_{T_2}) \\
K_{2G_{3/2}}(T_1) &= \frac{1}{2}[1 + p(a_E, a_{T_2})[1 - \frac{1}{3}s(a_E, a_{T_2})]]
\end{aligned} \tag{112}$$

From these relations the intervals of the $K_{iG_{3/2}}(T_1)$ values for certain vibronic constant values can be obtained. In particular, since $s(a_E, 0) = 0$ and $p(a_E, 0)$ lie between 0 and infinite, if $0 < a_E < \infty$, in the absence of vibronic coupling with T_2 vibrations $K_{1G_{3/2}}(T_1)|_{a_{T_2}=0} = 1$ and $\frac{1}{2} \leq K_{2G_{3/2}}(T_1)|_{a_{T_2}=0} \leq 1$. In the other limit case when $a_E = 0$, $a_{T_2} \neq 0$, the relation takes place

$$p(0, a_{T_2})[1 - s(0, a_{T_2})] = 1$$

and if a_{T_2} changes between 0 and ∞ , then

$$\frac{1}{2} < K_{1G_{3/2}}(T_1)|_{a_E=0} \leq 1 \quad \text{and} \quad \frac{2}{3} < K_{2G_{3/2}}(T_1)|_{a_E=0} \leq 1$$

At high temperatures by means of the approximation (96), the following formulas can be obtained:

$$\begin{aligned}
Q_{G_{3/2}}^{(12)}(E, \beta) &= Q_{G_{3/2}}(E, \beta) \\
Q_{G_{3/2}}^{(22)}(T_2, \beta) &= Q_{G_{3/2}}(T_2, \beta) \\
Q_{G_{3/2}}^{(1)}(T_1, \beta) &= 1 + \frac{2}{3}p(a_E^*, a_{T_2}^*)g(a_E^*, a_{T_2}^*) \\
Q_{G_{3/2}}^{(2)}(T_1, \beta) &= \frac{1}{2}[1 + p(a_E^*, a_{T_2}^*)[f(a_E^*, a_{T_2}^*) - \frac{1}{3}g(a_E^*, a_{T_2}^*)]]
\end{aligned} \tag{113}$$

from which follow the inequalities

$$\begin{aligned}
\frac{1}{2} < Q_{G_{3/2}}^{(2)}(T_1, \beta)|_{a_{T_2}=0} \leq 1, \quad Q_{G_{3/2}}^{(1)}(T_1, \beta)|_{a_{T_2}=0} = 1 \\
\frac{1}{2} < Q_{G_{3/2}}^{(1)}(T_1, \beta)|_{a_E=0} \leq 1, \quad \frac{2}{3} < Q_{G_{3/2}}^{(2)}(T_1, \beta)|_{a_E=0} < 1
\end{aligned} \tag{114}$$

If $a_E^*, a_{T_2}^* \ll 1$, within accuracy up to linear terms in $\beta E_{JT}(\bar{\Gamma})$, we obtain

$$\begin{aligned}
Q_{G_{3/2}}^{(1)}(T_1, \beta) &\approx 1 - \frac{2}{3}\beta E_{JT}(T_2) \\
Q_{G_{3/2}}^{(2)}(T_1, \beta) &\approx 1 - \frac{2}{3}\beta E_{JT}(E) - \frac{2}{3}\beta E_{JT}(T_2)
\end{aligned} \tag{115}$$

For $Q_{G_{3/2}}^{(12)}$ and $Q_{G_{3/2}}^{(22)}$ relations similar to (114) and (115) can be obtained from Eq. (113) by means of Eq. (102).

The preceding results show that the presence of degeneracy essentially redetermines the temperature dependence of the birefringence in both electric and magnetic fields. Most unusual is the manifestation of the degeneracy in the case of spherical-top molecules in which an orientational contribution to the birefringence occurs that is absent in nondegenerate states. The temperature dependence of this contribution is relatively simple for low temperatures when the population of the excited vibronic states can be neglected (quadratically or linear in β depending on whether the Zeeman (or Stark) effect in the initial electronic state takes place).

For intermediate and high temperatures the dependence of birefringence on β is complicated. In particular, it can change from linear to quadratic, even for diamagnetic and nonpolar molecules. In the traditional theory of the Kerr or Cotton-Mouton effect the quadratic dependence on temperature is related to the presence of a dipole or magnetic moment, respectively. In the case of degeneracy this interpretation is not unambiguous, since the quadratic contributions to the birefringence can arise owing to either the presence of a nonzero appropriate moment or the Jahn-Teller effect. This ambiguity can be removed, say, by means of the optical Kerr and Cotton-Mouton effects, in which the contribution due to the proper dipole or magnetic moments vanishes, whereas the quadratic contribution due to the Jahn-Teller effect is nonzero.

B. Depolarization of Light in Rayleigh, Hyper-Rayleigh, and Pure Rotational Raman Scattering

Another important method for investigation of the anisotropy of polarizabilities of molecules complementary to the Kerr and Cotton-Mouton effects is light scattering. The paper of Child and Longuet-Higgins (1961) was the first one devoted to the study of the manifestation of the degeneracy in Rayleigh and Raman light scattering by molecules of D_{3h} symmetry in electron degenerate states E' . In this work, by means of so-called primitive matrix elements describing the vibronic interaction, expressions were obtained for the coefficients of depolarization of the scattered light. The latter have unusual values due to the pseudovector-type scattering effective in the presence of degeneracy. Also the possibility of Raman transitions between different vibronic levels, which can be considered as the vibrational structure of the transition between different electronic states, and the type of possible scattering (scalar, quadrupole, or pseudovector), as well as the doubling of each Raman line due to the Jahn-Teller effect, were suggested. Further investigations of the effect of

degeneracy on the scattering were carried out in the works of Ogurtsov *et al.* (1978) and Ostrovski *et al.* (1983). In these works also the dependence of the scattering on the type of degeneracy of the ground electronic state was investigated.

Consider the scattering of light with ω frequency and I_0 intensity linearly polarized along the Z axis of the LSC and propagating along the X axis by a medium containing a large number (N) of molecules. The intensity of the light noncoherent scattered in the Y direction with a frequency $n\omega + \Delta\omega$ ($n = 1$ in the case of Rayleigh scattering, and $n = 2, 3$ in the cases of scattering in the second and third harmonics, respectively) and polarized along the i axis ($i = X, Z$) is given by the expression (Hellwarth, 1970; Alexievicz, 1975; Kielich, 1981)

$${}^{n\omega}I_i(\Delta\omega) = \frac{Na_n}{2\pi} \left(\frac{n\omega + \Delta\omega}{c} \right)^4 I_0^n \int_{-\infty}^{\infty} dt e^{i\Delta\omega t} \langle \hat{C}_{iZ\dots Z}^{n\omega\dagger}(t) \hat{C}_{iZ\dots Z}^{n\omega}(0) \rangle \quad (116)$$

in which c is the velocity of light propagation in the medium, $a_1 = 1$, $a_2 = \frac{1}{8}$, $a_3 = \frac{1}{288}$, $\hat{C}_{iZ\dots Z}^{n\omega}$ is the tensor of the scattering into the n th harmonic equal to the operators of dynamic polarizability $\hat{\alpha}_{iZ}(\omega)$, if $n = 1$, and hyperpolarizabilities $\hat{\beta}_{iZZ}(\omega)$ and $\hat{\gamma}_{iZZZ}(\omega)$, if $n = 2$ and 3 , respectively, and $\hat{A}(t)$ is the operator \hat{A} in the Heisenberg representation. Hereafter the index n in $\hat{C}_{iZ\dots Z}^{n\omega}$ is omitted keeping in mind that the number of indices Z in the tensor of scattering $\hat{C}_{iZ\dots Z}^{n\omega}$ coincides with n . Besides the intensities ${}^{n\omega}I_i(\Delta\omega)$, usually the depolarization coefficients are also considered, which are equal to the ratio

$$\Delta_v^{n\omega}(\Delta\omega) = \frac{{}^{n\omega}I_X(\Delta\omega)}{{}^{n\omega}I_Z(\Delta\omega)} \quad (117)$$

Using the transformation

$$\hat{C}_{iZ\dots Z} = \sum_{\nu JM} b_{iZ\dots Z}^{\nu JM} \hat{C}_M^{[\nu, J]} \quad (118)$$

we pass now from Cartesian components $\hat{C}_{iZ\dots Z}$ to the components of the spherical tensors $\hat{C}_M^{[\nu, J]}$ of the rank J . In Eq. (118) $b_{iZ\dots Z}^{\nu JM}$ are the coefficients given, e.g., in the work of Jerphagnon *et al.* (1978), and the index ν indicates the symmetry of the contributions in the expansion (118) with respect to the permutation of the index i with any of the indices Z [$\nu = s, a, m$ when the appropriate contribution is symmetrical, is antisymmetrical, or has no definite symmetry with respect to the permutation, respectively (Maker, 1970)]. The components of the spherical tensor $\hat{C}_M^{[\nu, J]}$ in the LSC and $\hat{C}_K^{[\nu, J]}$ in the MSC are related by the equation

$$\hat{C}_M^{[\nu, J]} = \sum_K \hat{C}_K^{[\nu, J]} D_{KM}^J(\Omega) \quad (119)$$

Neglecting the interaction of the internal degrees of freedom of the molecule with the rotations, we come to the following form of the correlation function of the tensor of scattering:

$$\begin{aligned} \langle \hat{C}_{iZ\dots Z}^\dagger(t) \hat{C}_{iZ\dots Z}(0) \rangle &= \sum_{vv'J'JKJ'M'K'} \rho_f b_{iZ\dots Z}^{\nu JM*} b_{iZ\dots Z}^{\nu'J'M'} \exp[i(\omega_f - \omega_{f'})t] \\ &\times \langle f' | \hat{C}_K^{[\nu,J]} | f \rangle^* \langle f' | \hat{C}_K^{[\nu',J']} | f \rangle \langle D_{KM}^{J*}[\Omega(t)] D_{K'M'}^{J'}[\Omega(0)] \rangle_{rot} \end{aligned} \quad (120)$$

where ρ_f and ω_f are the statistical Boltzmann factor and the energy of the state $|f\rangle$, respectively, $\langle D_{KM}^{J*}[\Omega(t)] D_{K'M'}^{J'}[\Omega(0)] \rangle_{rot}$ is the rotational correlation function.

1. Free-Rotating Systems

Consider first the case of free-rotating molecules for which the rotational correlation function is given by the expression

$$\begin{aligned} \langle D_{KM}^{J*}[\Omega(t)] D_{K'M'}^{J'}[\Omega(0)] \rangle_{rot} &= \sum_{\substack{J_1 M_1 K_1 \\ J_2 M_2 K_2}} \rho_{J_1 K_1} \exp[i(\omega_{J_1 K_1} - \omega_{J_2 K_2})t] \langle J_2 K_2 M_2 | D_{KM}^{J'} | J_1 K_1 M_1 \rangle^* \\ &\times \langle J_2 K_2 M_2 | D_{K'M'}^{J'} | J_1 K_1 M_1 \rangle \end{aligned} \quad (121)$$

Considering only symmetric-top or spherical-top molecules and presenting the rotational functions $|J_i K_i M_i\rangle$ as

$$|J_i K_i M_i\rangle = \sqrt{\frac{2J_i + 1}{8\pi^2}} D_{K_i M_i}^{J_i}(\Omega) \quad (122)$$

we obtain

$$\begin{aligned} \langle D_{KM}^{J*}[\Omega(t)] D_{K'M'}^{J'}[\Omega(0)] \rangle_{rot} &= \sum_{J_1 K_1 J_2 K_2} \rho_{J_1 K_1} \exp[i(\omega_{J_1 K_1} - \omega_{J_2 K_2})t] \\ &\times C_{J_1 K_1 J_2 K_2}^{J_2 K_2} C_{J_1 K_1 J_2 K_2}^{J_2 K_2} \sqrt{\frac{(2J_1 + 1)(2J_2 + 1)}{2J + 1}} \delta_{JJ'} \delta_{KK'} \{J_1 J_2 J\} \end{aligned} \quad (123)$$

where $\{J_1 J_2 J\}$ is the $3j$ symbol (Varshalovich *et al.*, 1975). Substituting Eqs. (123) and (120) into Eq. (118), one can present the intensity of scattering by free-rotating systems in the form

$$\begin{aligned} {}^{n\omega} I_l(\Delta\omega) &= S_n \sum_{\nu\nu'JK} B_{iZ\dots Z}^{\nu\nu'J} \\ &\times \sum_{\Gamma\Gamma'J_1 J_2 K_1 K_2} \rho_\Gamma \rho_{J_1 K_1} [G_{JK}^{\nu\nu'}(n\omega)] \Gamma' (b^J)_{J_1 K_1}^{J_2 K_2} \{J_1 J_2 J\} \\ &\times \delta(\omega_\Gamma - \omega_{\Gamma'} + \omega_{J_1 K_1} - \omega_{J_2 K_2} - \Delta\omega) \end{aligned} \quad (124)$$

where

$$S_n = Na_n \left(\frac{n\omega + \Delta\omega}{c} \right)^4 I_0^n$$

$$B_{iZ\dots Z}^{\nu\nu'J} = \sum_M b_{iZ\dots Z}^{\nu JM*} b_{iZ\dots Z}^{\nu'JM} \quad (125)$$

$$[G_{JK}^{\nu\nu'}(n\omega)]_{\Gamma}^{\Gamma'} = \sum_{\gamma\gamma'} \langle \Gamma\gamma | \hat{C}_K^{[\nu,J]}(n\omega) | \Gamma'\gamma' \rangle^* \langle \Gamma\gamma | \hat{C}_K^{[\nu',J]}(n\omega) | \Gamma'\gamma' \rangle \quad (126)$$

$$(b^J)_{J_1K_1}^{J_2K_2} = \sqrt{\frac{(2J_1 + 1)(2J_2 + 1)}{2J + 1}} (C_{J_1K_1J_2}^{J_2K_2})^2 \quad (127)$$

The coefficients $(b^J)_{J_1K_1}^{J_2K_2}$ for $J = 0, 1, 2$ are appropriate to the $b_{J_1K_1}^{(i)J_2K_2}$ ones with $i = 0, a, s$ introduced by Placzek (1935).

In cubic systems the rotational energy is independent of the rotational quantum number K , and hence in Eq. (124) one can perform the summation over K_1 and K_2 . As a result, for the intensity of the scattering by spherical-top molecules, we have

$$\begin{aligned} {}^{n\omega}I_i(\Delta\omega) &= S_n \sum_{\nu\nu'J} B_{iZ\dots Z}^{\nu\nu'J} \\ &\times \sum_{\Gamma\Gamma'J_1J_2} \rho_{\Gamma}\rho_{J_1}(2J_1 + 1) [G_{J_1}^{\nu\nu'}(n\omega)]_{\Gamma J_1}^{\Gamma' J_2} \\ &\times \delta(\omega_{\Gamma} - \omega_{\Gamma'} + \omega_{J_1} - \omega_{J_2} - \Delta\omega) \end{aligned} \quad (128)$$

In this formula

$$\begin{aligned} [G_{J_1}^{\nu\nu'}(n\omega)]_{\Gamma J_1}^{\Gamma' J_2} &= \frac{2J_2 + 1}{2J + 1} \{J_1 J_2 J\} \sum_{K\gamma\gamma'} (-1)^K \langle \Gamma\gamma | \hat{C}_K^{[\nu,J]}(n\omega) | \Gamma'\gamma' \rangle \\ &\times \langle \Gamma'\gamma' | \hat{C}_K^{[\nu',J]}(n\omega) | \Gamma\gamma \rangle \end{aligned} \quad (129)$$

determine the cross sections appropriate to different types of scattering. For instance, if $n = 1$, $[G_J^{\nu}(\omega)]_{\Gamma J_1}^{\Gamma' J_2}$ describes the contribution of scalar ($\nu = s, J = 0$), symmetric ($\nu = s, J = 2$), and antisymmetric ($\nu = a, J = 1$) scattering corresponding to the transition of the system between the states ΓJ_1 and $\Gamma' J_2$. Hereafter, if $\nu = \nu'$, only one index is used in the notations: $G_J^{\nu\nu} = G_J^{[\nu,J]}$.

a. Selection rules for vibronic-rotational Raman transitions. It follows from Eq. (128) that the n th harmonic consists of peaks corresponding to the transitions $\Gamma J_1 \rightarrow \Gamma' J_2$. In order to determine the selection rules one has to pass in Eq. (129) from spherical tensors $\hat{C}_K^{[\nu,J]}$ to irreducible

tensor operators $\hat{C}_{\bar{\Gamma}\bar{\gamma}}^{[\nu,J]}$ belonging to the representation $\bar{\Gamma}$ contained in the expansion of the full spherical group representation D^J with respect to irreducible representations of the point symmetry group of the molecule

$$\hat{C}_K^{[\nu,J]} = \sum_{\bar{\Gamma}\bar{\gamma}} b_{\bar{\Gamma}\bar{\gamma}}^{\nu JK} \hat{C}_{\bar{\Gamma}\bar{\gamma}}^{[\nu,J]} \quad (130)$$

Then, in accordance with Eqs. (129) and (130), the transitions between the states Γ and Γ' are allowed if the direct product $\Gamma \otimes \Gamma'$ contains at least one of the representations $\bar{\Gamma}$.

The selection rules with respect to the rotational quantum numbers are given by the $3j$ symbols $\{J_1 J_2 J\}$, which are nonzero and equal to one only if $\Delta J = |J_1 - J_2| \leq J$.

A special remark should be made concerning the transitions without changes of the energy of the internal degrees of freedom, i.e., about pure rotational Raman scattering. In the case of an even number of electrons, such transitions are possible if in the expansion of the even (odd) (with respect to time reversal) tensor operator $\hat{C}_K^{[\nu,J]}$ there are representations contained in the symmetric $[\Gamma^2]$ (antisymmetric $\{\Gamma^2\}$) quadrature of the representation Γ . In the case of an odd number of electrons, at least one of the representations $\bar{\Gamma}$ in the expansion of the even (odd) operator $\hat{C}_K^{[\nu,J]}$ (with respect to time reversal) is contained in $\{\Gamma^2\}(\{\Gamma^2\})$.

Let us use these selection rules for investigating the main features of the Rayleigh and pure rotational Raman scattering by spherical-top molecules in the lowest vibronic states (Ogurtsov *et al.*, 1978). The polarizability tensors $\hat{\alpha}_K^{[s,2]}$ and $\hat{\alpha}_K^{[g,1]}$ can be expanded into components of irreducible tensor operators that in cubic groups transform as E , T_2 , and T_1 , respectively. Here the behavior of the operators $\hat{\alpha}_K^{[\nu,J]}$ with respect to time reversal $\hat{\Theta}$ has to be taken into consideration. To do this, we use the explicit form of the operator $\hat{\alpha}_{ij}(\omega)$ in Cartesian coordinates:

$$\hat{\alpha}_{ij}(\omega) = \hat{d}_i \frac{1}{\hat{H} + \omega} \hat{d}_j + \hat{d}_j \frac{1}{\hat{H} - \omega} \hat{d}_i \quad (131)$$

Under the operation $\hat{\Theta}$ the operator \hat{V} transforms as

$$\hat{\Theta} \hat{V} \hat{\Theta}^{-1} = \hat{K} \hat{V}^\dagger \hat{K}^{-1} \quad (132)$$

where \hat{K} is the operator of complex conjugation. Since \hat{d}_i and \hat{H} are real Hermitian operators, we have

$$\begin{aligned} \hat{\Theta} \hat{\alpha}_{ij}(\omega) \hat{\Theta}^{-1} &= \hat{K} \hat{\alpha}_{ij}^\dagger(\omega) \hat{K}^{-1} \\ &= \hat{d}_j \frac{1}{\hat{H} + \omega} \hat{d}_i + \hat{d}_i \frac{1}{\hat{H} - \omega} \hat{d}_j = \hat{\alpha}_{ij}(-\omega) = \hat{\alpha}_{ji}(\omega) \end{aligned} \quad (133)$$

Using the explicit form of the relations between Cartesian $\hat{\alpha}_{ij}(\omega)$ and spherical $\hat{\alpha}_K^{[\nu, J]}$ components of polarizability and Eq. (133), we obtain

$$\hat{\Theta} \hat{\alpha}_K^{[\nu, J]} \hat{\Theta}^{-1} = (-1)^J \hat{\alpha}_K^{[\nu, J]} \quad (134)$$

Thus the operator $\hat{\alpha}_{\bar{1}\bar{2}}^{[s, 2]}$ is even and the $\hat{\alpha}_{\bar{1}\bar{2}}^{[a, 1]}$ one is odd with respect to the operation of time reversal.

b. Pure rotational Raman spectra. Let us use first the selection rules from the preceding subsection for elucidation of the possibility of pure rotational Raman spectra in the case of spherical-top molecules. In the case of a nondegenerate state A, all types of scattering except the scalar one ($J = 0$) are forbidden, since $[A^2] = A$ and $\{A^2\} = 0$, and hence in this case pure rotational Raman spectra are impossible. This conclusion coincides with the results of classical consideration.

In the case of degenerate E states we have $[E^2] = A_1 + E$ and $\{E^2\} = A_2$, and therefore here the pure rotational Raman spectra of quadrupole type are possible. In the case of T terms also, pseudovector scattering is allowed, since in this case $\{T^2\}$ contains T_1 . Finally, analogously one can make sure that in the states $E_{1/2}$ and $E_{5/2}$ pure rotational scattering of pseudovector type only is possible, while in the states $G_{3/2}$ both quadrupole and pseudovector scattering should take place.

Thus the selection rules show explicitly that in the case of electronic degeneracy pure rotational Raman spectra of light scattering by spherical-top molecules are possible. If the Jahn–Teller effect is taken into account, the degeneracy of the ground vibronic state coincides with that of the initial electronic one. Therefore in this case pure rotational Raman spectra are possible in spherical-top molecules already in the ground state. The type of scattering can be determined by using the selection rules in a manner quite similar to the earlier analysis.

Note that transitions with $\Gamma = \Gamma'$ should also be related to a pure rotational one. However, in the case of strong vibronic coupling there may be another low-lying vibronic state with a symmetry different from that of the ground state. Therefore in these cases the pure rotational Raman spectrum can be superposed by the spectrum of vibronic–rotational scattering.

For instance, in the case of the quadratic $E \otimes e$ problem, the lowest vibronic states are E and A_1 , divided by a small energy interval 2Δ (tunneling splitting) (Bersuker, 1961, 1962). The intensity of the split vibronic–rotational Raman transition is determined by the matrix elements $(G^{[\nu, J]})_{\Gamma\Gamma'}^2$, which may be presented in the form (Ogurtsov *et al.*, 1978)

$$\begin{aligned}
 (G^{[s,2]})_{EJ_1}^{EJ_1+\Delta J} &= [2(J_1 + \Delta J) + 1] \langle E \| \hat{\alpha}_E(\omega) \| E \rangle^2 \\
 (G^{[s,2]})_{EJ_1}^{AJ_1+\Delta J} &= (G^{[s,2]})_{EJ_1}^{EJ_1+\Delta J} \\
 &= [2(J_1 + \Delta J) + 1] \langle E \| \hat{\alpha}_E(\omega) \| E \rangle^2 \quad (\Delta J = 0, \pm 1, \pm 2) \\
 (G^{[a,1]})_{\Gamma\Gamma'}^{\Gamma\Gamma'} &= 0 \quad (\Gamma, \Gamma' = A_1, E)
 \end{aligned} \quad (135)$$

where $\langle \Gamma \| \hat{\alpha}_E(\omega) \| \Gamma' \rangle$ are the reduced matrix elements of the polarizability tensor that transform after the representation Γ and $|\Gamma\gamma\rangle$ and $|\Gamma'\gamma'\rangle$ are the vibronic functions.

It follows from these equations that in the case under consideration the pure rotational Raman spectrum consists of lines corresponding to three types of O, P, Q, R, and S transitions: $EJ_1 \rightarrow EJ_2$ (O, P, Q, R, S), $EJ_1 \rightarrow A_1J_2$ (O', P', Q', R', S'), and $AJ_1 \rightarrow EJ_2$ (O'', P'', Q'', R'', S''). The lines denoted by one and two primes are displaced with respect to the nonprimed ones by 2Δ and -2Δ , respectively. Note that the scalar scattering gives lines of the type Q only with cross section, as follows:

$$(G^{[s,0]})_{\Gamma\Gamma'}^{\Gamma\Gamma'} = (2J_1 + 1) \langle \Gamma \| \hat{\alpha}^{[s,0]}(\omega) \| \Gamma \rangle^2 \quad (\Gamma = A_1, E) \quad (136)$$

Consider now the depolarization coefficients. From the explicit form of the expansion of the Cartesian components of the polarization tensor $\hat{\alpha}_{XX}^{(s)}$, $\hat{\alpha}_{ZZ}^{(a)}$, and $\hat{\alpha}_{ZZ}^{(s)}$ with respect to the spherical one

$$\begin{aligned}
 \hat{\alpha}_{XX}^{(s)} &= \frac{1}{2} (\hat{\alpha}_{-1}^{[s,2]} - \hat{\alpha}_1^{[s,2]}) \\
 \hat{\alpha}_{XX}^{(a)} &= -\frac{1}{2} (\hat{\alpha}_{-1}^{[a,1]} + \hat{\alpha}_1^{[a,1]}) \\
 \hat{\alpha}_{ZZ}^{(s)} &= -\frac{1}{\sqrt{3}} \hat{\alpha}_0^{[s,0]} + \sqrt{\frac{2}{3}} \hat{\alpha}_0^{[s,2]}
 \end{aligned} \quad (137)$$

it follows that $B_{ZZ}^{s0} = \frac{1}{3}$, $B_{ZZ}^{s2} = \frac{2}{3}$, $B_{XX}^{s2} = B_{XX}^{a1} = \frac{1}{2}$. By means of these coefficients and the relations (117), (128), and (135), we find that the depolarization coefficients for all the transitions $(\Delta_v^{\omega})_{\Gamma\Gamma'}^{\Gamma\Gamma'+\Delta J}$ are equal to $\frac{3}{4}$, except the Q transitions, for which

$$(\Delta_v^{\omega})_{EJ_1}^{EJ_1} \leq \frac{3}{4} \quad (138)$$

In the case of systems with threefold degenerate terms interacting with T_2 displacements (the linear $T \otimes t$ problem), the lowest vibronic states are T and A. For the cross-section magnitudes $(G^{[v,J]})_{\Gamma\Gamma'}^{\Gamma\Gamma'}$ determined by Eq. (129), in the case of the $T \otimes t$ problem, we obtain

$$\left. \begin{aligned}
(G^{[s,2]})_{JJ_1}^{TJ_1+\Delta J} &= [2(J_1 + \Delta J) + 1] \langle T \| \hat{\alpha}_E(\omega) \| T \rangle^2 \\
&\quad + \langle T \| \hat{\alpha}_{T_2}(\omega) \| T \rangle^2 \\
(G^{[s,2]})_{JJ_1}^{TJ_1+\Delta J} &= (G^{[s,2]})_{JJ_1}^{AJ_1+\Delta J} = [2(J_1 + \Delta J) \\
&\quad + 1] \langle T \| \hat{\alpha}_{T_2} \| A \rangle^2
\end{aligned} \right\} \quad (\Delta J = 0, \pm 1, \pm 2) \quad (139)$$

$$\begin{aligned}
(G^{[a,1]})_{JJ_1}^{TJ_1+\Delta J} &= [2(J_1 + \Delta J) + 1] \langle T \| \hat{\alpha}_{T_1}(\omega) \| T \rangle^2 \quad (\Delta J = 0, \pm 1) \\
(G^{[s,0]})_{JJ_1}^{\Gamma J_1} &= (2J_1 + 1) \langle \Gamma \| \hat{\alpha}_{A_1}(\omega) \| \Gamma \rangle^2 \quad (\Gamma = A, T)
\end{aligned}$$

It follows from these relations that in the case of the $T \otimes t$ problem under consideration the number of branches of the vibronic-rotational Raman spectrum is the same as in the case of the $E \otimes e$ problem: $TJ_1 \rightarrow TJ_2(\text{O, P, Q, R, S})$, $TJ_1 \rightarrow AJ_2(\text{O}', \text{P}', \text{Q}', \text{R}', \text{S}')$, and $AJ_1 \rightarrow TJ_2(\text{O}'', \text{P}'', \text{Q}'', \text{R}'', \text{S}'')$.

However, in this case, as already mentioned, pseudovector scattering is also possible. This results in unusual depolarization coefficients not only for the Q transition, for which

$$(\Delta_v^\omega)_{JJ}^{TJ} \geq 0 \quad (140)$$

but also for P and R transitions,

$$(\Delta_v^\omega)_{JJ_1}^{TJ_1 \pm 1} \geq \frac{3}{4} \quad (141)$$

Thus high-symmetry molecular systems in degenerate vibronic states, in principle, should have a pure rotational Raman spectrum of light scattering. This spectrum consists of three types of the five branches O, P, Q, R, and S if the vibronic coupling is strong enough and the energy gap between the vibronic levels is comparable with the rotational quantum and only one type of the above branches in the opposite limit case.

The intensities of the spectral lines and the depolarization coefficients are functions of the reduced matrix elements of the polarizability tensor calculated by vibronic functions. In order to estimate the possibility of observation of the pure rotational Raman spectra under consideration, one has to consider in more detail the polarizability operator. Its components belonging to the line $\bar{\gamma}$ of representation $\bar{\Gamma}$ can be presented in the form of a power series with respect to the displacement $q_{\Gamma_2\gamma_2}$ active in the Jahn-Teller effect (the other components can be neglected as not active in the pure rotational Raman spectrum under consideration):

$$\hat{\alpha}_{\bar{\Gamma}\bar{\gamma}}(\omega, q) = \hat{\alpha}_{\bar{\Gamma}\bar{\gamma}}(\omega, 0) + \sum_{\Gamma_2\gamma_2} \left. \frac{\partial \hat{\alpha}_{\bar{\Gamma}\bar{\gamma}}(\omega, q)}{\partial q_{\Gamma_2\gamma_2}} \right|_{q=0} q_{\Gamma_2\gamma_2} + \dots \quad (142)$$

Thus in the linear in $q_{\Gamma_{2\gamma_2}}$ approximation any reduced matrix element consists of two terms corresponding to the matrix element of the electronic and nuclear polarizabilities, respectively. The reduced matrix elements of the electronic polarizability are equal to the matrix elements calculated by the electronic functions of the initial electronic term multiplied by the vibronic reduction factors. Since the latter decrease with increasing vibronic coupling, the contribution to the reduced matrix elements of the electronic polarizability is the smaller, the stronger the vibronic interaction. The contributions from the nuclear polarizability have an opposite trend—they are the larger, the stronger the vibronic coupling. Thus we state that the intensity of the pure rotational Raman spectrum is determined mainly by the electronic polarizability in the case of weak vibronic coupling and the nuclear polarizability together with the reduced electronic one in the case of strong vibronic coupling.

2. Scattering in a Viscous Medium

Consider now the main features of light scattering by vibronic systems in a viscous medium. As in the preceding subsection, we exclude the Raman and hyper-Raman transitions between vibronic levels of different energy. Assume that $\omega_f = \omega_{f'}$ and that only the ground vibronic degenerate state is populated, its wave functions belonging to the irreducible representation Γ .

Within the model of continuous rotational diffusion, the rotational correlation function for spherical-top molecules is given by the expression (Valiev and Ivanov, 1973)

$$\langle D_{KM}^{\Gamma*}[\Omega(t)] D_{K'M'}^{\Gamma'}[\Omega(0)] \rangle_{\text{rot}} = \frac{\delta_{JJ'} \delta_{KK'} \delta_{MM'}}{2J+1} \exp\left(-\frac{|t|}{\tau_{JK}}\right) \quad (143)$$

where

$$\tau_{JK}^{-1} = J(J+1)D_1 + K^2(D_3 - D_1) \quad (144)$$

Substituting Eq. (144) into Eq. (120) and using Eq. (116), we obtain

$${}^{n\omega}I_i(\Delta\omega) = S_n \sum_{\nu\nu'} \frac{B_{iZ\dots Z}^{\nu\nu'J}}{2J+1} G_J^{\nu\nu'}(n\omega, \Delta\omega) \quad (145)$$

where

$$G_J^{\nu\nu'}(n\omega, \Delta\omega) = \sum_K G_{JK}^{\nu\nu'}(n\omega) g_{JK}(\Delta\omega) \quad (146)$$

$$g_{JK}(\Delta\omega) = \frac{1}{\pi} \frac{\tau_{JK}}{1 + (\Delta\omega\tau_{JK})^2} \quad (147)$$

Beginning from Eqs. (145) and (146) the index Γ in the magnitudes $[G_J^{\nu\nu'}(n\omega, \Delta\omega)]_\Gamma^\Gamma$ and $[G_{JK}^{\nu\nu'}(n\omega)]_\Gamma^\Gamma$ is omitted.

In accordance with relation (144) and (147)

$$g_{00}(\Delta\omega) = \delta(\Delta\omega) \quad (148)$$

i.e., formally the half-width $g_{00}(\Delta\omega)$ equals zero. However, if one considers the fluctuations of entropy and density, one can show that the half-width of the spectrum of scalar-type scattering is in fact of the order of 1 cm^{-1} (Utarova, 1980). Therefore when the wing of Rayleigh or hyper-Rayleigh scattering ($\Delta\omega \sim 100 \text{ cm}^{-1}$) is considered, this contribution to the scattering can be neglected as compared with contributions of the fluctuation of anisotropy.

a. Rayleigh scattering. In the case of scattering into the first harmonic ($n = 1$), $J = 0, 1, 2$, the depolarization coefficient $\Delta_\omega^0(\Delta\omega)$ is

$$\Delta_\omega^0(\Delta\omega) = \frac{3G_2^s(\omega, \Delta\omega) + 5G_1^a(\omega, \Delta\omega)}{10G_0^s(\omega, \Delta\omega) + 4G_2^s(\omega, \Delta\omega)} \quad (149)$$

The determination of the types of scattering (scalar, quadrupole, or pseudovector) effective in scattering under consideration in a viscous medium can be carried out in accordance with the rules formulated earlier (Section III,A,1,a). The quadrupole and pseudovector scattering takes place if the representation $\Gamma_\xi^{(s)}$ and $\Gamma_\xi^{(a)}$ in the expansions $D_+^2 = \sum_\xi \Gamma_\xi^{(s)}$ and $D_+^1 = \sum_\xi \Gamma_\xi^{(a)}$ obey the relations

$$\Gamma_\xi^{(s)} \in [\Gamma^2] \quad \text{and} \quad \Gamma_\xi^{(a)} \in \{\Gamma^2\} \quad (150)$$

or

$$\Gamma_\xi^{(s)} \in \{\Gamma^2\} \quad \text{and} \quad \Gamma_\xi^{(a)} \in [\Gamma^2] \quad (151)$$

depending on whether the number of electrons in the molecule is even or odd, respectively.

Concerning the rules (150) and (151), the following remark seems to be worthwhile. Resulting from group-theoretical considerations, these rules allow us to predict the possibility, only in principle, of the appropriate type of scattering. However, in fact, some of the cross sections may be negligible in magnitude. By way of example consider the VCl_4 molecule in the ground ${}^2\text{E}$ state. In the double-valued group the term ${}^2\text{E}$ corresponds to the representation $\text{G}_{3/2}$. However, the antisymmetric scattering in the state $\text{G}_{3/2}$ allowed by the rules (151), in fact, becomes possible only if one takes into account the spin-orbital mixing of the ground state with the excited $\text{G}_{3/2}$ one originating from the electronic term ${}^2\text{T}_2$, resulting thus in an intensity proportional to the square of the small ratio of the spin-orbital constant to the energy gap between the ${}^2\text{E}$ and ${}^2\text{T}_2$ terms.

Using the rules (150) and (151), one can make sure that in the case of symmetric-top molecules both the symmetric and antisymmetric scattering are possible for all twofold degenerate states. Taking into account the notion about the half-width $g_{00}(\Delta\omega)$, we come to the conclusion that in the region of the wing of the Rayleigh scattering the depolarization coefficient is

$$\Delta_v^w(\Delta\omega) = \frac{3}{4} + \frac{5}{4} \frac{G_1^q(\omega, \Delta\omega)}{G_2^s(\omega, \Delta\omega)} \quad (152)$$

It is seen that the depolarization coefficient is larger than $\frac{3}{4}$ and depends on $\Delta\omega$ owing to the differences in the spectral functions $G_1^q(\omega, \Delta\omega)$ and $G_2^s(\omega, \Delta\omega)$.

For spherical-top molecules in the states T_1 , T_2 , and $G_{3/2}$ of cubic groups, both types of scattering are allowed, whereas in the state E the symmetric one only is allowed, while in the states $E_{1/2}$ and $E_{5/2}$ the antisymmetric one is allowed. Hence spherical-top molecules in the states T_1 , T_2 , and $G_{3/2}$ in accordance with Eq. (149) scatter linear polarized light with a depolarization coefficient larger than $\frac{3}{4}$ and determined by the Eq. (152). In the orbital state E, $G_2^s(\omega, \Delta\omega) \neq 0$ and $G_1^q(\omega, \Delta\omega) = 0$ and the depolarization coefficient in the region of the Rayleigh wing equals $\frac{3}{4}$ and is independent of $\Delta\omega$. In the states $E_{1/2}$ and $E_{5/2}$, on the contrary, $G_2^s(\omega, \Delta\omega) = 0$ and $G_1^q(\omega, \Delta\omega) \neq 0$ and therefore everywhere except the region of $\Delta\omega \sim 1 \text{ cm}^{-1}$, where $G_2^s(\omega, \Delta\omega) \neq 0$, the depolarization coefficient equals infinity; i.e., the scattered light is completely depolarized, and hence the component polarized as the incident light is absent.

Concerning the latter conclusion, note that in a series of works (see, e.g., Hamaguchi *et al.*, 1975; Hamaguchi and Shimanouchi, 1976) the Raman scattering by octahedral molecules in the states $E_{1/2}$ was experimentally investigated and the effect of the full depolarization of the lines appropriate to the excitation of totally symmetric vibration was observed. Owing to symmetry considerations the depolarization coefficients for the Rayleigh scattering have to be the same as they are for these lines.

b. Depolarization of scattering into the second harmonic. The tensor of hyperpolarizability of the first order determining the scattering into the second harmonic has the form

$$\begin{aligned} \hat{\beta}_{ijk}(\omega) = \hat{P}_{jk} \left[\hat{d}_i \frac{1}{\hat{H} + 2\omega} \hat{d}_j \frac{1}{\hat{H} + \omega} \hat{d}_k \right. \\ \left. + \hat{d}_j \frac{1}{\hat{H} - \omega} \hat{d}_i \frac{1}{\hat{H} + \omega} \hat{d}_k + \hat{d}_j \frac{1}{\hat{H} - \omega} \hat{d}_k \frac{1}{\hat{H} - 2\omega} \hat{d}_i \right] \end{aligned} \quad (153)$$

where \hat{P}_{jk} is the operator acting as follows:

$$\hat{P}_{jk}\hat{A}_{jk} = \hat{A}_{jk} + \hat{A}_{kj} \quad (154)$$

For group-theoretical selection of nonzero matrix elements of the hyperpolarizability components, one has to know the symmetry properties of the operator $\hat{\beta}_{ijk}(\omega)$. Owing to the definition (153), $\hat{\beta}_{ijk}(\omega)$ is symmetric with respect to the permutation of the indices j and k , but it has no definite symmetry with respect to the permutation of all the indices and has no definite parity with respect to the operation of time reversal:

$$\hat{\Theta}\hat{\beta}_{ijk}\hat{\Theta}^{-1} = \hat{\beta}_{ijk}(-\omega) \quad (155)$$

Nevertheless the group-theoretical considerations can be useful if one employs some approximation for the frequency dependence of $\hat{\beta}_{ijk}(\omega)$.

Following Christie and Lockwood (1971), the tensor $\hat{\beta}_{ijk}(\omega)$ can be presented in the form of the sum of two terms

$$\hat{\beta}_{ijk}(\omega) = \hat{\beta}_{ijk}^{(s)}(\omega) + \hat{\beta}_{ijk}^{(m)}(\omega) \quad (156)$$

in which $\hat{\beta}_{ijk}^{(s)}(\omega)$ is symmetric with respect to any permutation of the indices and

$$\hat{\beta}_{ijk}^{(m)}(\omega) = \frac{1}{3}[2\hat{\beta}_{ijk}(\omega) - \hat{\beta}_{kji}(\omega) - \hat{\beta}_{jki}(\omega)] \quad (157)$$

is the nonsymmetric part.

Next we employ the widespread assumption of the possibility of neglecting the nonsymmetric part $\hat{\beta}_{ijk}^{(m)}(\omega)$. This assumption is based on the fact that in the region far from the absorption band, and if the dispersion is neglected, $\hat{\beta}_{ijk}^{(m)}$ disappears [$\hat{\beta}_{ijk}^{(m)}(\omega = 0) = 0$]. In the framework of this approximation the operators $\hat{\beta}_{ijk}(\omega)$ become even with respect to the time reversal operation, and the components $\hat{\beta}_{zzz}$ and $\hat{\beta}_{xzz}$, using the coefficients $b_{ijk}^{[v,J]}$ tabulated by Maker (1970), can be written as

$$\begin{aligned} \hat{\beta}_{zzz} &= -\sqrt{\frac{3}{5}}\hat{\beta}_0^{[s,1]} + \sqrt{\frac{2}{5}}\hat{\beta}_0^{[s,3]} \\ \hat{\beta}_{xzz} &= -\frac{1}{\sqrt{30}}(\hat{\beta}_{-1}^{[s,1]} - \hat{\beta}_1^{[s,1]}) + \sqrt{\frac{2}{15}}(\hat{\beta}_{-1}^{[s,3]} - \hat{\beta}_1^{[s,3]}) \end{aligned} \quad (158)$$

By means of these relations the depolarization coefficient of the light scattered into the second harmonic can be presented in the form

$$\Delta_v^{2\omega}(\Delta\omega) = \frac{\frac{1}{3}G_1^s(2\omega, \Delta\omega) + \frac{1}{21}G_3^s(2\omega, \Delta\omega)}{G_1^s(2\omega, \Delta\omega) + \frac{1}{7}G_3^s(2\omega, \Delta\omega)} \quad (159)$$

Owing to the evenness of the operators $\hat{\beta}_M^{[s,J]}$ with respect to the time-reversal operation, the cross sections $G_j^s(2\omega, \Delta\omega)$ are nonzero if in the

expansion $D^J = \sum_{\zeta} b_{J\zeta} \Gamma_{\zeta}^{(s)}$, $\Gamma_{\zeta}^{(s)}$ obeys the condition

$$\Gamma_{\zeta}^{(s)} \in [\Gamma^2] \quad \text{or} \quad \Gamma_{\zeta}^{(s)} \in \{\Gamma^2\} \quad (160)$$

for molecules with even and odd numbers of electrons, respectively.

In accordance with the rules (160) G_1^s and G_3^s disappear in the case of molecules having an inversion center. In the absence of the latter, G_3^s is nonzero independent of the state and the point group of the molecule, since the decomposition of D^3 into representations of the appropriate point group (having no inversion center) always contains the totally symmetric one. The selection rules for the operator $\hat{\beta}_K^{[s,1]}$ determining the cross section $G_1^s(2\omega, \Delta\omega)$ coincide with that of the operator of the dipole moment. Therefore in all the states of nondipolar type (i.e., in the states for which the linear Stark effect is impossible), since $G_1^s(2\omega, \Delta\omega) = 0$, the depolarization coefficient $\Delta_v^{2\omega}$ is independent of $\Delta\omega$ and equals $\frac{2}{3}$. In the states of dipolar type (e.g., the degenerate states T_1 , T_2 , and $G_{3/2}$ in tetrahedral molecules and E' in molecules with D_{3h} symmetry), the depolarization coefficient is less than $\frac{2}{3}$ and, generally speaking, depends on $\Delta\omega$. In the limit case when $G_1^s \gg G_3^s$, the depolarization coefficient equals $\frac{1}{3}$.

c. Depolarization of the scattering into the third harmonic. The generation of the third harmonic is due to the hyperpolarizability of the second order with the following operator:

$$\begin{aligned} \hat{\gamma}_{ijkl}(\omega) = & \hat{P}_{jkl} \left[\hat{d}_i \frac{1}{\hat{H} + 3\omega} \hat{d}_j \frac{1}{\hat{H} + 2\omega} \hat{d}_k \frac{1}{\hat{H} + \omega} \hat{d}_l \right. \\ & + \hat{d}_j \frac{1}{\hat{H} - \omega} \hat{d}_i \frac{1}{\hat{H} + 2\omega} \hat{d}_k \frac{1}{\hat{H} + \omega} \hat{d}_l \\ & + \hat{d}_j \frac{1}{\hat{H} - \omega} \hat{d}_k \frac{1}{\hat{H} - 2\omega} \hat{d}_i \frac{1}{\hat{H} + \omega} \hat{d}_l \\ & \left. + \hat{d}_j \frac{1}{\hat{H} - \omega} \hat{d}_k \frac{1}{\hat{H} - 2\omega} \hat{d}_l \frac{1}{\hat{H} - 3\omega} \hat{d}_i \right] \quad (161) \end{aligned}$$

in which the operator \hat{P}_{jkl} realizes the summation over all permutations of the indices j , k , and l . Similar to the hyperpolarizability tensor of the first order, the operator $\hat{\gamma}_{ijkl}(\omega)$ has no permutation symmetry with respect to all the indices i , j , k , l , but it can be presented in the form of a sum as

$$\hat{\gamma}_{ijkl}(\omega) = \hat{\gamma}_{ijkl}^{(s)}(\omega) + \gamma_{ijkl}^{(m)}(\omega) \quad (162)$$

of the symmetric $\hat{\gamma}_{ijkl}^{(s)}(\omega)$ and nonsymmetric

$$\gamma_{ijkl}^{(m)}(\omega) = \frac{1}{4}[3\hat{\gamma}_{ijkl}(\omega) - \hat{\gamma}_{lij k}(\omega) - \hat{\gamma}_{kl i j}(\omega) - \hat{\gamma}_{j k l i}(\omega)] \quad (163)$$

contributions. As in the case of linear Rayleigh scattering and scattering into the second harmonic, in the absence of absorption and dispersion, only the symmetric part of the hyperpolarizability of the second order is nonzero [$\hat{\gamma}_{ijkl}^{(m)}(\omega = 0) = 0$]. This, again, if dispersion is neglected, allows us to consider the $\hat{\gamma}_{ijkl}$ operator as an even one with respect to time reversal. In this approximation the expansion of the Cartesian components $\hat{\gamma}_{zzzz}$ and $\hat{\gamma}_{xzzz}$ with respect to the spherical ones has the form

$$\begin{aligned}\hat{\gamma}_{zzzz} &= \frac{1}{\sqrt{5}} \hat{\gamma}_0^{[s,0]} - \frac{2}{\sqrt{7}} \hat{\gamma}_0^{[s,2]} + \frac{4}{\sqrt{70}} \hat{\gamma}_0^{[s,4]} \\ \hat{\gamma}_{xzzz} &\approx -\frac{\sqrt{3}}{2\sqrt{14}} (\hat{\gamma}_{-1}^{[s,2]} - \hat{\gamma}_1^{[s,2]}) + \frac{1}{\sqrt{14}} (\hat{\gamma}_{-1}^{[s,4]} - \hat{\gamma}_1^{[s,4]})\end{aligned}\quad (164)$$

Note that the tensor $\hat{\gamma}_{ijkl}$ transforms as a direct product $\hat{d}_i \otimes \hat{\beta}_{jkl}^{(s)}$, and therefore the spherical components of the operator $\hat{\gamma}$ with the value $J = 2$ originate from both the product $\hat{d} \otimes \hat{\beta}^{[s,1]}$ and $\hat{d} \otimes \hat{\beta}^{[s,3]}$. If the first one is denoted by $\hat{\gamma}^{(2,1)}$ and the second by $\hat{\gamma}^{(2,3)}$, then by means of genealogical coefficients (Kaplan, 1969) the components $\hat{\gamma}^{[s,2]}$ can be presented in form

$$\hat{\gamma}^{[s,2]} = \sqrt{\frac{7}{10}} \hat{\gamma}^{(2,1)} + \sqrt{\frac{3}{10}} \hat{\gamma}^{(2,3)} \quad (165)$$

Using Eqs. (164), (117), and (145) for the depolarization coefficient of the scattering into the third harmonic at the wing of the line, we have

$$\Delta_v^{3\omega}(\Delta\omega) = \frac{\frac{3}{20}G_2^s(3\omega, \Delta\omega) + \frac{1}{15}G_4^s(3\omega, \Delta\omega)}{\frac{4}{15}G_2^s(3\omega, \Delta\omega) + \frac{8}{45}G_4^s(3\omega, \Delta\omega)} \quad (166)$$

provided that the scalar contribution is neglected.

Since the decomposition of D_+^4 into the representations of the point-symmetry group contains the totally symmetric one, the cross section $G_4^s(3\omega, \Delta\omega)$ is nonzero for any molecule. The selection rules for $G_2^s(3\omega, \Delta\omega)$ coincide with the ones for the symmetric contribution to the Rayleigh scattering discussed earlier. In particular, for symmetrical-top molecules, independent of the multiplicity of their states, the contribution $G_2^s(3\omega, \Delta\omega)$ is nonzero. Therefore the degeneracy in such molecules does not result in any peculiarities in the depolarization of the scattering in the third harmonic.

In the case of molecules with cubic symmetry in a ground nondegenerate state of A type, $G_2^s(3\omega, \Delta\omega) = 0$ and $\Delta_v^{3\omega} = \frac{3}{8}$. In degenerate states T_1 , T_2 , and $G_{3/2}$, the depolarization coefficients are less than $\frac{3}{8}$ and depend on frequency, since $G_2^s(3\omega, \Delta\omega)$ and $G_4^s(3\omega, \Delta\omega)$ have different spectral width. Therefore the spherical-top molecules seem to be most convenient

for observation of the effects of degeneracy in the generation of the third harmonic.

Summarizing this section, we note that the degeneracy of the states essentially influences the characteristics of the light scattered into different harmonics. In some cases the degeneracy results in depolarization coefficients that usually are not inherent to high-symmetry molecules (e.g., in the case of the depolarization of Rayleigh scattering by spherical-top molecules in E states). In other cases the depolarization coefficient becomes dependent on the frequency of the scattered light.

However, numerical estimates of the effect of frequency dependence of the coefficients of depolarization based on the calculation of molecular cross sections $G_J^\nu(n\omega, \Delta\omega)$ are rather difficult. But it can be shown that in the cases when different G_J^ν magnitudes are nonzero by symmetry selection rules (neglecting the spin-orbital interaction), they are of the same order of magnitude, since they are determined by the same energy denominators and reduced matrix elements of the operator of the dipole moment.

For experimental investigation some sample systems can be suggested, among them VCl_4 ; ReF_6 ; IrF_6 (ground state $G_{3/2}$); C_nH_n , $n = 3, 5, 7$ (ground state E); and many other high-symmetry coordination compounds in different oxidation states (e.g., IrCl_6^{2-} , IrBr_6^{2-} , FeBr_4^- , and so on). The investigation of these systems is of special interest since different compounds with different ground state degeneracy may reveal different features of the effects under consideration.

C. Temperature-Dependent Optical Activity of Symmetric Molecules in Magnetic Fields

Interesting information about magnetic properties and anisotropy of polarizabilities and hyperpolarizabilities of molecules can also be obtained by investigation of light scattering in external fields. In particular, interest in the study of magnetic field-induced optical activity in linear light scattering has increased (Barron and Meehan, 1979; Barron *et al.*, 1982). The theoretical works devoted to this phenomenon (Barron and Buckingham, 1972; Barron, 1976) consider mainly the scattering by molecules with Kramer's degeneracy. A more general theory of magnetic activity in Rayleigh and hyper-Rayleigh scattering of molecules in arbitrary degenerate states was developed by Ostrovski *et al.* (1984).

1. Light Scattering in External Fields

Consider a medium in which the light of ω frequency and electric field vector E is propagating along the Z axis of the LSC. The intensity of the light incoherently scattered in the direction of the Y axis with the fre-

quency $n\omega + \Delta\omega$ and polarized along the q axis ($q = X, Z$) is given by the expression

$${}^{n\omega}I_q(\Delta\omega) = \frac{Na_n}{2\pi} \left(\frac{n\omega + \Delta\omega}{c} \right)^4 E_\alpha^* E_\beta^* \dots E_\delta^* E_{\alpha'} E_{\beta'} \dots E_{\delta'} \times \int_{-\infty}^{\infty} dt e^{-i\Delta\omega t} \langle \hat{C}_{q\alpha\beta\dots\delta}^{n\omega\dagger}(t) \hat{C}_{q\alpha'\beta'\dots\delta'}^{n\omega}(0) \rangle \quad (167)$$

where, as in Eq. (116), $\hat{C}_{q\alpha\beta\dots\delta}^{n\omega}$ are the tensors of scattering into the n th harmonic and the summation has to be performed over the repeating indices. If the light is polarized circularly, the electric vector can have two values:

$$E^{R/L} = (E_0/\sqrt{2}) (\mathbf{i} \mp \mathbf{j}) \quad (168)$$

which pertain to the right (index R and upper sign) or left (index L and lower sign) polarizations, respectively, \mathbf{i} and \mathbf{j} being the unit vectors directed along the X and Y axes.

Substituting Eq. (168) into Eq. (167), we obtain for the intensity difference of the right and left polarized light the expression

$${}^{n\omega}I_q^R(\Delta\omega) - {}^{n\omega}I_q^L(\Delta\omega) = \frac{2S_n}{\pi} \text{Im } J_{A^\dagger B}^{n\omega}(\Delta\omega) \quad (169)$$

in which

$$J_{A^\dagger B}^{n\omega}(\Delta\omega) = \int_{-\infty}^{\infty} dt e^{-i\Delta\omega t} \langle {}^{n\omega}\hat{A}_q^\dagger(t) {}^{n\omega}\hat{B}_q(0) \rangle \quad (170)$$

is the spectral density of the correlation function (Zubarev, 1971) of the operators ${}^{n\omega}\hat{A}_q^\dagger$ and ${}^{n\omega}\hat{B}_q$ related to the scattering tensors as follows:

$$\begin{aligned} {}^\omega\hat{A}_q &= \hat{C}_{qX}^\omega, & {}^\omega\hat{B}_q &= \hat{C}_{qY}^\omega \\ {}^{2\omega}\hat{A}_q &= \hat{C}_{qXX}^{2\omega} - \hat{C}_{qYY}^{2\omega}, & {}^{2\omega}\hat{B}_q &= 2\hat{C}_{qXY}^{2\omega} \\ {}^{3\omega}\hat{A}_q &= \hat{C}_{qYY}^{3\omega} - \hat{C}_{qXX}^{3\omega}, & {}^{3\omega}\hat{B}_q &= \hat{C}_{qXX}^{3\omega} - \hat{C}_{qYY}^{3\omega} \end{aligned} \quad (171)$$

In the absence of external fields, the medium is isotropic ${}^{n\omega}I_q^R(\Delta\omega) = {}^{n\omega}I_q^L(\Delta\omega)$, and hence the difference in the left side of Eq. (169) is zero. In order to answer the question of in which cases this difference is nonzero (i.e., the optical activity is possible), one has to consider the behavior of the spectral density $J_{VW, \mathcal{F}}(\Delta\omega)$ in the external field \mathcal{F} with respect to the time reversal operation $\hat{\Theta}$.

Let the operators \hat{V} and \hat{W} have a definite parity with respect to the operations of time reversal and Hermitian conjugation:

$$\begin{aligned}
\hat{\Theta} \hat{V} \hat{\Theta}^{-1} &= \varepsilon_V \hat{V}, & \hat{\Theta} \hat{W} \hat{\Theta}^{-1} &= \varepsilon_W \hat{W} \\
\hat{V}^\dagger &= \lambda_V \hat{V}, & \hat{W}^\dagger &= \lambda_W \hat{W} \\
(\varepsilon_{V,W} &= \pm 1, \quad \lambda_{V,W} = \pm 1) & & (172)
\end{aligned}$$

Then the spectral densities of the correlation function of the operators \hat{V} and \hat{W} in external electric \mathcal{E} or magnetic \mathcal{H} fields obey the relations

$$J_{VW,\mathcal{E}}(\Delta\omega) = \lambda_V \lambda_W \varepsilon_V \varepsilon_W J_{VW,\mathcal{E}}^*(\Delta\omega) \quad (173a)$$

$$J_{VW,\mathcal{H}}(\Delta\omega) = \lambda_V \lambda_W \varepsilon_V \varepsilon_W J_{VW,\mathcal{H}}^*(\Delta\omega) \quad (173b)$$

As mentioned earlier, the scattering tensors, generally speaking, have no definite parity with respect to time reversal and Hermitian conjugation. Therefore the relations (173) cannot be used directly for the analysis of the properties of the functions $J_{A+B,\mathcal{F}}^{n\omega}(\Delta\omega)$. However, in some approximation (e.g., in the case of hyperpolarizabilities of the first and second order by neglecting dispersion) ${}^{n\omega}\hat{A}_q$ and ${}^{n\omega}\hat{B}_q$ can be expressed by operators with definite parity with respect to the preceding operations. Since Cartesian coordinates of the scattering tensor $\hat{C}_{q\alpha\beta\ldots\delta}^{n\omega}$ are real, $\lambda = \varepsilon$ and $\lambda\varepsilon = 1$. Therefore it follows from Eq. (173a) that the functions $J_{A+B}^{n\omega}(\Delta\omega)$ are real and hence the electric field, distinguished from the magnetic one, cannot induce the optical activity in the geometry of scattering under consideration. Since for other polarization of the incident and scattered light, the optical activity of the molecule in electric fields is nevertheless possible (Buckingham and Raab, 1975; Graham, 1980), we consider subsequently the correlation function in arbitrary fields.

Where the group-theoretical analysis performed in this section is concerned, one has to note that by means of the formulas of the type (173), one can obtain the necessary conditions only of optical activity induced by the external field. The sufficient conditions are determined by the states of internal degrees of freedom. In order to formulate these conditions, consider a concrete form of the correlation function that determines the magnitude of optical activity.

If one neglects the translational motion of the molecules and the quantization of rotation, then

$$\begin{aligned}
&\langle \hat{C}_{q\alpha\beta\ldots\delta}^{n\omega\dagger}(t) \hat{C}_{q\alpha'\beta'\ldots\delta'}^{n\omega}(0) \rangle_{\mathcal{F}} \\
&= \int \frac{d\Omega}{8\pi^2} \frac{d\Omega_0}{\pi^2} \text{Sp} \{ \hat{\rho}_{\mathcal{F}}(\Omega, \Omega_0 | t) [\hat{C}_{q\alpha\beta\ldots\delta}^{n\omega\dagger}(\Omega; t) \hat{C}_{q\alpha'\beta'\ldots\delta'}^{n\omega}(\Omega_0; 0)]_{\mathcal{F}} \} \quad (174)
\end{aligned}$$

where Ω and Ω_0 are the sets of Euler angles determining the orientation of the molecule in the LSC at the moments of time t and $t = 0$, respectively; $\hat{\rho}_{\mathcal{F}}(\Omega, \Omega_0 | t)$ is the density matrix of the system calculated by taking into

account the influence of the field \mathcal{F} ; and Sp denotes the spur operations over the internal states of the molecule. The index \mathcal{F} at the angle brackets indicates that the time dependence of the scattering tensor is obtained by means of the eigenfunctions and eigenvalues of the molecule in the external field.

It follows from Eq. (174) that the change of the intensity of the scattering under the influence of the field is determined by the field dependence of two factors under the sign of the spur. The density matrix's ($\hat{\rho}_{\mathcal{F}}$) dependence on \mathcal{F} arises owing to the orientation of the molecules in the field \mathcal{F} , while the scattering tensor's dependence on \mathcal{F} is due to the field deformation of the molecule. If the light frequency falls into the region of the transparency of the medium, the deformation of the molecule can be neglected (Kielich, 1981), and then for the orientational contribution to the correlation function (174), we have the expression

$$\langle \hat{C}_{q\alpha\beta\dots\delta}^{n\omega\dagger}(t) \hat{C}_{q\alpha'\beta'\dots\delta'}^{n\omega}(0) \rangle_{\mathcal{F}}^{or} = \int \frac{d\Omega}{8\pi^2} \frac{d\Omega_0}{8\pi^2} \text{Sp}\{\hat{\rho}_{\mathcal{F}}(\Omega, \Omega_0 | t) e^{i\hat{H}t} \hat{C}_{q\alpha\beta\dots\delta}^{n\omega\dagger}(\Omega) e^{-i\hat{H}t} \hat{C}_{q\alpha'\beta'\dots\delta'}^{n\omega}(\Omega_0)\} \quad (175)$$

where \hat{H} is the Hamiltonian of the internal degrees of freedom of the molecule undistorted by the external field.

Using the transformation

$$\hat{C}_{q\alpha\beta\dots\delta}^{n\omega}(\Omega) = \sum_{\nu JM} b_{q\alpha\beta\dots\delta}^{\nu JM} D_{KM}^J(\Omega) \hat{C}_K^{[\nu, J]}(n\omega) \quad (176)$$

similar to the Eqs. (118) and (119) (explicit expressions for the coefficients $b_{q\alpha\beta\dots\delta}^{\nu JM}$ are given by Jerphagnon *et al.*, 1978) and restricting, as usual, the spur operation by vibronic states of the ground electronic term only, we obtain for the orientational contribution to the difference (169) the expression

$$\begin{aligned} & [{}^{n\omega}I_q^R(\Delta\omega) - {}^{n\omega}I_q^L(\Delta\omega)]^{or} \\ &= S_n \sum_{\nu JM} \sum_{\nu' J' M'} \{ [l_q^n(\nu JM, \nu' J' M') + l_q^n(\nu' J' M', \nu JM)] \\ & \times \int \frac{d\Omega}{8\pi^2} \frac{d\Omega_0}{8\pi^2} D_{KM}^{J*}(\Omega) D_{K'M'}^{J'}(\Omega_0) \int_{-\infty}^{\infty} \frac{dt}{8\pi} e^{-i\Delta\omega t} \\ & \times \text{Sp}_{\text{vibr}}[\hat{\rho}_{\mathcal{F}}(\Omega, \Omega_0 | t) e^{i\hat{H}_{\text{vibr}}t} \hat{C}_K^{[\nu, J]\dagger}(n\omega) e^{-i\hat{H}_{\text{vibr}}t} \hat{C}_{K'}^{[\nu', J']}(n\omega)] \} \quad (177) \end{aligned}$$

in which

$$\begin{aligned} l_q^1(\nu JM, \nu' J' M') &= \frac{1}{2} b_{qX}^{\nu JM} \text{Im } b_{qY}^{\nu' J' M'} \\ l_q^2(\nu JM, \nu' J' M') &= (b_{qXX}^{\nu JM} - b_{qYY}^{\nu JM}) \text{Im } b_{qXY}^{\nu' J' M'} \\ l_q^3(\nu JM, \nu' J' M') &= -\frac{1}{2} (b_{qXXX}^{\nu' J' M'} - 3b_{qXXY}^{\nu' J' M'}) \text{Im} (b_{qYY}^{\nu JM} - 3b_{qXXY}^{\nu JM}) \end{aligned} \quad (178)$$

In Eq. (177) in the presence of nonzero external fields, the spur operation over the internal degrees of freedom and the integration over the angles cannot be performed separately, since $\hat{\rho}_{\mathcal{F}}$ depends on the angles Ω and Ω_0 and is simultaneously the matrix in the basis of the vibronic states. The analysis of the density matrix $\hat{\rho}_{\mathcal{F}}$ is given in the next section.

2. The Rotational Diffusion of Molecules with Quantized Internal Degrees of Freedom in Anisotropic External Fields

Owing to the neglect of the quantization of rotations, the density matrix $\hat{\rho}_{\mathcal{F}}$ can be obtained in the framework of a semiclassical approximation in which the rotational degrees of freedom are considered classically, whereas the internal ones are investigated by considering the quantization. Let us assume that the medium is such a dense liquid that the rotation of each molecule can be described by means of the model of continuous rotational diffusion. The density matrix in this model obeys the Debye equation. Its generalization to the case in which the system with internal quantum degrees of freedom is in external fields can be realized by the following equation:

$$\frac{\partial \hat{\rho}_{\mathcal{F}}}{\partial t} = -\hat{\mathbf{J}} \cdot \hat{\mathbf{D}} \cdot \left\{ \hat{\mathbf{J}} \hat{\rho}_{\mathcal{F}} + i \frac{\beta}{2} [\hat{\mathbf{N}}^{\text{eff}}, \hat{\rho}_{\mathcal{F}}]_+ \right\} \quad (179)$$

where $\hat{\mathbf{J}}$ is the operator of the total angular momentum, $\hat{\mathbf{D}}$ is the tensor of rotational diffusion of the molecule, $\hat{\mathbf{N}}^{\text{eff}}$ is the operator of effective torque due to the action of the external force \mathcal{F} , and the material within brackets denotes the anticommutator, $\hat{\mathbf{N}}^{\text{eff}}$ being determined by the relation

$$\hat{\mathbf{J}} \exp[-\beta(\hat{H} + \hat{U})] + \frac{i\beta}{2} [\hat{\mathbf{N}}^{\text{eff}}, \exp[-\beta(\hat{H} + \hat{U})]]_+ = 0 \quad (180)$$

which emerges from the requirement that the density matrix appropriate to the equilibrium distribution of the molecules in the field with potential energy $\hat{U}(\Omega)$ obey Eq. (179). Since \hat{H} and \hat{U} are noncommutative, the effective torque $\hat{\mathbf{N}}^{\text{eff}}$ does not coincide with the classical value, $\hat{\mathbf{N}} = -i(\hat{\mathbf{J}}\hat{U})$, and it is given by the integral expression

$$\begin{aligned} \hat{\mathbf{N}}^{\text{eff}} &= \frac{2i}{\beta} \int_0^\beta d\tau \exp\{-\tau \exp[-\beta(\hat{H} + \hat{U})]\} \\ &\times \{\hat{\mathbf{J}} \exp[-\beta(\hat{H} + \hat{U})]\} \exp\{-\tau \exp[-\beta(\hat{H} + \hat{U})]\} \end{aligned} \quad (181)$$

Note that Eq. (179) is not the most general one (for the case under consideration), since its deduction is based on the assumption of the same diffusion tensor for all the internal states of the molecule. However, this approximation is not very restrictive, since one can expect that the $\hat{\mathbf{D}}$

values for different states will not be very much different. On the other hand, Eq. (179), if necessary, can be generalized considering the dependence of $\hat{\mathbf{D}}$ on the quantum numbers of internal degrees of freedom of the molecule.

Equation (179) has to be solved under the conditions that at $t = 0$, $\Omega = \Omega_0$, and that in the absence of the external field the diffusional tensor is isotropic ($D_{\alpha\beta} = D\delta_{\alpha\beta}$), while the density matrix has the form

$$\hat{\rho}^{(0)}(\Omega, \Omega_0 | t) = Z^{-1} \exp(-\beta\hat{H})G(\Omega, \Omega_0 | t) \quad (182)$$

where

$$G(\Omega, \Omega_0 | t) = \sum_{JMK} \frac{2J+1}{8\pi^2} \exp\left(-\frac{t}{\tau_J}\right) D_{KM}^J(\Omega) D_{KM}^{J*}(\Omega_0) \quad (183)$$

$\tau_J^{-1} = J(J+1)D$, and Z is the statistical sum of the internal degrees of freedom. Presenting the solution of Eq. (179) in the form of a power series with respect to the external field, one can obtain for the contributions linear in the field to the matrix elements of the operator $\hat{\rho}_{\mathfrak{F}}$ in the basis of the eigenfunctions $|m\rangle$ of the Hamiltonian \hat{H} the expression

$$\begin{aligned} \rho_{mm'}^{(1)}(\Omega, \Omega_0 | t) = & \sum_{JMKJ'M'K'} \frac{2J'+1}{8\pi^2} a_{mm'}(JMK, J'M'K') \\ & \times D_{KM}^J(\Omega) D_{K'M'}^{J'*}(\Omega_0) \end{aligned} \quad (184)$$

where

$$\begin{aligned} a_{mm'}(JMK, J'M'K' | t) = & Z^{-1} U_{mm'}(\bar{J}, M - M', K - K') \\ & \times \frac{\exp(-\beta\omega_m) - \exp(-\beta\omega_{m'})}{\omega_m - \omega_{m'}} C_{J'M'\bar{J}M-M'}^{JM} \left(R_{JK, J'K'}^{\bar{J}} \right. \\ & \times \frac{\exp(-t/\tau_{J'}) - \exp(-t/\tau_J)}{J(J+1) - J'(J'+1)} + C_{J'K'\bar{J}K-K'}^{JK} \exp(-t/\tau_J) \Big) \\ & (J' \neq J) \end{aligned} \quad (185a)$$

$$\begin{aligned} a_{mm'}(JMK, J'M'K' | t) = & Z^{-1} U_{mm'}(\bar{J}, M - M', K - K') \\ & \times \frac{\exp(-\beta\omega_m) - \exp(-\beta\omega_{m'})}{\omega_m - \omega_{m'}} C_{J'M'\bar{J}M-M'}^{JM} \\ & \times \left[R_{JK, JK'}^{\bar{J}} \frac{t}{J(J+1)\tau_J} + C_{J'K'JK-K'}^{JK} \right] \exp(-t/\tau_J) \\ & (J' = J) \end{aligned} \quad (185b)$$

$\hat{U}(\bar{J}, \bar{M}, \bar{K})$ are the coefficients in the expansion

$$\hat{U}(\Omega) = \sum_{\bar{J}\bar{M}\bar{K}} \hat{U}(\bar{J}, \bar{M}, \bar{K}) D_{\bar{K}\bar{M}}^{\bar{J}}(\Omega) \quad (186)$$

and

$$R_{JK,J'K'}^{\bar{J}} = \sum_{p=0,\pm 1} Q_{JK,J'K'}^{\bar{J}p} C_{J'K'-p}^{JK} \bar{J}_{K-K'+p}$$

$$Q_{JK,J'K'}^{\bar{J}p} = \begin{cases} \bar{J}(\bar{J} + 1) + K'(K - K') & (p = 0) \\ \frac{1}{2}[(J' \pm K')(J' \pm K' + 1)(\bar{J} \pm K \pm K')(\bar{J} \pm K \pm K' + 1)]^{1/2} & (p = \pm 1) \end{cases} \quad (187)$$

Now we use these results for the calculation of the circular difference of the intensities (177) in the case of a magnetic external field: $\hat{U} = \hat{\mu}_Z \mathcal{H}$. Substituting Eqs. (184) and (185) into Eq. (177), we obtain

$$[{}^{n\omega}I_q^R(\Delta\omega) - {}^{n\omega}I_q^L(\Delta\omega)] = -\frac{S_n \mathcal{H}}{Z} \sum_{\nu JK} \sum_{\nu' J' K'} \left\{ L_q^n(\nu J, \nu' J') \right. \\ \times \sum_{mm'm''} \left[\frac{\exp(-\beta\omega_{m'}) - \exp(-\beta\omega_m)}{\omega_m - \omega_{m'}} f(JK, J'K' | \Delta\omega + \omega_{m''} - \omega_{m'}) \right. \\ \left. \times \langle m | \hat{\mu}_{K-K'} | m' \rangle \langle m' | \hat{C}_{K'}^{[\nu, J] \dagger}(n\omega) | m'' \rangle \langle m'' | \hat{C}_{K'}^{[\nu', J']}(n\omega) | m \rangle \right] \left. \right\} \quad (188)$$

where

$$L_q^n(\nu J, \nu' J') = \sum_M \frac{C_{JM10}^{JM}}{2J+1} [l_q^n(\nu JM, \nu' J' M') \\ + l_q^n(\nu' J' M', \nu JM)] \quad (189)$$

$$f(JK, J'K' | x) = \begin{cases} R_{JK,J'K'}^1 \frac{g_{J'}(x) - g_J(x)}{J(J+1) - J'(J'+1)} + C_{JK1K-K'}^{JK} g_J(x) & (J' \neq J) \\ R_{JK,JK}^1 \frac{h_J(x)}{J(J+1)} + C_{JK1K-K'}^{JK} g_J(x) & (J' = J) \end{cases} \quad (190)$$

$$g_J(x) = g_{J0}(x), \quad h_J(x) = \begin{cases} \frac{\tau_J}{\pi} \frac{[1 - (x\tau_J)^2]}{[1 + (x\tau_J)^2]} & (J \neq 0) \\ 0 & (J = 0) \end{cases} \quad (191)$$

It can be seen from Eq. (188) that the circular intensity difference is a complicated function of $\Delta\omega$ that differs from a simple superposition of Lorentz functions. The temperature dependence is also rather complicated since in vibronic systems the matrix elements $\langle m | \hat{\mu}_{K-K'} | m' \rangle$ between the states $|m\rangle$ and $|m'\rangle$ of differing energy ($\omega_m \neq \omega_{m'}$) are nonzero.

In the next subsection we restrict the consideration by Rayleigh and hyper-Rayleigh scattering in the limit of low temperatures when the ground vibronic term only is populated. In this case, the summation in Eq. (188) has to be performed over m , m' , and m'' appropriate to the states

of the ground level. The temperature dependence then will be described by a linear in β function.

3. Selection Rules for Optical Active States in Rayleigh and Hyper-Rayleigh Scattering

The ranks of the spherical tensors of the scattering that give nonzero contribution to Eq. (188) are determined by Clebsh–Gordan coefficients C_{JM10}^{JM} under the restriction given by inequalities $|J - 1| \leq J' \leq J + 1$. In particular, in the case of linearly scattered light ($n = 1$) with the polarization $q = X$ the following pairs of values of the ranks of the scattering tensors, $(JJ') = (01), (10), (12), (21), (22)$ give nonzero contributions. The tensors with $J = 0, 1$, and 2 are responsible for the scalar, symmetric, and antisymmetric scattering, respectively, and they have different dependence on the frequency of incident light ω . For instance, for small ω values the antisymmetric part of the polarizability is negligibly small (Berestetskii *et al.*, 1971), whereas the scalar and symmetric parts remain finite. It follows that in this region of frequency the pair $(JJ') = (22)$ only contributes to the circular difference of intensities (188). Similarly, it can be shown that in the approximation under consideration in the case of generation of the second ($n = 2$) and third ($n = 3$) harmonics, the contribution with $(JJ') = (33)$ and $(JJ') = (22), (44)$, respectively, are effective.

The restrictions listed until now are of the type of necessary conditions. In order to obtain sufficient conditions for the observation of the effect of magnetic optical activity of molecules in Γ states, it is necessary to pass under the sign of the spur in the expression $\text{Sp}\{\hat{\mu}_{K-K'} \hat{C}_{\bar{K}}^{[p,J]} \hat{C}_{\bar{K}'}^{[\nu',J']}\}$ for allowed values of the pairs (JJ') to appropriate products of irreducible tensor operators for the point group of the molecule. Using the decomposition of the representation D^J of the full spherical group into irreducible representations of the molecular point group, one can present the result in the form of a sum of following terms:

$$\text{Sp}\{\hat{\mu}_{\bar{\Gamma}\bar{\gamma}} \hat{C}_{\Gamma'\gamma'}^\dagger \hat{C}_{\Gamma''\gamma''}\} \quad (192)$$

where $\bar{\Gamma}$ is the representation to which the components of the operator of the magnetic moment belong. Expressions of the type (192) are nonzero if the following conditions are fulfilled:

- (1) $\bar{\Gamma} \in \{\Gamma^2\}$ or $\bar{\Gamma} \in [\Gamma^2]$ for systems with even and odd number of electrons, respectively;
- (2) $\bar{\Gamma} \in \Gamma' \times \Gamma''$;
- (3) the matrix elements of the operators $\hat{C}_{\Gamma'\gamma'}^\dagger$ and $\hat{C}_{\Gamma''\gamma''}$ in the basis of states Γ are nonzero (see the discussion of Rayleigh and hyper-Rayleigh scattering, Section III,B,2).

The first of these conditions is equivalent to the requirement that the linear Zeeman effect be nonzero in the state Γ . This condition is fulfilled for the states $\Gamma = T_1, T_2, E_{1/2}$, and $G_{3/2}$ in cubic molecular systems and $\Gamma = E', E''$ for molecules of D_{3h} symmetry. The second condition in cubic groups ($\bar{\Gamma} = T_1$) is obeyed, if

$$(\Gamma'', \Gamma') = (A_1, T_1), (A_2, T_2), (E, T_2), (T_1, T_1), (T_1, T_2), (T_2, T_2) \quad (193)$$

(with any order of the Γ' and Γ'' representation in parentheses). For the D_{3h} group the pairs (Γ', Γ'') are (E', E') and (E'', E'') , since the products $E' \times E'$ and $E'' \times E''$ contain the representation A'_2 to which the Z component of the magnetic moment belongs.

Let us apply the formulated selection rules to the investigation of magnetic optical activity in degenerate states. Taking into account that in cubic groups $D_+^0 = A_1$, $D_+^1 = T_1$, and $D_+^2 = E + T$, while in the group D_{3h} $D_+^0 = A'_1$, $D_+^1 = A'_2 + E''$, and $D_+^2 = A'_1 + E' + E''$ (Koster *et al.*, 1963), one can easily see that molecules in nondegenerate states have no temperature-dependent optical activity in Rayleigh scattering. However, this activity takes place in the case of spherical-top molecules if the states belong to one of the representations $T_1, T_2, E_{1/2}, E_{5/2}$, and $G_{3/2}$. The activity in the states $E_{1/2}$ and $E_{5/2}$ is due to the antisymmetric part of the polarizability (Barron and Buckingham, 1972) effective only for relatively large frequencies ω . In the states T_1, T_2 , and $G_{3/2}$ the optical activity induced by the orientational influence of the magnetic field owing to the nonzero E and T_2 components of polarizability ($[T_1^2] = [T_2^2] = \{G_{3/2}^2\} = A_1 + E + T_2$) is possible also in the absence of antisymmetric scattering [a similar conclusion about the magnetic Raman optical activity is implicitly present in the works of Barron (1976) and Barron *et al.* (1982)]. Analogous optical activity nonrelated to the antisymmetric scattering should take place in E' and E'' states of molecules with D_{3h} symmetry.

As in the case of the linear scattering, the temperature-dependent magnetic optical activity in the nonlinear scattering is possible for degenerate states only. Indeed, as shown earlier, the generation of the second harmonic is determined by the components of the tensor of polarizability of the rank $J = 3$. In the symmetry group T_d , $D^3 = A_1 + T_1 + T_2$ (the generation of the second harmonic in the group O_h is forbidden because of the presence of an inversion center), and hence the conditions (193) are fulfilled for the states T_1, T_2 , and $G_{3/2}$ in which the matrix elements of T_2 components of the tensor of hyperpolarizability are nonzero. In the symmetry group D_{3h} , $D^3 = A'_1 + A'_2 + A''_2 + E' + E''$, and therefore the optical activity of orientational type in the generation of the second harmonic can take place in the states E' and E'' .

It can be seen easily that in all the cases of degenerate states men-

tioned, the conditions (193) are fulfilled also in the case of generation of the third harmonic.

In the conclusion of this section we focus our attention again on the fact that all the effects discussed so far result from a special anisotropy of the tensors of polarizability and hyperpolarizability in degenerate states. A prominent role is played by the degeneracy of orbital wave functions from which the spin-orbital ones are formed. The importance of this circumstance can be easily understood if one takes into account that the polarizability and hyperpolarizability are orbital operators and hence their reduced matrix elements in the basis of spin-orbital functions of the ground electronic term are expressed, at last, through matrix elements calculated by means of orbital functions only. This allows us by using the genealogy of the spin-orbital function to make some relative quantitative estimations of the effects that are due to anisotropy of degenerate states.

In order to illustrate this statement, consider the difference in cross-section values of antisymmetric scattering in the molecules ReF_6 and VCl_4 . Both these systems are in the ground electronic state $G_{3/2}$, but in ReF_6 this term originates from the orbital T_2 state, whereas in VCl_4 it originates from the E term. Owing to this difference, one can expect that in the magnetic field the optical activity of the molecule ReF_6 should be stronger than that of the VCl_4 molecule. Indeed, if the spin-orbital interaction is neglected, the spin and space degrees of freedom of the electron in the tetrahedral molecule in the 2E state are not coupled and hence the orientation of the spin magnetic moment in the magnetic field does not result in any anisotropy of the optical properties of the medium. [Note that the ellipsoid of the optical (hyper-) polarizabilities of the molecules has no initial orientation in space.] The spin-orbital interaction admixes the T functions of the excited states to the ground orbital term E. On the one hand, this results into a coupling of the magnetic moment to the (hyper-) polarizabilities. On the other hand, owing to this admixture, the T components of (hyper-) polarizability become nonzero. As a result, the optical anisotropy of the orientational type in VCl_4 is proportional to the quadrate of the ratio of the spin-orbital coupling constant to the energy gap between the E and T terms.

IV. Quadrupole Moments of Symmetric Systems and Their Manifestations in Intermolecular Interactions

As mentioned in the introduction to this chapter, the minimal multipole moment of a molecule with a given point symmetry in degenerate

states can be lower than in nondegenerate ones. For instance, for spherical-top molecules in the basis of states belonging to the E , T_1 , T_2 , and $G_{3/2}$ representations, the matrix elements of the quadrupole moment operator are nonzero. Hence, if the ground state of such a molecule with cubic symmetry belongs to one of the degenerate representations, its minimal moment will be the quadrupole one, and not the octupole or hexadecapole moment, as it is usually accepted. In molecules with lower symmetry, besides the matrix elements of totally symmetric components of the quadrupole moment, the degeneracy results in nonzero values of the matrix element of its anisotropic components.

These features of molecules in degenerate states should be manifest in the experiments that depend critically on the first nonzero moment of the charge distribution.

A. Birefringence in Inhomogeneous Electric Fields

Direct measurement of the quadrupole moment of molecules is possible by means of experiments on birefringence in gases in inhomogeneous external electric fields (Buckingham, 1959; Buckingham and Disch, 1968). Most convenient is the dependence of the electric field \mathcal{E} on the space coordinates when only two components of the electric field gradient from the nine are nonzero and obey the relation

$$-\partial\mathcal{E}_X/\partial X = \partial\mathcal{E}_Y/\partial Y = g \quad (194)$$

The constant gradient of the field g is created near the Z axis of the LSC along which the light wave with the frequency ω is propagating. The anisotropy of the medium induced by this electric field results in a difference between the refringence indices of light polarized along the X and Y axes, respectively. Their difference is

$$\Delta n = \rho \operatorname{Re}[\overline{\alpha_{XX}(\omega, \mathcal{E}, \Omega)} - \overline{\alpha_{YY}(\omega, \mathcal{E}, \Omega)}] \quad (195)$$

where ρ is the density of the medium under consideration and the polarizabilities α_{IK} are as determined by Eqs. (66)–(68) in which the Hamiltonian of the molecule, considering Eq. (194), is

$$\hat{H}(\mathcal{E}) = \hat{H} - \hat{\mathbf{d}}\mathcal{E} - g(\hat{\Theta}_{XX} - \hat{\Theta}_{YY}) \quad (196)$$

Here $\hat{\Theta}_{IK}$ are the components of the operator of the quadrupole moment of the molecule in the LSC. Usually in the measurement of the difference of the refraction indices (195) the contribution to the Kerr effect can be separated (Buckingham and Disch, 1968). Therefore in Eq. (196) one can neglect the contribution of the interaction of the dipole moment with the electric field and use the following Hamiltonian instead of $\hat{H}(\mathcal{E})$:

$$\hat{H}(g) = \hat{H} - g(\hat{\Theta}_{XX} - \hat{\Theta}_{YY}) \quad (197)$$

Assuming for small electric field gradients that the energy of interaction of the molecule with the inhomogeneous electric field is small compared with the thermal energy and with the difference between the energies of the ground and excited electronic terms, one can expand the difference of the refraction indices into a power series with respect to g (Ogurtsov and Ostrowski, 1985). This can be done by a procedure similar to that used in the investigation of the Kerr and Cotton-Mouton effects (Ogurtsov *et al.*, 1982, 1983a,b). As a result of the expansion with respect to g and after the averaging over the orientation of the molecules, the difference in the refraction indices can be presented in the form

$$\Delta n = \Delta n^{(\text{def})} + \Delta n^{(\text{or})} \quad (198)$$

where

$$\Delta n^{(\text{def})} = \rho g \sum_{ijkl} W^{ijkl} \langle \hat{\chi}_{ijkl}(\omega) \rangle \quad (199)$$

and

$$\Delta n^{(\text{or})} = \rho g \sum_{ijkl} W^{ijkl} \int_0^\beta d\lambda \langle e^{\lambda \hat{H}} \hat{\Theta}_{ij} e^{-\lambda \hat{H}} \hat{\alpha}_{kl}(\omega) \rangle \quad (200)$$

are the contributions to the birefringence due to the deformation and orientation of the molecules in the inhomogeneous electric field, respectively; i, j, k, l are indices used for denotation of the coordinates in the MSC; and $\hat{\chi}_{ijkl}(\omega)$ are the components of the operator of hyperpolarizability of the molecule in the inhomogeneous constant and variable electric fields [their mean values in the case of a nondegenerate electronic term coincide with the values $B_{ij,kl}$ used by Buckingham and Longuet-Higgins (1968)]. In Eqs. (199) and (200), as earlier, \hat{H} is the vibronic Hamiltonian of the ground electronic term.

1. Deformation Contribution

Since Eq. (198) is obtained by excluding that part of the interaction of the molecule with the field that mixes the orthogonal states of the ground and excited terms, $\hat{\chi}_{ijkl}$ is a pure electronic operator. As a consequence of this circumstance $\Delta n^{(\text{def})}$ is independent of temperature. Indeed, in the most general case the wave functions of any vibronic Γ_1 states $\psi_{n\Gamma_1\gamma_1}(r, q)$ originating from the electronic term Γ are

$$\psi_{n\Gamma_1\gamma_1}(r, q) = [\Gamma_1]^{1/2} \sum_{\gamma M_\mu} \psi_{\Gamma\gamma}(r) \varphi_{nM_\mu}(q) V_{(\gamma\mu\gamma_1)}^{(\Gamma M_\mu \Gamma_1)} \quad (201)$$

where r and q are the generalized coordinates of electrons and nuclei, respectively; $\psi_{\Gamma\gamma}(r)$ is the wave function of the ground electronic term; $\varphi_{nM\mu}(q)$ is the wave function of nuclear coordinate belonging to the representation M ; n is the index that numerates different states with the same M ; and $V(:::)$ is the 3Γ symbol (analogous to the $3jm$ symbol) (Griffith, 1962). The operators $\hat{\chi}_{ijkl}(\omega)$ can be presented in the form of a sum of irreducible tensor operators of the point group of the molecule,

$$\hat{\chi}_{ijkl}(\omega) = \sum_{\sigma\bar{\Gamma}\bar{\gamma}} \hat{\chi}_{\sigma\bar{\Gamma}\bar{\gamma}}^{ijkl}(\omega) \quad (202)$$

in which σ enumerates different contributions transforming after the same representation $\bar{\Gamma}$.

Substituting Eqs. (201) and (202) into Eq. (199) and using the Wigner–Eckart theorem and the rules of summation of the V coefficients (Griffith, 1962), we obtain the equation

$$\Delta n^{(\text{def})} = \rho g \sum_{\sigma ijkl} W^{ijkl} \langle \psi_{\Gamma} | \hat{\chi}_{\sigma A}^{ijkl}(\omega) | \psi_{\Gamma} \rangle \quad (203)$$

in which A is the totally symmetric representation of the point group of symmetry of the molecule under consideration. It follows from group-theoretical consideration that the reduced matrix elements $\langle \psi_{\Gamma} | \hat{\chi}_{\sigma A}^{ijkl}(\omega) | \psi_{\Gamma} \rangle$ are always nonzero because the totally symmetric representation A is present in both the antisymmetric product $\{\Gamma^2\}$ (for the case of odd numbers of electrons) and in the symmetric $[\Gamma^2]$ one (in the case of even numbers of electrons). Therefore in accordance with Eq. (203) the contribution to the birefringence originating from the quadrupole polarizability in the inhomogeneous electric field is nonzero and independent of temperature for any symmetry group of the molecule and any type of degeneracy of the electronic term.

2. Orientational Contribution

For the sake of convenience we rewrite the orientational contribution to Δn in the following form:

$$\Delta n^{(\text{or})} = \frac{\rho g}{15} \sum_{\bar{\Gamma}\bar{\gamma}} \int_0^{\beta} d\lambda \langle e^{\lambda \hat{H}} \hat{\Theta}_{\bar{\Gamma}\bar{\gamma}} e^{-\lambda \hat{H}} \hat{\alpha}_{\bar{\Gamma}\bar{\gamma}}^{(s)}(\omega) \rangle \quad (204)$$

where $\hat{\Theta}_{\bar{\Gamma}\bar{\gamma}}$ and $\hat{\alpha}_{\bar{\Gamma}\bar{\gamma}}^{(s)}(\omega)$ are the components of the irreducible tensor operators of the quadrupole moment and the symmetrical part of the dynamic polarizability, respectively, and $\bar{\Gamma}$ is the point-group representation in the expansion of D_+^2 .

If the vibronic interaction is neglected, then for the Γ state of the molecule, we have

$$\Delta n_{\Gamma}^{\text{or}} = \frac{\beta \rho g}{15} \sum_{\bar{\Gamma}} \langle \psi_{\Gamma} | \hat{\Theta}_{\bar{\Gamma}} | \psi_{\Gamma} \rangle \langle \psi_{\Gamma} | \hat{\alpha}_{\bar{\Gamma}}^{(s)}(\omega) | \psi_{\Gamma} \rangle \delta(\Gamma, \Gamma, \bar{\Gamma}) \quad (205)$$

Here $\delta(\Gamma, \Gamma, \bar{\Gamma})$ is nonzero and equals to one if and only if $\bar{\Gamma}$ is present in the $[\Gamma^2]$ or $\{\Gamma^2\}$ products, respectively, for the cases of even or odd numbers of electrons. In the case of nondegenerate states these conditions are fulfilled for anisotropic molecules only. For spherical-top molecules $\bar{\Gamma} = E, T_2$, and therefore in nondegenerate states $\delta(\Gamma, \Gamma, \bar{\Gamma}) = 0$. From this it follows that the temperature-dependent ($\sim \beta$) contribution to the birefringence is absent. In degenerate states $\Gamma = E, T_1, T_2$, and $G_{3/2}$ of cubic systems, $\delta(\Gamma, \Gamma, \bar{\Gamma}) = 1$, since $[E^2]$, $[T_1^2]$, $[T_2^2]$ and $\{G_{3/2}^2\}$ contain one or both representations $\bar{\Gamma} = E, T_2$, and hence the birefringence here is temperature dependent.

In order to take into account the vibronic interaction, we present the operator of quadrupole moment in the form of a sum:

$$\hat{\Theta}_{\bar{\Gamma}} = \Theta_{\bar{\Gamma}}^{(e)} \hat{C}_{\bar{\Gamma}} + \Theta_{\bar{\Gamma}}^{(n)} \mathbf{q}_{\bar{\Gamma}} \quad (206)$$

in which $\Theta_{\bar{\Gamma}}^{(e)}$ and $\hat{C}_{\bar{\Gamma}}$ are, respectively, the reduced matrix elements and the matrices of the electronic operator of the quadrupole moment calculated by the basis of the functions of electronic term Γ , the number of projections of the vector $\hat{A}_{\bar{\Gamma}}$ coincides with the dimension of representation $\bar{\Gamma}$, and $\Theta_{\bar{\Gamma}}^{(n)}$ is the effective quadrupole moment created by the nuclear displacements along the normal coordinates $\mathbf{q}_{\bar{\Gamma}}$. Substituting Eq. (206) into Eq. (204), we obtain

$$\begin{aligned} \Delta n^{(\text{or})} = & \frac{\beta \rho g}{15} \sum_{\bar{\Gamma}} [\Theta_{\bar{\Gamma}}^{(e)} Q_{\Gamma}^{(e)}(\bar{\Gamma}, \beta) + \Theta_{\bar{\Gamma}}^{(n)} Q_{\Gamma}^{(n)}(\bar{\Gamma}, \beta)] \\ & \times \langle \psi_{\Gamma} | \hat{\alpha}_{\bar{\Gamma}}^{(s)}(\omega) | \psi_{\Gamma} \rangle \delta(\Gamma, \Gamma, \bar{\Gamma}) \end{aligned} \quad (207)$$

where

$$Q_{\Gamma}^{(e)}(\bar{\Gamma}, \beta) = \frac{1}{\beta} \int_0^{\beta} d\lambda \langle \hat{C}_{\bar{\Gamma}}(\lambda) \hat{C}_{\bar{\Gamma}} \rangle \quad (208)$$

are the vibronic reduction parameters of electronic operators considered earlier [see Eqs. (10) and (95)],

$$Q_{\Gamma}^{(n)}(\bar{\Gamma}, \beta) = \frac{1}{\beta} \int_0^{\beta} d\lambda \langle \hat{\mathbf{q}}_{\bar{\Gamma}}(\lambda) \hat{C}_{\bar{\Gamma}} \rangle \quad (209)$$

Concerning the parameters $Q_{\Gamma}^{(e)}(\bar{\Gamma}, \beta)$ and $Q_{\Gamma}^{(n)}(\bar{\Gamma}, \beta)$, the following remark should be made. If the operator of vibronic interaction is linear with

respect to the nuclear displacements, i.e., if the Hamiltonian has the form

$$\hat{H} = \sum_{\bar{\Gamma}} \left[\frac{\omega_{\bar{\Gamma}}}{2} (\hat{\mathbf{p}}_{\bar{\Gamma}}^2 + \hat{\mathbf{q}}_{\bar{\Gamma}}^2) + \omega_{\bar{\Gamma}} a_{\bar{\Gamma}} \hat{\mathbf{C}}_{\bar{\Gamma}} \mathbf{q}_{\bar{\Gamma}} \right] \quad (210)$$

then $Q_{\bar{\Gamma}}^{(e)}(\bar{\Gamma}, \beta)$ and $Q_{\bar{\Gamma}}^{(n)}(\bar{\Gamma}, \beta)$ are not mutually independent. Indeed, in accordance with Eq. (210)

$$\hat{\mathbf{q}}_{\bar{\Gamma}} + a_{\bar{\Gamma}} \hat{\mathbf{C}}_{\bar{\Gamma}} = \frac{1}{i\omega_{\bar{\Gamma}}} [\hat{H}, \hat{\mathbf{p}}_{\bar{\Gamma}}]$$

and by means of the relation (8) one can show that

$$Q_{\bar{\Gamma}}^{(n)}(\bar{\Gamma}, \beta) = -a_{\bar{\Gamma}} Q_{\bar{\Gamma}}^{(e)}(\bar{\Gamma}, \beta) \quad (211)$$

Hence in the case of linear vibronic coupling the orientational contribution to the birefringence in the inhomogeneous electric field can be described by the expression

$$\Delta n^{(\text{or})} = \frac{\beta \rho g}{15} \sum_{\bar{\Gamma}} (\Theta_{\bar{\Gamma}}^{(e)} - a_{\bar{\Gamma}} \Theta_{\bar{\Gamma}}^{(n)}) \langle \Gamma \| \hat{\alpha}_{\bar{\Gamma}}(\omega) \| \Gamma \rangle Q_{\bar{\Gamma}}^{(e)}(\bar{\Gamma}, \beta) \delta(\Gamma, \Gamma, \bar{\Gamma}) \quad (212)$$

It follows that by increasing the constant of vibronic coupling the relative contribution of Jahn–Teller nuclear vibrations to the effective quadrupole moment determining the birefringence is increasing. Therefore $Q_{\bar{\Gamma}}^{(n)}(\bar{\Gamma}, \beta)$ [to be distinguished from the reduction parameters $Q_{\bar{\Gamma}}^{(e)}(\bar{\Gamma}, \beta)$] can be called the parameter of vibronic amplification of the vibrational contributions to the quadrupole moment.

Some features of the birefringence in inhomogeneous electric fields caused by the electronic degeneracy are considered in the following subsection.

a. Molecules with D_{3h} symmetry in ground electronic states E' . In this case $\delta(E', E', \bar{\Gamma}) = 1$ if $\bar{\Gamma} = A', E'$. Therefore in accordance with Eq. (212), the following relationship takes place:

$$\begin{aligned} \Delta n^{(\text{or})} = \frac{\beta \rho g}{15} [& \Theta_{A'} \langle E' \| \hat{\alpha}_{A'}(\omega) \| E' \rangle \\ & + (\Theta_{E'}^{(e)} - a_{E'} \Theta_{E'}^{(n)}) \langle E' \| \hat{\alpha}_{E'}(\omega) \| E' \rangle Q_{E'}^{(e)}(E', \beta)] \end{aligned} \quad (213)$$

in which $\langle \Gamma \| \hat{\alpha}_{\bar{\Gamma}}(\omega) \| \Gamma \rangle$ are the reduced matrix elements of the dynamic polarizability. The second term here arises because of the electronic degeneracy allowing nonzero matrix elements of the anisotropic components of the tensors of the quadrupole moment and dynamic polarizability that transforms after nontotally symmetric representation E' of the group D_{3h} . Due to this term the temperature dependence of the orientational

contribution to the birefringence may be subject to essential changes (the main features of the temperature dependence of $Q_E^{(e)}(E', \beta)$ were discussed as part of the investigation of the polarizability of molecules with D_{3h} symmetry in degenerate E' states; see Section II, A, 1).

b. Spherical-top molecules with electronic degeneracy. Molecules with cubic symmetry are of special interest since for them $\Delta n^{(or)}$ is identically equal to zero in the absence of degeneracy. For degenerate states the orientational contribution to the birefringence in inhomogeneous electric fields is nonzero and can be described by the expression

$$\begin{aligned} \Delta n^{(or)} = & \frac{\beta \rho g}{15} [(\langle \Gamma \| \Theta_E^{(e)} \| \Gamma \rangle - a_E \Theta_E^{(n)} \langle \Gamma \| \hat{\alpha}_E^{(s)}(\omega) \| \Gamma \rangle Q_\Gamma(E, \beta) \\ & + (\langle \Gamma \| \hat{\Theta}_{T_2}^{(e)} \| \Gamma \rangle - a_{T_2} \Theta_{T_2}^{(n)} \langle \Gamma \| \hat{\alpha}_{T_2}^{(s)}(\omega) \| \Gamma \rangle Q_\Gamma(T_2, \beta)] \\ & (\Gamma = E, T_1, T_2, G_{3/2}) \quad (214) \end{aligned}$$

Here the first term only in brackets is nonzero if $\Gamma = E$, since $\langle E \| \hat{F}_{T_2} \| E \rangle = 0$.

It follows that in the case of spherical-top molecules the orientational mechanism of birefringence in inhomogeneous electric fields becomes effective due to the degeneracy of the ground electronic term. In other words, molecules that traditionally have been considered to be isotropic polarizable systems having as the first nonzero moments the octupole or hexadecapole ones behave as anisotropic molecules having quadrupole moments, provided that their ground electronic state is degenerate. Besides, the temperature dependence of the birefringence in inhomogeneous fields is similar to the temperature dependence of the Kerr constant for these systems. For instance, in the case of $\Gamma = G_{3/2}$, Eq. (214) transforms into Eq. (94) if one substitutes the expression $(\rho g/15)(\langle G_{3/2} \| \hat{\Theta}_\Gamma^{(e)} \| G_{3/2} \rangle - a_\Gamma \Theta_\Gamma^{(n)})$ by $(\pi N/5)(\langle G_{3/2} \| \hat{\alpha}_\Gamma \| G_{3/2} \rangle)$.

The temperature dependencies were considered earlier for some concrete cases, and we present here some estimates of the effective quadrupole moment value for the molecule VCl_4 . The ground electronic term of this molecule, if the spin-orbital interaction is neglected, is an orbital doublet ($\Gamma = E$). If one neglects also the covalency, i.e., if one considers the electronic functions $|E\gamma\rangle$ as a pure 3d function of the vanadium atom, then the electronic contribution to the quadrupole moment $\Theta_E^{(e)}$ is approximately equal to the product of the electronic charge ($-e$) and the mean square of the distance of 3d electron from the nucleus in the free V atom ($\langle r^2 \rangle$). The magnitude of the quadrupole moment created by the nuclear displacements of E type $\Theta_E^{(n)}$ can be estimated by the equation $\Theta_E^{(n)} \simeq -eR_0 \sqrt{\hbar/2\pi\nu m_{Cl}}$, where R_0 is the V-Cl distance, m_{Cl} is the mass of the atom Cl, and ν is the frequency of E vibrations. Using the values $R_0 \sim$

$4.04 a_0$ (a_0 is the atomic unit of length), $\nu \sim 3.5 \cdot 10^4 \text{ Mhc}$, $a_E \sim 1.05$ (Morino and Uehara, 1966), $\langle r^2 \rangle \sim 2.4 a_0^2$ (Desclaux, 1973), and $Q_E(E, \beta)|_{T \sim 300 \text{ K}} \sim \frac{7}{9}$ (Ogurtsov *et al.*, 1983), we obtain for the effective quadrupole moment of the VCl_4 molecule $(\langle E | \hat{\Theta}_E^{(e)} | E \rangle - a_E \Theta_E^{(n)}) Q_E(E, \beta) \simeq -1.3 e a_0^2$. This value is comparable with the magnitude of quadrupole moments of diatomics (Stogryn and Stogryn, 1966).

B. Spectroscopic Manifestations of the Anisotropy of Intermolecular Interactions Induced by Degeneracy

In all the preceding cases of investigation of the internal anisotropy of molecules induced by degeneracy, the specificity of the interaction with external fields based on their point symmetry is employed, whereas the interaction among the molecules is neglected. In many cases this approximation is unacceptable. Moreover, intermolecular interactions in some cases result in new effects, their investigation giving additional information about the anisotropy of the molecules.

In this section some results of the theoretical investigation of possible manifestations of the degeneracy in intermolecular interactions are given. In particular, some special features of the light absorption induced by collisions in gases of spherical-top molecules with degenerate electronic terms and the influence of such a degeneracy on the line shapes in vibrational absorption and Raman spectra are considered (Ogurtsov, 1985).

1. Collision-Induced Light Absorption

The Coulomb interaction even among high-symmetry molecules results in formation of dipole moments due to which light absorption is possible. The theory of such a microwave absorption induced by collisions was developed in the work of Poll and Van Kranendonk (1961) and Gray (1971). The main characteristics of the absorption under consideration are the moment of the spectrum

$$\gamma = \frac{\beta}{2} \int_0^\infty \frac{A(\omega)}{\omega \text{th}(\omega\beta/2)} d\omega \quad (215)$$

and the integral intensity

$$\alpha = \int_0^\infty A(\omega) d\omega \quad (216)$$

where $A(\omega)$ is the coefficient of absorption of light of frequency ω per unit of length. In the case of nonpolar molecules, γ and α can be presented in the form of an expansion with respect to the gas density n ,

$$\gamma = \gamma_1 n^2 + \gamma_2 n^3 + \dots, \quad \alpha = \alpha_1 n^2 + \alpha_2 n^3 + \dots \quad (217)$$

where γ_1 and α_1 are determined by the relations (Gray, 1971)

$$\begin{aligned}\gamma_1 &= \frac{2\pi^2\beta}{3c} \int dR e^{-\beta V_0(R)} \int \frac{d\Omega_1 d\Omega_2}{(8\pi^2)^2} \langle \hat{\mu}(1, 2)^2 \rangle_{\text{int}} \\ \alpha_1 &= \frac{2\pi^2\beta}{3c} \int dR e^{-\beta V_0(R)} \int \frac{d\Omega_1 d\Omega_2}{(8\pi^2)^2} \langle [\hat{\mu}(1, 2), [\hat{\mathbf{K}}, \hat{\mu}(1, 2)]] \rangle_{\text{int}}\end{aligned}\quad (218)$$

in which R is the vector connecting molecules 1 and 2, $V_0(R)$ is the isotropic part of the intermolecular interaction, Ω_i is the set of Euler angles describing the orientation of the i th molecule, $\hat{\mu}(1, 2)$ is the operator of the dipole moment of the pair of molecules, and $\hat{\mathbf{K}}$ is the operator of kinetic energy of translational motion (changing the intermolecular distances) and rotational motion of molecules 1 and 2. Distinguished from the work of Gray (1971), in Eq. (218) the averaging over the internal vibronic states of colliding molecules is introduced. The necessity of such an averaging is due to the fact that in the case of Jahn–Teller systems the energy spacing of the vibronic levels may be comparable with the thermal energy, and hence the population of the excited vibronic levels cannot be neglected. Since we restrict our consideration by the region of only microwave absorption corresponding to pure rotational transitions, in the calculation of averaged values of the product of the operators related to the same molecule, the matrix elements of these operators for the states related to different eigenvalues should be excluded from Eq. (218).

If we restrict ourselves to only the multipolar mechanism of formation of the dipole moment, then using the gradient formula we obtain for the ν th spherical component ($\nu = 0, \pm 1$) of the operator of the dipole moment induced by the multipole moment \hat{Q}_{lm} of molecule 1 in polarizable molecule 2 the following expression:

$$\mu_\nu(1, 2) = \frac{4\pi}{R^{l+2}} \left(\frac{l+1}{2l+3} \right)^{1/2} \sum_{jm_2m_1\sigma\bar{n}} C_{lm_1\bar{1}\sigma}^{l+1\bar{n}} C_{jm_2\bar{1}\sigma}^{1\nu} \hat{Q}_{lm_1}^* \hat{\alpha}_{jm_2} Y_{l+1\bar{n}}(\Omega) \quad (219)$$

where $\hat{\alpha}_{jm_2}$ are spherical components of the tensor of the polarizability of molecule 2 of rank j in the LSC, $Y_{l+1\bar{n}}$ are the spherical harmonics, and Ω is the set of angles that characterize the orientation of the vector R in the LSC. For spherical-top molecules substituting Eq. (219) into Eq. (218) and passing to the MSC, after averaging over orientations of molecules 1 and 2 under the assumption that $V_0(R)$ is the Lennard–Jones potential, we have

$$\begin{aligned}
\gamma_1 &= \frac{2\pi^2}{3} (l+1) \beta \alpha^2(T) Q_l^2(T) \frac{I_{2l+4}}{c\sigma^{2l+1}} \\
\alpha_1 &= \frac{2\pi^2}{3} (l+1) \frac{\alpha^2(T) Q_l^2(T)}{mc\sigma^{2l+3}} \\
&\times \left\{ (l+2)(2l+3) I_{2l+6} + \frac{m\sigma^2}{I} I_{2l+4} \left[l(l+1) + \frac{\tilde{\alpha}^2(T)}{\alpha^2(T)} \right] \right\} \quad (220)
\end{aligned}$$

where m is the reduced mass of the pair of molecules, I is their moment of inertia, σ is the Lennard–Jones diameter,

$$I_n = \sigma^{-n+3} \int dR R^{-n} \exp[-\beta V_0(R)] \quad (221)$$

$$\begin{aligned}
\alpha^2(T) &= \sum_{j=0,2;n_2} \frac{(-1)^{j+n_2}}{2j+1} \langle \hat{\alpha}_{jn_2} \hat{\alpha}_{j-n_2} \rangle_{\text{int}2} \\
\tilde{\alpha}^2(T) &= \frac{6}{5} \sum_{n_2} (-1)^{n_2} \langle \hat{\alpha}_{2n_2} \hat{\alpha}_{2-n_2} \rangle_{\text{int}2} \quad (222)
\end{aligned}$$

$$Q_l^2(T) = \frac{4\pi}{2l+1} \sum_{n_1} (-1)^{n_1} \langle \hat{Q}_{ln_1} \hat{Q}_{l-n_1} \rangle_{\text{int}1}$$

\hat{Q}_{ln_1} and $\hat{\alpha}_{jn_2}$ are spherical components of the multipole moment and polarizability in the MSC, respectively, and $\langle \dots \rangle_{\text{int} i}$ denotes the averaging (of the type mentioned earlier) over the states of the i th molecule. Thus the values γ_1 and α_1 sought for are determined by the values of the effective temperature-dependent polarizabilities $\alpha(T)$ and $\tilde{\alpha}(T)$ and multipole moment $Q_l(T)$ of the colliding molecules. Note that the magnitudes of $\alpha(T)$ and $\tilde{\alpha}(T)$ in general are expressed by the values (averaged over the internal states) of both the scalar ($j=0$) and anisotropic ($j=2$) components of polarizability.

Consider now the selection rules for the minimal value l for which γ_1 and α_1 are nonzero. In order to do this, it is convenient to pass from the spherical components of the tensors \hat{Q}_{ln_1} and $\hat{\alpha}_{jn_2}$ to the components of irreducible tensor operators $\hat{Q}_{\Gamma\gamma l}$ and $\hat{\alpha}_{\Gamma\gamma j}$ that transform after the irreducible representation contained in the decomposition of D^l and D^j , respectively. If $|n\Gamma\gamma\rangle$ are the different vibronic states transforming after the representation Γ and corresponding to the vibronic level with the energy $\varepsilon_{n\Gamma}$, then for the collision-induced spectrum using the Wigner–Eckart theorem, we have

$$\begin{aligned}
\alpha^2(T) &= \sum_{n\Gamma} \frac{\exp(-\beta\epsilon_{n\Gamma})}{Z} \left[\langle n\Gamma \| \hat{\alpha}_{A_1} \| n\Gamma \rangle^2 + \frac{1}{5} \sum_{\bar{\Gamma}=E,T_2} \langle n\Gamma \| \hat{\alpha}_{\bar{\Gamma}} \| n\Gamma \rangle^2 \delta(\Gamma, \Gamma, \bar{\Gamma}) \right] \\
\tilde{\alpha}^2(T) &= \frac{6}{5} \sum_{n\Gamma} \frac{\exp(-\beta\epsilon_{n\Gamma})}{Z} \sum_{\bar{\Gamma}=E,T_2} \langle n\Gamma \| \hat{\alpha}_{\bar{\Gamma}} \| n\Gamma \rangle \delta(\Gamma, \Gamma, \bar{\Gamma}) \\
Q_l^2(T) &= \frac{4\pi}{2l+1} \sum_{n\Gamma_l} \frac{\exp(-\beta\epsilon_{n\Gamma})}{Z} \langle n\Gamma \| \hat{Q}_{\Gamma_l} \| n\Gamma \rangle^2 \delta(\Gamma, \Gamma, \Gamma_l)
\end{aligned} \tag{223}$$

Using the properties of the function $\delta(\Gamma, \Gamma, \bar{\Gamma})$ and the relation for cubic groups $D^1 = T_1$ or T_2 , $D^2 = E + T_2$, one can easily find by means of Eq. (223) that in nondegenerate states $l = 3$ for tetrahedral molecules and $l = 4$ for octahedral ones. For degenerate states E, T_1, T_2 , and $G_{3/2}$, $l = 2$ in octahedral systems; and for tetrahedral systems with T_1, T_2 , and $G_{3/2}$ states, $l = 1$. It follows that in the case of spherical-top molecules in all the preceding degenerate states the values γ_l and α_l are determined by multipole moments with $l = 2$ or $l = 1$, whereas in the nondegenerate states $l = 3$ or $l = 4$. It follows that in the case of the usually implicitly assumed nondegeneracy of the ground vibronic state the first nonzero multipole moment is the octupole one ($l = 3$) in molecules with T_d symmetry and the hexadecapole one ($l = 4$) for O_h symmetry molecules. In the case of electronic degenerate terms the ground vibronic term has the same symmetry as the electronic term (Bersuker and Polinger, 1983). Therefore in accordance with what has been said, in the case of spherical-top molecules, even if only the ground vibronic term is populated, the first nonzero multipole moment that is manifest in the collision-induced absorption is the quadrupole moment in octahedral molecules and the dipole moment in tetrahedral systems (in the states T_1, T_2 , and $G_{3/2}$).

Besides, as it follows from Eq. (223), in all the nondegenerate states $\alpha(T)$ is expressed by the isotropic part ($j = 0$) only of the polarizability and $\tilde{\alpha}(T) = 0$. In degenerate states there is also a contribution of the anisotropic components of the polarizability ($j = 2$) in the $\alpha^2(T)$ and $\tilde{\alpha}^2(T)$ magnitudes.

2. Intermolecular Torque in Gases of Cubic Systems with Electronic Degeneracy

In this section some manifestations of the degeneracy and the Jahn-Teller effect in the spectral line shapes of transitions between the states of the vibrational degrees of freedom not active in the Jahn-Teller effect are considered (Ogurtsov, 1985).

As is known from the theory of vibrational spectra of absorption and

Raman scattering, there are some simple relations between the second and fourth moments of the vibrational-rotational band and the mean-square value ($\langle \tau^2 \rangle$) of the torque that the absorbing or scattering molecule suffers due to the anisotropy of the interaction with the remaining molecules in the gas (Gordon, 1963, 1964a,b; Armstrong *et al.*, 1968). It can be shown that in the classical consideration of the rotations of the molecules the mean-squared torque, acting on molecule 1, is determined by the equation (Armstrong *et al.*, 1968)

$$\langle \tau^2 \rangle = \langle (\nabla_{\Omega_1} \hat{V})^2 \rangle \quad (224)$$

where ∇_{Ω_1} is the angular gradient operator in the space of the Euler angles of molecule 1, \hat{V} is the operator of the interaction between molecules 1 and 2, and the material in angle brackets denotes the usual thermodynamic averaging over the internal, rotational, and translational degrees of freedom of both molecules.

In the usual consideration neglecting the possible degeneracy of the interacting molecules, the simplifications of the calculation of $\langle \tau^2 \rangle$ can be achieved by employing the hypervirial relation (Hirschfelder, 1960)

$$\beta \langle (\nabla_{\Omega_1} \hat{V})^2 \rangle = \langle \Delta_{\Omega_1} \hat{V} \rangle \quad (225)$$

in which Δ_{Ω_1} is the angular Laplacian. In the case of high temperatures, Eq. (225) is fulfilled also for systems that are in degenerate states. By means of Eq. (225), assuming that the anisotropic part of the intermolecular interaction $\hat{V}_a(\mathbf{R}) = \hat{V}(\mathbf{R}) - \hat{V}_0(\mathbf{R})$ is small compared with kT , and in the first order with respect to the gas density n , we have

$$\begin{aligned} \langle \tau^2 \rangle = nkT \int d\mathbf{R} \exp[-\beta V_0(R)] \int \frac{d\Omega_1 d\Omega_2}{(8\pi^2)^2} \int_0^\beta d\lambda \\ \times \langle \exp[\lambda(\hat{H}_1 + \hat{H}_2)] \hat{V}_a(\mathbf{R}) \exp[-\lambda(\hat{H}_1 + \hat{H}_2)] \Delta_{\Omega_1} \hat{V}_a(\mathbf{R}) \rangle \end{aligned} \quad (226)$$

where \hat{H}_i is the Hamiltonian of the internal degrees of freedom of the i th molecule.

Later, a more concrete case of calculation of $\langle \tau^2 \rangle$ of the torque τ induced by perturbing molecule 2 with a multipole moment \hat{Q}_{l_2} on molecule 1 with the multipole moment \hat{Q}_{l_1} is considered. Substituting in Eq. (226) an appropriate operator of intermolecular Coulomb interaction (Gray, 1968; Armstrong *et al.*, 1968) and averaging over the orientations of the molecules, we find the following expression of the contribution in $\langle \tau^2 \rangle$ due to the direct Coulomb interaction:

$$\langle \tau^2 \rangle = l_1(l_1 + 1) \frac{[2(l_1 + l_2)]!}{(2l_1 + 1)(2l_2 + 1)} \frac{I_{2(l_1+l_2+1)} Q_{l_2}^2}{\sigma^{2(l_1+l_2)-1}} \bar{Q}_{l_1}^2(T) \quad (227)$$

where

$$\bar{Q}_{l_1}^2(T) = \frac{4\pi}{2l_1 + 1} \frac{1}{\beta} \int_0^\beta d\lambda \left\langle \sum_{\Gamma_{l_1}} \exp(\lambda \hat{H}_1) \hat{Q}_{\Gamma_{l_1}} \exp(-\lambda \hat{H}_1) \hat{Q}_{\Gamma_{l_1}} \right\rangle_1 \quad (228)$$

is the magnitude determining the effective value of the multipole moment Q_{l_1} , $\langle \dots \rangle_1$ denotes the thermodynamic averaging over the vibronic states of perturbed molecule 1, and Γ_{l_1} are the representations contained in the decomposition of the full spherical group representation D^l into the irreducible ones of the point group of symmetry of molecule 1. Hereafter for the sake of shortness the index 1 at l_1 will be omitted.

In order to elucidate the selection rules for the minimal value l resulting in a nonzero torque, we present the operators $\hat{Q}_{\Gamma_{l_1}}$, as earlier, in the form of a sum of the electronic and nuclear contributions, and we assume again that the operator of vibronic interaction is linear in the nuclear displacements. In this approximation, Eq. (228) can be transformed to the following form:

$$\bar{Q}_l^2(T) = \frac{4\pi}{2l + 1} \sum_{\Gamma} (\langle \Gamma \| \hat{Q}_{\Gamma_l}^{(e)} \| \Gamma \rangle - a_{\Gamma_l} \hat{Q}_{\Gamma_l}^{(n)})^2 Q_{\Gamma}(\Gamma_l, \beta) \delta(\Gamma, \Gamma, \Gamma_l) \quad (229)$$

From this it can be seen that the selection rules for the minimal multipole moment causing the torque of the molecule are the same as in the case of collision-induced absorption. Note, however, that the temperature dependence of the minimal effective moments (for instance, the quadrupole moment in the case of spherical-top molecules in degenerate states) are essentially different in different experiments [see Eqs. (223c) and (229)].

In a manner similar to the calculation of the contribution to $\langle \tau^2 \rangle$ due to the multipole Coulomb interaction, one can show that the contribution due to the induction interaction in cubic systems in the degenerate states under consideration is also determined by the quadrupole moment.

So far only the minimal multipole moments and their contribution to the γ_1 , α_1 , and $\langle \tau^2 \rangle$ values have been considered. However, they are not the only manifestations of the degeneracy in the characteristics of the absorption and Raman spectra under consideration. For instance, an important additional contribution to the torque can arise because of the anisotropy of the dispersion interaction between the molecules owing to the nonzero matrix elements of the anisotropic components of the polarizability tensor, i.e., the anisotropy of the cubic symmetry molecules in degenerate states.

It follows from these results that the interpretation of the line shapes

of the collision-induced absorption and Raman spectra appropriate to transitions between the states of Jahn–Teller nonactive vibrational degrees of freedom is essentially dependent on whether there is electronic degeneracy. The differences are due first of all to the different minimal multipole moments effective in the interactions and to the effectiveness of the anisotropic dispersion interaction in the case of degenerate states. However, the manifestations of the latter in the spectral characteristics γ_1 , α_1 , and $\langle\tau^2\rangle$ have not yet been investigated in any detail.

V. Conclusions

In the theory of electric properties of molecular systems in degenerate electronic states some unsolved problems remain. First, the problem of intermolecular interactions considering the degeneracy of the electronic states of the interacting molecules has not been solved completely. In this case, besides the lowering of the multipolarity of the interaction described in this paper, one can expect an essential contribution of anisotropic induction and dispersion interactions to different virial correction to the equations of state, refraction, and other electric characteristics of matter.

Second, the development of methods and concrete numerical calculations of the constants (reduced matrix elements of the dipole and quadrupole moments, polarizability, and hyperpolarizabilities, vibronic constant, etc.) determining the effects of electronic degeneracy on electric properties of molecules predicted in this paper seems to be one of the most up-to-date problem in the topics under consideration. Such calculations are quite possible, in principle, provided that the wave functions of the degenerate electronic term (for the calculation of the dipole moment), as well as the excited ones (for the calculation of the polarizabilities), are known. Considering the advances in quantum chemistry, the solution of the problem is quite possible from the practical point of view, especially if one takes into account that in the cases under consideration one can determine numerically the wave function of the system in the presence of an electric field instead of a calculation of excited states.

Third, in most cases in this paper, only the linear vibronic terms are considered. Meanwhile, it is known (Bersuker and Polinger, 1982, 1983) that the quadratic terms of vibronic interactions may be of primary importance in vibronic problems. Therefore the evaluation of the electric properties of molecules considering also the quadratic vibronic terms (in the cases where it has not been done yet) may result in new effects and regularities in this area.

Finally, the most important problem seems to be the further experi-

mental verification of the predicted effects. Considering the theoretical results, such experiments allow us to obtain additional information about the molecular structure, to determine the values of the vibronic constants and other parameters of the system, and to achieve a deeper understanding of the observed phenomena. Experiments on the depolarization of scattered light, the temperature dependence of the mean dipole moment, birefringence in external fields, dielectric losses, observation of pure rotational spectra of absorption and Raman scattering, among other areas, seem to be quite realizable.

We hope that this paper will stimulate further investigations into the electric properties of molecular systems in degenerate states.

REFERENCES

- Abraham, A., and Bleaney, B. (1970). "Electron Paramagnetic Resonance of Transition Ions." Oxford Univ. Press, New York.
- Alexiewicz, W. (1975). *Acta Phys. Pol.* **A47**, 657.
- Armstrong, R. L., Blumenfeld, S. M., and Gray, C. G. (1968). *Can. J. Phys.* **46**, 1331.
- Bates, C. A. (1978). *Phys. Rep.* **187**, 35.
- Barron, L. D. (1976). In "Molecular Spectroscopy" (R. F. Barrow, D. A. Long, and J. Sheridan eds.), Vol. 4, p. 96. The Chemical Society, London.
- Barron, L. D., and Buckingham, A. D. (1972). *Mol. Phys.* **23**, 145.
- Barron, L. D., and Meehan, C. (1979). *Chem. Phys. Lett.* **66**, 444.
- Barron, L. D., Meehan, C., and Vrbancich, J. (1982). *J. Raman Spectrosc.* **12**, 251.
- Berestetskii, V. B., Lifshitz, E. M., and Pitaevskii, L. P. (1971). "Relativistic Quantum Theory, Part 1." Pergamon, New York.
- Bernstein, E. R., and Webb, J. D. (1979). *Mol. Phys.* **37**, 191.
- Bersuker, I. B. (1961). *Opt. Spectrosc.* **11**, 319.
- Bersuker, I. B. (1962). *Zh. Eksp. Teor. Phys.* **43**, 1315.
- Bersuker, I. B. (1966). *Phys. Lett.* **20**, 589.
- Bersuker, I. B. (1969). *Teor. Eksp. Khim.* **5**, 293.
- Bersuker, I. B. (1975). *Coord. Chem. Rev.* **14**, 357.
- Bersuker, I. B. (1984). "The Jahn-Teller Effect and Vibronic Interactions in Modern Chemistry." Plenum, New York.
- Bersuker, I. B., Gorinchoy, N. N., and Polinger, V. Z. (1984). *Theoret. Chim. Acta* **66**, 161.
- Bersuker, I. B., Ogurtsov, I. Ya., and Shaparev, Yu. V. (1973). *Teor. Eksp. Khim.* **9**, 451.
- Bersuker, I. B., Ogurtsov, I. Ya., and Shaparev, Yu. V. (1974). *Opt. Spectrosc.* **36**, 315.
- Bersuker, I. B., and Polinger, V. Z. (1982). *Adv. Quantum Chem.* **15**, 85.
- Bersuker, I. B., and Polinger, V. Z. (1983). "Vibronnye Vzaimodeystviya v Molekulakh i Kristallakh" [Vibronic Interactions in Molecules and Crystals]. Nauka, Moscow.
- Bersuker, I. B., and Vekhter, B. G. (1965). *Tr. Komis. Spectroscop. Akad. Nauk SSSR, Vip. I: Mater. 15 Soveshch. Spectrosc., Minsk, 1963. Moscow.* **3**, 520.
- Bersuker, I. B., and Vekhter, B. G. (1978). *Ferroelectrics* **19**, 137.
- Bersuker, I. B., Vekhter, B. G., and Ogurtsov, I. Ya. (1975). *Usp. Fiz. Nauk* **116**, 605.
- Bir, G. L., and Pikus, G. E. (1972). "Simmetriya i Deformatsionnye Effecty v Poluprovodnikakh" [Symmetry and Deformation Effects in Semiconductors]. Nauka, Moscow.

- Blankenship, F. A., and Belford, R. L. (1962). *J. Chem. Phys.* **36**, 633.
- Brown, J. M. (1971). *Mol. Phys.* **20**, 817.
- Buckingham, A. D. (1959). *J. Chem. Phys.* **30**, 1580.
- Buckingham, A. D., and Disch, R. L. (1968). *Proc. R. Soc. London Ser. A* **273**, 275.
- Buckingham, A. D., and Longuet-Higgins, H. C. (1968). *Mol. Phys.* **14**, 63.
- Buckingham, A. D., and Raab, R. E. (1975). *Proc. R. Soc. London Ser. A* **345**, 365.
- Child, M. S. (1962). *Mol. Phys.* **5**, 391.
- Child, M. S., and Longuet-Higgins, H. C. (1961). *Philos. Trans. R. Soc. Ser. A* **244**, 1.
- Christie, J. H., and Lockwood, D. J. (1971). *J. Chem. Phys.* **54**, 1141.
- Clark, R. J. H., and Machin, L. J. (1963). *J. Chem. Soc.*, 4430.
- Debye, P. (1929). "Polar Molecules." Chemical Catalog Company, New York.
- Desclaux, J. P. (1973). *Atomic Data Nucl. Data Tables* **12**, 311.
- Englman, R. (1972). "The Jahn–Teller Effect in Molecules and Crystals." Wiley (Interscience), New York.
- Gemmel, D. S., Kanter, E. P., and Pietsch, W. J. (1980a). *J. Chem. Phys.* **72**, 1402.
- Gemmel, D. S., Kanter, E. P., and Pietsch, W. J. (1980b). *J. Chem. Phys.* **72**, 6818.
- Gehring, G. A., and Gehring, K. A. (1975). *Rep. Prog. Phys.* **38**, 1.
- Graham, C. (1980). *Proc. R. Soc. London Ser. A* **369**, 517.
- Gray, C. G. (1968). *Can. J. Phys.* **46**, 135.
- Gray, C. G. (1971). *J. Phys. B.: Atom. Mol. Phys.* **4**, 1661.
- Gordon, R. G. (1963). *J. Chem. Phys.* **39**, 2788.
- Gordon, R. G. (1964a). *J. Chem. Phys.* **40**, 1973.
- Gordon, R. G. (1964b). *J. Chem. Phys.* **41**, 1819.
- Griffith, J. S. (1962). "The Irreducible Tensor Method for Molecular Symmetry Groups." Prentice-Hall, Englewood Cliffs, New Jersey.
- Gyorgy, E. M., Le Gaw, R. C., and Sturge, M. D. (1966). *J. Appl. Phys.* **37**, 1303.
- Ham, F. S. (1965). *Phys. Rev. A* **138**, 1727.
- Ham, F. S. (1968). *Phys. Rev.* **166**, 307.
- Ham, F. S. (1972). In "Electronic Paramagnetic Resonance" (S. Geschwind, ed.), pp. 1–119. Plenum, New York.
- Ham, F. S., Leung, C. H., and Kleiner, W. H. (1976). *Solid State Commun.* **18**, 757.
- Hamaguchi, H., Harada, I., and Shimanouchi, T. (1975). *Chem. Phys. Lett.* **32**, 103.
- Hamaguchi, H., and Shimanouchi, T. (1976). *Chem. Phys. Lett.* **38**, 370.
- Hellwarth, R. W. (1970). *J. Chem. Phys.* **52**, 2128.
- Hirschfelder, J. O. (1960). *J. Chem. Phys.* **33**, 1462.
- Huber, D. L., and Van Vleck, J. H. (1966). *Rev. Mod. Phys.* **38**, 187.
- Jerphagnon, J., Chemla, D., and Bonneville, R. (1978). *Adv. Phys.* **27**, 609.
- Kaplan, I. G. (1969). "Simmetriya Mnogoelektronnykh Sistem" [The Symmetry of Many Electron Systems]. Nauka, Moscow.
- Kielich, S. (1981). "Molekulyarnaya Nelineinaya Optika" [Nonlinear Molecular Optics]. Nauka, Moscow.
- Koster, G. F., Dimmock, J. O., Wheeler, R. G., and Statz, H. (1963). "Properties of the Thirty-two Point Groups." M.I.T. Press, Cambridge, Massachusetts.
- Longuet-Higgins, H. C., Öpik, U., Pryce, M. H. L., and Sack, R. A. (1958). *Proc. R. Soc. London Ser. A* **244**, 1.
- Maker, P. D. (1970). *Phys. Rev. A* **1**, 923.
- Meredith, G. R., Webb, J. D., and Bernstein, E. R. (1977). *Mol. Phys.* **34**, 995.
- Mizushima, M., and Venkateswarlu, P. (1953). *J. Chem. Phys.* **21**, 705.
- Morino, Y., and Uehara, H. (1966). *J. Chem. Phys.* **45**, 4543.

- Ogurtsov, I. Ya. (1982). VI Vsesoyuznii Simpozium po Molekulyarnoi Spektroskopii Visokogo i Sverchvisokogo Razresheniya, p. 44. Tezisi dokladov, Tomsk.
- Ogurtsov, I. Ya. (1984). *Opt. Spectrosc.* **56**, 60.
- Ogurtsov, I. Ya. (1985). *Opt. Spectrosc.* **58**, 799.
- Ogurtsov, I. Ya., and Kazantseva, L. A. (1979). *J. Mol. Struct.* **55**, 301.
- Ogurtsov, I. Ya., and Kazantseva, L. A. (1981). *J. Mol. Struct.* **73**, 85.
- Ogurtsov, I. Ya., and Kazantseva, L. A. (1983). In "Cooperative Phenomena" (Proceedings of International Symposium "Synergetics and Cooperative Phenomena in Solids and Macromolecules"), p. 44. Valgus, Tallin.
- Ogurtsov, I. Ya., Kazantseva, L. A., and Ishchenko, A. A. (1977). *J. Mol. Struct.* **41**, 243.
- Ogurtsov, I. Ya., and Ostrovski, V. L. (1985). *Mol. Phys.* **54**, 119.
- Ogurtsov, I. Ya., Ostrovski, V. L., and Bersuker, I. B. (1982). *Opt. Spectrosc.* **53**, 356.
- Ogurtsov, I. Ya., Ostrovski, V. L., and Bersuker, I. B. (1983a). *Khim. Fiz.* **5**, 579.
- Ogurtsov, I. Ya., Ostrovski, V. L., and Bersuker, I. B. (1983b). *Mol. Phys.* **50**, 315.
- Ogurtsov, I. Ya., Shaparev, Yu. V., and Bersuker, I. B. (1978). *Opt. Spectrosc.* **45**, 672.
- Orgel, L. E. (1955). *J. Chem. Phys.* **23**, 1004.
- Ostrovski, V. L., Ogurtsov, I. Ya., and Bersuker, I. B. (1983a). *Mol. Phys.* **48**, 13.
- Ostrovski, V. L., Ogurtsov, I. Ya., and Bersuker, I. B. (1983b). *Opt. Spectrosc.*, **54**, 442.
- Ostrovski, V. L., Ogurtsov, I. Ya., and Bersuker, I. B. (1984). *Mol. Phys.* **51**, 1205.
- Ozier, I., and Rosenberg, A., (1973). *Can. J. Phys.* **51**, 1882.
- Placzek, G. (1935). "Relevenskoe Rasseyaniye i Raman-Effect" [Rayleigh scattering and Raman-effect]. GNTI Khaz'kov-Kiev.
- Perlin, Yu. E., and Tsukerblat, B. S. (1974). "Effecty Elektronno-Kolebatel'nogo Vzaimodeystviya v Opticheskikh Spectrakh Primesnykh Paramagnitnykh Ionov" [Vibronic Effects in Optical Spectra of Impurity Paramagnetic Ions]. Shtiintsa, Kishinev.
- Poll, J. D., and Van Kranendonk, J. (1961). *Can. J. Phys.* **39**, 189.
- Reinen, D., and Friebel, C. (1979). *Struct. Bonding (Berlin)* **37**, 1.
- Rosenberg, A., Ozier, I., and Kudian, A. K. (1971). *J. Chem. Phys.* **57**, 568.
- Steele, W. A. (1963). *J. Chem. Phys.* **38**, 2404.
- Stogryn, D. E., and Stogryn, A. P. (1966). *Mol. Phys.* **11**, 371.
- Truax, D. R., Geer, J. A., and Ziegler, M. (1974). *Theor. Chim. Acta* **33**, 229.
- Utarova, T. M. (1980). *Trudy FIAN* **118**, 3.
- Valiev, K. A., and Ivanov, Ye., N. (1973). *Usp. Fiz. Nauk* **109**, 31.
- Varshalovich, D. A., Moskalyov, A. N., and Khersonskii, V. K. (1975). "Kvantovaya Teoriya Uglovogo Momenta" [Quantum Theory of Angular Momentum]. Nauka, Leningrad.
- Wilson, E. B. (1935). *J. Chem. Phys.* **3**, 276.
- Zubarev, D. N. (1971). "Neravnovesnaya Statisticheskaya Termodinamika" [Nonequilibrium Statistical Thermodynamics]. Nauka, Moscow.

Quantum-Mechanical Prediction of Tautomeric Equilibria

JOZEF S. KWIATKOWSKI

*Institute of Physics
Nicholas Copernicus University
87-100 Torun, Poland**

and

THERESA JULIA ZIELINSKI

*Department of Chemistry
Niagara University
Niagara University, New York 14109†*

and

ROBERT REIN

*Unit of Theoretical Biology
Roswell Park Memorial Institute
Buffalo, New York 14263*

I. Introduction	85
II. Tautomeric Equilibrium: General Remarks	86
III. Tautomeric Equilibrium in an Electronic Ground State of a Molecule Existing in Vapor Phase	89
IV. Tautomeric Equilibrium in an Electronic Ground State of a Molecule Existing in Solution	104
V. Tautomeric Equilibrium in an Excited Electronic State of a Molecule Existing in the Vapor Phase and in Solution	114
VI. Role of Tautomers in Mutation Theory	121
References	127

I. Introduction

Considerable effort has been expended in the effort to understand the phenomenon of tautomerism, not only in relation to quantitative concepts

* Parts of this paper were prepared while J.S.K. was visiting the Chair for Theoretical Chemistry at the Friedrich-Alexander University in Erlangen-Nurnberg and the Laboratory of the National Foundation for Cancer Research at the University Erlangen-Nurnberg, Erlangen, Federal Republic of Germany.

† Parts of this paper were prepared during T.J.Z.'s affiliation with the Unit of Theoretical Biology and the National Foundation for Cancer Research Project at Roswell Park Memorial Institute, Buffalo, New York.

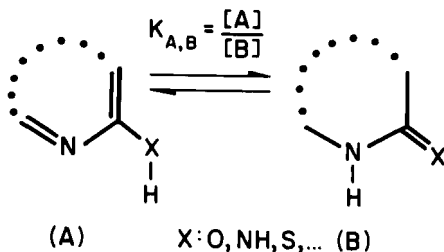
of chemical binding and structure–activity relationships in organic and physical chemistry (Katritzky and Lagowski, 1963; Katritzky and Ambler, 1963; Albert, 1968; Elguero *et al.*, 1975), but also in other fields such as molecular biology (e.g., in relation to spontaneous mutations as a consequence of mispairing by rare tautomeric forms of purines and pyrimidines (Löwdin, 1965; Cooper, 1978; Danilov and Kventsel, 1971; Rein *et al.*, 1983) or in relation to enzyme–substrate interactions (Metzler, 1979). During recent years a large amount of experimental and theoretical work has been carried out in order to elucidate the qualitative and quantitative aspects of prototropic tautomerism of heteroaromatic compounds that involves the movement of a proton between a cyclic nitrogen atom and a substituent atom directly adjacent to the ring. The information about the internal energy of the tautomers obtained by the computational methods of quantum chemistry is treated rather skeptically as compared with the data provided by experimental work (Beak, 1977). The purpose of this paper is to point out the scope and limitations of quantum-mechanical methods and to interpret several aspects of the tautomeric equilibria of heterocyclic compounds.

Quantum-mechanical studies on the tautomerism of heterocyclic compounds involve, in general, two aspects. The first deals with the prediction of physicochemical properties of defined tautomeric forms (e.g., ultraviolet spectra, dipole moments, ionization potentials, etc.). This seems to be easy to handle. Using any semiempirical or nonempirical quantum-mechanical computational method, depending on approximations involved in the method, we are able to calculate properties that, more or less, agree with experimental values. Calculations of this type do not contribute to a direct estimation of the relative stability of the tautomers, however; they are particularly important for cases in which a tautomeric form of a compound is so rare that it is not possible to measure it directly.

The second covers the prediction of the relative stability of tautomers in vapor phase and the estimation of the tautomeric constant in this phase, prediction of the influence of substituents (e.g., methyl group, halogen atom) on the shift of tautomeric equilibrium (the relative change of tautomeric constant caused by substituents), and even the estimation of the stability of defined tautomers in solution. Obtaining these properties is much more complicated. The difficulties connected with an attempt to apply quantum chemistry in this case will be discussed in the next section.

II. Tautomeric Equilibrium: General Remarks

Let us consider a molecule existing for simplicity in two tautomeric forms either A or B. The tautomeric equilibrium $A \rightleftharpoons B$ is characterized



Scheme 1

by a tautomeric constant $K_{A,B} = [A]/[B]$, a ratio of molar concentration of the tautomer A to that of the tautomer B. According to laws of statistical thermodynamics this constant is connected with the difference between the standard free energies of both forms $\Delta G_{A,B}^\circ$ through the formula:

$$K_{A,B} = \exp(-\Delta G_{A,B}^\circ/RT) \quad (1)$$

where R and T stand, respectively, for the gas constant and absolute temperature (Kelvin scale) and $\Delta G^\circ = \Delta H^\circ - T \Delta S^\circ$, where ΔH° and ΔS° represent the changes in standard enthalpy and entropy, respectively.

It is easy to show that for a tautomeric equilibrium the standard free energy change can be written as

$$\Delta G_{A,B}^\circ = \Delta E_{A,B}^{(0)} - T \Delta S_{A,B}^{\text{ovib}} \quad (2)$$

where $\Delta E_{A,B}^{(0)}$ is the sum of $\delta E_{A,B}^{\text{el}}$, the difference between the lowest energies of the tautomers E_A^{el} and E_B^{el} calculated as the minima of the potential energy surfaces of the respective tautomers, and $\delta E_{A,B}^{\text{vib}(0)}$, the zero-point vibrational energy difference between the two tautomers. The zero-point vibrational term and the vibronic entropy contribution for each tautomer can be calculated by using standard statistical thermodynamics (Herzberg, 1945):

$$E_A^{\text{vib}(0)} = \frac{N}{2} \sum_i h\nu_i \quad (3)$$

and

$$S_A^{\text{ovib}} = -R \sum_i d_i \ln \left(1 - \exp \frac{-\nu_i h}{kT} \right) + \frac{Rh}{kT} \sum_i \frac{d_i \nu_i \exp(-\nu_i h/kT)}{1 - \exp(-\nu_i h/kT)} \quad (4)$$

where ν_i is the vibrational frequency of the i th normal vibrational mode, N is Avogadro's number, d_i is the degeneracy of the i th mode, h is Planck's

constant, k is Boltzmann's constant, R is the gas constant, and T is temperature in Kelvin, so that

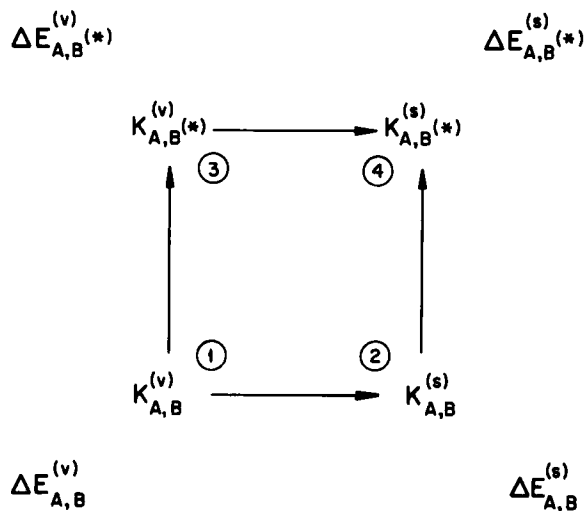
$$\delta E_{A,B}^{\text{vib}(0)} = E_A^{\text{vib}(0)} - E_B^{\text{vib}(0)} \quad (5)$$

and

$$\Delta S_{A,B}^{\text{ovib}} = S_A^{\text{ovib}} - S_B^{\text{ovib}} \quad (6)$$

From the second derivative of the potential energy surface for the tautomers, the frequencies necessary for Eqs. (3) and (4) can be obtained and the vibrational contribution to the free energy evaluated to allow calculation of the tautomeric equilibrium constant from theory.

When discussing the tautomeric equilibrium of a molecule, we should clearly specify the conditions of the equilibrium, i.e., the electronic state of the molecule (ground or excited state and its multiplicity) and the medium (vapor phase or solution) in which the equilibrium is considered. We shall restrict our attention to the four cases presented in Scheme 2,



Scheme 2

with the tautomeric equilibrium $A \rightleftharpoons B$ in a vapor phase (v) either in the electronic ground state, point 1 or in an excited state, point 3, and the tautomeric equilibrium $A \rightleftharpoons B$ in the corresponding states in solution(s), points 2 and 4. For simplicity we did not specify the multiplicity of the electronic state of the molecule.

In each case, the tautomeric equilibrium is characterized by the corresponding tautomeric constant $K_{A,B}$ or equivalently by the corresponding

difference between the lowest energies of the tautomers $\Delta E_{A,B}^{(0)}$ at absolute zero [in Scheme 2 we omitted the superscript (0) for simplicity of notation].

First of all, we shall discuss the estimation of the energy difference of vapor phase tautomers in the electronic ground state, $\Delta E_{A,B}^{(v)}$ (point 1). As we shall see later, the energy differences at points 2, 3, and 4 can be formally expressed by the energy difference at point 1 and some additional terms characterizing the change of this energy difference on excitation and/or on the change of environment.

III. Tautomeric Equilibrium in an Electronic Ground State of a Molecule Existing in Vapor Phase

The relative stability of the two tautomers A and B depends on the difference between their lowest energies $\Delta E_{A,B}^{(0)}$ (Fig. 1), which in the Born–Oppenheimer approximation is equal to the sum $\delta E_{A,B}^{el(eq)} + \delta E_{A,B}^{vib(0)}$, where the first term indicates the difference between the total electronic (el) energies of both tautomers at their corresponding geometric equilibrium (eq) positions and the second term stands for the difference between zero-point vibrational energies of the tautomers.

In many cases the estimation of the relative stability of tautomers is done only by consideration of $\delta E_{A,B}^{el(eq)}$ values, assuming that the contribution of the zero-point vibrational energies for both tautomers is the same, i.e., that $\delta E_{A,B}^{vib(0)} = 0$, and also assuming that $\Delta S_{A,B}^{ovib}$ is zero. In some cases, however, the values of $\delta E_{A,B}^{vib(0)}$ are calculated. In the case of uracil (1a), and its 4-hydroxyuracil tautomer (1b), the normal vibrational frequencies calculated by the MINDO/3 method gave $\delta E_{1a,1b}^{vib(0)} = -0.8 \text{ kJ mole}^{-1}$ (Shibata *et al.*, 1980). At 298 K this almost cancels the $-T \Delta S_{A,B}^{ovib}$ term, which is equal to $+1.3 \text{ kJ mole}^{-1}$. In the case of the lactim–lactam tautomeric pairs of oxopyridines (2, 3) and oxypyrimidines (4, 5) MINDO/3 calculations gave (Krebs *et al.*, 1980) $\delta E_{lactim,lactam}^{vib(0)} = -(2.5 - 3.1) \text{ kJ mole}^{-1}$. [Note, however, that calculation by means of the MNDO method gives for the same systems $\delta E_{lactim,lactam}^{vib(0)} = -(0.1-1.5) \text{ kJ mole}^{-1}$ (C. Krebs-Bartzsch, Leipzig, unpublished results).] The MINDO/3 energies are distinctly larger than the value of 0.4 kJ mole^{-1} estimated experimentally for 2-oxopyridine (Beak, 1977) and smaller than the value of 5 kJ mole^{-1} estimated for 2-oxo-6-methylpyrimidine (Nowak, 1979; Nowak *et al.*, 1980). Calculations of the vibrational frequencies of formamide (6a) and formimidic acid (6b) in the Hartree–Fock approximation using the 3-21G

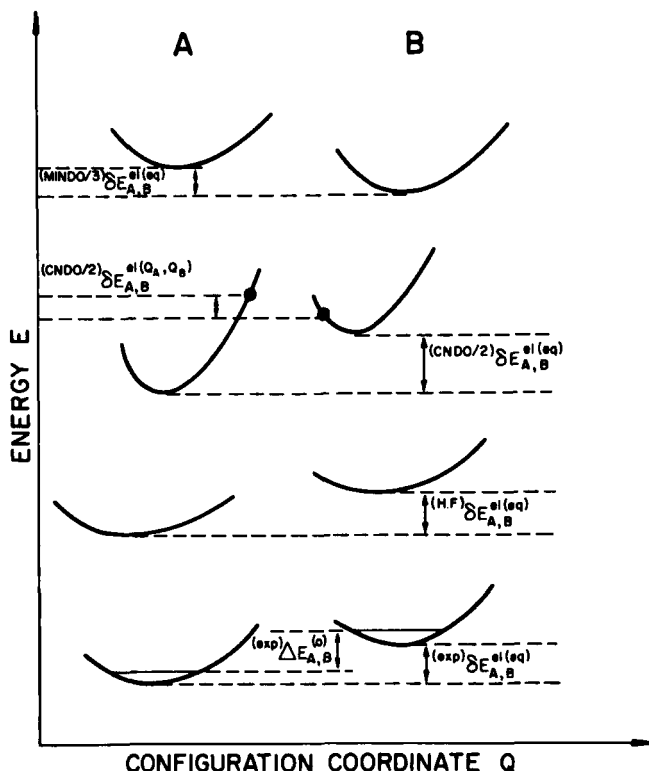
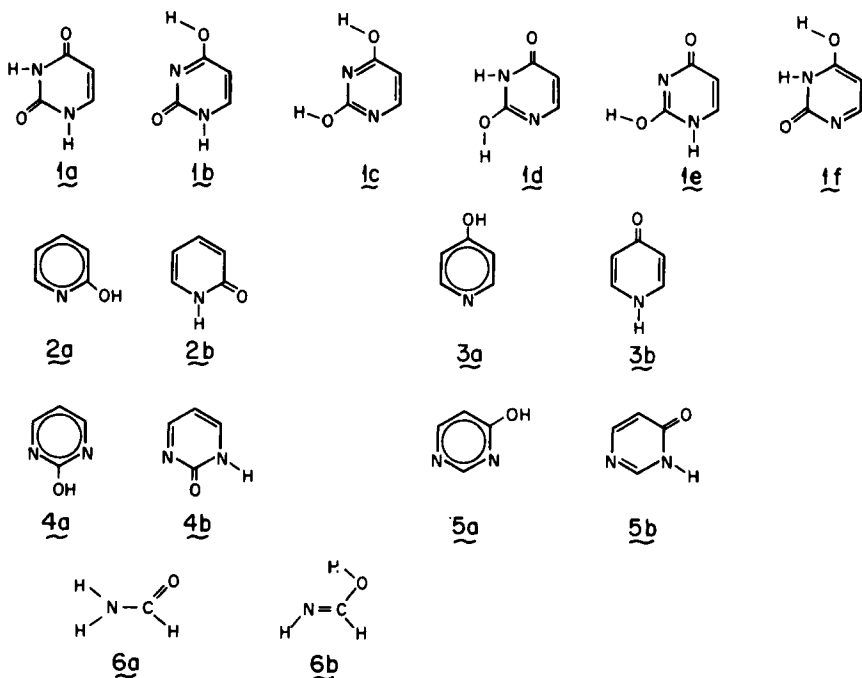


Fig. 1. Schematic representation of the potential energy surface for the electronic (el) ground state of a molecule existing in two tautomeric forms, A and B. Superscripts exp, HF, CNDO/2, MINDO/3 indicate that energy differences $\delta E_{A,B}^{el}$ calculated for potential energy surfaces determined either experimentally (exp) or calculated by means of *ab initio* method in the Hartree–Fock (HF) approximation or by semiempirical methods (CNDO/2, MINDO/3). The symbol eq stands for the geometrical equilibrium of both tautomers, while Q_A and Q_B indicate nonequilibrium geometries of tautomers A and B, respectively. Note that the theoretical potential surface calculated by sophisticated quantum-mechanical methods (“exact” solution of electronic Schrödinger equation includes electron correlation with geometry optimization) should be the same (or very similar) as that determined experimentally [in this case ${}^{(theor)}E^{el(eq)} \approx {}^{(exp)}E^{el(eq)}$ for both the tautomers, and then ${}^{(theor)}\delta E_{A,B}^{el(eq)} = {}^{(exp)}\delta E_{A,B}^{el(eq)}$].

basis set (HF/3-21G) also gave (Schlegel *et al.*, 1982) a small value, $\delta E_{6a,6b}^{vib(0)} = -1.2 \text{ kJ mole}^{-1}$. Unfortunately, as far as we are aware, the appropriate $\delta E_{A,B}^{vib(0)}$ and $\Delta S_{A,B}^{vib}$ values are not available for model systems exhibiting either amino–imino or thione–thiol tautomerism. In any case, due to the neglect of the $\delta E_{A,B}^{vib(0)}$ and $\Delta S_{A,B}^{vib}$ contribution to $\Delta E_{A,B}^{(0)}$, the estimate of the relative free energies of the tautomers may be in error by approximately 5



kJ mole^{-1} . This number may be smaller if as in the case of uracil the $\delta E_{A,B}^{\text{vib}(0)}$ and the $\Delta S_{A,B}^{\text{ovib}}$ terms cancel each other to some extent.

Since $\delta E_{A,B}^{\text{cl}(\text{eq})} = \Delta E_{A,B}^{(0)} - \delta E_{A,B}^{\text{vib}(0)}$ and the vibrational contributions $\delta E_{A,B}^{\text{vib}(0)}$ may be evaluated theoretically and sometimes experimentally, a comparison between theoretically and experimentally determined stabilities of two tautomers may be made by comparing the $^{(\text{exp})}\delta E_{A,B}^{\text{cl}(\text{eq})}$ and $^{(\text{theor})}\delta E_{A,B}^{\text{cl}(\text{eq})}$ values (Fig. 1).

Estimation of $\delta E_{A,B}^{\text{cl}(\text{eq})}$ for tautomers by means of the computational methods of quantum chemistry is not easy. An exact calculation of the potential energy surface for each tautomer is required followed by a comparison of the energies at the minimum points of both surfaces (these positions correspond to the optimized geometries of the tautomers).

Exact calculations of the potential energy surfaces for complex molecular systems are impossible to carry out from a practical point of view. Such calculations involve the solution of the electronic Schrödinger equation for the system including electron correlation effects and full geometry optimization. However, an estimate of the $\delta E_{A,B}^{\text{cl}(\text{eq})}$ value can be obtained in a different way. One can carry out an *ab initio* calculation in the Hartree-Fock (HF) approximation by using a simple basis set, e.g., (7s, 3p/3s), contracted to a minimal basis set, STO-3G, or 3-21G, etc., with full geom-

etry optimization. In general, these calculations predict geometries of molecular systems that do not differ very much from experimental geometries. Using the calculated equilibrium geometries of the tautomers, one can then calculate the electronic energies ${}^{(HF)}E_A^{\text{el}}$ and ${}^{(HF)}E_B^{\text{el}}$ by means of an *ab initio* method in the HF approximation with a better basis set (e.g., 6-31G*) and calculate the electron correlation energy for the tautomers. Final values ${}^{(\text{theor})}E_A^{\text{el}} = {}^{(HF)}E_A^{\text{el}} + {}^{(\text{corr})}E_A^{\text{el}}$ and ${}^{(\text{theor})}E_B^{\text{el}} = {}^{(HF)}E_B^{\text{el}} + {}^{(\text{corr})}E_B^{\text{el}}$ should not differ from values $E_A^{\text{el}(\text{eq})}$ and $E_B^{\text{el}(\text{eq})}$, respectively, calculated exactly or determined experimentally. In other words, ${}^{(\text{theor})}\delta E_{A,B}^{\text{el}} \approx {}^{(\text{theor})}\delta E_{A,B}^{\text{el}(\text{eq})} \approx {}^{(\text{exp})}\delta E_{A,B}^{\text{el}(\text{eq})}$.

As far as we are aware, this type of calculation has been performed for lactim and lactam tautomers of both 2- and 4-oxypyridines [(2), (3)] and for formamide (6a) and formimidic acid (6b) only (Schlegel *et al.*, 1982; Scanlan *et al.*, 1983). Since the calculations mentioned are expensive, one estimates the $\delta E_{A,B}^{\text{el}(\text{eq})}$ value by comparison of the electronic energies calculated in the HF approximation only [${}^{(HF)}\delta E_{A,B}^{\text{el}(\text{eq})}$], and even this has often been done by means of semiempirical methods [${}^{(\text{CNDO}/2)}\delta E_{A,B}$, ${}^{(\text{MINDO}/3)}\delta E_{A,B}$, ${}^{(\text{MNDO})}\delta E_{A,B}$, etc.).

One can justify this procedure with two assumptions: first, that the electron correlation contributions for both tautomers are the same or very similar to each other; second, that the errors existing in the calculation of the electron energies of the tautomers in the HF approximation (e.g., the errors connected with the fact that different basis sets are used or the errors caused by approximations involved in a semiempirical formulation of the HF approximation) are similar for both tautomers.

The first assumption is more or less justified. For example, calculations (Schlegel *et al.*, 1982) of the electron correlation energy by means of the Møller–Plesset second-order perturbation method (Møller and Plesset, 1934) gave the values of 2.5 to 3.4 kJ mole⁻¹ for relative electron correlation energies for the tautomers of 2- and 4-oxypyridines. For formamide (6a) and formimidic acid (6b) this relative energy is even smaller (0.4–0.8 kJ mole⁻¹). However, another type of calculation (configuration interaction including all singly and doubly excited configurations correct to the fourth order) for the tautomers of formamide gave a higher relative electron correlation energy (Schlegel *et al.*, 1982) (~7.1 kJ mole⁻¹).

The errors in prediction of the $\delta E_{A,B}^{\text{el}(\text{eq})}$ values when the contribution of the electron correlation is neglected are in fact smaller than the errors obtained in calculations within the HF approximation, particularly when semiempirical methods are used. Different computational methods give different potential energy surfaces (Fig. 1) and different theoretical values for $\delta E_{A,B}^{\text{el}(\text{eq})}$.

A good illustration of this type of discrepancy is presented in Tables I and II. In the case of 2-oxopyridine, semiempirical CNDO/2 and MNDO methods and *ab initio* HF/STO-3G calculations predict the lactim tautomer of the molecule to be more stable than the lactam one, while the MINDO/3 and HF/3-21G calculations give a reverse result. In view of the large uncertainty in the experimental value -1.3 ± 10.5 kJ mole⁻¹ (probably overestimated), it is not possible to draw any other conclusion than that the experimental values and the theoretical values are spanning the

TABLE I
THERMODYNAMIC QUANTITIES AND RELATIVE
ELECTRONIC ENERGIES $\delta E_{A,B}^{\text{el}(\text{eq})}$ FOR THE LACTIM (A)
AND LACTAM (B) TAUTOMERS OF 2-OXOPYRIDINE IN
THE VAPOR PHASE (THE LACTAM TAUTOMER
CONSIDERED AS THE REFERENCE SYSTEM)^a

<i>Experimental Data</i> (Beak <i>et al.</i> , 1976; Aue <i>et al.</i> , 1979) ^b		
Free Energy	ΔG°	-3.4
Enthalpy	ΔH°	-1.3 ± 1.3
	$\Delta E_{A,B}^{(0)}$	-1.3 ± 10.5
<i>Theoretical data</i> ^c		$\delta E_{A,B}^{\text{el}(\text{eq})}$
CNDO/2 (Krebs <i>et al.</i> , 1980)		-145.0
MINDO/3 (Krebs <i>et al.</i> , 1980; Czerminski <i>et al.</i> , 1979) ^d		+15.7
MNDO (Krebs <i>et al.</i> , 1980; Mirek and Sygula, 1981)		-40.8
HF/STO-3G (Schlegel <i>et al.</i> , 1982)		-64.4
HF/3-21G (Schlegel <i>et al.</i> , 1982)		+7.1
HF/3-21G (Scanlan <i>et al.</i> , 1983) ^e		+7.4
HF/6-31G** (Scanlan <i>et al.</i> , 1983)		-4.2

^a The minus sign indicates that the lactim form (A) is more stable. All values in kilojoules per mole.

^b The ΔG° value from x-ray photoelectron spectroscopy is $-(2.4 \pm 0.3)$ kJ mole⁻¹ (Brown *et al.*, 1980). Note that according to Beak (1977) $\text{exp} \Delta E_{A,B}^{\text{el}(\text{eq})} \approx \delta E_{A,B}^{\text{el}(\text{eq})}$ for 2-oxopyridine. ΔH° is also reported as -3 ± 0.4 kJ mole⁻¹ and ΔG° calculated as -3.7 kJ mole⁻¹ (Guimon *et al.*, 1979).

^c The calculations are with full-geometry optimization.

^d There is a typographical error for the MINDO/3 results (Krebs *et al.*, 1980), where a minus sign is given instead of a plus.

^e These authors used a slightly softer gradient condition for optimization.

TABLE II

THERMODYNAMIC QUANTITIES AND RELATIVE ELECTRONIC ENERGIES $\delta E_{A,B}^{\text{el(eq)}}$ FOR THE LACTIM (A) AND LACTAM (B) TAUTOMERS OF OXOPYRIDINES AND OXOPYRIMIDINES IN THE VAPOR PHASE^a

Molecule	Experimental results ^b		Theoretical results (with full-geometry optimization)				
	$\Delta G_{A,B}^\circ$	$\Delta E_{A,B}^{(0)}$	CNDO/2 ^f	MINDO/3 ^{e,f}	MNDO ^g	3-21G	6-31G**
2-Oxopyridine	-3.4	-1.3 ± 10	-145.0	+15.7	-40.8	+7.1 ^d	-4.2 ^c
4-Oxopyridine	-10	-29 ± 8	-195.1	-16.1	-62.2	-3.1 ^c	-14.9 ^c
						-2.9 ^d	
2-Oxopyrimidine	-10		-134.3	+29.5	-44.0	—	—
4-Oxopyrimidine	2.4 ± 5 1 ± 1 ^h	3 ± 1 ^h	-106.1	+19.6	-34.2	—	—

^a The minus sign indicates that the lactim (A) is more stable. All quantities in kilojoules per mole.

^b From Beak *et al.* (1976).

^c From Scanlan *et al.* (1983). These authors use a softer gradient condition for optimization.

^d From Schlegel *et al.* (1982).

^e From Krebs *et al.* (1980). There are typographical errors for the MINDO/3 results in this reference. The minus sign is given instead of the plus for 2-oxopyridine, 2-oxopyrimidine, and 4-oxopyrimidine.

^f From Czerminski *et al.* (1979b).

^g From Mirek and Syguła (1981) and Kwiatkowski and Lesyng (1983).

^h From Nowak *et al.* (1980). At 230°C.

same range. If zero-point energy and vibrational entropy contributions partially cancel in this case as for uracil/4-hydroxyuracil, then it seems reasonable to compare the calculated $\delta E_{A,B}^{\text{el(eq)}}$ directly to ΔH° . When this is done only the 6-31G** calculation is seen to give the best relative energies for the tautomer pair. Table II compares the available data for oxopyridines and oxopyrimidines. These data show further that conclusions concerning the relative stability of the tautomers cannot be drawn based on STO-3G or semiempirical calculations; CNDO/2 calculations give especially unrealistic $\delta E_{A,B}^{\text{el(eq)}}$ values. The lowest level of acceptable calculations seems to be the one employing the 3-21G basis, but even here there is an error of several kilojoules per mole.

In Table III lists the steps in the quantum-mechanical computation for 2-oxopyridine. The HF/STO-3G calculation with the full-geometry optimization gives an electronic energy for the lactim tautomer lower than that of the lactam by 64.4 kJ mole⁻¹ (step 1°). Calculations carried out with a better basis set (3-21G) and with full-geometry optimization give the lower energy for the lactam by 7.1 kJ mole⁻¹ (step 3°). This can be

TABLE III

ELECTRONIC ENERGIES E_A^{el} AND E_B^{el} AND RELATIVE ELECTRONIC ENERGIES $\delta E_{A,B}^{\text{el}}$ FOR THE LACTIM (A) AND LACTAM (B) TAUTOMERS OF 2-OXOPYRIDINE [*ab initio* HF LEVEL (SCHLEGEL *et al.*, 1983)]^a

Step of calculation	Method of calculation	E_A^{el} (a.u.)	E_B^{el} (a.u.)	$\delta E_{A,B}^{\text{el}}$ (kJ mole ⁻¹)
1°	HF/STO-3G geometry optimized	-317.49119	-317.46662	-64.4
2°	HF/3-21G geometry from step 1°	-319.76296	-319.76618	+8.4
3°	HF/3-21G geometry optimized	-319.76814	-319.77080	+7.1
4°	HF/6-31G geometry from step 3°	-321.43043	-321.43371	+8.6
5°	HF/6-31G* geometry from step 3°	-321.56564	-321.56653	+2.3
6°	MP2/6-31G ^b geometry from step 3°	-322.08181	-322.08640	+12.1
7°	Estimated value ^c			+5 ± 1.7 (+1.7 ± 2.3)

^a See Table I.

^b MP2-electron correlation energy calculated according to Møller and Plesset (1934).

^c For details see original text. The best theoretical estimate of $\Delta E_{A,B}^{(0)}$ after including the zero-point vibrational contributions is given in parentheses.

compared to the calculation at step 2° performed using the same 3-21G basis set but with optimized structures from step 1°. In this case, the electronic energies of both the A and B tautomers differ from those of step 3° by 13.6 and 12.1 kJ mole⁻¹, respectively, and $\delta E_{A,B}^{\text{el}}$ equal to 8.4 kJ mole⁻¹. This is due to the fact that both STO-3G and 3-21G basis sets give similar optimal geometric structures for the tautomers. The 3-21G structures are in general better than the STO-3G structures and should be used whenever they are available. In the steps 4° and 5° better basis sets were used. The electronic energies decrease, but the lowering of the energies for both the tautomers is not the same, giving different $\delta E_{A,B}^{\text{el}}$ values (8.6 kJ mole⁻¹ with the 6-31G basis and 2.3 kJ mole⁻¹ with the 6-31G* basis set). Calculations at step 6° predict similar electron correlation energy contributions for both the tautomers (in fact, the contribution for the lactam tautomer is slightly larger by 3.4 kJ mole⁻¹).

The calculation at step 5° gives the lowest electronic energies E_A^{el} and E_B^{el} in the HF approximation and a $\delta E_{A,B}^{\text{el}}$ value of 2.3 kJ mole⁻¹, while the

more-advanced calculation of step 6 (including electron correlation) gives $12.1 \text{ kJ mole}^{-1}$ for $\delta E_{A,B}^{\text{el}}$. As we see the results of step 5 are in better agreement with the experimental data for which $\Delta H^\circ = -1.3 \pm 1.3 \text{ kJ mole}^{-1}$ (see Table I) than the results calculated by means of the better method at step 6°. This, however, is a misleading discrepancy because as a matter of fact the electronic energies E_A^{el} and E_B^{el} calculated in step 6° are better than those of step 5°. It seems that the errors obtained in the calculation of E^{el} for the tautomers are better canceled in step 5° than in step 6° when the relative energies $\delta E_{A,B}^{\text{el}}$ are being calculated. This could be due to the absence of polarization functions in step 6°.

The last entry in Table III is what is called the best theoretical estimate. Schlegel *et al.* (1982) did not carry out additional more-advanced calculations. By studying their own results they were able to make suitable corrections to their best-calculated value. Their arguments are as follows. Because the optimization of geometry both in the STO-3G and 3-21G basis yields similar geometries for the tautomers (the values $\delta E_{A,B}^{\text{el}}$ calculated for different geometries in the same basis set are 8.4 and 7.1 kJ mole^{-1} , respectively; see steps 2° and 3°, Table III), it is conceivable that the change in $\delta E_{A,B}^{\text{el}}$ in optimizing the geometry in the 6-31G* basis would be no larger than $0.8 \pm 0.8 \text{ kJ mole}^{-1}$ in favor of the lactim form. Similarly, the authors estimate the probable changes of the $\delta E_{A,B}^{\text{el}}$ value that would be caused by including correlation effects and polarization functions in the basis set. The estimated (not calculated) value of $\delta E_{A,B}^{\text{el}}$ at this stage (Schlegel *et al.*, 1982) for 2-oxypyridine is $5 \pm 1.7 \text{ kJ mole}^{-1}$. Inclusion of the vibrational contribution $\delta E_{A,B}^{\text{vib}(0)}$ (Krebs *et al.*, 1980) calculated using the MINDO/3 method reduces $\delta E_{A,B}^{\text{el}}$ to give $1.7 \pm 2.3 \text{ kJ mole}^{-1}$ for $\Delta E_{A,B}^{(0)}$. If the MNDO vibronic contribution is used (C. Krebs-Bartzsch, Leipzig, unpublished results) $\Delta E_{A,B}^{(0)}$ is closer to $4 \pm 2 \text{ kJ mole}^{-1}$. Although the sign is incorrect, these results fall within the experimental error (Table I), which has a large deviation. Included in the set of reasonable theoretical results is the one obtained with the 6-31G** basis set at the 3-21G geometry, the last entry in Table I (Scanlan *et al.*, 1983). Using the Schlegel $\Delta E_{A,B}^{(0)}$ range of $+4.0$ to $-0.6 \text{ kJ mole}^{-1}$ and neglecting $\Delta S_{A,B}^{\text{ovib}}$, one obtains a range of 0.2 to 1.3 for $K_{\text{eq}}[\text{OH}]/[\text{NH}]$, which is from 20 to 4 times smaller than the experimental equilibrium constants reported as 4.0 at 50°C (Guimon *et al.*, 1979). A similar calculation using the Scanlan 6-31G** $\delta E_{A,B}^{\text{el}}$ and neglecting both the $\delta E_{A,B}$ and $\Delta S_{A,B}$ contributions yields a K_{eq} of 4.4 in agreement with the experimental value.

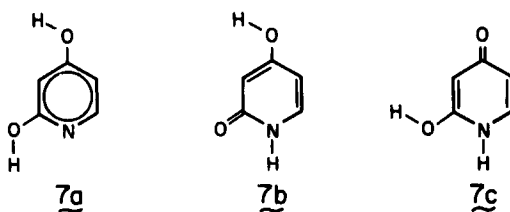
Similar calculations have been performed for 4-oxypyridine (Schlegel *et al.*, 1982). In this case the best theoretical estimate for $\Delta E_{A,B}^{(0)}$ is $-10 \pm 3 \text{ kJ mole}^{-1}$, which can be compared to the best experimental estimate of $-29 \pm 8 \text{ kJ mole}^{-1}$. Considering the success of the method for the 2-

hydroxypyridine/2-pyridone system, the agreement between theory and experiment is well outside the estimated errors of both the theoretical and experimental values. Schlegel *et al.* (1982) argue convincingly that since differences in tautomerization energies formally constitute isodesmic reactions, they can be obtained more accurately and with less effort than the $\Delta E_{A,B}^{(0)}$ themselves. The best theoretical estimate of the relative tautomerization energy $\Delta(\Delta E_{A,B}^{(0)})$ for 2-pyridone/4-pyridone is 12 ± 3 kJ mole⁻¹. This does not compare favorably with the experimental estimate of 28 ± 8 kJ mole⁻¹.

The experimental value is determined by subtracting the vapor phase enthalpy difference for 2-hydroxypyridine/2-pyridone (1 ± 1 kJ mole⁻¹) and the enthalpy difference for the corresponding methylated derivatives (32 ± 10 kJ mole⁻¹) to obtain a value of 31 kJ mole⁻¹ due to the difference in local bond energies (NH, OH versus NCH₃, OCH₃). This value is then subtracted from the gas phase enthalpy difference of 59.0 ± 8.2 kJ mole⁻¹ for the methyl derivatives of the 4-hydroxypyridine/4-pyridone to yield a gas phase enthalpy difference of 28 kJ mole⁻¹ for the 4-hydroxypyridine/4-pyridone system (keto form more stable) (Beak *et al.*, 1976). This too is an estimated quantity dependent on the transferability of the enthalpy due to the local bond energies mentioned earlier, i.e., that methylation affects both tautomers systems in the same manner.

Such a direct transfer must be examined more closely. Experiment and theory both show that there is significant interaction between the —OH bond and the adjacent nitrogen in 2-pyridone (Del Bene, 1979; Aue *et al.*, 1979). This interaction energy is about 36 kJ mole⁻¹. The interaction is lowered by 2 kJ mole⁻¹ when the hydrogen is replaced by a methyl group and lowered again by 6 kJ mole⁻¹ when the methyl group is rotated away from the carbonyl as calculated for methylformimidate and *N*-methylformamide (HF/3-21G, fully optimized geometries) (Schlegel *et al.*, 1982). When these effects are included in the correction for local bond energies, the experimental estimate becomes 21 ± 8 kJ mole⁻¹, closer to the calculated tautomerization energy. Only direct measurement of the 4-pyridone tautomerization will show whether these arguments are valid.

The same method has been applied to evaluate the tautomer energy differences among 2,4-pyridinediol, 4-hydroxy-2-pyridinone, and 2-hydroxy-4-pyridinone (7a–7c). These calculations were carried out at the HF/3-21G level with full-geometry optimization (Schlegel, 1983). The effects of polarization functions, electron correlation, and zero-point energy were included by using corrections from the 2- and 4-pyridine study. The results are summarized in Table IV. The most stable structure is 4-hydroxy-2-pyridinone in agreement with experiment (Beak *et al.*, 1972) after corrections for methyl group and condensed phase effects (Beak,



1977). Inspection of Table IV shows that the methodology is correctly predicting the order of stability of a series of tautomers but that the magnitudes of the values obtained by theory and experiment do not yet match closely. The reason for this is probably a complex mixture of inadequacy in theory and experimental difficulties indicated by the range of error associated with the experimental values.

The literature for uracil is about as extensive as that for 2-pyridone. A detailed analysis of the adequacy of different theoretical approaches applied to uracil/4-hydroxyuracil [U/U*; (1a)/(1b)] tautomerism up to and including the STO-3G with optimized geometries has been published (Mondragon and Ortega-Blake, 1982). These authors compare optimized geometries for U/U* obtained by a variety of methods to available experimental data and present the tautomerization energy for U/U* as a function of optimized geometry and method of calculation. These authors concluded that while semiempirical methods are adequate for predicting

TABLE IV
RELATIVE ELECTRONIC ENERGIES OF 2,4-PYRIDINEDIOL
TAUTOMERS (ALL QUANTITIES IN KILOJOULES PER MOLE)

Compound ^a	3-21G	Best theoretical estimate ^{b,c}	Best experimental estimate ^d
2-4-Pyridinediol	0.0	0.0	
4-Hydroxy-2-pyridinone	-13.8	-7.9	-1.3 ± 7.9
2-Hydroxy-4-pyridinone	+21.2	+29.3	+40.1 ± 7.9

^a Only the most stable of the possible hydroxyrotomers is included in the table.

^b Including estimates of polarization functions, electron correlation, and zero-point energy.

^c From Schlegel (1983).

^d From Beak *et al.* (1972) and correcting for methyl group and condensed phase effects (Beak, 1977).

the structures of tautomer pairs, they are inadequate for determining relative energies. The most consistent data obtained in this study involved the use of *ab initio* model potentials (Barthelat *et al.*, 1977; Durand and Barthelat, 1975; Teichteil *et al.*, 1977) with Gaussian-type functions optimized from the model potential (Les and Ortega-Blake, 1979, 1981). Their 2 ζ basis consisted of four Gaussians contracted to {3, 1}. Using this basis they obtained an average tautomerization energy for U/U* of 93.7 ± 10.0 kJ mole⁻¹ with PCILO, MNDO, MINDO/3, and STO-3G geometries.

The full set of uracil tautomers (1a–1f) has been examined by several methods. These results are summarized in Table V. The MINDO/3 method gives the diketo form of uracil (1a) as the most stable, followed by the 4-hydroxy form (1b) (Czerminski *et al.*, 1979a). The STO-3G and MNDO methods favor the dihydroxy (1c) as most stable (Goddard *et al.*, 1975; Buda and Syguła, 1983). Apparently the stability of the fully conjugated ring is overemphasized by these methods. In the next to last column the 3-21G data are summarized. Here, the most stable isomer is the diketo form (1a), followed by the 2-hydroxy tautomer (1d). The tautomerization energy for (1a)/(1b) is given as 81.8 kJ mole⁻¹ (Scanlan and Hillier, 1983). In the same basis set another estimate of the relative energies of (1a) and (1b) is 82.3 kJ mole⁻¹ (Zielinski, 1983). The differences in these last two energies are due to the different gradient convergence criteria used.

TABLE V

RELATIVE ELECTRONIC ENERGIES OF THE URACIL TAUTOMERS (ALL QUANTITIES IN KILOJOULES PER MOLE)

Structure	MINDO/3 ^a	STO-3G ^b	MNDO ^c	3-21G ^d	Experimental estimate ^e
1a	0.0	62.89	35.9	0.0	0.0
1b	21.3	80.79	38.8	81.8	79 \pm 25
1c	55.6 ^e	0.0	0.0	101.1 ^e	92 \pm 40
1d	41.0	77.45 ^e	30.4	72.1	—
1e	58.2	118.9	77.4	109.3	—
1f	33.1 ^f	127.1	66.7	119.6 ^f	—

^a From Czerminski *et al.* (1979a). All structures optimized uracils.

^b From Goddard *et al.* (1975). All structures were thymines designed by analogy to similar known structures.

^c From Buda and Syguła (1983). All structures were optimized uracils.

^d From Scanlan and Hillier (1983). All structures were optimized uracils.

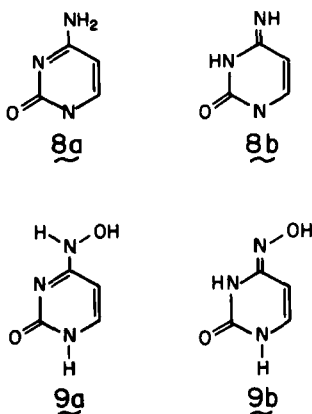
^e 2-Hydroxy group rotated by 180°.

^f 4-Hydroxy group rotated by 180°.

^g From Beak and White (1982).

Experimental estimates for the stability of 2,4-dihydroxyuracil and 4-hydroxyuracil relative to uracil have appeared in the literature (Beak and White, 1982). These are reported in the last column of Table V. As for the 2-hydroxy pyridine/pyridone case, the experimental estimate hinges on heats of isomerization and vaporization of representative methylated systems, namely, the *N*-methyl/*O*-methyl amide/imide pairs. For unstrained systems the amide is favored by 63 ± 12 kJ mole⁻¹, while for heteroaromatic ring systems it is favored by only 33 ± 12 kJ mole⁻¹. Studies on 1,3-dimethyl-2,4-pyrimidinedione, 2,4-dimethoxypyrimidine, 4-methoxy-1-methyl-2-pyrimidinone, and 2-methoxy-3-methyl-4-pyrimidine show that the amide/imide energy difference is quite different in these heteroaromatic systems. It was found that the energy of conversion of the methyl imide/amide for N₃ and C₄ of uracil is 113 kJ mole⁻¹. It is proposed that in this conversion, which involves the N₃ of the uracils, the N₃ is in a urea environment and that the urea/isourea energy difference is not adequately modeled by previously used imide/amide systems. The additive errors of the method are large but probably overestimated. The 3-21G predicted relative energies of uracil tautomers agree quite well with these experimental estimates. The 6-31G relative energy for (1a/1b) at the 3-21G geometry is 84.0 kJ mole⁻¹. If the methodology of Schlegel is used, then $\Delta(E_{A,B}^{(0)})$ for uracil/2-pyridone is 75.3 kJ mole⁻¹ at the 3-21G level. This energy should be within a few kilojoules of the best value of the relative tautomerization energy for these two systems as would be obtained with more extensive calculations including polarization functions and CI. When this relative value is combined with the experimental value for 2-pyridone (1.3 kJ mole⁻¹), 74.0 kJ mole is obtained for $U \rightleftharpoons U^*$. This is the best theoretical estimate for the (1a/1b) relative energies in close agreement with experiment.

The only other reported *ab initio* calculations at the HF level with full-geometry optimization are for the tautomers of cytosine (8a/8b) and *N*(4)-hydroxycytosine (9a/9b) (Kwiatkowski *et al.*, 1982; Palmer *et al.*, 1983). This study employed a (7s, 3p/3s) basis set of Gaussian functions contracted to a minimal basis set. There are also *ab initio* calculations on the HF level with partial-geometry optimization for 2-, 3-, and 4-oxypyridines (La Manna, 1981). All the other calculations for complicated systems such as purines and derivatives of pyridine and pyrimidines have been performed so far within the HF approximation, usually at the semiempirical level. For example, there also are MNDO calculations with geometry optimization for all tautomers of cytosine, adenine, and guanine (Buda and Syguła, 1983) and minimal basis set calculations with assumed geometries for cytosine, thymine, adenine, and guanine (Mezey and Ladik,



1979). These results should be treated with caution because of the limitations in both semiempirical and minimal basis set approaches.

In spite of the various difficulties and limitations, quantum-mechanical calculations may provide valuable information concerning the tautomeric equilibria of many molecules with similar structure, e.g., influence of substituents on tautomeric equilibria. It can be assumed that the errors in estimating the relative stabilities for a series of molecules with similar structures are of the same order. The results obtained for the amino and imino tautomers of cytosine (8a/8b) and *N*(4)-hydroxy cytosine (9a/9b) fall in this category.

In aqueous solutions $K_{8a/8b}$ is about 10^4 to 10^5 while $K_{9a/9b}$ is about 10^{-1} to 10^{-2} (Kwiatkowski and Pullman, 1975). This gives a value of 10^5 to 10^7 for the ratio $K_{8a/8b}/K_{9a/9b}$, which corresponds to a ΔG of about -29 to -40 kJ mole $^{-1}$. This can be compared (Kwiatkowski *et al.*, 1982; Palmer *et al.*, 1983) to the $\Delta(\delta E_{i,a}^{el}) = \delta E_{9i,a}^{el} - \delta E_{8i,a}^{el}$ values of -48 , -103 , and -56 kJ mole $^{-1}$ obtained by MINDO/3, MNDO, and *ab initio* HF/(7s, 3p/3s) methods with full-geometry optimization. The calculated changes in the relative total energies of the tautomers are qualitatively in good agreement with the large changes in the tautomeric equilibrium constant $K_{a,i}$ caused by $-\text{OH}$ substitution at the amino group of cytosine. In this respect it is interesting to note that an earlier CNDO/2 study (Kwiatkowski and Pullman, 1974) on cytosine and *N*(4)-hydroxycytosine tautomers, but without geometry optimization, yielded the result $\Delta(\delta E) = -58$ kJ mole $^{-1}$. It seems that in this instance the use of standardized geometric parameters rather than fully optimized geometries was adequate.

The *ab initio* structures for the two 4-amino-2-oxo tautomers (8a) and

(9a) are very slightly but significantly nonplanar. The external N4 and O2 atoms lie very close to the best ring plane. The N4 is slightly pyramidal with both hydrogens lying on the same side of the ring plane. The —OH group of (9a) is even further displaced from the best ring plane, 0.74 Å. Comparison of structure (8a) to (9a) and (8b) to (9b) shows that substitution of H by OH at the NH₂ or =NH group does not seriously change the bond lengths and angles of the parent rings except at the C4–N4 bond (Palmer *et al.*, 1983). This is as expected from the consideration of valence bond structures; a similar result was reported for the fluorobenzene radical and 2- and 4-monosubstituted pyridines (Hinde *et al.*, 1978; Del Bene, 1979).

In some cases, however, the results of theoretical studies seem to be less satisfactory. Zielinski (1982) reported HF/STO-3G calculations for both uracil (1a) and its 4-hydroxytautomeric form (1b) substituted by CH₃, F, and OCH₃ at the C5 position. The calculations were performed using the previously optimized HF/STO-3G geometries (Zielinski *et al.*, 1981) of the parent tautomeric forms (1a) and (1b) and standard geometries for the substituents. Calculated total energy indicated the diketo tautomeric forms [like (1a)] to be significantly more stable than the hydroxy forms [like (1b)] in each case. This result is consistent with experimental observations that do not detect the presence of hydroxy forms for 1-methyluracil and 1-methyl-5-fluorouracil in the vapor phase (Nowak *et al.*, 1978; Shugar and Szczepaniak, 1981). Numerous experimental studies in solution also show that uracil, 5-methyluracil (thymine), and 5-fluorouracil exist predominantly in the diketo form (Kwiatkowski and Pullman, 1975). On the other hand, the calculated relative changes in energy difference $\delta E_{1b,1a}^{\text{el}}$ between the 4-hydroxy form (1b) and diketo (1a) caused by 5-CH₃, 5-F, and 5-OCH₃ substitution seem to be in contradiction to expectation based on experimental evidence. The calculated value of $\delta E_{1b,1a}^{\text{el}} = 27.7 \text{ kJ mole}^{-1}$ increases by 0.6, 4.2, and 4.7 kJ mole⁻¹ upon 5-CH₃, 5-F, and 5-OCH₃ substitution, respectively. In other words, the calculations predict an increasing stability of the diketo form (1a) relative to the hydroxy form (1b) due to the substituents. This is contrary to experimental expectation for the effects of the substituents in question, which are postulated to increase the amount of the hydroxy forms (Kwiatkowski and Pullman, 1975).

The preceding discussion deserves some comment. First, the widely postulated mutagenesis induced by base analogs such as 5-halogeno-uracils has been questioned recently; some organisms readily tolerate, and replicate normally, when thymidine in DNA is replaced by 5-bromo-deoxyuridine (Shugar and Szczepaniak, 1981, and references therein).

Second, most of the experimental measurements have been done in solution, and as a matter of fact, for much more complicated systems (nucleosides, nucleotides) than those considered theoretically. Thus, there is a lack of appropriate experimental data on the relative stabilities of the tautomeric forms of the molecules in question. Finally, with respect to theoretical calculations, a definitive conclusion about the relative changes in the energy difference $\delta E_{\text{ib,1a}}^{\text{el}}$ caused by C5 substituents cannot be made owing to the lack of the full-geometry optimization for substituted uracils, neglect of the electron correlation, as well as neglect of the zero-point vibrational contributions. It seems that in order to be able to predict to what extent 5-substituted uracils exist in the hydroxy form relative to uracil itself, much more rigorous calculations similar to those performed by Schlegel (1983) for 2,4-dioxypyridine would be needed. This is also the conclusion of Zielinski (1982).

At the end of this section, it seems necessary to point out some misleading statements concerning the theoretical estimation of the relative energies of tautomers made in the past. Most of these calculations have been done without geometry optimization, i.e., using fixed geometries for the tautomers, and, of course, most using semiempirical methods. Under such conditions, the relative energy of two tautomers of a molecule not only differs from that calculated for optimal geometries, but can be of reversed sign [see Fig. 1: $^{(\text{CNDO}/2)}\delta E_{\text{A,B}}^{\text{el}}(Q_{\text{A}}, Q_{\text{B}})$, $^{(\text{CNDO}/2)}\delta E^{\text{el}(\text{eq})}$]. It is not unexpected then that the comparison of experimental and theoretical findings was found to be rather poor (Beak, 1977).

The most recent calculations seem to indicate some improvements in the theoretical evaluation of relative tautomer energies. At the 3-21G level the structures are accurate enough for higher-level calculations, which in turn clearly give better relative energies. Here the 6-31G** basis set shows the most promise. Another fact to consider is the almost uniform neglect to calculate $\Delta S_{\text{A,B}}^{\text{ovib}}$ and $\delta E_{\text{A,B}}^{\text{vib}(0)}$ even though the vibrational frequencies can be obtained with semiempirical methods. This makes the comparison of the calculated and experimental equilibrium constants even more difficult.

At this stage it is very difficult to systematically assess the agreement between predicted and experimentally obtained tautomeric equilibrium constants. In the cases of uracil and 2-pyridone the agreement between experiment and theory seems to narrow down to within one order of magnitude. Clearly, many more systems will have to be examined in order to make a more general statement. It should also be emphasized that more reliable comparisons are hampered to no lesser extent by experimental deficiency in the field than by deficiency in theory.

IV. Tautomeric Equilibrium in an Electronic Ground State of a Molecule Existing in Solution

It is well known that the information concerning experimental tautomeric equilibria for *N*-heterocyclic molecules is in most cases derived from measurements performed in solution and not in vapor (gas) phase. It was in the early 1970s when more systematic investigations on tautomeric equilibria in nonpolar solvents and particularly in the vapor phase were started together with some studies on the change of tautomeric equilibria caused by a change of environment (Beak *et al.*, 1980, and references therein). The latter studies are particularly important because of the possibility of verifying theoretical models describing the influence of environment on the shifts of the tautomeric equilibria.

An estimation of the absolute value of the tautomeric constant $K_{A,B}^{(s)}$ in solution [i.e., an estimation of $\Delta E_{A,B}^{(s)}$] by means of quantum-mechanical calculations is impossible due to practical considerations: a quantum-mechanical estimation of the $\Delta E_{A,B}^{(s)}$ value would require calculations of the potential surfaces for the tautomers interacting with all solvent molecules in the first two solvation shells at least.

An estimate of the relative change of the stabilities of tautomers caused by solvent prevents a less complicated problem. In practice it is necessary to calculate the interaction energies between tautomers and solvent and to compare the values of these energies. In calculations of this type it is usually assumed that the environment does not change the geometries of the tautomers and that the energy of the tautomer interacting with the solvent is estimated either classically or quantum mechanically.

If we denote the change of the ground state energies of the tautomers A and B when going from the vapor phase to solution (see Fig. 3) as $\delta\xi_A = E_A(S_0, s) - E_A(S_0, v)$ and $\delta\xi_B = E_B(S_0, s) - E_B(S_0, v)$, respectively, then the relative change of the energy caused by the environment will be $\Delta\xi_{A,B} = \delta\xi_B - \delta\xi_A$. A negative value of $\Delta\xi_{A,B}$ represents a stronger stabilization of form B by the solvent. Thus, the relation between the $\Delta E_{A,B}^{(s)}$ value for the ground state of tautomers in solution and the analogous quantity $\Delta E_{A,B}^{(v)}$ in the vapor phase (see point 2 on Scheme 2) can be formally presented as

$$\Delta E_{A,B}^{(s)} = \Delta E_{A,B}^{(v)} - \Delta\xi_{A,B}$$

If the information on the relative stability of the tautomers in a vapor phase is known (i.e., if the $\Delta E_{A,B}^{(v)}$ value is known from experimental measurement or from theoretical calculation), then a prediction of the

relative environmental effect on the stability of the tautomers is enough to estimate $\Delta E_{A,B}^{(s)}$.

An estimate of the influence of the environment on the relative stabilities of the tautomers and thus on the shifts of the tautomeric equilibria involves theoretical models describing the solvation phenomena for molecules. In spite of the progress made during the past few years in this field, the theoretical description of solvation of molecular systems is still handicapped by two main difficulties: the size of the molecules (particularly biomolecules) imposing the need for approximate methods and the lack of an unambiguous general theory describing the liquid state in general or liquid water in particular. Thus all "theoretical" results so far available must be treated with caution since the approximations of theoretical approaches are superimposed on the approximate models for the liquid state.

Traditional continuum, discrete, and mixed discrete-continuum models developed during the past few years have been reviewed in a number of papers (Bonaccorsi *et al.*, 1982; Claverie, 1982; Tapia, 1982). In spite of their obvious shortcomings, there is still hope that the models proposed so far may be suitable for describing, at least partially, some of the features of the solvation phenomena. We shall present an application of theoretical models of solvation to the estimation of the influence of the environment on the shift of the tautomeric equilibrium $A \rightleftharpoons B$. First, some comments on the models are given.

In continuum models, the solvent is considered as a homogeneous medium (structureless dielectric continuum), which is polarized by the solute molecule immersed in a solvent cavity. In this model, $\Delta\xi_{A,B}$ can be written as a sum of least three terms (Zielinski *et al.*, 1978; Sinanoglu, 1968):

$$\Delta\xi_{A,B} = \Delta\xi_{A,B}^{(cav)} + \Delta\xi_{A,B}^{(vdw)} + \Delta\xi_{A,B}^{(el)} \quad (7)$$

where $\Delta\xi_{A,B}^{(cav)}$ is the energy difference for both tautomers creating cavities within the solvent, $\Delta\xi_{A,B}^{(vdw)}$ is the difference in the van der Waals interaction energies between the tautomers embedded in the cavities and the surrounding solvent molecules, while $\Delta\xi_{A,B}^{(el)}$ is the difference in electrostatic interaction energies between the charge distributions of the tautomers and the solvent.

The several continuum models used to evaluate the terms given are, in fact, different versions of the classical reaction field theory introduced by Kirkwood (Kirkwood, 1934; Westheimer and Kirkwood, 1938) and Onsager (1936). The contributions of the first two terms $\Delta\xi_{A,B}^{(cav)}$ and $\Delta\xi_{A,B}^{(vdw)}$ to the $\Delta\xi_{A,B}$ value are small and partially compensate each other. Calcula-

tions carried out for the lactim and lactam hydroxyzine tautomers (Krebs *et al.*, 1982) have shown that the first term for (2a), (2b) and (5a), (5b) tautomers was $-(1.6-1.7)$ kJ mole $^{-1}$, while the second one for the same tautomers was of the order of $0.1-0.2$ kJ mole $^{-1}$. Therefore, these terms can be neglected. This is not unexpected, because these terms depend mainly on the cavity surfaces of the tautomers, which are only slightly different from each other in the case of two tautomers A and B of the same molecule. Thus, usually only the electrostatic contribution $\Delta\xi_{A,B}^{(el)}$ to the $\Delta\xi_{A,B}$ value is considered and compared with the experimentally determined value of $\Delta\xi_{A,B}$.

The continuum model has been applied to an experimental study of the solvent effect on the 6-chloro-2-hydroxypyridine/6-chloro-2-pyridone equilibrium in a variety of essentially non-hydrogen-bonding solvents (Beak *et al.*, 1980). In this study, a plot of $\log K_{t(NH/OH)}$ versus $(\epsilon - 1)/(2\epsilon + 1)$, the solvent dielectric term, yielded a linear least-squares fit with a slope of 2.5 ± 0.2 , an intercept of -1.71 , and a correlation coefficient of 0.9944 . This result was used to estimate the gas phase free-energy difference of 9.2 kJ mole $^{-1}$, which compares favorably with the observed value of 8.8 kJ mole $^{-1}$ for this system. The authors also reported that alcohol solvents are correlated fairly well in this study but that other solvents seem to be divided into two classes, those that are electron-pair donors and those that are electron-pair acceptors in a hydrogen bond. The hydrogen bonding effect is assumed to be independent from the reaction field effect and is included in the continuum model by means of the Kamlet and Taft (1976) empirical parameters. The interested reader is referred to the original paper for a detailed discussion of the method and its application.

An alternative to the continuum model is the discrete model. To estimate the influence of the aqueous environment on the tautomeric equilibrium $A \rightleftharpoons B$ within the discrete model, it is necessary first to find the structure of the hydration shell for each of the two tautomers and then to calculate and compare their hydration energies. While it is not easy to find the structures of the hydration shells with the methods of quantum chemistry, it can be done in two steps (Kwiatkowski and Szczodrowska, 1978).

Step 1. Find a monohydration sphere or a monohydration surface (limited only to the planes of the tautomers in the case of planar π -electron systems) for both the tautomers with a particular calculation method. This requires calculations (e.g., within the so-called "supermolecule" approach or with the use of electrostatic potentials) for the complex: tautomer plus water in different conformations. In other words, one must move the water molecule either in the space around the tautomer

(when considering the monohydration sphere) or in the plane of the tautomer (when considering the monohydration surface) and calculate the total energy (or interaction energy) at each point. A water molecule lying in the plane of the tautomer refers to the geometry of the complex for which the oxygen atom of the water molecule lies in the plane of the considered tautomer while the hydrogen atom may be out of the plane. If we choose the center of mass of the tautomer as a reference point, the monohydration sphere surrounding the tautomer is described as one for which a given point is determined by the position of the oxygen atom of water, the space configuration of water with respect to the tautomer, and the maximum value of interaction energy between the tautomer and the water molecule. The plane of the tautomer crossing the monohydration sphere determines the monohydration surface.

Step 2. The monohydration surface (in general a sphere) determined in step 1 is used for the construction of an approximate hydration or solvation shell (either in the plane of the tautomers or in space). The first water molecule is placed at the point of the global minimum of the monohydration surface (or sphere). This point corresponds to the maximum monohydration energy, i.e., to the most probable hydration site. The next water molecules are placed at points corresponding to additional local energy minima in the monohydration surface but in positions so as not to repel one another.

The hydration (polyhydration) energy may be presented in this case as

$$\delta\xi = \sum_i \xi^{h,i} + \sum_{k<l} \xi_{w-w}^{kl} \quad (8)$$

where $\xi^{h,i}$ is the monohydration energy of the tautomer by the water molecule placed at point i and ξ_{w-w}^{kl} is the interaction energy between the k th and l th water molecules of the shell [we do not consider here the method of estimating the water–water (w–w) interaction energy]. The difference

$$\Delta\xi_{A,B} = \delta\xi_B - \delta\xi_A \quad (9)$$

for the tautomers A and B determines the relative polyhydration effect (i.e., the influence of an aqueous solvent on the shift of the tautomeric equilibrium $A \rightleftharpoons B$ when going from a vapor phase to the solution).

The most-favored positions and orientations of water molecules around a solute can be determined by the use of electrostatic potentials. The electrostatic potential, evaluated from some molecular orbital wave function, is used to estimate the electrostatic interaction energy $\xi^{(el)}$ be-

tween the solute and a dipole simulating a water molecule (Hofmann *et al.*, 1981; Berndt and Kwiatkowski, 1978). Positions on a surface around the solute molecule that correspond to minimum values of $\xi^{(el)}$ are considered as the best monohydration sites. When applying the electrostatic approach to estimating the interaction energy of a tautomer with water, we cannot determine the components of the tautomer–water complex. It is necessary to construct an approximate shell by assuming a distance between the oxygen atom of the water molecules and the nitrogen (or oxygen) atoms of the tautomers to be equal to 2.8 to 2.9 Å [this distance is predicted by the *ab initio* SCF-MO calculations for the hydrogen bond in the *N*-heterocyclic molecule plus water molecule complex (Schuster, 1969 and 1976)]. Water molecules are placed on this predetermined contour and allowed to move along it, changing their orientation with respect to the tautomers at each point to obtain the lowest energy for that point. The electrostatic contribution to the interaction energy is calculated for each position and configuration, yielding the global minimum and local minima of the monohydration shell. The water molecules are then placed at the calculated minima at reasonable relative distances and the influence of aqueous solvent on the change of the tautomeric equilibrium is estimated from Eqs. (8) and (9).

Evaluation of $\Delta\xi_{A,B}^{(el)}$ by this method has been applied to the 2-pyridone and 4-pyridone tautomers systems using CNDO/2 wave functions. Three hydration sites were found for both 2-hydroxypyridine and 2-pyridone, yielding a net difference of 20 kJ mole⁻¹ in favor of 2-pyridone. Three hydration sites were found for both 4-hydroxypyridine and 4-pyridone, resulting in $\Delta\xi_{A,B}^{(el)} = 17.2$ kJ mole⁻¹. The preferred hydration sites determined by this method are in complete agreement with those obtained by the supermolecule and OMTP methods (see Table VI).

The overlap multipole procedure (OMTP), another approach to calculating the electrostatic interactions among molecules, utilizes a multipole expansion of *ab initio* wave functions for each of the interacting components. In this method, to determine the optimum positions for water around the solute (Kwiatkowski *et al.*, 1978; Pullman and Perahia, 1978; Goldblum *et al.*, 1978) one water molecule is moved around the solute along a predetermined grid that fixes the water oxygen relative to the solute. At each point the H₂O is rotated about its three local axes to find the best orientation. Positions with minimum ξ^{el} are the desired sites of hydration. Water molecules are then placed at each of these sites of hydration and the position of each one is cyclically optimized in the presence of all other water molecules until the computed total interaction energy does not change significantly. This method also has been applied

TABLE VI

DISCRETE MODEL RELATIVE POLYHYDRATION ENERGIES $\Delta\xi_{A,B}$ (IN KILOJOULES PER MOLE) FOR 2- AND 4-OXOPYRIDINES^a

	2-Oxopyridine	4-Oxopyridine
Supermolecule Model		
CNDO/2		
Kwiatkowski and Szczodrowska (1978)	29 15 ^b	33
Electrostatic Model		
OMTP, <i>ab initio</i> SCF MO		
Kwiatkowski <i>et al.</i> (1978)	11–41 ^c	5.4–9.6 ^c
Kwiatkowski (1980)	11 ^d	17
Point dipole, CNDO/2		
Berndt and Kwiatkowski (1978)	13	13
<i>n</i> PD-MEP, CNDO/2 ^e		
Hofmann <i>et al.</i> (1981) ^f	48.5 (19.7)	17.2
Tempczyk (1983)	20.5	20.5
<i>n</i> PD-MEP, CNDO/S CI		
Tempczyk (1983)	27.6	17.6
Monte Carlo Simulation		
Danilov <i>et al.</i> (1981)	20–30	
Corongiu <i>et al.</i> (1979)		6.3
La Manna and Venuti (1982)	27	
Experimental		
Beak <i>et al.</i> (1976)	19.6	≥29.7

^a In this table positive $\Delta\xi_{A,B}$ indicates a stronger stabilization of the lactam (B) by the solvent.

^b Calculation of $\Delta\xi_{A,B}$ carried out with a radius of hydration $r = 2.85$ Å.

^c The value for the polyhydration energy depends on the number of waters of hydration included.

^d Only two water molecules were used.

^e *n*-Point dipoles—molecular electrostatic potential method.

^f In this reference the value of $\Delta\xi_{A,B}$ is incorrectly estimated. The authors consider three water molecules around the lactam tautomer and only two waters for the lactam. The water–water interactions were also omitted from consideration. The correct value of $\Delta\xi_{A,B}$ is given by us in parentheses.

to the determination of the hydration scheme of 2- and 4-hydroxypyridine tautomers (Kwiatkowski *et al.*, 1978). A 3.0-Å minimum approach of the water oxygen to the pyridine-type nitrogens and a 2.85-Å minimum approach of the oxygen to other heavy atoms of the pyridines was maintained in order to avoid false zones of apparent stability due to the neglect of the exchange repulsion (Goldblum *et al.*, 1978).

When estimating the polyhydration energy of the tautomer, one can also perform supermolecule calculations. In this model

$$\delta\xi = E(t + n \text{ H}_2\text{O}) - (E(t) + nE(\text{H}_2\text{O})) \quad (10)$$

where the first term of the difference indicates the total energy value of the complex (supermolecule) consisting of the tautomer (t) and n water molecules, while $E(t)$ and $E(\text{H}_2\text{O})$ are the total energies of the isolated tautomer and water molecules, respectively. The exact positions of the water molecules in the hydration shell are determined by minimizing the total energy of the complex with respect to the relative water positions. Then the polyhydration energy of the exact shell for each tautomer is calculated according to the formula

$$\delta\xi = E_{\min}(t + n \text{ H}_2\text{O}) - (E(t) + nE(\text{H}_2\text{O})) \quad (11)$$

and the relative influence of the aqueous medium on the shift of the tautomeric equilibrium is estimated from relation (9).

There are many practical considerations surrounding the method described. Of these approaches to evaluating the hydration shell the supermolecule calculations are the most time-consuming. Hydration shells determined from electrostatic potentials or by use of the OMTP procedure yield the same most-favored hydration sites (Hofmann *et al.*, 1981; Kwiatkowski *et al.*, 1978; Berndt and Kwiatkowski, 1978) with considerable savings in computation. Polyhydration sites determined by these two electrostatic potential approaches probably offer the most economical preparation for supermolecule calculations of the polyhydration energy. Also, in the case of planar π -electron systems, one usually considers only the water molecules placed in the hydration surface because the interaction energy between the tautomer and the water molecule is much larger when the water lies in the plane of the tautomers than when it is located out of the plane (Kwiatkowski *et al.*, 1978; Kwiatkowski, 1980). Finally, since the tautomeric rearrangement induces structural changes only in part of the molecule, it is necessary to determine the hydration shell in only that part of the molecule immediately involved in the tautomeric rearrangement as in Scheme 3.

The Monte Carlo method can also be used to study the effect of solvent on the position of tautomeric equilibrium (Metropolis *et al.*, 1953). This method models a dilute solution as N solvent molecules ($N \approx 10^2$) and 1 solute molecule. The fundamental requirement for a Monte Carlo simulation of tautomer solvation is a set of pair potentials for the solvent-solvent and solvent-solute interactions because approximately 10^6 config-



Scheme 3

urations of water molecules are randomly chosen and weighted by using the Boltzmann factor. A suitable potential for water-solute interactions has been developed by Clementi and co-workers (Clementi *et al.*, 1977; Scordamaglia *et al.*, 1977; Bolis and Clementi, 1977):

$$E = \sum_i \sum_{j \neq i} \left(-\frac{A_{ij}^{ab}}{r_{ij}^6} + \frac{B_{ij}^{ab}}{r_{ij}^{12}} + \frac{C_{ij}^{ab}}{r_{ij}} \right) + E(\text{solute}) + E(\text{water})$$

for i solute atoms and j water atoms. The various electronic environments in the solute are distinguished by the index a , while b distinguishes between the hydrogens and oxygen in water. The constants A , B , and C were fitted using *ab initio* methods; $E(\text{solute})$ and $E(\text{water})$ are the *ab initio* total energies of the solute and water molecules, respectively, at infinite separation.

Forty-nine classes describing the H, C, N, O, and S atoms in different molecules interacting with water have been developed. These classes can be transferred to other molecules, provided that each atom in the solute and its nearest neighbors have previously been studied (Bolis and Clementi, 1977). Net charge and molecular orbital valency state energy are used to assign atoms with the same atomic number to different classes (Carozzo *et al.*, 1978; Corongiu *et al.*, 1979).

Water-water interactions can be evaluated by using the potential function of Matsuoka *et al.* (Matsuoka *et al.*, 1976) when the oxygen atoms are less than 3 Å apart. At larger separations a simpler potential function may be used (Owicki and Sheraga, 1977).

Results obtained using the various discrete models applied to 2- and 4-oxypyridines are summarized in Table VI. Similar data for continuum models are summarized in Table VII. All methods used to estimate the effect of solvent on the position of these tautomeric equilibria are qualitatively correct in that they all show greater stabilization of the lactam form in agreement with experiment. Quantitatively the various discrete models yield a disappointing array of results. For 2-oxypyridine several methods yield relative polyhydration energies close to the experimental value but then predict the same or lower relative polyhydration energy for the 4-oxypyridine system, a direction opposite to that found experimentally.

TABLE VII

CONTINUUM MODEL RELATIVE POLYHYDRATION ENERGIES $\Delta\xi_{A,B}$ (IN KILOJOULES PER MOLE) FOR 2- AND 4-OXOPYRIDINE ACCORDING TO KREBS *et al.* (1982)^a

	2-Oxopyridine	4-Oxopyridine
Theoretical Method		
Solvaton model		
Classical ^b	63.4	64.9
Quantum mechanical ^c	97.9	98.6
Reaction-field model		
Classical ^d	22.9	52.0
Quantum mechanical ^e	27.0	61.7
Experimental Values		
Beak <i>et al.</i> (1976)	19.6	29.7
Krebs <i>et al.</i> (1982)	20.3	50.3 ^f

^a Here positive value indicates a stronger stabilization of the lactam (B) tautomer by the solvent.

^b Classical electrostatic calculation of solvatons interacting with the charge distribution of a molecule (Klopman, 1967).

^c Solvaton interaction with the electrons and cores of a molecule included in the Hamiltonian.

^d Electrostatic interaction energy calculated classically (Birnstock *et al.*, 1976).

^e The reaction field introduced into the Hamiltonian.

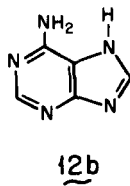
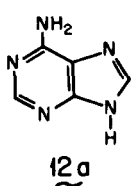
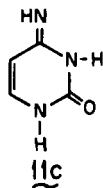
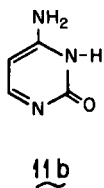
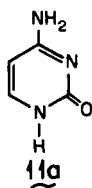
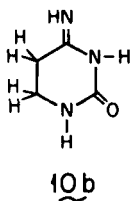
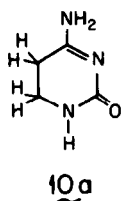
^f Calculated using the assumption that $\Delta S = -4 \text{ J mole}^{-1} \text{ K}^{-1}$.

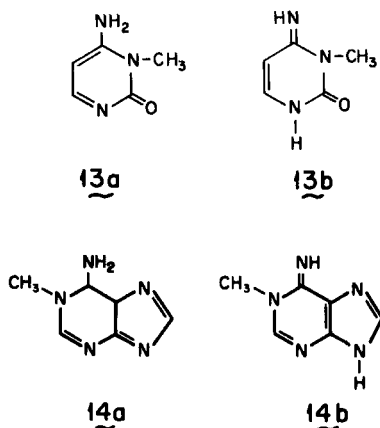
The results in Table VII are not much better. The solvation model, both classical and quantum mechanical, overestimates the solvation energy by a factor of 2 to 5 and does not distinguish between the polyhydration energy for 2- and 4-oxopyridine. In contrast to this both the classical and quantum-mechanical reaction-field results are close to the experimental values, especially when the entropy effect is included in the 4-oxopyridine experimental value.

An improved form of the reaction-field model (Huron and Claverie, 1974; Claverie *et al.*, 1978) has been used to study various tautomers of cytosine and adenine in solution (Bartzsch *et al.*, 1984) using NDDO relative energies for MINDO/3 optimized structures under the assumption that in the gas phase $\Delta G^{(v)} = \delta E_{A,B}^{\text{el}}$ and that in solution $\Delta G^{(s)} = \delta E_{A,B}^{\text{el}} + \Delta G_{\text{solvation}}$. In this way, the imino form of 5,6-dihydrocytosine is found to be predominant in nonpolar solvents with the equilibrium shifting to favor the amino form in aqueous solution. The experimental change in free energy when transferring from chloroform to water solvent is 13.7 kJ

mole⁻¹, which can be compared to the calculated value of 6.8 kJ mole⁻¹. Qualitatively similar results were obtained for the detectable tautomers of cytosine (11a–11c). The calculated energy differences in water are $\Delta G_{(11b,11a)} = 31.7$ kJ mole⁻¹ and $\Delta G_{(11c,11a)} = 53.7$ kJ mole⁻¹, while the corresponding experimental values are 14.9 and 27.0 kJ mole⁻¹, respectively (Dreyfus *et al.*, 1976). Likewise, for the two important tautomers of adenine (12a, 12b), the measured $\Delta G = 3.2$ kJ mole⁻¹ in aqueous solution (Dreyfus *et al.*, 1975) can be compared to the calculated value, $\Delta G = 9.4$ kJ mole⁻¹. Better agreement with experiment is obtained for the amino and imino forms of 3-methylcytosine (13a and 13b). The calculated and experimental (Dreyfus *et al.*, 1976) relative energies $\Delta G_{(13b,13a)}$ in aqueous solution are 5.6 and 8.7 kJ mole⁻¹, respectively. Similarly, for the amino and imino forms of 1-methyladenine (14a and 14b), the calculated and experimental (Dreyfus *et al.*, 1977) relative energies in aqueous solution are 10.4 and 11.5 kJ mole⁻¹, respectively.

These results obtained by Bartzsch *et al.* (1984) show in most cases only qualitative agreement with experimental relative tautomer energies in solution in that the calculated values exceed the experimental ones by up to a factor of 3. In the 1-methyladenine the good agreement between





theory and experiment is encouraging. Of course, those results must be viewed cautiously because of the less rigorous calculation of the relative energies of the tautomer in the gas phase. The NDDO method probably suffers from the same limitations found for other semiempirical methods and some *ab initio* methods, namely, an overestimation of the stability of aromatic rings. Clearly, much more work is needed for accurate prediction of tautomeric equilibria in solution.

V. Tautomeric Equilibrium in an Excited Electronic State of a Molecule Existing in the Vapor Phase and in Solution

The difference between the lowest energies of the corresponding excited state of both tautomers in the vapor phase (point 3 on Scheme 2) is equal to (see Figs. 2 and 3)

$$\Delta E_{A,B}^{(v)}(*) = \Delta E_{A,B}^{(v)} + hc(\bar{\nu}_A(v) - \bar{\nu}_B(v))$$

where the last term corresponds to the difference between O—O (or at least maximum) absorption band positions of both tautomers in the vapor phase. This term characterizes the change of $\Delta E_{A,B}^{(v)}$ caused by electronic excitation. Thus, an estimate of the relative stability of the tautomers in an excited state can be experimentally obtained by measuring the absorption band positions for both tautomers if their relative stability in the ground state is already known. This is, of course, also true for the theoretical $\Delta E_{A,B}^{(v)}(*)$ value.

Quantum-mechanical estimation of $\Delta E_{A,B}^{(v)}$ according to the relation given in the preceding is difficult due to problems associated both with the

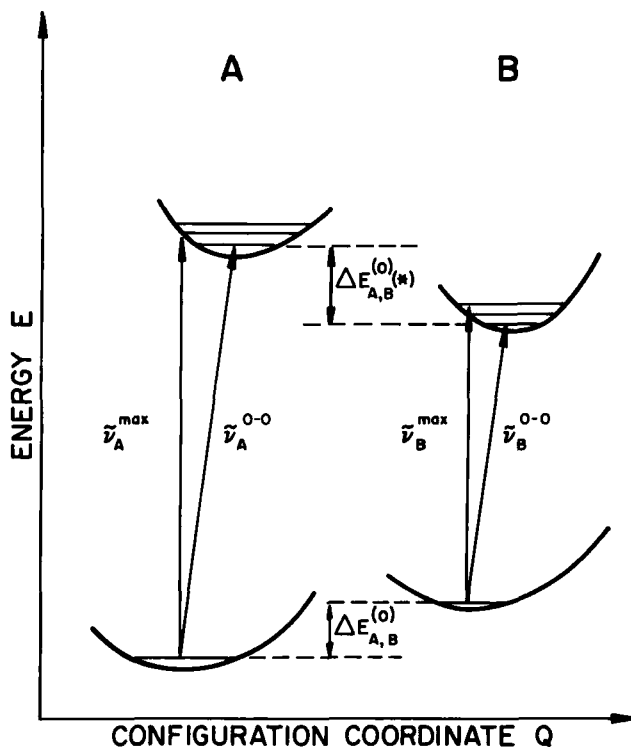


Fig. 2. Schematic representation of the potential energy surfaces for the electronic ground state and excited states of a molecule existing in two tautomeric forms A and B. The relationship between the quantities characterizing the tautomeric equilibrium in a ground state and an excited state is $\Delta E_{A,B}^{(0)(*)} = \Delta E_{A,B}^{(0)} + hc(\bar{\nu}_A^{0-0} - \bar{\nu}_B^{0-0}) \approx \Delta E_{A,B}^{(0)} + hc(\bar{\nu}_A^{\max} - \bar{\nu}_B^{\max})$.

prediction of the relative stability of the tautomers in their ground states as discussed in Section III and with the quantum-mechanical treatment of the transition energies of molecules. There are two main sources of uncertainty connected with the prediction of transition energies. The first is due to the fundamental relationship between theoretical calculation and electronic absorption spectra. The calculated transition energies, of course, do not correspond to the O–O transition energies, but they are usually compared to maximum band positions (Franck–Condon transitions); this is not quite true (Trogler, 1981). It is difficult to estimate the magnitude of the various energy corrections that can amount to uncertainties when comparing the calculated transition energies with the experimental maximum band positions; in the case of transition metal complexes this uncertainty can be of the order of 1000 cm^{-1} ($0.01 \text{ kJ mole}^{-1}$) (Trogler, 1981). These small errors can be neglected when comparing two tautomeric

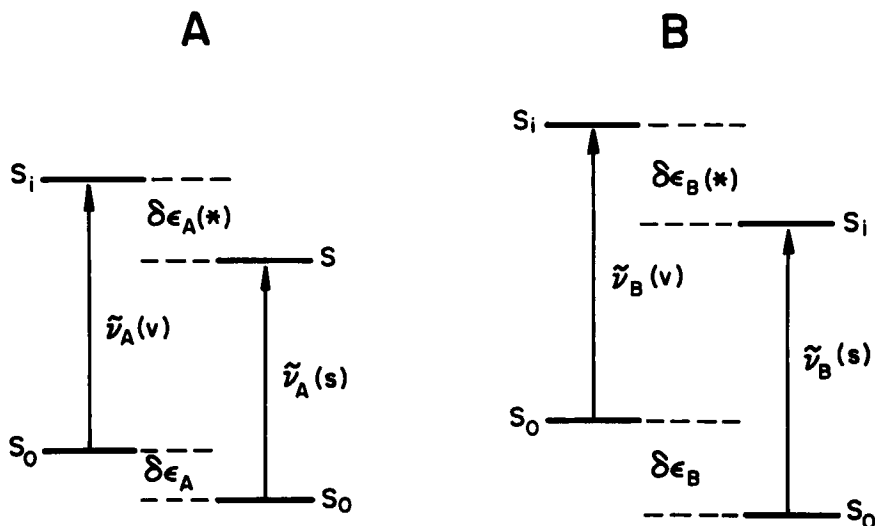


Fig. 3. Schematic representation of the energetic changes of the ground state S_0 and i th excited state S_i of tautomers A and B on going from vapor phase (v) to solution (s).

forms of a molecule, particularly when the larger uncertainties connected with approximations involved in the quantum-mechanical methods used for calculating transition energies are considered. For the complex molecular systems considered here, the calculations of the transition energies have been performed so far only by means of semiempirical methods (*ab initio* calculations have been performed in some cases; however, they are not interesting from the point of view of tautomeric rearrangement). Usually various versions of the π -SCF MO CI method (Parr, 1972) or all-valence electron SCF MO CI approach such as the CNDO/S CI (Del Bene and Jaffe, 1968) have been used to calculate the transition energies of π -electronic planar compounds. It can be stated that the transition energies are predicted by π -SCF MO CI methods with an accuracy of 0.1 to 0.2 eV (± 9.6 kJ mole⁻¹) compared to experimental data. Calculation of the $n \rightarrow \pi^*$ and $\pi \rightarrow \pi^*$ transition energies by the methods including all-valence electrons gives in general poorer results.

It is also worth noting that calculations of transition energies have been in most cases carried out for one form of a molecule without regard for the possible existence of different tautomeric forms. For instance, most calculations of transition energies for nucleic acid bases have been performed for the most stable forms of the compounds (Kwiatkowski and Pullman, 1975; Callis, 1983). Some time ago, the π -SCF MO CI calculations of transition energies were carried out for different tautomeric forms

of *N*-heterocyclic compounds substituted by simple donor groups such as OH, SH, and NH₂ (calculations involving the nucleic acid bases) (Kwiatkowski and Pullman, 1975, and references therein; Kwiatkowski and Lesyng, 1979). In general, the calculations correctly predict the differences in absorption spectra for tautomeric forms of molecules. However, while the relatively good agreement between experimental data and predicted transition energies of the lactim, thiol, or amino forms have been obtained (forms A on Scheme 1), the discrepancy between calculated and experimental absorption band positions for the lactam, thione, or imine forms (forms B on Scheme 1) were greater. Thus, the discrepancies between predicted and measured absorption band position of two tautomeric forms A and B of the same molecules are not of the same order. The same conclusion seems to be valid for the all-valence electron SCF MO CI calculations (Morita *et al.*, 1981, 1982). Since calculations of this type are rather rare, it is difficult to draw any general conclusion at this time. Anyway, it can be said that the calculation of $\tilde{\nu}_A^{\max}(\nu) - \tilde{\nu}_B^{\max}(\nu)$ involves an error, the amount of which is difficult to estimate, and additional uncertainty is introduced with the substitution of $\tilde{\nu}_A^{O-O}(\nu) - \tilde{\nu}_B^{O-O}(\nu)$ by $\tilde{\nu}_A^{\max}(\nu) - \tilde{\nu}_B^{\max}(\nu)$.

Although the calculations of the transition energies of different tautomeric forms of molecules have been performed in a few cases, the discussion has been restricted to the difference in electronic absorption band positions and not to the change in relative stabilities of the tautomers caused by electronic excitation. The latter problem, however, has been the subject of a few theoretical considerations for nucleic acid base pairs. Most of these studies were motivated by the need for a potential function for double proton transfer between nucleic acid bases that would allow calculation of proton tunneling probabilities for the Lowdin model of mutagenesis (Lowdin, 1965).

A series of studies on the effect of electronic state on proton transfer reactions has been carried on by Julio Maranon and Oscar M. Sorarrain with the CNDO/S-CI method. Their conclusion was that for guanine, cytosine, adenine, and thymine proton tunneling from one position on the base to another position on the base is negligible in the ground state but large enough in some excited states to warrant further investigation (Maranon and Sorarrain, 1978, 1979). These studies were extended to consider the double proton transfer between adenine and thymine to form the A*-T* tautomer pair by using the CNDO/S-CI approximation. They report that the normal Watson-Crick A-T base pair is the most stable of all the excited states studied and that increasing the energy of the excited states would increase the probability of double proton transfer by the tunnel effect (Grinberg *et al.*, 1981; Maranon *et al.*, 1982).

Phototautomerism in G, C, and G-C base pairs was also examined by Srivastava and Mishra (1981), who used the VE-PPP molecular orbital method. They conclude that C* cannot phototautomerize utilizing the first two singlet $\pi-\pi^*$ excitations, while for G* the first, third, and higher $\pi-\pi^*$ singlet transitions will allow phototautomerism to a greater extent than in the ground state. For the biprotonic transition from G-C to G*-C* the differences in total energies of the lowest purine localized or charge transfer transitions are less in these excited states than in the ground state by 39 and 23 kJ mole⁻¹, respectively. By combining these results with those of Abdunur (1976) and Rein and Harris (1964), they estimate an increase in the rate of tautomerization due to excitation by a factor of 10 to 10³. It is difficult to assess the significance of these results since the authors themselves point out that only the qualitative aspect of their work may be reliable. This caution must be doubly stressed when the quality of the molecular orbital methods used is considered; the same thing can be said for the earlier CNDO/2 studies of Bertran *et al.* (1970). These authors reported that the tautomeric equilibrium constant is increased in the first excited singlet and triplet states of adenine, in the first excited singlet state of uracil and thymine, and in the first excited triplet state of cytosine. More recently, the same system was examined with a modified INDO scheme including consideration of the effect of Mg²⁺ ions on the G-C double proton transfer (DPT) (Lipinski and Gorzkowska, 1983). They conclude that in the ground state a divalent cation at N7 of G in the G-C dimer reduces the probability of DPT and that in some locally excited $\pi-\pi^*$ states the same cation increases the probability of DPT. Considering the biological significance of the DPT process and the complexity of the problem, when dealing with nucleic acid base pairs, it must be understood that more accurate calculations will be needed to determine DPT probabilities in the ground state and excited states (Agresti and Ranfagni, 1981).

Some experimental evidence for a DPT process in the excited state leading to tautomerization not observed in the ground state has been reported (Chang *et al.*, 1980; Sepiol and Wild, 1982) for solutions of 1-azacarbazole in 3-methylpentane and mixed 1-azacarbazole/7-azaindol solutions in the same solvent. For these systems the tautomeric forms that are unstable in the ground state are formed adiabatically from the excited state hydrogen-bonded dimers via a DPT and detected in the fluorescence spectra. These results are especially relevant to excited state DPT processes possible for nucleic acid base pairs. Clearly, further experimental and theoretical studies on heterocyclic dimer systems are needed.

This leads us to a consideration of the difference between the energies of the corresponding excited states of two tautomers in solution (point 4

on Scheme 2) that can formally be expressed by the energy difference for ground states of the tautomers (point 1 on Scheme 2) and some additional terms characterizing the change of this energy difference on excitation and/or on the change of environment as follows (see Figs. 2 and 3):

$$\begin{aligned}\Delta E_{A,B}^{(s)}(*) &= \Delta E_{A,B}^{(s)} + hc(\bar{\nu}_A(s) - \bar{\nu}_B(s)) \\ &= \Delta E_{A,B}^{(v)}(*) - \{\Delta\xi_{A,B} + hc(\Delta\bar{\nu}_A - \Delta\bar{\nu}_B)\} \\ &= \Delta E_{A,B}^{(v)}(*) - \Delta\xi_{A,B}(*)\end{aligned}$$

Here the difference in solvation energy of two tautomers in their excited state is defined as $\Delta\xi_{A,B}(*) = \Delta\xi_{A,B} + hc(\Delta\bar{\nu}_A - \Delta\bar{\nu}_B)$, where $\Delta\bar{\nu} = \bar{\nu}(v) - \bar{\nu}(s)$ indicates the shift of the O—O (or maximum) absorption band positions of the tautomers on going from vapor phase to solution.

As can be seen from Scheme 2, an estimation of the relative stability of the tautomers in their corresponding excited state when a molecule exists in solution can be made in two independent ways: (1) through estimation of the change of $\Delta E_{A,B}^{(v)}(*)$ value upon solvation (transition 3 \rightarrow 4) or (2) through estimation of the change of $\Delta E_{A,B}^{(s)}$ value on excitation (transition 2 \rightarrow 4). In both cases the estimation of the stability of the tautomers is done by calculation of the $\Delta\xi_{A,B}(*)$ value. In the second case, transition 2 \rightarrow 4 calculations are performed for transition energies of isolated tautomers (in the vapor phase) and for tautomers existing in solution because

$$\Delta E_{A,B}^{(v)} + hc(\bar{\nu}_A(v) - \bar{\nu}_B(v)) - \{\Delta E_{A,B}^{(s)} + hc(\bar{\nu}_A(s) - \bar{\nu}_B(s))\} = \Delta\xi_{A,B}(*)$$

Two independent quantum-mechanical models have been proposed to realize the estimation of the $\Delta\xi_{A,B}(*)$ value in two ways mentioned here (Tempczyk, 1983; Kwiatkowski and Tempczyk, 1984). One of the models (n PD-MEP model) has been used to estimate relative environmental effect on the stability of the tautomers in a given excited electronic state (transition 3 \rightarrow 4). In this model, the solvent molecule is approximated by a point dipole \mathbf{u} (PD), while the tautomer (solute molecule) is represented by the corresponding molecular electrostatic potential (MEP). Based on the MEP values in a given excited state of the tautomer, the electrostatic interaction energy $E^{(es)}$ between a tautomer and a point dipole \mathbf{u} simulating the solvent molecule has been calculated by means of the formula $E^{(es)}(\mathbf{r}) = -\mathbf{u} \cdot \nabla V(\mathbf{r})$, where $V(\mathbf{r})$ is the MEP value at the position \mathbf{r} . In a practical realization of the approach, the CNDO/S CI wave function has been used to calculate the MEP values in the ground state as well as in excited states of the tautomers. For consideration of the effect of aqueous medium on tautomeric equilibrium, the water molecule was simulated by a point dipole with $|\mathbf{u}|$ value equal to 1.85 Debye units. As suggested previously (Section IV), hydration surfaces around the tautomers using a

radius of 2.85 Å around each heavy atom were calculated. Comparison of the stabilization energies of the polyhydrated tautomers in their excited states determines the trend of the influence of water solvent on the tautomeric equilibrium in excited state of the molecule. The second model (*n* P-DQ model) has been used to estimate the influence of electronic excitation on the change of the relative stability of tautomers in solution (transition 2 → 4). In the first step, transition energies were calculated for the isolated tautomers (vapor phase) and in the second step for the tautomers in solution. In the second step, the same semiempirical method (CNDO/S CI) is used with the modification whereby the solvent (water) is simulated by a set of *n* point dipoles and quadrupoles. In this treatment, the solvent modifies the solute Hamiltonian via an electrostatic interaction contribution (the multipole expansion for the potential due to the solvent is used and additional terms describing electronic charge-dipole, nuclei charge-dipole, electronic charge-quadrupole, and nuclei charge-quadrupole are explicitly considered in the Hamiltonian prior to the SCF procedure).

Both models mentioned have been used to investigate the simultaneous influence of electronic excitation and solvation (hydration) on the tautomeric equilibrium in the first two excited states of 2- and 4-oxopyridine tautomers (2a), (2b) and (3a), (3b). The relative stabilization energies $\Delta\xi_{A,B}^*$ in the first two excited electronic states of the tautomers in question are given with the available experimental data in Table VIII. Comparison with experimental data can only be done for the second excited state (the appropriate experimental data for the first $n \rightarrow \pi^*$ state are not available). In the case of 2-oxopyridine the value of $\Delta\xi_{2a,2b}^*$ is estimated to be equal to $-(5.4-11.7)$ kJ mole⁻¹ from shifts of the absorption bands of the lactim and lactam tautomers of 2-oxopyridine and the

TABLE VIII

RELATIVE STABILIZATION ENERGIES $\Delta\xi_{A,B}^*$ IN EXCITED STATE
OF A MOLECULE CAUSED BY SOLVATION (ALL VALUES IN
KILOJOULES PER MOLE)

Electronic state	<i>n</i> PD-MEP model	<i>n</i> P-DQ model	Experimental ^a
2-Oxopyridine Tautomers			
S ₁ (<i>n</i> , π^*)	+13.7	+61.7	
S ₂ (π , π^*)	-13.0	- 5.3	-(5.4 - 11.7)
4-Oxopyridine Tautomers			
S ₁ (<i>n</i> , π^*)	+15.5	+60.4	
S ₂ (π , π^*)	+13.0	+ 5.0	+(0.7 - 2.8)

^a For details see the text.

model systems (1-methyl-2-pyridinone and 2-methoxypyridine) on going from vapor phase to water solution and including the difference between stabilization energies of both tautomers in their ground states caused by solvation energies ($\Delta\xi_{2a,2b} = -(16.7-18.8)$ kJ mole⁻¹). The predicted values of $\Delta\xi_{2a,2b}^*$ by means of both models agree qualitatively with the experimental data. It is worth noting that both models predict stronger stabilization of the lactim form of 2-oxopyridine in $S_1(n, \pi^*)$ state and stronger stabilization of the lactam form in $S_2(\pi, \pi^*)$ state. On the other hand, the behavior of the first triplet (π, π^*) state is different from that of the first singlet (π, π^*) state. Specifically, the phosphorescence study by Sakurai and Inoue (1981) indicates a strong shift of tautomeric equilibrium in the triplet (π, π^*) state of 2-oxopyridine 1-oxide towards the lactim form.

In the case of 4-oxopyridine, the comparison of theoretical results with experimental data is somewhat more difficult than for the case of 2-oxopyridine (due to problems in assignment of absorption bands of the lactam tautomer of 4-oxopyridine). Two values of $\Delta\xi_{3a,3b}^*$ for the $S_2(\pi, \pi^*)$ state of 4-oxopyridine have been suggested: (a) $-(25.3-27.4)$ kJ mole⁻¹ when the change of the sequence of $S_2(\pi, \pi^*)$ and $S_4(\pi, \pi^*)$ states on going from vapor phase to water solution is not considered; and (b) $+(0.7-2.8)$ kJ mole⁻¹ when one includes the change of the sequence of both excited states on solvation. In both estimates of $\Delta\xi_{3a,3b}^*$ the difference between stabilization energies of the lactim and lactam tautomers of 4-oxopyridine in their ground states caused by solvation, $\Delta\xi_{3a,3b} = -(20-25)$ kJ mole⁻¹, has been included. Thus, it was concluded that the values of $\Delta\xi_{3a,3b}^*$ predicted by means of both models are in qualitative agreement with the experimental value estimated only on assumption of the change of the sequence of the excited states caused by aqueous medium.

Although the proposed estimate of the change of the relative stability of tautomers in their excited state caused by solvation should not be used in a quantitative way because of the numerous uncertainties involved in the approximate models, qualitatively it appears to account correctly for the general trend of both electronic excitation and solvation effects on the tautomeric equilibrium of a molecule.

VI. Role of Tautomers in Mutation Theory

Since the proposal of the double helical structure of DNA, it has been recognized that the fidelity of replication of genetic information depends on the hydrogen bonding interaction between the purine and pyrimidine bases of DNA, i.e., the cytosine-guanine and thymine-adenine complementarity. The importance of hydrogen bonds for fidelity depends on two

factors: first, the electronic complementarity of the bases and, second, the geometric invariance of the glycosidic bond distance, 10.7 Å. Nevertheless, both in experimental and theoretical studies, it was shown that there are many alternative hydrogen bonding possibilities between the base pairs. These, however, do not satisfy the aforementioned geometric invariance.

From biological data, it has been recognized that the fidelity of copying is very high, or the error rate during replication, is very low. Errors occur in only about 1 out of 10^9 base pairs (Fowler *et al.*, 1974). This copying fidelity involves at least three different molecular discrimination steps. The first of these is at the template base, and it is assumed to be governed by the free-energy difference between correct and incorrect base pairing (Goodman *et al.*, 1980). Proofreading and postreplicative repair constitute the second and third steps. Thermodynamically, the first of these steps, misinsertion frequency, can be evaluated by examining the stability differences that may arise from different types of hydrogen bonding and backbone deformations.

On the hydrogen bonding level, there is the possibility of mispairing through involvement of minor tautomer forms of the bases (Watson and Crick, 1953), wobble-type mispairs (Rein, 1978), or mispairs involving both minor tautomer forms and syn isomers (Topal and Fresco, 1976). One must also consider any hydrogen bonding scheme in which the glycosidic distance is not 10.7 Å. In this case an additional input of energy due to deformation of the backbone is required. Even superficial examination of the available data indicates that the energy difference between a mispair and the normal G-C or A-T base pair added to the backbone deformation energy is not sufficient for the observed high rates of discrimination of errors. So, in addition to this intrinsic or thermodynamically controlled energy difference in base selection, there must exist additional mechanisms that improve fidelity. Any discussion of error introduction into DNA must include consideration of all thermodynamic and enzymatic factors.

The suggestion that the rare tautomeric forms of the bases may play a role in mutations is based on the observation that some tautomers of the nucleic acid bases mimic other bases. For example, a tautomer of thymine can mimic cytosine. An advantage for using tautomers is that the basic geometry of the tautomer hydrogen-bonded complex mimics the normal base pairs and maintains the 10.7-Å glycosidic bond distance, eliminating the need to estimate backbone deformation energies. This simplifies the thermodynamic problem to one of estimating or calculating by theoretical means the relative energies of the tautomers. In other words, without considering backbone deformation, hydrogen bonding energy differences,

or stacking energy differences, it seems that the principle factor governing the error rate is the tautomerization energy if this mechanism is correct. This consideration focused attention on the tautomerization energies and started a long sequence of studies stretching over 30 years.

Tautomer studies were given a great impetus when Löwdin published his hypothesis for spontaneous mutations (Löwdin, 1965). This hypothesis states that spontaneous mutations may be a result of proton transfer in complementary DNA base pairs. The Lowdin mechanism of proton transfer depends on the observation that in DNA each base pair has at least two hydrogen bonds. This implies two double-well potentials, each depending on its local electronic environment. The probability of locating a proton in a particular well is treated quantum mechanically; i.e., the proton may penetrate the potential barrier separating two wells by means "tunneling." Tunneling of one proton in one direction will very likely induce a tunneling of the other proton in the other direction, thus maintaining the neutral charge of the base pair. Tunneling probabilities express the equilibrium populations of A^*-T^* and G^*-C^* in a large number of A-T and G-C base pairs. These rearranged hydrogen bonds may be immortalized at the time of replication since the tautomeric forms of the bases have altered pairing schemes, i.e., A^*-C and G^*-T . The result would be a transition-type mutation, assuming that the bases do not revert to their normal isomeric forms during the DNA opening step or while the DNA is in the open state. Since mutations are very rare, the double-well potential for double-proton transfer is rather asymmetric. This explains the enormous stability of the genetic code (Löwdin, 1965).

Lowdin also suggested that single-proton rearrangement could occur. This would lead to ionic pairs such as A^--T^+ or G^+-C^- . Such pairs would have extra stability owing to ionic forces of attraction. No normal nucleotide would pair with A^+ or T^+ , which may result in deletions, while any nucleotide could bind to A^- and T^- . Use of ionized bases further presumes that the charged forms are stable enough to undergo one cycle of replication. It is difficult to imagine how these ionized bases could remain stable enough to participate in replication under cellular conditions or how one would experimentally detect these events.

Initial examination of these suggestions was made in the 1960s (Rein and Ladik, 1964; Rein and Harris, 1964) for single-proton tunneling using PPP-type calculations. These authors report the presence of a double-well potential for the G-C pair that would allow much higher fidelity than actually observed in nature, making enzymatic contributions to fidelity unnecessary. Later, calculations on the G-C pair by Clementi *et al.* (1971) at the *ab initio* level failed to detect a double-well potential for the motion of single-hydrogen-bonded atoms. They also examined double-

proton transfer in a smaller system, the formic acid dimer, when a double-well potential was obtained, but its shape was found to be sensitive to the choice of basis set.

More recent work on the double-proton transfer in benzoic acid dimer and the acetic acid dimer has been reported by Nagaoka *et al.* (1982, and references therein). They carried out full-geometry optimization for the acetic acid monomer, and dimer, and DPT transition state at the STO-3G and 4-31G levels. These authors also show that the double-well potential exists for this system and that the barrier separating the two wells depends on the basis set, as shown before, but that it also depends on relaxation of the geometry along the double-proton reaction path. Much more work is needed to evaluate accurately the height and thickness of the potential barriers to double-proton transfer before anything conclusive can be said about double-proton transfer in more complicated systems such as base pairs in DNA (Agresti *et al.*, 1981).

The work on the formic acid dimer focused on the double-well potential for a highly symmetric system. An attempt to locate a double-well potential for a less symmetric system was made by Zielinski and Poirier (1984). They studied the formamide dimer and isolated a possible structure for the transition state for a double-proton transfer along the reaction path to the formimidic acid dimer (a dimer of the enol form of formamide) using the 3-21G basis set. The proposed transition state is only slightly less stable than the formimidic acid dimer. In other words, a very asymmetric double-well potential was found with a very shallow well on the formimidic acid dimer side of the reaction. It will be interesting to see the shape of the function for a double-proton transfer between formamide and amidine, which would more closely mimic the double-proton transfer that may be possible for the A-T pair.

This brings us back to the consideration of single tautomers. The rate of incorporation of the tautomeric forms into a growing DNA strand would be proportional to the equilibrium population of these tautomers in solution. A review of the experimental efforts to determine the presence and equilibrium population of nucleic acid base tautomers in solution has been made (Kwiatkowski and Pullman, 1975). Most of the workers in the field have used the indirect *pK* method. The underlying principle of this method is the blocking of one or more of the labile hydrogens by replacing them with a methyl group. This freezes in one of the tautomeric forms for *pK* measurements and assumes that methyl substitution will not affect the tautomeric equilibrium of interest in solution. The accuracy of this assumption with respect to the electronic properties controlling tautomeric proton transfer is not known. Disregarding this reservation, these experiments estimate that the equilibrium population of the tautomers is 10^{-4} to

10^{-5} in aqueous solution, obviously too low for any direct concentration measurements but certainly plausible for fidelity considerations. This means that the tautomerization energies are in the range of 6 to 8 kcal mole⁻¹, which would amount to a discrimination of errors of about 1 out of 10,000 to 1 out of 100,000. Some support of this mechanism comes from experiments measuring the rate of error introduction in *in vitro*.

Another variation of the tautomer model was suggested by Topal and Fresco (1976). Base substitution point mutations can be classified as transitions or transversions. In transitions, one changes the base pairs but not the purine–pyrimidine polarity, while in transversion one changes the polarity. Analysis reveals that transversions require purine–purine or pyrimidine–pyrimidine mispairing. The normal glycosidic bond distance cannot be preserved in this case. Topal and Fresco tried to avoid this by proposing that some purine–purine pairs involved both a tautomer and a syn isomer of one of the bases. In this way base pairs that preserve closely the glycosidic distance are built, but at the expense of requiring two endergonic events instead of one.

An alternative to these two tautomer models for point mutations assumes non-Watson–Crick base pairing schemes between normal tautomer forms in which the glycosidic bonds are displaced relative to their normal position in DNA. In other words, incorporation of these wobble mispairs requires appropriate adjustment of the DNA backbone resulting in glycosidic distances different from the usual 10.7 Å.

One is then led to ask how the tautomer mechanism can be distinguished from the alternatives, i.e., wobble mispairs of mispairs involving minor tautomer forms base paired to syn isomers. The approach is to compare the energies of the various proposed models including interaction energies, deformation energies, and tautomerization energies to determine which model is more plausible.

It has been quantitatively shown (Rein *et al.*, 1983) that at least in some instances the pairs proposed by Topal and Fresco were energetically highly unlikely. First, the tautomerization required was the highly endergonic one between the second and sixth position of the purine, not between two adjacent atoms as is usually the case. Second, both purine–purine and pyrimidine–pyrimidine base pairs are possible from a purely geometrical analysis. In fact, the uracil–uracil wobble has been shown by crystallography to be utilized in some RNAs. Determining which of the various mispairing schemes are energetically feasible emphasizes the importance of trying to deal, from a theoretical point of view, both with the determination of the tautomer relative energies and with the evaluation of the energy of base pairs in the DNA environment with appropriate backbone deformation. This requires calculation of base pairing energies,

tautomer energies, minihelix conformation energies, and interaction energies between various components of a minihelix. Calculation of the energetics for mispair formation in a helical environment is quite complicated. *Ab initio* calculations are impractical; the systems are too large and are complicated by ionic and solvent effects. A suitable approach is to mix better calculations for the tautomerization energies with some form of empirical potential function estimate of the helix energy coupled to a suitable approximation of the solvent effect. Such calculations have been performed (Rein *et al.*, 1983; Rein and Shibata, 1983). Rein *et al.* used MINDO/3 tautomerization energies, which consistently agree with the available experimental data obtained by the *pK* method in solution. They then compared the energetics of misinsertion for the tautomer mechanism, the wobble mechanism, and the Topal–Fresco mechanism, which involves the imino–enol tautomer of guanine hydrogen bonded to adenine in the syn conformation.

Solvent effect on tautomers energies was included by means of the simple reaction-field model with MINDO/3 dipole moments. Entropic effects and zero-point vibrational energy differences were neglected. The major results are the following.

1. The imino–enol tautomer of guanine is energetically highly unfavorable (92.6 kJ mole⁻¹). This makes the tautomer mechanism for transversion highly unlikely.
2. Structures incorporating G–T and A–G in a minihelical environment show that such mispairs can be incorporated in DNA with only modest changes in the backbone conformation.
3. In general, mispairing involving normal bases, not minor tautomers, is most probably responsible for error incorporation at a template terminus.

ACKNOWLEDGMENTS

The authors wish to dedicate this paper to Professor Per-Olov Löwdin, whose suggestion in 1962 that proton tunneling between nucleic acid base pairs may lead to spontaneous point mutations has inspired a wealth of experimental and theoretical research in the field. His enthusiasm for the application of theoretical methods to problems in biochemical structure and function has been an inspiration to the three of us.

J.S.K. wishes to express his gratitude to Professor David Shugar (Polish Academy of Sciences, Warsaw) for many valuable discussions on tautomerism. This work was supported in part by the Ministry of Science, Higher Education, and Technology (Poland) within project MR I.5. J.S.K. also wishes to acknowledge that the support of his stay in Erlangen, where part of this paper was written, was made possible pursuant to a contract with the National Foundation for Cancer Research.

T.J.Z. and R.R. acknowledge partial support of this paper pursuant to a contract with the National Foundation for Cancer Research. R.R. also acknowledges support of NASA grant #NSG-7305. We would like to thank Masayuki Shibata for his careful reading of the manuscript. Deborah Raye's assistance in the preparation of the manuscript is gratefully acknowledged.

REFERENCES

- Abdulnur, S. F. (1976). In "Quantum Science: Methods and Structures" (J.-L. Calais, O. Goscinski, J. Linderberg, and Y. Ohrn, eds.), p. 567. Plenum, New York.
- Agresti, A., Bacci, M., and Ranfagni, A. (1981). *Chem. Phys. Lett.* **79**, 100.
- Albert, A. (1968). "Heterocyclic Chemistry." Athlone Press, London.
- Aue, D. H., Betowski, L. D., Davidson, W. R., Bowers, M. T., Beak, P., and Lee, J. (1979). *J. Am. Chem. Soc.* **101**, 1361.
- Barthelat, J. C., Durand, Ph., and Serafini, A. (1977). *Mol. Phys.* **33**, 159.
- Bartzsch, C., Weiss, C., and Hofmann, H.-J. (1984). *J. Prakt. Chem. (Leipzig)* **324**, 407.
- Beak, P. (1977). *Acc. Chem. Res.* **10**, 186.
- Beak, P., Covington, J. B., and White, J. M. (1980). *J. Org. Chem.* **45**, 1347.
- Beak, P., Fry, F. S., Jr., Lee, J., and Steele, F. (1976). *J. Am. Chem. Soc.* **98**, 171.
- Beak, P., and White, J. M. (1982). *J. Am. Chem. Soc.* **104**, 7073.
- Beak, P., Woods, T. S., and Mueller, D. S. (1972). *Tetrahedron* **28**, 5507.
- Berndt, M., and Kwiatkowski, J. S. (1978). *Theoret. Chim. Acta (Berlin)* **50**, 223.
- Bertran, J., Chalvet, O., and Daudel, R. (1970). *Anales de Fisica* **66**, 247.
- Birnstock, F., Hofmann, H.-J., and Kohler, H.-J. (1976). *Theoret. Chim. Acta (Berlin)* **42**, 311.
- Bolis, G., and Clementi, E. (1977). *J. Am. Chem. Soc.* **99**, 5550.
- Bonaccorsi, R., Ghio, C., and Tomasi, J. (1982). In "Current Aspects of Quantum Chemistry 1981" (R. Carbo, ed.), p. 407. Elsevier, Amsterdam.
- Brown, R. S., and Tse, A. (1980). *J. Am. Chem. Soc.* **102**, 5222.
- Brown, R. S., Tse, A., and Vederas, J. C. (1980). *J. Am. Chem. Soc.* **102**, 1174.
- Buda, A., and Syguła, A. J. (1983). *J. Mol. Struct. (THEOCHEM)* **92**, 255, 267.
- Callis, P. R. (1983). *Ann. Rev. Phys. Chem.* **34**, 329.
- Carozzo, L., Corongiu, G., Petrongolo, C., and Clementi, E. (1978). *J. Chem. Phys.* **68**, 787.
- Chang, C., Shabestary, N., and El-Bayoumi, M. A. (1980). *Chem. Phys. Lett.* **75**, 107.
- Claverie, P. (1982). In "Quantum Theory of Chemical Reactions" (R. Daudel, A. Pullman, L. Salem, and A. Veillard, eds.), Vol. III, p. 151. Reidel, Dordrecht.
- Claverie, P., Daudey, J. P., Langlet, J., Pullman, B., Piazzola, D., and Huron, M. J. (1978). *J. Phys. Chem.* **82**, 405.
- Clementi, E., Cavallone, F., and Scordamaglia, R. (1977). *J. Am. Chem. Soc.* **99**, 5531.
- Clementi, E., Mehl, J., and von Niessen, W. (1971). *J. Chem. Phys.* **54**, 508.
- Cooper, W. G. (1978). *Intl. J. Quantum Chem.* **14**, 71.
- Corongiu, G., Clementi, E., Dagnino, M., and Paoloni, L. (1979). *Chem. Phys.* **40**, 439.
- Czerminski, R., Lesyng, B., and Pohorille, A. (1979a). *Intl. J. Quantum Chem.* **16**, 605.
- Czerminski, R., Lesyng, B., and Pohorille, A. (1979b). *Intl. J. Quantum Chem.* **16**, 1141.
- Danilov, V. I., and Kventsel, G. F. (1971). "Electronic Representation in Point Mutation Theory" [in Russian]. Naukova Dumka, Kiev.
- Danilov, V. I., Kwiatkowski, J. S., Lesyng, B., and Poltev, V. I. (1981). *Int. J. Quantum Chem.* **QBS8**, 359.

- Del Bene, J. E. (1979). *J. Am. Chem. Soc.* **101**, 6184.
- Del Bene, J. E., and Jaffe, H. H. (1968a). *J. Chem. Phys.* **48**, 1807 and 4050.
- Del Bene, J. E., and Jaffe, H. H. (1968b). *J. Chem. Phys.* **49**, 1221.
- Dreyfus, M., Dodin, G., Bensaude, O., and Dubois, J. E. (1977). *J. Am. Chem. Soc.* **99**, 7027.
- Dreyfus, M., Bensaude, O., Dodin, G., and Dubois, J. E. (1976). *J. Am. Chem. Soc.* **98**, 6338.
- Dreyfus, M., Dodin, G., Bensaude, O., and Dubois, J. E. (1975). *J. Am. Chem. Soc.* **97**, 2369.
- Durand, Ph., and Barthelat, J. C. (1975). *Theoret. Chim. Acta (Berlin)* **38**, 283.
- Elguero, J., Marzin, C., Katritzky, A. R., and Linda, P. (1975). *Adv. Heterocyclic Chem.*, Suppl. No. 1.
- Fowler, R. G., Degnen, G. E., and Cox, E. C. (1974). *Mol. Gen. Genet.* **133**, 179.
- Goddard, J. D., Mezey, P. G., and Csizmadia, I. G. (1975). *Theoret. Chim. Acta (Berlin)* **39**, 1.
- Goldblum, A., Perahia, D., and Pullman, A. (1978). *FEBS Lett.* **91**, 213.
- Goodman, M. F., Hopkins, R. L., Watanabe, S. M., Clayton, L. K., and Guidotti, S. (1980). In "Mechanistic Studies of DNA Recombination." (B. Alberts and F. F. Fox, eds.), p. 685. Academic Press, New York.
- Grinberg, H., Capparelli, A. L., Spina, A., Maranon, J., and Sorarrain, O. M. (1981). *J. Phys. Chem.* **85**, 2751.
- Guimon, C., Garrabe, G., and Pfister-Guillouzo, G. (1979). *Tetrahedron Lett.* (No. 28), 2585.
- Herzberg, G. (1945). "Molecular Spectra and Molecular Structure II. Infrared and Raman Spectra of Polyatomic Molecules." Van Nostrand Reinhold, New York.
- Hinde, A. L., Poppinger, D., and Radom, L. (1978). *J. Am. Chem. Soc.* **100**, 4681.
- Hofmann, H.-J., Peinel, G., Krebs, C., and Weiss, C. (1981). *Intl. J. Quantum Chem.* **20**, 785.
- Huron, M.-J. and Claverie, P. (1974). *J. Phys. Chem.* **78**, 1853.
- Kamlet, M. J., and Taft, R. W. (1976). *J. Am. Chem. Soc.* **98**, 377, 2886.
- Katritzky, A. R., and Ambler, A. P. (1963). In "Physical Methods in Heterocyclic Chemistry" (A. R. Katritzky, ed.), Vol. II, p. 161. Academic Press, New York.
- Katritzky, A. R., and Lagowski, J. M. (1963). *Adv. Heterocyclic Chem.* **1**, 311.
- Kirkwood, J. G. (1934). *J. Chem. Phys.* **2**, 351.
- Klopman, G. (1967). *Chem. Phys. Lett.* **1**, 200.
- Krebs, C., Forster, W., Weiss, C., and Hofmann, H.-J. (1982). *J. Prakt. Chem. (Leipzig)* **324**, 369.
- Krebs, C., Hofmann, H. J., Kohler, H.-J., and Weiss, C. (1980). *Chem. Phys. Lett.* **69**, 537.
- Kwiatkowski, J. S. (1980). In "Biomolecular Structure, Conformation, Function, and Evolution" (R. Srinivasan, ed.), Vol. 2, p. 311. Pergamon, Oxford.
- Kwiatkowski, J. S., and Lesyng, B. (1983). Unpublished results.
- Kwiatkowski, J. S., and Lesyng, B. (1979). *Intl. J. Quantum Chem.* **QBS6**, 391.
- Kwiatkowski, J. S., Lesyng, B., Palmer, M. H., and Saenger, W. (1982). *Z. Naturforsch.* **37c**, 937.
- Kwiatkowski, J. S., Perahia, D., and Pullman, B. (1978). *Intl. J. Quantum Chem.* **QCS12**, 249.
- Kwiatkowski, J. S., and Pullman, B. (1974). *Acta Phys. Polon.* **A45**, 693.
- Kwiatkowski, J. S., and Pullman, B. (1975). *Adv. Heterocyclic Chem.* **18**, 199.
- Kwiatkowski, J. S., and Szczodrowska, B. (1978). *Chem. Phys.* **27**, 389.
- Kwiatkowski, J. S., and Tempczyk, A. (1984). *Chem. Phys.* **85**, 397.
- La Manna, G. (1981). *J. Mol. Structure (THEOCHEM)* **85**, 389.
- La Manna, G., and Venuti, E. (1982). *J. Comput. Chem.* **3**, 593.

- Les, A., and Ortega Blake, I. (1979). *Intl. J. Quantum Chem.* **QBS6**, 189.
- Les, A., and Ortega Blake, I. (1981). *Intl. J. Quantum Chem.* **19**, 719.
- Lipinski, J., and Gorzkowska, E. (1983). *Chem. Phys. Lett.* **94**, 479.
- Löwdin, P.-O. (1965). *Adv. Quantum Chem.* **2**, 213.
- Maranon, J., Grinberg, H., and Nudelman, N. S. (1982). *Intl. J. Quantum Chem.* **22**, 69.
- Maranon, J., and Sorarrain, O. M. (1979). *Z. Naturforsch.* **34a**, 315.
- Maranon, J., and Sorarrain, O. M. (1978). *Z. Naturforsch.* **33c**, 23.
- Matsuoka, O., Clementi, E., and Yoshimine, M. (1976). *J. Chem. Phys.* **64**, 1351.
- Metropolis, N., Rosenbluth, A. W., Rosenbluth, M. N., Teller, A. H., and Teller, E. (1953). *J. Chem. Phys.* **21**, 1087.
- Metzler, D. E. (1979). *Adv. Enzymology* **50**, 1.
- Mezey, P. G., and Ladik, J. J. (1979). *Theoret. Chim. Acta (Berlin)* **52**, 129.
- Mirek, J., and Sygula, A. (1981). *J. Mol. Struct.* **86**, 81.
- Møller, C., and Plesset, M. S. (1934). *Phys. Rev.* **46**, 618.
- Mondragon, A., and Ortega-Blake, I. (1982). *Intl. J. Quantum Chem.* **22**, 89.
- Morita, H., Kwiatkowski, J. S., and Tempczyk, A. (1981). *Bull. Chem. Soc. Jpn.* **54**, 1797.
- Morita, H., Kwiatkowski, J. S., and Tempczyk, A. (1982). *Bull. Chem. Soc. Jpn.* **55**, 2715.
- Nagaoka, S., Hirota, N., Matsushita, T., and Nishimoto, K. (1982). *Chem. Phys. Lett.* **92**, 498.
- Nowak, M. J. (1979). Ph.D. Thesis, Institute of Physics, Polish Academy of Sciences, Warsaw.
- Nowak, M. J., Szczepaniak, K., Barski, A., and Shugar, D. (1978). *Z. Naturforsch.* **33c**, 876.
- Nowak, M. J., Szczepaniak, K., Barski, A., and Shugar, D. (1980). *J. Mol. Struct.* **69**, 47.
- Onsager, L. (1936). *J. Am. Chem. Soc.* **58**, 1486.
- Owicky, J. C., and Scheraga, H. A. (1977). *J. Am. Chem. Soc.* **99**, 7403.
- Palmer, M. H., Wheeler, J. S., Kwiatkowski, J. S., and Lesyng, B. (1983). *J. Mol. Structure (THEOCHEM)* **92**, 283.
- Parr, R. G. (1972). "The Quantum Theory of Molecular Electronic Structure." Benjamin, Reading, Massachusetts.
- Pullman, A., and Perahia, D. (1978). *Theoret. Chim. Acta (Berlin)* **48**, 29.
- Ragazzi, M., Ferro, D. R., and Clementi, E. (1979). *J. Chem. Phys.* **70**, 1040.
- Rein, R. (1978). In "Intermolecular Interactions from Diatomics to Biopolymers" (B. Pullman, ed.), p. 308. Wiley, New York.
- Rein, R., and Harris, F. E. (1964). *J. Chem. Phys.* **41**, 3393.
- Rein, R., and Ladik, J. (1964). *J. Chem. Phys.* **40**, 2466.
- Rein, R., and Shibata, M. (1983). In "Nucleic Acids: The Vectors of Life" (B. Pullman and J. Jortner, eds.), p. 479. Reidel, Dordrecht.
- Rein, R., Shibata, M., Garduno-Juarez, R., and Kieber-Emmons, T. (1983). In "Structure and Dynamics: Nucleic Acids and Proteins" (E. Clementi and R. H. Sarma, eds.), p. 269. Adenine, New York.
- Sakurai, T., and Inoue, H. (1981). *J. Chem. Soc. Chem. Commun.*, 1004.
- Scanlan, M. J., and Hillier, I. H. (1983). *Chem. Phys. Lett.* **98**, 545.
- Scanlan, M. J., Hillier, I. H., and MacDowell, A. A. (1983). *J. Am. Chem. Soc.* **105**, 3568.
- Schlegel, H. B. (1983). *Intl. J. Quantum Chem.* **22**, 1041.
- Schlegel, H. B., Gund, P., Fluder, E. M. (1982). *J. Am. Chem. Soc.* **104**, 5347.
- Schuster, P. (1976). In "The Hydrogen Bond—Recent Developments in Theory and Experiments" (P. Schuster, G. Zundel, and C. Sandorfy, eds.), p. 25. North-Holland, Amsterdam.
- Schuster, P. (1969). *Intl. J. Quantum Chem.* **3**, 851.
- Scordamaglia, R., Cavallone, F., and Clementi, E. (1977). *J. Am. Chem. Soc.* **99**, 5545.

- Sepiol, J., and Wild, U. P. (1982). *Chem. Phys. Lett.* **93**, 204.
- Shibata, M., Zielinski, T. J., and Rein, R. (1980). *Intl. J. Quantum Chem.* **18**, 323.
- Shugar, D., and Szczepaniak, K. (1981). *Intl. J. Quantum Chem.* **20**, 573.
- Sinanoglu, O. (1968). In "Molecular Associations in Biology" (B. Pullman, ed.), p. 427. Academic Press, New York.
- Srivastava, S. K. and Mishra, P. C. (1981). *J. Theor. Biol.* **93**, 655.
- Tapia, O. (1982). In "Molecular Interactions" (H. Ratajczak, and W. J. Orville-Thomas, eds.), Vol. 3, p. 47. Wiley, New York.
- Teichteil, Ch., Mahieu, J. P., and Barthelat, J. C. (1977). *Mol. Phys.* **33**, 181.
- Tempczyk, A. (1983). Ph.D. Thesis, University of Gdansk, Gdansk.
- Topal, M. D., and Fresco, J. R. (1976). *Nature (London)* **263**, 285.
- Trogler, W. C. (1981). *J. Mol. Struct. (THEOCHEM)* **85**, 1.
- Watson, J. P., and Crick, F. H. C. (1953). *Nature (London)* **171**, 964.
- Westheimer, F. H., and Kirkwood, J. G. (1938). *J. Chem. Phys.* **6**, 513.
- Zielinski, T. J. (1983). *J. Comp. Chem.* **4**, 345.
- Zielinski, T. J. (1982). *Intl. J. Quantum Chem.* **22**, 639.
- Zielinski, T. J., Breen, D. L., Haydock, K., Rein, R., and McElroy, R. D. (1978). *Intl. J. Quantum Chem. QBS5*, 355.
- Zielinski, T. J., and Poirier, R. A. (1984). *J. Comp. Chem.* **5**, 466.
- Zielinski, T. J., Shibata, M., and Rein, R. (1981). *Intl. J. Quantum Chem.* **19**, 171.

NOTE ADDED IN PROOF. The present review covers the most important papers on theoretical studies of tautomeric equilibria up to the beginning of 1984. The reader is referred to the following more recent papers concerning the theoretical studies on tautomerism of nucleic acid bases and their model systems:

- Berndt, M., and Kwiatkowski, J. S. (1986). In "Theoretical Chemistry of Biological Systems" (G. Naray-Szabo, ed.). Elsevier, Amsterdam (in press)—review on hydration of biomolecules including theoretical studies on the effect of solvation on tautomeric equilibria, bibliography of theoretical papers on this subject up to 1984.
- Cieplak, P., and Geller, M. (1985). *J. Mol. Struct. (THEOCHEM)* **121**, 247—Monte Carlo simulation of water effects on tautomeric equilibrium of 2-oxypyrimidine.
- Cieplak, P., and Geller, M. (1985). *J. Mol. Struct. (THEOCHEM)* **124**, 249—Monte Carlo simulation of CCl₄ effect on tautomeric equilibrium of 2-oxypyrimidine.
- Jaworski, A., Kwiatkowski, J. S., and Lesyng, B. (1986). *Intl. J. Quantum Chem. QBS12*, 209—discussion of the relationship between tautomerism of isocytosine, isoguanine, and genetic code.
- La Manna, G. (1984). *J. Mol. Struct. (THEOCHEM)* **110**, 183—*ab initio* (3-21G, 6-31G*) calculations for tautomers of 2-oxypyrimidine.
- Latajka, Z., Person, W. B., and Morokuma, K. (1986). *J. Mol. Struct. (THEOCHEM)* **135**, 253—*ab initio* (STO-3G, 3-21G) calculations for tautomers of guanine.
- Les, A., and Ortega-Blake, I. (1985). *Intl. J. Quantum Chem.* **27**, 567—semiempirical (PCILO,MNDO) and *ab initio* pseudopotential calculations for relative stabilities of tautomers of 2- and 4-oxypyrimidine.
- Scanlan, M. J., and Hillier, I. H. (1984). *J. Am. Chem. Soc.* **106**, 3737—*ab initio* (3-21G) calculations for different tautomers of uracil, thymine, 5-fluorouracil, and cytosine; solvent effects (continuous model) on stabilities of the tautomers.
- Shibata, M. (1985). "Theoretical Study of Point Mutation," Ph.D. Thesis, p. 249. Roswell Park Memorial Institute, Buffalo, N.Y.—thesis includes a discussion on relationship between tautomeric equilibria and point mutations.
- Syguła, A., and Buda, A. (1985). *J. Mol. Struct. (THEOCHEM)* **121**, 133—MNDO calculations for amino-type tautomers of cytosine, adenine, and guanine.

Dynamics of Molecular Crystals

W. J. BRIELS,* A. P. J. JANSEN, and A. VAN DER AVOIRD

*Institute of Theoretical Chemistry
University of Nijmegen
6525 ED Nijmegen, The Netherlands*

I. Introduction	131
II. Intermolecular Interactions and the Crystal Hamiltonian	135
A. Atom-Atom Potentials	136
B. Intermolecular Potential in Terms of Symmetry-Adapted Functions	137
C. Expansion of Atom-Atom Potentials in Symmetry-Adapted Functions	141
D. The Crystal Hamiltonian	144
III. Harmonic and Quasi-harmonic Theories of Lattice Dynamics	149
A. Harmonic Approximation	150
B. Anharmonic Corrections by Perturbation Theory	153
C. The Self-Consistent Phonon Method	159
IV. Dynamical Models for Large-Amplitude Motions	162
A. Classical Molecular Dynamics and Monte Carlo Methods	163
B. The Mean Field Model	165
C. The Random Phase or Time-Dependent Hartree Approximation	170
D. Stability Conditions for the Mean Field Solution	173
V. Molecular Motions in Solid Nitrogen	175
A. Theory for Linear Molecules	175
B. Results from Harmonic and Quasi-Harmonic Models	178
C. Large-Amplitude Motions in the Ordered Phases	181
D. The Plastic Phase and the Orientational Order-Disorder Phase Transition	186
VI. Dynamics and Magnetism of Solid Oxygen	191
A. Lattice Dynamics and Spin Wave Calculations	193
B. The Complete Crystal Hamiltonian and the Coupling between Lattice Vibrations and Spin Dynamics	195
Appendix	200
References	203

I. Introduction

Molecular crystals are solids in which the atoms group together in well-defined stable entities arranged in some periodic way. In general, these entities can be molecules or molecular ions, but in this paper we mainly restrict ourselves to crystals built from neutral molecules. The binding forces keeping the atoms together in the molecules are much

* Present address: Van't Hoff Laboratorium voor Fysische-en Colloidchemie, 3584 CH Utrecht, The Netherlands.

stronger than the van der Waals forces that cause the condensation of the molecules in the crystal. As a consequence, the atoms in the solid take part in two types of motions that, to a good approximation, can be assumed to be uncoupled. First, they perform rapid oscillations around instantaneous positions in such a way as to keep the positions, orientations, and geometries of the molecules nearly unchanged. These motions are called intramolecular vibrations. In the solid, when their frequencies are slightly shifted by the crystal field and they are very weakly coupled, they are called vibrons. Second, the equilibrium positions of the atoms undergo displacements that are such that they amount to translations and rotations of the molecules as a whole. These motions, the intermolecular vibrations, usually called lattice vibrations, are much slower than the intramolecular vibrations, and they are the subject of this paper.

Because we are dealing with molecules, two types of lattice vibrations can be distinguished: translational and rotational. In order to describe these motions we have to know the potential energy of the crystal, expressed as a function of the center of mass positions and the orientations of all molecules. In Section II, we give a fairly detailed description of the different ways in which the potential can be expressed, each way having its own merits, depending on the subsequent calculations in which it has to be used.

Depending on the character of the molecular motions, one can distinguish several physical situations. In most cases, the molecules are trapped in relatively deep potential wells. Then, they perform small translational and orientational oscillations around well-defined equilibrium positions and orientations. Such motions are reasonably well described by the harmonic approximation. The collective vibrational excitations of the crystal, which are considered as a set of harmonic oscillators, are called phonons. Those phonons that represent pure angular oscillations, or librations, are called librons. For some properties it turns out to be necessary to look at the effects of anharmonicities. Anharmonic corrections to the harmonic model can be made by perturbation theory or by the self-consistent phonon method. These methods, which are summarized in Section III under the name quasi-harmonic theories, can be considered to be the standard tools in lattice dynamics calculations, in addition to the harmonic model. They are only applicable in the case of fairly small amplitude motions. Only the simple harmonic approximation is widely used; the calculation of anharmonic corrections is often hard in practice. For detailed descriptions of these methods, we refer the reader to the books and reviews by Maradudin *et al.* (1968, 1971, 1974), Cochran and Cowley (1967), Barron and Klein (1974), Birman (1974), Wallace (1972), and Califano *et al.* (1981).

A second situation occurs when the molecules perform angular oscillations, usually with large amplitudes, around one of a set of equilibrium orientations and randomly jump from one orientation to the other. Sometimes the librations are so violent that the molecules perform more or less hindered rotations. An extreme case is solid hydrogen, at normal pressure, in which the free-molecule rotations are only weakly perturbed and one speaks of rotons instead of librons. In all these cases the molecular crystal is called orientationally disordered or plastic, in contrast with the ordered or localized crystals discussed in the preceding paragraph. The only standard method to deal with this type of molecular motion is the mean field or (time-independent) Hartree approximation. By using the mean-field single-particle states as a basis, the collective motions of all molecules in the crystal can be described via the random phase approximation or time-dependent Hartree method. These methods are outlined in Section IV. Mostly the centers of mass of the molecules are thought of as being fixed. This approximation will rarely be justified in practice, however. Most molecular crystals are rather closely packed, which forces the molecules to separate before they can substantially change their orientations. As a result, there will be considerable coupling between the translational vibrations of the molecules and their rotational motions and mixing of the translational phonons and librons. The effects of such coupling on the properties of molecular crystals have been discussed by Michel and co-workers (Michel and Naudts, 1978; de Raedt *et al.*, 1981; Michel, 1984), and by Raich *et al.* (1983) and illustrated by semiempirical model calculations. A way to deal with this coupling via the time-dependent Hartree method has been proposed by ourselves (Briels *et al.*, 1984). This extension of the theory is included in Section IV.

All the lattice dynamics methods that we have just mentioned neglect the exchange of identical molecules. The mean-field method, for instance, is based on the Hartree approximation rather than on the Hartree-Fock model. This concerns, of course, the exchange of identical nuclei, since we are dealing with the nuclear motions and the effects of electron exchange are already contained in the intermolecular potential used. In practically all cases, even for the lightest nuclei, the nuclear wave functions have negligible overlap and the exchange effects may be safely omitted.

Let us now discuss to what extent the lattice vibrations are important for the macroscopic properties of molecular crystals. First of all, we have to consider the zero-point vibrations, i.e., the energy difference between the quantum-mechanical ground state of the system and the minimum of its potential energy. Since the van der Waals interactions among the molecules are rather weak, their zero-point motions affect the cohesion

energy of the crystal to a nonnegligible extent. Second, the characteristic excitation energies of the lattice vibrations are of the same order of magnitude as $k_B T$ (k_B being the Boltzmann constant) in most experimental circumstances. The excited states are populated and thus contribute to the properties of the system. Their effective contributions are strongly dependent on the size of the excitation energies and may vary considerably from one system to the other. As an illustration, let us briefly discuss the phase transition between the ordered and disordered modifications that often exist for the same material. Usually the ordered phase is thermodynamically stable at low temperatures, the plastic phase at high temperatures. The stability of the ordered phase is mainly due to the packing of the molecules in such a manner that the ground-state energy of the system is as low as possible. The stability of the disordered phase at high temperature is caused by its excitation energies, which are typically those of hindered rotors, being much lower than the excitation energies of the ordered phase, which are more like those of harmonic oscillators. Consequently, the excited states in the plastic phase will be more populated, its entropy will be larger, and its free energy ($A = E - TS$) will be lower at high temperature. It will be clear from this example that in order to give a reasonable account of any phase transition, one must accurately calculate the ground state and the excitation energies of the phases involved. The comparison between the calculated and observed phase transition temperatures and pressures yields a sensitive test, both for the potential and for the method used to describe the lattice dynamics.

In most cases, the crystal potential is not known *a priori*. The usual procedure is to introduce some model potential containing several parameters, which are subsequently found by fitting the calculated crystal properties to the observed data available. This procedure has the drawback that the empirical potential thus obtained includes the effects of the approximations made in the lattice dynamics model, which is mostly the harmonic model. It is very useful to have independent and detailed information about the potential from quantum-chemical *ab initio* calculations. Such information is available for nitrogen (Berns and van der Avoird, 1980) and oxygen (Wormer and van der Avoird, 1984), and we have chosen the results calculated for solid nitrogen and solid oxygen to illustrate in Sections V and VI, respectively, the lattice dynamics methods described in Sections III and IV. Nitrogen is the simplest typical molecular crystal;* as such it has received much attention from theorists and

* Hydrogen is even simpler, but solid hydrogen is very atypical. Because of the large splitting between the rotational states of the free H_2 molecule and the weak anisotropy of the H_2 - H_2 interaction potential, the free molecule rotations are nearly unperturbed in the solid. This system has been extensively discussed by van Kranendonk (1983).

experimentalists and many data have been collected. It has several phases, ordered as well as disordered. Oxygen is especially interesting because it combines the properties of a molecular crystal with those of a magnetic material. It exhibits both structural and magnetic order-disorder phase transitions.

II. Intermolecular Interactions and the Crystal Hamiltonian

In the Born–Oppenheimer approximation the potential energy of a molecular crystal depends on the internal and external degrees of freedom of all molecules. As mentioned before, it is a very good approximation in most cases to separate the intramolecular vibrations from the center of mass vibrations and rotations of the molecules, i.e., the lattice vibrations. Then one can average the potential energy over the vibrational wave functions of the molecules and obtain the effective potential for the lattice vibrations. If one wishes to obtain this effective intermolecular potential by calculation, it is a good approximation to use the vibrationally averaged molecular geometries from theory or experiment. The (average) geometry of the molecules in the crystal is usually not very different from the free-molecule geometry.

A further approximation, which is applied in almost all practical treatments, is to write the intermolecular potential for the crystal as a sum over molecular pair potentials. For van der Waals solids—in which the electrostatic interactions, the exchange repulsion, and the London dispersion attraction are the main contributors to the potential—this is fairly well justified. However, when the molecules have large dipole moments (in ice, for example) or even more so in ionic crystals, the induction (multipole-induced multipole) interactions become substantial, and the three-body interaction energy will be comparable in size to the pair energy. This is because one has to add pairwise the polarizing electric fields from all neighbors in order to calculate the polarization energy of a given molecule that is quadratic in the field strength. Moreover, one has to take into account self-consistently the mutual interactions among the induced dipole moments. In the present paper, we focus on molecules with relatively small dipole moments, for which we estimate the exchange, induction, and dispersion three-and-more-body contributions to be not larger than about 10% of the pair potential (van der Avoird *et al.*, 1980), and we further neglect these deviations from pairwise additivity.

In order to be useful in crystal dynamics calculations, the intermolecular potential must be represented in a manageable, preferably analytic, form. The form chosen to express the potential will depend on the type of application. If, for example, the intermolecular potential is to be deduced

from the agreement between calculated and observed crystal properties, it is important to have a representation that is as simple as possible, depending only on a few parameters. The same requirement has to be fulfilled when during the calculation the numerical value of the intermolecular potential is needed many times, for instance, in classical molecular dynamics or Monte Carlo simulations. For such purposes a representation in terms of atom-atom interaction potentials is convenient. On the other hand, if one intends to make statistical mechanics calculations with an “*ab initio*” potential without loosing too much accuracy, an expansion of the potential in terms of orthogonal symmetry-adapted functions is suitable. In the sequel, we briefly describe in Section II,A the atom-atom potential model, in Section II,B the representation of the potential in terms of symmetry-adapted functions, and in Section II,C the relation between the two formalisms. Finally, in Section II,D we discuss the full crystal Hamiltonian.

A. Atom-Atom Potentials

The concept of an atom-atom potential (Kitaigorodsky, 1973) is based on the idea that the interaction potential between two molecules P and P' can be approximated by pairwise additive interactions between the constituent atoms, $\alpha \in P$ and $\beta \in P'$, which, in practice, are nearly always taken to be isotropic, i.e., dependent only on the interatomic distances $r_{\alpha\beta}$:

$$V_{PP'} = \sum_{\alpha \in P} \sum_{\beta \in P'} v^{X_\alpha X_\beta}(r_{\alpha\beta}) \quad (1)$$

The labels X_α and X_β denote the types of the atoms α and β . Popular forms for the atom-atom potentials are the Lennard-Jones 12-6 form

$$v^{X_\alpha X_\beta}(r_{\alpha\beta}) = A^{X_\alpha X_\beta} r_{\alpha\beta}^{-12} - B^{X_\alpha X_\beta} r_{\alpha\beta}^{-6} \quad (2)$$

and the Buckingham exp -6 or exp -6-1 form

$$v^{X_\alpha X_\beta}(r_{\alpha\beta}) = A^{X_\alpha X_\beta} \exp(-B^{X_\alpha X_\beta} r_{\alpha\beta}) - C^{X_\alpha X_\beta} r_{\alpha\beta}^{-6} (+ q^{X_\alpha} q^{X_\beta} r_{\alpha\beta}^{-1}) \quad (3)$$

The first term always represents the exchange repulsion and the second term the London dispersion attraction. The Coulomb term is sometimes added in order to represent the electrostatic interactions among molecules, with fractional atomic point charges q^{X_α} and q^{X_β} used. Alternatively, one has included these electrostatic contributions by adding the leading molecular multipole-multipole interaction term to an atom-atom potential of 12-6 or exp -6 type.

The interaction parameters $A^{X_\alpha X_\beta}$, $B^{X_\alpha X_\beta}$, $C^{X_\alpha X_\beta}$, and q^{X_α} are mostly obtained by fitting calculated crystal properties to experimental data. The quality of the resulting empirical potentials is rather uncertain, however,

since the fit will try to compensate for the inaccuracies in the dynamical model used and in the atom-atom model itself. Moreover, the different parameters are often strongly correlated. This implies that such empirical potentials are usually not very effective in predicting properties other than those to which they have been fitted.

In some cases (see van der Avoird *et al.*, 1980, and references therein) atom-atom potentials, which are subsequently used to calculate crystal properties, have been obtained from an independent source, viz., from *ab initio* quantum-chemical calculations. The individual terms in an atom-atom potential of the form in Eq. (3), for example, are then fitted to the corresponding interaction energy contributions calculated for a more or less extensive set of geometries of a molecular pair. It appears that the Buckingham form (in Eq. 3) especially can yield a reasonably accurate representation of an *ab initio* calculated potential, provided that the individual terms are given different force centers (sites) whose positions are shifted away from the atomic nuclei and optimized in fitting the *ab initio* data.

It is convenient for further use to summarize the various atom-atom potentials as given in Eqs. (2) and (3) in the single formula

$$V^{X_a X_\beta}(r_{\alpha\beta}) = \sum_{n, \text{exp}} A_{n/\text{exp}}^{X_a X_\beta} f^{(n/\text{exp})}(r_{\alpha\beta}) \quad (4)$$

with parameters $A_{n/\text{exp}}^{X_a X_\beta}$, $A_{\text{exp}}^{X_a X_\beta}$ and distance functions $f^{(n)}(r_{\alpha\beta}) = r_{\alpha\beta}^{-n}$ (e.g., $n = 12, 6, 1$) and $f^{(\text{exp})}(r_{\alpha\beta}) = \exp(-B^{X_a X_\beta} r_{\alpha\beta})$.

B. Intermolecular Potential in Terms of Symmetry-Adapted Functions

In order to describe the orientation of a given molecule we attach a rectangular coordinate frame M to it and specify the Euler angles $\omega = \{\alpha, \beta, \gamma\}$ of this frame relative to a fixed global frame G . The position vector of the center of mass of the molecule is denoted by \mathbf{r} . The potential between two molecules at \mathbf{r}_P and $\mathbf{r}_{P'}$, respectively, can then be expanded (Steele, 1963; Yasuda and Yamamoto, 1971; Egelstaff, Gray and Gubbins, 1975; van der Avoird *et al.*, 1980; Briels, 1980) in a complete set of functions of the variables ω_P , $\omega_{P'}$, and $\hat{r}_{PP'}$, where $\hat{r}_{PP'}$ is the unit vector in the direction of $\mathbf{r}_{PP'} = \mathbf{r}_{P'} - \mathbf{r}_P$. The coefficients of the expansion depend on $r_{PP'}$, the length of $\mathbf{r}_{PP'}$. As a basis for the expansion we use the products

$$D_{n_1 m_1}^{(l_1)}(\omega_P) D_{n_2 m_2}^{(l_2)}(\omega_{P'}) C_{m_3}^{(l_3)}(\hat{r}_{PP'})$$

where the $D_{nm}^{(l)}(\omega)$ are Wigner functions and $C_m^{(l)}(\hat{r})$ is a Racah spherical harmonic. For these functions as well as for the Euler angles, we use the definitions of Edmonds (1957). This expansion can be greatly simplified if we exploit the full symmetry of the molecular pair.

In order to incorporate the symmetry requirements into our expansion, we need the transformation properties of the Wigner functions, both with respect to rotations $R^G(\omega)$ of the global frame and with respect to rotations $R^M(\omega)$ of the molecular frames. If we rotate the global frame through the Euler angles $\tilde{\omega}$, then a scalar quantity that was described in the original frame by a function F will be described in the new frame by $R^G(\tilde{\omega})F$; the two functions are related by $R^G(\tilde{\omega})F(\omega) = F(\omega')$, where ω and ω' are the Euler angles of the molecular frame relative to the new and old global frames, respectively. Similarly, if we rotate a molecular frame through the Euler angles $\tilde{\omega}$, F will transform into $R^M(\tilde{\omega})F$. With the conventions that we have adopted, the transformed Wigner functions are given by

$$R^G(\tilde{\omega})D_{nm}^{(l)}(\omega) = \sum_{m'} D_{nm'}^{(l)}(\omega) D_{m'm}^{(l)}(\tilde{\omega}) \quad (5)$$

$$R^M(\tilde{\omega})D_{nm}^{(l)}(\omega) = \sum_{n'} D_{n'm}^{(l)}(\omega) D_{n'n}^{(l)}(\tilde{\omega}) \quad (6)$$

The well-known transformation properties of the Racah spherical harmonics can be obtained from the relation

$$C_m^{(l)}(\hat{r}) = C_m^{(l)}(\theta, \phi) = D_{0m}^{(l)}(\phi, \theta, 0) \quad (7)$$

and Eq. (5):

$$R^G(\tilde{\omega})C_m^{(l)}(\hat{r}) = \sum_{m'} C_{m'}^{(l)}(\hat{r}) D_{m'm}^{(l)}(\tilde{\omega}) \quad (8)$$

The expression for the intermolecular potential must satisfy two symmetry requirements. First, it must be invariant if we rotate the molecular frame of either of the two molecules through specific Euler angles $\tilde{\omega}_g$ that correspond with a symmetry element of the molecule in question. This means that our basis must be invariant under rotations of the outer direct product group $G_P \otimes G_{P'}$, where G_P is the symmetry group of molecule P and $G_{P'}$ that of molecule P' . Acting with the projection operator of the totally symmetric irreducible representation of the group G_P (of order $\#G_P$),

$$P = \frac{1}{\#G_P} \sum_{g \in G_P} R^M(\tilde{\omega}_g) \quad (9)$$

on the Wigner functions, and using Eq. (6), we construct linear combinations

$$G_m^{(l)}(\omega_P) = \sum_n A_n^{(l)} D_{nm}^{(l)}(\omega_P) \quad (10)$$

which are invariant under the group G_P . We choose as the expansion basis the set of all products:

$$G_{m_1}^{(l_1)}(\omega_P) G_{m_2}^{(l_2)}(\omega_{P'}) C_{m_3}^{(l_3)}(\hat{r}_{PP'}). \quad (11)$$

It may happen that for certain values of l more than one totally symmetric combination (10) may exist. In that case, the l index should be understood as a composite label. As an example, we list in Table I, for values of l up to 10, the tetrahedral rotation functions that transform according to the totally symmetric representation of the tetrahedral group T . These functions are normalized such that

$$(8\pi^2)^{-1} \int d\omega T_{m_1}^{(l_1)}(\omega) * T_{m_2}^{(l_2)}(\omega) = \delta_{l_1 l_2} \delta_{m_1 m_2} (2l_1 + 1)^{-1}$$

The coefficients $A_n^{(l)}$ in these functions depend on the way in which the molecular coordinate frame is fixed on the molecule, for which we use the standard convention in this example (see Table I).

TABLE I
TETRAHEDRAL ROTATION FUNCTIONS^a

l	Function
0	$T_0^{(0)} = D_{00}^{(0)}$
3	$T_m^{(3)} = -\frac{1}{2} i (2)^{1/2} \{D_{2m}^{(3)} - D_{-2m}^{(3)}\}$
4	$T_m^{(4)} = \frac{1}{2} (\frac{7}{3})^{1/2} \{D_{0m}^{(4)} + (\frac{5}{14})^{1/2} (D_{4m}^{(4)} + D_{-4m}^{(4)})\}$
6	$T_m^{(6)} = \frac{1}{4} (2)^{1/2} \{D_{0m}^{(6)} - (\frac{7}{2})^{1/2} (D_{4m}^{(6)} + D_{-4m}^{(6)})\}$ $T_m^{(6)} = \frac{1}{4} (\frac{11}{2})^{1/2} \{D_{2m}^{(6)} + D_{-2m}^{(6)} - (\frac{5}{11})^{1/2} (D_{6m}^{(6)} + D_{-6m}^{(6)})\}$
7	$T_m^{(7)} = -\frac{1}{4} i (\frac{13}{3})^{1/2} \{(D_{2m}^{(7)} - D_{-2m}^{(7)}) + (\frac{11}{13})^{1/2} (D_{6m}^{(7)} - D_{-6m}^{(7)})\}$
8	$T_m^{(8)} = \frac{1}{8} (33)^{1/2} \{D_{0m}^{(8)} + (\frac{14}{99})^{1/2} (D_{4m}^{(8)} + D_{-4m}^{(8)}) + (\frac{65}{198})^{1/2} (D_{8m}^{(8)} + D_{-8m}^{(8)})\}$
9	$T_m^{(9)} = -\frac{1}{4} i (\frac{3}{2})^{1/2} \{(D_{2m}^{(9)} - D_{-2m}^{(9)}) - (\frac{13}{3})^{1/2} (D_{6m}^{(9)} - D_{-6m}^{(9)})\}$ $T_m^{(9)} = -\frac{1}{4} i (\frac{17}{3})^{1/2} \{(D_{4m}^{(9)} - D_{-4m}^{(9)}) - (\frac{7}{17})^{1/2} (D_{8m}^{(9)} - D_{-8m}^{(9)})\}$
10	$T_m^{(10)} = \frac{1}{8} (\frac{65}{6})^{1/2} \{D_{0m}^{(10)} - (\frac{66}{65})^{1/2} (D_{4m}^{(10)} + D_{-4m}^{(10)}) - (\frac{187}{130})^{1/2} (D_{8m}^{(10)} + D_{-8m}^{(10)})\}$ $T_m^{(10)} = \frac{1}{16} (\frac{247}{3})^{1/2} \{(D_{2m}^{(10)} + D_{-2m}^{(10)}) + (\frac{1}{26})^{1/2} (D_{6m}^{(10)} + D_{-6m}^{(10)}) - (\frac{255}{494})^{1/2} (D_{10m}^{(10)} + D_{-10m}^{(10)})\}$

^a The z axis of the molecule fixed system is a two-fold axis; the $[1, 1, 1]$ axis is a threefold axis.

The second symmetry requirement that the expression for the intermolecular potential has to meet is that it must be invariant under any rotation of the global coordinate frame. The transformation properties of the symmetry-adapted functions $G_m^{(l)}(\omega)$ under such a rotation are easily obtained from Eqs. (10) and (5):

$$R^G(\tilde{\omega})G_m^{(l)}(\omega) = \sum_{m'} G_{m'}^{(l)}(\omega)D_{m'm}^{(l)}(\tilde{\omega}) \quad (12)$$

We now construct the invariant basis in which we shall expand the intermolecular potential by acting on the products (11) with the projection operator

$$(8\pi^2)^{-1} \int d\tilde{\omega} R^G(\tilde{\omega}) \quad (13)$$

using the transformation formulas (8) and (12) and the relation

$$\begin{aligned} (8\pi^2)^{-1} \int d\tilde{\omega} D_{m'_1 m_1}^{(l_1)}(\tilde{\omega}) D_{m'_2 m_2}^{(l_2)}(\tilde{\omega}) D_{m'_3 m_3}^{(l_3)}(\tilde{\omega}) \\ = \begin{pmatrix} l_1 & l_2 & l_3 \\ m'_1 & m'_2 & m'_3 \end{pmatrix} \begin{pmatrix} l_1 & l_2 & l_3 \\ m_1 & m_2 & m_3 \end{pmatrix} \end{aligned} \quad (14)$$

The symbols on the right-hand side are 3- j coefficients.

The expansion of the intermolecular potential then reads

$$\begin{aligned} V(\omega_P, \omega_{P'}, \mathbf{r}_{PP'}) = \sum_{\mathbf{l}} v_{\mathbf{l}}(r_{PP'}) \sum_{\mathbf{m}} \begin{pmatrix} l_1 & l_2 & l_3 \\ m_1 & m_2 & m_3 \end{pmatrix} \\ \times G_{m_1}^{(l_1)}(\omega_P) G_{m_2}^{(l_2)}(\omega_{P'}) C_{m_3}^{(l_3)}(\hat{r}_{PP'}) \end{aligned} \quad (15)$$

The summation labels are defined as $\mathbf{l} = \{l_1, l_2, l_3\}$ and $\mathbf{m} = \{m_1, m_2, m_3\}$. We note again that for certain values of l_1 and l_2 more than one symmetry-adapted function $G_m^{(l)}$ exists and that in this case $\sum_{\mathbf{l}}$ includes all these functions.

From Eq. (15) we observe that the intermolecular potential is completely specified by the coefficients $v_{\mathbf{l}}(r_{PP'})$. These expansion coefficients can be obtained in various ways. If the intermolecular potential is given in terms of atom-atom potentials, it is possible to obtain explicit expressions for these coefficients (see Section II,C). If the long-range part of the potential is known from perturbation theory calculations in the multipole expansion, the expansion coefficients, after some angular momentum recoupling, can also be obtained from explicit formulas (see van der Avoird *et al.*, 1980). If the (short- and intermediate-range) potential is known

numerically from *ab initio* calculations for a grid of distances $r_{PP'}$ and molecular orientations ω_P and $\omega_{P'}$, the expansion coefficients can be found by numerical integration for each value of $r_{PP'}$:

$$\begin{aligned} v_l(r_{PP'}) &= (2l_1 + 1)(2l_2 + 1)(2l_3 + 1)(8\pi^2)^{-2} \\ &\times \int d\omega_P \int d\omega_{P'} \sum_m \begin{pmatrix} l_1 & l_2 & l_3 \\ m & -m & 0 \end{pmatrix} \\ &\times G_m^{(l_1)}(\omega_P) G_{-m}^{(l_2)}(\omega_{P'}) V(\omega_P, \omega_{P'}, r_{PP'}) \end{aligned}$$

Here we have used the fact that one can always choose to perform the *ab initio* calculations on the pair PP' in a coordinate frame with the z axis along $\mathbf{r}_{PP'}$. Then we have $\hat{r}_{PP'} = (\theta, \phi) = (0, 0)$ and $C_m^{(l)}(\hat{r}_{PP'}) = \delta_{m0}$. The integral can be further simplified by noting that the internal geometry of any molecular pair can be specified by at most five Euler angles, so that one of the six angles $\omega_P, \omega_{P'}$ can also be set to zero and left out of the integration. In special cases, even more simplifications can be made. For example, if the molecules P and P' are linear, two more Euler angles can be omitted. Once the coefficients $v_l(r_{PP'})$ are calculated for several values of $r_{PP'}$, it is convenient to fit their $r_{PP'}$ dependence by means of simple analytic forms (r^{-n} in the long range, $\exp(-Br)$ in the short range). For further details of this procedure we refer to the review by van der Avoird *et al.* (1980) and the references therein.

Finally, we observe that, in principle, one may truncate the expansion (15) after a few terms and thus model the anisotropy of the potential (the term $l = \{0, 0, 0\}$ is the isotropic part). Simple parameterized $r_{PP'}$ functions for the expansion coefficients $v_l(r_{PP'})$ can then be introduced and the parameters can be fitted empirically. The latter procedure is similar to the empirical way of obtaining atom-atom model potentials and the same questions can be raised regarding the validity of the resulting potentials.

C. Expansion of Atom-Atom Potentials in Symmetry-Adapted Functions

In atom-atom potentials the anisotropy of the intermolecular potential, i.e., its dependence on the molecular orientations ω_P and $\omega_{P'}$, is implicitly determined by the model. One can make this dependence explicit by expanding a given atom-atom potential in the form (15). It has been demonstrated by Sack (1964), Yasuda and Yamamoto (1971), and Downs *et al.* (1979) that analytic expressions can be derived for the expansion coefficients $v_l(r_{PP'})$ in (15) for atom-atom potentials (see Section II,A) with $f^{(n)}(r_{\alpha\beta}) = r_{\alpha\beta}^{-n}$ dependence and by Briels (1980) that they can be derived for atom-atom interactions with exponential dependence

$f^{(\text{exp})}(r_{\alpha\beta}) = \exp(-r_{\alpha\beta})$. In order to derive such expressions these authors use the two-center expansion of the functions:

$$f^{(n/\text{exp})}(r_{\alpha\beta}) = f^{(n/\text{exp})}(|\mathbf{r}_{PP'} - \mathbf{d}_\alpha + \mathbf{d}_\beta|)$$

where \mathbf{d}_α is the position vector of atom α relative to the center of mass of the molecule P to which it belongs and \mathbf{d}_β is the same vector for atom β in molecule P' . The result is the formula (Briels, 1980):

$$f^{(n/\text{exp})}(r_{\alpha\beta}) = \sum_{\mathbf{l}} \begin{pmatrix} l_1 & l_2 & l_3 \\ 0 & 0 & 0 \end{pmatrix} g_{\mathbf{l}}^{(n/\text{exp})}(d_\alpha, d_\beta, r_{PP'}) \\ \times \sum_{\mathbf{m}} \begin{pmatrix} l_1 & l_2 & l_3 \\ m_1 & m_2 & m_3 \end{pmatrix} C_{m_1}^{(l_1)}(\hat{d}_\alpha) C_{m_2}^{(l_2)}(\hat{d}_\beta) C_{m_3}^{(l_3)}(\hat{r}_{PP'}) \quad (16)$$

with

$$g_{\mathbf{l}}^{(1)}(d_\alpha, d_\beta, r_{PP'}) = \delta_{l_1+l_2, l_3} (-1)^{l_2/2} [\mathbb{I}] \frac{(2l_3)!}{(2l_1+1)!(2l_2+1)!} \frac{l_1! l_2!}{l_3!} \\ \times \frac{1}{r_{PP'}} \left(\frac{d_\alpha}{r_{PP'}} \right)^{l_1} \left(\frac{d_\beta}{r_{PP'}} \right)^{l_2} \quad (17)$$

$$g_{\mathbf{l}}^{(n)}(d_\alpha, d_\beta, r_{PP'}) = (-1)^{l_2/2} \frac{[\mathbb{I}]}{(n-2)!} \left(\frac{1}{r_{PP'}} \right)^n \left(\frac{d_\alpha}{r_{PP'}} \right)^{l_1} \left(\frac{d_\beta}{r_{PP'}} \right)^{l_2} \\ \times \sum_{m_1=0}^{\infty} \sum_{m_2=0}^{\infty} \left(\frac{d_\alpha}{r_{PP'}} \right)^{2m_1} \left(\frac{d_\beta}{r_{PP'}} \right)^{2m_2} \\ \times \frac{(n-2+l_1+l_2-l_3+2m_1+2m_2)!}{(2l_1+2m_1+1)!!(2m_1)!!(2l_2+2m_2+1)!!(2m_2)!!} \\ \times \frac{(n-2+l_1+l_2+l_3+2m_1+2m_2)!!}{(n-2+l_1+l_2-l_3+2m_1+2m_2)!!} \quad (18)$$

for $n \geq 2$, and

$$g_{\mathbf{l}}^{(\text{exp})}(d_\alpha, d_\beta, r_{PP'}) = (-1)^{l_2+1} [\mathbb{I}] \{ (1+l_1+l_2+l_3) J_{l_1}(d_\alpha) J_{l_2}(d_\beta) K_{l_3}(r_{PP'}) \\ + d_\alpha J_{l_1+1}(d_\alpha) J_{l_2}(d_\beta) K_{l_3}(r_{PP'}) \\ + d_\beta J_{l_1}(d_\alpha) J_{l_2+1}(d_\beta) K_{l_3}(r_{PP'}) \\ - r_{PP'} J_{l_1}(d_\alpha) J_{l_2}(d_\beta) K_{l_3+1}(r_{PP'}) \} \quad (19)$$

We use the abbreviated notation $[\mathbb{I}] = (2l_1+1)(2l_2+1)(2l_3+1)$. The functions $J_l(z)$ and $K_l(z)$ are related to the modified spherical Bessel

functions (Antosiewicz, 1970) of the first and third kind, respectively, by $J_l(z) = (\pi/2z)^{1/2} J_{l+(1/2)}(z)$ and $(\pi/2) K_l(z) = (\pi/2z)^{1/2} K_{l+(1/2)}(z)$. It is interesting to notice that Eq. (19) is in closed form, whereas Eq. (18) contains an infinite sum.

Using the general expressions (1) with (4) for an atom-atom model and substituting the two-center expansion (16), we write the intermolecular atom-atom potential as

$$\begin{aligned}
 V_{PP'} = V(\omega_P, \omega_{P'}, \mathbf{r}_{PP'}) &= \sum_l \begin{pmatrix} l_1 & l_2 & l_3 \\ 0 & 0 & 0 \end{pmatrix} \sum_{a \in P} \sum_{b \in P'} \\
 &\times \sum_{n, \exp} A_{n/\exp}^{X_a X_b} g_l^{(n/\exp)}(d_a, d_b, r_{PP'}) \\
 &\times \sum_{\mathbf{m}} \begin{pmatrix} l_1 & l_2 & l_3 \\ m_1 & m_2 & m_3 \end{pmatrix} \left\{ \sum_{\alpha \in a} C_{m_1}^{(l_1)}(\hat{d}_\alpha) \right\} \\
 &\times \left\{ \sum_{\beta \in b} C_{m_2}^{(l_2)}(\hat{d}_\beta) \right\} C_{m_3}^{(l_3)}(\hat{r}_{PP'}) \quad (20)
 \end{aligned}$$

Here we have partitioned the sums over all atoms α and β in the molecules P and P' in the following manner. First, we sum over equivalent atoms within the same class $\alpha \in a$ and $\beta \in b$, which have the same chemical nature $X_\alpha = X_a$ and $X_\beta = X_b$ and the same distance $d_\alpha = d_a$ and $d_\beta = d_b$ to the respective molecular center of mass. Next, we sum over classes $a \in P$ and $b \in P'$. The orientations \hat{d}_α and \hat{d}_β of the position vectors of the atoms \mathbf{d}_α and \mathbf{d}_β , relative to the molecular centers of mass, are still given with respect to the global coordinate frame. If we denote the polar angles of \mathbf{d}_α and \mathbf{d}_β in the molecule fixed frames by \hat{d}_α^0 and \hat{d}_β^0 and remember that the molecular frames are related to the global frame by rotations through the Euler angles ω_P and $\omega_{P'}$, respectively, we find that

$$\begin{aligned}
 \sum_{\alpha \in a} C_{m_1}^{(l_1)}(\hat{d}_\alpha) &= \sum_{n_1} \left\{ \sum_{\alpha \in a} C_{n_1}^{(l_1)}(\hat{d}_\alpha^0) \right\} D_{n_1 m_1}^{(l_1)}(\omega_P) \\
 &= k_a^{(l_1)} G_{m_1}^{(l_1)}(\omega_P) \quad (21)
 \end{aligned}$$

and a similar expression for atoms $\beta \in b \in P'$. The latter equality, which is related to Eq. (10), follows from the fact that the left-hand side must be invariant under all rotations of the molecular point group G_P ; these rotations just interchange the equivalent atoms $\alpha \in a$. Introducing Eq. (21) and the corresponding result for atoms $\beta \in b$ into Eq. (20), the general atom-atom potential is expressed in the form of Eq. (15), with

$$v_l(r_{PP'}) = \begin{pmatrix} l_1 & l_2 & l_3 \\ 0 & 0 & 0 \end{pmatrix} \sum_{a \in P} \sum_{b \in P'} k_a^{(l_1)} k_b^{(l_2)} \sum_{n, \exp} A_{n/\exp}^{x_a x_b} \times g_l^{(n/\exp)}(d_a, d_b, r_{PP'}) \quad (22)$$

D. The Crystal Hamiltonian

Now that we have expressed the intermolecular potential, it is easy to write down the crystal Hamiltonian. We associate with each point $P = \{\mathbf{n}, i\}$ of the lattice a molecule with position vector $\mathbf{r}_P = \mathbf{R}_P + \mathbf{u}_P$. The vector \mathbf{R}_P denotes the position of the lattice point P , i.e., $\mathbf{R}_P = \mathbf{R}_n + \mathbf{R}_i$ with \mathbf{R}_n being the position vector of the origin of the unit cell to which P belongs and \mathbf{R}_i the position vector of P relative to this origin. The displacement vector \mathbf{u}_P describes the position of the center of mass of the molecule at P relative to the lattice point P . The Hamiltonian then reads

$$H = \sum_P \{T(\mathbf{u}_P) + L(\omega_P)\} + \frac{1}{2} \sum_{P \neq P'} V_{PP'}(\mathbf{u}_P, \omega_P; \mathbf{u}_{P'}, \omega_{P'}) \quad (23)$$

where

$$V_{PP'}(\mathbf{u}_P, \omega_P; \mathbf{u}_{P'}, \omega_{P'}) = V(\omega_P, \omega_{P'}, \mathbf{r}_{PP'}) \quad (24)$$

In the latter equation $\mathbf{r}_{PP'} = \mathbf{r}_{P'} - \mathbf{r}_P = \mathbf{R}_{P'} - \mathbf{R}_P + \mathbf{u}_{P'} - \mathbf{u}_P = \mathbf{R}_{PP'} + \mathbf{u}_{P'} - \mathbf{u}_P$, from which the dependence of $V_{PP'}$ on $\mathbf{u}_{P'}$ and \mathbf{u}_P follows. In Eq. (23) the kinetic energy operators for the translational and rotational motions are defined, respectively, as

$$T(\mathbf{u}_P) = -\frac{\hbar^2}{2M} \Delta(\mathbf{u}_P) \quad (25)$$

$$L(\omega_P) = \frac{J_a^2(\omega_P)}{2I_a} + \frac{J_b^2(\omega_P)}{2I_b} + \frac{J_c^2(\omega_P)}{2I_c} \quad (26)$$

Here $\Delta(\mathbf{u}_P)$ is the Laplacian and J_a, J_b , and J_c are the components of the angular momentum operator with respect to the principal a, b , and c axes of the molecule; I_a, I_b , and I_c are the principal values of the molecular moment of inertia. For simplicity we have assumed that the crystal is composed of just one type of molecules. Otherwise, the molecular mass M and the moments of inertia have to carry the sublattice label i , appearing in $P = \{\mathbf{n}, i\}$.

The dependence of the potential $V_{PP'}$ on the translational degrees of freedom \mathbf{u}_P is rather intricate, and in order to use this potential in lattice dynamics calculations, we have to rewrite it in more tractable form. Beforehand, we make some remarks concerning the case when only rotational motions are considered. This is useful when the rotation-transla-

tion coupling is weak, for instance, as in hydrogen or methane crystals, or, in general, at certain points of high symmetry in the Brillouin zone, where the rotation and translation modes are decoupled because of this symmetry. In these cases, the potential for the rotational problem is an effective potential in the sense that it can be obtained from the complete intermolecular potential by averaging over the translational motions. This effective potential can be written in the form of Eq. (15) with coefficients $\langle v_l(r_{PP'}) \rangle = v_l(R_{PP'})$. The crystal Hamiltonian then reads

$$H = U^C + \sum_P \{L(\omega_P) + V_P(\omega_P)\} + \frac{1}{2} \sum_{P \neq P'} \Phi_{PP'}(\omega_P, \omega_{P'}) \quad (27)$$

The two-body potential $\Phi_{PP'}$ consists of those terms that depend on the orientations of both molecules; i.e., $\Phi_{PP'}$ is equal to $V_{PP'}$ minus the terms, with one or both of l_1 and l_2 equal to zero. The terms with either l_1 or l_2 equal to zero are contained in V_P , which depends only on the orientation of molecule P , and the isotropic term $l_1 = l_2 = 0$ is just the constant U^C :

$$U^C = \frac{1}{2} \sum_{P \neq P'} \sum v_{0,0,0}(R_{PP'}) = \sum_P U_P \quad (28)$$

$$V_P(\omega_P) = \sum'_{l,m} V_m^{(l)}(P) G_m^{(l)}(\omega_P) \quad (29)$$

$$\Phi_{PP'}(\omega_P, \omega_{P'}) = \sum'_{l_1, m_1} \sum'_{l_2, m_2} G_{m_1}^{(l_1)}(\omega_P) X_{m_1, m_2}^{(l_1, l_2)}(P, P') G_{m_2}^{(l_2)}(\omega_{P'}) \quad (30)$$

with

$$\begin{aligned} V_m^{(l)}(P) &= (2l+1)^{-1/2} (-1)^l \frac{1}{2} \sum_{P'} \{v_{l,0,l}(R_{PP'}) C_m^{(l)}(\hat{R}_{PP'})^* \\ &\quad + v_{0,l,l}(R_{PP'}) C_m^{(l)}(-\hat{R}_{PP'})^*\} \\ &= (2l+1)^{-1/2} (-1)^l \sum_{P'} v_{l,0,l}(R_{PP'}) C_m^{(l)}(\hat{R}_{PP'})^* \end{aligned} \quad (31)$$

$$X_{m_1, m_2}^{(l_1, l_2)}(P, P') = \sum_{l_3, m_3} v_l(R_{PP'}) \begin{pmatrix} l_1 & l_2 & l_3 \\ m_1 & m_2 & m_3 \end{pmatrix} C_{m_3}^{(l_3)}(\hat{R}_{PP'}) \quad (32)$$

In Eq. (31) we have used the relation $v_{0,l,l}(R_{PP'}) = (-1)^l v_{l,0,l}(R_{PP'})$ (Briels, 1980). The primes on the summation signs indicate that the terms with $l = 0$ have to be omitted.

The term $V_P(\omega_P)$ in Eq. (27) is called the crystal field term. From Eqs. (29) and (31) it is clear that this term is invariant under all rotations of the global frame that correspond to symmetry operations on the lattice. As a

result $V_P(\omega_P)$ contains only linear combinations of the functions $G_m^{(l)}(\omega_P)$, which transform according to the totally symmetric representation of the site group S_P . Note that S_P contains all rotations around P that leave the point lattice invariant; this group is larger than the point group of the crystal, which is not yet defined as long as the equation of motion is not solved. The functions adapted to the site symmetry can be obtained by acting with the projection operator:

$$P_S = \frac{1}{\#S_P} \sum_{g \in S_P} R^G(\tilde{\omega}_g) \quad (33)$$

on the functions $G_m^{(l)}(\omega_P)$. In Table II we have given the results for the octahedral group $S_P = O$, which is the site group of all sites in the fcc lattice.

In order to obtain the explicit translational dependence of the complete intermolecular potential (15), we expand the translationally dependent part of Eq. (15) as a Taylor series in the displacement vectors \mathbf{u}_P and $\mathbf{u}_{P'}$:

$$v_l(r_{PP'}) C_{m_3}^{(l_3)}(\hat{r}_{PP'}) = \sum_{\alpha_1, \alpha_2} \frac{(-\mathbf{u}_P \cdot \nabla)^{\alpha_1}}{\alpha_1!} \frac{(\mathbf{u}_{P'} \cdot \nabla)^{\alpha_2}}{\alpha_2!} v_l(R_{PP'}) C_{m_3}^{(l_3)}(\hat{R}_{PP'}) \quad (34)$$

In principle, the sums over α_1 and α_2 must be extended to infinity. In practice, we apply the truncation condition $\alpha_1 + \alpha_2 \leq \alpha_{\max}$. The terms with $\alpha_1 = \alpha_2 = 0$ give rise to the purely rotational part of the Hamiltonian, which we have just treated. The other terms can be most easily evaluated by applying the gradient formula in spherical tensor form (Edmonds, 1957):

$$\begin{aligned} \mathbf{u}_P \cdot \nabla F(R_{PP'}) C_{m_3}^{(l_3)}(\hat{R}_{PP'}) &= u_P \sum_k A_{l_3 k}(R_{PP'}) F(R_{PP'}) \\ &\times [C^{(1)}(\hat{u}_P) \otimes C^{(k)}(\hat{R}_{PP'})]_{m_3}^{(l_3)} \end{aligned} \quad (35)$$

where A_{lk} is an operator defined by

$$\begin{aligned} A_{lk}(R) &= -\delta_{k,l-1} \left[\frac{l(2l-1)}{2l+1} \right]^{1/2} \left(\frac{d}{dR} + \frac{l+1}{R} \right) \\ &+ \delta_{k,l+1} \left[\frac{(l+1)(2l+3)}{2l+1} \right]^{1/2} \left(\frac{d}{dR} - \frac{l}{R} \right) \end{aligned} \quad (36)$$

The irreducible tensor product between the brackets represents the usual angular momentum coupling

$$[C^{(l_1)}(\hat{r}_1) \otimes C^{(l_2)}(\hat{r}_2)]_{m_3}^{(l_3)} = (-1)^{l_1+l_2-m_3} \sum_{m_1 m_2} \begin{pmatrix} l_1 & l_2 & l_3 \\ m_1 & m_2 & -m_3 \end{pmatrix} C_{m_1}^{(l_1)}(\hat{r}_1) C_{m_2}^{(l_2)}(\hat{r}_2) \quad (37)$$

between two tensors $\{C_{m_1}^{(l_1)}(\hat{r}_1); m_1 = -l_1, \dots, l_1\}$ and $\{C_{m_2}^{(l_2)}(\hat{r}_2); m_2 = -l_2, \dots, l_2\}$ to an irreducible tensor that transforms as $C_{m_3}^{(l_3)}$ under rotations of the global frame. Applying Eq. (35) repeatedly to Eq. (34), we find after some tedious algebra (Briels *et al.*, 1984)

$$\begin{aligned} v_{\mathbf{k}}(r_{PP'}) C_{m_3}^{(l_3)}(\hat{r}_{PP'}) &= \sum_{\alpha_1, \alpha_2} \frac{(-u_P)^{\alpha_1}}{\alpha_1!} \frac{(u_{P'})^{\alpha_2}}{\alpha_2!} \\ &\times \sum_{\mathbf{k}} \sum_j {}^j W_{\mathbf{k}}^{(1)}(R_{PP'} | \alpha_1, \alpha_2) \\ &\times [[C^{(k_1)}(\hat{u}_P) \otimes C^{(k_2)}(\hat{u}_{P'})]^{(j)} \otimes C^{(k_3)}(\hat{R}_{PP'})]_{m_3}^{(l_3)} \quad (38) \end{aligned}$$

TABLE II

TETRAHEDRAL ROTATION FUNCTIONS ADAPTED TO THE SITE GROUP O [SEE EQ. (33)]^a

l	Function
0	$O_T^{(0)} = T_0^{(0)}$
3	$O_T^{(3)} = -\frac{1}{2}i(2)^{1/2}\{T_2^{(3)} - T_{-2}^{(3)}\}$
4	$O_T^{(4)} = \frac{1}{2}(\frac{7}{3})^{1/2}\{T_0^{(4)} + (\frac{5}{14})^{1/2}(T_4^{(4)} + T_{-4}^{(4)})\}$
6	$O_T^{(6)} = \frac{1}{4}(2)^{1/2}\{T_0^{(6)} - (\frac{7}{2})^{1/2}(T_4^{(6)} + T_{-4}^{(6)})\}$ $O_T^{(6)} = \frac{1}{4}(\frac{11}{2})^{1/2}\{(T_2^{(6)} + T_{-2}^{(6)}) - (\frac{5}{11})^{1/2}(T_6^{(6)} + T_{-6}^{(6)})\}$
7	$O_T^{(7)} = -\frac{1}{4}i(\frac{13}{3})^{1/2}\{(T_2^{(7)} - T_{-2}^{(7)}) + (\frac{11}{13})^{1/2}(T_6^{(7)} - T_{-6}^{(7)})\}$
8	$O_T^{(8)} = \frac{1}{8}(33)^{1/2}\{T_0^{(8)} + (\frac{14}{99})^{1/2}(T_4^{(8)} + T_{-4}^{(8)}) + (\frac{65}{198})^{1/2}(T_8^{(8)} + T_{-8}^{(8)})\}$
9	$O_T^{(9)} = -\frac{1}{4}i(\frac{3}{2})^{1/2}\{(T_2^{(9)} - T_{-2}^{(9)}) - (\frac{13}{3})^{1/2}(T_6^{(9)} - T_{-6}^{(9)})\}$ $O_T^{(9)} = -\frac{1}{4}i(\frac{17}{3})^{1/2}\{(T_4^{(9)} - T_{-4}^{(9)}) - (\frac{7}{17})^{1/2}(T_8^{(9)} - T_{-8}^{(9)})\}$
10	$O_T^{(10)} = \frac{1}{8}(\frac{65}{6})^{1/2}\{T_0^{(10)} - (\frac{66}{85})^{1/2}(T_4^{(10)} + T_{-4}^{(10)}) - (\frac{187}{150})^{1/2}(T_8^{(10)} + T_{-8}^{(10)})\}$ $O_T^{(10)} = \frac{1}{16}(\frac{247}{3})^{1/2}\{(T_2^{(10)} + T_{-2}^{(10)}) + (\frac{1}{26})^{1/2}(T_6^{(10)} + T_{-6}^{(10)}) - (\frac{255}{484})^{1/2}(T_{10}^{(10)} + T_{-10}^{(10)})\}$

^a Tetrahedral rotational functions as in Table I.

Site group: z-axis is 4-fold axis, [1, 1, 1] direction is 3-fold axis.

with the following recursion relation for the coefficients:

$$\begin{aligned}
 {}^j W_{k_1, k_2, k_3}^{(l)}(R_{PP'} | \alpha_1 + 1, \alpha_2) &= (-1)^{k_2 + k_3 + l_3} (2j + 1)(2k_1 + 1) \\
 &\times \sum_{k'_1 k'_2} \sum_{j'} \begin{pmatrix} 1 & k'_1 & k_1 \\ 0 & 0 & 0 \end{pmatrix} \begin{Bmatrix} k_1 & k_2 & j \\ j' & 1 & k'_1 \end{Bmatrix} \begin{Bmatrix} j & k_3 & l_3 \\ k'_3 & j' & 1 \end{Bmatrix} \\
 &\times A_{k'_3 k_3}(R_{PP'}) {}^j W_{k'_1, k_2, k'_3}^{(l)}(R_{PP'} | \alpha_1, \alpha_2)
 \end{aligned} \quad (39)$$

and an analogous relation to raise the index α_2 . The symbols between braces are 6- j coefficients, which arise from recoupling the spherical harmonics (Edmonds, 1957; Brink and Satchler, 1975). The introduction of Eq. (38) into (15) then yields the final expression for the intermolecular potential:

$$\begin{aligned}
 V_{PP'}(\mathbf{u}_P, \omega_P; \mathbf{u}_{P'}, \omega_{P'}) &= \sum_{\alpha_1, \alpha_2} \frac{(-u_P)^{\alpha_1}}{\alpha_1!} \frac{(u_{P'})^{\alpha_2}}{\alpha_2!} \sum_l \sum_k \sum_j {}^j W_k^{(l)}(R_{PP'} | \alpha_1, \alpha_2) \\
 &\times \sum_{\mathbf{m}} \begin{pmatrix} l_1 & l_2 & l_3 \\ m_1 & m_2 & m_3 \end{pmatrix} G_{m_1}^{(l_1)}(\omega_P) G_{m_2}^{(l_2)}(\omega_{P'}) \\
 &\times [[C^{(k_1)}(\hat{u}_P) \otimes C^{(k_2)}(\hat{u}_{P'})]^{(j)} \otimes C^{(k_3)}(\hat{R}_{PP'})]_{m_3}^{(l_3)}
 \end{aligned} \quad (40)$$

Another, equivalent, form in which the potential can be written is

$$\begin{aligned}
 V_{PP'}(\mathbf{u}_P, \omega_P; \mathbf{u}_{P'}, \omega_{P'}) &= \sum_{\alpha_1, \alpha_2} \frac{(-u_P)^{\alpha_1}}{\alpha_1!} \frac{(u_{P'})^{\alpha_2}}{\alpha_2!} \sum_l \sum_{j_1, j_2} \sum_{k_1, k_2} \\
 &\times B_{j_1, k_1; j_2, k_2}^{(l)}(R_{PP'} | \alpha_1, \alpha_2) \sum_{\mathbf{m}} \begin{pmatrix} l_1 & l_2 & l_3 \\ m_1 & m_2 & m_3 \end{pmatrix} [G^{(j_1)}(\omega_P) \otimes C^{(k_1)}(\hat{u}_P)]_{m_1}^{(l_1)} \\
 &\times [G^{(j_2)}(\omega_{P'}) \otimes C^{(k_2)}(\hat{u}_{P'})]_{m_2}^{(l_2)} C_{m_3}^{(l_3)}(\hat{R}_{PP'})
 \end{aligned} \quad (41)$$

The expansion coefficients are related to those of Eq. (40) by

$$\begin{aligned}
 B_{j_1, k_1; j_2, k_2}^{(l)}(R_{PP'} | \alpha_1, \alpha_2) &= (-1)^{k_1 + k_2} (2l_1 + 1)(2l_2 + 1) \\
 &\times \sum_{a, b} (-1)^a \begin{Bmatrix} l_1 & l_2 & l_3 \\ k_1 & k_2 & a \\ j_1 & j_2 & b \end{Bmatrix} {}^a W_{k_1, k_2, l_3}^{(j_1, j_2, b)}(R_{PP'} | \alpha_1, \alpha_2)
 \end{aligned} \quad (42)$$

and they satisfy the recursion relations

$$\begin{aligned}
 B_{j_1, k_1; j_2, k_2}^{(l_1, l_2, l_3)}(R_{PP'} | \alpha_1 + 1, \alpha_2) &= (-1)^{1+j_1+l_1+l_2} (2k_1 + 1)(2l_1 + 1) \\
 &\times \sum_{l'_1, l'_2, k'_1} \begin{pmatrix} 1 & k'_1 & k_1 \\ 0 & 0 & 0 \end{pmatrix} \begin{Bmatrix} k_1 & j_1 & l_2 \\ l'_1 & 1 & k'_1 \end{Bmatrix} \begin{Bmatrix} l_1 & l_3 & l_2 \\ l'_3 & l'_1 & 1 \end{Bmatrix} A_{l'_3 l_3}(R_{PP'}) \\
 &\times B_{j_1, k_1; j_2, k_2}^{(l'_1, l'_2, l'_3)}(R_{PP'} | \alpha_1, \alpha_2)
 \end{aligned} \quad (43)$$

These results [(41) and (42)] are obtained from Eq. (40) by angular momentum recoupling (Brink and Satchler, 1975); the symbol between braces in Eq. (42) is a 9- j coefficient. The recursion relation (43) is derived analogously to Eq. (39) (see Briels *et al.*, 1984).

By introducing the expanded potential [Eq. (40) or Eq. (41)] into the crystal Hamiltonian [Eq. (23)], we can write the latter as

$$\begin{aligned}
 H = & U^C + \sum_P \{T(\mathbf{u}_P) + V_P^T(\mathbf{u}_P)\} + \sum_P \{L(\omega_P) + V_P^R(\omega_P)\} \\
 & + \sum_P V_P^{TR}(\mathbf{u}_P, \omega_P) + \frac{1}{2} \sum_{P \neq P'} \sum \{\Phi_{PP'}^T(\mathbf{u}_P; \mathbf{u}_{P'}) \\
 & + \Phi_{PP'}^R(\omega_P; \omega_{P'}) + \Phi_{PP'}^{TR}(\mathbf{u}_P, \omega_P; \mathbf{u}_{P'}, \omega_{P'})\}
 \end{aligned} \quad (44)$$

in terms of one-body operators and two-body operators affecting the molecular translations T , rotations R , and their coupling TR . This partitioning can give some physical insight; in specific cases, one can study the importance of the different contributions. Just as we did for pure rotational motions, we can use the site symmetry to simplify the expressions. For the crystal field terms V_P^T and V_P^R this can be done exactly as before. For the mixed field terms V_P^{TR} it is somewhat more difficult; one finds that

$$\begin{aligned}
 V_P^{TR}(\mathbf{u}_P, \omega_P) = & \sum_{\alpha} (u_P)^{\alpha} \sum_{l_1, l_2} \sum_{\mu} V_{l_1, l_2}^{(\mu)}(P | \alpha) \\
 & \times \sum_i C_i^{(l_1, \mu)}(\hat{u}_P)^* G_i^{(l_2, \mu)}(\omega_P)
 \end{aligned} \quad (45)$$

where $C_i^{(l_1, \mu)}$, $i = 1, \dots, n_{\mu}$, are linear combinations of $C_m^{(l)}$ that transform according to the unitary representation $\Gamma^{(\mu)}$ of the site group S_P ; n_{μ} is the dimension of this representation. Similarly, $G_i^{(l, \mu)}$, $i = 1, \dots, n_{\mu}$, are linear combinations of $G_m^{(l)}$ transforming in the same way. These functions are coupled to an invariant of S_P . An explicit inspection of the separate contributions in Eq. (45) is only useful for small values of α_{\max} , since l_1 is at most equal to α_{\max} [see Eqs. (34)–(36)]. Otherwise, the separation becomes too complicated to provide any insight. For the two-body terms this applies *a fortiori*. However, even without the partitioning given by Eq. (44), the crystal Hamiltonian (23) with the potential expanded by Eq. (40) or (41) forms a good basis for discussing any lattice dynamics treatment.

III. Harmonic and Quasi-Harmonic Theories of Lattice Dynamics

In this section we briefly discuss the harmonic and quasi-harmonic models that are commonly used to describe the molecular motions, i.e.,

the lattice vibrations, in molecular crystals. We use the term *quasi-harmonic* for any theory in which the harmonic approximation plays a central role, although strictly speaking the quasi-harmonic model (Barron and Klein, 1974) is a special theory in this category. We include in this section a description of perturbation theory around the harmonic model and of the self-consistent phonon method. In general, as will be clear from the following, quasi-harmonic theories are suitable for describing anharmonic motions with fairly small amplitudes, for example, the translational motions in most crystals. If, however, the vibrational amplitudes are larger, for instance, for the librational motions, especially of small molecules or in the neighborhood of phase transitions, the quasi-harmonic models are of very limited value. They break down completely if the molecules perform hindered rotations as in plastic crystals. In these cases one must resort to completely different treatments, which we discuss in Section IV.

A. Harmonic Approximation

The harmonic approximation consists of expanding the potential up to second order in the atomic or molecular displacements around some local minimum and then diagonalizing the quadratic Hamiltonian. In the case of molecular crystals the rotational part of the kinetic energy, expressed in Euler angles, must be approximated, too. The angular momentum operators that occur in Eq. (26) are given by

$$\begin{aligned} J_a(\omega) &= \frac{\hbar}{i} \left(-\frac{\cos \gamma}{\sin \beta} \frac{\partial}{\partial \alpha} + \sin \gamma \frac{\partial}{\partial \beta} + \cot \beta \frac{\partial}{\partial \gamma} \right) \\ J_b(\omega) &= \frac{\hbar}{i} \left(\frac{\sin \gamma}{\sin \beta} \frac{\partial}{\partial \alpha} + \cos \gamma \frac{\partial}{\partial \beta} - \cot \beta \frac{\partial}{\partial \gamma} \right) \\ J_c(\omega) &= \frac{\hbar}{i} \frac{\partial}{\partial \gamma} \end{aligned} \quad (46)$$

where $\omega = \{\alpha, \beta, \gamma\}$ are the Euler angles of the molecule fixed coordinate frame relative to the global frame. The harmonic approximation implies that one replaces the angles ω in Eq. (46) by their equilibrium values $\omega_0 = \{\alpha_0, \beta_0, \gamma_0\}$ and then substitutes the result into the quadratic kinetic energy expression (26). Thus, one neglects the terms linear in the operators $\partial/\partial\beta$ and $\partial/\partial\gamma$, which occur in the exact expression (26); these terms arise by commuting $\partial/\partial\beta$ and $\partial/\partial\gamma$ with the sine and cosine functions of β and γ in the exact Eq. (46). At the same time, the volume element $\sin \beta \, d\alpha \, d\beta \, d\gamma$ becomes $\sin \beta_0 \, d\alpha \, d\beta \, d\gamma$ and the angular displacement coordinates $\Delta\omega = \omega - \omega_0$ become rectilinear and formally run from $-\infty$ to ∞ . For

linear molecules this approximation has been applied by Goodings and Henkelman (1971), Schnepf and Jacobi (1972), and Walmsley (1975).

The crystal Hamiltonian now reads

$$H = \frac{1}{2} \sum_P \sum_{\lambda, \lambda'} G_P^{\lambda, \lambda'} P_P^\lambda P_P^{\lambda'} + \frac{1}{2} \sum_{P, P'} \sum_{\lambda, \lambda'} F_{P, P'}^{\lambda, \lambda'} Q_P^\lambda Q_{P'}^{\lambda'} \quad (47)$$

where

$$Q_P^\lambda = u_P^\lambda \quad \text{for } \lambda = 1, 2, 3$$

$$Q_P^\lambda = \Delta \omega_P^{\lambda-3} \quad \text{for } \lambda = 4, 5, 6$$

and

$$P_P^\lambda = \frac{\hbar}{i} \frac{\partial}{\partial Q_P^\lambda}$$

are the momenta conjugate to these coordinates. These operators satisfy the usual commutation rules:

$$[Q_P^\lambda, P_{P'}^{\lambda'}] = i\hbar \delta_{P, P'} \delta_{\lambda, \lambda'}$$

The first term in Eq. (47) represents the kinetic energy operator. The 6×6 matrices \mathbf{G}_P follow from the foregoing discussion; they contain the inverse molecular mass M^{-1} and the inverse inertia tensor depending on the equilibrium angles $\omega_0 = \{\alpha_0, \beta_0, \gamma_0\}$ with respect to the global frame. The second term represents the potential; linear terms are absent because this potential is expanded around a local minimum. The 6×6 matrices $\mathbf{F}_{P, P'}$ are defined as the second derivatives

$$F_{P, P'}^{\lambda, \lambda'} = \left[\frac{\partial^2 V_{PP'}}{\partial Q_P^\lambda \partial Q_{P'}^{\lambda'}} \right]_0, \quad F_{P, P'}^{\lambda, \lambda'} = \sum_{P'} \left[\frac{\partial^2 V_{PP'}}{\partial Q_P^\lambda \partial Q_{P'}^{\lambda'}} \right]_0 \quad (48)$$

taken at the equilibrium positions and orientations. The Hamiltonian (47) can easily be diagonalized exactly. First we introduce the operators

$$Q_i^\lambda(\mathbf{q}) = \frac{1}{\sqrt{N}} \sum_{\mathbf{n}} \exp(i\mathbf{q} \cdot \mathbf{R}_{\mathbf{n}}) Q_P^\lambda$$

$$P_i^\lambda(\mathbf{q}) = \frac{1}{\sqrt{N}} \sum_{\mathbf{n}} \exp(-i\mathbf{q} \cdot \mathbf{R}_{\mathbf{n}}) P_P^\lambda \quad (49)$$

with $P = \{\mathbf{n}, i\}$, where N is the number of unit cells in the crystal and \mathbf{q} is a vector in the Brillouin zone. The Hamiltonian transforms into

$$H = \sum_{\mathbf{q}} H(\mathbf{q}) \quad (50)$$

with

$$H(\mathbf{q}) = \frac{1}{2} \sum_i \sum_{\lambda, \lambda'} G_i^{\lambda, \lambda'} P_i^\lambda(\mathbf{q}) P_i^{\lambda'}(\mathbf{q})^\dagger + \frac{1}{2} \sum_{i, i'} \sum_{\lambda, \lambda'} F_{i, i'}^{\lambda, \lambda'}(\mathbf{q}) Q_i^\lambda(\mathbf{q}) Q_{i'}^{\lambda'}(\mathbf{q})^\dagger \quad (51)$$

and

$$F_{i, i'}^{\lambda, \lambda'}(\mathbf{q}) = \sum_{\mathbf{n}} F_{\{\mathbf{0}, i\} \{\mathbf{n}, i'\}}^{\lambda, \lambda'} \exp(i\mathbf{q} \cdot \mathbf{R}_{\mathbf{n}}) = F_{i', i}^{\lambda', \lambda}(-\mathbf{q}) = F_{i', i}^{\lambda', \lambda}(\mathbf{q})^* \quad (52)$$

Here we have used the property that \mathbf{G}_P and $\mathbf{F}_{PP'}$, are translationally invariant. The commutation rules for the wave-vector-dependent operators are

$$[Q_i^\lambda(\mathbf{q}), P_{i'}^{\lambda'}(\mathbf{q}')] = i\hbar \delta_{i, i'} \delta_{\lambda, \lambda'} \delta_{\mathbf{q}, \mathbf{q}'}$$

Every $H(\mathbf{q})$, depends on $6Z$ operators $Q_i^\lambda(\mathbf{q})$ and $6Z$ operators $P_i^\lambda(\mathbf{q})$ if Z is the number of sublattices, i.e., the number of molecules in the unit cell. Finally, we introduce linear combinations

$$\begin{aligned} \bar{Q}_r(\mathbf{q}) &= \sum_{i=1}^Z \sum_{\lambda=1}^6 (\mathbf{c}(\mathbf{q})^{-1})_{i, \lambda}^r Q_i^\lambda(\mathbf{q}) \\ \bar{P}_r(\mathbf{q}) &= \sum_{i=1}^Z \sum_{\lambda=1}^6 c_r^{i, \lambda}(\mathbf{q}) P_i^\lambda(\mathbf{q}) \end{aligned} \quad (53)$$

such that $H(\mathbf{q})$ can be written as

$$H(\mathbf{q}) = \frac{1}{2} \sum_r \{ \bar{P}_r^\dagger(\mathbf{q}) \bar{P}_r(\mathbf{q}) + \omega_r(\mathbf{q})^2 \bar{Q}_r^\dagger(\mathbf{q}) \bar{Q}_r(\mathbf{q}) \} \quad (54)$$

The coefficients $\mathbf{c}_r(\mathbf{q}) = \{c_r^{i, \lambda}(\mathbf{q}), i = 1, \dots, Z, \lambda = 1, \dots, 6\}$ can be obtained from the generalized eigenvalue problem

$$\mathbf{F}(\mathbf{q}) \mathbf{c}_r(\mathbf{q}) = \mathbf{G}^{-1} \mathbf{c}_r(\mathbf{q}) \omega_r(\mathbf{q})^2 \quad (55)$$

with the normalization condition

$$\mathbf{c}_r^\dagger \mathbf{G}^{-1} \mathbf{c}_{r'} = \delta_{rr'} \quad (56)$$

The choice of the transformation (53) ensures that

$$[\bar{Q}_r(\mathbf{q}), \bar{P}_{r'}(\mathbf{q}')] = i\hbar \delta_{r, r'} \delta_{\mathbf{q}, \mathbf{q}'} \quad (57)$$

Introducing phonon creation and annihilation operators

$$\begin{aligned} a_r^\dagger(\mathbf{q}) &= [2\hbar\omega_r(\mathbf{q})]^{-1/2}\{\omega_r(\mathbf{q})\bar{Q}_r^\dagger(\mathbf{q}) - i\bar{P}_r(\mathbf{q})\} \\ a_r(\mathbf{q}) &= [2\hbar\omega_r(\mathbf{q})]^{-1/2}\{\omega_r(\mathbf{q})\bar{Q}_r(\mathbf{q}) + i\bar{P}_r^\dagger(\mathbf{q})\} \end{aligned} \quad (58)$$

with the commutation relations

$$[a_r(\mathbf{q}), a_{r'}^\dagger(\mathbf{q}')] = \delta_{r,r'} \delta_{\mathbf{q},\mathbf{q}'} \quad (59)$$

which follow from Eqs. (57) and (58), we can write the Hamiltonian in its well-known form:

$$H = \sum_{\mathbf{q}} \sum_r \hbar\omega_r(\mathbf{q}) \left\{ a_r^\dagger(\mathbf{q})a_r(\mathbf{q}) + \frac{1}{2} \right\} \quad (60)$$

representing a sum of independent harmonic oscillators whose excitations are called phonons. The properties of the crystal can be obtained (see Appendix) from the thermodynamic partition function and its derivatives. The partition function for a system of harmonic oscillators reads

$$Z = \text{Tr}(e^{-\beta H}) = \prod_{\mathbf{q}} \prod_r \left\{ 2 \sinh \left(\frac{1}{2} \beta \hbar \omega_r(\mathbf{q}) \right) \right\}^{-1} \quad (61)$$

with $\beta = (k_B T)^{-1}$, k_B being the Boltzmann constant and T the temperature.

B. Anharmonic Corrections by Perturbation Theory

In contrast with atoms and small molecules, the energy levels of extended systems almost invariably appear as broad bands. Degeneracy and near-degeneracy are the rule rather than the exception, and as a consequence, only weak interactions are needed to obtain intermixings of many states. This intermixing will also be caused by external perturbations applied in measurements, such as the electromagnetic fields in spectroscopic experiments. Another consequence of such close-lying states is that many of these states will be thermally populated. The (measured) properties of the system are not determined by the expectation values of operators over pure states, but by thermodynamic (Boltzmann) averages. These two aspects make it less useful to apply straightforward quantum-mechanical perturbation theory to single eigenstates of the Hamiltonian, as one mostly does for atoms and molecules. Instead, it is desirable to use a perturbation theory that describes the response of the whole system. The most powerful theory of this kind is based on the thermal, or imaginary time, Green's function.

In the perturbation theory of lattice dynamics one starts from the

harmonic approximation. The cubic and higher terms in the Taylor expansion of the potential around some local minimum, which are neglected in this approximation, are taken as perturbations of the harmonic model. Accordingly, the Hamiltonian can be written as (Califano, 1981)

$$\begin{aligned}
 H &= H_0 + H_I \\
 &= \sum_{\mathbf{q}} \sum_r \hbar \omega_r(\mathbf{q}) \left\{ a_r^\dagger(\mathbf{q}) a_r(\mathbf{q}) + \frac{1}{2} \right\} \\
 &\quad + \sum_{m=3}^{\infty} \sum_{\mathbf{q}_1, \dots, \mathbf{q}_m} \sum_{r_1, \dots, r_m} \Phi_{r_1, \dots, r_m}(\mathbf{q}_1, \dots, \mathbf{q}_m) A_{r_1}(\mathbf{q}_1) \dots A_{r_m}(\mathbf{q}_m) \quad (62)
 \end{aligned}$$

The operators appearing in the interaction Hamiltonian $H_I = \sum_{m=3}^{\infty} H_m$ are defined as

$$A_r(\mathbf{q}) = a_r(\mathbf{q}) + a_r^\dagger(-\mathbf{q}) \quad (63)$$

and the coupling constants $\Phi_{r_1, \dots, r_m}(\mathbf{q}_1, \dots, \mathbf{q}_m)$ are the derivatives of the potential with respect to the coordinates $\bar{Q}_r(\mathbf{q})$, multiplied by some constant factors. These coupling constants differ from zero only when $\mathbf{q}_1 + \dots + \mathbf{q}_m$ equals a reciprocal lattice vector. In molecular crystals, the difference between the exact rotational kinetic energy and its harmonic oscillator approximation (see Section III,A) should also be considered as a perturbation. As far as we know, this has never actually been done, however.

The thermal Green's function, or phonon propagator, that is used in lattice dynamics theory is defined as

$$\begin{aligned}
 G_{r,r'}(\mathbf{q}; \tau) &= \Theta(\tau) \langle e^{\tau H} A_r(\mathbf{q}) e^{-\tau H} A_{r'}(-\mathbf{q}) \rangle \\
 &\quad + \Theta(-\tau) \langle A_{r'}(-\mathbf{q}) e^{\tau H} A_r(\mathbf{q}) e^{-\tau H} \rangle \quad (64)
 \end{aligned}$$

where $\Theta(\tau)$ is the Heaviside step function and $\langle X \rangle$ denotes the thermodynamic average of an operator X over the eigenstates of H , i.e.,

$$\langle X \rangle = Z^{-1} \text{Tr}(X e^{-\beta H}) \quad (65)$$

with

$$Z = \text{Tr}(e^{-\beta H})$$

being the partition function and $\beta = (k_B T)^{-1}$. Using the invariance of the trace for cyclic permutations of the operators, one easily demonstrates that the phonon propagator (64) is a periodic function of the imaginary time τ with period β ; we may therefore confine the values of τ to the interval $0 \leq \tau \leq \beta$. The time-dependent perturbation expansion of the

phonon propagator for the Hamiltonian $H = H_0 + H_1$ is given by the formula (Fetter and Walecka, 1971)

$$G_{r,r'}(\mathbf{q}; \tau) = \langle S(\beta) \rangle_0^{-1} \sum_{n=0}^{\infty} \frac{(-1)^n}{n!} \int_0^{\beta} d\tau_1 \dots \int_0^{\beta} d\tau_n \times \langle T[\tilde{H}_1^{\tau_1} \dots \tilde{H}_1^{\tau_n} \tilde{A}_r^{\tau}(\mathbf{q}) \tilde{A}_{r'}^0(-\mathbf{q})] \rangle_0 \quad (66)$$

with

$$S(\beta) = \sum_{n=0}^{\infty} \frac{(-1)^n}{n!} \int_0^{\beta} d\tau_1 \dots \int_0^{\beta} d\tau_n T[\tilde{H}_1^{\tau_1} \dots \tilde{H}_1^{\tau_n}] \quad (67)$$

where \tilde{X}^{τ} denotes the operator X in the (imaginary time) interaction representation

$$\tilde{X}^{\tau} = \exp(\tau H_0) X \exp(-\tau H_0) \quad (68)$$

and $\langle X \rangle_0$ is the thermodynamic average of X over the eigenstates of the unperturbed Hamiltonian H_0 . The so-called time-ordering operator T places the operators to its right in the order of decreasing times, from left to right. Introduction of the anharmonic interaction operator $H_1 = \sum_{m=3}^{\infty} H_m$ defined in Eq. (62) into the expansions (66) and (67) yields many terms of the type written in Eq. (69) below. These can be evaluated by means of the (generalized) Wick theorem (Fetter and Walecka, 1971; Abrikosov *et al.*, 1965):

$$\begin{aligned} & \langle T[\tilde{A}_r^{\tau_1}(\mathbf{q}_1) \dots \tilde{A}_{r'2n}^{\tau_{2n}}(\mathbf{q}_{2n})] \rangle_0 \\ &= \sum_p \langle T[\tilde{A}_r^{\tau_i}(\mathbf{q}_i) \tilde{A}_{r'j}^{\tau_j}(\mathbf{q}_j)] \rangle_0 \dots \langle T[\tilde{A}_k^{\tau_k}(\mathbf{q}_k) \tilde{A}_l^{\tau_l}(\mathbf{q}_l)] \rangle_0 \end{aligned} \quad (69)$$

The summation runs over all $(2n - 1)!!$ pairings of the operators $\tilde{A}_i^{\tau_i}(\mathbf{q}_i)$. The corresponding expectation value for a product of an odd number of operators is zero. The building blocks are the harmonic propagators

$$\langle T[\tilde{A}_r^{\tau}(\mathbf{q}) \tilde{A}_{r'}^{\tau'}(\mathbf{q}')] \rangle_0 = \delta_{-\mathbf{q}, \mathbf{q}'} G_{r,r'}^{(0)}(\mathbf{q}; \tau - \tau') \quad (70)$$

given by Eq. (64) for $H = H_0$; they differ from zero only when $\mathbf{q}' = -\mathbf{q}$ and $r' = r$ and can be easily calculated.

The terms in the expansion (66), after substituting Eq. (62) and applying Wick's theorem (69), are usually represented by diagrams, according to the following recipe. For any interaction H_m given by Eq. (62) draw a vertex with m lines. When two operators $\tilde{A}_i^{\tau_i}(\mathbf{q}_i)$ and $\tilde{A}_j^{\tau_j}(\mathbf{q}_j)$ are paired in Eq. (69), the corresponding two lines are connected. The two operators $\tilde{A}_r^{\tau}(\mathbf{q})$ and $\tilde{A}_{r'}^{\tau'}(\mathbf{q}')$ defining the propagator (64) appear as vertices with just

a single line. As an example we show

$$\begin{aligned}
 & \tau \frac{\mathbf{q}, r}{\tau_1} \bigcirc \frac{-\mathbf{q}, r'}{\tau_2} 0 = 18 \sum_{\mathbf{q}_1, \mathbf{q}_2} \sum_{r_1, r_2} \Phi_{r, r_1, r_2}(-\mathbf{q}, \mathbf{q}_1, \mathbf{q}_2) \\
 & \times \Phi_{r_1, r_2, r'}(-\mathbf{q}_1, -\mathbf{q}_2, \mathbf{q}) \frac{(-1)^2}{2!} \int_0^\beta d\tau_1 \int_0^\beta d\tau_2 \\
 & \times \langle T[\tilde{A}^r(\mathbf{q}) \tilde{A}^{r_1}(-\mathbf{q})] \rangle_0 \langle T[\tilde{A}^{r_1}(\mathbf{q}_1) \tilde{A}^{r_2}(-\mathbf{q}_1)] \rangle_0 \\
 & \times \langle T[\tilde{A}^{r_2}(\mathbf{q}_2) \tilde{A}^{r'}(-\mathbf{q}_2)] \rangle_0 \langle T[\tilde{A}^{r'}(\mathbf{q}) \tilde{A}^0(-\mathbf{q})] \rangle_0 \quad (71)
 \end{aligned}$$

The factor 18 appears because there are 18 pairings consistent with this diagram, which all yield the same result; one obtains another 18 diagrams with this result by interchanging the vertices τ_1 and τ_2 . There are two kinds of diagrams, those with all lines connected to (\mathbf{q}, r) and/or $(-\mathbf{q}, r')$, which are called connected, and those diagrams consisting of a connected part and one or more parts connected neither to (\mathbf{q}, r) nor to $(-\mathbf{q}, r')$, which are called disconnected. The summation in Eq. (66) contains the contributions from all diagrams, connected or disconnected, that have just two external lines, the (\mathbf{q}, r) and the $(-\mathbf{q}, r')$ lines. It is a simple combinatorial problem to demonstrate that this sum is equal to $\langle S(\beta) \rangle_0$ times the sum over all contributions from connected diagrams only. Thus the expansion (66) for the propagator can be simplified to

$$\begin{aligned}
 G_{r, r'}(\mathbf{q}; \tau) &= \sum_{n=0}^{\infty} \frac{(-1)^n}{n!} \int_0^\beta d\tau_1 \dots \int_0^\beta d\tau_n \\
 &\times \langle T[\tilde{H}_I^{\tau_1} \dots \tilde{H}_I^{\tau_n} \tilde{A}_r^r(\mathbf{q}) \tilde{A}_{r'}^0(-\mathbf{q})] \rangle_{0, \text{connected}} \quad (72)
 \end{aligned}$$

where the subscript “connected” indicates that only connected diagrams must be taken into account. A final simplification is possible because a permutation of the interaction vertices of equal order does not affect the numerical value of a diagram. Considering only topologically distinct diagrams removes the factor $1/n!$; this is essential for the derivation of the Dyson equation [Eq. (78) below].

In order to relate the thermal or imaginary time propagator to the measured properties of the system, we shall need its Fourier components:

$$\bar{G}_{r, r'}(\mathbf{q}; i\omega_l) = \beta^{-1} \int_0^\beta d\tau G_{r, r'}(\mathbf{q}; \tau) \exp(i\omega_l \tau) \quad (73)$$

where $\omega_l = 2\pi l\beta^{-1}$ with integer l , since the thermal propagator has the period β . For the harmonic propagator one derives

$$\begin{aligned}\bar{G}_{r,r'}^{(0)}(\mathbf{q}; i\omega_l) &= \delta_{r,r'}(\beta\hbar)^{-1} \frac{2\omega_r(\mathbf{q})}{\omega_r(\mathbf{q})^2 + \omega_l^2} \\ &= \delta_{r,r'}\bar{G}_r^{(0)}(\mathbf{q}; i\omega_l)\end{aligned}\quad (74)$$

The Fourier representation of the anharmonic propagator is obtained from Eqs. (73) and (72), by using Wick's theorem (69), together with the Fourier representation of the harmonic phonon propagators. The "time" integrations can then explicitly be performed, yielding the condition $\sum_i \omega_i = 0$ and a factor β at every interaction vertex.

The Fourier components of the imaginary time propagator are defined on the imaginary frequency axis. We are interested in the Fourier transform of its real time analog, whose singularities, on the real frequency axis, yield the excitation energies of the system. Therefore, we need expressions for the Fourier components of the thermal phonon propagator that can be analytically continued in the complex plane in such a manner that they correctly yield the shifts of the singularities on the real axis caused by the perturbation. The perturbation expansion (72), truncated at any finite order n , does not satisfy this requirement. In order to calculate the frequency shifts caused by specific interactions, one must sum the corresponding diagrams to infinity. The result can be simplified if we define a "proper" diagram as a diagram that cannot be broken into two parts, each of which as two external lines, by cutting a single phonon line. Then the infinite sum can be symbolically written as

$$\bar{G}_{r,r'}(\mathbf{q}; i\omega_l) = \text{---} + \text{---} \bigcirc \text{---} + \text{---} \bigcirc \text{---} \bigcirc \text{---} + \cdots \quad (75)$$

where the first contribution, the simple line, is the harmonic result $\delta_{r,r'}\bar{G}_r^{(0)}(\mathbf{q}; i\omega_l)$. The second term represents the sum of contributions from all proper diagrams, the third term arises from all diagrams consisting of two proper parts connected by an intermediate line, and so on. The second term is usually written as

$$\text{---} \bigcirc \text{---} = \bar{G}_r^{(0)}(\mathbf{q}; i\omega_l) S_{r,r'}(\mathbf{q}; i\omega_l) \bar{G}_{r'}^{(0)}(\mathbf{q}; i\omega_l) \quad (76)$$

thus defining the "self-energy" matrix $S(\mathbf{q}; i\omega_l)$. Then, one can show that because of the conditions $\sum_i \mathbf{q}_i = 0$ and $\sum_i \omega_i = 0$ at any vertex, which causes all intermediate lines to have momentum \mathbf{q} and frequency ω_l , the third term yields

$$\begin{aligned}\text{---} \bigcirc \text{---} \bigcirc \text{---} &= \bar{G}_r^{(0)}(\mathbf{q}; i\omega_l) \sum_{r''} S_{r,r''}(\mathbf{q}; i\omega_l) \\ &\times \bar{G}_{r''}^{(0)}(\mathbf{q}; i\omega_l) S_{r'',r'}(\mathbf{q}; i\omega_l) \bar{G}_{r'}^{(0)}(\mathbf{q}; i\omega_l)\end{aligned}\quad (77)$$

This relation can be generalized to diagrams with any number of bubbles, and one can sum Eq. (75) to infinity. The result is the Dyson equation:

$$\bar{\mathbf{G}}(\mathbf{q}; i\omega_l) = \{\mathbf{1} - \bar{\mathbf{G}}^{(0)}(\mathbf{q}; i\omega_l)\mathbf{S}(\mathbf{q}; i\omega_l)\}^{-1}\bar{\mathbf{G}}^{(0)}(\mathbf{q}; i\omega_l) \quad (78)$$

All matrices are of dimension $6Z$ and the harmonic propagator matrix $\bar{\mathbf{G}}^{(0)}(\mathbf{q}; i\omega_l)$ is diagonal. The problem of calculating the phonon propagators thus reduces to the calculation of the self-energy matrices $\mathbf{S}(\mathbf{q}; i\omega_l)$ that contain all anharmonic information. It is not difficult to demonstrate that the self-energy matrix is a Hermitian function of ω_l^2 from which it follows that its analytic continuation in the complex frequency plane, in the neighborhood of the real axis, has the form

$$\lim_{\varepsilon \rightarrow 0^+} \mathbf{S}(\mathbf{q}; \omega \pm i\varepsilon) = -\beta\hbar\{\Delta(\mathbf{q}; \omega) \mp i\Gamma(\mathbf{q}; \omega)\} \quad (79)$$

where Δ and Γ are real symmetric and antisymmetric matrices, respectively.

Now we can show the explicit relation with experiment. What is usually measured in spectroscopic or scattering experiments is the spectral density function $I(\omega)$, which is the Fourier transform of some correlation function. For example, the absorption intensity in infrared spectroscopy is given by the Fourier transform of the time-dependent dipole-dipole correlation function $\langle[\mu(t), \mu(0)]\rangle$. If one expands the observables, i.e., the dipole operator in the case of infrared spectroscopy, as a Taylor series in the molecular displacement coordinates, the absorption or scattering intensity corresponding to the phonon branch r at wave vector \mathbf{q} can be written as (Kobashi, 1978)

$$I_{\mathbf{q},r}(\omega) \sim \lim_{\varepsilon \rightarrow 0^+} i\{\bar{G}_{r,r}(\mathbf{q}; \omega + i\varepsilon) - \bar{G}_{r,r}(\mathbf{q}; \omega - i\varepsilon)\} \quad (80)$$

Usually it is justifiable to neglect the nondiagonal elements of the self-energy matrix; if not so, these can be taken into account as a small perturbation. Then, we arrive at the result

$$I_{\mathbf{q},r}(\omega) \sim (\beta\hbar)^{-1} \frac{8\omega_r(\mathbf{q})^2\Gamma_{r,r}(\mathbf{q}; \omega)}{\{-\omega^2 + \omega_r(\mathbf{q})^2 + 2\omega_r(\mathbf{q})\Delta_{r,r}(\mathbf{q}, \omega)\}^2 + 4\omega_r(\mathbf{q})^2\Gamma_{r,r}(\mathbf{q}; \omega)^2} \quad (81)$$

If $\Delta_{r,r}(\omega)$ and $\Gamma_{r,r}(\omega)$ do not vary much with ω , they may be interpreted as the frequency shift, i.e., the resonance shifts from $\omega_r(\mathbf{q})$ to $\omega_r(\mathbf{q}) + \Delta_{r,r}(\mathbf{q}; \omega)$, and the bandwidth, respectively. Note that the actual calculation of these quantities will not be easy, however, since the diagrams involved contain summations over the entire Brillouin zone [see Eq. (71), for instance]. Some simplification may arise from the lattice

symmetry. A perturbation theory has been developed (Briels, 1983; Hammer and Irving, 1984) in which successive perturbation corrections are associated with an increasing sequence of clusters on the (real) lattice, thus avoiding the multiple sums over the Brillouin zone. Up until now, this method has only been applied to relatively simple Hamiltonians.

C. The Self-Consistent Phonon Method

Just as the perturbation theory described in the previous section, the self-consistent phonon (SCP) method applies only in the case of small oscillations around some equilibrium configuration. The SCP method was originally formulated (Werthamer, 1976) for atomic, rare gas, crystals. It can be directly applied to the translational vibrations in molecular crystals and, with some modification, to the librations. The essential idea is to look for an effective harmonic Hamiltonian H_0 , which approximates the exact crystal Hamiltonian as closely as possible, in the sense that it minimizes the free energy A_{var} . This minimization rests on the thermodynamic variation principle:

$$A_{\text{var}} = A_0 + \langle H - H_0 \rangle_0 \geq A \quad (82)$$

The angle brackets denote a thermal average over the eigenstates of H_0 [cf. Eq. (65)]. The free energies A and A_0 correspond to the Hamiltonians H and H_0 , respectively:

$$\begin{aligned} A &= -k_B T \ln Z, & Z &= \text{Tr}[\exp(-\beta H)] \\ A_0 &= -k_B T \ln Z_0, & Z_0 &= \text{Tr}[\exp(-\beta H)] \end{aligned} \quad (83)$$

The exact crystal Hamiltonian H is given by Eq. (23) and H_0 is of the form given by Eq. (47); the force constants $F_{P,P'}^{\lambda,\lambda'}$ are not given by Eq. (48), however, but they are chosen such as to minimize A_{var} . Neglecting the difference between the exact kinetic energy operators [(25) and (26)] and their harmonic approximations (see Section III,A), one obtains

$$H - H_0 = \frac{1}{2} \sum_{P,P'} V_{PP'}(\mathbf{u}_P, \omega_P; \mathbf{u}_{P'}, \omega_{P'}) - \frac{1}{2} \sum_{P,P'} \sum_{\lambda,\lambda'} F_{P,P'}^{\lambda,\lambda'} Q_P^\lambda Q_{P'}^{\lambda'} \quad (84)$$

with effective force constants $F_{P,P'}^{\lambda,\lambda'}$ that still have to be optimized. The displacement coordinates Q_P^λ are assumed to be rectilinear, as described in Section III,A. The effective harmonic free energy A_0 is given by Eq. (83) with Z_0 as in Eq. (61). The expectation value of the harmonic potential, i.e., the second term in Eq. (84), can be written as

$$- \frac{1}{2} \sum_{P,P'} \sum_{\lambda,\lambda'} F_{P,P'}^{\lambda,\lambda'} D_{P,P'}^{\lambda,\lambda'} \quad (85)$$

in terms of the effective force constants and the displacement–displacement correlation functions:

$$D_{P,P'}^{\lambda,\lambda'} = \langle Q_P^\lambda Q_{P'}^{\lambda'} \rangle_0 \quad (86)$$

The expectation value of the exact potential, the first term in Eq. (84), is somewhat more difficult to calculate. Using the properties of the harmonic oscillator eventually leads to (Choquard, 1967; Werthamer, 1976)

$$\begin{aligned} & \langle V_{PP'}(\mathbf{u}_P, \omega_P; \mathbf{u}_{P'}, \omega_{P'}) \rangle_0 \\ &= \left\langle \exp \left\{ \sum_{\lambda} (Q_P^\lambda \nabla_P^\lambda + Q_{P'}^\lambda \nabla_{P'}^\lambda) \right\} \right\rangle_0 V_{PP'}(\mathbf{0}, \omega_{0P}; \mathbf{0}, \omega_{0P'}) \\ &= \exp \left\{ \frac{1}{2} \sum_{\lambda, \lambda'} (D_{P,P'}^{\lambda,\lambda'} \nabla_P^\lambda \nabla_{P'}^{\lambda'} + 2D_{P,P'}^{\lambda,\lambda'} \nabla_P^\lambda \nabla_{P'}^{\lambda'} \right. \\ & \quad \left. + D_{P',P'}^{\lambda,\lambda'} \nabla_{P'}^\lambda \nabla_{P'}^{\lambda'}) \right\} V_{PP'}(\mathbf{0}, \omega_{0P}; \mathbf{0}, \omega_{0P'}) \end{aligned} \quad (87)$$

with $\nabla_P^\lambda = \partial/\partial Q_P^\lambda$ acting only on $V_{PP'}$. Substituting the expression for A_0 and the results (85) and (87) for $\langle H - H_0 \rangle_0$ into A_{var} [Eq. (82)] and applying the minimization conditions

$$\partial A_{\text{var}} / \partial F_{P,P'}^{\lambda,\lambda'} = 0$$

one finds the expression for the optimized force constants:

$$F_{P,P'}^{\lambda,\lambda'} = \left\langle \frac{\partial^2 V_{PP'}}{\partial Q_P^\lambda \partial Q_{P'}^{\lambda'}} \right\rangle_0, \quad F_{P,P'}^{\lambda,\lambda'} = \sum_{P'} \left\langle \frac{\partial^2 V_{PP'}}{\partial Q_P^\lambda \partial Q_{P'}^{\lambda'}} \right\rangle_0 \quad (88)$$

So, instead of using the second derivatives of the potential in the equilibrium configuration as force constants, the SCP method employs the thermal averages of these derivatives. Equation (88) and the corresponding dynamical equations, given by the generalized eigenvalue problem (55), have to be solved self-consistently. One can do this via the usual iterative procedure, starting with trial values for the effective force constants (88), which can be taken from the harmonic model. The averaging in Eqs. (82) and (88) can be most easily performed (Werthamer, 1976) by first Fourier transforming the function to be averaged, next applying Eq. (87), and then transforming back to the original coordinates, which yields

$$\begin{aligned} & \langle V_{PP'}(\mathbf{u}_P, \omega_P; \mathbf{u}_{P'}, \omega_{P'}) \rangle_0 \\ &= \int d^6 Q_P \int d^6 Q_{P'} \rho_{PP'}(Q_P^1, \dots, Q_{P'}^6) V_{PP'}(Q_P^1, \dots, Q_{P'}^6) \end{aligned} \quad (89)$$

and a similar expression for the second derivatives (88). The width of the Gaussian probability distribution $\rho_{PP'}$ is determined by the Hessian of the

quadratic exponent. This Hessian is the inverse of the 12-dimensional matrix

$$\begin{pmatrix} \mathbf{D}_{PP} & \mathbf{D}_{PP'} \\ \mathbf{D}_{P'P} & \mathbf{D}_{P'P'} \end{pmatrix} \quad (90)$$

with elements given by Eq. (86). These elements, the displacement-displacement correlation functions, can easily be calculated by using Eqs. (49), (53), and (58). The result for the minimized free energy A_{var} is

$$\begin{aligned} A = & \sum_{\mathbf{q}, r} k_B T \ln \left\{ 2 \sinh \left(\frac{1}{2} \beta \hbar \omega_r(\mathbf{q}) \right) \right\} \\ & + \frac{1}{2} \sum_{P \neq P'} \sum \langle V_{PP'}(\mathbf{u}_P, \omega_P; \mathbf{u}_{P'}, \omega_{P'}) \rangle_0 \\ & - \frac{1}{4} \sum_{\mathbf{q}, r} \hbar \omega_r(\mathbf{q}) \coth \left(\frac{1}{2} \beta \hbar \omega_r(\mathbf{q}) \right) \end{aligned} \quad (91)$$

The calculation of this quantity, and of the displacement-displacement correlation functions, involves a single summation over all wave vectors \mathbf{q} in the Brillouin zone.

From the free energy all thermodynamic properties of the system can be calculated. For example, the entropy is $S = -\partial A / \partial T$ and the energy is $E = A + TS$. For more details we refer to the review by Werthamer (1976). One important point should be mentioned. Expanding the potential $V_{PP'}(Q_P^1, \dots, Q_{P'}^6)$ as a Taylor series in the displacement coordinates Q_P^i , we observe, using the analog of Eq. (87) for the force constants (88), that the odd power terms do not contribute to the effective force constants; the SCP method neglects these terms. Their relative importance can, of course, be estimated by perturbation techniques as described in Section III,B.

Here we have formulated the SCP method for molecular crystals. We could easily include the librations because the orientational dependence of the potential $V_{PP'}$ has been explicitly given, in Sections II,B and II,C, in terms of the Euler angles ω_P and thus in terms of the angular displacements $\Delta\omega_P = \omega_P - \omega_{0P}$. In two earlier applications of the SCP method to molecular crystals, one has used atom-atom potentials, however, whose orientational dependence was implicit and the description of librations was still a problem. Raich *et al.* (1974) in their calculations on α -nitrogen (see Section V) have avoided this problem by including the librations implicitly. They did this by considering a molecular crystal as a collection of atoms interacting via strong chemical bonds with their partners within the same molecule and via weak van der Waals potentials with all other

atoms belonging to neighboring molecules. Then they applied the original SCP method to the atomic motions. This approach is, of course, confined to the use of intermolecular potentials of the atom-atom type (see Section II,A). Wasiutynski (1976) has considered the molecular librations explicitly. He has expressed the atom-atom potential as a function of the translational and librational molecular displacements by writing a linear relation between these displacements and the atomic displacements. This relation holds only for small angular displacements.

IV. Dynamical Models for Large-Amplitude Motions

The methods outlined in the preceding section obviously cannot be applied when the molecules in a crystal perform large-amplitude librations or even (hindered) rotations. In this case, one has the tendency to emphasize the motions of the individual molecules rather than the collective motions. Indeed, the most generally applicable method to describe large-amplitude motions is the mean field theory (Kirkwood, 1940; James and Keenan, 1959), which treats the molecules as moving in a field that represents the mean interaction with the neighboring molecules. In a quantum-mechanical description, it is then possible to use the low-lying single-particle states to construct a basis for the whole solid in which the complete crystal Hamiltonian can be diagonalized. Adaptation of this basis to the translational symmetry of the crystal makes this diagonalization practically possible. At the same time, it leads to a labeling of the crystal states by the wave vectors in the Brillouin zone, thus reintroducing the collective aspect of the lattice vibrations. In order to make the frequencies of the acoustical lattice modes go to zero when the wave vector approaches the center of the Brillouin zone, the crystal Hamiltonian has to be diagonalized at the time-dependent Hartree (TDH) or random phase approximation (RPA) level (Fredkin and Werthamer, 1965).

A scheme as described here is indispensable for a quantum dynamical treatment of strongly delocalized systems, such as solid hydrogen (van Kranendonk, 1983) or the plastic phases of other molecular crystals. We have shown, however (Jansen *et al.*, 1984), that it is also very suitable to treat the anharmonic librations in ordered phases. Moreover, the RPA method yields the exact result in the limit of a harmonic crystal Hamiltonian, which makes it appropriate to describe the weakly anharmonic translational vibrations, too. We have extended the theory (Briels *et al.*, 1984) in order to include these translational motions, as well as the coupled rotational-translational lattice vibrations. In this section, we outline the general theory and present the relevant formulas for the coupled

problem. First, we briefly sketch some classical methods, however, that have been used in the literature to study large-amplitude motions in molecular systems.

A. Classical Molecular Dynamics and Monte Carlo Methods

In classical mechanics there exist, apart from the mean field theory, two popular methods to describe the dynamics of molecular systems, viz., the molecular dynamics (MD) method and the Monte Carlo (MC) method (Hansen and McDonald, 1976). In both methods the system is represented by a finite number, usually about 100 to 300, of molecules. In order to reduce boundary effects, this finite system is periodically repeated in all directions.

In the MD method (Rahman, 1966; Verlet, 1967) one specifies the initial conditions, i.e., the positions and orientations of all molecules and their (angular) velocities, and one integrates the classical equations of motion numerically by means of some finite difference scheme. The choice of the time step is mainly determined by the error allowed and the time scale in which one is interested. Usually, one takes time steps of order 10^{-14} sec and follows the trajectory for some 10^3 to 10^5 steps. Along the whole or part of the trajectory all kinds of quantities can be averaged. The method is especially suitable for calculating time-dependent correlation functions that yield information on the dynamics of the system. An example is the so-called intermediate scattering function:

$$F(\mathbf{q}, t) = \frac{1}{4N} \sum_{P, P'}^N \langle M_P(\mathbf{q}, t) M_{P'}(\mathbf{q}, 0) \rangle \quad (92)$$

where N is the number of molecules in the system, and the operator

$$M_P(\mathbf{q}, t) = \exp[i\mathbf{q} \cdot \mathbf{r}_P(t)] \sum_{\alpha \in P} \exp[i\mathbf{q} \cdot \mathbf{d}_\alpha(t)] \quad (93)$$

is related to the scattering of neutrons with scattering vector \mathbf{q} by a molecule at the instantaneous position $\mathbf{r}_P(t)$. The atoms α belonging to this molecule have (instantaneous) position vectors $\mathbf{d}_\alpha(t)$ relative to its center of mass; these vectors depend on the orientation of the molecule. The Fourier transform of this particular correlation function

$$S(\mathbf{q}, \omega) = (2\pi)^{-1} \int_{-\infty}^{\infty} dt F(\mathbf{q}, t) e^{i\omega t} \quad (94)$$

is called the dynamic structure factor, and it describes the response of the system to a transfer of momentum \mathbf{q} and energy $\hbar\omega$. By the nature of the

MD method, the system studied has constant energy. Its temperature can be defined via the mean kinetic energy. Other thermodynamic properties can be calculated from the numerical derivatives of the energy or by using their relations to certain fluctuations of the system. The specific heat, for instance, can be obtained from the derivative of the energy with respect to the temperature or from the temperature fluctuations. It will be clear that for these derived quantities the uncertainties are larger than for the trajectory itself.

The Monte Carlo method is most easily explained by means of a discrete model. One assumes that the system can only be in a configuration corresponding to one of a finite but large number of grid points on a very fine mesh. The idea is to sample this configuration space and to calculate various mean values. Even with the largest computers, however, it is not possible to sample a substantial part of configuration space, and the possibility exists that one samples many highly improbable configurations. The way to avoid this problem is to generate a Markov chain of successive configurations with step probabilities p_{ij} to get from state i to state j . The probabilities p_{ij} are chosen such that the stationary state of the chain has occupation probabilities in accordance with the canonical Boltzmann distribution law. It is also possible to simulate other thermodynamic ensembles, in which case the Boltzmann distribution has to be replaced by the appropriate probability distribution. Of course, the requirement just stated is not sufficient to completely specify the transition matrix p_{ij} . Among the possible choices for p_{ij} the most popular one, proposed by Metropolis *et al.* (1953), leads to the following scheme. Given a configuration, randomly generate a new one that differs not too much from the previous one and accept it as a sample point if its energy is lower than that of the previous state. If its energy is higher, accept it with probability $\exp(-\beta \Delta V_{ij})$, where $\Delta V_{ij} = V(j) - V(i)$. This method is very suitable for calculating static correlation functions. The calculation of thermodynamic properties is similar to that in the MD method; one can use the derivatives of the mean energy or the average fluctuations. Another way is to connect the system reversibly to a model system whose properties are known.

Both the MD and MC methods have some limitations that are mainly due to the finite size of the system and to the periodic boundary conditions. Generally, when the number of molecules is 100 or more, the fluctuations are sufficiently weak for the average properties to approach the bulk properties. Because of the periodic boundary conditions, however, it is impossible to study fluctuations with a wavelength that is larger than the length of the box. This is most unsatisfactory for two-dimensional

systems or for systems in the neighborhood of (second-order) phase transitions, because in these cases the large-scale fluctuations constitute an interesting part of the theory. The same limitation holds in MD calculations for the time-dependent correlations. These may contain spurious contributions when local perturbations are not sufficiently damped, so that they reappear because of the periodic boundary conditions. Another problem occurring especially in small systems is that they can be locked in a small region of phase space. Consequently, it is often difficult to locate phase transitions, because the system remains in a metastable state for a very long time. A third problem is that short-range and long-range interactions have to be included via different methods.

B. The Mean Field Model

Just as the self-consistent phonon method, the mean field approximation (Kirkwood, 1940; James and Keenan, 1959) is based on the thermodynamic variation principle for the Helmholtz free energy:

$$A_{\text{var}} = A_0 + \langle H - H_0 \rangle_0 \geq A \quad (95)$$

The meaning of the symbols is explained in Section III,C [Eq. (83)]; H is the exact crystal Hamiltonian [Eq. (23)]. This time, however, we choose as the approximate Hamiltonian H_0 a sum of single-particle Hamiltonians:

$$H_0 = \sum_P H_P^{\text{MF}}(\mathbf{u}_P, \omega_P) \quad (96)$$

In order to obtain the conditions on $H_P^{\text{MF}}(\mathbf{u}_P, \omega_P)$ that guarantee that H_0 is the best possible Hamiltonian with the form of Eq. (96) in the sense that A_{var} adopts its minimum value, we vary every single-particle Hamiltonian by an arbitrary amount $h_P(\mathbf{u}_P, \omega_P)$:

$$H_0 \rightarrow H_0 + h = \sum_P \{H_P^{\text{MF}}(\mathbf{u}_P, \omega_P) + h_P(\mathbf{u}_P, \omega_P)\} \quad (97)$$

and calculate the corresponding variation of the free energy:

$$\begin{aligned} \Delta A_{\text{var}} &= A_{\text{var}}(H_0 + h) - A_{\text{var}}(H_0) \\ &= A(H_0 + h) - A(H_0) \\ &\quad + \text{Tr}[(H - H_0)\{\rho(H_0 + h) - \rho(H_0)\}] \\ &\quad - \text{Tr}[h\rho(H_0 + h)] \end{aligned} \quad (98)$$

This result can easily be obtained by writing the thermodynamic expectation value of an arbitrary operator X as

$$\langle X \rangle = \text{Tr}\{X\rho(H)\} \quad (99)$$

in terms of the density operator

$$\rho(H) = Z^{-1} e^{-\beta H} \quad (100)$$

with

$$Z = \text{Tr } e^{-\beta H}$$

To first order in the perturbation h , ΔA_{var} must be zero, while to second order it must be positive for arbitrary h . In order to calculate ΔA_{var} and the density operator on which it depends, up to the second order, we can use the perturbation expansion

$$\begin{aligned} \exp\{-\beta(H_P^{\text{MF}} + h_P)\} &= \exp(-\beta H_P^{\text{MF}}) \\ &\times \sum_{n=0}^{\infty} \frac{(-1)^n}{n!} \int_0^{\beta} d\tau_1 \dots \int_0^{\beta} d\tau_n T[\tilde{h}_P^{\tau_1} \dots \tilde{h}_P^{\tau_n}] \end{aligned} \quad (101)$$

with

$$\tilde{h}_P^{\tau} = \exp(\tau H_P^{\text{MF}}) h_P \exp(-\tau H_P^{\text{MF}}) \quad (102)$$

This expansion lies also at the basis of the perturbation expansion given by Eq. (66). The time-ordering operator T orders the (imaginary) times τ_1, \dots, τ_n . For brevity we have momentarily stopped indicating the dependence of all quantities on the coordinates \mathbf{u}_P and ω_P . Using the notation $\rho_P^{\text{MF}} = \rho(H_P^{\text{MF}})$ and $\langle X \rangle_{\text{MF}} = \text{Tr}(X\rho_P^{\text{MF}})$, we readily derive

$$\rho(H_P^{\text{MF}} + h_P) = \rho_P^{\text{MF}} + \Delta\rho_P^{(1)} + \Delta\rho_P^{(2)} + \dots \quad (103)$$

with

$$\Delta\rho_P^{(1)} = \rho_P^{\text{MF}} \{ \beta \langle h_P \rangle_{\text{MF}} - \int_0^{\beta} d\tau_1 \tilde{h}_P^{\tau_1} \} \quad (104)$$

The explicit expression for $\Delta\rho_P^{(2)}$ will not be needed. Using the perturbation expansion (101) in Eq. (98) we arrive, after some algebra (van der Avoird *et al.*, 1984), at

$$\Delta A_{\text{var}} = \Delta A_{\text{var}}^{(1)} + \Delta A_{\text{var}}^{(2)} + \dots \quad (105)$$

with

$$\Delta A_{\text{var}}^{(1)} = \sum_P \text{Tr}\{(T_P + L_P + V_P^{\text{MF}} - H_P^{\text{MF}}) \Delta\rho_P^{(1)}\} \quad (106)$$

and

$$\begin{aligned}
 \Delta A_{\text{var}}^{(2)} = & \sum_P \text{Tr}\{(T_P + L_P + V_P^{\text{MF}} - H_P^{\text{MF}}) \Delta \rho_P^{(2)}\} \\
 & + \frac{1}{2} \sum_{P \neq P'} \text{Tr}\{\Delta \rho_P^{(1)} V_{PP'} \Delta \rho_{P'}^{(1)}\} \\
 & + \beta^{-1} \sum_P \int_0^\beta d\tau_1 \tau_1 \langle \tilde{h}_P^\tau h_P \rangle_{\text{MF}} \\
 & - \frac{1}{2} \beta \sum_P \langle h_P \rangle_{\text{MF}}^2
 \end{aligned} \tag{107}$$

The kinetic energy operators $T_P = T(\mathbf{u}_P)$ and $L_P = L(\omega_P)$ are defined in Eqs. (25) and (26); the mean field potential is given by

$$V_P^{\text{MF}} = \sum_{P' \neq P} \text{Tr}^{(P')}(V_{PP'} \rho_{P'}^{\text{MF}}) = \sum_{P' \neq P} \langle V_{PP'} \rangle_{P'} \tag{108}$$

From the extremum condition that $\Delta A_{\text{var}}^{(1)}$ should be zero for arbitrary variations h_P and thus for arbitrary changes $\Delta \rho_P^{(1)}$ in the density operator, we derive the expression for the optimized single-particle Hamiltonian

$$H_P^{\text{MF}}(\mathbf{u}_P, \omega_P) = T(\mathbf{u}_P) + L(\omega_P) + \sum_{P' \neq P} \langle V_{PP'}(\mathbf{u}_P, \omega_P; \mathbf{u}_{P'}, \omega_{P'}) \rangle_{P'} \tag{109}$$

This defines a set of equations for the mean field Hamiltonians H_P^{MF} . These equations have to be solved self-consistently since the thermodynamic values within the angle brackets in (109) involve the mean field Hamiltonians $H_{P'}^{\text{MF}}$. In principle, all H_P^{MF} can be different; in practice, we impose symmetry relations. Therefore, we choose a unit cell, compatible with the symmetry of the lattice introduced in Section II,D, and we put $H_{P'}^{\text{MF}}$ equal to H_P^{MF} whenever P' and P belong to the same sublattice. Moreover, we apply unit cell symmetry that relates the mean field Hamiltonians on different sublattices. By using the symmetry-adapted functions introduced in Section II,B, the latter symmetry can be imposed as follows. We select a set of molecules constituting the asymmetric part of the unit cell. Then we assign to all other molecules P' Euler angles $\tilde{\omega}_{P'}$ through which the mean field Hamiltonian of some molecule P in the asymmetric part has to be rotated in order to obtain $H_{P'}^{\text{MF}}$. As a result, we find

$$\begin{aligned}\langle C_m^{(l)} \rangle_{P'} &= \sum_n \langle C_n^{(l)} \rangle_P D_{nm}^{(l)}(\hat{\omega}_{P'}) \\ \langle G_m^{(l)} \rangle_{P'} &= \sum_n \langle G_n^{(l)} \rangle_P D_{nm}^{(l)}(\hat{\omega}_{P'})\end{aligned}\quad (110)$$

If we substitute these transformation relations into Eq. (109), we observe that the latter equation involves only the mean field Hamiltonians of the molecules in the asymmetric part of the unit cell.

In order to perform the calculations in practice, we introduce a basis in which we diagonalize the mean field Hamiltonians. The density operators ρ_P^{MF} become diagonal, too, and the calculation of the thermodynamic averages is obvious. The most convenient basis consists of the products

$$D_{m_1 m_2}^{(l)}(\omega_P) \Psi_{k, m_3}^{(n)}(\mathbf{u}_P) \quad (111)$$

of Wigner functions $D_{m_1 m_2}^{(l)}(\omega)$ and three-dimensional harmonic oscillator functions

$$\Psi_{k, m}^{(n)}(\mathbf{u}_P) = A \left(\frac{2}{u_P} \right)^{1/2} \Lambda_{1/2(n-k)}^{k+1/2} (A^2 u_P^2) S_m^{(k)}(\hat{u}_P) \quad (112)$$

with

$$\Lambda_l^\alpha(t) = \left[\Gamma(\alpha + 1) \binom{l + \alpha}{l} \right]^{-1/2} e^{-t/2} t^{\alpha/2} L_l^\alpha(t) \quad (113)$$

The functions $S_m^{(k)}$ are tesseral (i.e., real combinations of spherical) harmonics, L_l^α are Laguerre functions, and $\Gamma(\alpha)$ are gamma functions (Powell and Craseman, 1961); k is restricted to $0 \leq k \leq n$ and it must have the same parity as n . The constant A , in the case of a finite basis, can be used to optimize this basis. The matrix elements required in this basis can be easily computed from Eq. (14) and the relation

$$\begin{aligned}& \int_0^\infty u^2 du \Lambda_{1/2(n_1-k_1)}^{k_1+1/2}(u^2) \frac{u^\alpha}{u} \Lambda_{1/2(n_2-k_2)}^{k_2+1/2}(u^2) \\ &= \frac{1}{2} (-1)^{a_1+a_2} \left[\frac{\Gamma(a_1+1)}{\Gamma(a_1+b_1+1)} \frac{\Gamma(a_2+1)}{\Gamma(a_2+b_2+1)} \right]^{1/2} \\ &\times \sum_{l=l_{\min}}^{l_{\max}} \binom{c-b_1}{a_1-l} \binom{c-b_2}{a_2-l} \binom{c+1}{l} \Gamma(c+1)\end{aligned}\quad (114)$$

with

$$\begin{aligned} a_i &= \frac{1}{2}(n_i - k_i), & b_i &= k_i + \frac{1}{2} \\ c &= \frac{1}{2}(k_1 + k_2 + \alpha + 1), & d &= \max(a_1 + b_1, a_2 + b_2) - c \\ l_{\min} &= \begin{cases} d & \text{if } c \text{ is half-integer and } d > 0, \\ 0 & \text{otherwise,} \end{cases} & l_{\max} &= \min(a_1, a_2) \end{aligned}$$

The factor u^2 in the integrand originates from the volume element in \mathbf{u} space. Matrix elements of the translational kinetic energy operator $T(\mathbf{u}_P)$ follow from the identity

$$-\Delta(\mathbf{u}_P) = A^2[-\Delta(A\mathbf{u}_P) + A^2u_P^2] - A^4u_P^2 \quad (115)$$

The operator between the brackets is the harmonic oscillator Hamiltonian, which has the basis functions (112) as its eigenfunctions; the remaining term is taken into account via Eq. (114). The rotational kinetic energy operator $L(\omega_P)$ [Eq. (26)] can be written in terms of the shift operators $J_{\pm} = J_a \mp iJ_b$ and the operator J_c , which act on the basis as

$$\begin{aligned} J_c D_{mn}^{(l)}(\omega) &= m D_{mn}^{(l)}(\omega) \\ J_{\pm} D_{mn}^{(l)}(\omega) &= \{(l \mp m)(l \pm m + 1)\}^{1/2} D_{m \pm 1, n}^{(l)}(\omega) \end{aligned} \quad (116)$$

At this point let us make a remark concerning the size of the basis. In order to obtain convergence, one must sometimes include (Briels *et al.*, 1984) basis functions with high values of l and n . High values of l are needed in particular when the orientations of the molecules are fairly well localized. This leads to a rapidly increasing size of the basis. Two measures can be taken to simplify the problem. First, one can adapt the basis of molecule P to the site symmetry at P , which block-diagonalizes the secular problem. If this does not sufficiently reduce the problem, the mean field model Hamiltonian (96) can be further separated by writing

$$H_P^{\text{MF}}(\mathbf{u}_P, \omega_P) = H_P^T(\mathbf{u}_P) + H_P^L(\omega_P) \quad (117)$$

As a result, we now have two "particles" at every lattice point P , one translating and one librating. Expressions for the separate mean field Hamiltonian can be derived as before. The translating particle experiences the mean field of all its neighbors, translating and librating, and of its accompanying librating particle; for the librating particle this relation holds in reverse. The advantage of this separation is that the basis to be used in any cycle of the iterative mean field calculation is either a pure translational basis or a pure rotational basis, and the secular problems are

much smaller than before. The price that we pay is the neglect of correlation between the single-particle translations and librations. This correlation is recovered in the RPA calculations described in the following section.

Once we have obtained the mean field Hamiltonians, we can calculate the thermodynamic properties of the system. The free energy can be found from Eq. (95) and other quantities follow from it:

$$\begin{aligned}
 A &= -k_B T \sum_P \ln Z_P^{\text{MF}} - \frac{1}{2} \sum_P \langle V_P^{\text{MF}} \rangle_P \\
 S &= -\frac{\partial A}{\partial T} = k_B \sum_P \ln Z_P^{\text{MF}} + T^{-1} \sum_P \langle H_P^{\text{MF}} \rangle_P \\
 E &= A + TS = \sum_P \langle H_P^{\text{MF}} \rangle_P - \frac{1}{2} \sum_P \langle V_P^{\text{MF}} \rangle_P
 \end{aligned} \tag{118}$$

The mean field partition function is $Z_P^{\text{MF}} = Z(H_P^{\text{MF}})$. In order to obtain the entropy in its final form, we have used the relation

$$\sum_P \left\langle \frac{\partial H_P}{\partial T} \right\rangle_P = \frac{1}{2} \sum_P \frac{\partial}{\partial T} \langle V_P^{\text{MF}} \rangle_P \tag{119}$$

which follows from Eq. (109).

Before we discuss the stability condition $\Delta A_{\text{var}}^{(2)} \geq 0$ on the mean field solution, we first describe the RPA formalism.

C. The Random Phase or Time-Dependent Hartree Approximation

The mean field model outlined in the preceding section provides us with a set of single-particle states

$$H_P^{\text{MF}} |\psi_P^{(\alpha)}\rangle = \varepsilon_P^{(\alpha)} |\psi_P^{(\alpha)}\rangle \tag{120}$$

from which we construct the crystal states

$$|\psi_{\{\alpha\}}^{\text{MF}}\rangle = \prod_P |\psi_P^{(\alpha_P)}\rangle \tag{121}$$

For all α_P equal to zero, Eq. (121) represents the ground state of the crystal. In order to keep the equations as simple as possible, we have again stopped explicitly indicating the coordinates on which all functions and operators depend. When the mean field Hamiltonian has the form of Eq. (117), the index P , from now on, must be interpreted as $P = \{\mathbf{n}, i, K\}$,

where $K = T, L$ distinguishes between the translating and librating "particles."

The shortcoming of the mean field method is that it admits no correlation between the motions of the individual particles. This correlation can be introduced by means of the random phase approximation (RPA) or time-dependent Hartree (TDH) method. In order to formulate this method, we introduce excitation operators $(E_p^\alpha)^\dagger$, which replace $\psi_p^{(0)}$ by $\psi_p^{(\alpha)}$ when applied to the mean field ground state of the crystal; when applied to any other state, they yield zero. Then, we write the Hamiltonian as a quadratic form in the excitation operators $(E_p^\alpha)^\dagger$ and their Hermitian conjugates E_p^α

$$H = \sum_{P \neq P'} \sum_{\alpha, \alpha'} \{ A_{P, P'}^{\alpha, \alpha'} (E_P^\alpha)^\dagger E_{P'}^{\alpha'} + B_{P, P'}^{\alpha, \alpha'} (E_P^\alpha)^\dagger (E_{P'}^{\alpha'})^\dagger + (B_{P, P'}^{\alpha, \alpha'})^* E_P^\alpha E_{P'}^{\alpha'} \} \quad (122)$$

Linear terms are absent because of the Brillouin theorem. The coefficients $A_{P, P'}^{\alpha, \alpha'}$ and $B_{P, P'}^{\alpha, \alpha'}$ can be calculated by equating the nonzero matrix elements of the RPA Hamiltonian [Eq. (122)], in the basis of Eq. (121), to the corresponding matrix elements of the exact Hamiltonian [Eq. (23)] in the same basis. From the translational symmetry of the mean field states it follows that the A and B coefficients do not depend on the complete labels $P = \{\mathbf{n}, i, K\}$ and $P' = \{\mathbf{n}', i', K'\}$, but only on the sublattice labels $\{i, K\}$ and $\{i', K'\}$. The second ingredient of the RPA formalism is that we assume boson commutation relations for the excitation and de-excitation operators (Raich and Etters, 1968; Dunmore, 1972).

The RPA Hamiltonian [Eq. (122)] can be easily diagonalized. A partial diagonalization is already obtained by writing it in terms of operators

$$E_{i, K}^\alpha(\mathbf{q}) = \frac{1}{\sqrt{N}} \sum_{\mathbf{n}} \exp(i\mathbf{q} \cdot \mathbf{R}_{\mathbf{n}}) E_P^\alpha \quad (123)$$

with $P = \{\mathbf{n}, i, K\}$, adapted to the translational symmetry of the crystal. Just as in Section III,A, the commutation relations are preserved under this transformation. The next step is to define operators $a_\lambda^\dagger(\mathbf{q})$ that represent the exact excitation operators of the crystal, which satisfy the equations of motion

$$\begin{aligned} [H, a_\lambda^\dagger(\mathbf{q})] &= \omega_\lambda(\mathbf{q}) a_\lambda^\dagger(\mathbf{q}) \\ [H, a_\lambda(\mathbf{q})] &= -\omega_\lambda(\mathbf{q}) a_\lambda(\mathbf{q}) \end{aligned} \quad (124)$$

Expressing these operators as

$$a_\lambda^\dagger(\mathbf{q}) = \sum_{\alpha, i, K} \{ x_{\alpha, i, K}^\lambda(\mathbf{q}) E_{i, K}^\alpha(\mathbf{q})^\dagger + y_{\alpha, i, K}^\lambda E_{i, K}^\alpha(-\mathbf{q}) \} \quad (125)$$

leads to the RPA eigenvalue problem for the coefficients $x_{\alpha,i,K}^\lambda$ and $y_{\alpha,i,K}^\lambda$:

$$\begin{pmatrix} \chi - \Phi(\mathbf{q}) & -\Phi(\mathbf{q}) \\ \Phi(\mathbf{q}) & -\chi + \Phi(\mathbf{q}) \end{pmatrix} \begin{pmatrix} \mathbf{x}^\lambda(\mathbf{q}) \\ \mathbf{y}^\lambda(\mathbf{q}) \end{pmatrix} = \begin{pmatrix} \mathbf{x}^\lambda(\mathbf{q}) \\ \mathbf{y}^\lambda(\mathbf{q}) \end{pmatrix} \omega_\lambda(\mathbf{q}) \quad (126)$$

The diagonal matrix χ contains the mean field excitation energies

$$\chi_{\alpha,i,K;\alpha',i',K'} = \delta_{\alpha,\alpha'} \delta_{i,i'} \delta_{K,K'} [\varepsilon_{\{i,K\}}^{(\alpha)} - \varepsilon_{\{i,K\}}^{(0)}] \quad (127)$$

and the elements of the matrix $\Phi(\mathbf{q})$ are defined as

$$\begin{aligned} \Phi_{\alpha,i,K;\alpha',i',K'}(\mathbf{q}) = & \sum_{\mathbf{n}} \exp(i\mathbf{q} \cdot \mathbf{R}_{\mathbf{n}}) \langle \psi_P^{(\alpha)} \psi_{P'}^{(0)} | \langle V_{\{0,i\}\{\mathbf{n},i'\}} \rangle_{P_c, P_c'} | \psi_P^{(0)} \psi_{P'}^{(\alpha')} \rangle \\ & + \delta_{i,i'} \delta_{K,K_c} \sum_{\mathbf{n}''} \sum_{i''} \langle \psi_P^{(\alpha)} \psi_{P_c}^{(0)} | \langle V_{\{0,i\}\{\mathbf{n}'',i''\}} \rangle_{Q, Q_c} | \psi_P^{(0)} \psi_{P_c}^{(\alpha')} \rangle \end{aligned} \quad (128)$$

with $P = \{0, i, K\}$, $P' = \{\mathbf{n}, i', K'\}$, $Q = \{\mathbf{n}'', i'', K\}$, $P_c = \{0, i, K_c\}$, K_c is the complement of K and $|\psi_P^{(\alpha)} \psi_{P'}^{(0)}\rangle = |\psi_P^{(\alpha)}\rangle |\psi_{P'}^{(0)}\rangle$. When the mean field problem is separated for the translations and librations, as reflected by Eq. (117), the matrix $\Phi(\mathbf{q})$ will have a block structure. The blocks $\Phi^{\text{TT}}(\mathbf{q})$ and $\Phi^{\text{LL}}(\mathbf{q})$ correlate the translational and librational motions of the molecules, respectively, and the off-diagonal blocks $\Phi^{\text{TL}}(\mathbf{q})$ and $\Phi^{\text{LT}}(\mathbf{q})$ account for the translation-rotation coupling. The second term of the elements of the latter matrices, given by Eq. (128), includes the coupling between the single-particle librations and translations. The eigenvalues $\omega_\lambda(\mathbf{q})$ in Eq. (126) provide the excitation energies of the crystal. The eigenvectors can be conceived as the polarization vectors that, in general, correspond to mixed translational-rotational modes. In using a quadratic Hamiltonian, the RPA model is similar to the harmonic model. The motions in the RPA model can be strongly anharmonic, however; they may even be hindered rotations.

The RPA formalism that we have just presented only applies at zero temperature. It is possible, however, to derive similar eigenvalue equations for the excitation frequencies $\omega_\lambda(\mathbf{q})$ by means of the time-dependent Hartree method (Fredkin and Werthamer, 1965; Hüller, 1974; Jansen *et al.*, 1984). The TDH equations are valid for finite temperature; in the limit of $T \rightarrow 0$ K, they become identical to the RPA equations. The TDH matrix that replaces the RPA matrix in the eigenvalue equations (126) can be written as

$$\mathbf{M}(\mathbf{q}) = \begin{pmatrix} -\mathbf{P} & \mathbf{0} \\ \mathbf{0} & \mathbf{P} \end{pmatrix} \begin{pmatrix} \Phi(\mathbf{q}) - \chi & \Phi(\mathbf{q}) \\ \Phi(\mathbf{q}) & \Phi(\mathbf{q}) - \chi \end{pmatrix} = \begin{pmatrix} -\mathbf{P} & \mathbf{0} \\ \mathbf{0} & \mathbf{P} \end{pmatrix} \mathbf{N}(\mathbf{q}) \quad (129)$$

where the diagonal matrix χ is given by

$$\chi_{\alpha,\beta,i,K;\alpha',\beta',i',K'} = \delta_{\alpha,\alpha'} \delta_{\beta,\beta'} \delta_{i,i'} \delta_{K,K'} \frac{\varepsilon_P^{(\alpha)} - \varepsilon_P^{(\beta)}}{P_P^{(\alpha)} - P_P^{(\beta)}} \quad (\alpha > \beta) \quad (130)$$

and the matrix $\Phi(\mathbf{q})$ by

$$\begin{aligned} \Phi_{\alpha,\beta,i,K;\alpha',\beta',i',K'}(\mathbf{q}) &= \sum_{\mathbf{n}} \exp(i\mathbf{q} \cdot \mathbf{R}_{\mathbf{n}}) \langle \psi_P^{(\alpha)} \psi_{P'}^{(\beta')} | \langle V_{\{0,i\}\{\mathbf{n},i'\}} \rangle_{P_C, P'_C} | \psi_P^{(\beta)} \psi_{P'}^{(\alpha')} \rangle \\ &+ \delta_{i,i'} \delta_{K,K'} \sum_{\mathbf{n}''} \sum_{i''} \\ &\langle \psi_P^{(\alpha)} \psi_{P'_C}^{(\beta')} | \langle V_{\{0,i\}\{\mathbf{n}'',i''\}} \rangle_{Q, Q_C} | \psi_P^{(\beta)} \psi_{P'_C}^{(\alpha')} \rangle \end{aligned} \quad (131)$$

while \mathbf{P} is a diagonal matrix containing population differences:

$$P_{\alpha,\beta,i,K;\alpha',\beta',i',K'} = \delta_{\alpha,\alpha'} \delta_{\beta,\beta'} \delta_{i,i'} \delta_{K,K'} [P_P^{(\alpha)} - P_P^{(\beta)}] \quad (132)$$

with

$$P_P^{(\alpha)} = \langle \psi_P^{(\alpha)} | \rho_P^{\text{MF}} | \psi_P^{(\alpha)} \rangle = \exp(-\beta \varepsilon_P^{(\alpha)}) / \sum_{\alpha} \exp(-\beta \varepsilon_P^{(\alpha)}) \quad (133)$$

In the limit of $T \rightarrow 0$ K, $P_P^{(0)} = 1$ and $P_P^{(\beta)} = 0$ for $\beta > 0$; the matrix \mathbf{P} becomes the unit matrix \mathbf{I} , and obviously, the TDH matrix $\mathbf{M}(\mathbf{q})$ given by Eqs. (129) to (132) reduces to the RPA matrix [see Eqs. (126)–(128)].

D. Stability Conditions for the Mean Field Solution

Just as there exist the so-called Thouless stability conditions on the Hartree–Fock solutions in nuclear physics (Thouless, 1960, 1961; Rowe, 1970) and in quantum chemistry (Čížek and Paldus, 1971), one has stability conditions on the mean field solutions in lattice dynamics problems (Fredkin and Werthamer, 1965). The mean field solutions are obtained from the condition $\Delta A_{\text{var}}^{(1)} = 0$ (see Section IV, A). They are stable; i.e., they correspond with a local minimum in the free energy if $\Delta A_{\text{var}}^{(2)} > 0$. Substituting the mean field solution (109) into the equation (107) for $\Delta A_{\text{var}}^{(2)}$, the term with $\Delta \rho_P^{(2)}$ vanishes and we can express the stability condition as

$$\begin{aligned} \Delta A_{\text{var}}^{(2)} &= \frac{1}{2} \sum_{P \neq P'} \sum \text{Tr} \{ \Delta \rho_P^{(1)} V_{PP'} \Delta \rho_{P'}^{(1)} \} \\ &+ \beta^{-1} \sum_P \int_0^\beta d\tau_1 \tau_1 \langle \bar{h}_P^\dagger h_P \rangle_{\text{MF}} - \frac{1}{2} \beta \sum_P \langle h_P \rangle_{\text{MF}}^2 > 0 \end{aligned} \quad (134)$$

This condition must hold for arbitrary variations h_P , with the corresponding changes in the density operators $\Delta\rho_P^{(1)}$ as given by Eq. (104). Writing Eq. (134) in the main field basis $|\psi_P^{(\alpha)}\rangle$ and substituting the matrix elements of Eq. (104) in this basis, we find

$$\begin{aligned} \Delta A_{\text{var}}^{(2)} = & \frac{1}{2} \sum_P \sum_{P'} \sum_{\alpha, \alpha'} \sum_{\beta, \beta'} \langle \psi_P^{(\alpha)} | \Delta\rho_P^{(1)} | \psi_P^{(\beta)} \rangle \langle \psi_{P'}^{(\beta')} | \Delta\rho_{P'}^{(1)} | \psi_{P'}^{(\alpha')} \rangle \\ & \times \left[\langle \psi_P^{(\beta)} \psi_{P'}^{(\alpha')} | V_{PP'} | \psi_P^{(\alpha)} \psi_{P'}^{(\beta')} \rangle \right. \\ & \left. - \delta_{\alpha, \alpha'} \delta_{\beta, \beta'} \delta_{P, P'} \frac{\varepsilon_P^{(\alpha)} - \varepsilon_{P'}^{(\beta)}}{P^{(\alpha)} - P^{(\beta)}} \right] \end{aligned} \quad (135)$$

The matrix elements of the variations in the density operators $\Delta\rho_P^{(1)}$ can be interpreted as arbitrary variation coefficients

$$c_{\alpha, \beta, P} = \langle \psi_P^{(\alpha)} | \Delta\rho_P^{(1)} | \psi_P^{(\beta)} \rangle \quad (136)$$

The second-order change in the free energy $\Delta A_{\text{var}}^{(2)}$ thus appears to be a quadratic form in these coefficients. If $\Delta A_{\text{var}}^{(2)}$ has to be positive for arbitrary variation coefficients $c_{\alpha, \beta, P}$, the Hessian of this form has to be positive definite. By Fourier transforming the coefficients, the Hessian can be block-diagonalized with blocks

$$\begin{pmatrix} \Phi(\mathbf{q}) - \chi & \phi(\mathbf{q}) & \Phi(\mathbf{q}) \\ \phi(\mathbf{q})^\dagger & \mathbf{f}(\mathbf{q}) - \mathbf{g} & \phi(\mathbf{q})^\dagger \\ \Phi(\mathbf{q}) & \phi(\mathbf{q}) & \Phi(\mathbf{q}) - \chi \end{pmatrix} \quad (137)$$

which each have to be positive definite. The matrices χ and $\Phi(\mathbf{q})$ are defined in Eqs. (130) and (131); the other submatrices have similar definitions (van der Avoird *et al.*, 1984), which are not relevant for the conclusion, however. Not only the matrices (137) have to be positive definite, but also all of their diagonal submatrices, in particular the matrices $\mathbf{N}(\mathbf{q})$, defined in Eq. (129), which we obtain from Eq. (137) by omitting the central rows and columns. From Eq. (129) it is not difficult to demonstrate that the eigenvalues of $\mathbf{N}(\mathbf{q})$ will all be positive if and only if the eigenvalues of $\mathbf{M}(\mathbf{q})$, which are the RPA frequencies, are all real (van der Avoird *et al.*, 1984). In that case the matrix $\mathbf{N}(\mathbf{q})$ is positive definite. Therefore, we find the following stability condition: $\Delta A_{\text{var}}^{(2)}$ will only be positive, i.e., the mean field solution will only be stable, if the matrix $\mathbf{N}(\mathbf{q})$ is positive definite. This implies that all TDH frequencies must be real. If at least one of these frequencies is complex, and one can prove that it will be purely imaginary, one finds negative eigenvalues of $\mathbf{N}(\mathbf{q})$ and one can choose variations $\Delta\rho_P^{(1)}$ around the mean field solution ρ_P^{MF} that make $\Delta A_{\text{var}}^{(2)}$ negative. In that case, the mean field solution does not correspond

to a local minimum in the free energy, but to a saddle point [or even a maximum if all eigenvalues of $\mathbf{N}(\mathbf{q})$ would be negative]. Following the direction(s) indicated by the variations that make $\Delta A_{\text{var}}^{(2)}$ negative, one can find a mean field solution of lower free energy.

V. Molecular Motions in Solid Nitrogen

Solid nitrogen is a very suitable system to illustrate the various lattice dynamics theories and to verify how well they describe the different motions that molecules can perform in a solid. Nitrogen has ordered phases in which the molecules librate around well-defined equilibrium orientations, as well as plastic, i.e., orientationally disordered, phases. In the latter case, the x-ray and neutron diffraction studies (Streib *et al.*, 1962; Jordan *et al.*, 1964; Schuch and Mills, 1970; Powell *et al.*, 1983) cannot determine the molecular orientations, and the nature of the molecular motions [i.e., (hindered) rotations or precessions or jumps between different equilibrium orientations] is still uncertain (Schuch and Mills, 1970; Press and Hüller, 1978; Powell *et al.*, 1983). Even in the ordered phases the amplitudes of the molecular librations are not very small, however, especially near the order-disorder phase transition, where "orientational melting" takes place. The ordered α and γ phases that exist at low temperature for pressures below and above 4 kbar, respectively, and the plastic β phase that occurs above $T = 35.6$ K (at zero pressure) have been subject to many experimental investigations. The structures of these phases are shown in Fig. 1. The results prior to 1976 have been collected by Scott (1976). Additional data are still becoming available, and new phases that are stable at higher pressures have been discovered (LeSar *et al.*, 1979; Cromer *et al.*, 1981), for which the molecular ordering is not as yet well established. All the lattice dynamics methods that we have described in Sections III and IV have been applied to the α and γ phases, the methods of Section IV also to the β phase. In this section we discuss the most characteristic results and compare them, with some emphasis on the formalism developed by ourselves, which holds both for small- and large-amplitude motions.

A. Theory for Linear Molecules

The orientations of linear molecules, relative to the global frame, can be specified by two Euler angles $\omega_P = \{\theta_P, \phi_P\}$; the symmetry-adapted functions $G_m^{(l)}(\omega_P)$ that occur in the intermolecular potential [Eq. (15)] reduce to Racah spherical harmonics $C_m^{(l)}(\theta_P, \phi_P)$. If the molecules possess a center of inversion such as N_2 (when we disregard the occurrence of mixed isotopes $^{14}\text{N}^{15}\text{N}$, the natural abundance of ^{15}N being only 0.37%),

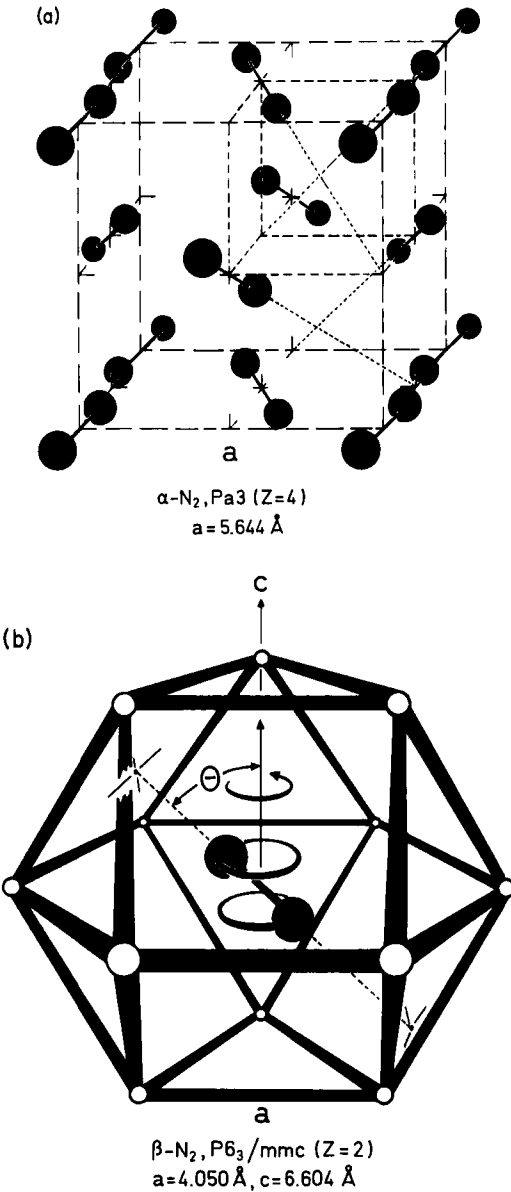


Fig. 1. Crystal structures of (a) α -, (b) β -, and (c) γ -nitrogen, according to Scott (1976).

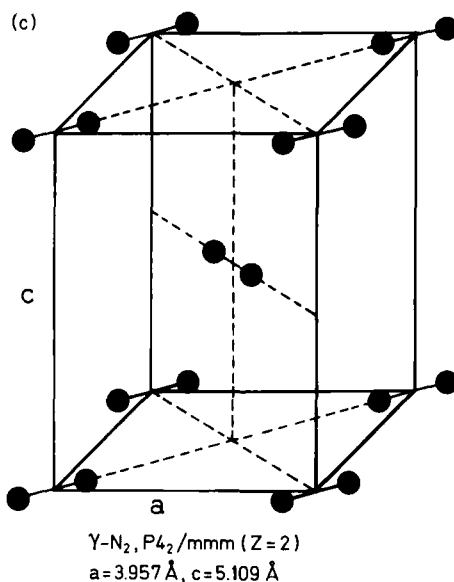


Fig. 1. (Continued)

just the even l values occur. The expression (26) for the rotational kinetic energy becomes simply

$$L(\omega_P) = BJ^2(\theta_P, \phi_P) \quad (138)$$

with the rotational constant $B = (2I)^{-1} = (2\mu r_0^2)^{-1}$. For $^{14}\text{N}^{14}\text{N}$ the average internuclear distance $r_0 = 1.094 \text{ \AA}$, the reduced mass $\mu = 7 \text{ amu}$, and $B = 2.013 \text{ cm}^{-1}$. The Wigner $D_{nm}^{(l)}(\omega_P)$ functions in the orientational basis [Eq. (111)] can also be replaced by spherical harmonics $C_m^{(l)}(\theta_P, \phi_P)$, with further restrictions on l depending on the nuclear permutation-inversion symmetry, which is related to the nuclear spin species. Therefore, for ^{14}N the nuclear spin $I = 1$ and the $^{14}\text{N}^{14}\text{N}$ molecules can be classified as *ortho*-N₂ with $I = 0$ or $I = 2$, and rotational basis functions with even l , and *para*-N₂ with $I = 1$ and a rotational basis with odd l . In lattice dynamics calculations (Dunmore, 1972; Jansen *et al.*, 1984; van der Avoird *et al.*, 1984), one has assumed that the crystal is composed of pure *ortho*-N₂ or pure *para*-N₂. The difference between the libron frequencies for ortho and para crystals is a measure for the quenching of the free N₂ rotations, i.e., the degree of orientational localization, caused by the rotational barriers from the anisotropic potential. In most cases, except for the delocalized solutions in β -nitrogen (van der Avoird *et al.*, 1984), one has found

very small ortho-para differences, which indicate a rather strong localization.

B. Results from Harmonic and Quasi-Harmonic Models

A large majority of the lattice dynamics calculations on nitrogen have employed the harmonic model. Naturally, these calculations concern the

TABLE IIIA
LATTICE FREQUENCIES IN α -N₂ (IN CM⁻¹), $T = 0$ K, $p = 0$

	Experiment ^a	Semiempirical harmonic ^b	<i>Ab initio</i> harmonic ^c	SCP ^c	RPA ^d
a (Å)	5.644	5.644	5.611	5.796	5.699
$\Gamma(0, 0, 0)$					
Librations	$\begin{cases} E_g & 32.3 \\ T_g & 36.3 \\ T_g & 59.7 \end{cases}$	$\begin{cases} 37.5 \\ 47.7 \\ 75.2 \end{cases}$	$\begin{cases} 42.4 \\ 52.9 \\ 77.7 \end{cases}$	$\begin{cases} 41.1 \\ 50.7 \\ 73.7 \end{cases}$	$\begin{cases} 31.0 \\ 41.0 \\ 68.0 \end{cases}$
Translational vibrations	$\begin{cases} A_u & 46.8 \\ T_u & 48.4 \\ E_u & 54.0 \\ T_u & 69.4 \end{cases}$	$\begin{cases} 45.9 \\ 47.7 \\ 54.0 \\ 69.5 \end{cases}$	$\begin{cases} 52.8 \\ 52.6 \\ 58.9 \\ 78.8 \end{cases}$	$\begin{cases} 49.2 \\ 49.0 \\ 54.1 \\ 73.3 \end{cases}$	$\begin{cases} 47.2 \\ 48.8 \\ 55.6 \\ 73.1 \end{cases}$
$M\left(\frac{\pi}{a}, \frac{\pi}{a}, 0\right)$					
Mixed	$\begin{cases} M_{12} & 27.8 \\ M_{12} & 37.9 \\ M_{12} & 46.8 \\ M_{12} & 54.9 \\ M_{12} & 62.5 \end{cases}$	$\begin{cases} 29.6 \\ 40.6 \\ 51.8 \\ 59.0 \\ 66.4 \end{cases}$	$\begin{cases} 34.9 \\ 46.4 \\ 59.1 \\ 64.4 \\ 72.3 \end{cases}$	$\begin{cases} 32.7 \\ 43.8 \\ 55.8 \\ 60.4 \\ 67.6 \end{cases}$	$\begin{cases} 27.6 \\ 39.1 \\ 50.2 \\ 59.1 \\ 66.5 \end{cases}$
$R\left(\frac{\pi}{a}, \frac{\pi}{a}, \frac{\pi}{a}\right)$					
Translational vibrations	$\begin{cases} R_{12}^- & 33.9 \\ R_{23}^- & 34.7 \\ R_{23}^- & 68.6 \end{cases}$	$\begin{cases} 34.4 \\ 35.7 \\ 68.3 \end{cases}$	$\begin{cases} 37.1 \\ 39.2 \\ 77.6 \end{cases}$	$\begin{cases} 34.7 \\ 36.5 \\ 72.3 \end{cases}$	$\begin{cases} 34.4 \\ 35.8 \\ 72.3 \end{cases}$
Librations	$\begin{cases} R_{12}^+ & 43.6 \\ R_{23}^+ & 47.2 \end{cases}$	$\begin{cases} 50.7 \\ 57.8 \end{cases}$	$\begin{cases} 58.1 \\ 61.0 \end{cases}$	$\begin{cases} 55.2 \\ 58.4 \end{cases}$	$\begin{cases} 47.9 \\ 50.8 \end{cases}$
rms deviation of librational frequencies		10.6	14.8	12.2	5.0
rms deviation of translational frequencies		0.6	6.3	2.4	2.1
rms deviation of all lattice frequencies		6.1	10.4	7.6	3.4

^a From Kjems and Dolling (1975).

^b From Raich and Gillis (1977).

^c From Luty *et al.* (1980).

^d From Briels *et al.* (1984).

ordered α and γ phases, although sometimes the translational vibrations in the β phase have been considered, too, with the molecular rotations neglected. The only nontechnical difference between these harmonic treatments lies in the potentials used, which are practically always empirical model potentials mostly of the atom–atom and/or quadrupole–quadrupole type (see Section II). It is generally believed that, particularly, the phonon frequencies are very sensitive to the shape of the intermolecular potential, the translational frequencies to its distance dependence and the librational modes to its anisotropy. The experimental phonon frequencies from infrared and Raman spectroscopy (for wave vector $\mathbf{q} = 0$) and from inelastic neutron scattering (for any \mathbf{q}) have been used to optimize the parameters in the model potentials. As an example of the most sophisticated work of this type, we quote the paper by Raich and Gillis (1977). The results listed in the second columns of Tables IIIA and IIIB are characteristic: fairly good agreement with experiment for the pure translational phonon frequencies and substantially worse agreement for the librational modes even after optimizing the parameters. The discrepancy has been ascribed to the strong anharmonicity and rather large amplitudes of the librations, even at the lowest temperatures. A study by Luty *et al.* (1980) using a nonempirical N_2 – N_2 site–site potential obtained from quantum-chemical *ab initio* calculations (Berns and van der Avoird, 1980) yields similar results (see the third columns of Tables IIIA, B). The overall agreement in the *ab initio* treatment, which involves no parameter

TABLE IIIB

LATTICE FREQUENCIES IN γ - N_2 (IN CM^{-1}), $T = 0 \text{ K}$, $p = 4 \text{ KBAR}$

		Experiment ^a	Semiempirical harmonic ^b	<i>Ab initio</i> harmonic ^c	SCP ^c	RPA ^d
<i>a</i> (Å)		3.957	3.940	4.032	4.100	3.961
<i>c</i> (Å)		5.109	5.086	5.000	5.188	5.104
Γ(0, 0, 0)						
Librations	E_g	55.0	50.5	60.1	58.7	67.6
	B_{1g}	98.1	74.8	89.2	87.9	103.3
	A_{2g}		105.1	111.2	108.6	124.4
Translational vibrations	E_u	65.0	58.3	71.4	68.7	65.2
	B_{1u}		103.1	113.8	110.9	114.9
rms deviation			14.2	7.0	6.6	7.9

^a From Thiéry and Fabre (1976) and Fondère *et al.* (1981).^b From Raich and Gillis (1977).^c From Luty *et al.* (1980).^d From Briels *et al.* (1980).

optimization, is slightly worse. We shall illustrate, however, that this is largely due to the harmonic approximation made in the lattice dynamics calculation. We observe, at this point, a weakness of the semiempirical procedure: optimizing a parameterized potential by comparing approximate, mostly harmonic, lattice dynamics results with measured data might lead to incorrect potentials and, at the same time, partly hide the flaws of the approximate lattice dynamics model.

Harris and Coll (1972), Kobashi (1978), and Kuchta and Luty (1983) have used anharmonic perturbation theory (see Section III,B) to study the effect of the cubic and quartic anharmonicities on the libron and phonon frequencies in α -nitrogen. The results are conflicting, however, and the shifts appear to depend very sensitively on the potential. Harris and Coll (1972), using only the quadrupole-quadrupole interactions, find a reduction of the libron frequencies by about 12%, whereas Kobashi (1978), using a 12-6 atom-atom potential, finds an increase in all libron and phonon frequencies by 4 to 14 cm^{-1} , i.e., 7 to 17%. Kuchta and Luty (1983), using a perturbed uncoupled oscillator model starting from the *ab initio* potential of Berns and van der Avoird (1980), obtain a decrease of the harmonic libron frequencies by 18 to 27%. The agreement of the latter results, after the perturbation correction, with experimental data must probably be regarded as fortuitous, however, since the anharmonic corrections for the librations are too large to be treated by perturbation theory up to the second order.

A similar influence of the potential chosen occurs if one tries to calculate the anharmonic effects by the self-consistent phonon (SCP) method. The calculation by Raich *et al.* (1974) is based on the atomic version of the SCP method (see Section III,C). Using an empirical 12-6 atom-atom potential, they found a consistent increase of the harmonic phonon and libron frequencies by 3 to 10%. The calculation by Luty *et al.* (1980), who use the SCP method of Wasiutynski (1976) and the *ab initio* N_2 - N_2 potential of Berns and van der Avoird (1980), yields a consistent lowering by about the same amount. It is striking (see Tables IIIA,B, fourth columns) that the *ab initio* results for the pure translational phonon frequencies in α - and γ -nitrogen agree remarkably well with experiment, without any parameter optimization, while the librational frequencies and those of the mixed modes are still substantially too high. Apparently the anharmonicity in the distance dependence of the intermolecular potential, which affects the translational vibrations, is very well accounted for by the SCP method. The orientational dependence of the potential is strongly anharmonic. In combination with the fairly large amplitudes of the rotational oscillations, this causes the SCP method to fail in describing the librational motions. This failure may be related to the additional approximations made in generalizing this method to molecular crystals.

Raich *et al.* (1974) and Goldman and Klein (1975) have applied the SCP method to the translational phonons in β -nitrogen. The molecular rotations were assumed to be completely free and the effective isotropic intermolecular potential used was a rotationally averaged, empirical atom-atom 12-6 potential. The results of such models that completely neglect any translation-rotation coupling are mainly of qualitative interest.

C. Large-Amplitude Motions in the Ordered Phases

Since it became clear from various observations that the librational motions of the molecules, even in the ordered α and γ phases of nitrogen at low temperature, have too large amplitudes to be described correctly by (quasi-) harmonic models, we have resorted to the alternative lattice dynamics theories that were described in Section IV. Most of these theories have been developed for large-amplitude rotational oscillations, hindered or even free rotations, and remain valid when the molecular orientations become more and more localized.

Weis and Klein (1975) made classical molecular dynamics (MD) calculations for 250 N_2 molecules in a cubic box, with periodic boundary conditions. These molecules were initially arranged in the cubic Pa3 structure of α -nitrogen, and they were made to interact via a 12-6 atom-atom potential. The molecular motions were mainly characterized via the calculated dynamic structure factor $S(\mathbf{q}, \omega)$, which describes the response of the system to a transfer of momentum \mathbf{q} and energy $\hbar\omega$ (see Section IV,A). Because for given wave vector \mathbf{q} the peaks in $S(\mathbf{q}, \omega)$ can be identified with phonons, the results of these calculations could be compared with (quasi-) harmonic lattice dynamics studies. The phonon frequencies appeared to be substantially different from the quasi-harmonic results calculated with the same atom-atom potential, and the temperature shifts of some of the peaks were much larger in the MD calculations. These differences and the corresponding peak broadenings have been ascribed by Weis and Klein to the occurrence of strongly anharmonic, large-amplitude motions that cause the breakdown of the quasi-harmonic model. At a temperature, of 35 K, close to the α - β phase transition point, the MD calculations even indicate the existence of "quasi-free" rotations.

Jacobi and Schnepf (1972) and Raich (1972) were the first to develop a quantum-dynamical model for the large-amplitude librations in α -nitrogen. Their formalism is essentially described in Section IV,C. They first calculated single-molecule mean field states that may be localized as well as delocalized, depending on the height of the rotation barriers from the anisotropic potential. These states were used to construct a basis of excitonlike wave functions for the whole crystal. The final step in their calcu-

lation, the diagonalization of the full-crystal Hamiltonian in this basis, amounts to diagonalizing the upper left block of the RPA matrix, Eq. (126). Therefore, this theory is more approximate than the RPA formalism; one of the consequences is that it does not converge to the harmonic solution in the limit of an exactly harmonic crystal Hamiltonian. If the excitonlike model were applied to the translational phonons rather than to the librations, the acoustical modes would not go to zero frequency for $\mathbf{q} = 0$. Employing the full RPA method, as described in Section IV,C, ensures the convergence to the correct limits; this method has been applied to the librations in α -nitrogen by Dunmore (1972, 1976), Raich *et al.* (1974), and Mandell (1974, 1975).

All these authors have used semiempirical N_2 - N_2 potentials, often simplified to the utmost by retaining only pure quadrupole-quadrupole interactions or atom-atom 12-6 interactions. Moreover, they have always fixed the molecules with their centers of mass to the lattice points, thus neglecting the translational vibrations and the effects of libron-phonon coupling. We applied the RPA formalism to α - and γ -nitrogen (Jansen *et al.*, 1984) by using the *ab initio* potential of Berns and van der Avoird (1980). This potential was not approximated by a site-site model this time, but expanded in symmetry-adapted functions as in Section II,B. In a subsequent paper (Briels *et al.*, 1984) we extended the theory in order to account explicitly for the translational phonons and for libron-phonon coupling after expanding the crystal Hamiltonian as in Section II,D. The extended formalism is described in Section IV,C. Since this treatment is more complete than any of the previous ones, we shall use its results as an illustration.

We have started by assuming the observed lattice symmetry and by theoretically optimizing the cell parameters for the given *ab initio* potential as follows. For α -nitrogen we have calculated the minimum of the free energy in the mean field approximation as a function of the cubic cell parameter a . This yields the optimum value $a = 5.699 \text{ \AA}$, experimentally (Scott, 1976) $a = 5.644 \text{ \AA}$, and the mean field lattice cohesion energy at $T = 0 \text{ K}$ of $\Delta E = 5.92 \text{ kJ/mol}$, experimentally $\Delta E = 6.92 \text{ kJ/mol}$. For the γ phase we have calculated the free energy A for several values of the tetragonal cell parameters a and c and fitted $A(a, c)$ by a second-order polynomial. On each curve of constant molar volume $v = Na^2c/2$, we have determined the optimum a and c by minimizing A . Using the optimum points and the corresponding free energies, we have calculated the pressure as $p = -\partial A/\partial v$. Thus we found at $p = 4 \text{ kbar}$ that $a = 3.961 \text{ \AA}$ and $c = 5.104 \text{ \AA}$, in excellent agreement with the experimental values $a = 3.957 \text{ \AA}$ and $c = 5.109 \text{ \AA}$ (Scott, 1976).

The mean field approximation yields a picture of the single-molecule

motions as determined by the anisotropic *ab initio* potential. The orientational probability distributions in α - and γ -nitrogen are shown in Fig. 2a,b, respectively. We clearly observe that the librations of the molecules in the α phase are localized about the cubic body diagonals, i.e., the $[1, 1, 1]$ direction and three equivalent directions. In γ -nitrogen the N_2 molecules appear to librate about the $[1, 1, 0]$ and $[1, -1, 0]$ directions. Both these findings agree with experiment, cf. Fig. 1. For temperatures up to at least 40 K, these pictures remain qualitatively similar. The amount of delocalization is measured by the decreasing order parameter $S = \langle P_2(\cos \theta) \rangle$ (see Fig. 3), with θ now defined relative to the equilibrium axis. Even at $T = 0$ K the root-mean-square amplitude of the librations is already substantial, however, about 16° in the α -phase. Similar parameters, including the translational vibrations, are listed in Table IV. We observe that the molecular motions, both librational and translational, in γ -nitrogen at $p = 4$ kbar are more restricted than in the α phase, at zero pressure.

After calculating the ground and excited mean field states of α - and γ -nitrogen, we have included the correlation between the molecular motions, as well as the translational-rotational coupling, by determining the eigenvalues of the RPA matrix $\mathbf{M}(\mathbf{q})$ [Eq. (129)]. The expansion of the potential in the translational displacements (\mathbf{u}_p) of the molecules [see Eq.

TABLE IV
TRANSLATIONAL AND LIBRATIONAL AMPLITUDES FROM
MEAN FIELD CALCULATIONS

α -N ₂	$T = 0$ K	$p = 0$
$\langle u_{\parallel}^2 \rangle^{1/2} = 0.112 \text{ \AA}$		$u_{\parallel} = u_{[1,1,1]}$
$\langle u_{\perp}^2 \rangle^{1/2} = 0.107 \text{ \AA}$		
$\langle u^2 \rangle^{1/2} = 0.189 \text{ \AA}$		
$\arccos(\langle \cos^2 \theta \rangle^{1/2}) = 16.1^\circ$		
γ -N ₂	$T = 0$ K	$p = 4$ kbar
$\langle u_{\parallel}^2 \rangle^{1/2} = 0.100 \text{ \AA}$		$u_{\parallel} = u_{[1,1,0]}$
$\langle u_{\perp ab}^2 \rangle^{1/2} = 0.086 \text{ \AA}$		$u_{\perp ab} = u_{[1,-1,0]}$
$\langle u_{\perp c}^2 \rangle^{1/2} = 0.087 \text{ \AA}$		$u_{\perp c} = u_{[0,0,1]}$
$\langle u^2 \rangle^{1/2} = 0.159 \text{ \AA}$		
$\arccos(\langle \cos^2 \theta \rangle^{1/2}) = 12.9^\circ$		
asymmetry parameter (rotation out of <i>ab</i> plane – rotation		
in <i>ab</i> plane): $\frac{\langle \sin^2 \theta (\sin^2 \varphi - \cos^2 \varphi) \rangle}{\langle \sin^2 \theta \rangle} = 0.05$		

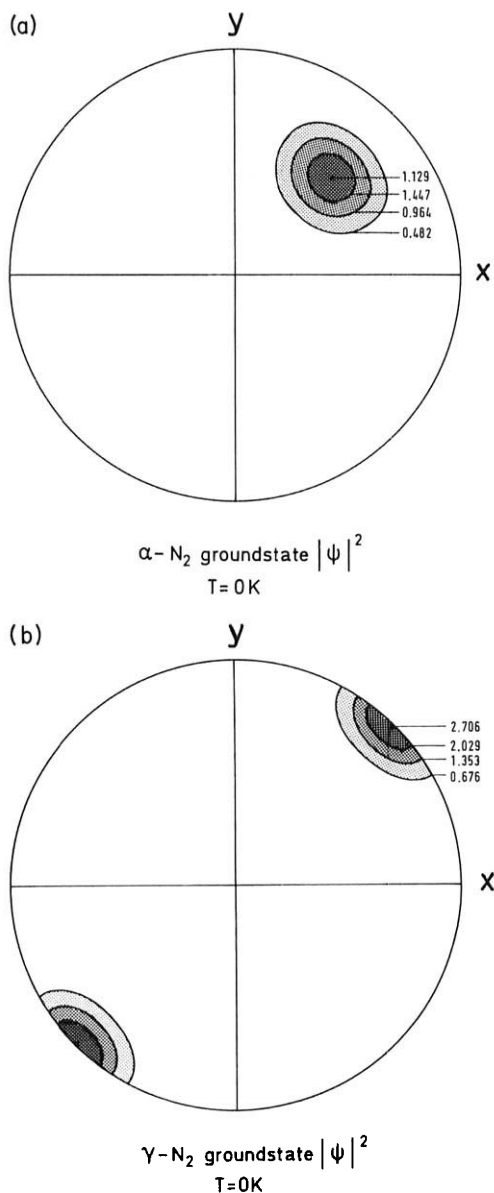


Fig. 2. Orientational probability distributions of the molecular axes in (a) α -nitrogen and (b) γ -nitrogen. Contours of constant probability for the molecule in the origin, calculated in the mean field model, are plotted as functions of the polar angles (θ , ϕ) with respect to the crystal axes (Fig. 1). The angle θ increases linearly with the radius of the plots from 0 (in the center) to $\pi/2$ (at the boundary); ϕ is the phase angle.

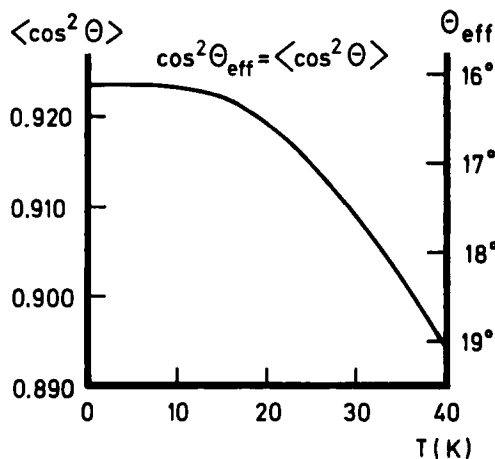


Fig. 3. Temperature dependence of the (mean field) order parameter in α -N₂.

(40)] has been truncated at three different levels. Taking $\alpha_{\text{max}} = 2$ corresponds to a harmonic model for the translational phonons; taking $\alpha_{\text{max}} = 3$ and $\alpha_{\text{max}} = 4$ includes the cubic and quartic anharmonicities, respectively. The orientational (ω_p) dependence of the *ab initio* potential has always been included exactly, which is important because of the large amplitude of the librations. Some typical results are shown in Table V. The size of the anharmonic corrections to the translational phonon frequencies is comparable with that of the self-consistent phonon corrections calculated with the same *ab initio* potential (Luty *et al.*, 1980); the corrected frequencies agree equally well with experiment. There is an important difference, however, between our RPA formalism and the SCP method. The latter neglects those terms in the potential that depend on the odd powers of the molecular displacements. The cubic terms have sometimes been added perturbationally (Goldman *et al.*, 1968; Koehler, 1969), but not so by Luty *et al.* (1980). Our formalism includes the effects of the cubic terms directly in the mean field and RPA results. In α -nitrogen, however, because of the inversion symmetry, they vanish at the mean field level and have no effect on the purely translational phonon frequencies of Table V. In the mixed phonon-libron modes the cubic corrections mostly lower the frequencies, while the quartic corrections are always positive and dominant.

We wish to emphasize that the most essential advantage of the RPA method discussed here over the previous (quasi-) harmonic treatments is the correct description of the large-amplitude libron modes and the mixed libron-phonon modes. This is reflected by the substantial anharmonic corrections in the frequencies of these modes; compare the last column of

TABLE V
 α_{\max} DEPENDENCE OF SOME RPA LATTICE FREQUENCIES FOR α -N₂
 ($a = 5.644$ Å, $T = 0$ K)

		Frequency ω (cm ⁻¹)		
		$\alpha_{\max} = 2^a$	$\alpha_{\max} = 3$	$\alpha_{\max} = 4$
$\Gamma(0, 0, 0)$				
Librations	E_g	32.8	32.8	32.8
	T_g	43.4	43.4	43.4
	T_g	71.6	71.6	71.5
Translations	A_u	42.3	42.3	50.6
	T_u	48.7	48.7	52.7
	E_u	55.7	55.7	60.2
	T_u	73.0	73.0	79.4
$M\left(\frac{\pi}{a}, \frac{\pi}{a}, 0\right)$				
Mixed	M_{12}	28.8	25.7	28.8
	M_{12}	40.4	38.5	41.5
	M_{12}	52.2	51.7	53.3
	M_{12}	60.0	61.2	63.7
	M_{12}	67.0	68.6	72.0

^a Harmonic model for translations.

Table III with the preceding columns. The new results calculated with the *ab initio* potential agree very well with the frequencies from inelastic neutron scattering (Kjems and Dolling, 1975) and from infrared and Raman spectroscopy (Thiéry and Fabre, 1976; Fondère *et al.*, 1981) for all types of modes. Also the phonon dispersion relations, displayed in Fig. 4, are in good agreement with the neutron-scattering data. Since most of the lattice modes are actually mixed libron-phonon modes, this indicates that the translation-rotation coupling is correctly included in the RPA formalism.

D. The Plastic Phase and the Orientational Order-Disorder Phase Transition

Lattice dynamics calculations on the plastic β -nitrogen phase are relatively scarce because, obviously, the standard (quasi-) harmonic theory cannot be applied to this phase. Classical Monte Carlo calculations have been made by Gibbons and Klein (1974) and Mandell (1974) on a face-centered cubic (α -nitrogen) lattice of 108 N₂ molecules, while Mandell has also studied a 32-molecule system and a system of 96 N₂ molecules on a hexagonal close-packed (β -nitrogen) lattice. Gibbons and Klein used 12-6

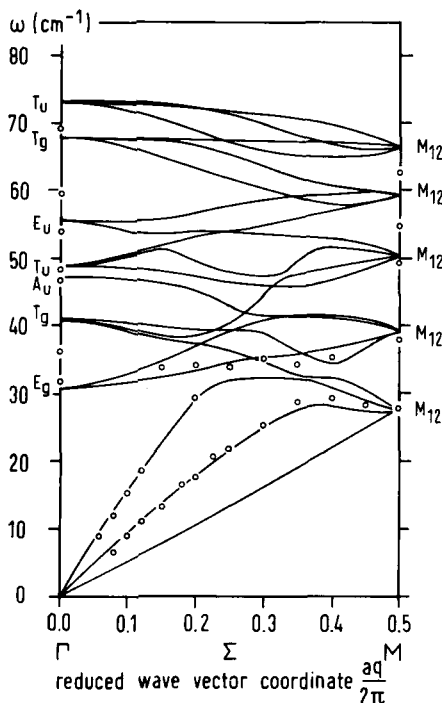


Fig. 4. Calculated (TDH) dispersion curves for α -N₂, for phonon-libron modes propagating along the [110] direction. The circles correspond to inelastic neutron scattering data measured at $T = 15$ K by Kjems and Dolling (1975).

and 9–6 atom–atom potentials and fairly high temperatures, $T = 96$ and 192 K; they found only complete orientational disorder. Mandell made his N₂ molecules interact as pure point quadrupoles, and he showed that even the smaller 32-molecule system already yields a fairly realistic order–disorder phase transition.

Another simple, quantum-mechanical, model for the phase transition has been proposed by Raich and Etters (1972). They studied N₂ molecules on an fcc lattice, again interacting as pure point quadrupoles. Using a mean field model for the librations in the α phase, a free rotor model for β -nitrogen, and calculating the corresponding free-energy curves, they found an α – β phase transition at somewhat too high a temperature. This model has been refined by Raich *et al.* (1974) and Goldman and Klein (1975), who applied the self-consistent phonon method to the translational and librational motions in the α phase and to the pure translational phonons in the β phase (cf. Section V,B). The rotational motions in β -nitrogen were still assumed to be completely free, however, and any

translation-rotation coupling was neglected. Classical molecular dynamics calculations by Klein *et al.* (1977, 1981) on a 288-molecule model for β -nitrogen at $T = 47$ K indicate that this coupling is probably important, since the translational phonon frequencies derived from these MD calculations, while using the same 12-6 atom-atom potential, are substantially different from the SCP results of Raich *et al.* (1974). The rotational motions in the β phase were found to be "quasi-free" in the classical MD model.

Finally, we discuss the mean field and RPA calculations made on β -nitrogen (van der Avoird *et al.*, 1984) by using the *ab initio* potential of Berns and van der Avoird (1980) again. We started our calculations on this phase, just as those for α - and γ -nitrogen, by assuming the experimentally observed lattice symmetry. Thus, the two molecules in the hexagonal unit cell (see Fig. 1) were given translationally equivalent mean field solutions. The orientational probability distribution that results for the pure *ortho*-N₂ crystal is shown in Fig. 5a. The ground state of the *para*-N₂ species is twofold degenerate; the average probability distribution $\frac{1}{2}|\psi_1|^2 + \frac{1}{2}|\psi_2|^2$ is similar to Fig. 5a. This picture suggests that the orientational motions in β -nitrogen are quasi-free precessions around the crystal c axis, modulated by small sixfold barriers. In accordance with the ideas of Press and Hüller (1978) and the earlier mean field calculations by Dunmore (1976), the precession angle θ between the molecular axis and the c axis is not sharply defined, but it shows a rather broad distribution with the maximum at the "experimental" value of $\theta = 56^\circ$ (Scott, 1976).

The mean field ground state yielding this delocalized picture appeared to be unstable, however. This could be concluded from the ensuing RPA calculations yielding imaginary libron frequencies and the stability conditions in Section IV,D. We have searched for a stable mean field solution by independently varying the orientational wave functions of the two molecules in the unit cell, and we have indeed found such a solution, which is lower in (free) energy by 0.87 kJ/mol than the previous delocalized solution at $T = 0$ K. In this new solution the orientations of the N₂ molecules are clearly localized (see Fig. 5b). They librate about an equilibrium axis that makes an angle of 52° with the crystal c axis. The equilibrium axes for the two neighboring molecules in the hexagonal unit cell are not the same, but they are rotated through 180° about the c axis. This 180° rotation avoids the steric hindrance between neighbors that would occur when the molecules were freely precessing (Schuch and Mills, 1970) and, thus, leads to the lower free energy.

The problem with this localized, stable, mean field solution is that it has a much lower symmetry than the experimentally observed hexagonal symmetry of β -nitrogen. We have conjectured that the higher symmetry is

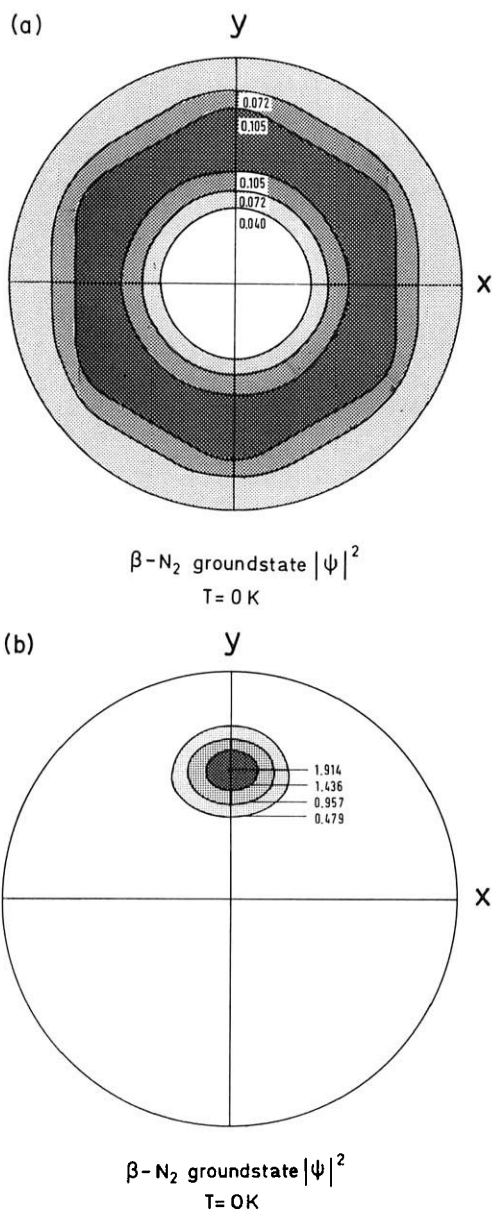


Fig. 5. Orientational probability distribution of the molecular axes for the delocalized (a) and localized (b) mean field states in β -nitrogen. (a) applies to both molecules in the unit cell. (b) is drawn for one molecule in the unit cell; the other molecule in the cell is rotated over $\phi = 180^\circ$. The distribution does not change qualitatively up to (at least) $T = 70$ K; it just becomes slightly wider with increasing temperature. Reading of the contour plot as in Fig. 2.

observed because of rapid jumps of the molecular axes between six localized librational states of the type found in the final mean field calculation. The six equilibrium axes will be located at $\theta \approx 52^\circ$ and $\phi = 0^\circ, 60^\circ, 120^\circ, 180^\circ, 240^\circ$, and 300° . The characteristic time for these jumps should be less than the inverse frequency of the nuclear quadrupole resonance measurements (de Reggi *et al.*, 1969), i.e., about 10^{-7} sec. In order to preserve the lower energy of the stable mean field solution, the jumps of neighboring molecules must be correlated; two neighbors have the tendency to remain 180° out of phase in their ϕ angles.

With the different models emerging for the molecular motions in the β phase and the mean field model for localized, large-amplitude librations in the α phase (see Section V,C), we have studied the α - β phase transition. The calculated free-energy curves corresponding with these models are shown in Fig. 6. The free energy for the delocalized precession model of β -nitrogen decreases much more steeply, with increasing temperature, than that for α -nitrogen. This is caused by the spectrum of the delocalized β -N₂ model being like a free rotor, with considerably smaller excitation

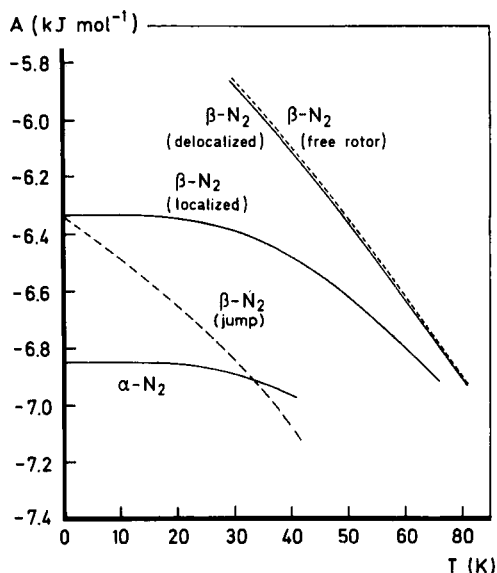


Fig. 6. Free energy (at zero pressure) for α -nitrogen and β -nitrogen, in different mean field models (closed lines). The dashed free rotor curve has been calculated from the isotropic $(l_1, l_2, l_3) = (0, 0, 0)$ term of the *ab initio* potential by adding the free rotor expression for the free energy. The dashed jump model curve has been obtained from the localized mean field solution (with the full anisotropic potential) by adding an entropy term $-k_B T \ln 6$ (see the text).

energies than the harmonic oscillatorlike spectrum of α -N₂. As shown in Fig. 6, a free rotor model for β -N₂ yields almost the same free-energy curve as the delocalized precession model. However, both these models cannot give a free energy lower than that for α -N₂, and thus a phase transition, at any reasonable temperature. On the other hand, the localized librational solution for β -N₂ is much lower in energy, but its free-energy curve does not sufficiently fall off with temperature to cross the α -N₂ curve. Now we invoke the jumps of the molecules between the localized solutions. Ignoring, for the moment, the correlations between these jumps and assuming that each molecule has access to six localized states yields an entropy term $-k_B T \ln 6$. Adding this term to the free-energy curve of a particular localized solution leads to the curve in Fig. 6 marked " β -N₂ jump." This model predicts an α - β phase transition temperature of 34 K, very close to the experimental value $T = 35.6$ K.

Starting from the localized mean field wave functions, we have also calculated the libron frequencies in β -nitrogen via the RPA formalism. All frequencies appeared to be real, as they should be for a stable mean field solution. The infrared spectrum (Medina and Daniels, 1976) shows two very broad peaks around 25 to 36 cm⁻¹ and 50 to 68 cm⁻¹, depending on the pressures. The first one has been interpreted as a translational phonon band, the second one as a libron band. Neutron scattering (Kjems and Dolling, 1975) yields broad peaks at 25 and 64 cm⁻¹ attributed to translational phonons. We have calculated optical libron frequencies of 34, 41, 56, and 59 cm⁻¹. The observed broad peaks may well contain these libron excitations in addition to the translational phonon bands. We assign the broadening of these peaks to the occurrence of more or less random transitions, classically called jumps, between the different localized libron states.

In summary, we think that our calculations suggest a model with localized librations and 60° jumps for the orientational motions in β -nitrogen. This model gives a reasonable account of the α - β phase transition and the libron spectrum of β -N₂. A dynamical model for the 60° jumps, which must include strong short-range pair correlations, is still lacking, however. Possibly this correlation can be introduced by using Jastrov functions (van Kranendonk, 1983).

VI. Dynamics and Magnetism of Solid Oxygen

Oxygen, with its $^3\Sigma_g^-$ ground state, is one of the few stable molecules with a nonvanishing electronic spin momentum. The potential between O₂ molecules is not only determined by the usual van der Waals interactions occurring between closed shell molecules, but it contains, moreover, the

coupling between the electronic spins. In addition to their positional and orientational coordinates, the O_2 molecules have an extra degree of freedom: the orientations of their triplet spin momenta. Consequently, in the solid we must consider the molecular motions, translational and rotational, as well as the spin dynamics.

This extra degree of freedom makes solid O_2 one of the most interesting molecular crystals. Even at low pressure one finds three different phases: the α phase between 0 and 23.8 K, the β phase between 23.8 and 43.8 K, and the γ phase between 43.8 K and the melting point at 54.4 K. These phases have structural as well as magnetic order. The α and β phases are orientationally ordered; the γ phase is plastic. The α phase is antiferromagnetic, with the usual (spin up, spin down) two-sublattice structure; α -oxygen is the only homogeneous antiferromagnet known. The β phase probably has short-range antiferromagnetic order with a three-sublattice 120° spin arrangement. The γ phase is paramagnetic, just like liquid oxygen. Both in the α and β phases the molecules are packed in layers, the a - b planes, with their axes perpendicular to these planes (see Fig. 7). In the β phase this packing is hexagonal; in the monoclinic α phase the hexagons are slightly distorted by a contraction in the a direction and a dilation in the b direction. This distortion is driven by the magnetic coupling: the α - β phase transition is called magnetoelastic. The spins in the α phase are preferentially directed in the $\pm b$ directions.

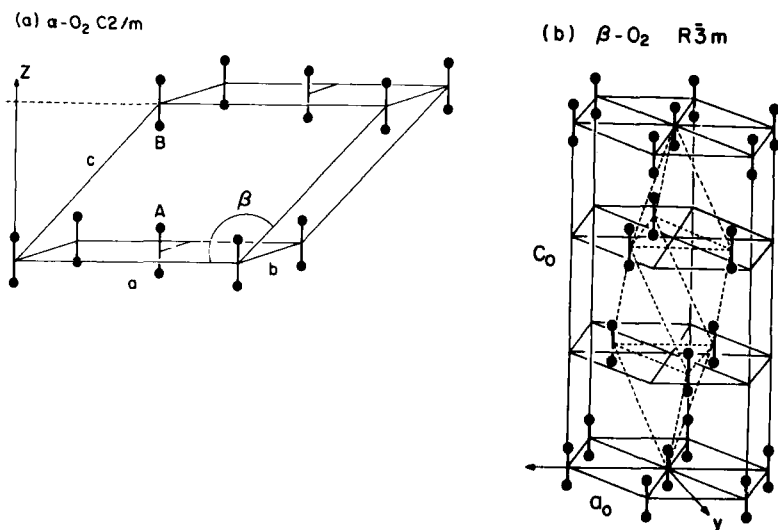


Fig. 7. Crystal structures of (a) α -oxygen and (b) β -oxygen, according to De Fotis (1981).

The excitations in such a magnetic solid are not only due to the lattice vibrations, phonons, and librations, but also to the spin waves; the corresponding quasi-particles are called magnons. The magnetic excitations in α -O₂ have been directly observed by infrared and Raman spectroscopy and by inelastic neutron scattering. In general, they determine, of course, the magnetic properties of the system, susceptibilities, spin flop processes, etc. They also affect other properties, though, such as the specific heat and the thermal expansion coefficients. For the experimental and theoretical work prior to 1981 we refer to De Fotis's (1981) review, which begins by stating that "the magnetic, structural, thermodynamic and spectroscopic properties of the condensed phases of oxygen have been under study for nearly a century. Yet important aspects of their behavior remain poorly understood." Work by Slyusarev *et al.* (1980, 1981), Gaididei and Loktev (1981), Stephens *et al.* (1983), Meier *et al.* (Meier *et al.*, 1982; Meier and Helmholtz, 1984; Meier, 1984), Etters *et al.* (Etters *et al.*, 1983; Helmy *et al.*, 1984), and van der Avoird *et al.* (van Hemert *et al.*, 1983; Wormer and van der Avoird, 1984; Jansen and van der Avoird, 1985) has provided additional information.

A. Lattice Dynamics and Spin Wave Calculations

Until very recently, the lattice vibrations in solid O₂ and its magnetic properties have always been treated separately. As far as the packing in the crystal and the lattice vibrations are concerned, one can consider the O₂ molecules as resembling N₂. An important quantitative difference lies in the O₂ molecule's quadrupole moment, however, which is about four times smaller than that of N₂ (in absolute value). This smaller quadrupole moment, together with the exchange coupling between the open-shell O₂ molecules (see the subsequent discussion), probably explains why the packing in the ordered α and β phases of solid O₂ (see Fig. 7) is very different from the ordered N₂ structures (see Fig. 1) (English and Venables, 1974; English *et al.*, 1974). The lattice dynamics calculations that have been made for α - and β -oxygen (Kobashi *et al.*, 1979; Etters *et al.*, 1983; Kuchta, 1985) are very similar to the standard harmonic calculations made on solid nitrogen (see Section V); they have used empirical atom-atom 12-6 or exp -6 potentials. The calculated optical libron frequencies are generally in reasonable agreement with the experimental data. One important observation could not be explained by these calculations, however. In β -oxygen there is a degenerate optical ($\mathbf{q} = 0$) libron mode of E_g symmetry with a frequency of about 50 cm⁻¹. This mode corresponds with the in-phase librations of all O₂ molecules around the crystal **a** and **b** axes, and the degeneracy occurs because of the equivalence of these axes in the hexagonal β phase. When the hexagonal sym-

metry is distorted by going through the β - α phase transition, this mode will be split, in principle. The librations around the monoclinic **b** axis in α -O₂ have A_g symmetry; those around the **a** axis have B_g symmetry. The splitting actually observed by Raman spectroscopy is so large, however, that it cannot be explained by any of the lattice dynamics calculations. The experimental spectrum of α -O₂ shows two peaks at 43 and 79 cm⁻¹, whereas the lattice dynamics calculations yield a splitting of about 10 cm⁻¹ at most. The latter result is not surprising in view of the small structural distortion that accompanies the β - α phase transition. Most authors have assumed, therefore, that the A_g and B_g modes remain very nearly degenerate in α -O₂ and that the higher-frequency peak represents a two-libron, two-phonon, or libron-magnon transition. Experiments by Bier and Jodl (1984) indicate, however, that the mode at 43 cm⁻¹ is probably the B_g mode and the mode at 79 cm⁻¹ the A_g mode. We shall give an explanation of this phenomenon in the next section.

The magnetic properties of α -O₂, which is the most extensively studied phase, have always been interpreted on the basis of the following phenomenological spin Hamiltonian:

$$H_{\text{spin}} = -\frac{1}{2} \sum_{P \neq P'} \sum_P 2J_{PP'} \mathbf{S}_P \cdot \mathbf{S}_{P'} + \sum_P (AS_x^2 + BS_y^2) \quad (139)$$

where z is the preferred magnetization axis, the **b** axis, the x axis is the orientation of the molecular axes (i.e., the crystallographic **c*** direction), and the y axis coincides with the crystal **a** axis. The first term in this Hamiltonian is the Heisenberg exchange coupling between the triplet O₂ molecules. The dominant, intersublattice exchange coupling is antiferromagnetic, i.e., $J_{PP'} < 0$, and it occurs between a given molecule and its four nearest neighbors in the a - b plane. In the more recent work, moreover, the in-plane intrasublattice coupling with the two next-nearest neighbors and the interplanar coupling with four additional neighbors have been included. The interplanar coupling was found (Burakhovich *et al.*, 1977; Stephens *et al.*, 1983) to be very weak, which makes α -oxygen, and β -oxygen, a quasi-two-dimensional magnetic system. The single-particle term AS_x^2 is due to the intramolecular spin-orbit and spin-spin interactions; the free-molecule value of A is equal to 3.96 cm⁻¹ = 5.72 K. This term tends to keep the directions of the molecular spin momenta perpendicular to the molecular axes, such that in α - and β -oxygen the spins will lie in the a - b plane. The additional single-particle term BS_y^2 is then added *ad hoc* in order to impose the observed in-plane anisotropy that forces the spins to lie parallel to the **b** axis. Classical dipole models yielding the preferred magnetization axis and the order of magnitude of the empirical

B values suggest that the term BS_y^2 actually represents the magnetic dipole-dipole interactions between the molecular spin moments.

With the use of the phenomenological spin Hamiltonian [Eq. (139)], mean field and spin-wave calculations have been made that yield the observed magnetic, optical, and thermodynamic properties. The antiferromagnetic spin-wave calculations are mostly based on the RPA method outlined in Section IV,C. The formalism is very simple in this case, because the basis for every molecule consists only of the three triplet spin states. By taking the mean field ground state on each molecule and the first excited state, which provides the single magnon states, the RPA equations can be solved exactly for the magnon frequencies. The calculated properties have been compared with experimental data and the coupling constants J , A , and B in the Hamiltonian (139) have thus been determined empirically. The situation is not very satisfactory, however, since the various semiempirical studies on α -O₂ have yielded substantially different sets of coupling constants, depending on the type of experimental data fitted. The discrepancies have been pointed out most clearly by De Fotis (1981), but also the more recent studies still yield rather different J , A , and B values. Moreover, most of the empirical A and B values in solid O₂ deviate considerably from the values corresponding with the free-molecule zero-field splitting and the magnetic dipole moment, respectively. This is surprising since we expect the distortions of the molecular electronic charge distributions, due to the weak van der Waals interactions in the solid, to be minor.

B. The Complete Crystal Hamiltonian and the Coupling between Lattice Vibrations and Spin Dynamics

In a recent paper (Jansen and van der Avoird, 1985), two of us have proposed replacing the phenomenological spin Hamiltonian (139) by a spin Hamiltonian from first principles. By this qualification we mean that our Hamiltonian can be derived directly from the known properties of the O₂ molecules and their interactions. Such a Hamiltonian, which applies not only to α -O₂, but also to any of the condensed phases, looks as follows:

$$\begin{aligned}
 H_{\text{spin}} = & -\frac{1}{2} \sum_{P \neq P'} \sum 2J(\omega_P, \omega_{P'}, \mathbf{r}_{PP'}) \mathbf{S}_P \cdot \mathbf{S}_{P'} \\
 & + \sum_P \sum_m (-1)^m A_{-m}(\omega_P) [\mathbf{S}_P \otimes \mathbf{S}_P]_m^{(2)} \\
 & + \frac{1}{2} \sum_{P \neq P'} \sum_m \sum (-1)^m T_{-m}(\mathbf{r}_{PP'}) [\mathbf{S}_P \otimes \mathbf{S}_{P'}]_m^{(2)} \quad (140)
 \end{aligned}$$

The irreducible tensor product between two (spherical) vectors is defined in Eq. (37). An important feature of this Hamiltonian is that it explicitly describes the dependence of the coupling "constants" J , A_m , and T_m on the distance vectors $\mathbf{r}_{PP'}$ between the molecules and on the orientations $\omega_P = \{\theta_P, \phi_P\}$ of their axes, in contrast with the phenomenological Hamiltonian (139). Another important difference with the latter is that the *ad hoc* single-particle spin anisotropy term BS_y^2 , which probably stands implicitly for the magnetic dipole-dipole interactions, has been replaced by a two-body operator that correctly represents these interactions. The distance and orientational dependence of the coupling parameters J , A_m , and T_m has been obtained as follows.

The Heisenberg exchange coupling parameter J is a scalar quantity; its dependence on $\mathbf{r}_{PP'}$, ω_P , and $\omega_{P'}$ is described by expanding it in symmetry-adapted angular functions, just as the intermolecular potential in Eq. (15). The distance-dependent expansion coefficients have been explicitly obtained from *ab initio* quantum-chemical calculations (van Hemert *et al.*, 1983; Wormer and van der Avoird, 1984). These coefficients could be represented by steeply decaying exponential functions of the distance. The *ab initio* calculations refer to $(\text{O}_2)_2$ dimers with the triplet O_2 spins coupled to a singlet, a triplet, or a quintet. The exchange splitting between the dimer spin states has been obtained from a second-quantized hole-particle formalism, generalized to nonorthogonal orbitals (Wormer and van der Avoird, 1984). It was found that this exchange splitting could indeed be represented accurately by a Heisenberg effective spin Hamiltonian. The coupling parameter J appeared to depend very sensitively on the distance between the O_2 molecules and, particularly, on their orientations (see Fig. 8). In Fig. 9 we have plotted the dependence of J on the librational coordinates in α -oxygen.

The molecular spin-anisotropy term, the second term in Eq. (140), depends on the angle between the O_2 spin momentum \mathbf{S}_P and the molecular axis. With respect to the global frame, this dependence can be expressed as in Eq. (140) with the second-rank tensor

$$A_m(\omega_P) = \frac{1}{3}A\sqrt{30}C_m^{(2)}(\theta_P, \phi_P) \quad (141)$$

The constant $A = 3.96 \text{ cm}^{-1}$ has been obtained from the free-molecule zero-field splitting (Mizushima, 1975) and $C_m^{(2)}$ is a Racah spherical harmonic with $l = 2$. The tensor that describes the interaction between the magnetic dipole moments $g_e\mu_B\mathbf{S}_P$, where g_e equals 2.0023 and μ_B is the Bohr magneton, can be written immediately as

$$T_m(\mathbf{r}_{PP'}) = -g_e^2\mu_B^2\sqrt{30}r_{PP'}^{-3}C_m^{(2)}(\hat{r}_{PP'}) \quad (142)$$

In summing this term over the lattice, in the calculations described subsequently, the Ewald method (Born and Huang, 1954) had to be invoked.

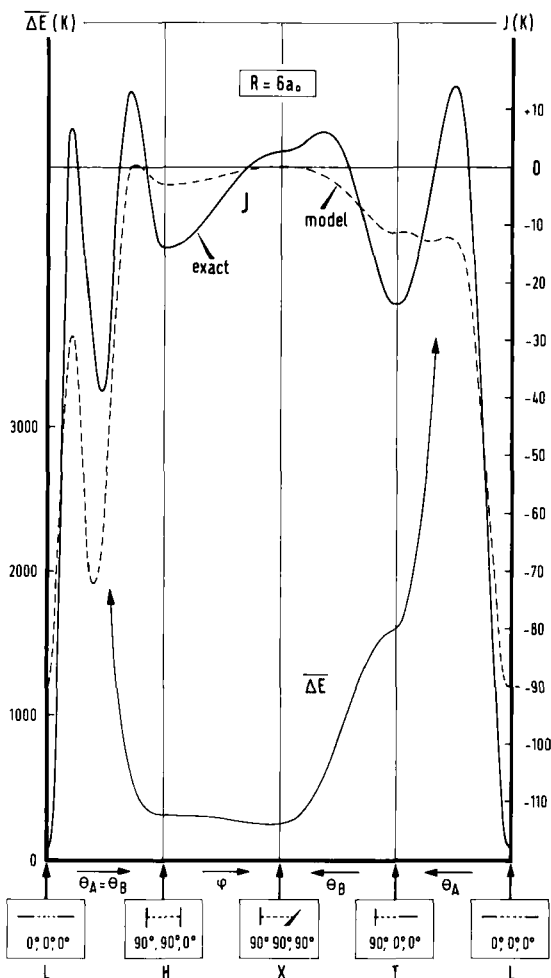


Fig. 8. Orientational dependence of the average (spin-independent) exchange interaction energy $\overline{\Delta E} = V(\omega_p, \omega_{p'}, \mathbf{r}_{pp'})$ and the Heisenberg exchange coupling constant $J(\omega_p, \omega_{p'}, \mathbf{r}_{pp'})$ in the $\text{O}_2\text{-O}_2$ dimer at $r_{pp'} = 6$ bohrs. The full lines represent the results of all-electron calculations; the dashed line refers to a four-electron model. The multipole contributions to $\overline{\Delta E}$ are now drawn explicitly because they are negligible at $r_{pp'} = 6a_0$.

Since the O_2 molecule carries a triplet spin momentum, the spin Hamiltonian (140) has to be added to the Hamiltonian (23), which contains the kinetic energies and the spin-independent part of the intermolecular $\text{O}_2\text{-O}_2$ potential, in order to obtain the crystal Hamiltonian for solid O_2 . The spin-independent $\text{O}_2\text{-O}_2$ potential can be partly extracted from the *ab initio* calculations on the $(\text{O}_2)_2$ dimer by averaging the calculated interac-

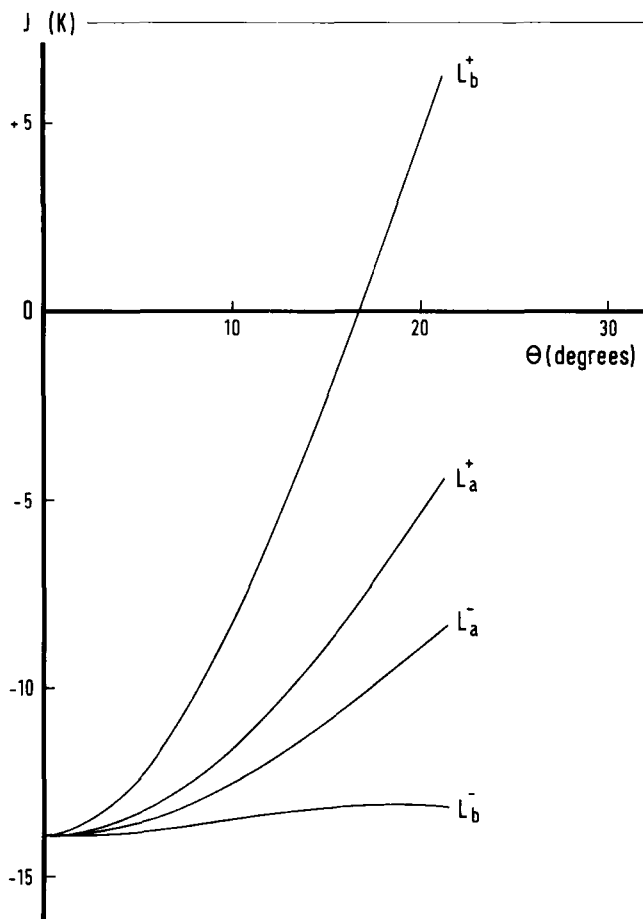


Fig. 9. Variation of the (intersublattice) exchange coupling parameter J between the nearest neighbors in solid α -O₂ along some normal coordinates of libration. The labels L_a and L_b refer to librations around the crystal **a** and **b** axes, respectively; see Fig. 7. The plus and minus signs denote in-phase and out-of-phase librations of the molecules on different sublattices.

tions over the dimer spin multiplets. The *ab initio* calculations do not yet contain the long-range dispersion attractions, however, and so the corresponding terms in the potential must still be included semiempirically. The approximate solutions for the complete crystal Hamiltonian, which describe the coupled lattice vibrations (phonons, librations, mixed modes) and spin waves (magnons), can be obtained very elegantly via the mean field and RPA methods described in Sections IV,B and IV,C. This has

actually been done by Jansen and van der Avoird (1985) for α - and β -oxygen. All they had to add to the formalism applied by Briels *et al.* (1984) to solid nitrogen, was to multiply the basis (111) by the triplet spin functions

$$\Theta_{M_S}^S(\sigma_P) \quad \text{with } S = 1 \quad \text{and } M_S = 1, 0, -1$$

to add a spin term $H_P^S(\sigma_P)$ to the mean field Hamiltonian (117) and to extend the particle label $P = \{\mathbf{n}, i, K\}$ in the RPA Hamiltonian (122) to translations, librations, and spin "motions": $K = \{T, L, S\}$. This extension leads to extra blocks in the RPA eigenvalue equations (126) that correlate the spin excitations and couple them to the phonons and librons. In principle, one can obtain mixed phonon-libron-magnon modes. Such modes are not found in solid oxygen, however. The bilinear coupling terms between the lattice modes and the single-magnon spin modes vanish from the RPA Hamiltonian (122) because of symmetry. The excitations are either pure lattice vibrations, of (mixed) phonon-libron type, or pure magnons. The effective Hamiltonian for the lattice modes is obtained from the complete Hamiltonian by spin averaging Eq. (140), i.e., replacing \mathbf{S}_P by $\langle \mathbf{S}_P \rangle$, and adding it to Eq. (23). The amplitude of the librations, 11° in α -oxygen at $T = 0$ K, appears to be substantially smaller than in solid nitrogen. This agrees with the experimental data (Cahill and Leroi, 1969). The effective spin Hamiltonian is given by Eq. (140) with the coupling constants $\langle J(\omega_P, \omega_{P'}, \mathbf{r}_{PP'}) \rangle$, $\langle A_m(\omega_P) \rangle$, and $\langle T_m(\mathbf{r}_{PP'}) \rangle$ averaged over the translations and librations. Proceeding in this way, several of the problems outlined in Section VI,A can be solved.

The problem of the splitting of the E_g libron in β -oxygen into an A_g , B_g doublet in α -oxygen appears to have the following explanation. Given the small structural distortion at the β - α phase transition, this splitting is indeed far too large to be obtained from lattice dynamics calculations employing the usual spin-independent Hamiltonian (23). The spin orderings in β and α -oxygen are very different, however, yielding a strong discontinuity of $\langle \mathbf{S}_P \rangle \cdot \langle \mathbf{S}_{P'} \rangle$ at the β - α transition. More precisely, one finds for the 120° spin arrangement in β -O₂ that $\langle \mathbf{S}_P \rangle \cdot \langle \mathbf{S}_{P'} \rangle \simeq -0.5$ and for the antiferromagnetic ordering in α -O₂ that $\langle \mathbf{S}_P \rangle \cdot \langle \mathbf{S}_{P'} \rangle \simeq -1$ for nearest neighbors. Introducing these values into the effective Hamiltonian for the lattice modes, the Heisenberg coupling parameter $J(\omega_P, \omega_{P'}, \mathbf{r}_{PP'})$ in Eq. (140) gets a very different weight in the β and α phases. We have mentioned already that this parameter is extremely anisotropic, and thus it has a strong influence on the librational motions (see Fig. 9). The A_g mode in α -O₂ indeed obtains a much higher frequency than the E_g mode in β -O₂, while the B_g mode is somewhat lowered. Using the anisotropic $J(\omega_P, \omega_{P'}, \mathbf{r}_{PP'})$ from *ab initio* calculations (Wormer and van der Avoird, 1984) gives

quantitative agreement with the experimental splitting and shifts. Omitting the Heisenberg term yields a small splitting, just as in the earlier lattice dynamics calculations. This confirms the crucial role of this term in the libron-splitting mechanism.

Jansen and van der Avoird (1985) have also made spin-wave calculations as described earlier. The RPA equations with the effective spin Hamiltonian (140), averaged over the translations and librations, could be solved analytically for any wave vector \mathbf{q} . The optical ($\mathbf{q} = 0$) magnon frequencies emerging from these calculations are 6.3 and 20.9 cm^{-1} , in reasonable agreement with the experimental values 6.4 and 27.5 cm^{-1} . This agreement is very satisfactory if we realize that the spin Hamiltonian has been obtained from first principles, with none of its parameters fitted to the magnetic data.* We conclude that the RPA model, both for the lattice modes and the spin waves, when based on a complete crystal Hamiltonian from first principles, yields a realistic description of several properties of solid O_2 that were not well understood before.

Appendix

In this article we have used some of the concepts of quantum-statistical mechanics. These concepts can, of course, be found in the textbooks (Ter Haar, 1966; Feynman, 1972; McQuarrie, 1976), but the ideas that are most relevant to this paper are summarized in this appendix. In particular, we prove the thermodynamic variation principle, which has been applied several times.

In quantum-statistical physics, just as in the classical counterpart, one introduces a density operator ρ such that the average value of any mechanical observable X can be calculated as

$$\langle X \rangle = \text{Tr}(\rho X) \quad (\text{A.1})$$

Depending on the boundary conditions imposed on the system and on the specific form of ρ , several ensembles are distinguished. Most often the system is assumed to have constant volume V and the density operator is chosen to be

$$\rho = e^{\beta(A-H)} \quad (\text{A.2})$$

* Actually, the long-range dispersion term in the spin-independent potential of Eq. (23), which affects the lattice vibrations and thus the averaged coupling parameters in Eq. (140), has been fitted to obtain the best lattice constants in $\alpha\text{-O}_2$. The magnetic data, and the libron splitting discussed, are very insensitive to this term, however.

The corresponding ensemble is therefore called canonical. The constant A is chosen such that $\text{Tr}(\rho) = 1$, from which it follows that ρ can be interpreted as defining a probability distribution over the eigenstates of the Hamiltonian H . It is easy to demonstrate that

$$A = -\beta^{-1} \ln Z \quad (\text{A.3})$$

with $Z = \text{Tr}(e^{-\beta H})$ and $\beta^{-1} = k_B T$, k_B being the Boltzmann constant. The quantity A corresponds with the Helmholtz free energy of the system.

The thermodynamic variation principle reads

$$A \leq A_0 + \langle H - H_0 \rangle_0 \quad (\text{A.4})$$

with the free energy A_0 and the average $\langle \rangle_0$ referring to an approximate Hamiltonian H_0 . The inequality holds for any H_0 . In the classical limit it is a simple consequence of Jensen's inequality known from integration theory (Rudin, 1966). In the quantum-mechanical case, its proof is more elaborate (Girardeau and Mazo, 1973; Feynman, 1972). Here we reproduce the proof of Girardeau and Mazo and define

$$Z(\lambda) = \text{Tr}(e^{X+\lambda Y}) \quad (\text{A.5})$$

We need the derivatives of this quantity with respect to λ . The derivatives of an exponential operator are given by the rule

$$\frac{d}{d\lambda} e^{H(\lambda)} = e^{H(\lambda)} \int_0^1 dx e^{-xH(\lambda)} \frac{dH(\lambda)}{d\lambda} e^{xH(\lambda)} \quad (\text{A.6})$$

This rule is proved by writing

$$\frac{d}{d\lambda} e^{yH(\lambda)} = e^{yH(\lambda)} F(y)$$

and demonstrating, via some simple differentiations, that

$$\frac{dF(y)}{dy} = e^{-yH(\lambda)} \frac{dH(\lambda)}{d\lambda} e^{yH(\lambda)}$$

Since

$$\lim_{y \rightarrow 0} F(y) = 0$$

it follows that

$$F(y) = \int_0^y dx e^{-xH(\lambda)} \frac{dH(\lambda)}{d\lambda} e^{xH(\lambda)}$$

which, for $y = 1$, proves the rule (A.6). Applying this rule, with $H(\lambda) = X + \lambda Y$, and using the invariance of the trace with respect to cyclic permutations of the operators, one finds for the derivatives of the quantity $Z(\lambda)$ defined by Eq. (A.5) that

$$Z'(\lambda) = \text{Tr}(Y e^{X+\lambda Y}) \quad (\text{A.7})$$

$$Z''(\lambda) = \text{Tr}\left(Y \frac{d}{d\lambda} e^{X+\lambda Y}\right) \quad (\text{A.8})$$

Applying the rule (A.6) to Eq. (A.8) and using the cyclic invariance of the trace again, it follows for Hermitian operators X and Y that

$$Z''(\lambda) = \int_0^1 dx \text{Tr}\{C(x)C(x)^\dagger\} \quad (\text{A.9})$$

with

$$C(x) = e^{1/2x(X+\lambda Y)} Y e^{1/2(1-x)(X+\lambda Y)}$$

Knowing the derivatives of the quantity $Z(\lambda)$, we can expand it as a Taylor series:

$$Z(\lambda) = Z(0) + \lambda Z'(0) + \frac{1}{2} \lambda^2 Z''(\lambda')$$

for some λ' lying in the interval $0 \leq \lambda' \leq \lambda$. Since the second derivative, expressed as in Eq. (A.9), must satisfy the relation

$$Z''(\lambda) \geq 0 \quad (\text{A.10})$$

we find the inequality

$$Z(1) \geq Z(0) + Z'(0) \quad (\text{A.11})$$

When choosing

$$X = -\beta H_0 - \beta \langle H - H_0 \rangle_0, \quad Y = -\beta(H - H_0) + \beta \langle H - H_0 \rangle_0$$

it can be shown, using Eq. (A.7), that $Z'(0) = 0$, and the inequality (A.11) becomes

$$\begin{aligned} \text{Tr}[\exp(-\beta H)] &= \text{Tr}[\exp(X + Y)] \geq \text{Tr}[\exp(X)] \\ &= \text{Tr}[\exp(-\beta H_0)] \exp(-\beta \langle H - H_0 \rangle_0) \end{aligned} \quad (\text{A.12})$$

Taking the logarithm of this inequality and multiplying by $-\beta^{-1}$ yields the thermodynamic variation principle, Eq. (A.4).

When the free energy A is given as a function of its characteristic variables, viz., T and V , it is possible to calculate all thermodynamic properties of the system. We list, for instance, the

$$\text{(entropy)} \quad S = - \left(\frac{\partial A}{\partial T} \right)_V$$

$$\text{(energy)} \quad E = A + TS$$

$$\text{(pressure)} \quad p = - \left(\frac{\partial A}{\partial V} \right)_T$$

$$\text{(specific heat)} \quad C_v = T \left(\frac{\partial S}{\partial T} \right)_V = -T \left(\frac{\partial^2 A}{\partial T^2} \right)_V$$

$$C_p = T \left(\frac{\partial S}{\partial T} \right)_p = C_v + \alpha_p^2 \frac{TV}{\kappa_T}$$

$$\text{(thermal expansion coefficient)} \quad \alpha_p = \frac{1}{V} \left(\frac{\partial V}{\partial T} \right)_p$$

$$\text{(compressibility)} \quad \kappa_T = - \frac{1}{V} \left(\frac{\partial V}{\partial p} \right)_T$$

For details we refer the reader to the textbooks mentioned.

ACKNOWLEDGMENT

This investigation was supported in part by the Netherlands Foundation for Chemical Research (SON) with financial aid from the Netherlands Organization for the Advancement of Pure Research (ZWO).

One of us (W.J.B.) is grateful to the Van't Hoff Laboratory for granting him the time to spend on writing this article.

REFERENCES

- Abrikosov, A. A., Gorkov, L. P., and Dzyaloshinski, I. E. (1965). "Methods of Quantum Field Theory in Statistical Physics." Dover, New York.
- Antosiewicz, H. A., (1970). In "Handbook of Mathematical Functions" (M. Abramowitz and I. A. Stegun, eds.). Dover, New York.
- van der Avoird, A., Wormer, P. E. S., Mulder, F., and Berns, R. M. (1980). *Top. Curr. Chem.* **93**, 1.
- van der Avoird, A., Briels, W. J., and Jansen, A. P. J. (1984). *J. Chem. Phys.* **81**, 3658.
- Barron, T. H. K., and Klein, M. L. (1974). In "Dynamical Properties of Solids" (G. K. Horton and A. A. Maradudin, eds.), Vol. 1. North Holland, Amsterdam, p. 391.
- Berns, R. M., and van der Avoird, A. (1980). *J. Chem. Phys.* **72**, 6107.
- Bier, K. D., and Jodl, H. J. (1984). *J. Chem. Phys.* **81**, 1192.

- Birman, J. L. (1974). In "Dynamical Properties of Solids" (G. K. Horton and A. A. Maradudin, eds.), Vol. 1. North Holland, Amsterdam, p. 83.
- Born, M., and Huang, K. (1954). "Dynamical Theory of Crystal Lattices." Clarendon, Oxford.
- Briels, W. J. (1980). *J. Chem. Phys.* **73**, 1850.
- Briels, W. J. (1983). *J. Chem. Phys.* **79**, 969.
- Briels, W. J., Jansen, A. P. J., and van der Avoird, A. (1984). *J. Chem. Phys.* **81**, 4118.
- Brink, D. M., and Satchler, G. R. (1975). "Angular Momentum." Clarendon, Oxford.
- Burakhovich, I. A., Krupskii, I. N., Prokhvatilov, A. I., Freiman, Yu. A., and Erenburg, A. I. (1977). *JETP Lett.* **25**, 32.
- Cahill, J. E., and Leroi, G. E. (1969). *J. Chem. Phys.* **51**, 97.
- Califano, S., Schettino, V., and Neto, N. (1981). "Lattice Dynamics of Molecular Crystals." Lecture Notes in Chemistry, Vol. 26. Springer, Berlin.
- Choquard, P. F. (1967). "The Anharmonic Crystal." Benjamin, New York.
- Čížek, J., and Paldus, J. (1971). *Phys. Rev.* **A3**, 525.
- Cochran, W., and Cowley, R. A. (1967). In "Encyclopedia of Physics," Vol. XXV, 2a. Springer, Berlin.
- Cromer, D. T., Mills, R. L., Schiferl, D., and Schwalbe, L. A. (1981). *Acta Crystallogr.* **B37**, 8.
- DeFotis, G. C. (1981). *Phys. Rev.* **B23**, 4714.
- Downs, J., Gubbins, K. E., Murad, S., and Gray, C. G. (1979). *Mol. Phys.* **37**, 129.
- Dunmore, P. V. (1972). *J. Chem. Phys.* **57**, 3348.
- Dunmore, P. V. (1976). *J. Low Temp. Phys.* **24**, 397.
- Dunmore, P. V. (1977). *Can. J. Phys.* **55**, 554.
- Edmonds, A. R. (1957). "Angular Momentum in Quantum Mechanics." Princeton Univ. Press, Princeton, New Jersey.
- Egelstaff, P. A., Gray, C. G., and Gubbins, K. E. (1975). In "Molecular Structure and Properties" (Physical Chemistry, Ser. 2, Vol. 2). MTP Internatl. Rev. Sci., Butterworths, London.
- English, C. A., and Venables, J. A. (1974). *Proc. R. Soc. London Ser. A* **340**, 57.
- English, C. A., Venables, J. A., and Salahud, D. R. (1974). *Proc. R. Soc. London Ser. A* **340**, 81.
- Etters, R. D., Helmy, A. A., and Kobashi, K. (1983). *Phys. Rev.* **B28**, 2166.
- Fetter, A. L., and Walecka, J. D. (1971). "Quantum Theory of Many Particles Systems." McGraw-Hill, New York.
- Feynman, R. P. (1972). "Statistical Mechanics." Benjamin, Reading, Massachusetts.
- Fondère, F., Obriot, J., Marteau, Ph., Allavena, M., and Chakroun, H. (1981). *J. Chem. Phys.* **74**, 2675.
- Fredkin, D. R., and Werthamer, N. R. (1965). *Phys. Rev.* **A138**, 1527.
- Gaididei, Yu. B., and Loktev, V. M. (1981). *Sov. J. Low Temp. Phys.* **7**, 1305.
- Gibbons, T. G., and Klein, M. L. (1974). *Chem. Phys. Lett.* **29**, 463.
- Girardeau, M. D., and Mazo, R. M. (1973). *Adv. Chem. Phys.* **24**, 187.
- Goldman, V. V., Horton, G. K., and Klein, M. L. (1968). *Phys. Rev. Lett.* **21**, 1527.
- Goldman, V. V., and Klein, M. L. (1975). *J. Chem. Phys.* **64**, 5121.
- Goodings, D. A., and Henkelman, M. (1971). *Can. J. Phys.* **49**, 2898.
- ter Haar, D. (1966). "Elements of Thermostatistics." Holt, New York.
- Hamer, C. J., and Irving, A. C. (1984). *Nucl. Phys.* **B230**(FS10), 336.
- Hansen, J. P., and McDonald, I. R. (1976). "Theory of Simple Liquids." Academic Press, New York.
- Harris, A. B., and Coll, C. F. (1972). *Solid State Commun.* **10**, 1029.

- Helmy, A. A., Kobashi, K., and Etters, R. D. (1984). *J. Chem. Phys.* **80**, 2782.
- van Hemert, M. C., Wormer, P. E. S., and van der Avoird, A. (1983). *Phys. Rev. Lett.* **51**, 1167.
- Hüller, A. (1974). *Phys. Rev.* **B10**, 4403.
- Jacobi, N., and Schnepf, O. (1972). *Chem. Phys. Lett.* **13**, 344.
- James, H. M., and Keenan, T. A. (1959). *J. Chem. Phys.* **31**, 12.
- Jansen, A. P. J., Briels, W. J., and van der Avoird, A. (1984). *J. Chem. Phys.* **81**, 3648.
- Jansen, A. P. J., and van der Avoird, A. (1985). *Phys. Rev.* **B31**, 7500.
- Jordan, T. H., Smith, H. W., Streib, W. E., and Lipscomb, W. N. (1964). *J. Chem. Phys.* **41**, 756.
- Kirkwood, J. G. (1940). *J. Chem. Phys.* **8**, 205.
- Kitaigorodsky, A. I. (1973). "Molecular Crystals and Molecules." Academic Press, New York.
- Kjems, J. K., and Dolling, G. (1975). *Phys. Rev.* **B11**, 1639.
- Klein, M. L., and Weis, J. J. (1977). *J. Chem. Phys.* **67**, 217.
- Klein, M. L., Lévesque, D., and Weis, J. J. (1981). *J. Chem. Phys.* **74**, 2566.
- Kobashi, K. (1978). *Mol. Phys.* **36**, 225.
- Kobashi, K., Klein, M. L., and Chandrasekharan, V. (1979). *J. Chem. Phys.* **71**, 843.
- Koehler, T. R. (1969). *Phys. Rev. Lett.* **22**, 777.
- van Kranendonk, J. (1983). "Solid Hydrogen." Plenum, New York.
- Kuchta, B., and Luty, T. (1983). *J. Chem. Phys.* **78**, 1447.
- Kuchta, B. (1985). *Chem. Phys.* **95**, 391.
- LeSar, R., Ekberg, S. A., Jones, L. H., Mills, R. L., Schwalbe, L. A., and Schiferl, D. (1979). *Solid State Commun.* **32**, 131.
- Luty, T., van der Avoird, A., and Berns, R. M. (1980). *J. Chem. Phys.* **73**, 5305.
- McQuarrie, D. A. (1976). "Statistical Mechanics." Harper, New York.
- Mandell, M. J. (1974). *J. Chem. Phys.* **60**, 1432.
- Mandell, M. J. (1974). *J. Chem. Phys.* **60**, 4880.
- Mandell, M. J. (1974). *J. Low Temp. Phys.* **17**, 169.
- Mandell, M. J. (1975). *J. Low Temp. Phys.* **18**, 273.
- Maradudin, A. A., Montroll, E. W., Weiss, G. H., and Ipatova, P. (1971). "Theory of Lattice Dynamics in the Harmonic Approximation." Academic Press, New York.
- Maradudin, A. A., and Vosko, S. H. (1968). *Rev. Mod. Phys.* **40**, 1.
- Maradudin, A. A. (1974). In "Dynamical Properties of Solids" (G. K. Horton and A. A. Maradudin, eds.), Vol. 1. North Holland, Amsterdam, p. 1.
- Medina, F. D., and Daniels, W. B. (1976). *J. Chem. Phys.* **64**, 150.
- Meier, R. J., Schinkel, C. J., and de Visser, A. (1982). *J. Phys.* **C15**, 1015.
- Meier, R. J., and Helmholdt, R. B. (1984). *Phys. Rev.* **B29**, 1387.
- Meier, R. J. (1984). Unpublished thesis, University of Amsterdam.
- Metropolis, M., Rosenblut, A. W., Rosenblut, M. N., Teller, A. N., and Teller, E. (1953). *J. Chem. Phys.* **21**, 1087.
- Michel, K. H., and Naudts, J. (1978). *J. Chem. Phys.* **68**, 216.
- Michel, K. H. (1984). *Z. Physik* **B54**, 129.
- Mizushima, M. (1975). "The Theory of Rotating Diatomic Molecules." Wiley, New York.
- Powell, B. M., Dolling, G., and Nieman, H. F. (1983). *J. Chem. Phys.* **79**, 982.
- Powell, J. L., and Craseman, B. (1961). "Quantum Mechanics." Addison-Wesley, Reading, Massachusetts.
- Press, W., and Hüller, A. (1978). *J. Chem. Phys.* **68**, 4465.
- de Raedt, B., Binder, K., and Michel, K. H. (1981). *J. Chem. Phys.* **75**, 2977.
- Rahman, A. (1966). *J. Chem. Phys.* **45**, 258.

- Raich, J. C., and Etters, R. D. (1968). *Phys. Rev.* **168**, 425.
- Raich, J. C. (1972). *J. Chem. Phys.* **56**, 2395.
- Raich, J. C., and Etters, R. D. (1972). *J. Low Temp. Phys.* **7**, 449.
- Raich, J. C., Gillis, N. S., and Anderson, A. B. (1974). *J. Chem. Phys.* **61**, 1399.
- Raich, J. C., Gillis, N. S., and Koehler, T. R. (1974). *J. Chem. Phys.* **61**, 1411.
- Raich, J. C., and Gillis, N. S. (1977). *J. Chem. Phys.* **66**, 846.
- Raich, J. C., Yasuda, H., and Bernstein, E. R. (1983). *J. Chem. Phys.* **78**, 6209.
- de Reggi, A. S., Canepa, P. C., and Scott, T. A. (1969). *J. Magn. Reson.* **1**, 144.
- Rowe, D. J. (1970). "Nuclear Collective Motion." Methuen, London.
- Rudin, W. (1966). "Real and Complex Analysis." McGraw-Hill, New York.
- Sack, R. A. (1964). *J. Math. Phys.* **5**, 260.
- Scott, T. A. (1976). *Phys. Rep.* **27**, 89.
- Schnepp, O., and Jacobi, N. (1972). *Adv. Chem. Phys.* **22**, 205.
- Schuch, A. F., and Mills, R. L. (1970). *J. Chem. Phys.* **52**, 6000.
- Slyusarev, V. A., Freiman, Yu. A., and Yankelevich, R. P. (1980). *Sov. J. Low Temp. Phys.* **6**, 105.
- Slyusarev, V. A., and Freiman, Yu. A., and Yankelevich, R. P. (1981). *Sov. J. Low Temp. Phys.* **7**, 265.
- Steele, W. A. (1963). *J. Chem. Phys.* **39**, 3197.
- Stephens, P. W., Birgenau, R. J., Majkrzak, C. F., and Shirane, G. (1983). *Phys. Rev.* **B28**, 452.
- Streib, W. E., Jordan, T. H., and Lipscomb, W. N. (1962). *J. Chem. Phys.* **37**, 2962.
- Thiéry, M. M., and Fabre, D. (1976). *Mol. Phys.* **32**, 257.
- Thouless, D. J. (1960). *Nucl. Phys.* **21**, 225.
- Thouless, D. J. (1961). "The Quantum Mechanics of Many-Body Systems." Academic Press, New York.
- Verlet, L. (1967). *Phys. Rev.* **159**, 98.
- Wallace, D. C. (1972). "Thermodynamics of Crystals." Wiley, New York.
- Walmsley, S. H. (1975). In "Lattice Dynamics and Intermolecular Forces" (S. Califano, ed.) (Proc. Enrico Fermi, Vol. 55). North Holland, Amsterdam.
- Wasiutynski, T. (1976). *Phys. Status Solidi* **B76**, 175.
- Weis, J. J., and Klein, M. L. (1975). *J. Chem. Phys.* **63**, 2869.
- Werthamer, N. R. (1976). In "Rare Gas Solids" (M. L. Klein and J. Venables, eds.), Vol. I. Academic Press, London.
- Wormer, P. E. S., and van der Avoird, A. (1984). *J. Chem. Phys.* **81**, 1929.
- Yasuda, H., and Yamamoto, T. (1971). *Progr. Theor. Phys.* **45**, 1458.

A Full Coupled-Cluster Singles, Doubles, and Triples Model for the Description of Electron Correlation

MARK R. HOFFMANN* and HENRY F. SCHAEFER, III

*Department of Chemistry
University of California
Berkeley, California 94720*

I. Introduction	207
II. Renormalization	211
III. Coupled-Cluster Equations	219
IV. Diagrams and Rules	223
V. Matrix Elements	234
VI. Final Equations	264
VII. Discussion and Conclusions	276
References	278

I. Introduction

The computationally viable description of electron correlation for stationary state molecular systems has been the subject of considerable research in the past two decades. A recent review¹ gives a historical perspective on the developments in the field of quantum chemistry. The predominant methods for the description of electron correlation have been configuration interactions (CI) and perturbation theory (PT); more recently, the variant of CI involving reoptimization of the molecular orbitals [i.e., multiconfiguration self-consistent field (MCSCF)] has received much attention.¹ As is reasonable to expect, neither CI nor PT is wholly satisfactory; a possible alternative is the use of cluster operators, in the electron excitations, to describe the correlation.^{2,3}

Two ongoing developments support the tenability of the coupled-cluster method, an inherently complicated procedure. The first is the increas-

* Present address: James Franck Institute, University of Chicago, Chicago, Illinois 60637.

ing understanding of the applicability of elegant methods from nuclear and particle physics to chemistry. The other development is the decreasing ratio of cost to operations per second in modern high-speed computers, especially the advent of superminicomputers.

The present work details the derivation of a full coupled-cluster model, including single, double, and triple excitation operators. Second quantization and time-independent diagrams are used to facilitate the derivation; the treatment of (diagram) degeneracy and permutational symmetry is adapted from time-dependent methods. Implicit formulas are presented in terms of products of one- and two-electron integrals, over (molecular) spin-orbitals and cluster coefficients. Final formulas are obtained that restrict random access requirements to rank 2 modified integrals and sequential access requirements to the rank 3 cluster coefficients.

The coupled-cluster method (CCM) is based on the ansatz that an exact many-particle wave function can be written as an exponential cluster operator acting on an independent-particle function,

$$|\Psi\rangle = \exp(T)|\Phi_0\rangle \quad (1)$$

where

$$|\Phi_0\rangle = \prod_{i=1}^N X_i^+ |\text{vac}\rangle \quad (2)$$

$$T = T_1 + T_2 + T_3 + \dots \quad (3)$$

and

$$T_m = \sum_{\substack{i < j < k < \dots \\ a < b < c < \dots}} t_{ijk\dots}^{abc\dots} X_a^+ X_i X_b^+ X_j X_c^+ X_k \dots \quad (4)$$

and X_i^+ (X_i) is used to denote the creation (annihilation) of an electron in spin-orbital i . The exponential cluster expansion was introduced by Ursell and Mayer in the context of statistical mechanics; Coester and Kümmerl first applied the method to problems in nuclear physics between 1958 and 1962;⁴ Cizek and Paldus were the first to use the method to address atomic and molecular problems.^{5,6} In the terminology of Löwdin, the cluster operator [cf. Eq. (3)] is the logarithm of the wave operator.⁷

With the exponential matrix defined in the usual fashion,

$$\exp(T) = 1 + T + \frac{1}{2!}T^2 + \frac{1}{3!}T^3 + \dots \quad (5)$$

the exact wave function can be written as

$$\begin{aligned}
|\Psi\rangle = & \left\{ (1) + (T_1) + \left(T_2 + \frac{1}{2!}T_1^2\right) + \left(T_3 + T_2T_1 + \frac{1}{3!}T_1^3\right) \right. \\
& + \left(T_4 + T_3T_1 + \frac{1}{2!}T_2T_1^2 + \frac{1}{2!}T_2^2 + \frac{1}{4!}T_1^4\right) \\
& + \left(T_5 + T_4T_1 + T_3T_2 + \frac{1}{2!}T_3T_1^2 + \frac{1}{2!}T_2^2T_1 + \frac{1}{3!}T_2T_1^3 + \frac{1}{5!}T_1^5\right) \\
& \left. + \dots \right\} |\Phi_0\rangle
\end{aligned} \tag{6}$$

The parentheses have been included to facilitate comparison with the method of configuration interaction. Defining C_i consecutively with the terms in parentheses, the exact wave function can be written as

$$|\Psi\rangle = \{1 + C_1 + C_2 + C_3 + C_4 + C_5 + \dots\} |\Phi_0\rangle \tag{7}$$

Variational determination of the C_i coefficients in Eq. (7) without truncation is referred to as "full CI" and is the exact wave function subject to approximations in the operator (e.g., nonrelativistic) and in the independent-particle reference (e.g., basis set limit).

Essentially all problems of chemical interest require, owing to computational constraints, limiting the level of excitation used to correlate electrons. The necessary truncation is the key distinction between the coupled-cluster method and the method of configuration interaction. In truncated CI, the coefficients in Eq. (7) are determined variationally; however, unlike full CI, unlinked terms remain (i.e., are not canceled) in the expressions determining the amplitudes and the energy.^{3,8} In contrast, any truncation of Eq. (6) leads solely to linked terms in the equations for the amplitudes and the energy, provided that the individual T_m 's are connected.^{3,8} Hence, truncated CCM is size-extensive, whereas CI is not.^{3,8,9,10} The energy of a "supermolecule," in a size-extensive method, is linear in the number of noninteracting molecules included,^{8,9}

$$E(nM) = nE(M) \tag{8}$$

Size-extensivity can be seen to be of particular importance when a consistent description is needed over a large portion of a correlated potential energy surface.

Various approximations of Eq. (6), the exact wave function in the coupled-cluster formalism, have been discussed in the chemical literature. In particular, Cizek's coupled-pair many-electron theory (CPMET),⁵ also referred to as coupled-cluster doubles (CCD) by Bartlett,⁸ has re-

ceived considerable attention.^{6,11-15} In this approach, the wave operator is approximated by

$$\exp(T) \approx \exp(T_2) \quad (9)$$

The success of this rather abrupt truncation for closed-shell molecular systems is not too surprising when one considers that the dominant terms of a perturbation expansion have been included.^{2,6,16} The next more complete approximation to attain recognition is the extended coupled-pair many-electron theory (ECPMET) of Paldus, Cizek, and Shavitt,^{6,17,18} which includes connected single and triple excitations,

$$\exp(T) \approx \exp(T_2) + T_1 + T_3 \quad (10)$$

Again the terms to be included were based on a perturbation order argument.^{6,16} The contribution of connected triples was shown numerically to be not inconsequential in applications of perturbation theory.^{19,20} More recently, Purvis and Bartlett¹⁶ reported the equations and initial implementation of a full coupled-cluster singles and doubles model (CCSD); this theory includes all terms in the first five parentheses, C_0 – C_4 , of Eq. (6) except for T_3 , T_4 , and T_1T_3 . The inclusion of disconnected terms is known to enhance the numerical stability of the coupled equations.^{21,22}

In consideration of the complementary importances of connected triples and a full treatment of disconnected terms, it seems reasonable to investigate coupled-cluster models that incorporate both features. This present work details the derivation of a computationally tractable full coupled-cluster singles, doubles, and triples model (CCSDT). Such a theory includes all terms in the six parentheses given in Eq. (6), except for T_4 , T_5 , and T_4T_1 . It should be noted that Lee, Kucharski, and Bartlett^{23,24} have presented the triples part of CCSDT in explicit spin-orbital form to augment Bartlett and Purvis's earlier CCD^{8,9} and CCSD¹⁶ papers; they have obtained computational results for partial inclusion of the connected triples operator (CCSDT-1). Also, Kümmel and Lührmann²⁵ have derived CCSDT equations and presented numerical results with some terms neglected.

It would be remiss not to mention multireference techniques for the high-level description of correlation within the coupled-cluster framework.^{2,3,26} Consider that double excitations from reference functions that are doubly excited relative to each other incorporate quadruple excitations (e.g., T_4) from a single reference. However, further discussion of MR-CCM is beyond the scope of the present article, and we refer the interested reader to Refs. 2, 3, and 26.

It is perhaps appropriate at this point to examine a few of the key words in coupled-cluster theory. Using the word *connected* may lead to

confusion since it is used in reference to component diagrams (e.g., the wave operator) and to complete or resulting diagrams. The wave operator may have connected as well as disconnected (but linked) components; however, the requirement of Cizek's connected-cluster theorem⁵ is that only connected resulting diagrams contribute to the amplitudes and the energy. A connected diagram is a diagram in which a line (solid, dashed, or squiggly) can be found between any two vertices. A set of linked diagrams includes the subset of connected diagrams together with those disconnected diagrams that would be connected if lines were drawn between the ends of line segments with only one vertex (i.e., dangling lines). Another word used in two contexts is *complete* or *full*. A complete reference is one in which all possible occupations—subject to conservation of particle number, correct description of spin statistics, and possibly spin and molecular point group symmetry restrictions—of a subset of the independent particle basis are subject to the action of the wave operator. Examples of this use of complete or full are full CI or complete active space self-consistent field (CASSCF); the space of a singles and doubles excitation CI would be considered incomplete by this definition. The other usage of *complete* or *full* is to describe the inclusion in the exponential cluster operator, or wave operator, all possible terms, connected and disconnected, subject to the restriction of connected diagrams, consistent with a given truncation of the cluster operator. This is the definition appropriate to the occurrence of *full* in the title of Purvis and Bartlett's paper.¹⁶ A subtle, but illustrative, point: CPMET is complete, but ECPMET is not. A final word to be examined that is used in two different ways is *truncated*. A cluster operator is said to be truncated when not all ranks of cluster operators up to and including T_N , where N is the total number of electrons in the system, are included. With this first usage, ECPMET and CCSDT have the same truncation, CCSD is more truncated, and CPMET is more yet. The second usage is similar but not identical to the first: a wave operator is said to be truncated when terms are neglected. Under this definition, ECPMET is quite truncated in comparison to CCSDT. We hope that this lexicographic digression will enhance the clarity of this writing.

II. Renormalization

Both the topology of resulting diagrams and the forms of the coupled-cluster equations themselves are considerably simplified by the use of operators in normal product form.^{5,12,27–29} The resulting diagrams are simplified in that certain connections, which would otherwise be legal, are eliminated, reducing the number of unique diagrams. This aspect will be

discussed in Section IV after the diagrams are introduced. The coupled-cluster equations are simplified through the elimination of reference to the uncorrelated energy; this rather direct manifestation of renormalization will be detailed in the following section on the coupled-cluster equations themselves. It is the purpose of this section then to derive, following the general procedure of Cizek and Paldus,^{5,27} the normal product form of the Hamiltonian operator, to demonstrate how this suggests a particularly appropriate renormalized vacuum, and to examine the excitation operators with respect to normal ordering. The tensorial properties of the operators are discussed, especially the connection between rank and normal product form.

Under the Born–Oppenheimer approximation, the spin-independent, nonrelativistic electronic Hamiltonian for molecular systems can be written as

$$H = Z + V \quad (11)$$

where the first-quantized forms of the operators are

$$Z = \sum_i z(i) \quad (12)$$

and

$$V = \sum_{i<j} v(i, j) \quad (13)$$

with

$$z(i) = -\frac{1}{2} \nabla_i^2 - \sum_a Q_a r_{ia}^{-1} \quad (14)$$

and

$$v(i, j) = r_{ij}^{-1} \quad (15)$$

In Eqs. (12)–(15), i and j refer to electrons and a to nuclei, r is the metric, ∇^2 is the Laplacian, and Q is the (nuclear) charge. Then the second-quantized forms of the operators are given by^{27,30–32}

$$Z = \sum_{pq} \langle p|z|q \rangle X_p^+ X_q \quad (16)$$

and

$$V = \frac{1}{2} \sum_{pqrs} \langle pq|v|rs \rangle X_p^+ X_q^+ X_s X_r \quad (17)$$

with

$$\langle p|z|q\rangle = \int \phi_p^*(1)z(1)\phi_q(1) d\tau_1 \quad (18)$$

and

$$\langle pq|v|rs\rangle = \int \phi_p^*(1)\phi_q^*(2)v(1,2)\phi_r(1)\phi_s(2) d\tau_1 d\tau_2 \quad (19)$$

where p, q, r , and s label spin-orbitals, ϕ is the spatial representation of a spin-orbital, and integrations are over the spin and spatial coordinates of the subscripted particle.

The normal product form of the Hamiltonian operator is obtained by the use of the time-independent Wick theorem^{5,27} (also known as Wick's first theorem²⁹); i.e.,

$$M_1 \dots M_{i_k} = N[M_1 \dots M_{i_k}] + \sum N[M_1 \dots M_{i_k}] \quad (20)$$

where M_i can represent either a creation or an annihilation operator and the summation extends over all possible contractions. Here $N[\dots]$ is used to designate the normal product of the enclosed operators: the product of operators in which all the creation operators appear to the left of all the annihilation operators, multiplied by $(-1)^p$, where p is the parity of the Fermi permutations. Similarly,

$$N[\dots \dots]$$

is the normal product with pairings.

Application of the time-independent Wick theorem to the rank 1 component of the Hamiltonian [cf. Eq. (16)] gives

$$Z = \sum_{pq} \langle p|z|q\rangle N[X_p^+ X_q] + \sum_{pq} \langle p|z|q\rangle N[\overline{X_p^+ X_q}] \quad (21)$$

$$Z = \sum_{pq} \langle p|z|q\rangle N[X_p^+ X_q] + \sum_{pq} \langle p|z|q\rangle h(p)\delta_{pq} \quad (22)$$

where $h(p)$ is the hole function defined by Paldus and Cizek and δ_{pq} is the Kronecker delta. We have made implicit use of the orthonormality of the spin-orbitals in obtaining Eq. (22) from Eq. (21). The convention we will abide by throughout this section is that p, q, r , and s extend over all spin-orbitals; i, j, k , and l refer to spin-orbitals occupied in $|\Phi_0\rangle$; and a, b, c , and d refer to spin-orbitals unoccupied in the reference. Then,

$$Z = \sum_{pq} \langle p|z|q \rangle N[X_p^+ X_q] + \sum_i \langle i|z|i \rangle \quad (23)$$

so

$$Z = Z_1 + Z_0 \quad (24)$$

where the subscripts refer now to the irreducible rank.

Likewise, application of the Wick theorem to the rank 2 component gives

$$V = V_2 + V_1 + V_0 \quad (25)$$

where

$$V_2 = \frac{1}{2} \sum_{pqrs} \langle pq|v|rs \rangle N[X_p^+ X_q^+ X_s X_r] \quad (26)$$

$$V_1 = \sum_{pq} \langle p|g|q \rangle N[X_p^+ X_q] \quad (27)$$

$$V_0 = \frac{1}{2} \sum_{ij} \langle ij||ij \rangle \quad (28)$$

and

$$\langle p|g|q \rangle = \sum_i \langle pi||qi \rangle \quad (29)$$

$$\langle pq||rs \rangle = \langle pq|v|rs \rangle - \langle pq|v|sr \rangle \quad (30)$$

Now, gathering terms of the same rank, we can write

$$H_0 = \sum_i \langle i|z|i \rangle + \frac{1}{2} \sum_{ij} \langle ij||ij \rangle \quad (31)$$

$$H_1 = \sum_{pq} \{ \langle p|g|q \rangle + \langle p|z|q \rangle \} N[X_p^+ X_q] \quad (32)$$

$$H_2 = \frac{1}{2} \sum_{pqrs} \langle pq|v|rs \rangle N[X_p^+ X_q^+ X_s X_r] \quad (33)$$

Defining

$$f_{pq} = \langle p|f|q \rangle = \langle p|z + g|q \rangle \quad (34)$$

Eq. (32) may be written

$$H_1 = \sum_{pq} f_{pq} N[X_p^+ X_q] \quad (35)$$

Using Eq. (30), the definition of the antisymmetrized two-electron integral, and the anticommutation relation of fermion annihilation operators, Eq. (33) may be written

$$H_2 = \frac{1}{4} \sum_{pqrs} \langle pq || rs \rangle [X_p^+ X_q^+ X_s X_r] \quad (36)$$

Hence the Hamiltonian can be decomposed in terms of irreducible tensors

$$H = H_0 + H_1 + H_2 \quad (37)$$

i.e., written in normal product form.

Careful examination of Eq. (31) reveals that H_0 is identical to the energy matrix element of the reference determinant,

$$\langle \Phi_0 | H | \Phi_0 \rangle = H_0 \quad (38)$$

as given by the Slater–Condon rules.^{30,31} Hence, we are motivated to choose the reference determinant as the renormalized, or Fermi, vacuum.

The terminology of tensor operators is used extensively in this work and warrants further comment. Let us consider the action of the operator

$$[X_r^+ X_s, \cdot] = L_r^s \quad (39)$$

on a creation operator

$$[X_r^+ X_s, X_u^+] = (X_r^+ X_s X_u^+ - X_u^+ X_r^+ X_s) \quad (40)$$

$$= X_r^+ (X_s X_u^+ + X_u^+ X_s) \quad (41)$$

$$= X_r^+ \delta_{su} \quad (42)$$

where use has been made of the fermion anticommutation relations,

$$[X_p^+, X_q^+]_+ = [X_p, X_q]_+ = 0 \quad (43)$$

$$[X_p^+, X_q]_+ = \delta_{pq} \quad (44)$$

The operator L_r^s acting on the vector field of the creation operators satisfies the transformation law for covariant vectors (e.g., tensor rank 1).³³ The form of the transformation operator is reasonable in light of the following two observations, although it is to be emphasized that the legitimacy of referring to the creation operators as covariant vectors resides in Eq. (42). As Moshinsky noted, annihilation operators can be thought of as

differentiation operators with respect to creation operators;³⁴ then similarly,

$$X_r^+ \sim \frac{\partial}{\partial X_r} \quad (45)$$

Secondly, the commutator is the Lie product³³ of the operators $X_r^+ X_s$ and X_u^+ ; this choice of "multiplication" is particularly appropriate when one realizes that the $X_r^+ X_s$ are the generators of the semisimple compact Lie group U_n , which is associated with the infinitesimal unitary transformations of the Euclidean vector space R_n (e.g., the space of the creation operators).³⁴ With the preceding comments, the action of the transformation operator on the creation operators can formally be written in the usual form of the transformation law for covariant vectors,³³

$$X_r^+ = \sum_s \left(\frac{\partial X_s^+}{\partial X_r} \right) X_s \quad (46)$$

where the indices on the annihilation operators have been written as superscripts in anticipation of the results of the following paragraph.

Next consider the action of the same operator L_r^s on the annihilation operator

$$[X_r^+ X_s, X_u] = X_r^+ X_s X_u - X_u X_r^+ X_s \quad (47)$$

$$= -(X_r^+ X_u + X_u X_r^+) X_s \quad (48)$$

$$= -\delta_{ru} X_s \quad (49)$$

Whence, the operator $-L_r^s$ acting on the vector field of the annihilation operators satisfies the transformation law for contravariant vectors.³³ Making the analogous observations as before now for the annihilation operators, the action of the transformation operator on the annihilation operators can formally be written in the usual form of the transformation law for contravariant vectors,³³

$$X^r = \sum_s \left(\frac{\partial X_r^+}{\partial X_s^+} \right) X^s \quad (50)$$

The index on the annihilation operator will usually continue to be written in the conventional subscript position, except when added emphasis of the contravariant transformation property is deemed useful; in either case the same operator is intended.

A useful test on the consistency of the definition of the transformation operator for creation operators and for annihilation operators is provided

by considering the action of L_r^s on a rank 1 (in both covariant and contravariant indices) operator

$$[X_r^+ X_s, X_u^+ X_v] = X_r^+ X_s X_u^+ X_v - X_u^+ X_v X_r^+ X_s \quad (51)$$

$$= \delta_{su} X_r^+ X_v - \delta_{vr} X_u^+ X_s \quad (52)$$

For spin-orbitals, the creation and annihilation operator pair is a generator of the unitary group, and so Eq. (52) can be written

$$[e_{rs}, e_{uv}] = \delta_{su} e_{rv} - \delta_{vr} e_{us} \quad (53)$$

and Eq. (53) is the correct equation defining the structure constants of the Lie algebra.^{33,34}

Having established that creation and annihilation operators are rank 1 covariant and contravariant tensors, respectively, with respect to the operator $(\pm)L_r^s$, we can define an n th-rank boson operator as consisting of a like number of fermion creation and annihilation operators. Then the normal product of an n th-rank boson operator is a natural definition for the irreducible tensor.

Tensors, from the same or different fields, can be combined by outer multiplication, denoted by juxtaposing indices with order preserved on the resultant tensor.³³ It is possible that an index is present both in the covariant and contravariant index sets; then with the repeated index summation convention, both are eliminated and a tensor of lower rank results. The elimination of pairs of indices is known as contraction, and outer multiplication followed by contraction is inner multiplication.³³ In multiplication between tensors, contractions cannot take place entirely within one normal product (i.e., the generalized time-independent Wick theorem; see Section IV); hence such tensors are called irreducible.

Thus far we have only considered one (boson) vector field, namely, the direct product field $R_{n \times n}$ of creation and annihilation operators. The coefficients of the creation and annihilation operator pairs in fact also constitute vector fields; this can be shown rigorously by construction, but the result can also be inferred. Consider that the Hamiltonian and the cluster operators are index free or scalar operators; then the excitation operators, which form part of the said operators, must be contracted, in the sense of tensors, by the coefficients. But then we have the result that the coefficients themselves behave like tensors. This conclusion is not of immediate use, but will be important in the manipulation of the final equations (i.e., after the diagrams have contracted the excitation operators). Also, the sense of the words *rank* and *irreducible rank* as they have been used to describe components of the Hamiltonian is now clear: they refer to the excitation operator (or, equivalently, the coefficient) part of the operator.

Finally, it should be stressed that the position of an index in a sequence is significant, since all operators (and coefficients) will eventually be written in antisymmetrized form. We can shed some light on the sign change for the transformation operator for covariant and contravariant tensors by examining the following equations:

$$L_r^s X_u^+ = (LX)_{r^s u} = \delta_{su} X_r^+ \quad (54)$$

but

$$L_r^s X^u = (LX)^{su} = \delta_{ru} X^s \quad (55)$$

In words, the transformation operator transforms a covariant vector into a covariant vector [cf. Eq. (54)], but the transformation operator transforms a contravariant vector into a contravariant rank 1 tensor that is not a traditional vector. Since L_r^s is antisymmetric, the rank 1 contravariant tensor in Eq. (55) can be converted into a vector by interchanging indices, which results in a minus sign. However, in cases in which there is no ambiguity, the covariant and contravariant indices will be collimated to make the notation more compact.

Questions concerning possible modifications to the descriptions of excited determinants and cluster operators T_m due to the renormalization and/or the use of normal product operators must be addressed. Excited determinants with respect to the Fermi vacuum can be written straightforwardly using creation and annihilation operators; a singly excited determinant is given by

$$|i^a\rangle = X_a^+ X_i |\Phi_0\rangle \quad (56)$$

a doubly excited determinant by,

$$|ij^{ab}\rangle = X_a^+ X_i X_b^+ X_j |\Phi_0\rangle \quad (57)$$

and a triply excited determinant by

$$|ijk^{abc}\rangle = X_a^+ X_i X_b^+ X_j X_c^+ X_k |\Phi_0\rangle \quad (58)$$

The cluster operators [cf. Eq. (4)], like the Hamiltonian operator, are independent of the choice of vacuum level.

Application of the time-independent Wick theorem to the single-excitation operator $X_a^+ X_i$, present in both the description of singly excited determinants with respect to the Fermi vacuum and in the cluster operator T_1 , gives

$$X_a^+ X_i = N[X_a^+ X_i] + N[\overline{X_a^+ X_i}] \quad (59)$$

$$X_a^+ X_i = N[X_a^+ X_i] + h(a)\delta_{ai} \quad (60)$$

so

$$X_a^+ X_i = N[X_a^+ X_i] \quad (61)$$

since a and i are members of disjoint sets, i.e., $i \in \{FS\}$, $a \notin \{FS\}$. Similarly for the double-excitation operator,

$$\begin{aligned} X_a^+ X_i X_b^+ X_j &= N[X_a^+ X_i X_b^+ X_j] + N[\overbrace{X_a^+ X_i X_b^+ X_j}^{(a,b)}] + N[\overbrace{X_a^+ X_i X_b^+ X_j}^{(a,i)}] + N[\overbrace{X_a^+ X_i X_b^+ X_j}^{(a,j)}] \\ &\quad + N[\overbrace{X_a^+ X_i X_b^+ X_j}^{(i,b)}] + N[\overbrace{X_a^+ X_i X_b^+ X_j}^{(i,j)}] + N[\overbrace{X_a^+ X_i X_b^+ X_j}^{(b,j)}] \\ &\quad + N[\overbrace{X_a^+ X_i X_b^+ X_j}^{(a,b,i)}] + N[\overbrace{X_a^+ X_i X_b^+ X_j}^{(a,b,j)}] + N[\overbrace{X_a^+ X_i X_b^+ X_j}^{(a,i,j)}] \end{aligned} \quad (62)$$

Contractions between the creation operators or the annihilation operators vanish identically because of the Fermi–Dirac statistics obeyed by electrons [cf. Eq. (43)]; and as in the single-excitation operator case, contractions between creation and annihilation operators are zero, because the indices belong to disjoint sets [cf. Eq. (44)]. Hence, Eq. (62) becomes

$$X_a^+ X_i X_b^+ X_j = N[X_a^+ X_i X_b^+ X_j] \quad (63)$$

Further use of the anticommutation relation of fermions for orthonormal orbitals gives

$$X_a^+ X_i X_b^+ X_j = N[X_a^+ (-X_b^+ X_i) X_j] \quad (64)$$

$$= -N[X_a^+ X_i X_b^+ X_j] \quad (65)$$

and the Kronecker delta vanishes identically because the field operators are known to be uncontracted. Finally,

$$X_a^+ X_i X_b^+ X_j = N[X_a^+ X_b^+ X_j X_i] \quad (66)$$

and we are led to the interesting conclusion that the double-excitation operator, like the single-excitation operator, is implicitly in normal product form. The same conclusion holds for the triple-excitation operator, with

$$X_a^+ X_i X_b^+ X_j X_c^+ X_k = N[X_a^+ X_b^+ X_c^+ X_k X_j X_i] \quad (67)$$

III. Coupled-Cluster Equations

The truncated many-particle wave function in the coupled-cluster method is required to satisfy the Schrödinger equation

$$H|\Psi\rangle = E|\Psi\rangle \quad (68)$$

i.e.,

$$H \exp(T)|\Phi_0\rangle = E \exp(T)|\Phi_0\rangle \quad (69)$$

The reference energy can be removed^{5,27} from the Schrödinger equation by defining

$$\Delta E = E - \langle \Phi_0 | H | \Phi_0 \rangle \quad (70)$$

then, since H_1 and H_2 are normal product operators of greater than zero rank,

$$E = \Delta E + \langle \Phi_0 | H_0 | \Phi_0 \rangle \quad (71)$$

Recalling that H_0 is a scalar,

$$\langle \Phi_0 | H_0 | \Phi_0 \rangle = H_0 \langle \Phi_0 | \Phi_0 \rangle \quad (72)$$

so, with a normalized reference,

$$E = \Delta E + H_0 \quad (73)$$

and the Schrödinger equation can be written

$$H_N \exp(T)|\Phi_0\rangle = \Delta E \exp(T)|\Phi_0\rangle \quad (74)$$

where $H_N = H_1 + H_2$.

Multiplying Eq. (74) through from the left by $\exp(-T)$, we obtain

$$\exp(-T)H_N \exp(T)|\Phi_0\rangle = \Delta E|\Phi_0\rangle \quad (75)$$

The connected cluster theorem of Cizek⁵ states that

$$\exp(-T)A \exp(T) = \{A \exp(T)\}_C \quad (76)$$

where A is any operator of the same number of creation and annihilation operators in normal product form and the subscript C means that only connected diagrams are to be included.¹⁷ Then the Schrödinger equation, with no further approximation beyond the exponential ansatz, may be written

$$\{H_N \exp(T)\}_C |\Phi_0\rangle = \Delta E |\Phi_0\rangle \quad (77)$$

Projection of Eq. (77) onto the set of α -excited determinants ($\alpha = 1, 2, 3$) yields a set of coupled equations in the cluster coefficients:

$$\langle \alpha | \{H_N \exp(T)\}_C | \Phi_0 \rangle = \Delta E \langle \alpha | \Phi_0 \rangle = 0 \quad (78)$$

Also, projection onto the reference determinant allows ΔE , and hence the correlated energy, to be calculated once the cluster coefficients are known:

$$\langle \Phi_0 | \{H_N \exp(T)\}_C | \Phi_0 \rangle = \Delta E \langle \Phi_0 | \Phi_0 \rangle = \Delta E \quad (79)$$

It is clear that the necessary and sufficient number of equations in the coupled set [Eq. (78)] is equal to the number of unique cluster coefficients, provided that a solution exists. Since the coupled-cluster equations are non-Hermitian and nonlinear, the existence of solutions and the reality of eigenvalues corresponding to solutions are not guaranteed. However, Zivkovic and Monkhorst^{35,36} have recently shown, using analytic continuations of solutions to the CI problem, that for physically reasonable cases both the existence of solutions and the reality of eigenvalues are assured.

The specific equations used to determine the cluster coefficients in the CCSDT model will now be given. Projection of the Schrödinger equation [cf. Eq. (77)] onto the singly excited space gives

$$\langle \beta_u | \left\{ H_N \left(1 + T_1 + T_2 + \frac{1}{2} T_1^2 + T_3 + T_2 T_1 + \frac{1}{3!} T_1^3 \right) \right\} c | \Phi_0 \rangle = 0 \quad (80)$$

$\forall u \in \{FS\}, \forall \beta \notin \{FS\}$; projection onto the doubly excited space gives

$$\begin{aligned} \langle \beta\gamma_{uv} | \left\{ H_N \left(1 + T_1 + T_2 + \frac{1}{2} T_1^2 + T_3 + T_2 T_1 + \frac{1}{3!} T_1^3 \right. \right. \\ \left. \left. + T_3 T_1 + \frac{1}{2} T_2^2 + \frac{1}{2} T_2 T_1^2 + \frac{1}{4!} T_1^4 \right) \right\} c | \Phi_0 \rangle = 0 \end{aligned} \quad (81)$$

$\forall u < v, u, v \in \{FS\}, \forall \beta < \gamma, \beta, \gamma \notin \{FS\}$; and projection onto the triply excited space gives

$$\begin{aligned} \langle \beta\gamma\epsilon_{uvw} | \left\{ H_N \left(T_1 + T_2 + \frac{1}{2} T_1^2 + T_3 + T_2 T_1 + \frac{1}{3!} T_1^3 \right. \right. \\ \left. \left. + T_3 T_1 + \frac{1}{2} T_2^2 + \frac{1}{2} T_2 T_1^2 + \frac{1}{4!} T_1^4 \right. \right. \\ \left. \left. + T_3 T_2 + \frac{1}{2} T_3 T_1^2 + \frac{1}{2} T_2^2 T_1 + \frac{1}{3!} T_2 T_1^3 + \frac{1}{5!} T_1^5 \right) \right\} c | \Phi_0 \rangle = 0 \end{aligned} \quad (82)$$

$\forall u < v < w, u, v, w \in \{FS\}, \forall \beta < \gamma < \epsilon, \beta, \gamma, \epsilon \notin \{FS\}$. The correlated energy can similarly be written as

$$\langle \Phi_0 | \left\{ H_N \left(1 + T_1 + T_2 + \frac{1}{2} T_1^2 \right) \right\} c | \Phi_0 \rangle = \Delta E \quad (83)$$

It should be emphasized that the absence of terms in the wave operators in the preceding equations does not reflect further truncation [e.g., with respect to $\exp(T_1 + T_2 + T_3)$]; rather it is a consequence of the triangle inequalities involving the (irreducible) ranks of the Hamiltonian, the external space operators, and the cluster operators. More specifically, a matrix element vanishes identically unless it has an overall rank of 0; from

elementary vector analysis, this can only occur if the component contributions obey a triangle inequality,

$$|r(H_N) - \sum_i m_i| \leq \alpha \leq r(H_N) + \sum_i m_i \quad (84)$$

where the m_i refer to the ranks of the individual T_m operators in a term and α is the rank of the external space operator. The generalized time-independent Wick theorem, which will be discussed in the following section, justifies the strict addition of the m_i 's in Eq. (84). Equations (80)–(83) reflect the triangle inequality for $\max r(H_N) = r(H_N) = 2$; of course, the potent range of the wave operator is even smaller for matrix elements involving H_1 .

As shown by Paldus *et al.*,⁶ antisymmetrized (e.g., degenerate) T matrix elements

$$\begin{aligned} t_{uvw\dots}^{\beta\gamma\varepsilon\dots} &= \langle \beta\gamma\varepsilon\dots | T | uvw\dots \rangle_A \\ &= \langle \beta\gamma\varepsilon\dots | T | P(u|v|w|\dots) uvw\dots \rangle \end{aligned} \quad (85)$$

are the most appropriate for use in the coupled-cluster equations. The permutation operator used in Eq. (85) is our adaptation of the (symmetric) permutation operator of Bogoliubov and Shirkov²⁹ used in the formal power series expansion of the scattering matrix and will be discussed in greater detail in the following section. The permutation operator, as used in Eq. (85), represents the signed summation over all possible permutations of hole indices. With the T matrix elements as defined in Eq. (85), the following specific relations hold:

$$t_{uv}^{\beta\gamma} = -t_{vu}^{\beta\gamma} = -t_{uv}^{\gamma\beta} = t_{vu}^{\gamma\beta} \quad (86)$$

and

$$t_{uvw}^{\beta\gamma\varepsilon} = -t_{vuw}^{\beta\gamma\varepsilon} = t_{uvw}^{\beta\gamma\varepsilon} = -t_{wvu}^{\beta\gamma\varepsilon} = t_{wvu}^{\beta\gamma\varepsilon} = -t_{uwv}^{\beta\gamma\varepsilon} = -t_{uwv}^{\gamma\beta\varepsilon}, \text{ etc.} \quad (87)$$

We have implicitly used the permutational symmetry of the T matrix elements in writing Eqs. (4), (81), and (82). In particular, the restrictions on the external indices are a direct consequence of there being only one unique T matrix element for a given set of indices.

Perhaps it is appropriate in closing this section on the coupled-cluster equations to comment on the relation between perturbation theory and the coupled-cluster method. The iterative scheme used to solve the coupled-cluster equations can be seen as a method to simultaneously generate and evaluate diagrams of arbitrarily high order in perturbation theory.¹² Of course, diagrams corresponding to high-order connected terms (e.g., T_4 in CCSDT) will not be so generated.¹² It is this property, generat-

ing arbitrarily high-order diagrams, that makes the coupled-cluster method, in principle, less subject to the issue of the "smallness" of the perturbation than perturbation theory. If one wished to speculate, it is reasonable to suppose that the coupled-cluster method will prove superior to perturbation theory especially in the calculation of excited electronic states.

IV. Diagrams and Rules

As was first realized by Feynman, field operators and their interactions can be represented graphically by lines and points, respectively. The evaluation of matrix elements proceeds in two steps: all topologically distinct diagrams capable of being formed from the given component diagrams are assembled and then the resulting diagrams are converted back to algebraic expressions using relatively straightforward rules.

The original rules and diagrams, as formulated by Feynman for quantum electrodynamics (QED), are unnecessarily general for our intended application. Rather, the time-independent formulations of Hugenholtz³⁷ and Brandow,³⁸ developed primarily for use in perturbation treatments of problems in nuclear physics, are more suitable for our needs. Cizek and Paldus^{5,6,12,27} were the first to apply the time-independent diagrammatic approach to atomic and molecular problems, and it is their notation that we will conform to most often. A key feature of our implementation of the diagrammatic technique is the use of formal concepts used in the functional expansion of the scattering matrix in quantum electrodynamics, in a time-independent approach.

A formal similarity arises because both the scattering matrix in quantum electrodynamics and the wave operator in a full coupled-cluster method [cf. Equations (1) and (4)] are exponential operators. In Bogoliubov's axiomatic formulation of the scattering matrix,²⁹

$$|\Phi(\infty)\rangle = S(g)|\Phi(-\infty)\rangle \quad (88)$$

with

$$S(g) = 1 + \sum_{n \geq 1} \frac{1}{n!} \int S_n(x_1, \dots, x_n) g(x_1) \dots g(x_n) dx_1 \dots dx_n \quad (89)$$

where the x_i are coordinates of space-time and the $g(x_i)$ are functions describing the intensity of switching on the interaction. The two specific features that we adapt from Bogoliubov and Shirkov's²⁹ formulation of Feynman's rules for use in the time-independent approach involve the use of formal permutation operators and the analysis of the symmetry factor.

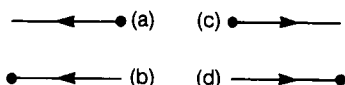


Fig. 1. Parts of diagrams representing (a) the creation of an electron, (b) the annihilation of an electron, (c) the annihilation of a hole, and (d) the creation of a hole.

We turn now to the description of the requisite component diagrams for a CCSDT theory. The basic interaction in our application of spinor electrodynamics is the absorption of an electron (or hole) and the emission of an electron (or hole), together with the absorption or emission of a photon. Solid lines will be used to represent operators of the Dirac field; since both positive and negative energy single-particle states are admissible,^{29,32,40} the diagrammatic representation of the spinors must be directed. A left-pointed arrow will designate an electron, and a right-pointed will then denote a hole. A solid dot will be used to designate an interaction; spinor lines emerging from the dot will then correspond to electron creation operators, and spinor lines converging upon the dot will represent electron annihilation operators. The four possible relations of one spinor line and an interaction dot are shown in Fig. 1. It is clear then that under the constraint of requiring one incoming line and one outgoing line that there are four versions of the basic interaction, denoted pp, ph, hp, and hh.

Different types of diagrams are used to represent nondegenerate and degenerate (i.e., antisymmetrized) operators. The time-independent nondegenerate diagrams in common usage were first suggested by Goldstone.¹⁰ In Goldstone diagrams, operators of the electromagnetic field (e.g., photons) are represented by dashed lines; the background, or averaged, electromagnetic field of the other electrons and the nuclei is represented by a small triangle. The Goldstone diagram for the hh version of an H_1 operator (i.e., an F vertex) is given in Fig. 2a. Hugenholtz³⁷ was the first to suggest the use of time-independent degenerate diagrams. Since all of the operators required in the CCSDT model are, or can be made, degenerate (cf. Sections II and III), and there are most certainly fewer

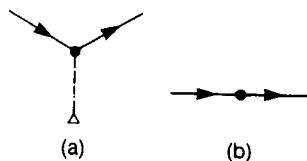


Fig. 2. (a) Goldstone and (b) degenerate diagrams for the hh version of an F vertex.

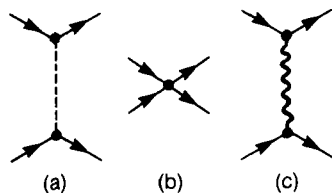


Fig. 3. (a) Goldstone, (b) Hugenholtz, and (c) Brandow diagrams for hh-hh V vertices.

degenerate than nondegenerate resulting diagrams, we will use degenerate diagrams. A potential difficulty in using degenerate diagrams is some ambiguity of absolute phase; Brandow³⁸ proposed a solution to this problem in the context of MBPT by combining the Goldstone and Hugenholtz forms. Bartlett and Silver³⁹ and Paldus¹² were the first to deduce the equivalent changes for coupled-cluster theory. These hybrid diagrams may be referred to either as antisymmetrized CC diagrams³⁹ or as Brandow diagrams,¹² where it is assumed that the extension to coupled cluster has been made. Figure 3 shows the different topological representations of an hh-hh version H_2 operator (V vertex).

Symbols for nondegenerate T operators are not needed, and no further discussion is afforded them. Antisymmetrized T operators, for (irreducible) ranks 1, 2, and 3, are shown in Fig. 4.

As usual in degenerate time-independent diagrammatic methods,^{5,12,27,37,38} excited determinants are represented by external space operators rather than by pair creation-annihilation operators. Diagrammatically, an external line is a ray, whereas an internal line is a line segment. The four possible types of rays and line segments that arise in a CCSDT method are shown in Fig. 5. The indexing convention we will use for the rest of the chapter is that u , v , and w will denote external holes; i and j internal holes; β , γ , and ε external particles (i.e., electrons); and a and b internal particles.

The component diagrams necessary for a CCSDT model have now

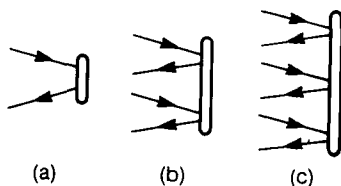


Fig. 4. Diagrams for (a) single, (b) double, and (c) triple antisymmetrized cluster operators.

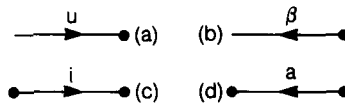


Fig. 5. (a) External hole line, (b) external particle line, (c) internal hole line, and (d) internal particle line.

been introduced and briefly described. We continue with a short exposition on the rules for the construction and subsequent evaluation of the resulting, or final, diagrams.

RULE 1. Juxtapose antisymmetrized versions of all component diagrams, representing operators of the matrix element in question, to form all possible time-ordered, topologically distinct, nonvanishing, connected, canonical resulting diagrams.

The relative positions of the component diagrams can be established by considering the time order of the operators that they represent. Hugenholtz³⁷ and Brandow³⁸ have shown the correspondence of the order of appearance, read right to left, of operators in perturbation theory matrix elements and their time order. Cizek and Paldus^{5,27} have extended this idea to truncated versions of coupled-cluster theory. The questions that remain in our minds are whether all T operators are always “simultaneous” and whether the Hamiltonian vertex is always at a “later” time. Rather direct answers to these questions are obtained by considering the relation between commutation and time ordering, as discussed in Bogoliubov and Shirkov’s text.²⁹ In particular, local Bose operators (i.e., field operators having the same number of fermion creation and annihilation operators) that commute have a spacelike relation (e.g., they are simultaneous); conversely, local Bose operators that do not commute are separated in time. It is not difficult to verify that

$$[T_m, T_n] = 0, \quad 1 \leq m, n \leq 3 \quad (90)$$

and

$$[T_m, H] \neq 0, \quad 1 \leq m \leq 3 \quad (91)$$

So the cluster operators are seen to have a spacelike relation with each other and a timelike relation with the Hamiltonian. Then, in keeping with the choice of directions for the Dirac spinors shown in Fig. 1, the topological arrangement of component diagrams is a column of cluster operators to the far right, followed by a Hamiltonian diagram to the left, followed by the external space operators on the extreme left. In agreement with the



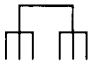
Fig. 6. Vanishing contractions of Dirac spinor lines.

convention of Hugenholtz³⁷ (and Cizek and Paldus^{5,27}), “time flows from right to left” in our diagrams.

Component diagrams are assembled into resulting diagrams by attaching the free ends of spinor lines. A resulting diagram with the property that a continuous line exists between each pair of interaction vertices is said to be connected. (N.B.: The aforementioned line may consist of a set of Dirac spinor line segments, electromagnetic line segments, or a combination of the two.)

A large number of connected, time-ordered resulting diagrams can be eliminated from further consideration by recognizing that two of four possible types of contractions of Dirac spinor lines are vanishing.²⁷ The values of the two potentially nonzero joinings are given by Kronecker delta functions (i.e., for orthonormal orbitals).²⁷ Additionally, consideration of connections between different T operators (cf. Fig. 8d later) can now be categorically eliminated. Of the four possible single connections between different T operators, two are identically zero “because the arrows don’t match up” (cf. Fig. 6). The other two possibilities, representing an annihilation operator of one T operator being contracted with a creation operator of the other T operator, give Kronecker delta contributions to the matrix element (cf. Fig. 7). However, the last two possibilities are also zero in this case, because the particle and hole index sets are disjoint. Hence, no diagrams containing connections between different T operators need be considered.

The topology of contractions is determined by the generalized time-independent Wick theorem^{27,29} and the fact that matrix elements of uncontracted operators are identically zero.²⁷ The generalized time-independent Wick theorem can be written in the form

$$M_1 \dots M_{i_1} N[M_{i_1+1} \dots M_{i_2}] M_{i_2+1} \dots M_{i_3} N[M_{i_3+1} \dots M_{i_4}] \dots M_{i_k} \\ = N[M_1 \dots M_{i_k}] + \sum' N[M_1 \dots \dots M_{i_k}] \quad (92)$$


where M_i can represent either a creation or an annihilation operator and the prime indicates that contractions between operators originating in the



Fig. 7. Possibly nonvanishing contractions of Dirac spinor lines.

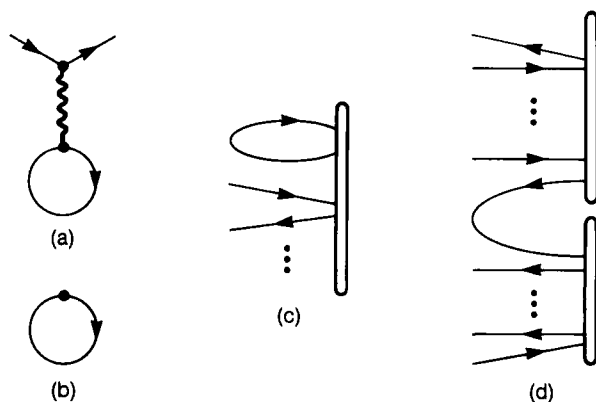


Fig. 8. (a) $V-V$, (b) $F-F$, (c) $T-T$, and (d) $T-T'$ diagrams.

same normal product are to be neglected. Since F , V , and T vertices represent normal product operators [cf. Eqs. (35), (36), (61), (66), and (67)], it is clear that the diagrams shown in Fig. 8a-c do not occur in the coupled-cluster method.

A canonical diagram is a resulting, or final, diagram in which the external line labels conform to a specific pattern or ordering.¹² The pattern that will be designated canonical in our diagrams has both the electron (β , γ , ϵ) and hole (u , v , w) indices progressing from top to bottom. Note that the position of an electron index relative to a hole index is in no way specified in a canonical diagram. A consequence of considering only canonical diagrams is that external lines from a common set (i.e., electron or hole) may not cross. Canonical diagrams with crossed lines from a common set are in fact topologically equivalent to a related noncanonical diagram. The noncanonical, but otherwise valid, diagrams related to a given canonical diagram by the interchange of external line indices can be generated by the action of the permutation operator on the canonical diagram and hence will be considered at a later stage.

The final requirement for an otherwise valid resulting diagram is that it be topologically distinct from all permutations (including the identity) of all previous resulting canonical diagrams. Two diagrams are topologically distinct if there does not exist any continuous transformation (e.g., stretching, bending) converting one into the other. Heuristically, one needs to "cut and paste" in order to convert one topologically distinct diagram into another.

RULE 2. Determine the algebraic expression, up to phase and degeneracy, corresponding to each resulting canonical diagram using the fol-

lowing rules: (a) Assign f_{pq} , $\langle pq||rs \rangle$, and $t_{pq}^{rs\dots}$ to each F , V , and T vertex, respectively, consistent with extant line indexing; (b) sum over each internal line.

Note that p exits an F vertex (i.e., p represents electron creation or hole annihilation), and q enters an F vertex (i.e., q represents electron annihilation or hole creation). Also, p and q exit V vertices, and r and s enter; but p and q enter T vertices, while r and s exit. Since V and T vertices are degenerate, the assignment of values to these vertices is determined only up to phase [cf. Eqs. (85)–(87)]. It will expedite the establishment of the overall phase factor of the matrix element (cf. Rule 3 later) if antisymmetrized component matrix elements with the same ordering of indices as the corresponding direct matrix elements are used. Hence, p and r , q and s , etc., are associated or considered participants in the same basic interaction.

The sum over internal lines is unrestricted; so (linked) exclusion principle violating (e-v³⁸ or EPV²⁷) terms are included in the sums. Note that either restricting sums to eliminate both unlinked and linked EPV diagrams or unrestricting summations and doing a simple cancellation of unlinked terms satisfies the Pauli exclusion principle.²⁷

RULE 3. Determine the prefactor for each resulting diagram by multiplying the phase factor and the weight of the diagram:

$$\phi = \eta w \quad (93)$$

The overall phase can be established by considering any one of the mixed Goldstone–Brandow diagrams included in a given resulting diagram. It is simplest to work with the direct mixed Goldstone–Brandow diagram, since that diagram looks like the corresponding Brandow diagram except that the degenerate V vertex is replaced by a nondegenerate V vertex, but with index labels intact. The phase, or sign, factor of the degenerate diagram is then equal to the phase factor of the nondegenerate diagram; i.e.,^{12,27,29,38}

$$\eta = (-1)^{l+h+p} \quad (94)$$

where l is the number of closed loops, h is the number of internal hole lines, and p is the parity of the permutation yielding the canonical labeling of external lines.¹² Of course, $p = 0$ for all canonical diagrams, but this contribution to the phase must be considered in the permutation operators used to generate the noncanonical diagrams related to a given canonical resulting diagram (cf. Rule 4 later).

The symmetry factor, and hence the weight, is determined by an adaptation of Bogoliubov and Shirkov's²⁹ prescription for obtaining the sym-

metry factor in (time-dependent) quantum electrodynamics. The three contributions to the symmetry factor are the following.

1. The $n_i \dots n_j$ th term of the expansion of the wave operator contains the factor $(n_i!)^{-1} \dots (n_j!)^{-1}$. This is always compensated by the factor $(n_i!) \dots (n_j!)$, which takes into account permutation of the vertices.

2. The rank 2 Hamiltonian contains two identical creation operators and two identical annihilation operators, which introduces the factor $(2!)(2!) = 4$. This compensates the numerical factor $\frac{1}{4}$ associated with a V vertex.

3. In case there exist c topologically equivalent variants of pairings of internal lines, they must be taken into account only once. This corresponds to the introduction of the factor $(c!)^{-1}$.

For Hamiltonians with no greater than rank 2 components, the third rule simplifies to the following.

1. Unless altered by the following rules, $c_p = c_h = c_{ph} = 1$.
2. If two hole lines begin at the same vertex and end at the same vertex, $c_h = 2$.
3. If two particle lines begin at the same vertex and end at the same vertex, $c_p = 2$.
4. If simultaneous interchange of the particle lines and the hole lines yields a topologically equivalent diagram and the hole and particle lines are not independently interchangeable, $c_{ph} = 2$.
5. The weight of the diagram is given by

$$w = \frac{1}{c_p c_h c_{ph}} \quad (95)$$

There are two points we would like to emphasize at this time. The first is that the weight factor detailed in the preceding is in accord with the usual " $\frac{1}{4}$ rule" for weights in perturbation theory^{27,37,38} and truncated coupled-cluster expansions.^{5,6,12,18} The value then of the somewhat extended treatment of weight factors given in the present work is that the straightforward " $\frac{1}{4}$ rule" can justifiably be used in a full coupled-cluster method. In particular, it was not transparent to us that the presence of the numerical factors $(n!)^{-1}$, $n \geq 3$, in the wave operator would be exactly offset in every matrix element. It should be noted that the star product treatment developed by Cizek⁵ is correct and justified for the determination of the weight factor in a full coupled-cluster method; however, the procedure is a bit cumbersome when there are more than about two cluster operators.

The second point is that the use of rules originally developed for a time-dependent formalism in a time-independent diagrammatic approach is appropriate, provided that the diagrams are topologically similar and that the rules consider only topological (e.g., not physical) aspects of the theory. The structural similarities of the (exponential) scattering matrix and the wave operator [cf. Eqs. (88), (89), (1), and (4)], and the physical particles and the excited (bra) determinant, have already been discussed. A subtlety is that the interaction vertices in a time-dependent formalism represent components of the Lagrangian, while the interaction vertices in a time-independent formalism represent components of the Hamiltonian. The topological equivalence is assured with the realization that the basic interaction in both versions is the entering and exiting of a spinor line together with the emission or absorption of a photon. Hence, the efficient symmetry rules set out by Bogoliubov and Shirkov²⁹ can straightforwardly be used in a time-independent formalism.

RULE 4. Generate the algebraic expressions corresponding to the non-canonical diagrams directly from the algebraic expressions for the canonical diagrams by applying permutation operators.

The generalized time-independent Wick theorem [cf. Eq. (92)] requires that all sets of contractions between operators (from different N products) be included in the summation. The inclusion of only canonical diagrams, as defined earlier, can be seen to represent all possible contractions between the Hamiltonian and the wave operator but restricted contraction between the bra configuration and these combined operator products. The noncanonical diagrams then complete the set of all possible contractions between operator expressions. A noncanonical diagram is characterized by crisscrossing external lines or equivalently (i.e., fermion operators anticommute) noncrossing external lines with permuted indices with respect to the canonical ordering.

Consider a permutation operator that generates all topologically distinct noncanonical diagrams from a given canonical diagram; essentially, this operator just relabels external lines. Since the noncanonical diagrams are structurally the same as their parent resulting diagram, the algebraic expressions for the noncanonical diagrams must be the same as the algebraic expression for the parent diagram up to a reordering of external indices. It can be seen then that the permutation operator acting on the algebraic expression for a canonical diagram will produce algebraic expressions corresponding to noncanonical diagrams permutationally related to the parent resulting diagram.

Two properties of the permutation operator, spin statistics and topo-

logical distinctness, warrant further discussion. As pointed out by Paldus,¹² the phase factor of a noncanonical diagram must include the contribution $(-1)^p$, where p is here the parity of the permutation yielding the canonical labeling of external lines. The origin of this term is the anticommutation of fermion field operators [cf. Eq. (43)]. So, in order for the permutation operator to generate algebraic expressions for noncanonical diagrams with the correct overall phase, the contribution to the phase factor from the ordering of external indices must be included in the permutation operator. A second major concern is that the sum over resulting diagrams include only topologically distinct diagrams. Hence, we require that the algebraic expressions generated by the permutation operator correspond to topologically distinct noncanonical diagrams.

Since both the particle and hole labels are in general permuted, and it is often the case that the permutations are independent, it is efficacious to (always) write the permutation operator as the binary product of operators acting on the disjoint sets,

$$\begin{aligned} p(u_i, \beta_i) &= P(u_i)P'(\beta_i) \\ &= P'(\beta_i)P(u_i), \quad i = 1, 2, 3 \end{aligned} \quad (96)$$

In Eq. (96), the u_i and β_i represent hole and particle labels, respectively, and P and P' denote single-index set permutation operators. In the cases that the particle and hole permutations are dependent, the decomposition of the permutation operator into single-index set permutation operators is ambiguous; i.e., two correct descriptions exist,

$$p(u_i, \beta_i) = P(u_i)P'(\beta_i) = P''(u_i)P'''(\beta_i) \quad (97)$$

It is found that for such permutations, any correct description is adequate.

The particular form of the single-index permutation operators we will use is an antisymmetrized generalization of Bogoliubov and Shirkov's²⁹ (symmetric) permutation operators used in the power series expansion of the scattering matrix. Vertical lines demarcate topologically distinct environments and hence define the permutation patterns. It should be noted that a null intersection between external lines of a given index set and a topologically distinct environment is suppressed in the notation. Under the action of the permutation operator, the labels in the algebraic expression lose their original significance (e.g., they become placeholders or "dummy variables"), but the ordering in the parent resulting diagram is preserved by the list of labels in the permutation operator. Hence it can be

seen that the list of labels, which specifies the identity permutation, together with the placement of vertical lines completely specify the single-index set permutation operators.

There are four types of nontrivial single-index set permutation operators required in a CCSDT model; i.e.,

$$P(x_1 | x_2) = I - (x_1 x_2) \quad (98)$$

$$P(x_1 x_2 | x_3) = I - (x_1 x_2) - (x_2 x_3) \quad (99)$$

$$P(x_1 | x_2 x_3) = I - (x_1 x_2) - (x_1 x_3) \quad (100)$$

and

$$\begin{aligned} P(x_1 | x_2 | x_3) &= I - (x_1 x_2) - (x_1 x_3) - (x_2 x_3) \\ &\quad + (x_1 x_2)(x_2 x_3) + (x_1 x_3)(x_2 x_3) \end{aligned} \quad (101)$$

or

$$\begin{aligned} &= I - (x_1 x_2) - (x_1 x_3) - (x_2 x_3) \\ &\quad + (x_1 x_2 x_3) + (x_1 x_3 x_2) \end{aligned} \quad (102)$$

In Eqs. (98)–(102), cyclic notation was used, with I denoting the identity permutation and x_i representing either particles β_i or holes u_i . The trivial permutation operator, $P = I$, will not be explicitly used. It should be noted that the signs are in agreement with the parities of the permutation cycles, so that the criterion of correct phase for noncanonical diagrams is implemented on the single index set permutation operator level.

Application of an appropriate single-index set permutation operator on the algebraic expression corresponding to a canonical resulting diagram produces only algebraic expressions corresponding to topologically distinct noncanonical diagrams, since indices are switched between topologically nonequivalent environments. However, subsequent application of the complementary (e.g., particle–hole) single-index set permutation operator may produce algebraic expressions corresponding to topologically indistinct resulting diagrams, because the action of the first operator rendered two distinct topological environments equivalent. Effectively, a specious vertical line exists in the second operator, the removal of which correctly reflects the physical situation and leads to the correct number of topologically distinct noncanonical diagrams. It is to be emphasized that the recognition of topologically distinct environments is relatively straightforward diagrammatically and is actually a strong recommendation for a diagrammatic approach.

In summary, the rules for the construction and subsequent evaluation of diagrams corresponding to matrix elements in the CCSDT model have been given. The adaptation of certain features from time-dependent diagrams, not usually found in time-independent approaches, have been seen to clarify and/or expedite time-independent diagrams.

V. Matrix Elements

The equations for the cluster coefficients and the correlated energy in a CCSDT model were given in operator form in Section III [cf. Eqs. (80)–(83)]; this form is, of course, not amenable to calculations. In Section V the time-independent techniques discussed in Section IV are applied to evaluate the requisite matrix elements in terms of cluster coefficients and one- and two-electron integrals over the spin-orbital basis.

Table I lists all possible nonvanishing matrix elements arising from the projection of the Schrödinger equation onto the reference, singly, doubly, and triply excited spaces. The matrix elements are assigned an ordinal number. The diagrams generated in the application of Rule 1 from the preceding section to a given matrix element are listed on the right-hand side of the table, below the particular matrix element. Multiple diagrams from a given matrix element are distinguished by lowercase roman letters. Algebraic expressions, up to phase and symmetry, corresponding to a given diagram are evaluated by using Rule 2; they are designated with the letter *d*, and the subscript associated with the diagram. Contributions to the symmetry and phase factors are also listed if they are different from the following default values: $l = 0$, $h = 0$, $c_p = 1$, $c_h = 1$, $c_{ph} = 1$. The prefactor corresponding to a given diagram is then evaluated by using Rule 3; it is symbolized by the greek letter ϕ and the subscript of the diagram. The permutation operator generating all noncanonical diagrams related to a given diagram (cf. Rule 4) is listed, provided that either the hole or the particle permutation operator is different than the identity. The permutation operator is symbolized by the letter *p* and the subscript of the diagram. Hence each diagram has between two and four lines of text written opposite to it (e.g., left-hand side) in Table I.

The expression for a given matrix element *m* without reference to field operators is then given by

$$[m] = \sum_{\zeta} p_{m\zeta} \phi_{m\zeta} d_{m\zeta} \quad (103)$$

where the summation runs over all valid (canonical) diagrams derivable from *m*.

TABLE I

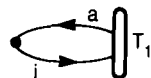
DIAGRAMMATIC EVALUATION OF ALL NONVANISHING MATRIX ELEMENTS OCCURRING
IN THE CCSDT MODEL^a

$$[1] = \langle \Phi_0 | \{H_1 T_1\}_C | \Phi_0 \rangle$$

$$d_1 = \sum_{ia} f_{ia} t_i^a$$

$$l = 1, \quad h = 1$$

$$\phi_1 = 1$$

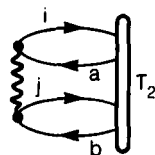


$$[2] = \langle \Phi_0 | \{H_2 T_2\}_C | \Phi_0 \rangle$$

$$d_2 = \sum_{ijab} \langle ij || ab \rangle t_{ij}^{ab}$$

$$l = 2, \quad h = 2, \quad c_h = 2, \quad c_p = 2$$

$$\phi_2 = \frac{1}{4}$$

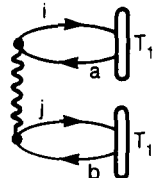


$$[3] = \langle \Phi_0 | \{H_2 \frac{1}{2} T_1^2\}_C | \Phi_0 \rangle$$

$$d_3 = \sum_{ijab} \langle ij || ab \rangle t_i^a t_j^b$$

$$l = 2, \quad h = 2, \quad c_{ph} = 2$$

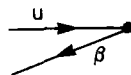
$$\phi_3 = \frac{1}{2}$$



$$[4] = \langle \Phi_u^\beta | \{H_1 1\}_C | \Phi_0 \rangle$$

$$d_4 = f_{u\beta}$$

$$\phi_4 = 1$$

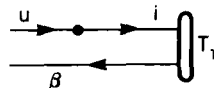


$$[5] = \langle \Phi_u^\beta | \{H_1 T_1\}_C | \Phi_0 \rangle$$

$$d_{5a} = \sum_i f_{ui} t_i^\beta$$

$$h = 1$$

$$\phi_{5a} = -1$$

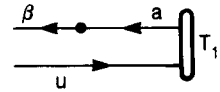


^a See text for explanation of symbols.

TABLE I (Continued)

$$d_{5b} = \sum_a f_{a\beta} t_u^a$$

$$\phi_{5b} = 1$$

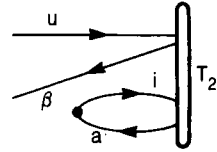


$$[6] = \langle \beta_u | \{H_1 T_2\}_C | \Phi_0 \rangle$$

$$d_6 = \sum_{ia} f_{ia} t_{ui}^{\beta a}$$

$$l = 1, \quad h = 1$$

$$\phi_6 = 1$$

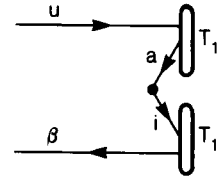


$$[7] = \langle \beta_u | \{H_1 \frac{1}{2} T_1^2\}_C | \Phi_0 \rangle$$

$$d_7 = \sum_{ia} f_{ia} t_u^a t_i^\beta$$

$$h = 1$$

$$\phi_7 = -1$$

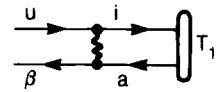


$$[8] = \langle \beta_u | \{H_2 T_1\}_C | \Phi_0 \rangle$$

$$d_8 = \sum_{ia} \langle \beta i || a u \rangle t_i^a$$

$$h = 1$$

$$\phi_8 = -1$$

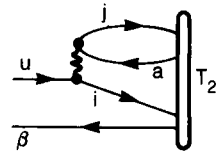


$$[9] = \langle \beta_u | \{H_2 T_2\}_C | \Phi_0 \rangle$$

$$d_{9a} = \sum_{ija} \langle ij || u a \rangle t_{ij}^{\beta a}$$

$$l = 1, \quad h = 2, \quad c_h = 2$$

$$\phi_{9a} = -\frac{1}{2}$$



$$d_{9b} = \sum_{iab} \langle \beta i || a b \rangle t_{ui}^{ab}$$

$$l = 1, \quad h = 1, \quad c_p = 2$$

$$\phi_{9b} = \frac{1}{2}$$

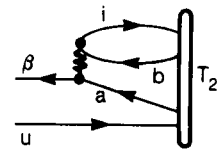


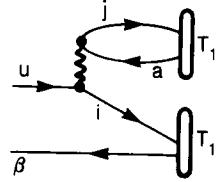
TABLE I (Continued)

$$[10] = \langle \beta_u | \{H_2 \frac{1}{2} T_1^2\}_C | \Phi_0 \rangle$$

$$d_{10a} = \sum_{ija} \langle ij || ua \rangle t_i^\beta t_j^a$$

$$l = 1, \quad h = 2$$

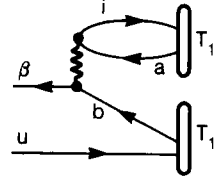
$$\phi_{10a} = -1$$



$$d_{10b} = \sum_{iab} \langle i\beta || ab \rangle t_i^a t_u^b$$

$$l = 1, \quad h = 1$$

$$\phi_{10b} = 1$$

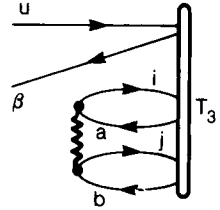


$$[11] = \langle \beta_u | \{H_2 T_3\}_C | \Phi_0 \rangle$$

$$d_{11} = \sum_{ijab} \langle ij || ab \rangle t_{uij}^{\beta ab}$$

$$l = 2, \quad h = 2, \quad c_h = 2, \quad c_p = 2$$

$$\phi_{11} = \frac{1}{4}$$



$$[12] = \langle \beta_u | \{H_2 T_2 T_1\}_C | \Phi_0 \rangle$$

$$d_{12a} = \sum_{ijab} \langle ij || ab \rangle t_{ui}^{\beta a} t_j^b$$

$$l = 2, \quad h = 2$$

$$\phi_{12a} = 1$$

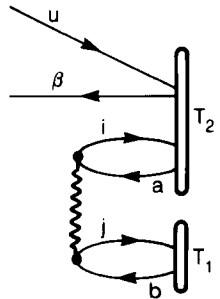
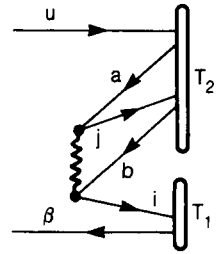


TABLE I (Continued)

$$d_{12b} = \sum_{ijab} \langle ji \| ab \rangle t_{ij}^{ab} t_i^\beta$$

$$h = 2, \quad c_p = 2$$

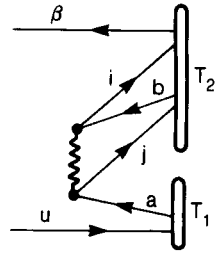
$$\phi_{12b} = \frac{1}{2}$$



$$d_{12c} = \sum_{ijab} \langle ij \| ba \rangle t_{ij}^{\beta b} t_u^a$$

$$h = 2, \quad c_h = 2$$

$$\phi_{12c} = \frac{1}{2}$$

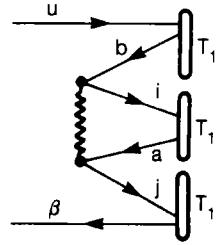


$$[13] = \langle \beta_u | \left\{ H_2 \frac{1}{3!} T_1^3 \right\} c | \Phi_0 \rangle$$

$$d_{13} = \sum_{ijab} \langle ij \| ba \rangle t_u^b t_i^a t_j^\beta$$

$$h = 2$$

$$\phi_{13} = 1$$



$$[14] = \langle \beta_\gamma | \{ H_1 T_2 \} c | \Phi_0 \rangle$$

$$d_{14a} = \sum_i f_{ui} t_{iv}^{\beta\gamma}$$

$$h = 1$$

$$\phi_{14a} = -1$$

$$p_{14a} = P(u | v)$$

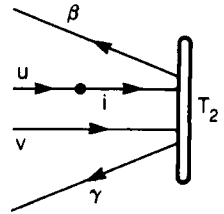
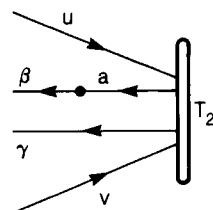


TABLE I (Continued)

$$d_{14b} = \sum_a f_{a\beta} t_{uv}^{a\gamma}$$

$$\phi_{14b} = 1$$

$$p_{14b} = P(\beta | \gamma)$$

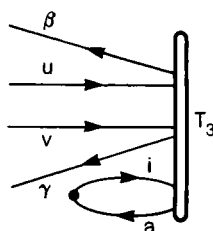


$$[15] = \langle \beta\gamma | \{H_1 T_3\}_C | \Phi_0 \rangle$$

$$d_{15} = \sum_{ia} f_{ia} t_{uvi}^{\beta\gamma a}$$

$$l = 1, \quad h = 1$$

$$\phi_{15} = 1$$



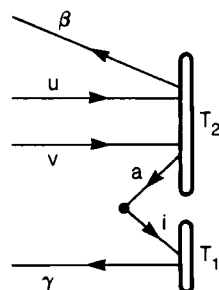
$$[16] = \langle \beta\gamma | \{H_1 T_2 T_1\}_C | \Phi_0 \rangle$$

$$d_{16a} = \sum_{ia} f_{ai} t_{uv}^{\beta a} t_i^{\gamma}$$

$$h = 1$$

$$\phi_{16a} = -1$$

$$p_{16a} = P(\beta | \gamma)$$



$$d_{16b} = \sum_{ia} f_{ai} t_{ui}^{\beta\gamma} t_v^a$$

$$h = 1$$

$$\phi_{16b} = -1$$

$$p_{16b} = P(u | v)$$

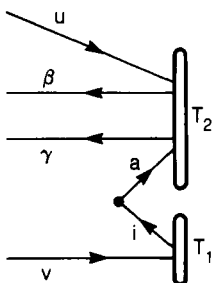
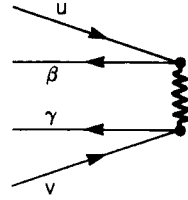


TABLE I (Continued)

$$[17] = \langle \beta\gamma | \{H_2 1\}_C | \Phi_0 \rangle$$

$$d_{17} = \langle \beta\gamma | uv \rangle$$

$$\phi_{17} = 1$$



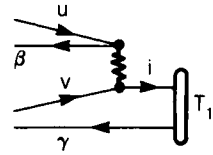
$$[18] = \langle \beta\gamma | \{H_2 T_1\}_C | \Phi_0 \rangle$$

$$d_{18a} = \sum_i \langle \beta i | uv \rangle t_i^\gamma$$

$$h = 1$$

$$\phi_{18a} = -1$$

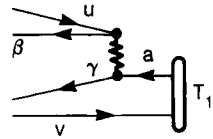
$$p_{18a} = P(\beta | \gamma)$$



$$d_{18b} = \sum_a \langle \beta\gamma | ua \rangle t_v^a$$

$$\phi_{18b} = 1$$

$$p_{18b} = P(u | v)$$



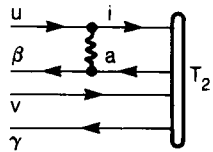
$$[19] = \langle \beta\gamma | \{H_2 T_2\}_C | \Phi_0 \rangle$$

$$d_{19a} = \sum_{ia} \langle \beta i | au \rangle t_{iv}^{a\gamma}$$

$$h = 1$$

$$\phi_{19a} = -1$$

$$p_{19a} = P(\beta | \gamma)P(u | v)$$



$$d_{19b} = \sum_{ij} \langle ij | uv \rangle t_{ij}^{\beta\gamma}$$

$$h = 2, \quad c_h = 2$$

$$\phi_{19b} = \frac{1}{2}$$

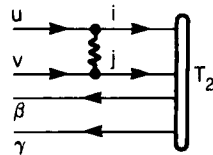


TABLE I (Continued)

$d_{19c} = \sum_{ab} \langle \beta\gamma ab \rangle t_{uv}^{ab}$ $c_p = 2$ $\phi_{19c} = \frac{1}{2}$	
$[20] = \langle \beta\gamma \{H_2 \frac{1}{2} T_1^2\}_C \Phi_0 \rangle$ $d_{20a} = \sum_{ia} \langle \beta i av \rangle t_u^a t_i^\gamma$ $h = 1$ $\phi_{20a} = -1$ $p_{20a} = P(\beta \gamma) P(v u)$	
$d_{20b} = \sum_{ab} \langle \beta\gamma ab \rangle t_u^a t_v^b$ $\phi_{20b} = 1$	
$d_{20c} = \sum_{ij} \langle ij uv \rangle t_i^\beta t_j^\gamma$ $h = 2$ $\phi_{20c} = 1$	
$[21] = \langle \beta\gamma \{H_2 T_3\}_C \Phi_0 \rangle$ $d_{21a} = \sum_{iab} \langle \gamma i ab \rangle t_{uvi}^{\beta ab}$ $l = 1, \quad h = 1, \quad c_p = 2$ $\phi_{21a} = \frac{1}{2}$ $p_{21a} = P(\gamma \beta)$	

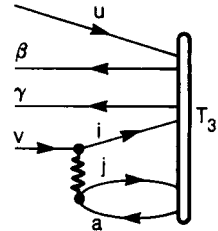
TABLE I (Continued)

$$d_{21b} = \sum_{ija} \langle ij || va \rangle t_{uij}^{\beta\gamma a}$$

$$l = 1, \quad h = 2, \quad c_h = 2$$

$$\phi_{21b} = -\frac{1}{2}$$

$$p_{21b} = P(v | u)$$



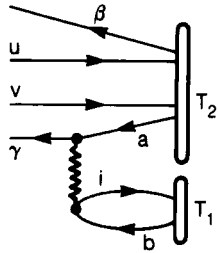
$$[22] = \langle \beta\gamma_{uv} | \{H_2 T_2 T_1\}_C | \Phi_0 \rangle$$

$$d_{22a} = \sum_{iab} \langle \gamma i || ab \rangle t_{uv}^{\beta a} t_i^b$$

$$l = 1, \quad h = 1$$

$$\phi_{22a} = 1$$

$$p_{22a} = P(\gamma | \beta)$$

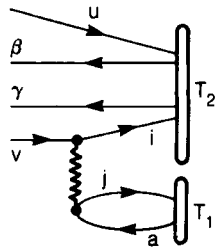


$$d_{22b} = \sum_{ija} \langle ij || va \rangle t_{ui}^{\beta\gamma} t_j^a$$

$$l = 1, \quad h = 2$$

$$\phi_{22b} = 1$$

$$p_{22b} = P(v | u)$$



$$d_{22c} = \sum_{ija} \langle ij || av \rangle t_{ui}^{\beta a} t_j^\gamma$$

$$l = 1, \quad h = 2$$

$$\phi_{22c} = -1$$

$$p_{22c} = P(\beta | \gamma) P(v | u)$$

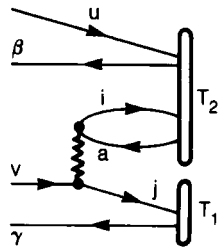


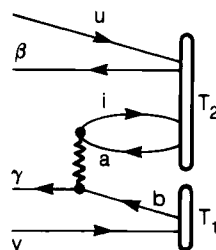
TABLE I (Continued)

$$d_{22d} = \sum_{iab} \langle i\gamma || ab \rangle t_{ui}^{\beta a} t_v^b$$

$$l = 1, \quad h = 1$$

$$\phi_{22d} = 1$$

$$\phi_{22d} = P(\gamma | \beta) P(u | v)$$

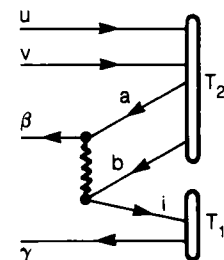


$$d_{22e} = \sum_{iab} \langle \beta i || ab \rangle t_{uv}^{ab} t_i^\gamma$$

$$h = 1, \quad c_p = 2$$

$$\phi_{22e} = -\frac{1}{2}$$

$$p_{22e} = P(\beta | \gamma)$$

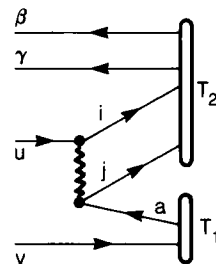


$$d_{22f} = \sum_{ija} \langle ij || ua \rangle t_{ij}^{\beta\gamma} t_v^a$$

$$h = 2, \quad c_h = 2$$

$$\phi_{22f} = \frac{1}{2}$$

$$\phi_f = P(u | v)$$



$$[23] = \langle \beta\gamma | \left\{ H_2 \frac{1}{3} T_1^3 \right\}_C | \Phi_0 \rangle$$

$$d_{23a} = \sum_{ija} \langle ij || av \rangle t_u^a t_i^\beta t_j^\gamma$$

$$h = 2$$

$$\phi_{23a} = 1$$

$$p_{23a} = P(v | u)$$

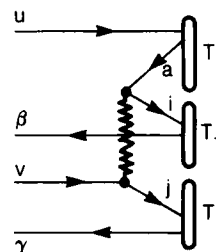


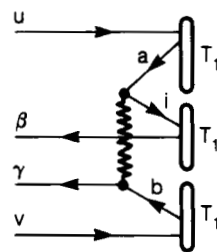
TABLE I (Continued)

$$d_{23b} = \sum_{iab} \langle i\gamma || ab \rangle t_u^a t_i^\beta t_v^b$$

$$h = 1$$

$$\phi_{23b} = -1$$

$$p_{23b} = P(\gamma | \beta)$$

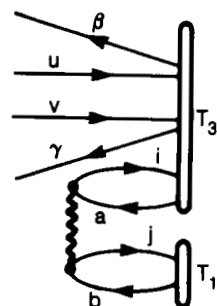


$$[24] = \langle \beta\gamma | \{H_2 T_3 T_1\}_C | \Phi_0 \rangle$$

$$d_{24a} = \sum_{ijab} \langle ij || ab \rangle t_{uvi}^{\beta\gamma a} t_j^b$$

$$l = 2, \quad h = 2$$

$$\phi_{24a} = 1$$

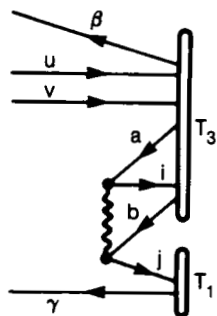


$$d_{24b} = \sum_{ijab} \langle ij || ab \rangle t_{uvi}^{\beta\gamma a} t_j^\gamma$$

$$h = 2, \quad c_p = 2$$

$$\phi_{24b} = \frac{1}{2}$$

$$p_{24b} = P(\beta | \gamma)$$



$$d_{24c} = \sum_{ijab} \langle ij || ab \rangle t_{uij}^{\beta\gamma a} t_v^b$$

$$h = 2, \quad c_h = 2$$

$$\phi_{24c} = \frac{1}{2}$$

$$p_{24c} = P(u | v)$$

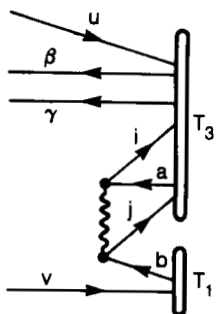


TABLE I (Continued)

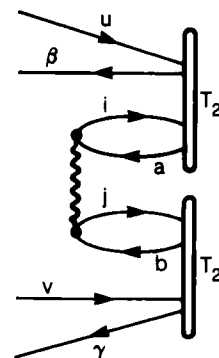
$$[25] = \langle \beta\gamma | \{H_{2\frac{1}{2}} T_2^2\} c | \Phi_0 \rangle$$

$$d_{25a} = \sum_{ijab} \langle ij || ab \rangle t_{ui}^{\beta a} t_{jv}^{b\gamma}$$

$$l = 2, \quad h = 2$$

$$\phi_{25a} = 1$$

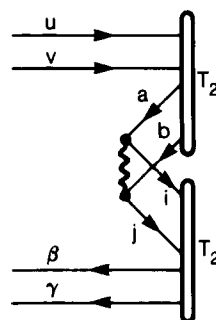
$$p_{25a} = P(\beta | \gamma)$$



$$d_{25b} = \sum_{ijab} \langle ij || ab \rangle t_{uv}^{ab} t_{i\gamma}^{\beta\gamma}$$

$$h = 2, \quad c_p = 2, \quad c_h = 2$$

$$\phi_{25b} = \frac{1}{4}$$



$$d_{25c} = \sum_{ijab} \langle ij || ab \rangle t_{ui}^{\beta a} t_{jv}^{b\gamma}$$

$$h = 2, \quad c_p = 2$$

$$\phi_{25c} = \frac{1}{2}$$

$$p_{25c} = P(u | v)$$

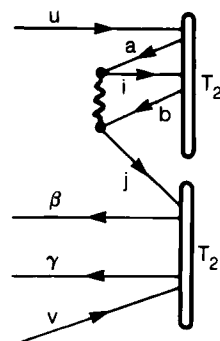


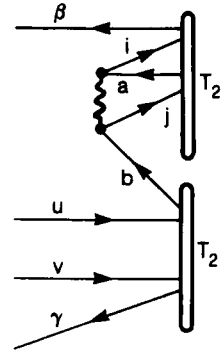
TABLE I (Continued)

$$d_{25d} = \sum_{ijab} \langle ij || ab \rangle t_{ij}^{\beta a} t_{uv}^{\gamma b}$$

$$h = 2, \quad c_h = 2$$

$$\phi_{25d} = \frac{1}{2}$$

$$p_{25d} = P(\beta \mid \gamma)$$



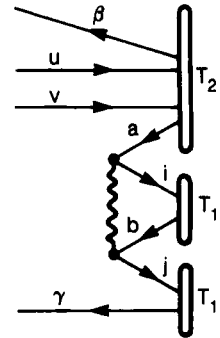
$$[26] = \langle \beta \gamma | \{ H_2 \frac{1}{2} T_2 T_1^2 \} | \Phi_0 \rangle$$

$$d_{26a} = \sum_{ijab} \langle ij || ab \rangle t_{uv}^{\beta a} t_i^b t_j^{\gamma}$$

$$h = 2$$

$$\phi_{26a} = 1$$

$$p_{26a} = P(\beta \mid \gamma)$$



$$d_{26b} = \sum_{ijab} \langle ij || ab \rangle t_{ui}^{\beta \gamma} t_j^a t_v^b$$

$$h = 2$$

$$\phi_{26b} = 1$$

$$p_{26b} = P(u \mid v)$$

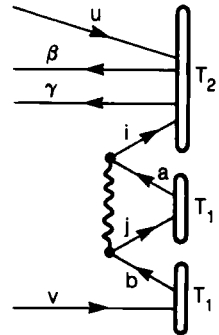


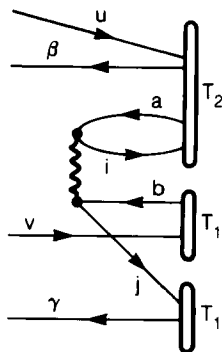
TABLE I (Continued)

$$d_{26c} = \sum_{ijab} \langle ij || ab \rangle t_{ui}^{\beta a} t_v^b t_j^\gamma$$

$$l = 1, \quad h = 2$$

$$\phi_{26c} = -1$$

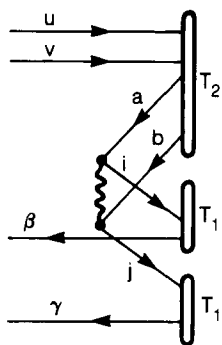
$$p_{26c} = P(\beta | \gamma) P(u | v)$$



$$d_{26d} = \sum_{ijab} \langle ij || ab \rangle t_{uv}^{ab} t_i^\beta t_j^\gamma$$

$$h = 2, \quad c_p = 2$$

$$\phi_{26d} = \frac{1}{2}$$



$$d_{26e} = \sum_{ijab} \langle ij || ab \rangle t_{ij}^{\beta\gamma} t_u^a t_v^b$$

$$h = 2, \quad c_h = 2$$

$$\phi_{26e} = \frac{1}{2}$$

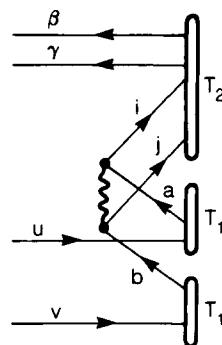


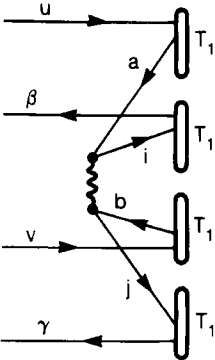
TABLE I (Continued)

$[27] = \langle \beta\gamma | \left\{ H_2 \frac{1}{4!} T_1^4 \right\}_C | \Phi_0 \rangle$

$d_{27} = \sum_{ijab} \langle ij || ab \rangle t_u^a t_i^\beta t_v^b t_j^\gamma$

$h = 2$

$\phi_{27} = 1$



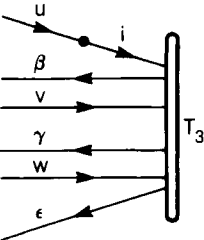
$[28] = \langle \beta\gamma\epsilon | \{ H_1 T_3 \}_C | \Phi_0 \rangle$

$d_{28a} = \sum_i f_{ui} t_{iuv}^{\beta\gamma\epsilon}$

$h = 1$

$\phi_{28a} = -1$

$p_{28a} = P(u \mid v\epsilon)$



$d_{28b} = \sum_a f_{a\beta} t_{uvw}^{a\gamma\epsilon}$

$\phi_{28b} = 1$

$p_{28b} = P(\beta \mid \gamma\epsilon)$

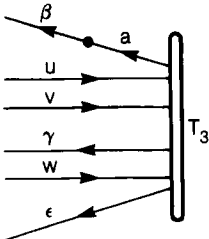


TABLE I (Continued)

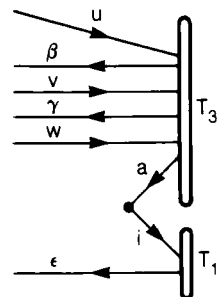
$$[29] = \langle \beta\gamma\epsilon | \{H_1 T_3 T_1\}_C | \Phi_0 \rangle$$

$$d_{29a} = \sum_{ia} f_{ia} t_{uvw}^{\beta\gamma a} t_i^\epsilon$$

$$h = 1$$

$$\phi_{29a} = -1$$

$$p_{29a} = P(\beta\gamma \mid \epsilon)$$

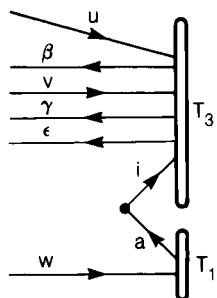


$$d_{29b} = \sum_{ia} f_{ia} t_{uvi}^{\beta\gamma\epsilon} t_w^a$$

$$h = 1$$

$$\phi_{29b} = -1$$

$$p_{29b} = P(uv \mid w)$$



$$[30] = \langle \beta\gamma\epsilon | \{H_1 \frac{1}{2} T_2^2\}_C | \Phi_0 \rangle$$

$$d_{30} = \sum_{ia} f_{ia} t_{uv}^{\beta a} t_{iw}^{\gamma\epsilon}$$

$$h = 1$$

$$\phi_{30} = -1$$

$$p_{30} = P(\beta \mid \gamma\epsilon) P(uv \mid w)$$

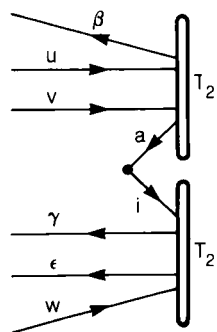


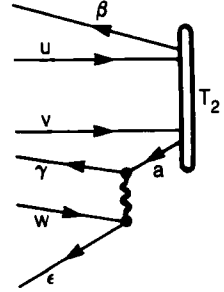
TABLE I (Continued)

$$[31] = \langle \beta \gamma \epsilon | \{H_2 T_2\}_C | \Phi_0 \rangle$$

$$d_{31a} = \sum_a \langle \gamma \epsilon || a w \rangle t_{uv}^{\beta a}$$

$$\phi_{31a} = 1$$

$$p_{31a} = P(\gamma \epsilon | \beta) P(w | uv)$$

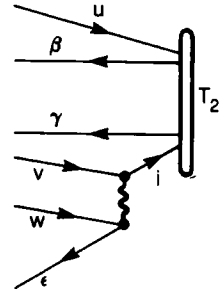


$$d_{31b} = \sum_i \langle i \epsilon || v w \rangle t_{ui}^{\beta \gamma}$$

$$h = 1$$

$$\phi_{31b} = -1$$

$$p_{31b} = P(\epsilon | \beta \gamma) P(vw | u)$$



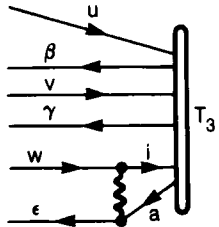
$$[32] = \langle \beta \gamma \epsilon | \{H_2 T_3\}_C | \Phi_0 \rangle$$

$$d_{32a} = \sum_{ia} \langle \epsilon i || a w \rangle t_{uvi}^{\beta \gamma a}$$

$$h = 1$$

$$\phi_{32a} = -1$$

$$p_{32a} = P(\epsilon | \beta \gamma) P(w | uv)$$



$$d_{32b} = \sum_{ij} \langle ij || v w \rangle t_{uij}^{\beta \gamma \epsilon}$$

$$h = 2 \quad c_h = 2$$

$$\phi_{32b} = \frac{1}{2}$$

$$p_{32b} = P(vw | u).$$

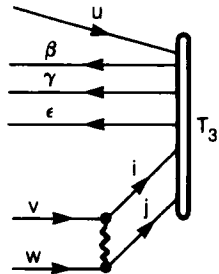


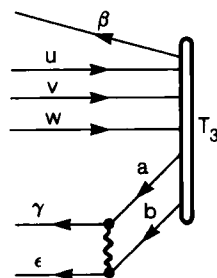
TABLE I (Continued)

$$d_{32c} = \sum_{ab} \langle \gamma \epsilon \| ab \rangle t_{uvw}^{\beta ab}$$

$$c_p = 2$$

$$\phi_{32c} = \frac{1}{2}$$

$$p_{32c} = P(\gamma \epsilon \mid \beta)$$



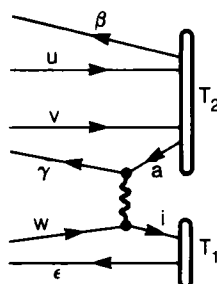
$$[33] = \langle \beta \gamma \epsilon | \{H_2 T_2 T_1\}_C | \Phi_0 \rangle$$

$$d_{33a} = \sum_{ia} \langle \gamma i \| aw \rangle t_{uv}^{\beta a} t_i^\epsilon$$

$$h = 1$$

$$\phi_{33a} = -1$$

$$p_{33a} = P(\gamma \mid \beta \mid \epsilon) P(w \mid uv)$$

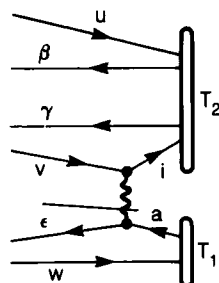


$$d_{33b} = \sum_{ia} \langle \epsilon i \| av \rangle t_{ui}^{\beta \gamma} t_w^a$$

$$h = 1$$

$$\phi_{33b} = -1$$

$$p_{33b} = P(\epsilon \mid \beta \gamma) P(v \mid u \mid w)$$



$$d_{33c} = \sum_{ij} \langle ij \| vw \rangle t_{ui}^{\beta \gamma} t_j^\epsilon$$

$$h = 2$$

$$\phi_{33c} = 1$$

$$p_{33c} = P(\beta \gamma \mid \epsilon) P(vw \mid u)$$

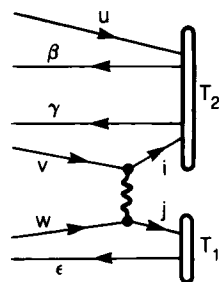
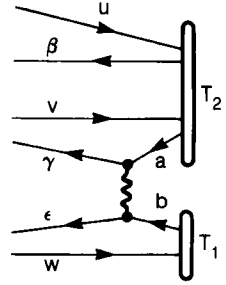


TABLE I (Continued)

$$d_{33d} = \sum_{ab} \langle \gamma \epsilon \| ab \rangle t_{uv}^{\beta a} t_w^b$$

$$\phi_{33d} = 1$$

$$p_{33d} = P(\gamma \epsilon \mid \beta) P(uv \mid w)$$



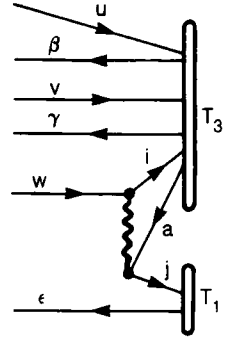
$$[34] = \langle \beta \gamma \epsilon | \{H_2 T_3 T_1\}_C | \Phi_0 \rangle$$

$$d_{34a} = \sum_{ija} \langle ij \| wa \rangle t_{uvi}^{\beta \gamma a} t_j^\epsilon$$

$$h = 2$$

$$\phi_{34a} = 1$$

$$p_{34a} = P(\beta \gamma \mid \epsilon) P(w \mid uv)$$



$$d_{34b} = \sum_{iab} \langle \gamma i \| ab \rangle t_{uvw}^{\beta ab} t_i^\epsilon$$

$$h = 1, \quad c_p = 2$$

$$\phi_{34b} = -\frac{1}{2}$$

$$p_{34b} = P(\gamma \mid \beta \mid \epsilon)$$

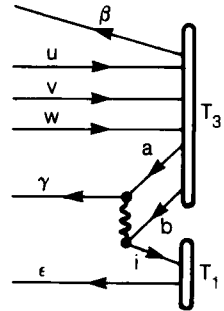


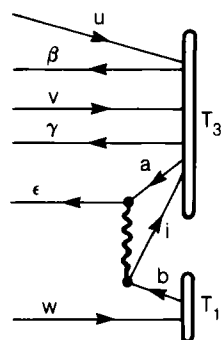
TABLE I (Continued)

$$d_{34c} = \sum_{iab} \langle \varepsilon i \| ab \rangle t_{uvi}^{\beta\gamma a} t_w^b$$

$$h = 1$$

$$\phi_{34c} = -1$$

$$p_{34c} = P(\varepsilon \mid \beta\gamma)P(uv \mid w)$$

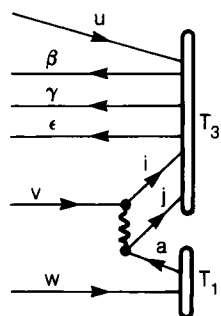


$$d_{34d} = \sum_{ija} \langle ij \| va \rangle t_{uij}^{\beta\gamma e} t_w^a$$

$$h = 2, \quad c_h = 2$$

$$\phi_{34d} = \frac{1}{2}$$

$$p_{34d} = P(v \mid u \mid w)$$



$$d_{34e} = \sum_{iab} \langle \varepsilon i \| ab \rangle t_{uvw}^{\beta\gamma a} t_i^b$$

$$l = 1, \quad h = 1$$

$$\phi_{34e} = 1$$

$$p_{34e} = P(\varepsilon \mid \beta\gamma)$$

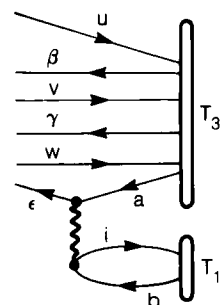


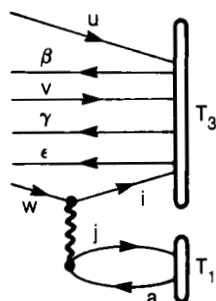
TABLE I (Continued)

$$d_{34f} = \sum_{ija} \langle ij || wa \rangle t_{uvi}^{\beta\gamma\epsilon} t_j^a$$

$$l = 1, \quad h = 2$$

$$\phi_{34f} = -1$$

$$p_{34f} = P(w | uv)$$



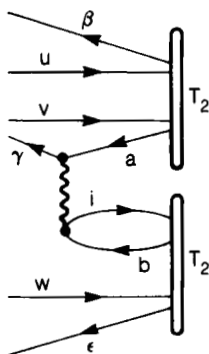
$$[35] = \langle uvw | \{H_2 \frac{1}{2} T_2^2\}_C | \Phi_0 \rangle$$

$$d_{35a} = \sum_{iab} \langle \gamma i || ab \rangle t_{uv}^{\beta a} t_{iw}^{b\epsilon}$$

$$l = 1, \quad h = 1$$

$$\phi_{35a} = 1$$

$$p_{35a} = P(\gamma | \beta | \epsilon) P(uv | w)$$



$$d_{35b} = \sum_{ija} \langle ij || va \rangle t_{ui}^{\beta\gamma} t_{jw}^{a\epsilon}$$

$$l = 1, \quad h = 2$$

$$\phi_{35b} = -1$$

$$p_{35b} = P(\beta\gamma | \epsilon) P(v | u | w)$$

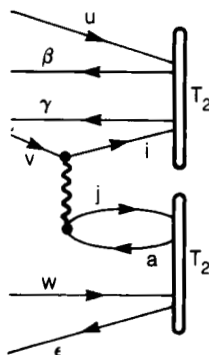


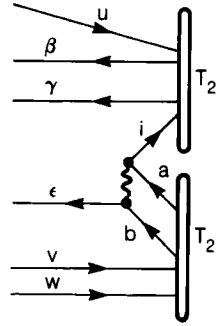
TABLE I (Continued)

$$d_{35c} = \sum_{iab} \langle \epsilon i \| ba \rangle t_{ui}^{\beta\gamma} t_{vw}^{ab}$$

$$h = 1, \quad c_p = 2$$

$$\phi_{35c} = -\frac{1}{2}$$

$$p_{35c} = P(\epsilon \mid \beta\gamma)P(u \mid vw)$$

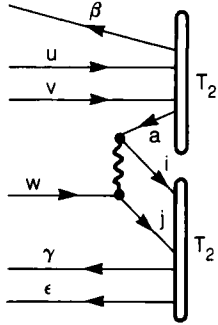


$$d_{35d} = \sum_{ija} \langle ij \| aw \rangle t_{uv}^{\beta a} t_{ij}^{\gamma \epsilon}$$

$$h = 2, \quad c_h = 2$$

$$\phi_{35d} = \frac{1}{2}$$

$$p_{35d} = P(\beta \mid \gamma\epsilon)P(w \mid uv)$$



$$[36] = \langle \beta\gamma\epsilon | \{H_2 \frac{1}{2} T_2 T_1^2\}_C | \Phi_0 \rangle$$

$$d_{36a} = \sum_{ija} \langle ij \| aw \rangle t_{uv}^{\beta a} t_i^{\gamma} t_j^{\epsilon}$$

$$h = 2$$

$$\phi_{36a} = 1$$

$$p_{36a} = P(\beta \mid \gamma\epsilon)P(w \mid uv)$$

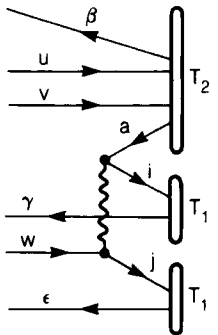


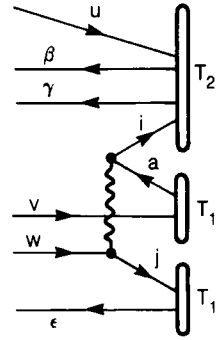
TABLE I (Continued)

$$d_{36b} = \sum_{ija} \langle ij \| aw \rangle t_{ui}^{\beta\gamma} t_v^a t_j^e$$

$$h = 2$$

$$\phi_{36b} = 1$$

$$p_{36b} = P(\beta\gamma \mid \varepsilon)P(w \mid u \mid v)$$

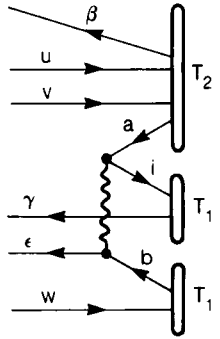


$$d_{36c} = \sum_{iab} \langle i\varepsilon \| ab \rangle t_{uv}^{\beta a} t_i^{\gamma} t_w^b$$

$$h = 1$$

$$\phi_{36c} = -1$$

$$p_{36c} = P(\varepsilon \mid \beta \mid \gamma)P(uv \mid w)$$



$$d_{36d} = \sum_{iab} \langle i\varepsilon \| ab \rangle t_{ui}^{\beta\gamma} t_v^a t_w^b$$

$$h = 1$$

$$\phi_{36d} = -1$$

$$p_{36d} = P(\varepsilon \mid \beta\gamma)P(u \mid vw)$$

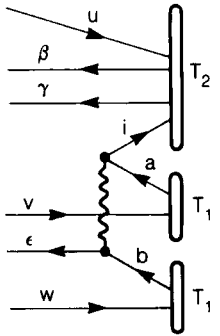


TABLE I (Continued)

$$[37] = \langle \beta\gamma\epsilon | \{H_2 T_3 T_2\}_C | \Phi_0 \rangle$$

$$d_{37a} = \sum_{ijab} \langle ij || ab \rangle t_{uvi}^{\beta ab} t_{jw}^{\gamma\epsilon}$$

$$h = 2, \quad c_p = 2$$

$$\phi_{37a} = \frac{1}{2}$$

$$p_{37a} = P(\beta | \gamma\epsilon) P(uv | w)$$

$$d_{37b} = \sum_{ijab} \langle ij || ab \rangle t_{uij}^{\beta\gamma a} t_{vw}^{\epsilon b}$$

$$h = 2, \quad c_h = 2$$

$$\phi_{37b} = \frac{1}{2}$$

$$p_{37b} = P(\beta\gamma | \epsilon) P(u | vw)$$

$$d_{37c} = \sum_{ijab} \langle ij || ab \rangle t_{uvj}^{\beta\gamma a} t_{iw}^{\epsilon b}$$

$$l = 1, \quad h = 2$$

$$\phi_{37c} = -1$$

$$p_{37c} = P(\beta\gamma | \epsilon) P(uv | w)$$

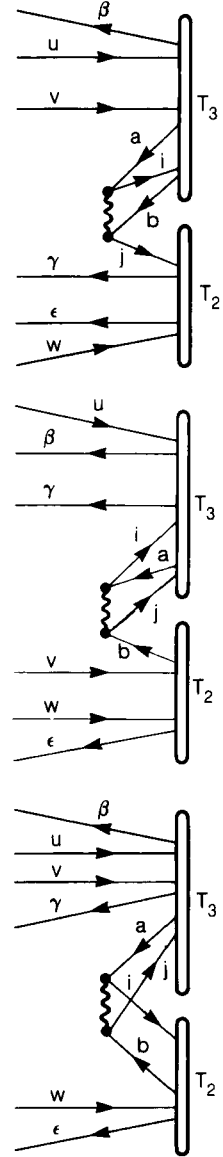


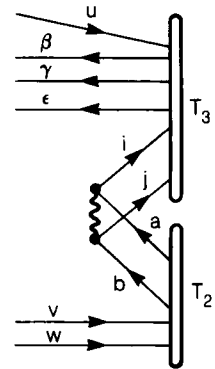
TABLE I (Continued)

$$d_{37d} = \sum_{ijab} \langle ij || ab \rangle t_{uij}^{\beta\gamma\epsilon} t_{vw}^{ab}$$

$$h = 2, \quad c_p = 2, \quad c_h = 2$$

$$\phi_{37d} = \frac{1}{4}$$

$$p_{37d} = P(u \mid vw)$$

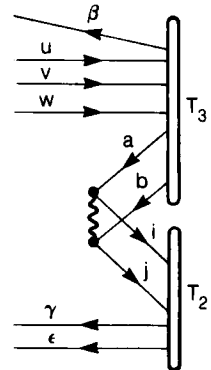


$$d_{37e} = \sum_{ijab} \langle ij || ab \rangle t_{uvw}^{\beta ab} t_{ij}^{\gamma\epsilon}$$

$$h = 2, \quad c_p = 2, \quad c_h = 2$$

$$\phi_{37e} = \frac{1}{4}$$

$$p_{37e} = P(\beta \mid \gamma\epsilon)$$



$$d_{37f} = \sum_{ijab} \langle ij || ab \rangle t_{uvw}^{\beta\gamma a} t_{ij}^{b\epsilon}$$

$$h = 2, \quad c_h = 2$$

$$\phi_{37f} = \frac{1}{2}$$

$$p_{37f} = P(\beta\gamma \mid \epsilon)$$

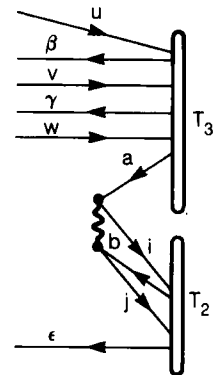


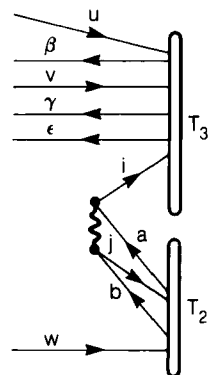
TABLE I (Continued)

$$d_{37g} = \sum_{ijab} \langle ij || ab \rangle t_{uvi}^{\beta\gamma\epsilon} t_{jw}^{ab}$$

$$h = 2, \quad c_p = 2$$

$$\phi_{37g} = \frac{1}{2}$$

$$p_{37g} = P(uv \mid w)$$



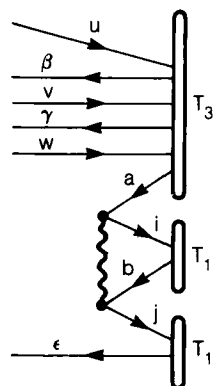
$$[38] = \langle \beta\gamma\epsilon | \{ H_2 \frac{1}{2} T_3 T_1^2 \}_C | \Phi_0 \rangle$$

$$d_{38a} = \sum_{ijab} \langle ij || ab \rangle t_{uvw}^{\beta\gamma a} t_i^b t_j^\epsilon$$

$$h = 2$$

$$\phi_{38a} = 1$$

$$p_{38a} = P(\beta\gamma \mid \epsilon)$$



$$d_{38b} = \sum_{ijab} \langle ij || ab \rangle t_{uvi}^{\beta\gamma\epsilon} t_j^a t_w^b$$

$$h = 2$$

$$\phi_{38b} = 1$$

$$p_{38b} = P(uv \mid w)$$

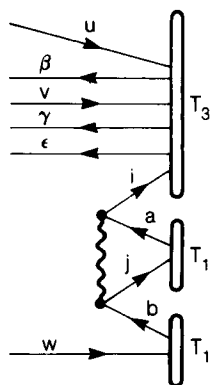


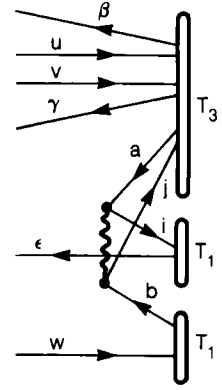
TABLE I (Continued)

$$d_{38c} = \sum_{ijab} \langle ij || ab \rangle t_{uvj}^{\beta\gamma a} t_i^\epsilon t_w^b$$

$$h = 2$$

$$\phi_{38c} = 1$$

$$p_{38c} = P(\beta\gamma | \epsilon) P(uv | w)$$

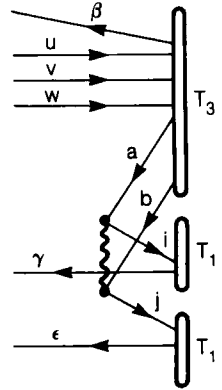


$$d_{38d} = \sum_{ijab} \langle ij || ab \rangle t_{uvw}^{ab} t_i^\gamma t_j^\epsilon$$

$$h = 2, \quad c_p = 2$$

$$\phi_{38d} = \frac{1}{2}$$

$$p_{38d} = P(\beta | \gamma\epsilon)$$



$$d_{38e} = \sum_{ijab} \langle ij || ab \rangle t_{uij}^{\beta\gamma\epsilon} t_v^a t_w^b$$

$$h = 2, \quad c_h = 2$$

$$\phi_{38e} = \frac{1}{2}$$

$$p_{38e} = P(u | vw)$$

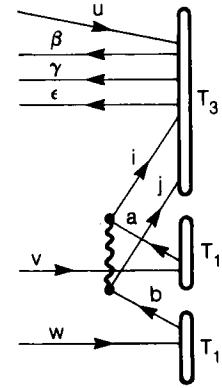


TABLE I (Continued)

$$[39] = \langle \beta \gamma \epsilon | \{ H_2 \frac{1}{2} T_2^2 T_1 \}_C | \Phi_0 \rangle$$

$$d_{39a} = \sum_{ijab} \langle ij || ab \rangle t_{uv}^{\beta a} t_i^b t_{jw}^{\gamma \epsilon}$$

$$h = 2$$

$$\phi_{39a} = 1$$

$$p_{39a} = P(\beta | \gamma \epsilon) P(uv | w)$$

$$d_{39b} = \sum_{ijab} \langle ij || ab \rangle t_{uv}^{ab} t_i^{\beta} t_{jw}^{\gamma \epsilon}$$

$$h = 2, \quad c_p = 2$$

$$\phi_{39b} = \frac{1}{2}$$

$$p_{39b} = P(\beta | \gamma \epsilon) P(uv | w)$$

$$d_{39c} = \sum_{ijab} \langle ij || ab \rangle t_{ui}^{\beta a} t_v^b t_{jw}^{\gamma \epsilon}$$

$$l = 1, \quad h = 2$$

$$\phi_{39c} = -1$$

$$p_{39c} = P(\beta | \gamma \epsilon) P(u | v | w)$$

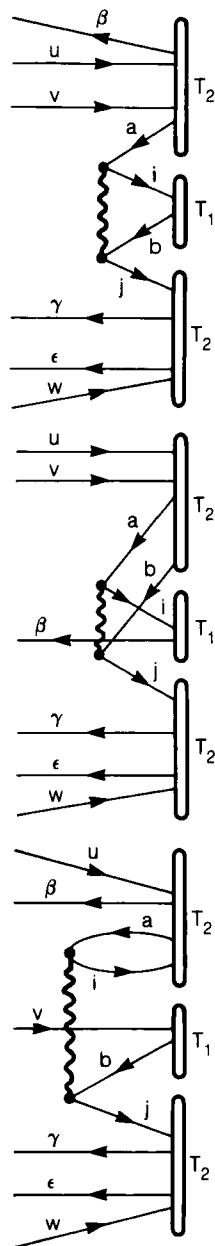


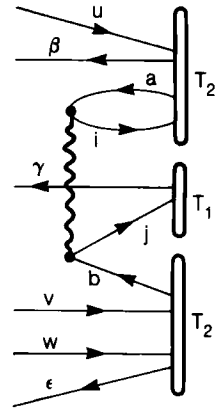
TABLE I (Continued)

$$d_{39d} = \sum_{ijab} \langle ij || ab \rangle t_{ui}^{\beta a} t_j^{\gamma} t_{vw}^{b \varepsilon}$$

$$l = 1, \quad h = 2$$

$$\phi_{39d} = -1$$

$$p_{39d} = P(\beta \mid \gamma \mid \varepsilon) P(u \mid vw)$$



$$d_{39e} = \sum_{ijab} \langle ij || ab \rangle t_{ij}^{\beta \gamma} t_u^a t_{vw}^{b \varepsilon}$$

$$h = 2, \quad c_h = 2$$

$$\phi_{39e} = \frac{1}{2}$$

$$p_{39e} = P(\beta \gamma \mid \varepsilon) P(u \mid vw)$$

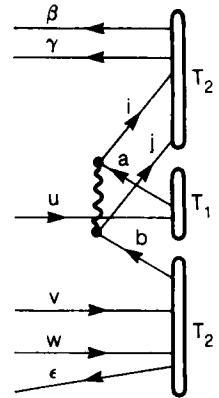


TABLE I (Continued)

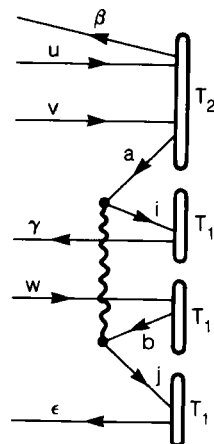
$$[40] = \langle \beta \gamma \epsilon | \left\{ H_2 \frac{1}{3!} T_2 T_1^3 \right\}_C | \Phi_0 \rangle$$

$$d_{40a} = \sum_{ijab} \langle ij || ab \rangle t_{uv}^{\beta a} t_i^{\gamma} t_w^b t_j^{\epsilon}$$

$$h = 2$$

$$\phi_{40a} = 1$$

$$p_{40a} = P(\beta \mid \gamma \epsilon) P(uv \mid w)$$

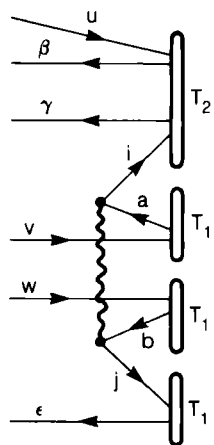


$$d_{40b} = \sum_{ijab} \langle ij || ab \rangle t_{ui}^{\beta \gamma} t_v^a t_w^b t_j^{\epsilon}$$

$$h = 2$$

$$\phi_{40b} = 1$$

$$p_{40b} = P(\beta \gamma \mid \epsilon) P(u \mid vw)$$



VI. Final Equations

The expressions for the matrix elements obtained in the preceding section, together with Eqs. (80)–(83), enable us to write implicit equations determining the cluster coefficients and the correlated energy in terms of the cluster coefficients and the one- and two-electron integrals over the spin-orbital basis. We may write Eq. (80), the projection of the Schrödinger equation for the CCSDT wave function on the singly excited space, as

$$0 = \sum_{m=4}^{13} [m] \quad (104)$$

Similarly Eq. (81), the projection on the doubly excited space, can be written

$$0 = \sum_{m=14}^{27} [m] \quad (105)$$

and Eq. (82), the projection on the triply excited space, can be written as

$$0 = \sum_{m=28}^{40} [m] \quad (106)$$

The equation for the correlated energy [Eq. (83)] may similarly be written as

$$\Delta E = \sum_{m=1}^3 [m] \quad (107)$$

where $[m]$, the symbol for a possibly nonvanishing matrix element, is related to entries in Table I by Eq. (103). The preceding equations are, however, of dubious computational value: Practical random access is restricted by the size of core memory, and sequential access is limited by the size of disk storage. For small polyatomic molecules, these limits translate to $O(n^2)$ and $O(n^3)$ matrices, respectively, where n is the dimension of the binary direct product space of spin-orbitals, i.e., $n = (\text{number of spin-orbitals})^2$. We will show that the judicious choice of the order in which cluster coefficients and integrals are combined in a multiple product (i.e., the “vertical” factorization³) results in a procedure that satisfies the preceding computational constraints at all stages.

Individual cluster coefficients, as well as integrals, cannot in general be freely reordered in expressions for matrix elements. In particular, the rearrangement of coefficients can be seen to correspond to a topological deformation of a diagram that alters the sequence of topologically distinct

environments (cf. Rule 4); it is hardly surprising that the permutation operator, which is partially defined by the sequence, must reflect the change. To examine the specific effect of rearrangement, let $f(x_i)$ and $g(x_i)$ be arbitrary single-index functions, which may, however, depend parametrically on other variables, and let $P(x_1 | x_2)$ be the single-index set permutation operator defined in Eq. (98); then

$$P(x_1 | x_2)f(x_1)g(x_2) = f(x_1)g(x_2) - f(x_2)g(x_1) \quad (108)$$

$$= g(x_2)f(x_1) - g(x_1)f(x_2) \quad (109)$$

$$= P(x_2 | x_1)g(x_2)f(x_1) \quad (110)$$

$$= P(x_2 | x_1)g(x_1)f(x_2) \quad (111)$$

Equation (111) can be obtained from Eq. (110) because the action of the permutation operator renders the argument index set dummy. Consider next the permutation operator $P(x_1x_2 | x_3)$, defined in Eq. (99), and let $h(x_1, x_2)$ be an arbitrary, antisymmetrized two-index function; then

$$P(x_1x_2 | x_3)h(x_1, x_2)g(x_3) \\ = h(x_1, x_2)g(x_3) - h(x_3, x_2)g(x_1) - h(x_1, x_3)g(x_2) \quad (112)$$

$$= g(x_3)h(x_1, x_2) - g(x_1)h(x_3, x_2) - g(x_2)h(x_1, x_3) \quad (113)$$

$$= P(x_3 | x_1x_2)g(x_1)h(x_2, x_3) \quad (114)$$

Note that $P(x_3 | x_1x_2)$ is the single-index set permutation operator defined in Eq. (100).

A complication arising through the switching of coefficients and the necessary corresponding switching of permutation operators is the generation of permutation operators with noncanonical index lists [e.g., if x_1, x_2, x_3 in Eq. (112) represents a canonical list, then x_3, x_1, x_2 in Eq. (114) certainly cannot]. Hence, we must examine the symmetry properties of the permutation operators. As before let us first consider the simplest single-index set permutation operator, $P(x_1 | x_2)$;

$$P(x_2 | x_1)f(x_1)g(x_2) = f(x_2)g(x_1) - f(x_1)g(x_2) \quad (115)$$

$$= -\{-f(x_2)g(x_1) + f(x_1)g(x_2)\} \quad (116)$$

$$P(x_2 | x_1)f(x_1)g(x_2) = -P(x_1 | x_2)f(x_1)g(x_2) \quad (117)$$

i.e., functionally,

$$P(x_2 | x_1) = -P(x_1 | x_2) \quad (118)$$

Next, consider the permutation operator $P(x_1x_2 | x_3)$. One can imagine two kinds of permutations: within a topologically distinct region and be-

tween topologically distinct regions. We now examine the first kind:

$$P(x_2x_1 \mid x_3)h(x_1, x_2)g(x_3) \\ = h(x_2, x_1)g(x_3) - h(x_3, x_1)g(x_2) - h(x_2, x_3)g(x_1) \quad (119)$$

$$= -\{-h(x_2, x_1)g(x_3) + h(x_3, x_1)g(x_2) + h(x_2, x_3)g(x_1)\} \quad (120)$$

$$= -\{h(x_1, x_2)g(x_3) - h(x_1, x_3)g(x_2) - h(x_3, x_2)g(x_1)\} \quad (121)$$

$$= -P(x_1x_2 \mid x_3)h(x_1, x_2)g(x_3) \quad (122)$$

i.e., functionally,

$$P(x_2x_1 \mid x_3) = -P(x_1x_2 \mid x_3) \quad (123)$$

Equation (121) was obtained from Eq. (120) by use of the antisymmetry of the test function h . Now let us consider the permutation of indices between topologically distinct regions:

$$P(x_1x_3 \mid x_2)h(x_1, x_2)g(x_3) \\ = h(x_1, x_3)g(x_2) - h(x_2, x_3)g(x_1) - h(x_1, x_2)g(x_3) \quad (124)$$

$$= -\{-h(x_1, x_3)g(x_2) + h(x_2, x_3)g(x_1) + h(x_1, x_2)g(x_3)\} \quad (125)$$

$$= -\{-h(x_1, x_3)g(x_2) - h(x_3, x_2)g(x_1) + h(x_1, x_2)g(x_3)\} \quad (126)$$

$$= -P(x_1x_2 \mid x_3)h(x_1, x_2)g(x_3) \quad (127)$$

i.e., functionally,

$$P(x_1x_3 \mid x_2) = -P(x_1x_2 \mid x_3) \quad (128)$$

The symmetry properties of the permutation operator $P(x_1 \mid x_2x_3)$ need not be separately considered in light of the relation between $P(x_1 \mid x_2x_3)$ and $P(x_1x_2 \mid x_3)$ [cf. Eq. (114)]. The remaining permutation operator used in Table I but thus far not discussed in this section is $P(x_1 \mid x_2 \mid x_3)$, defined in Eq. (102). We now show that $P(x_1 \mid x_2 \mid x_3)$ is the composite of two single-index set permutation operators already examined. In addition to f and g , let $k(x_i)$ be an arbitrary single-index function, which may depend parametrically on other variables; then

$$P(x_1x_2 \mid x_3)P(x_1 \mid x_2)f(x_1)g(x_2)k(x_3) \\ = P(x_1x_2 \mid x_3)\{f(x_1)g(x_2) - f(x_2)g(x_1)\}k(x_3) \quad (129)$$

$$= \{f(x_1)g(x_2) - f(x_2)g(x_1)\}k(x_3) \\ - \{f(x_3)g(x_2) - f(x_2)g(x_3)\}k(x_1) \\ - \{f(x_1)g(x_3) - f(x_3)g(x_1)\}k(x_2) \quad (130)$$

$$\begin{aligned}
&= f(x_1)g(x_2)k(x_3) - f(x_2)g(x_1)k(x_3) \\
&\quad - f(x_3)g(x_2)k(x_1) - f(x_1)g(x_3)k(x_2) \\
&\quad + f(x_2)g(x_3)k(x_1) + f(x_3)g(x_1)k(x_2)
\end{aligned} \tag{131}$$

$$= P(x_1 | x_2 | x_3) f(x_1)g(x_2)k(x_3) \tag{132}$$

i.e., functionally,

$$P(x_1x_2 | x_3)P(x_1 | x_2) = P(x_1 | x_2 | x_3) \tag{133}$$

Hence the symmetry and argument exchange properties of $P(x_1 | x_2 | x_3)$ can be understood in terms of the already-examined permutation operators $P(x_1x_2 | x_3)$ and $P(x_1 | x_2)$.

We have shown that although the cluster coefficients and the integrals do not in general commute, the commutation relations can be understood in terms of changes in the permutation operator. Furthermore, the symmetry properties of the permutation operators found in a CCSDT model have been characterized. The symmetry properties enable a canonical ordering of (external) indices regardless of the ordering of the cluster coefficients and integrals.

We now show that the projection of the Schrödinger equation for the CCSDT wave function on the triply excited space [cf. Eq. (106)] can be written in terms of (at worst) products of unmodified rank 3 cluster coefficients and modified rank 2 integrals. Tensor notation with repeated index summation convention will be used, except, of course, for the permutation operator.

Consider breaking the sum in Eq. (106) into eight parts, designated by roman numerals,

$$[I] = [28a] + [29b] + [34f] + [37g] + [38b] \tag{134}$$

$$[II] = [28b] + [29a] + [34e] + [37f] + [38a] \tag{135}$$

$$[III] = [32a] + [34a] + [34c] + [37c] + [38c] \tag{136}$$

$$[IV] = [32b] + [34d] + [37d] + [38e] \tag{137}$$

$$[V] = [32c] + [34b] + [37e] + [38d] \tag{138}$$

$$[VI] = [30] + [39a] \tag{139}$$

$$\begin{aligned}
[VII] &= [31b] + [33b] + [33c] + [35b] + [36b] + [35c] \\
&\quad + [36d] + [37a] + [39c] + [39b] + [40b]
\end{aligned} \tag{140}$$

$$\begin{aligned}
[VIII] &= [31a] + [33a] + [33d] + [35a] + [36c] + [35d] \\
&\quad + [36a] + [37b] + [39d] + [39e] + [40a]
\end{aligned} \tag{141}$$

Let us examine each of these partial sums in turn:

$$[I] = -P(u | vw) f_u^i t_{uvw}^{\beta\gamma\epsilon} - f_a^i P(uv | w) t_{uvi}^{\beta\gamma\epsilon} t_w^a - P(u | vw) v_{ua}^{ij} t_{vwi}^{\beta\gamma\epsilon} t_j^a \\ + v_{ab}^{ij} P(uv | w) \{ \frac{1}{2} t_{uvi}^{\beta\gamma\epsilon} t_{jw}^{ab} + t_{uvi}^{\beta\gamma\epsilon} t_j^a t_w^b \} \quad (142)$$

where $v_{ab}^{ij} = \langle ij || ab \rangle$. Equation (142) can be rewritten

$$[I] = P(uv | w) t_{uvi}^{\beta\gamma\epsilon} \{ -f_w^i - (ft_1)_{aw}^{ia} - (vt_1)_{waj}^{ija} + (vt_2)_{abjw}^{ijab} \} \quad (144)$$

where $t_2' = \frac{1}{2} t_2 + t_1 t_1$. The ambiguity in removing paired indices, when multiple pairs exist, can be eliminated if we adopt the convention that the first covariant summation index is implicitly paired with the first possible contravariant summation index, etc. [N.B.: The cluster coefficients and the integrals are irreducible tensors of the appropriate rank (cf. Section II) and contractions between different cluster operators also cannot occur (cf. Section IV).] It should also be noted that the ranges of the contractions are preserved by the tensor notation since covariant indices of cluster coefficients must be elements of the Fermi sea and contravariant indices cannot be elements of the Fermi sea. Then

$$[I] = P(uv | w) t_{uvi}^{\beta\gamma\epsilon} (f^{(3)})_w^i \quad (146)$$

where the modified one-electron integral $(f^{(3)})_w^i$ is defined as

$$(f^{(3)})_w^i = -f_w^i - (ft_1)_w^i - (vt_1)_w^i + (vt_2')_{..w}^i \quad (147)$$

Similarly, the second partial sum

$$[II] = P(\beta | \gamma\epsilon) f_a^{\beta} t_{uvw}^{\alpha\gamma\epsilon} - f_a^i P(\beta\gamma | \epsilon) t_{uvw}^{\beta\gamma a} t_i^\epsilon + P(\beta | \gamma\epsilon) v_{ab}^{\beta i} t_{uvw}^{\gamma\epsilon a} t_i^b \\ + v_{ab}^{ij} P(\beta\gamma | \epsilon) \{ \frac{1}{2} t_{uvw}^{\beta\gamma a} t_{ij}^{be} + t_{uvw}^{\beta\gamma a} t_i^b t_j^\epsilon \} \quad (148)$$

becomes

$$[II] = P(\beta\gamma | \epsilon) t_{uvw}^{\beta\gamma a} (f^{(3)})_a^\epsilon \quad (149)$$

where

$$(f^{(3)})_a^\epsilon = f_a^\epsilon - (ft_1)_a^\epsilon + (vt_1)_a^\epsilon + (vt_2')_{a..}^\epsilon \quad (150)$$

The third partial sum is

$$[III] = -P(\beta | \gamma\epsilon) P(u | vw) v_{au}^{\beta i} t_{vwi}^{\gamma\epsilon a} + P(\beta\gamma | \epsilon) P(u | vw) v_{ua}^{ij} t_{vwi}^{\beta\gamma a} t_j^\epsilon \\ - P(\beta | \gamma\epsilon) P(uv | w) v_{ab}^{\beta i} t_{uvi}^{\gamma\epsilon a} t_w^b + v_{ab}^{ij} P(\beta\gamma | \epsilon) P(uv | w) t_{uij}^{\beta\gamma a} t_w^{be} \\ + v_{ab}^{ij} P(\beta\gamma | \epsilon) P(uv | w) t_{uij}^{\beta\gamma a} t_i^\epsilon t_w^b \quad (151)$$

and can be written

$$[III] = P(\beta\gamma | \epsilon) P(uv | w) t_{uvi}^{\beta\gamma a} (v^{(3)})_{aw}^{ei} \quad (152)$$

with the modified two-electron integral

$$(v^{(3)})_{aw}^{ei} = -v_{aw}^{ei} + (vt_1)_{wa}^i \varepsilon - (vt_1)_{aw}^{ei} + (vt_2)_{aw}^i \varepsilon + (vt_1 t_1)_{aw}^{ie} \quad (153)$$

Note that the required inner multiplication of the three-tensor product $(vt_1 t_1)$ is rank 2 at all stages; i.e.,

$$(vt_1 t_1)_{aw}^{ie} = (vt_1)_{ab}^{ie} t_w^b \quad (154)$$

The fourth partial sum is

$$\begin{aligned} [\text{IV}] = & \frac{1}{2} P(uv | w) v_{uv}^{ij} t_{wij}^{\beta\gamma\varepsilon} - \frac{1}{2} P(u | v | w) v_{ua}^{ij} t_{vij}^{\beta\gamma\varepsilon} t_w^a \\ & + \frac{1}{2} v_{ab}^{ij} P(u | vw) t_{uij}^{\beta\gamma\varepsilon} (\frac{1}{2} t_{vw}^{ab} + t_v^a t_w^b) \end{aligned} \quad (155)$$

which gives

$$[\text{IV}] = \frac{1}{2} P(u | vw) t_{uij}^{\beta\gamma\varepsilon} (v^{(3)})_{vw}^{ij} \quad (156)$$

with the modified two-electron integral

$$(v^{(3)})_{vw}^{ij} = v_{vw}^{ij} + P(v | w) (vt_1)_{vw}^{ij} + (vt_2')_{vw}^{ij} \quad (157)$$

Similarly the fifth partial sum

$$\begin{aligned} [\text{V}] = & \frac{1}{2} P(\beta\gamma | \varepsilon) v_{ab}^{\beta\gamma} t_{uvw}^{\varepsilon ab} + \frac{1}{2} P(\beta | \gamma | \varepsilon) v_{ab}^{\beta i} t_{uvw}^{\gamma ab} t_i^\varepsilon \\ & + \frac{1}{2} v_{ab}^{ij} P(\beta | \gamma\varepsilon) t_{uvw}^{\beta ab} \{ \frac{1}{2} t_{ij}^{\gamma\varepsilon} + t_i^\gamma t_j^\varepsilon \} \end{aligned} \quad (158)$$

can be written as

$$[\text{V}] = \frac{1}{2} P(\beta | \gamma\varepsilon) t_{uvw}^{\beta ab} (v^{(3)})_{ab}^{\gamma\varepsilon} \quad (159)$$

with

$$(v^{(3)})_{ab}^{\gamma\varepsilon} = v_{ab}^{\gamma\varepsilon} - P(\gamma | \varepsilon) (vt_1)_{ab}^{\gamma\varepsilon} + (vt_2')_{ab}^{\gamma\varepsilon} \quad (160)$$

The sixth partial sum is

$$[\text{VI}] = -f_a^i P(\beta | \gamma\varepsilon) P(uv | w) t_{uv}^{\beta a} t_{iw}^{\gamma\varepsilon} + v_{ab}^{ij} P(\beta | \gamma\varepsilon) P(uv | w) t_{uv}^{\beta a} t_i^b t_{jw}^{\gamma\varepsilon} \quad (161)$$

Although a more symmetric formulation is possible, the following suffices:

$$[\text{VI}] = P(\beta\gamma | \varepsilon) P(u | vw) t_{ui}^{\beta\gamma} (v^{(3')})_{vw}^{ie} \quad (162)$$

with

$$(v^{(3')})_{vw}^{ie} = (ft_2)_{vw}^{ie} + (vt_1 t_2)_{vw}^{i\varepsilon} \quad (163)$$

The required inner multiplication of the three-tensor product $(vt_1 t_2)$ is rank 2 or less at all stages; i.e.,

$$(vt_1 t_2)_{vw}^{i\varepsilon} = (vt_1)_a^i t_{vw}^{\varepsilon a} \quad (164)$$

The seventh partial sum is

$$\begin{aligned}
 [\text{VII}] = & -P(\beta \mid \gamma \varepsilon)P(uv \mid w)v_{uv}^{i\beta}t_{wi}^{\gamma\varepsilon} + P(\beta \mid \gamma \varepsilon)P(u \mid v \mid w)v_{au}^{\beta i}t_{vi}^{\gamma\varepsilon}t_w^a \\
 & + P(\beta \gamma \mid \varepsilon)P(uv \mid w)v_{uv}^{ij}t_{wi}^{\beta\gamma}t_j^\varepsilon + P(\beta \gamma \mid \varepsilon)P(u \mid v \mid w)v_{ua}^{ij}t_{vi}^{\beta\gamma}t_{jw}^{a\varepsilon} \\
 & - P(\beta \gamma \mid \varepsilon)P(u \mid v \mid w)v_{ua}^{ij}t_{vi}^{\beta\gamma}t_w^a t_j^\varepsilon \\
 & + P(\beta \mid \gamma \varepsilon)P(u \mid vw)v_{ab}^{\beta i}t_{ui}^{\gamma\varepsilon}\{\frac{1}{2}t_{vw}^{ab} + t_v^a t_w^b\} \\
 & + \frac{1}{2}v_{ab}^{ib}P(\beta \mid \gamma \varepsilon)P(uv \mid w)t_{uvi}^{\beta ab}t_{jw}^{\gamma\varepsilon} \\
 & - v_{ab}^{ij}P(\beta \mid \gamma \varepsilon)P(u \mid v \mid w)t_{ui}^{\beta a}t_v^b t_{jw}^{\gamma\varepsilon} \\
 & + \frac{1}{2}v_{ab}^{ib}P(\beta \mid \gamma \varepsilon)P(uv \mid w)t_{uv}^{ab}t_i^\beta t_{jw}^{\gamma\varepsilon} \\
 & + v_{ab}^{ij}P(\beta \gamma \mid \varepsilon)P(u \mid vw)t_{ui}^{\beta\gamma}t_v^a t_w^b t_j^\varepsilon
 \end{aligned} \tag{165}$$

which can be written as

$$[\text{VII}] = P(\beta \gamma \mid \varepsilon)P(u \mid vw)t_{ui}^{\beta\gamma}(v^{(3)})_{vw}^{i\varepsilon} \tag{166}$$

with

$$\begin{aligned}
 (v^{(3)})_{vw}^{i\varepsilon} = & -v_{vw}^{i\varepsilon} - P(v \mid w)(vt_1)_{vw}^{ei} + (vt_1)_{vw}^i{}^\varepsilon + P(v \mid w)(vt_2)_{v.w}^i{}^\varepsilon \\
 & + P(v \mid w)(vt_1 t_1)_{v.w}^{i\varepsilon} + (vt_2')_{vw}^{ei} - \frac{1}{2}(vt_3)_{vw}^{i\varepsilon} \\
 & + P(v \mid w)(vt_2 t_1)_{v.w}^{i\varepsilon} - (vt_2' t_1)_{vw}^{i\varepsilon}
 \end{aligned} \tag{167}$$

The required inner multiplication of the three-tensor products $(vt_2 t_1)$ and $(vt_2' t_1)$ are rank 2 at all stages; i.e.,

$$(vt_2 t_1)_{v.w}^{i\varepsilon} = (vt_2)_{av}^{i\varepsilon} t_w^a \tag{168}$$

$$(vt_2' t_1)_{vw}^{i\varepsilon} = (vt_2')_{vw}^{ji} t_j^\varepsilon \tag{169}$$

and construction of $(vt_1 t_1)$ was discussed in Eq. (154). Similarly, the eighth partial sum

$$\begin{aligned}
 [\text{VIII}] = & P(\beta \gamma \mid \varepsilon)P(u \mid vw)v_{au}^{\beta\gamma}t_{vw}^{\varepsilon a} + P(\beta \mid \gamma \mid \varepsilon)P(u \mid vw)v_{au}^{\beta i}t_{vw}^{\gamma a}t_i^\varepsilon \\
 & + P(\beta \gamma \mid \varepsilon)P(uv \mid w)v_{ab}^{\beta\gamma}t_{uv}^{\varepsilon a}t_w^b - P(\beta \mid \gamma \mid \varepsilon)P(uv \mid w)v_{ab}^{\beta i}t_{uv}^{\gamma a}t_{iw}^{b\varepsilon} \\
 & + P(\beta \mid \gamma \mid \varepsilon)P(uv \mid w)v_{ab}^{\beta i}t_{uv}^{\gamma a}t_i^\varepsilon t_w^b \\
 & - P(\beta \mid \gamma \varepsilon)P(u \mid vw)v_{ua}^{ij}t_{vw}^{\beta\gamma}\{\frac{1}{2}t_{ij}^{\gamma\varepsilon} + t_i^\gamma t_j^\varepsilon\} \\
 & + \frac{1}{2}v_{ab}^{ij}P(\beta \gamma \mid \varepsilon)P(u \mid vw)t_{uij}^{\beta\gamma a}t_{vw}^{b\varepsilon} \\
 & - v_{ab}^{ij}P(\beta \mid \gamma \mid \varepsilon)P(u \mid vw)t_{ui}^{\beta a}t_j^\gamma t_{vw}^{b\varepsilon} \\
 & + \frac{1}{2}v_{ab}^{ij}P(\beta \gamma \mid \varepsilon)P(u \mid vw)t_{ij}^{\beta\gamma}t_u^a t_{vw}^{b\varepsilon} \\
 & + v_{ab}^{ij}P(\beta \mid \gamma \varepsilon)P(uv \mid w)t_{uv}^{\beta a}t_i^\gamma t_w^b t_j^\varepsilon
 \end{aligned} \tag{170}$$

can be written as

$$[\text{VIII}] = P(\beta \mid \gamma \varepsilon) P(uv \mid w) t_{uv}^{\beta a} (v^{(3)})_{aw}^{\gamma \varepsilon} \quad (171)$$

with

$$\begin{aligned} (v^{(3)})_{aw}^{\gamma \varepsilon} = & v_{aw}^{\gamma \varepsilon} - P(\gamma \mid \varepsilon) (vt_1)_{aw}^{\gamma \varepsilon} + (vt_1)_{aw}^{\gamma \varepsilon} - P(\gamma \mid \varepsilon) (vt_2)_{a \cdot w}^{\gamma \varepsilon} \\ & - P(\gamma \mid \varepsilon) (vt_1 t_1)_{a \cdot w}^{\gamma \varepsilon} - (vt_2')_{wa}^{\gamma \varepsilon} - \frac{1}{2} (vt_3)_{\cdot aw}^{\gamma \varepsilon} \\ & + P(\gamma \mid \varepsilon) (vt_2 t_1)_{\cdot aw}^{\gamma \varepsilon} - (vt_2' t_1)_{\cdot a}^{\gamma \varepsilon} \end{aligned} \quad (172)$$

The required inner multiplications of the three-tensor products $(vt_2 t_1)$ and $(vt_2' t_1)$ are rank 2 at all stages; i.e.,

$$(vt_2 t_1)_{\cdot aw}^{\gamma \varepsilon} = (vt_2)_{\cdot aw}^{j \gamma} t_j^{\varepsilon} \quad (173)$$

$$(vt_2' t_1)_{\cdot a}^{\gamma \varepsilon} = (vt_2')_{ba}^{\gamma \varepsilon} t_b^{\varepsilon} \quad (174)$$

We next show that the projection of the Schrödinger equation for the CCSDT wave function on the doubly excited space can be written in terms of (at worst) products of unmodified rank 3 cluster coefficients and modified rank 2 integrals. We consider breaking the sum in Eq. (105) into eight parts; the first six being

$$[\text{IX}] = [14a] + [16b] + [22b] + [25c] + [26b] \quad (175)$$

$$[\text{X}] = [14b] + [16a] + [22a] + [25d] + [26a] \quad (176)$$

$$[\text{XI}] = [15] + [24a] \quad (177)$$

$$[\text{XII}] = [25a] + [26c] \quad (178)$$

$$[\text{XIII}] = [25b] + [26d] + [26e] + [27] \quad (179)$$

$$\begin{aligned} [\text{XIV}] = & [17] + [18a] + [18b] + [19a] + [19b] + [20c] \\ & + [20a] + [19c] + [20b] + [21a] + [21b] + [22c] \\ & + [22d] + [22e] + [23b] + [22f] + [23a] \end{aligned} \quad (180)$$

the remaining two partial sums are the single diagrams [24b] and [24c]. Aside from satisfying the computational constraints, the partial summations were chosen (1) to expose (double) cluster coefficients one index removed from the $(\beta \gamma)_{uv}$ component of the external space [cf. Eq. (81)] and (2) to utilize tensors already required for the triply excited space. The first consideration facilitates the solution of the coupled-cluster equations by the method of iteration (i.e., successive substitution).^{16,17} The second obviously reduces the computational effort. The appropriate forms of the preceding two considerations were used in the choice of partial summations for the triply excited space and will be used for the singly excited space, although it should be noted that the constraints imposed by rank seriously restricted the options in the triples case.

As before, let us examine each of the partial sums in turn:

$$\begin{aligned}
 [\text{IX}] = & -P(u | v) f_u^i t_{iv}^{\beta\gamma} - P(u | v) f_a^i t_{ui}^{\beta\gamma} t_v^a + P(u | v) v_{ua}^{ij} t_{vi}^{\beta\gamma} t_j^a \\
 & + \frac{1}{2} v_{ab}^{ij} P(u | v) t_{ui}^{\beta\gamma} t_{jv}^{\beta\gamma} + v_{ab}^{ij} P(u | v) t_{ui}^{\beta\gamma} t_j^a t_v^b
 \end{aligned} \quad (181)$$

which can be written

$$[\text{IX}] = P(u | v) t_{ui}^{\beta\gamma} (f^{(2)})_v^i \quad (182)$$

where

$$(f^{(2)})_v^i = -f_v^i - (ft_1)_v^i - (vt_1)_v^i + (vt_2')_{..v}^i \quad (183)$$

Observe that the modified one-electron integral, with both indices from the Fermi sea, for the projection on the doubly excited space $(f^{(2)})_v^i$ is identical with the corresponding integral for the triply excited space $(f^{(3)})_v^i$ [cf. Eq. (147)].

Now let us consider the second partial sum

$$\begin{aligned}
 [\text{X}] = & P(\beta | \gamma) f_a^{\beta} t_{uv}^{a\gamma} - P(\beta | \gamma) f_a^i t_{uv}^{\beta a} t_i^{\gamma} - P(\beta | \gamma) v_{ab}^{\beta i} t_u^{\gamma a} t_i^b \\
 & + \frac{1}{2} v_{ab}^{ij} P(\beta | \gamma) t_{ij}^{\beta a} t_{uv}^{b\gamma} + v_{ab}^{ij} P(\beta | \gamma) t_{uv}^{\beta a} t_i^b t_j^{\gamma}
 \end{aligned} \quad (184)$$

which gives

$$[\text{X}] = P(\beta | \gamma) t_{uv}^{\beta a} (f^{(2)})_a^{\gamma} \quad (185)$$

with

$$(f^{(2)})_a^{\gamma} = f_a^{\gamma} - (ft_1)_a^{\gamma} + (vt_1)_a^{\gamma} + (vt_2')_{a..}^{\gamma} \quad (186)$$

As before, note that $(f^{(2)})_a^{\gamma} = (f^{(3)})_a^{\gamma}$. The third partial sum is

$$[\text{XI}] = f_a^i t_{uvi}^{\beta\gamma a} + v_{ab}^{ij} t_{uvi}^{\beta\gamma a} t_j^b \quad (187)$$

and can be written

$$[\text{XI}] = t_{uvi}^{\beta\gamma a} (f^{(2)})_a^i \quad (188)$$

where

$$(f^{(2)})_a^i = f_a^i + (vt_1)_a^i \quad (189)$$

The fourth partial sum is

$$[\text{XII}] = v_{ab}^{ij} P(\beta | \gamma) t_{ui}^{\beta a} t_{jv}^{b\gamma} - v_{ab}^{ij} P(\beta | \gamma) P(u | v) t_{ui}^{\beta a} t_v^b t_j^{\gamma} \quad (190)$$

or

$$[\text{XII}] = -P(\beta | \gamma) P(u | v) (t_2')_{ui}^{a\beta} (v^{(2)})_{av}^{i\gamma} \quad (191)$$

where

$$(v^{(2)})_{av}^{i\gamma} = (vt_2)_{av}^{i\gamma} \quad (192)$$

Similarly, the fifth partial sum

$$[\text{XIII}] = \frac{1}{4}v_{ab}^{ij}t_{uv}^{ab}t_{ij}^{\beta\gamma} + \frac{1}{2}v_{ab}^{ij}t_{uv}^{ab}t_i^{\beta}t_j^{\gamma} + \frac{1}{2}v_{ab}^{ij}t_{ij}^{\beta\gamma}t_u^at_v^b + v_{ab}^{ij}t_u^at_i^{\beta}t_v^bt_j^{\gamma} \quad (193)$$

can be written as

$$[\text{XIII}] = (t_2')_{uv}^{ab}(v^{(2)})_{ab}^{\beta\gamma} \quad (194)$$

where

$$(v^{(2)})_{ab}^{\beta\gamma} = (vt_2')_{ab}^{\beta\gamma} \quad (195)$$

The fourth and fifth terms, [XII] and [XIII], are anomalous in that modified cluster coefficients (e.g., rank 2) are used in the final tensor products. The particular modified cluster coefficients involved, t_2' , have already been used in several intermediate tensor products [cf. Eqs. (145), (157), (160), (169), and (174)].

The sixth partial sum is

$$\begin{aligned} [\text{XIV}] = & v_{uv}^{\beta\gamma} - P(\beta | \gamma)v_{uv}^{\beta i}t_i^{\gamma} + P(u | v)v_{ua}^{\beta\gamma}t_v^a - P(\beta | \gamma)P(u | v)v_{au}^{\beta i}t_{iv}^{a\gamma} \\ & + v_{uv}^{ij}\{\frac{1}{2}t_{ij}^{\beta\gamma} + t_i^{\beta}t_j^{\gamma}\} + P(\beta | \gamma)P(u | v)v_{au}^{\beta i}t_v^at_i^{\gamma} + v_{ab}^{\beta\gamma}\{\frac{1}{2}t_{uv}^{ab} + t_u^at_v^b\} \\ & - \frac{1}{2}P(\beta | \gamma)v_{ab}^{\beta i}t_{uvi}^{\gamma ab} + \frac{1}{2}P(u | v)v_{ua}^{ij}t_{vij}^{\beta\gamma a} \\ & + P(\beta | \gamma)P(u | v)v_{au}^{ij}t_{vi}^{\beta a}t_j^{\gamma} \\ & - P(\beta | \gamma)P(u | v)v_{ab}^{i\beta}t_{ui}^{\gamma a}t_v^b - \frac{1}{2}P(\beta | \gamma)v_{ab}^{\beta i}t_{uv}^{\gamma ab}t_i^{\gamma} \\ & + P(\beta | \gamma)v_{ab}^{i\beta}t_u^at_i^{\gamma}t_v^b \\ & + \frac{1}{2}P(u | v)v_{ua}^{ij}t_{ij}^{\beta\gamma}t_v^a - P(u | v)v_{au}^{ij}t_v^at_i^{\beta}t_j^{\gamma} \end{aligned} \quad (196)$$

which can be rewritten as

$$\begin{aligned} [\text{XIV}] = & (v^{(2)})_{uv}^{\beta\gamma} \\ = & v_{uv}^{\beta\gamma} - P(\beta | \gamma)(vt_1)_{uv}^{\beta\gamma} + P(u | v)(vt_1)_{uv}^{\beta\gamma} \\ & - P(\beta | \gamma)P(u | v)(vt_2)_{uv}^{\beta\gamma} \\ & + (vt_2')_{uv}^{\beta\gamma} + P(\beta | \gamma)P(u | v)(vt_1t_1)_{uv}^{\beta\gamma} + (vt_2')_{uv}^{\beta\gamma} \\ & - \frac{1}{2}P(\beta | \gamma)(vt_3)_{uv}^{\beta\gamma} + \frac{1}{2}P(u | v)(vt_3)_{uv}^{\beta\gamma} \\ & + P(\beta | \gamma)P(u | v)(vt_2t_1)_{uv}^{\beta\gamma} - P(\beta | \gamma)P(u | v)(vt_2t_1)_{uv}^{\beta\gamma} \\ & - P(\beta | \gamma)(vt_2't_1)_{uv}^{\beta\gamma} + P(u | v)(vt_2't_1)_{uv}^{\beta\gamma} \end{aligned} \quad (198)$$

Three-tensor products were previously considered in Eqs. (154), (168), (169), (173), and (174).

The seventh partial sum consists of only one term, which may be written

$$[24b] = \frac{1}{2}P(\beta | \gamma)t_i^\beta(v^{(2)})_{uv}^{i\gamma} \quad (199)$$

with

$$(v^{(2)})_{uv}^{i\gamma} = (vt_3)_{uv}^{i\gamma} \quad (200)$$

Likewise, the eighth partial sum may be written as

$$[24c] = \frac{1}{2}P(u | v)t_u^a(v^{(2)})_{av}^{\beta\gamma} \quad (201)$$

with

$$(v^{(2)})_{av}^{\beta\gamma} = (vt_3)_{a-v}^{\beta\gamma} \quad (202)$$

We next show that the projection on the singly excited space can be written in terms of (at worst) products of unmodified rank 3 cluster coefficients and modified rank 2 integrals. We consider breaking the sum in Eq. (104) into four parts:

$$[XV] = [5a] + [7] + [10a] + [12b] + [13] \quad (203)$$

$$[XVI] = [5b] + [7] + [10b] + [12c] + [13] \quad (204)$$

$$[XVII] = [4] + [6] + [8] + [9a] + [9b] + [11] + [12a] \quad (205)$$

$$[XVIII] = -[7] - [13] \quad (206)$$

We have added to and subtracted from the sum in order to use the same modified one-electron integrals for the projection on the singly excited space as for the doubly and triply excited spaces [cf. the text following Eqs. (183) and (186)]. Let us consider each of the partial sums in turn:

$$[XV] = -f_u^i t_i^\beta - f_a^i t_u^a t_i^\beta - v_{ua}^{ij} t_i^\beta t_j^a - \frac{1}{2} v_{ab}^{ij} t_{ij}^{ab} t_i^\beta - v_{ab}^{ij} t_u^b t_i^a t_j^\beta \quad (207)$$

which can be written

$$[XV] = t_i^\beta (f^{(1)})_u^i \quad (208)$$

where

$$(f^{(1)})_u^i = -f_u^i - (ft_1)_u^i - (vt_1)_u^i + (vt_2')_{..u}^i \quad (209)$$

Comparison with Eqs. (147) and (183) shows that the same modified one-electron integrals, with both indices from the Fermi sea, can be used for all projections; i.e.,

$$(f')_u^i = (f^{(1)})_u^i = (f^{(2)})_u^i = (f^{(3)})_u^i \quad (210)$$

Similarly, for the second partial sum,

$$[\text{XVI}] = f_a^\beta t_u^a - f_a^i t_u^a t_i^\beta + v_{ab}^{i\beta} t_i^a t_u^b - \frac{1}{2} v_{ab}^{ij} t_{ij}^{\beta b} t_u^a - v_{ab}^{ij} t_u^b t_i^a t_j^\beta \quad (211)$$

or

$$[\text{XVI}] = t_u^a (f^{(1)})_a^\beta \quad (212)$$

where

$$(f^{(1)})_a^\beta = f_a^\beta - (ft_1)_a^\beta + (vt_1)_a^\beta + (vt_2')_a^{\beta\beta} \quad (213)$$

As before, comparison with the modified one-electron integrals for the doubly and triply excited spaces [Eqs. (150) and (186)] gives

$$(f')_a^\beta = (f^{(1)})_a^\beta = (f^{(2)})_a^\beta = (f^{(3)})_a^\beta \quad (214)$$

The third partial sum

$$\begin{aligned} [\text{XVII}] = & f_u^\beta + f_a^i t_{ui}^{\beta a} - v_{au}^{\beta i} t_i^a - \frac{1}{2} v_{ua}^{ij} t_{ij}^{\beta a} + \frac{1}{2} v_{ab}^{\beta i} t_{ui}^{ab} \\ & + \frac{1}{4} v_{ab}^{ij} t_{uij}^{\beta ab} + v_{ab}^{ij} t_{ui}^{\beta a} t_j^b \end{aligned} \quad (215)$$

can be written as

$$[\text{XVII}] = (f^{(1)})_u^\beta \quad (216)$$

$$\begin{aligned} = & f_u^\beta - (ft_2)_u^\beta - (vt_1)_u^\beta - \frac{1}{2} (vt_2)_u^{\beta\beta} + \frac{1}{2} (vt_2)_u^\beta \\ & + \frac{1}{4} (vt_3)_{..u}^\beta + (vt_2 t_1)_{..u}^\beta \end{aligned} \quad (217)$$

The fourth partial sum, which compensates for the added terms, is

$$[\text{XVIII}] = f_a^i t_u^a t_i^\beta + v_{ab}^{ij} t_u^b t_i^a t_j^\beta \quad (218)$$

which we can rewrite as

$$[\text{XVIII}] = t_i^\beta (f^{(1')})_i^i \quad (219)$$

where

$$(f^{(1')})_u^i = (ft_1)_u^i - (vt_1 t_1)_{..u}^i \quad (220)$$

Finally, the projection of the Schrödinger equation for the CCSDT wave function on the reference determinant [Eq. (107)] may be written as

$$\Delta E = f_a^i t_u^a + \frac{1}{4} v_{ab}^{ij} t_{ij}^{ab} + \frac{1}{2} v_{ab}^{ij} t_i^a t_j^b \quad (221)$$

Hence the correlated energy can be expressed in terms of contractions of modified one- and two-electron integrals

$$\Delta E = (ft_1) + \frac{1}{2} (vt_2') \quad (222)$$

VII. Discussion and Conclusions

The algebraic expressions obtained from a diagrammatic evaluation of the coupled-cluster equations for a CCSDT model are resolvable into products of unmodified cluster coefficients (or trivially modified in the case of t'_2) and modified one- and two-electron integrals. At no stage of the calculation are tensors of rank greater than 2 required, except for the initial contraction and final expansion of the rank 3 triples cluster coefficients.

The coupled-cluster equations for a CCSDT model are linear in the triples coefficients, even though the wave operator is full with respect to the logarithmic wave operator truncated at rank 3. This suggests that a single sequential pass of the triples cluster coefficients suffices for each iteration. The algorithm for the determination of the cluster coefficients would appear to be divisible into three parts: construction of the modified integrals [except $(v t_3)$], list-directed multiplication of the triples coefficients and the modified integrals, and final contraction with t_1 , t_2 , and t'_2 . The final forms of the coupled-cluster equations derived in the preceding section are eminently compatible with this algorithm.

A key aspect in the implementation of a full coupled-cluster method is the rearrangement of the cluster equations to enable a solution by the method of iteration or successive substitution. As discussed by Purvis and Bartlett in their paper¹⁶ on a full coupled-cluster method including single and double excitations (CCSD), a convergent solution can usually be obtained by casting the equations in a form reminiscent of perturbation theory (i.e., factor the appropriate diagonal elements of the Fock matrix). The analogous rearrangement from implicit to iterative forms can be done for the cluster equations in the CCSDT model presented in the preceding section.

An interesting variant iterative scheme is motivated by the near invariance of the intraset modified one-electron integrals to external space excitation level in the cluster equations. Consider that the cluster equations for arbitrary external space rank r (>0) may be written as

$$0 = P(u_1 \dots u_{r-1} | u_r) t_{u_1 \dots u_{r-1} i}^{\beta_1 \dots \beta_r} (f')^i_{u_r} \\ + P(\beta_1 \dots \beta_{r-1} | \beta_r) t_{u_1 \dots u_r}^{\beta_1 \dots \beta_{r-1} a} (f')^{\beta_r}_a + R_r, \quad (223)$$

where P is the single-index set permutation operator, R_r represents terms that are currently not of interest, f' is an intraset modified one-electron integral, and the repeated index summation convention is used with the appropriate modification (cf. Section IV) when an argument of the permutation operator is involved. Equation (223) may be rewritten

$$\begin{aligned}
& -P(u_1 \dots u_{r-1} | u_r) t_{u_1 \dots u_r}^{\beta_1 \dots \beta_r}(f')_{u_r}^{u_r} - P(\beta_1 \dots \beta_{r-1} | \beta_r) t_{u_1 \dots u_r}^{\beta_1 \dots \beta_r}(f')_{\beta_r}^{\beta_r} \\
& = P(u_1 \dots u_{r-1} | u_r) \{ t_{u_1 \dots u_{r-1}}^{\beta_1 \dots \beta_r}(f')_{u_r}^i - t_{u_1 \dots u_r}^{\beta_1 \dots \beta_r}(f')_{u_r}^{u_r} \} \\
& + P(\beta_1 \dots \beta_{r-1} | \beta_r) \{ t_{u_1 \dots u_r}^{\beta_1 \dots \beta_{r-1} a}(f')_a^{\beta_r} - t_{u_1 \dots u_r}^{\beta_1 \dots \beta_r}(f')_{\beta_r}^{\beta_r} \} + R_r \quad (224)
\end{aligned}$$

Then consideration of the action of a permutation operator on an already antisymmetric tensor allows us to obtain

$$\begin{aligned}
t_{u_1 \dots u_r}^{\beta_1 \dots \beta_r} &= \frac{-1}{(f')_p} \{ P(u_1 \dots u_{r-1} | u_r) t_{u_1 \dots u_{r-1} i'}^{\beta_1 \dots \beta_r}(f')_{u_r}^{i'} \\
&+ P(\beta_1 \dots \beta_{r-1} | \beta_r) t_{u_1 \dots u_r}^{\beta_1 \dots \beta_{r-1} a'}(f')_{a'}^{\beta_r} + R_r \} \quad (225)
\end{aligned}$$

as iterative forms of the coupled-cluster equations. In Eq. (225), the index sets are given by $p \in \{u_1, \dots, u_r, \beta_1, \dots, \beta_r\}$, $i' \in \{\bar{u}_j\} \wedge \{FS\}$, and $a' \in \{\bar{\beta}_j\} \wedge \{\bar{FS}\}$. We have just shown that a modification to the final (implicit) equations to obtain iterative equations in a CCSDT model can be found that localizes changes to the contractions of the intraset modified one-electron integrals and the appropriate cluster coefficients. Specifically, unrestricted sums in Eqs. (146), (149), (182), (185), (208), and (212) are replaced by the appropriate restricted sums. It must be emphasized that the conclusions concerning algorithm structure and required tensor ranks are equally valid for the iterative and implicit forms of the final coupled-cluster equations.

The CCSDT model has been shown not to make excessive demands on either the core memory or the disk memory of modern computers when applied to small polyatomic molecules. A complementary concern in assessing the potential usefulness of the method is the central processing unit (CPU) requirement relative to other techniques in computational chemistry. The bulwark methods, configuration interaction including all single and double excitations (CISD) and fourth-order perturbation theory (PT4), have computational complexities of $O(m^6)$ and $O(m^7)$, respectively, where m is the number of orbitals. Including triples in the CI wave function increases the algorithm to $O(m^8)$, quadruples to $O(m^{10})$, etc. The portions of MCSCF calculations dealing with the orbital rotations are $O(m^6)$; hence, the overall order of an MCSCF procedure is the same as the order of the corresponding configuration interaction calculation. The computational complexity of the CCSDT model, as presented in this work, is easily found to be $O(m^8)$; that of the CCSD model is $O(m^6)$. Since the CCSDT model includes all (connected) single, double, and triple excitations and the dominant (connected) quadruple and quintuple excitations, it ought to be compared in reliability with CISDTQQ. Hence, the CCSDT model appears to be a computationally viable, size-extensive method for the very high level description of electron correlation, at an only moderately high cost.

ACKNOWLEDGMENTS

This work was supported by the Director, Office of Energy Research, Office of Basic Energy Sciences, Chemical Sciences Division of the U.S. Department of Energy under Contract No. DE-AC03-76SF00098. We would like to thank Prof. R. J. Bartlett of the University of Florida for his useful comments on this manuscript.

REFERENCES

1. H. F. Schaefer, "Quantum Chemistry." Clarendon, Oxford, 1984.
2. R. J. Bartlett, *Ann. Rev. Phys. Chem.* **32**, 359 (1981).
3. R. J. Bartlett, C. E. Dykstra, and J. Paldus, In "Advanced Theories and Computational Approaches to the Electronic Structure of Molecules," pp. 127-159 (C. E. Dykstra, ed.). Reidel, Dordrecht, 1984.
4. F. Coester, *Nucl. Phys.* **7**, 421 (1958); F. Coester and H. Kümmel, *Nucl. Phys.* **17**, 477 (1960); H. Kümmel, *Nucl. Phys.* **22**, 177 (1961).
5. J. Cizek, *J. Chem. Phys.* **45**, 4256 (1966); J. Cizek, *Adv. Chem. Phys.* **14**, 35 (1969).
6. J. Paldus, J. Cizek, and I. Shavitt, *Phys. Rev. A* **5**, 50 (1972).
7. P.-O. Löwdin, *Adv. Chem. Phys.* **14**, 283 (1969).
8. R. J. Bartlett and G. D. Purvis, *Int. J. Quantum Chem.* **14**, 561 (1978).
9. R. J. Bartlett and G. D. Purvis, *Phys. Scripta* **21**, 255 (1980).
10. J. Goldstone, *Proc. Phys. Soc. (London)* **A239**, 267 (1957).
11. J. Cizek, J. Paldus, and J. Sroubkova, *Int. J. Quantum Chem.* **3**, 149 (1969).
12. J. Paldus, *J. Chem. Phys.* **67**, 303 (1977).
13. R. J. Bartlett, I. Shavitt, and G. D. Purvis, *J. Chem. Phys.* **71**, 281 (1979).
14. J. A. Pople, R. Krishnan, H. B. Schlegel, and J. S. Binkley, *Int. J. Quantum Chem.* **14**, 545 (1978).
15. G. D. Purvis and R. J. Bartlett, *J. Chem. Phys.* **71**, 548 (1979).
16. G. D. Purvis and R. J. Bartlett, *J. Chem. Phys.* **76**, 1910 (1982).
17. V. Kvasnicka, *Phys. Rev. A* **25**, 671 (1982).
18. B. G. Adams and J. Paldus, *Phys. Rev. A* **20**, 1 (1979).
19. R. Krishnan, M. J. Frisch, and J. A. Pople, *J. Chem. Phys.* **72**, 4244 (1980).
20. M. J. Frisch, R. Krishnan, and J. A. Pople, *Chem. Phys. Lett.* **75**, 66 (1980).
21. G. D. Purvis and R. J. Bartlett, *J. Chem. Phys.* **75**, 1284 (1981).
22. A. Banerjee and J. Simons, *J. Chem. Phys.* **76**, 4548 (1982).
23. Y. S. Lee and R. J. Bartlett, *J. Chem. Phys.* **80**, 4371 (1984).
24. Y. S. Lee, S. K. Kucharski, and R. J. Bartlett, *J. Chem. Phys.* **81**, 5906 (1984).
25. H. Kümmel, K. H. Lührmann, and J. G. Zabolitzky, *Phys. Rep.* **36**, 1 (1978).
26. W. D. Laidig and R. J. Bartlett, *Chem. Phys. Lett.* **104**, 424 (1984).
27. J. Paldus and J. Cizek, *Adv. Quantum Chem.* **9**, 105 (1975).
28. N. N. Bogoliubov and D. V. Shirkov, "Introduction to the Theory of Quantized Fields." Nauka Press, Moscow, 1957 [Engl. transl., Wiley (Interscience), New York, 1959].
29. N. N. Bogoliubov and D. V. Shirkov, "Quantum Fields." Nauka Press, Moscow, 1980 [Engl. transl., Benjamin/Cummings, Reading, Massachusetts, 1982].
30. E. U. Condon and G. H. Shortley, "The Theory of Atomic Spectra." Cambridge Univ. Press, Cambridge, 1935.

31. E. U. Condon and H. Odabasi, "Atomic Structure." Cambridge Univ. Press, New York, 1980.
32. P. A. M. Dirac, "The Principles of Quantum Mechanics." Oxford Univ. Press, Oxford, 1930.
33. R. D. Richtmyer, "Principles of Advanced Mathematical Physics," Vol. II. Springer-Verlag, New York, 1981.
34. M. Moshinsky, *J. Math. Phys.* **4**, 1128 (1963).
35. T. P. Zivkovic, *Int. J. Quantum Chem.* **S11**, 413 (1977).
36. T. P. Zivkovic and H. J. Monkhorst, *J. Math. Phys.* **19**, 1007 (1978).
37. N. M. Hugenholtz, *Physica* **23**, 481 (1957).
38. B. H. Brandow, *Rev. Mod. Phys.* **9**, 771 (1967).
39. R. J. Bartlett and D. M. Silver, *Int. J. Quantum Chem.* **S9**, 183 (1975).
40. J. J. Sakurai, "Advanced Quantum Mechanics." Addison-Wesley, Reading, Massachusetts, 1967.

Fifth-Order Many-Body Perturbation Theory and Its Relationship to Various Coupled-Cluster Approaches*

STANISLAW A. KUCHARSKI† and RODNEY J. BARTLETT

*Quantum Theory Project
Departments of Chemistry and Physics
University of Florida
Gainesville, Florida 32611*

I. Introduction	281
II. Review of the Rayleigh–Schrödinger Theory	283
III. Synopsis of Coupled-Cluster Theory	289
IV. Diagrammatics	292
A. Many-Body Perturbation Theory Diagrams	292
B. Coupled-Cluster Diagrams.	298
V. Generation of the MBPT Diagrams by CC Iterations	306
A. Relevant CC Equations	306
B. Second-Order MBPT Energy E_2	306
C. Third-Order MBPT Energy E_3	308
D. Fourth-Order MBPT Energy E_4	308
E. Computational Scheme for the Fourth-Order Energy Terms	310
F. Generation of Fifth-Order MBPT Diagrams	311
VI. Remarks and Comments.	320
VII. Computational Strategy in a Fifth-Order MBPT Calculation	328
VIII. Summary	333
Appendix A. Choice of Skeleton Diagrams and MBPT Diagram Rules	334
Appendix B. Systematic Generation of MBPT Energy Diagrams	337
Appendix C. Diagram Factorization and Basis Set Size Dependence in MBPT–CC Computations	340
References	343

I. Introduction

The coupled-cluster (CC) method has been recognized in recent years as a very powerful method for the calculation of correlation effects.^{1–14} It became an attractive alternative to more common configuration interac-

* This research has been supported by the U.S. Air Force Office of Scientific Research.

† Permanent address: Institute of Chemistry, Szkolna 9, 40-006 Katowice, Poland.

tion (CI) approaches owing to the so-called "size extensivity" property^{6,7} that ensures correct scaling with size for large molecules and owing to some computational advantages in the inclusion of higher-order excitation effects that are normally not possible to include fully in CI.

Foundations to the CC methods were laid by Coester and Kuemmel,¹ Cizek,² Hubbard,³ Sinanoglu,⁴ and Primas,⁵ while Cizek² first presented the CC equations in explicit form. Also Hubbard³ called attention to the equivalence of CC methods and infinite-order many-body perturbation theory (MBPT) methods. From this latter viewpoint, the CC method is a device to sum to infinity certain classes of MBPT diagrams or all possible MBPT diagrams when the full set of coupled-cluster equations is solved. The latter possibility would require solving a series of coupled equations involving up to N -fold excitations for N electrons. Practical applications require the truncation of the cluster operators to low N values.

Following the pair correlation approach of Sinanoglu,⁴ Cizek² introduced the coupled-pair many-electron theory (CPMET) method, which takes into account only double excitation clusters T_2 . In the present paper we prefer our more systematic nomenclature for different versions of the CC method, consistently used in our previous papers. Thus the original Cizek approach will be denoted CCD (CC doubles), while its linearized version will be denoted as LCCD. By including in the CC equations single excitation clusters T_1 , we arrive at the CCSD method, exploited in a series of papers by Bartlett and co-workers.⁹⁻¹¹ We will also consider the linearized version of the CCSD method, LCCSD,¹⁵ the full CCSDT model that includes effects of triple excitation clusters T_3 , and the CCSDTQ model that also considers T_4 .

One of the unattractive characteristics of MBPT is the rapidly growing number of diagrams in higher order. For the HF-SCF reference state there are 1, 3, and 39^{6,7} antisymmetrized diagrams in the second, third, and fourth order, respectively. According to our analysis, in fifth order there are 840 such antisymmetrized diagrams. However, in order to calculate the fifth-order energy we do not necessarily need to approach the problem in a diagram-by-diagram manner. A more efficient way to do this would be to follow the CC scheme, from which we can obtain the wave function at a certain order without explicit consideration of its lower-order structure. In this way, the number of diagrams to be considered is reduced to the much smaller set of CC diagrams. We have shown elsewhere in high-order MBPT studies that fifth-order MBPT coupled with the [2, 1] Padé approximant extrapolation has prospects of being an attractive model for electron correlation.¹⁶ It is also possible that for other properties than the energy, MPBT(5) might offer important corrections.¹⁷⁻²⁰

The aim of the present paper is to present the fifth-order terms generated by several different CC approaches and to compare them with all fifth-order MBPT diagrams. This will enable us to analyze the steps required to compute these terms. Several simplifications are identified. In particular, *all* the fifth-order diagrams arising from T_4 may be obtained with only an n^6 algorithm. To enumerate the fifth-order terms, we also introduce a modified type of diagram that reduces the overall number of fifth-order diagrams to 210.

II. Review of the Rayleigh–Schrödinger Theory

The nonrelativistic Hamiltonian within the Born–Oppenheimer approximation is given as

$$H = \sum_i h(i) + \sum_{i>j} \frac{1}{r_{ij}} \quad (1)$$

where the one-electron operator is defined as

$$h(i) = -\frac{1}{2} \nabla_i^2 - \sum_{\alpha} \frac{Z_{\alpha}}{r_{i\alpha}} \quad (2)$$

In the formalism of perturbation theory we assume the exact Hamiltonian H to be composed of two components: the zero-order H_0 and the perturbation V

$$H = H_0 + V \quad (3)$$

In the Møller–Plesset type of perturbation theory, we define H_0 as

$$H_0 = \sum f(i) \quad (4)$$

$$f(i) = h(i) + u(i) \quad (5)$$

$$f\phi_r = \varepsilon_r \phi_r \quad (6)$$

and $H\Phi_0 = E_0\Phi_0$, with Φ_0 the antisymmetrized product of spin orbitals $\{\phi_r\}$. Here $u(i)$ is an effective one-electron operator. The perturbation operator then becomes

$$V = \sum_{i>j} \frac{1}{r_{ij}} - \sum_i u(i) \quad (7)$$

In order to develop a diagrammatic approach to perturbation theory, it is convenient to work within a second-quantized formalism. The expressions for H_0 and V then become

$$H_0 = \sum_r \varepsilon_r r^\dagger r \quad (8)$$

$$V = V_2 + V_1 \quad (9a)$$

$$V_2 = \frac{1}{4} \sum_{pqrs} \langle pq || rs \rangle p^\dagger q^\dagger sr \quad (9b)$$

$$V_1 = - \sum_{p,q} \langle p | u | q \rangle p^\dagger q \quad (9c)$$

and $\langle pq || rs \rangle = \int d\tau_1 \int d\tau_2 \phi_p^*(1) \phi_q^*(2) r_{12}^{-1} (1 - P_{12}) \phi_r(1) \phi_s(2)$, the antisymmetrized integral. We use our normal convention that the indices i, j, k, l, \dots represent spin orbitals and associated operators corresponding to orbitals occupied in some reference function while the indices a, b, c, d, \dots correspond to unoccupied spin orbitals and operators, with p, q, r, s unrestricted. The Schrödinger equation for the zeroth order and the exact problem are then

$$H_0 |\Phi_r\rangle = E_r^0 |\Phi_r\rangle \quad (10)$$

$$H |\psi\rangle = E |\psi\rangle \quad (11)$$

with $\{\Phi_r\}$ the set of determinants composed of the spin orbitals in Eq. (6).

The form [Eq. (3)] of the perturbation operator points out that formally we obtain a double perturbation expansion with the two-electron V_2 and one-electron V_1 perturbations. However, in the case of a Hartree–Fock potential the one-electron part of the perturbation is exactly canceled by some terms of the two-electron part. This becomes more transparent when we switch to the normal product form of the second-quantized operators^{2,21} indicated by the symbol $\{\dots\}$. We define normal orders for second-quantized operators by moving all a (“particle” annihilation) and i^\dagger (“hole” annihilation) operators to the right by virtue of the usual anti-commutation relations $[a^\dagger, b]_+ = \delta_{ab}$, $[i^\dagger, j] = \delta_{ij}$ since $a|\Phi_0\rangle = i^\dagger|\Phi_0\rangle = 0$. Then

$$H_N = H - \langle \Phi_0 | H | \Phi_0 \rangle \quad (12)$$

$$H_N = H_N^0 + V_N \quad (13)$$

$$H_N^0 = \sum_r \varepsilon_r \{r^\dagger r\} \quad (14)$$

$$V_N = V_1^N + V_2^N \quad (15)$$

$$V_1^N = \sum_{pq} \langle p | w - u | q \rangle \{p^\dagger q\} \quad (15a)$$

$$V_2^N = \sum_{pq} \langle pq || rs \rangle \{p^\dagger q^\dagger sr\} \quad (15b)$$

where H_N , H_N^0 , V_1^N , and V_2^N are normal-ordered operators corresponding to the operators in Eqs. (8) and (9). This operator form is accomplished by Wick's theorem, which says that for a string of m second-quantized operators, $ABC\cdots = \{ABC\cdots\}$ (the normal product) plus all single, double, ... up to m -fold contractions,²¹ or symbolically, $ABC\cdots = \{ABC\cdots\} + \overline{\{ABC\cdots\}} + \cdots + \overline{\overline{\{ABC\cdots\}}}$. Furthermore, the only nonvanishing contractions are $\overline{i^\dagger j} = \delta_{ij}$ and $\overline{ab^\dagger} = \delta_{ab}$. Hence, the $\langle p|w|q\rangle\{p^\dagger q\}$ term is a component of the V_2 operator (9b) containing one contraction

$$\langle p|w|q\rangle = \sum_i \langle pi || qi \rangle \quad (16)$$

If the one-electron potential $u(i)$ used to generate one-particle states according to Eq. (6) is the usual Fock potential, then the one-electron perturbation (15a) vanishes. With the preceding definition of the Hamiltonians, the Schrödinger equations (10) and (11) take the form

$$H_N^0 |\Phi_r\rangle = \Delta E_r^0 |\Phi_r\rangle \quad (17)$$

$$H_N |\psi\rangle = \Delta E |\psi\rangle \quad (18)$$

where

$$\Delta E_r^0 = E_r^0 - E_0$$

$$\Delta E = E - E_0$$

The RS formulas for the energy expansion are well known and are given in many places (e.g., Ref. 22). A thorough development of the wave-reaction operator perturbation theory has been presented by Löwdin.²³ Using conventional first quantized operators, we may write down the expressions for the n th-order energy $E^{(n)}$, for instance, as

$$E^{(n)} = \langle \Phi_0 | V | \Psi^{(n-1)} \rangle \quad (19)$$

and

$$\Psi^{(n)} = R_0 V \Psi^{(n-1)} - \sum_{\kappa=1}^{n-1} E^{(\kappa)} R_0 \Psi^{(n-\kappa)} \quad (20)$$

where

$$R_0 = \frac{Q}{E_0 - H_0}, \quad Q = \sum_{s(\neq 0)} |\Phi_s\rangle \langle \Phi_s| \quad (21)$$

By recursive iteration of Eq. (20) we may obtain explicit formulas for $E^{(n)}$, which in general would look like

$$E^{(n)} = \langle \Phi_0 | V(R_0 V)^{n-1} | \Phi_0 \rangle + \text{renormalization terms} \quad (22a)$$

Thus, the RS energy expression consists of two parts: the first one, which will be called the principal part, is given explicitly in Eq. (22a), and the second one, called the renormalization part, involves many terms, the number of which rapidly grows with the order of perturbation. For example, at the third order there is 1 such term; at the fourth order, 4; at the fifth order, 13; etc. Perhaps the easiest procedure for generating these terms is the "bracketing technique" of Brueckner.²⁴

One of the virtues of the diagrammatic expansion lies in the fact that we do not need to consider the renormalization part, but, formally, we can limit ourselves to the principal one. The other terms are automatically accounted for by (a) eliminating from the diagrammatic expansion all the unlinked terms [by virtue of the linked diagram theorem (LDT)²⁴⁻²⁷] and (b) admitting to the expansion the so-called exclusion principle violating (EPV) diagrams.²⁶⁻²⁹ The EPV diagrams, which have been called the "conjoint" part of the renormalization terms,⁶ are very convenient from a computational point of view, since they allow an unrestricted summation over the "particle" or "hole" orbital labels. Of course, invoking the linked-diagram theorem also ensures the size-extensive property.⁶

Hence, a statement of the linked diagram theorem is that

$$\Psi_{\text{MBPT}} = \Phi_0 + \sum_{k=1}^{\infty} (R_0 V)^k | \Phi_0 \rangle_{\text{L}} \quad (22b)$$

and that

$$E_{\text{MBPT}} = \langle \Phi_0 | H | \Phi_0 \rangle + \sum_{k=1}^{\infty} \langle \Phi_0 | V(R_0 V)^k | \Phi_0 \rangle_{\text{L}} \quad (22c)$$

where the L indicates the limitation to "linked" diagrams. Computational methods based on MBPT were introduced into chemistry by Bartlett and co-workers^{6-8,30-33} with the current state of the art being the evaluation of all diagrams through fourth-order perturbation theory.^{11,34}

The analogous expansion may be developed for the n th-order perturbed wave function $\Psi^{(n)}$ in Eq. (22b), but they must be expressed in terms of open diagrams, i.e., those in which all the lines are not closed into loops. Strictly speaking, such diagrams occur in the expansion of the wave operator, a concept studied at length by Löwdin,³⁵ since their algebraic equivalents are second-quantized operators. The n th-order wave

operator that takes Φ_0 into $\Psi^{(n)}$ is defined as

$$|\Psi^{(n)}\rangle = \Omega^{(n)}|\Phi_0\rangle \quad (23)$$

We express contributions to $\Omega^{(n)}$ diagrammatically, but they can be automatically identified through Eq. (23) with contributions to the $\Psi^{(n)}$. These are shown for the first- and second-order MBPT wave function in Fig. 1. In the wave operator expansion, we encounter *disconnected* but *linked* diagrams, i.e., diagrams that are composed of two or more separate parts like



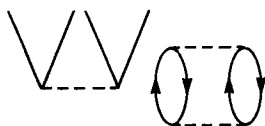
and, of course, all wave operator diagrams are “open” (since they have external lines). The LDT, of course, holds for this case, since no *unlinked*

$$\psi_{\text{MBPT}}^{(1)} = \text{V} + \text{V}_x$$

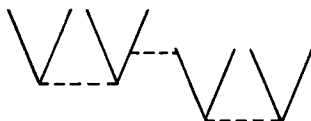
$$\begin{aligned} \psi_{\text{MBPT}}^{(2)} = & \text{V} \text{V} + \text{V} \text{V}_x + \text{V}_x \text{V} + \text{V}_x \text{V}_x \\ & + \text{V} \text{V}_x \text{V} + \text{V}_x \text{V}_x \text{V} + \text{V}_x \text{V}_x \text{V}_x + \text{V}_x \text{V}_x \text{V}_x \\ & + \text{V} \text{V}_x \text{V}_x + \text{V}_x \text{V}_x \text{V}_x + \text{V}_x \text{V}_x \text{V}_x + \text{V}_x \text{V}_x \text{V}_x \\ & + \text{V}_x \text{V}_x + \text{V}_x \text{V}_x + \text{V}_x \text{V}_x + \text{V}_x \text{V}_x \\ & + \text{V}_x \text{V}_x + \text{V}_x \text{V}_x + \text{V}_x \text{V}_x \end{aligned}$$

Fig. 1. MBPT wave function diagrams for first and second order.

terms are allowed, where *unlinked* means composed of two or more disconnected parts in which at least one is closed like



(closed means no external lines). The diagram



is connected and linked. Illustratively speaking, the presence of the disconnected terms prevents us from obtaining the higher-order wave function $\Psi^{(n+1)}$ by merely operating with V on $\Psi^{(n)}$, since such a procedure would lead also to an occurrence of unlinked terms in the $\Psi^{(n+1)}$ expansion, which would be compensated by an addition to $V|\Psi^{(n)}\rangle$ of renormalization terms. This, however, would be equivalent to $(V|\Psi^{(n)})_L$, where L means linked diagrams only.

The same observation refers also to the different energy formulas. We can express the n th-order energy given in Eq. (19) as

$$E^{(n)} = \langle \Phi_0 | V | \Psi^{(n-1)} \rangle \equiv \langle \Psi^{(1)} | E_0 - H_0 | \Psi^{(n-1)} \rangle \quad (24a)$$

$$\begin{aligned} &= \langle \Psi^{(1)} | V | \Psi^{(n-2)} \rangle + A \equiv \langle \Psi^{(2)} | E_0 - H_0 | \Psi^{(n-2)} \rangle + A \\ &\equiv \langle \Psi^{(2)} | E_0 - H_0 | \Psi^{(n-2)} \rangle_L \end{aligned} \quad (24b)$$

$$\begin{aligned} &= \langle \Psi^{(2)} | V | \Psi^{(n-3)} \rangle + B \equiv \langle \Psi^{(3)} | E_0 - H_0 | \Psi^{(n-3)} \rangle + B \\ &\equiv \langle \Psi^{(3)} | E_0 - H_0 | \Psi^{(n-3)} \rangle_L \end{aligned} \quad (24c)$$

where A, B, \dots are the renormalization terms that must be added when changing the order of the wave function occurring in the expression of $E^{(n)}$ and that account for the different unlinked terms arising from the modified first term.

It turns out to be very convenient to separate contributions to the wave operator $\Omega^{(n)}$ [and by Eq. (23) to the wave function $\Psi^{(n)}$] into several classes

$$\Omega^{(n)} = \Omega_1^{(n)} + \Omega_2^{(n)} + \dots + \Omega_{2n}^{(n)} \quad (25)$$

where $\Omega_k^{(n)}$ refers to that part of $\Omega^{(n)}$ that involves only k -tuple substitutions in the reference determinant $|\Phi_0\rangle$. The Ω_k contributions can be further analyzed by expressing them in terms of a cluster operator T_i ,

$$\Omega_k = T_k + \sum \prod_{i=1}^p \frac{1}{n_i!} T_i^{n_i} \quad (26)$$

where the summation runs over those n_i and i values that fulfill the condition $\sum_{i=1}^p n_i i = k$, $1 \leq n_i \leq k$, $p < k$. The T_l cluster operator is given as

$$T_l = \frac{1}{(l!)^2} \sum_{\substack{abc\dots \\ ij k\dots}} t_{ijk\dots}^{abc\dots} a^\dagger b^\dagger c^\dagger \dots kji \quad (27a)$$

and are naturally in normal product form

$$T_l = \sum_{\substack{a>b>c\dots \\ i>j>k\dots}} t_{ijk\dots}^{abc\dots} \{a^\dagger i b^\dagger j c^\dagger k \dots\} \quad (27b)$$

where the number of creation (annihilation) operators equals l . We also assume that $t_{ijk\dots}^{abc\dots}$ is antisymmetrized.

Another way of introducing cluster operators is to define the operator T_l to sum only “connected” l -fold excitation diagrams in Ψ_{MBPT} , and by virtue of defining $\Omega = \exp(T)$ the “disconnected” but “linked” Ψ_{MBPT} diagrams are summed as the quadratic and higher terms in the $\exp(T)$ expansion. This is the essential relationship of MBPT to coupled-cluster theory.

III. Synopsis of Coupled-Cluster Theory

In the coupled-cluster theory^{1,2,6} the perturbed wave function may be expressed in terms of cluster operators T as

$$|\Psi_{\text{CC}}\rangle = e^T |\Phi_0\rangle \quad (28)$$

where

$$T = \sum_i T_i$$

Similarly the CC correlation energy ΔE is given by

$$\Delta E = \langle \Phi_0 | VT_1 | \Phi_0 \rangle + \langle \Phi_0 | VT_1^2 | \Phi_0 \rangle + \langle \Phi_0 | VT_2 | \Phi_0 \rangle \quad (29)$$

which simply corresponds to inserting Eq. (28) into the Schrödinger equation and projecting by the reference function Φ_0 .

The T_i coefficients are solutions of the CC equations, which may be generally formulated as

$$\langle \Phi_{ij\dots}^{ab\dots} | (E_0 - H_0) e^T | \Phi_0 \rangle = \langle \Phi_{ij\dots}^{ab\dots} | (V - \Delta E) e^T | \Phi_0 \rangle \quad (30)$$

by projection of the Schrödinger equation onto the other possible excitations, although a simpler procedure is possible.

As already stated, the T operators are in normal-ordered form. Hence, by introducing H_N from Eqs. (13)–(15) into Eq. (30), we have

$$\exp(-T)H_N \exp(T)|\Phi_0\rangle = \Delta E|\Phi_0\rangle \quad (31a)$$

The Campbell–Baker–Hausdorff commutator formula tells us that the quantity

$$\exp(-T)H_N \exp(T)|\Phi_0\rangle = H_N \exp(T)|\Phi_0\rangle_C \quad (31b)$$

where C indicates the limitation to “connected” diagrams. It is important to distinguish connected from linked as discussed earlier. The MBPT wave function consists only of linked diagrams, but some are disconnected. By virtue of defining T to sum only connected diagrams, its insertion into $\exp(T)$ introduces the remaining linked but disconnected diagrams of the MBPT wave function via the exponential expansion.

Projecting Eq. (32) on the left by $\langle\Phi_0|$ gives ΔE ,

$$\Delta E = \langle\Phi_0|H_N \exp(T)|\Phi_0\rangle_C \quad (32)$$

while projection onto some excitation $\langle\Phi_{ij\ldots}^{ab\ldots}|$ provides equations for the T amplitudes,

$$\langle\Phi_{ij\ldots}^{ab\ldots}|H_N \exp(T)|\phi_0\rangle_C = 0 \quad (33)$$

Limiting ourselves up to triple excitation clusters T_1, T_2, T_3 , where $T_4 = T_5 = \cdots = 0$, we obtain the operator equations for T_1 from projection by single excitations, T_2 from projection by double excitations, and T_3 by projection by triple excitations. Hence,

$$0 = \langle\Phi_i^a|V_1^N + \overbrace{\{H_N T_2\}}^2 + \overbrace{\{H_N T_1\}}^3 + \overbrace{\{H_N T_3\}}^4 + \overbrace{\{H_N T_1 T_2\}}^5 + \overbrace{\{H_N T_1^2\}}^6/2 + \overbrace{\{H_N T_1^3\}}^7/3!|0\rangle_C \quad (34a)$$

$$0 = \langle\Phi_{ij}^{ab}|V_2^N + \overbrace{\{H_N T_2\}}^2 + \overbrace{\{H_N T_1\}}^3 + \overbrace{\{H_N T_3\}}^4 + \overbrace{\{H_N T_1^2\}}^5/2 + \overbrace{\{H_N T_1 T_2\}}^6 + \overbrace{\{H_N T_1^2\}}^7 + \overbrace{\{H_N T_1 T_3\}}^8 + \overbrace{\{H_N T_1^2 T_2\}}^9/2 + \overbrace{\{H_N T_1^3\}}^{10}/3! + \overbrace{\{H_N T_1^4\}}^{11}/4!|0\rangle_C. \quad (34b)$$

$$0 = \langle\Phi_{ijk}^{abc}| \overbrace{\{H_N T_2\}}^1 + \overbrace{\{H_N T_1^2\}}^2/2 + \overbrace{\{H_N T_3\}}^3 + \overbrace{\{H_N T_1 T_2\}}^4 + \overbrace{\{H_N T_2 T_3\}}^5 + \overbrace{\{H_N T_1 T_3\}}^6 + \overbrace{\{H_N T_1^2 T_2\}}^7/2 + \overbrace{\{H_N T_1 T_2^2\}}^8/2 + \overbrace{\{H_N T_1^2 T_3\}}^9/2 + \overbrace{\{H_N T_1^3 T_2\}}^{10}/3!|0\rangle_C \quad (34c)$$

The symbol $\overbrace{\{ABCD \dots\}}$ indicates all possible contractions among the

different normal-ordered operators. There are no contractions within a normal-ordered operator. The easiest way to work out explicit spin-orbital formulas for the amplitudes in the operator T_i is to use diagrammatic techniques. This is done in Section IV,B.

Limiting ourselves to the HF reference case for convenience, by combining a cluster-type expansion of Ω given in Eq. (26) and its order-by-order series, the low-order contributions to the wave operator may be expressed as

$$\Omega^{(1)} = T_2^{(1)} \quad (35a)$$

$$\Omega^{(2)} = T_1^{(2)} + T_2^{(2)} + T_3^{(2)} + T_2^{(1)}T_2^{(1)}/2 \quad (35b)$$

$$\begin{aligned} \Omega^{(3)} = & T_1^{(3)} + T_2^{(3)} + T_3^{(3)} + T_1^{(2)}T_2^{(1)} + T_4^{(3)} \\ & + T_2^{(1)}T_2^{(2)} + T_2^{(1)}T_3^{(2)} + T_2^{(1)}T_2^{(1)}T_2^{(1)}/3! \end{aligned} \quad (35c)$$

where we took into account the fact that

$$T_3^{(1)} = T_4^{(1)} = T_4^{(2)} = 0$$

and similar conditions for low-order T_5 , T_6 , etc. Also due to the Brillouin theorem

$$T_1^{(1)} = 0$$

Diagrammatic expressions for the operators $\Omega^{(1)}$ to $\Omega^{(3)}$ are presented in Fig. 2, in which the diagrams appear in the same order as in Eq. (35). The

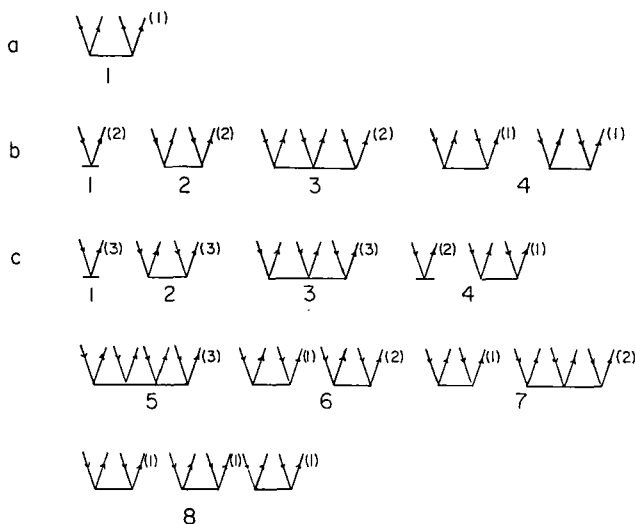


Fig. 2. Diagrammatic representation of the wave operators (a) $\Omega^{(1)}$, (b) $\Omega^{(2)}$, and (c) $\Omega^{(3)}$. A Hartree-Fock reference state is assumed.

meaning of these diagrams will become clear after the discussion in Section IV,B.

IV. Diagrammatics

A. Many-Body Perturbation Theory Diagrams

The second-quantized form of the perturbation operators given by Eqs. (9) or (15) is most suitable for the transformation of the algebraic expansion into a diagrammatic one. In this section we will briefly discuss the relationship between algebraic Rayleigh–Schrödinger perturbation theory (RSPT) terms and the MBPT diagrams they generate without going into details of the proof of the linked diagram theorem.^{24–26} As was mentioned in the preceding section, to obtain a diagrammatic expansion we need to consider only the lead term in the expansion of Eq. (22a). In order to have in this expression a sequence of second-quantized operators without any restrictions, we will replace the projector Q in the resolvent by the operator $1 - P_0$, where $P_0 = |\Phi_0\rangle\langle\Phi_0|$. In this way we obtain

$$\sum_n \langle\Phi_0| V \left(\frac{1 - P_0}{E_0 - H_0} V \right)^{n-1} |\Phi_0\rangle + \text{renormalization terms} \quad (36)$$

Now we can divide all the terms in the preceding equation into three groups: (a) leading term $E_L^{(n)}$, (b) terms originating from the first term of Eq. (36) but containing the P_0 operator, and (c) the original renormalization terms. We can now single out the term $E_L^{(n)}$, which is

$$E_L^{(n)} = \langle\Phi_0| V \left(\frac{1}{E_0 - H_0} V \right)^{n-1} |\Phi_0\rangle \quad (37)$$

and in this way we have obtained an expression analogous to that obtained by Goldstone in the time-dependent (TD) proof of the linked diagram theorem.²⁵ The unlinked terms generated by Eq. (37) are in analogy to the TD scheme: (1) The first group contains those diagrams that are due to the inclusion of P_0 into the resolvent and that are canceled by the terms of group *b*. They always have one or more vacuum states between adjacent vertices. (2) The second group includes unlinked diagrams in which unlinked parts overlap each other and that are canceled by the renormalization terms present in the RS expansion.

As we develop the diagrammatic procedure, it is interesting to examine how enormous numbers of diagrams are initially reduced by the introduction of more sophisticated graphic representations. Assuming, for in-

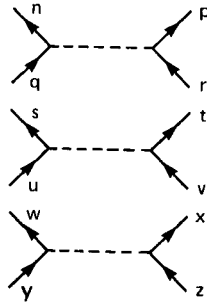
stance, that the perturbation operator is of two-electron character only,

$$V = V_2 = \frac{1}{2} \sum \langle pq|rs \rangle p^\dagger q^\dagger sr \quad (38)$$

in the n th order we will have a sequence of $4n$ creation and annihilation operators

$$2^{-n} \sum \langle np|qr \rangle n^\dagger p^\dagger r q \dots \langle st|uv \rangle s^\dagger t^\dagger v u \dots \langle wx|yz \rangle w^\dagger x^\dagger z y \quad (39)$$

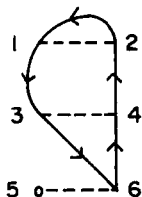
This can be presented diagrammatically as n vertices not yet connected together:



Then we use Wick's theorem, which states that nonvanishing contributions to the energy come only from fully contracted terms. A contraction between two operators in diagrammatic language means that two lines corresponding to two operators being contracted must be tied together. Thus Wick's theorem in diagrammatic language states that in order to have a nonvanishing contribution to the energy all the lines in the diagram must be connected into loops and no diagram with an open line survives. It is straightforward to see that n sets of the operators of the type $p^\dagger q^\dagger sr$ can be fully contracted into $(2n)!$ ways. This can be illustrated with the second-order expression in which we have the sequence of operators

$$p^\dagger q^\dagger s r t^\dagger u^\dagger w v$$

We can assign to the creation operators the numbers 1, 2, 3, 4, and contracting them in all possible ways with operators $srwu$ will be equivalent to taking all the permutations of the latter ones. On the other hand, it may be observed that to each permutation of $2n$ numbers we can assign an n th-order diagram. For instance, taking $n = 3$ we can pick at random a permutation, say, 241653, and assign to it a diagram



in which we have numbered the ends of each vertex with the numbers 1 to 6 and have drawn the diagram according to the prescription that the number j placed in the i th position means that we ought to draw the line directed from the point j to the point i . The number of cycles in the permutation is equal to the number of loops in the diagram. In this way we would obtain 2 diagrams in first order, 24 diagrams in second order, 720 diagrams in third order, etc. (cf. the first row of Table I).

These enormous numbers of diagrammatic terms are obviously useless, and there are methods to reduce them substantially. This can be done in several steps:

Step 1: Introduction of the linked diagram theorem. The diagrams obtained so far are generated by the expression in Eq. (37), which is the leading term in the expansion of Eq. (36), the remaining terms of which are ignored. Introduction of the LDT in our scheme is equivalent to the inclusion into the diagrammatic expansion all the remaining terms in Eq. (36), whose role will be to cancel all the unlinked terms originating from the leading one. Actually, the LDT should not be considered just a

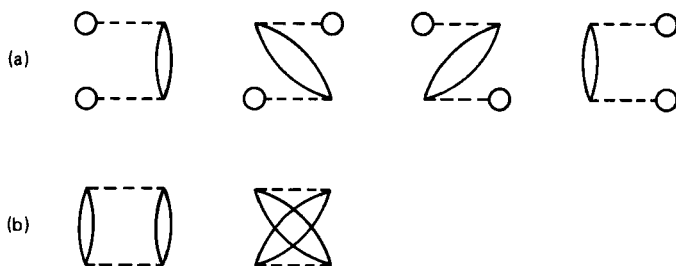
TABLE I

NUMBER OF VARIOUS TYPES OF DIAGRAMS FOR THE FIVE LOWEST ORDERS OF PERTURBATION THEORY

Type of diagrams	Order of perturbation theory				
	1st	2nd	3rd	4th	5th
Topologically equivalent	2	24	720	40,320	3,628,800
Linked	2	20	592	33,888	3,134,208
Topologically distinct (Goldstone)	2	6	76	2,124	97,968
Antisymmetrized	1	2	14	201	4,704
Hartree-Fock reference state	1	1	3	39	840
Antisymmetrized skeleton	1	1	1	15	210
Hugenholtz skeleton	1	1	1	12	148

method of reducing the number of diagrams, since this is just a "side effect," although a desirable one. The LDT itself ensures that all non-physical terms, i.e., the unlinked diagrams that are size inextensive, are eliminated. The number of terms left after applying the LDT in the second and third order, respectively, is 20 and 592. See the second row of Table I for higher-order terms. It follows from the derivation that with each n th-order diagram we have to attach a factor 2^{-n} .

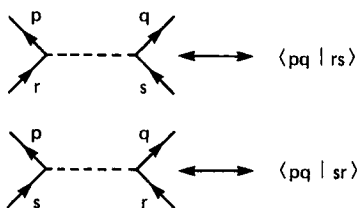
Step 2. In this step we introduce so-called topologically nonequivalent or Goldstone diagrams.²⁵ Each group of topologically equivalent diagrams contains all those terms that can be obtained one from another without cutting any line, i.e., by turning one or more vertices around the vertical axis. It follows from this that there are 2^n topologically equivalent diagrams in one group (or 2^{n-1} when there is a vertical symmetry plane in the diagram). Replacing such a group with a single diagram will be equivalent to removing the factor 2^n from the corresponding algebraic expression. This is visualized in the following figure, in which two groups of topologically equivalent diagrams are presented for the second order:



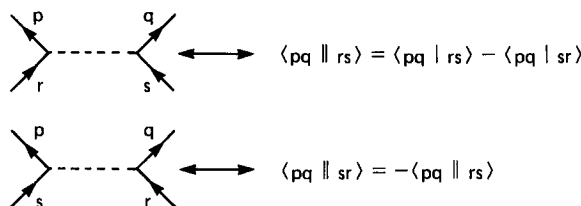
Group (a) consists of four diagrams and group (b) consists of two diagrams (there is a symmetry plane in this group). In (b) the factor 2^{-n} is not entirely canceled, and so we attach with the resulting Goldstone diagram a factor $\frac{1}{2}$ (in accordance with the Goldstone rule). The procedure of taking only topologically nonequivalent diagrams, which, of course, also adds the "exchange" diagrams of those above, reduces the overall number of terms to be considered to 2, 6, and 76 for the first to third order (cf. Table I, third row).

Step 3. The next decrease in the number of diagrams is realized by the introduction of antisymmetrized diagrams, which arise when replacing a Goldstone vertex by an antisymmetrized one, which is our normal convention for MBPT³⁶ and CC⁶ methods. The difference between the two is revealed in the integral attached with the vertex. In the Goldstone dia-

gram we have the relation



whereas for the antisymmetrized diagram



This means that switching outgoing or incoming lines that are not a topological transformation in the case of Goldstone diagrams leads to a new diagram (i.e., exchange diagrams), while in the case of antisymmetrized diagrams this results in the same diagram. Therefore, a group of Goldstone diagrams then can be obtained one from another by switching pairs of incoming or outgoing lines at any vertex corresponds to the same antisymmetrized diagram. Any member of the group may be selected, but it is convenient to take those that contain a maximum number of loops.^{36,37}

The number of Goldstone diagrams corresponding to the antisymmetrized one is determined by the number of pairs of equivalent lines according to the formula $2^n - N_p + \delta_{N_p n}$, where n denotes an order of perturbation, N_p is a number of pairs of equivalent lines, and $\delta_{N_p n}$ is the Kronecker delta. Two lines are said to be equivalent³⁷ if they go in the same direction and both of them begin at the same interaction line and end at the same interaction line. After antisymmetrization we obtain, respectively, in first through fifth order 1, 2, 14, 201, 4704 antisymmetrized diagrams.

Step 4. When we happen to develop a perturbation expansion with respect to the Hartree–Fock reference state, the number of diagrams is further reduced. In this case, all diagrams produced by a contraction *within* an operator, which results in Goldstone terminology to a “bubble” line $|\text{---}\bigcirc$, are canceled (with an exception of the first order) by the negative of the Hartree–Fock one-particle potential $|\text{---}\times$. This is clearly seen when one uses the normal-order form of the perturbation operator,

since then the V_1^N operator [Eq. (15a)] vanishes. [In our notation used in all figures $|\text{---}\times = |\text{---}\otimes = |\text{---}\bigcirc + |\text{---}\times$ (Goldstone) unlike the Goldstone convention.] By assuming an HF reference state, the number of diagrammatic terms goes down to 1, 1, 3, 39, and 840 from first to fifth order (see Table I). Also in Fig. 1 once our $|\text{---}\times = 0$, the second term in $\Psi_{\text{MBPT}}^{(1)}$ and 11 of the terms in $\Psi_{\text{MBPT}}^{(2)}$ would disappear.

Step 5. The preceding numbers point out that up to fourth order, the diagrams are manageable. To make them more manageable in fifth order, it is convenient to introduce a further reduction by ignoring arrows in the antisymmetrized diagrams. In this way we obtain antisymmetrized skeleton diagrams (or just skeleton diagrams) to distinguish them from the ordinary antisymmetrized diagrams. The skeleton diagrams carry practically as much information as the antisymmetrized ones, since providing the arrows is an automatic procedure and assigning the algebraic formula to them is as straightforward as for the antisymmetrized diagrams. However, as is explained in Appendix A, not every one of a group of equivalent antisymmetrized diagrams may be selected as the skeleton, and this requires some attention. By introducing skeleton diagrams we reduce the number of SCF graphs in the third order from 3 to 1, in the fourth order from 39 to 15, and in the fifth order from 840 to 210. See Ref. 10a for a similar analysis for the CCSDT equation.

Step 6. Another option would be to use Hugenholtz skeletons, i.e., those obtained by ignoring the arrows in the Hugenholtz diagrams.³⁸ In this way we can achieve another reduction (see the last row of Table I). However, as we discuss in Appendix A, the loss of information when going from antisymmetrized skeleton to Hugenholtz skeleton diagrams does not correspond to the reduction in the number of terms. Hence, in this paper we will mostly use the directed and skeleton diagrams that combine the Goldstone form with antisymmetrized vertices as popularized by Bartlett and co-workers.⁶⁻¹¹ Assigning an algebraic expression (usually more than one) for a skeleton diagram is as trivial as for the antisymmetrized directed diagrams (this is also discussed in Appendix A), but their number is much smaller. For example, in fifth order, it is four times less. Moreover, when reproducing MBPT diagrams by diagrammatically performing CC iterations, we can also use the CC equations in arrowless form, which makes the generation of the perturbation terms transparent.

None of the foregoing states how to actually generate *all* possible MBPT energy diagrams in each order. Such a procedure is presented in Appendix B.



B. Coupled-Cluster Diagrams

The diagrammatic equations for CC theory are in many respects easier to generate than are those of MBPT. It is apparent from the foregoing discussion that using fully antisymmetrized integrals is preferable to other possibilities. Once we have the CC diagrammatic expressions we can then make the transition to MBPT by iteration of the CC equations.

Returning to Eqs. (32)–(34) and temporarily suppressing the external indices on the configuration $\Phi_{ij\dots}^{ab\dots}$, we can quickly diagram the $H_N \exp(T)|\Phi_0\rangle_C$ part for the T amplitudes. This is accomplished as follows:

1. Pick an excitation level of interest (zero, single, double, etc.). This specifies the number of unpaired lines in the resultant diagrams.

2. Symbolize T_1 by , T_2 by ,

T_3 by , and T_4 by .

Upward arrows represent "particle" lines and downward "hole" lines.

Hence, $T_2^2 =$ .

3. Symbolize $H_N = H_N^0 + V_1^N + V_2^N$ as

$$H_N^0 + V_1^N = \left| \text{---} \times \right| = \left| \text{---} \uparrow \right| + \left| \text{---} \downarrow \right| + \left| \text{---} \wedge \right| + \left| \text{---} \vee \right|$$

0 0 -1 +1

$$V_2^N = \left| \text{---} \right| = \left| \text{---} \uparrow \uparrow \right| + \left| \text{---} \downarrow \downarrow \right| + \left| \text{---} \wedge \vee \right| + \left| \text{---} \wedge \uparrow \right| + \left| \text{---} \wedge \downarrow \right|$$

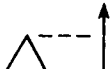
0 0 0 -1 -1

$$+ \left| \text{---} \vee \uparrow \right| + \left| \text{---} \vee \downarrow \right| + \left| \text{---} \wedge \wedge \right| + \left| \text{---} \vee \vee \right|$$

+1 +1 -2 +2

The interaction $|\text{---}\times$ stands for the operator $\epsilon_p\{p^\dagger p\} + \langle p|w - u|q\rangle\{p^\dagger q\}$, while >---< stands for the antisymmetrized operator $\langle pq||rs\rangle\{p^\dagger q^\dagger sr\}$. The labels at the bottom of the $H_N^0 + V_1^N$ and V_2^N operators refer

to the change in excitation level caused by that form of the operator.

Hence,  reduces the excitation level by 1.

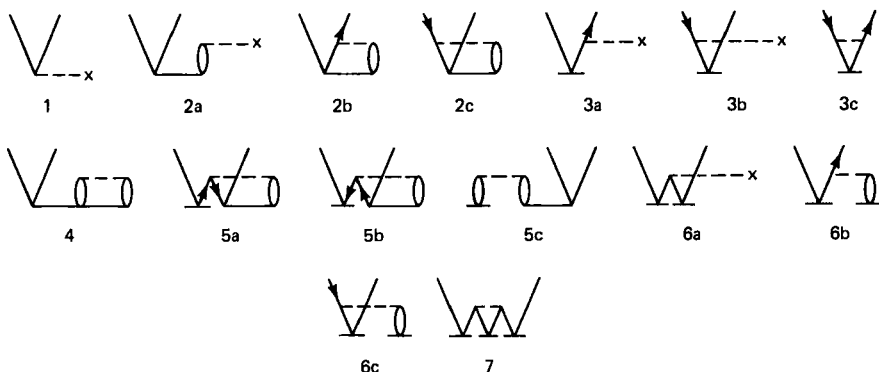
4. Construct the quantity $H_N \exp(T)|\Phi_0\rangle_C$. First we expand $\exp(T)$ subject to the limitation on the excitation level in step 1 above. Then we add the correct components of H_N to each T vertex or combination of T vertices to retain the correct excitation level and the connected requirement on the diagram. This procedure exploits the fact that the only contractions that need to be considered are those among different normal-ordered operators.

The simplest example is the energy in Eq. (29). Diagrammatically this is

$$\Delta E = \left(\text{diagram 1} \right) + \left(\text{diagram 2} \right) + \left(\text{diagram 3} \right) \quad (40)$$

since only the third term in $H_N^0 + V_1^N$ and the penultimate term in V_2^N "close" the diagrams from the T_1 and T_2 contributions to result in a net zero excitation.


To illustrate the amplitude equations, consider the T_1 equations in CC theory. Since our net excitation level is a single, we have Eq. (34a), which is arranged by orders in H_N . The seven terms from Eq. (34a) generate the following diagrams:



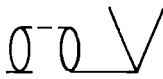
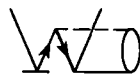
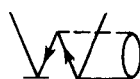
The first term in Eq. (34a), V_1^N , has only one term (diagram) that corresponds to a single excitation, the fourth in number 3 above. The next term, $\{H_N T_2\}$, has contributions from both V_1^N and V_2^N . Each must reduce the double excitation quantity T_2 by one excitation; hence the third term

from V_1^N and the fourth and fifth from V_2^N are required. The resulting diagrams are shown as 2a, 2b, and 2c above. Because of the antisymmetric vertices, there is only one *distinct* way each of the perturbations can be connected to the T_2 vertex. We can make this clear with an example that serves to illustrate a combinational convention we have developed that is guaranteed to generate *each* distinct diagram and will generate it *only* one time, so that there can be no question about redundancy or topological equivalence.

Consider the $\{H_N T_1 T_2\}$ term. Label each vertex with a plus sign for an upward-going line and a minus sign for a downward-going line. Since $T_1 T_2$

corresponds to , we have $+ - | + + - -$ for the two

vertices. Notice that the order of the pluses and minuses is irrelevant since all lines going in the same direction and originating from the same vertex are equivalent. Since this corresponds to a triple excitation, we require the (-2) de-excitation operator from H^N to reduce to a single excitation, and this can only come from V_2^N . We can similarly label this perturbation as $+ + - -$. The combinations are generated by taking two pluses and two minuses from the available vertices to satisfy the perturbation. We may do this in three distinct ways that lead to connected diagrams, namely, $+ - | + -$, $+ | + - -$, $- | + + -$, where the vertical separates the two vertices. This may be systematized into the following table:

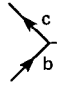
Vertices	Perturbation	Combinations	Diagrams
$+ - + + - -$	$+ + - -$	$+ - + -$	
		$+ + - -$	
		$- + + -$	

Hence, we have the three distinct T_1 amplitude diagrams.

To interpret the diagram algebraically, we have the following rules.

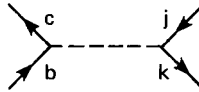
1. Each upgoing line is labeled with a "particle" label a, b, c, d, \dots and each downgoing line with a "hole" label i, j, k, l, \dots . Open lines should be labeled in sequence as $a, i; b, j; c, k$, etc.

2. Each one-particle vertex should be interpreted as the integral $\langle \text{left out} | \text{operator} | \text{right in} \rangle$. Hence



$$x = \langle c | f | b \rangle$$

3. Each two-particle vertex corresponds to the antisymmetrized integral $\langle \text{left out}, \text{right out} | | \text{left in}, \text{right in} \rangle$, and so



$$= \langle ck || bj \rangle$$

4. Cluster vertices correspond to $i \downarrow a = t_i^a$, $i \downarrow a j \downarrow b = t_{ij}^{ab}$,

etc., and are antisymmetric as well; hence $t_{ij}^{ab} = -t_{ji}^{ab} = -t_{ij}^{ba} = t_{ji}^{ba}$ and similarly for t_{ijk}^{abc} .

5. All the orbital labels are summed over "internal" lines, i.e., lines terminating below the last H_N .

6. The sign of the diagram is obtained from (-1) raised to the power of the sum of hole lines and loops. For the purpose of getting the sign, open lines are closed into fictitious loops by pairing $i, a; j, b$; etc. In the preceding example, in the first diagram we have three loops and three hole lines, giving a positive sign. In the second and third diagrams we have two loops and three hole lines, giving a negative sign.

7. The weight factor for the diagram is specified by $(1/2)^m$, where m is the number of pairs of "equivalent" lines. A pair of equivalent lines is defined as being two lines originating at the same vertex and ending at another, but same vertex, and going in the same direction. In the preceding example, there is one pair of equivalent lines in the second and third diagrams.

8. To maintain full antisymmetry of an amplitude, the algebraic expression for a diagram should be preceded by a permutation operator permuting the open lines in all distinct ways, $\sum_P (-1)^P P$.

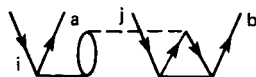
The final rule pertains to the number of distinct permutations that are possible among the open lines. For any single excitation diagram there can only be one. However, for double excitations and higher, there is normally more than one distinct way for a double Φ_{ij}^{ab} , triple Φ_{ijk}^{abc} , etc.,

excitation to label the diagram. As an example consider the T_2^2 contribution, to the T_2 amplitude. Using our convention, in which Σ implies sum over all permutations and all internal hole or particle labels, such as $\Sigma_{c,d,k,l}^P$ in the diagrams that follow, we have

Vertices	Perturbation	Combinations	Diagrams	Interpretation
$++-- ++--$	$++--$	$+- +-$		$\Sigma(-1)^P P(ij) \langle kl \ cd \rangle t_{ik}^{ac} t_{jl}^{bd}$
$++-- +$				$-\frac{1}{2} \Sigma(-1)^P P(ab) \langle kl \ cd \rangle t_{ij}^{ac} t_{kl}^{bd}$
$++-- -$				$-\frac{1}{2} \Sigma(-1)^P P(ij) \langle kl \ cd \rangle t_{ik}^{ab} t_{jl}^{cd}$
$++-- --$				$\frac{1}{4} \Sigma \langle kl \ cd \rangle t_{ij}^{cd} t_{kl}^{ab}$

In the first diagram, interchanging a with b or i with j gives a distinct term, while interchanging both is indistinguishable since the vertical axis of a diagram is irrelevant. Hence, the preceding permutation is $\Sigma_P(-1)^P P(ij) = \Sigma_P(-1)^P P(ab)$, where the symbol $P(ij)$ means that in addition to the identity permutation (parity factor $+1$) there is a single permutation of i with j (parity factor -1) in the succeeding algebraic expression.

Note that one cannot always depend on the symmetry of the diagram to indicate such an equivalent permutation since the diagram may equally well be written as



since it only requires that a plus-minus combination be taken from each T_2 vertex. (Of course, in this form the diagram has a minus sign and a corresponding interchange in the t_{jl}^{db} amplitude.) However, this should be evident immediately when the same combinations of plus-minus are being taken from equivalent vertices in the diagram generation step.

When two lines from the same vertex are quasi-equivalent, that is, when they would be equivalent once the diagram was closed by a projecting determinant, there can be no distinct permutations among those lines. Hence, the second diagram has $P(ab)$ since i and j are quasi-equivalent, while the third must have $P(ij)$. The final diagram has no permutations. Here it is important to recognize the two continuous loops generated by connecting i with a and j with b .

In a more complicated case, such as the $T_1^2 T_2$ contribution to T_3 , we have

Vertices	Perturbation	Combinations	Diagrams	Interpretation
$+- +- ++--$	$++-(\uparrow \cdots \wedge)$	$+ - +$		$-\sum(-1)^p P(i/jk abc) \langle lb de \rangle t_i^d t_j^a t_k^{ec}$
		$+ + -$		$-\sum(-1)^p P(k/ij a/bc) \langle al de \rangle t_i^d t_j^a t_k^{bc}$
	$+--(\uparrow \cdots \wedge)$	$+ - -$		
		$- - +$		

Here $P(i/jk|abc)$ means that i may be permuted with j or k , but not j or k with themselves, while all permutations among abc are allowed. In the second diagram even though i and j are from different vertices, they arise from taking the same line direction from equivalent vertices and so i to j permutations are not distinct.

The T_2 and T_3 CC amplitude diagrams are shown in Figs. 3 and 4 in which the labels, as in the preceding discussion for T_1 , indicate which of the terms in Eq. (34b,c) leads to the diagram. A little practice using the rules makes the generation of these diagrams automatic. Detailed interpretation of the triple excitation diagrams in CC theory is presented in Lee *et al.*¹⁰

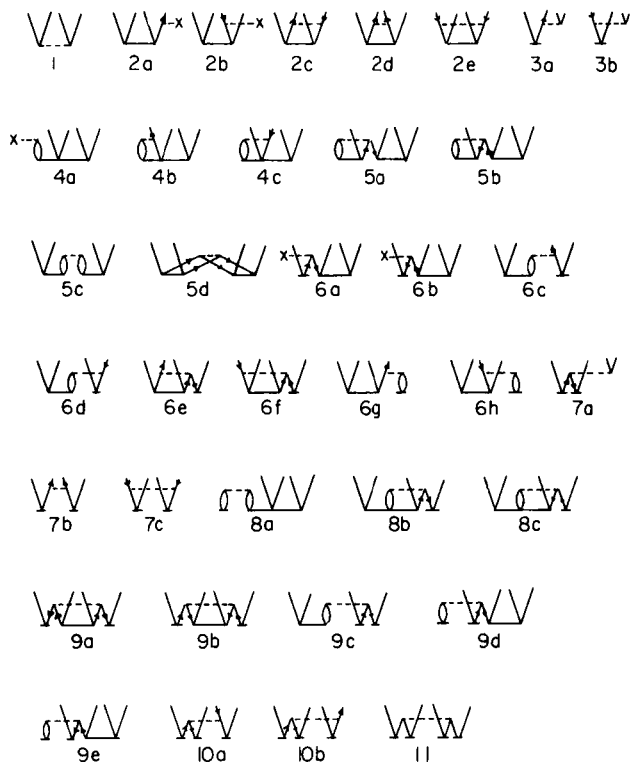


Fig. 3. Diagrammatic representation of the T_2 coupled-cluster equation [Eq. (34b)] from CCSDT with directed lines. Henceforth referred to as the D equation.

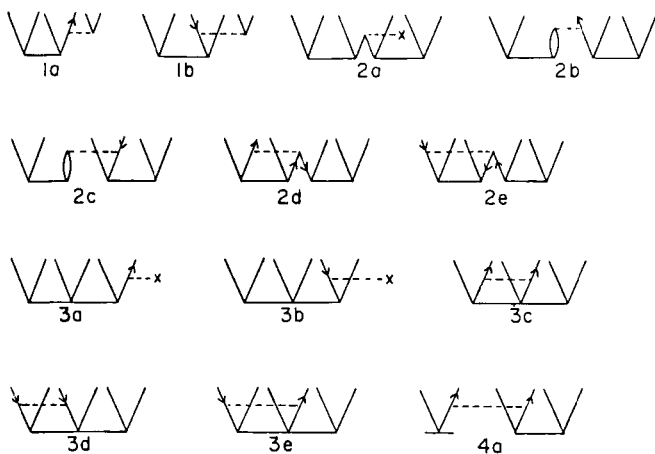


Fig. 4. Diagrammatic representation of the T_3 coupled-cluster equation [Eq. (34c)] from CCSDT with directed lines. Henceforth referred to as the T equation.

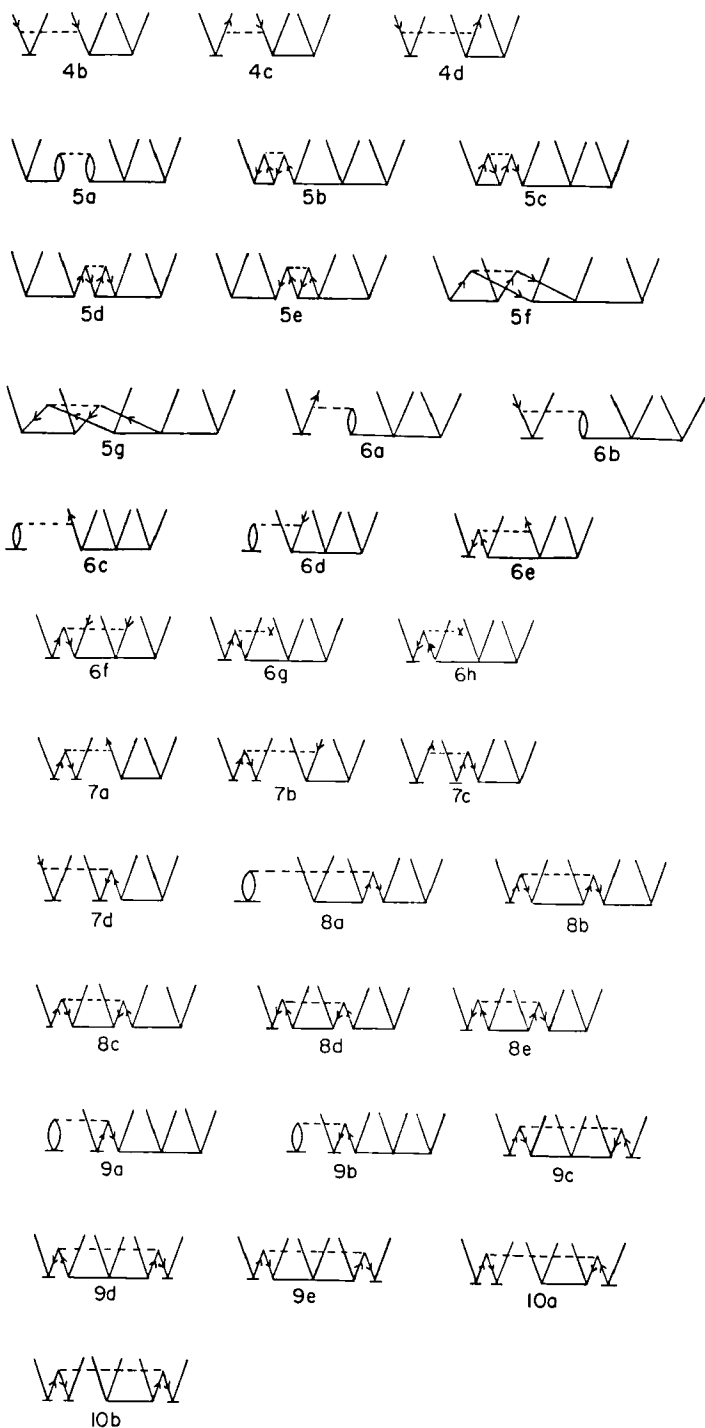


Fig. 4. (Continued)

V. Generation of the MBPT Diagrams by CC Iterations

A. Relevant CC Equations

In order to analyze how MBPT terms through fifth order are generated by the coupled-cluster iterations, we present in Fig. 5a–d the CC skeleton diagrams for single, double, triple, and quadruple amplitudes, respectively. These assume a Hartree–Fock reference state and include only those terms that contribute to the energy up to fifth order. Ordinary antisymmetrized directed diagrams as used in Figs. 3 and 4 may be easily obtained from them by providing arrows, which is a fairly automatic procedure.

B. Second-Order MBPT Energy E_2

The CC energy is given by Eq. (29) or by the equivalent diagrammatic expression in Eq. (40). This means that up to fourth order only the last term will contribute, since the second one would involve first-order $T_1^{(1)}$, which, by virtue of Brillouin's theorem, is equal to zero. Thus, in order to obtain the second-order energy we need to plug $T_2^{(1)}$ in place of the bottom iteration line in Eq. (40). We say that $T_2^{(1)}$ is obtained in the zeroth-order iteration of the CCD equation, which means that it is merely computed by

$$\begin{aligned}
 \text{a} \quad \text{V} &= \text{V}_1^{\text{V}} + \text{V}_2 + \text{V}_3 \\
 \text{b} \quad \text{VV} &= \text{V}_1^{\text{VV}} + \text{V}_2^{\text{VV}} + \text{V}_{3\text{a}}^{\text{VV}} + \text{V}_{3\text{b}}^{\text{VV}} + \text{V}_4^{\text{VV}} \\
 &\quad + \text{V}_{5\text{a}}^{\text{VV}} + \text{V}_{5\text{b}}^{\text{VV}} + \text{V}_6^{\text{VV}} + \text{V}_7^{\text{VV}} \\
 \text{c} \quad \text{VVV} &= \text{V}_1^{\text{VVV}} + \text{V}_2^{\text{VVV}} + \text{V}_3^{\text{VVV}} \\
 \text{d} \quad \text{VVVV} &= \text{V}_1^{\text{VVVV}} + \text{V}_2^{\text{VVVV}}
 \end{aligned}$$

Fig. 5. Terms in (a) S , (b) D , (c) T , and (d) Q amplitude equations contributing to the fifth-order energy E_5 . An HF reference state is assumed in all figures henceforth.

providing a denominator to the corresponding integral according to the formula

$$t_{ij}^{ab(1)} = \frac{\langle ab || ij \rangle}{\varepsilon_i + \varepsilon_j - \varepsilon_a - \varepsilon_b}$$

This is even easier to see with diagrams since

$$T_2^{(1)} = \text{---} \bigvee \bigvee \text{---}$$

(the denominator is attached above the dashed interaction line according to MBPT wave function rules), and by using the CC correlation energy diagrammatic expression [Eq. (40)]. The first term never contributes in the HF case and the second only in fifth and higher order. Hence we have the term in Fig. 6a.

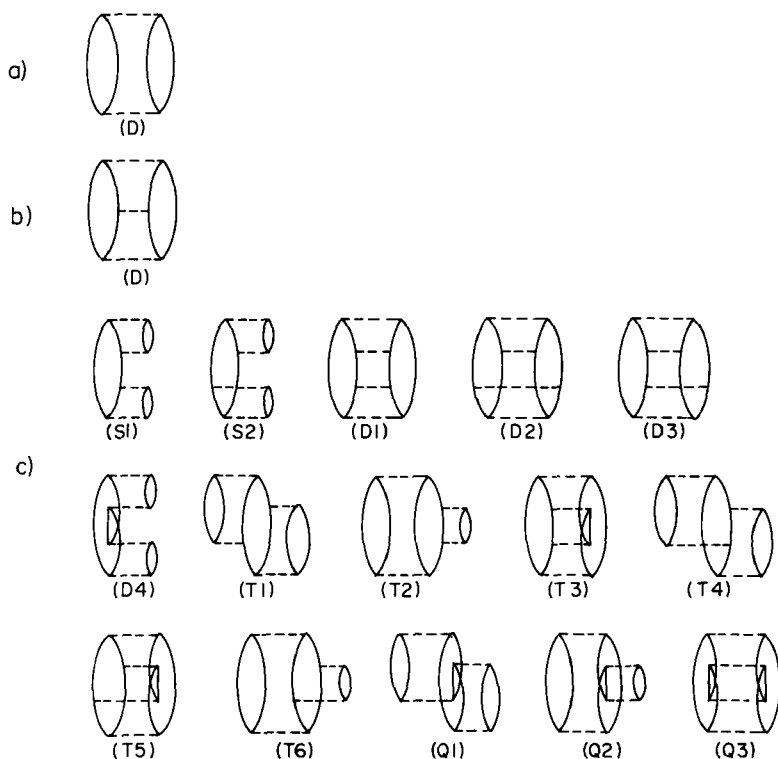



Fig. 6. Antisymmetrized skeleton energy diagrams for (a) E_2 , (b) E_3 , and (c) E_4 . These diagrams are labeled by the intermediate vertex as double excitation (D), single excitation (S), triple excitation (T), or quadruple excitation (Q) type.

C. Third-Order MBPT Energy E_3

It is well known that the third-order MBPT energy with an HF reference state can be obtained from the LCCD method.⁶ The LCCD equation is expressed when using skeleton diagrams by

$$\text{Diagram 1} = \text{Diagram 2} + \text{Diagram 3}$$

Replacing the bottom interaction of the second term by $T_2^{(1)}$, ,

which is equivalent to carrying out one iteration, we obtain the second-order $T_2^{(2)}$ amplitude. By inserting the latter into the third diagram of Eq. (40), we obtain the third-order energy, Fig. 6b.

D. Fourth-Order MBPT Energy E_4

In order to obtain the fourth-order energy we need first to generate T_2 amplitudes of one order lower, that is, $T_2^{(3)}$. This can be realized by doing the required number of iterations of the doubles (i.e., D) equation, Fig. 5b. (We use the terminology D equation to mean the T_2 part of the full coupled-cluster equations to avoid any confusion with CCD, which means approximating $T \approx T_2$ only.) It follows from this that only five terms in this equation will contribute to the third-order T_2 , b(1), b(2), b(4), b(5a), and b(5b). Other than b(1), which is only first order, the remaining terms generate higher-order T_2 amplitudes and will contribute for the first time to the fifth-order energy. It is already a well-established procedure in the literature⁶ to classify fourth-order terms into four groups according to the type of diagram in the CC equation to which they correspond, i.e., singles, doubles, triples, and quadruples as shown in Fig. 6c. Although their generation by the CC method is already well known,⁶ for the sake of completeness we will briefly discuss how they arise from the CC iterations.

1. Fourth-Order Singles E_4^S

In order to obtain the E_4^S terms we need to put the $T_1^{(2)}$ amplitude in place of the T_1 vertex in diagram b(1) in Fig. 5. The second-order $T_1^{(2)}$, in turn, should be obtained from the S equation as given in Fig. 5a. It is obvious that to the second-order T_1 , only the term 5a(2) contributes. By substituting it into b(1) in Fig. 5 we obtain the diagrams in Fig. 7a. By inserting these diagrams into the third term of Eq. (40), we then obtain the two S skeleton diagrams presented in Fig. 6c, which may be converted by providing arrows into four antisymmetrized diagrams (see Appendix A for

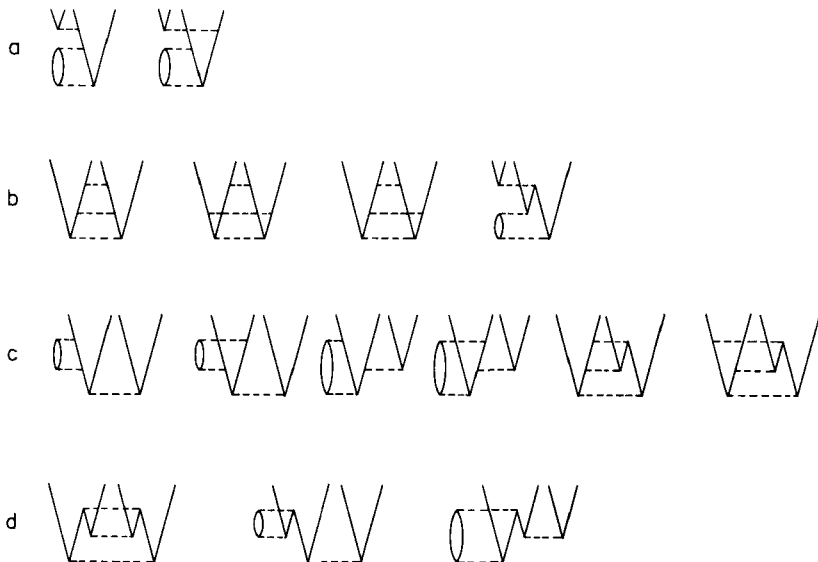


Fig. 7. Third-order T_2 diagrams: (a) single excitation type; (b) double excitation type; (c) triple excitation type; and (d) quadruple excitation type.

the procedure for directing the lines in skeleton diagrams). Thus, to obtain this contribution we have to employ both the T_2 equation—to obtain $T_2^{(3)}$ —and the T_1 equation—to generate $T_1^{(2)}$. The E_4^S may be obtained then only in the CCSD method, by performing one iteration of the S equation and one of the D equation.

2. Fourth-Order Doubles E_4^D

This group of terms is obtained by substituting $T_2^{(2)}$ into the b(2) diagram in Fig. 5. In order to obtain the fourth-order contribution we have to carry out two iterations of the D equation: in the first iteration we obtain $T_2^{(2)}$ given in Fig. 8b, and then by plugging $T_2^{(2)}$ again into the b(2) term, we obtain $T_2^{(3)}$ (D) shown in Fig. 7b. By adding the final interaction, which is equivalent to substituting $T_2^{(3)}$ into the third diagram of Eq. (40), we obtain

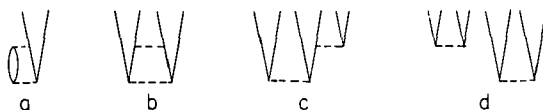


Fig. 8. All possible second-order amplitudes for an HF reference state.

all the fourth-order double excitation diagrams shown as 4 skeleton diagrams in Fig. 6c, which are equivalent to 12 antisymmetrized diagrams.

3. Fourth-Order Triples E_4^T

This is the largest group of fourth-order diagrams, obtained from the diagram b(4) in Fig. 5 by replacing the T_3 vertex with the second-order T_3 coefficient. The latter, presented in Fig. 8c, may be considered as a result of a single iteration of the T equation (Fig. 5c) engaging only the first diagram c(1). The substitution of diagram c in Fig. 8 into b(4) of Fig. 5 results in the six $T_3^{(3)}$ skeleton diagrams given in Fig. 7c. They may be directly related to the 6 T diagrams of Fig. 6c or the 16 antisymmetrized fourth-order triple diagrams shown elsewhere.⁷ The procedure used to obtain the E_4^T diagrams requires a single iteration of the T equation and a single iteration of the D equation. Hence, they are generated by the simplest version of the CCSDT method, which is denoted as CCSDT-1.¹⁰

4. Fourth-Order Quadruples E_4^Q

This class of the fourth-order MBPT terms originates from the diagrams b(5a) and b(5b) in Fig. 5. In order to have third-order T_2 we have to substitute two $T_2^{(1)}$ for both vertices. In this way to obtain the fourth-order energy we need to iterate the D equation only once. By inserting $(T_2^{(1)})^2$ into diagrams b(5a) and b(5b) in Fig. 5, we obtain the three Q contributions to T_2 in Fig. 7d, which once closed correspond to the Q diagram in Fig. 6c. The three skeleton diagrams presented in Fig. 6 may be transformed, after adding arrows, into the usual seven fourth-order antisymmetrized diagrams involving quadruple excitations.⁶

E. Computational Scheme for the Fourth-Order Energy Terms

To conclude this subsection devoted to the generation of the fourth-order energy diagrams by CC iteration, it should be stressed that in the actual computations we use a different algorithm to compute the fourth-order energy. It turns out to be simpler to perform only a single iteration of the LCCSDT method and to obtain in this manner $T_1^{(2)}$, $T_2^{(2)}$, and $T_3^{(2)}$ amplitudes. Then by using the $2n + 1$ rule for the MBPT energy (or strictly speaking the $2n$ rule),^{32,39} we can compute the fourth-order energy according to the formulas

$$E_4^S = \sum_{ai} (t_i^{a(2)})^2 \cdot D_i^a$$

$$E_4^D = \sum_{\substack{a>b \\ i>j}} (t_{ij}^{ab(2)})^2 \cdot D_{ij}^{ab}$$

$$E_4^T = \sum_{\substack{a>b>c \\ i>j>k}} (t_{ijk}^{abc(2)})^2 \cdot D_{ijk}^{abc}$$

The E_4^S computations exhibit an n^5 type of basis set size dependence, with E_4^D , n^6 and E_4^T , n^7 .

There is no convenient $2n + 1$ rule to compute fourth-order quadruples. It is possible to create second-order $T_4^{(2)}$ by taking all 18 distinct permutations of indices in the $(T_2^{(1)})^2$ term. This, however, although easy to program, would require an n^8 basis set size dependence asymptotically. It turns out that the more efficient way to program the $(T_2)^2$ contribution to the energy is to use so-called vertical factorization of the diagram, which makes it possible to do the computations with still an n^6 basis set size dependence. This was described in detail by Bartlett and Purvis.⁶ The more exhaustive discussion of the different types of factorization of the CC and MBPT diagrams will be presented in subsequent subsections and systematized in Appendix C.

F. Generation of Fifth-Order MBPT Diagrams

In analogy to previous examples, our starting point is Eq. (29) or its diagrammatic version, Eq. (40). It follows from this that for the Hartree–Fock case in the fifth-order energy, two terms contribute: $T_2^{(4)}$ and $T_1^{(2)} \cdot T_1^{(2)}$, which is the connected and disconnected $T_2^{(4)}$ contribution. Considering the connected term $T_2^{(4)}$ first, we need to go through all the terms, one by one, occurring in Fig. 5b, since it shows from which terms $T_2^{(4)}$ receives a contribution. Thus the connected contribution to E_5 can be divided, according to Fig. 5b, into six parts, corresponding to the terms 1 to 6 in Fig. 5b. This term can be classified by the type of excitation occurring below the top interaction line. Since this interaction line corresponds to one order lower in perturbation theory, below it we have third-order quantities.

Hence, to the connected $T_2^{(4)}$ we have contributions from

1. $T_1^{(3)}$ —first term in Fig. 5b—fifth-order energy diagrams originating from this term will be called singles or E_5^S ;
2. $T_2^{(3)}$ —second term in Fig. 5b—these will be called doubles or E_5^D ;
3. $T_2^{(1)} \cdot T_1^{(2)}$ —third and fourth, i.e., 3a and 3b terms in Fig. 5b—these terms will be called disconnected triples or E_5^{Tds} ;
4. $T_3^{(3)}$ —term 4 in Fig. 5b—this generates diagrams that will be called connected triples (or triples) or E_5^T ;
5. $T_2^{(1)} \cdot T_2^{(2)}$ —terms 5a and 5b in Fig. 5b—these will give rise to the diagrams that are classified as disconnected quadruples or E_5^{Qds} ;
6. $T_4^{(3)}$ —the sixth term in Fig. 5b—these terms will be called connected quadruples (or quadruples) or E_5^Q .

In the following six subsections we will analyze each of the six types of terms contributing to E_5 , and in the last subsection we will give diagrams that enter E_5 via $T_1^{(2)} \cdot T_1^{(2)}$, i.e., from disconnected $T_2^{(4)}$.

1. Fifth-Order Singles E_5^S

All the E_5^S terms are obtained by substituting $T_1^{(3)}$ into the first term of the D equation in Fig. 5b, but in order to obtain $T_1^{(3)}$ we need to use the equation in Fig. 5a. From this equation it follows that to have a complete $T_1^{(3)}$ we need to consider three terms, numbered one to three in Fig. 5a, which correspond to the three amplitudes at the second-order level, namely, $T_1^{(2)}$, $T_2^{(2)}$, $T_3^{(2)}$. Because of that we can further divide the fifth-order singles into three subclasses: E_5^{SS} , E_5^{SD} , and E_5^{ST} , in which the additional superscripts refer to the type of second-order amplitude contributing to $T_1^{(3)}$.

Figure 8a–c presents all possible second-order amplitudes in the form of skeleton diagrams. By providing arrows we obtain two antisymmetrized diagrams for $T_1^{(2)}$, three antisymmetrized diagrams for $T_2^{(2)}$, and two such diagrams for $T_3^{(2)}$. The remaining nonzero amplitudes at the second-order level arise from $T_4^{(2)}$, which, being composed of two $T_2^{(1)}$ contributions shown in Fig. 8d, is of disconnected character. By inserting the appropriate second-order diagrams given in Fig. 8 in place of the lower vertex in Fig. 5a(1–3) we obtain all possible $T_1^{(3)}$ diagrams presented in Fig. 9.

The next step to recover the fifth-order energy diagrams is to operate with V_2^N on the $T_1^{(3)}$ amplitude in order to obtain $T_2^{(4)}$. Since at the third-order level we have a single excitation operator and at the fourth-order level we need a double excitation operator, we have to use the form of the V_2^N operator that increases the level of excitation, i.e., $|_{---}\nabla$. When com-

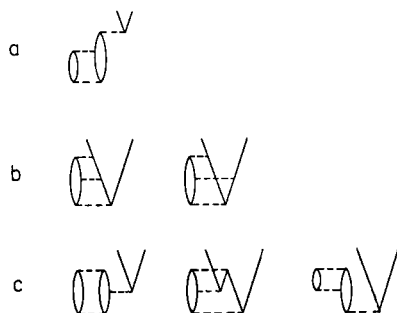


Fig. 9. Third-order T_1 amplitudes arising from (a) second-order singles $T_1^{(3)}(S)$, (b) second-order doubles $T_1^{(3)}(D)$, and (c) second-order triples $T_1^{(3)}(T)$.

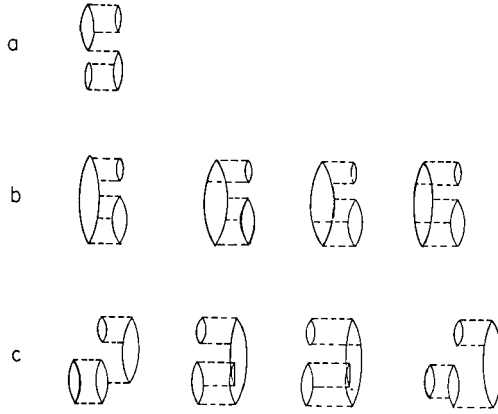


Fig. 10. The fifth-order diagrams originating from the first term in the D equation in Fig. 5b. (a), (b), and (c) correspond, respectively, to different subclasses of E_5^S , i.e., E_5^{SS} , E_5^{SD} , and E_5^{ST} .

binning this V_2^N diagram with those given in Fig. 9, we obtain 9 $T_2^{(4)}$ skeleton diagrams and the same number of E_5^S diagrams. All of the latter are shown in Fig. 10. In this way we obtain 4 E_5^{SS} diagrams (one skeleton diagram in Fig. 10a), 16 E_5^{SD} diagrams (4 skeleton diagrams in Fig. 10b) and 16 E_5^{ST} diagrams (4 skeleton diagrams in Fig. 10c).

2. Fifth-Order Doubles E_5^D

This class of diagrams is obtained by substituting $T_2^{(3)}$ into the second term, Fig. 5b(2). In order to obtain $T_2^{(3)}$ we have to use again the same equation for $T_2^{(2)}$, but we do not need to pay attention to the terms in which the lower vertices must exceed the second order, i.e., diagrams b(3) and b(6) in Fig. 5. Thus, to obtain $T_2^{(3)}$ we have to use diagrams from Fig. 8a–d and put them in place of the lower vertex in diagrams 1, 2, 4, 5 of Fig. 5b. The resulting new third-order diagrams are presented in Fig. 7a–d. They correspond to the full $T_2^{(3)}$, and the total number of the $T_2^{(3)}$ antisymmetrized diagrams must be equal to the number of diagrams occurring for E_4 (the final closing interaction line can be added in only one way to the corresponding $T_2^{(3)}$ amplitude). Figure 7a generates 4 diagrams, which are termed $T_2^{(3)}(S)$ since they are obtained by inserting $T_1^{(2)}$ into the first term of Fig. 5b. Figure 7b presents 12 antisymmetrized diagrams $T_2^{(3)}(D)$. In a similar way the remaining 16 antisymmetrized triple excitation diagrams derive from $T_2^{(3)}(T)$ in Fig. 7c, and Fig. 7d corresponds to the 7 diagrams obtained from $T_2^{(3)}(Q)$. Thus the different types of $T_2^{(3)}$ amplitudes corre-

spond to the number of different diagrams in the fourth-order energy expression.^{6,7}

In order to obtain $T_2^{(4)}(D)$ and, consequently, E_5^D we have to operate on $T_2^{(3)}$ with the V_2^N operator. This time we have to retain the level of excitation so that we will operate with the V_2^N diagram of the form $|\dots|$. We can connect the V_2^N skeleton to each skeleton diagram in Fig. 7a in two different ways, thus obtaining the 4 skeleton diagrams shown in Fig. 11a, which correspond to 16 antisymmetrized E_5^{DS} diagrams. Operating with $|\dots|$ on the skeleton in Fig. 7b, we obtain 16 E_5^{DD} skeleton diagrams (Fig. 11b), which correspond to the 56 antisymmetrized E_5^{DD} diagrams.

In an analogous way Fig. 7c will give rise to the 20 skeleton diagrams (presented in Fig. 11c) corresponding to 80 antisymmetrized E_5^{DT} diagrams. Finally, the last class of the fifth-order doubles arises by operation with the above form of V_2^N operator on each of the skeleton diagrams presented in Fig. 7d. This gives the 8 skeletons shown in Fig. 11d. By providing arrows we can easily obtain the 28 antisymmetrized E_5^{DQ} diagrams.

Thus, the second term in the CC equation in Fig. 5b generates the class of fifth-order diagrams classified as doubles, which, in turn, are further divided into four groups according to the origin of the $T_2^{(3)}$ amplitude into E_5^{DS} , E_5^{DD} , E_5^{DT} , and E_5^{DQ} . The number of antisymmetrized diagrams in each subclass is, respectively, 16, 56, 80, and 28, which gives the total number of 180 E_5^D antisymmetrized diagrams.

3. Fifth-Order Disconnected Triples E_5^{Tds}

Diagrams (3a) and (3b) in Fig. 5b contribute to the fifth-order energy in only one way. By taking the first-order T_2 , i.e., $T_2^{(1)}$, and combining it with the second-order T_1 , i.e., $T_1^{(2)}$, we have a third-order $T_3^{(3)}$ of disconnected character. Replacing then the T_2 amplitude with $T_2^{(1)}$ and the T_1 amplitude with $T_1^{(2)}$ in Fig. 5b(3a) and closing the diagrams with an energy interaction on the top, we obtain the fifth-order skeleton diagrams presented in Fig. 12a. Analogously, working in the same way on the diagram in Fig. 5b(3b), we obtain the skeleton diagrams given in Fig. 12b. The skeleton diagrams in Fig. 12a,b can be factorized into two and one, respectively. This comes from the observation that the first three diagrams in Fig. 12a are obtained from each other by switching the order of the lowest three interactions. The same refers to the second group of the three diagrams in Fig. 12a and to the diagrams in Fig. 12b. After factorization we no longer need a triple excitation denominator, i.e., a denominator involving three particle and three hole labels. Instead, we can write out the algebraic formula by using

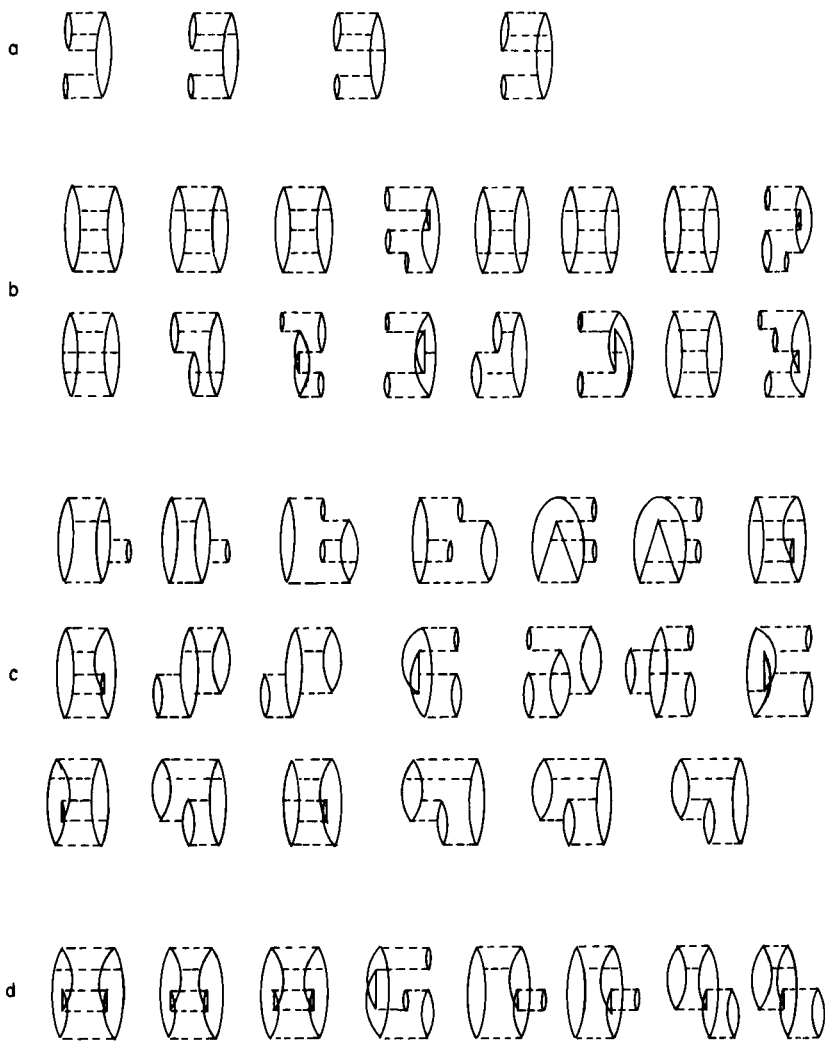


Fig. 11. The fifth-order energy diagrams arising from the third-order T_2 amplitudes, i.e., the second term in the D equation in Fig. 5b. (a) E_5^{DS} diagrams, (b) E_5^{DD} diagrams, (c) E_5^{DT} diagrams, and (d) E_5^{DQ} diagrams.

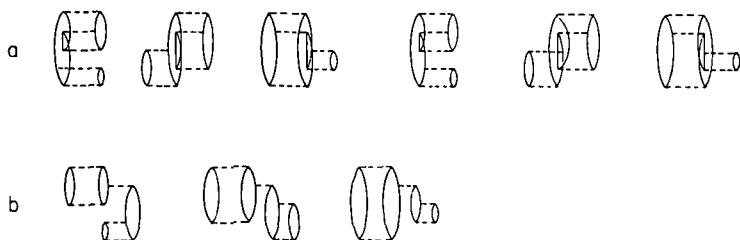


Fig. 12. The fifth-order energy diagrams E_5^{Tds} arising from disconnected triple excitation amplitudes. Diagrams in (a) derive from Fig. 5b(3a), and those in (b) are generated by Fig. 5b(3b).

only the T_1 and T_2 denominators, i.e., in the way typical of the CC method.

Thus, this group of fifth-order energy diagrams contains 9 skeletons corresponding to the 36 antisymmetrized diagrams for E_5^{Tds} .

4. Fifth-Order Connected Triples E_5^T

This is the largest class of E_5 diagrams. It is generated by inserting a $T_3^{(3)}$ amplitude in place of the lower vertex in Fig. 5b(4), since $T_3^{(3)}$ can be, as it may be observed from Fig. 5c, obtained in three different ways. By employing the $T_2^{(2)}$ amplitude according to Fig. 5c(1), by employing $T_3^{(2)}$ as it is in Fig. 5c(2), and by substituting a disconnected $T_4^{(2)}$ operator into the third diagram in Fig. 5c, we can divide this group into three different subclasses: E_5^{TD} , E_5^{TT} , and E_5^{TQ} . Figure 13a–c presents these three types of $T_3^{(3)}$ amplitudes, which can be denoted as $T_3^{(3)}(D)$, $T_3^{(3)}(T)$, and $T_3^{(3)}(Q)$. In order to obtain $T_4^{(3)}$ we have to combine each diagram in Fig. 13 with the

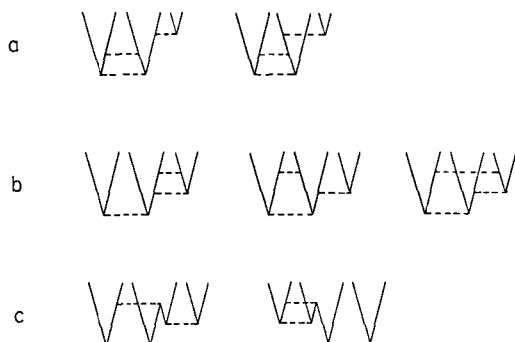


Fig. 13. Third-order T_3 amplitudes: (a) doubles, (b) triples, and (c) quadruples.

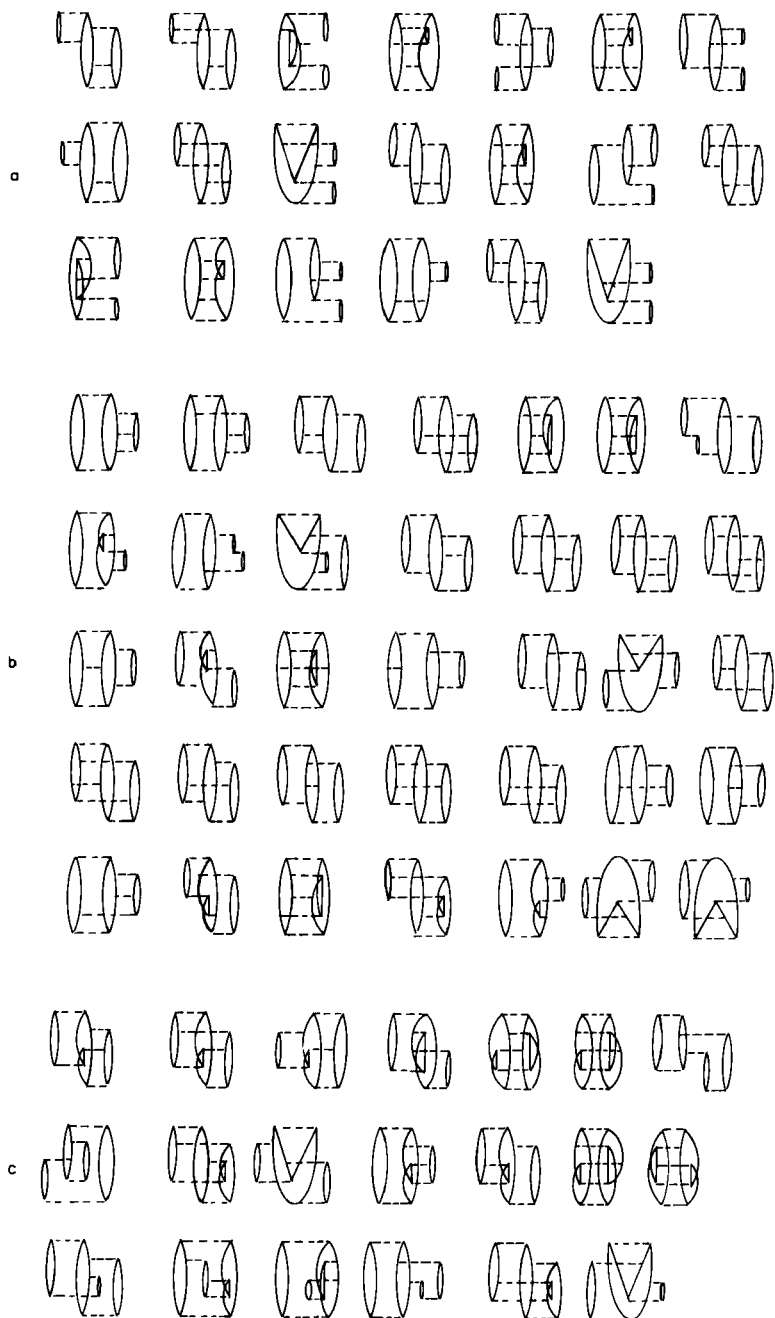


Fig. 14. Fifth-order energy diagrams arising from connected triple excitations, i.e., Fig. 5b(4): (a) E_5^{TD} , (b) E_5^{TT} , and (c) E_5^{TQ} .

V_2^N operator of the form $|\text{---}\wedge$, which decreases by one the excitation level; and as the second step, by adding the final interaction. The first step may be accomplished in many ways, which can be seen from Fig. 14, in which we have three groups of diagrams. The first group, in Fig. 14a, is a result of the operation with V_2^N on the diagrams shown in Fig. 13a and then closing. This gives 20 skeleton diagrams denoted as E_5^{TD} , corresponding to 80 antisymmetrized ones. When applying the same procedure to the three skeleton diagrams in Fig. 13b, we can generate the 35 skeletons shown in Fig. 14b, equivalent to 164 antisymmetrized diagrams of triple excitation origin. Repeating this for the $T_3^{(3)}(Q)$ amplitudes from Fig. 13c, we are able to create all the fifth-order triple excitation diagrams of quadruple origin, i.e., E_5^{TQ} . There are 20 such skeletons that correspond to 80 antisymmetrized diagrams.

Thus the total number of the E_5^{T} antisymmetrized diagrams is equal to 324.

5. Fifth-Order Energy Diagrams Originating from the Disconnected Quadruple Contribution E_5^{Qds}

The E_5^{Qds} diagrams are generated by the b(5a) and b(5b) terms in the D equation in Fig. 5b. The combined order of the lower vertices in Fig. 5b(5a,b) must be equal to 3, and so this can be realized by taking $T_2^{(1)}$ and $T_2^{(2)}$ amplitudes. The V_2^N operator present in the CC equation, i.e., the upper vertex in Fig. 5b(5a,b) terms can be joined to the combined $T_2^{(1)}$ and $T_2^{(2)}$ in 84 ways. Thus, we will have 84 E_5^{Qds} antisymmetrized diagrams, 36

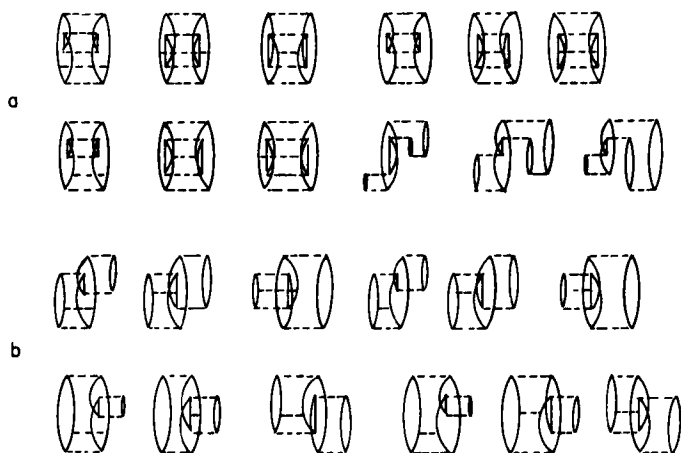


Fig. 15. Fifth-order energy diagrams arising from disconnected quadruple excitations, i.e., from (a) Fig. 5b(5a) and (b) Fig. 5b(5b).

of them due to the term (5a) and 48 due to the term (5b). Both groups of diagrams are presented in the form of skeleton diagrams in Fig. 15a,b. Similarly, as in the case of E_5^{Tds} we can avoid "long," i.e., quadruple, excitation denominators by factoring each group of three antisymmetrized diagrams differing only by "time" order into one via the factorization theorem.^{26,40} In this way instead of 84 we would have 28 "short" denominator diagrams, which are much simpler computationally.

6. Fifth-Order Quadruples E_5^Q

This group of diagrams is generated by Fig. 5b(6), i.e., by replacing the bottom interaction line in this diagram by the $T_4^{(3)}$ amplitudes given in Fig. 16. Here $T_4^{(3)}$ operators can be obtained with the help of the equation presented in Fig. 5d from $T_3^{(2)}$ and $T_2^{(1)} \cdot T_2^{(1)}$ operators. In the first case we would have the two $T_4^{(3)}(T)$ skeleton diagrams presented in Fig. 16a, corresponding to eight antisymmetrized diagrams, while the second term would result in the four antisymmetrized diagrams shown in Fig. 16b as one skeleton diagram. The substitution of $T_4^{(3)}$ into Fig. 5d would lead finally to the fifth-order energy diagrams pictured in Fig. 17. Figure 17a derives from $T_4^{(3)}(T)$ or E_5^{TQ} , which are represented by 112 antisymmetrized diagrams or 28 skeleton diagrams. Figure 17b derives from the $T_4^{(3)}(Q)$, i.e., E_5^{QQ} , and represents 56 antisymmetrized diagrams or 14 skeleton diagrams.

The total number of E_5^Q diagrams produced by the connected $T_4^{(3)}$ contribution amounts to 168. Adding the 84 fifth-order disconnected quadruple excitation diagrams, E_5^{Qds} , results in a total of 252 antisymmetrized diagrams of quadruple excitation type.

7. Disconnected Contribution to E_5

This kind of contribution originates from the second term of Eq. (29) or (40). As was mentioned at the beginning of this section, this term can contribute to the energy only through $T_1^{(2)} \cdot T_1^{(2)}$. The diagrams generated in

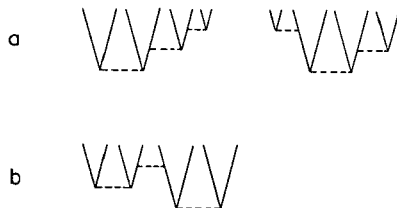


Fig. 16. Third-order T_4 diagrams: (a) diagrams arising from connected triples $T_3^{(2)}$ and (b) diagrams arising from disconnected $T_2^{(1)} \cdot T_2^{(1)}$.

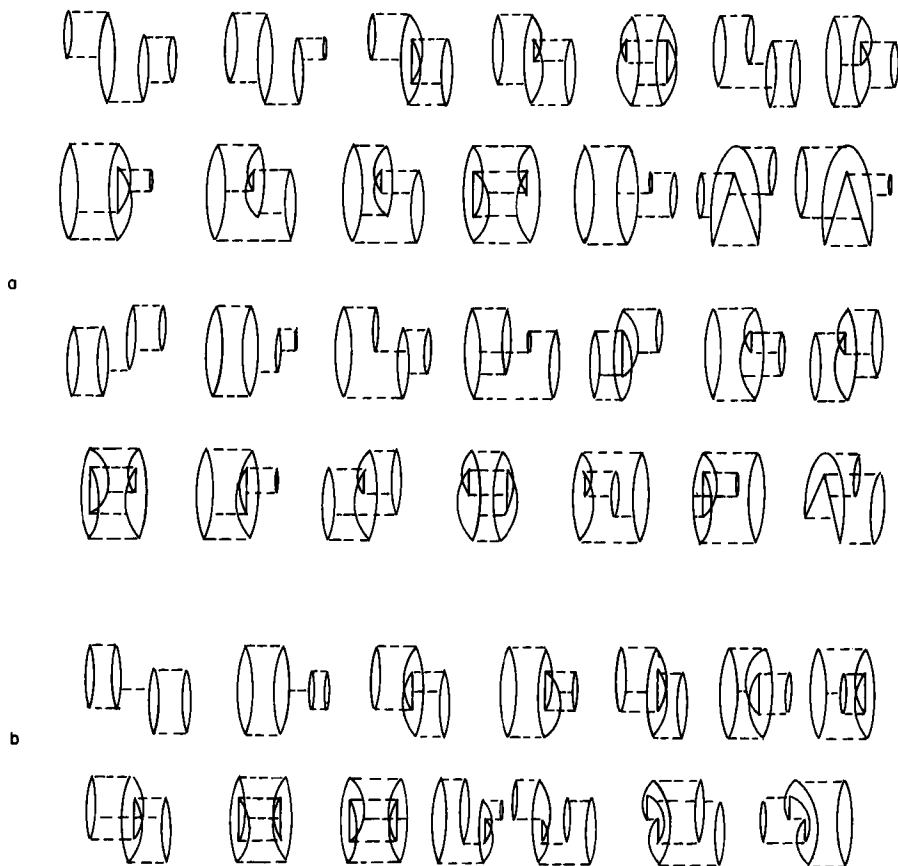


Fig. 17. Fifth-order energy diagrams derived from $T_4^{(3)}$, Fig. 16: (a) diagrams from $T_4^{(2)}(T)$, E_5^{QT} ; (b) diagrams from $T_4^{(3)}(Q)$, E_5^{QQ} .

this way are presented in Fig. 18. There are 12 antisymmetrized diagrams corresponding to 3 skeleton diagrams. It can be easily observed that the 3 diagrams in Fig. 18 can be obtained by switching the “time orders” of the lowest three interactions. Analogous to the case of E_5^{Qds} we can factorize these diagrams; this would result in 1 skeleton diagram or 3 antisymmetrized diagrams with simpler denominators.

VI. Remarks and Comments

A summary of the analysis of the fifth-order terms is given in Table II. The columns refer to all possible contributions to the fifth-order energy

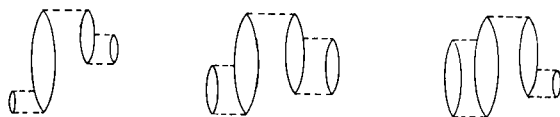


Fig. 18. Fifth-order energy diagrams that arise from disconnected contributions of T_2^2 .

E_5 , while the various CC approaches are placed in the rows. A crossmark indicates that the group of energy diagrams is generated by the relevant CC approach.

In order to further clarify the generation of the fifth-order terms we demonstrate pictorially in Table III how, by the CC iterations, particular groups of E_5 are obtained.

The simplest of all CC schemes, LCCD, generates 16/56 (skeleton/antisymmetrized) diagrams, i.e., the whole E_5^{DD} group (cf. col. 6 of Table II). Table III demonstrates that this can be achieved by straightforward threefold iteration of the T_2 diagrams.

Inclusion of the nonlinear terms in CCD, i.e., $\{\overline{H_N T_2^2}\}$, results in an additional 112 terms, grouped in E_5^{DQ} (col. 8 of Table II) and E_5^{Qds} (col. 13). The latter are obtained (see Table III) by combining $T_2^{(2)}$, obtained from the first iteration and $T_2^{(1)}$, calculated in zeroth iteration, to obtain in one more iteration $T_2^{(4)}$. Similarly, the E_5^{DQ} diagrams are obtained in two iterations: $T_2^{(3)}$ in the first and $T_2^{(4)}$ in the second.

Inclusion of the T_1 coefficients results in the creation of several additional groups of diagrams, depending on whether a linear or full CCSD method is considered. The former case provides 9/36 additional diagrammatic terms, compared to LCCD, while the full CCSD produces 69/252 diagrams, i.e., 8 out of 15 classes. These are placed in Table III under S and D entries. It may be seen there what type of mutual interrelation between S and D leads to the fifth-order diagrams. In order to reproduce the fifth-order terms according to the CC scheme, we need to carry out two iterations of the S equation and three iterations of the D equation.

The most dramatic improvement over former methods is obtained by an inclusion of triple excitation amplitudes. The simplest version of CCSDT, CCSDT-1, proposed elsewhere,¹⁰ reproduces an additional 44/176 terms. It is possible to develop another approximation to CCSDT, denoted as CCSDT-2 (see Table II), which is still computationally very efficient. It arises from including $T_2^2/2$ into the CCSDT equations. In this manner we can account for an additional 20/80 diagrammatic terms. The full inclusion of T_3 generates an additional 35/164 diagrams or 99/420 more diagrams compared to the CCSD method. In order to obtain that, we need

TABLE

SUMMARY OF THE DIAGRAMMATIC TERMS IN FIFTH-ORDER ENERGY

1	2	3	4	5	6	7	8	9 ^a	9 ^b
								E_5^{Tds}	
	E_5^{SS}	E_5^{SD}	E_5^{ST}	E_5^{DS}	E_5^{DD}	E_5^{DT}	E_5^{DQ}	$E_5^{(TS)}$	$E_5^{(TQ)}$
Figure	10a	10b	10c	11a	11b	11c	11d	12	9
Number of skeleton diagrams	1	4	4	4	16	20	8	3	6
Number of antisymm. diagrams	4	16	16	16	56	80	28	36	
								12	24
LCCD					×				
CCD					×		×		
LCCSD	×	×		×	×				
CCSD	×	×		×	×		×		×
CCSDT-1	×	×	×	×	×	×	×		×
CCSDT-2	×	×	×	×	×	×	×		×
CCSDT	×	×	×	×	×	×	×		×
CCSDTQ	×	×	×	×	×	×	×		×

^a See explanation in the text.

^b The first number refers to the number of skeleton diagrams; the second to the number

to perform two T_3 iterations, although some $T_3^{(3)}$ contributions are obtained already in the first iteration (see Table III).

An inclusion of T_4 will generate the missing 42/168 diagrams. It may be seen from Table III that we need only one iteration of T_4 to obtain E_5^{QT} and E_5^{QQ} .

It follows from the preceding presentation that the CCSDTQ method can reproduce all the terms occurring in the fifth-order energy expansion. It can be observed that many of the diagrams are equivalent to each other due to some sort of symmetry. This can be demonstrated by comparing, for instance, groups of diagrams denoted as E_5^{DS} (Fig. 11a) with those denoted as E_5^{SD} (Fig. 10b). The latter are just Hermitian conjugates of the former ones, or putting it in a more illustrative way, one group can be obtained from the other by turning it upside down. In terms of real orbitals the two sets are numerically equal. In general, we should obtain a Hermi-

II

EXPANSION GENERATED BY VARIOUS CC APPROACHES

10	11	12	13a	13b	14	15	16a	16b		
			E_5^{Qds}				E_5^{ds}		$^a\text{Total}$	Basis set size dependence
$^aE_5^{\text{TD}}$	E_5^{TT}	E_5^{TQ}	$E_5^{(\text{QD})}$	$E_5^{(\text{QQ})}$	$^aE_5^{\text{QT}}$	E_5^{QQ}	$E_5^{(\text{TS})}$	$E_5^{(\text{TQ})}$		
14a	14b	14c	15		17a	17b	18			
			24				3			
20	35	20			28	14			210	
			8	16			1	2		
			84				12			
80	164	80			112	56			840	
			28	56			4	8		
									16/56 ^b	n^6
									48/168	n^6
									25/92	n^6
									69/252	n^6
									133/428	n^7
									133/508	n^7
									168/672	n^8
									210/840	n^9

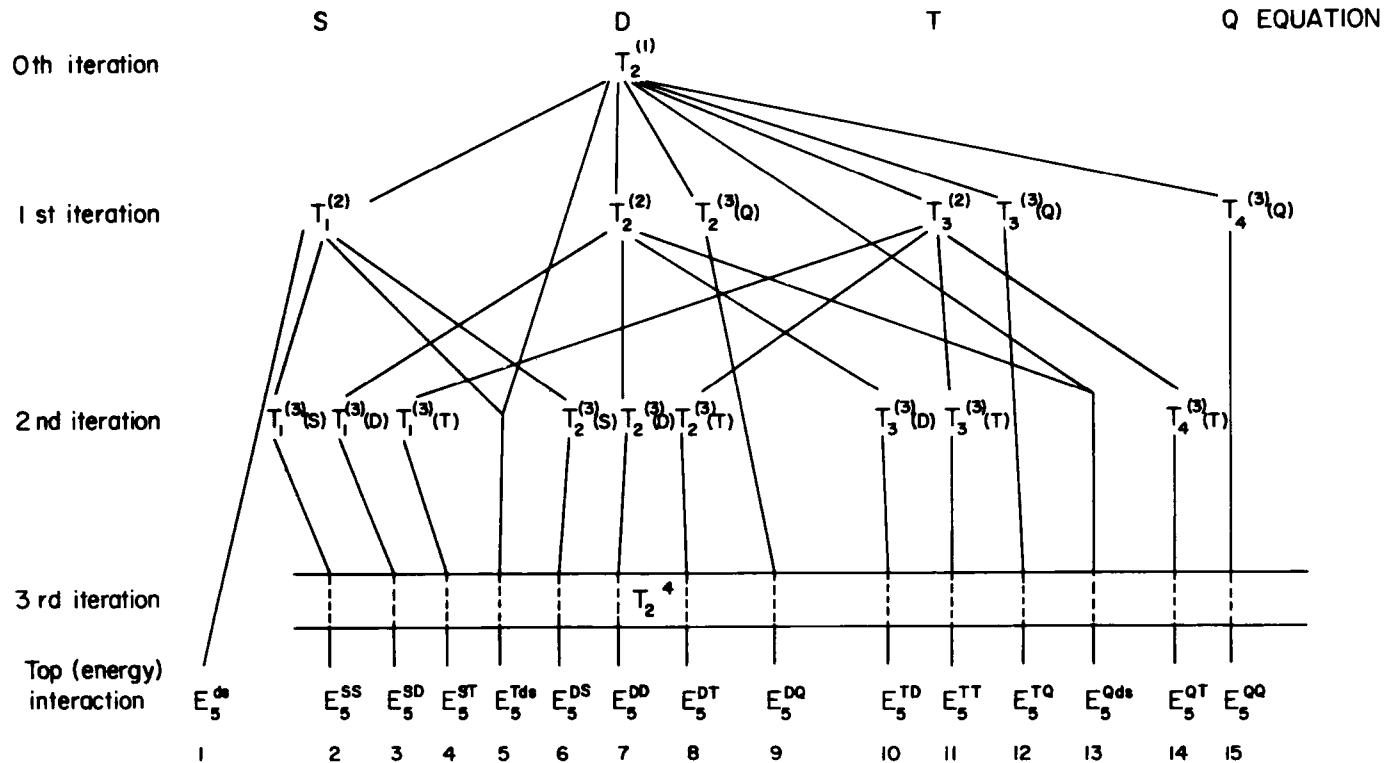
of antisymmetrized diagrams.

tian conjugate by switching superscripts in the E_5 symbol, for instance, E_5^{DT} to E_5^{TD} . This is true, however, only for two pairs of groups: $E_5^{\text{SD}}-E_5^{\text{DS}}$ and $E_5^{\text{DT}}-E_5^{\text{TD}}$. This may be seen even by comparing the number of skeleton or antisymmetrized diagrams belonging to each group and given in columns 3 and 5 or 7 and 10 in Table II. When comparing other types of diagrams, e.g., E_5^{TQ} and E_5^{QT} , the number of terms in each group is not the same. This is due to the inherent asymmetric nature of the CC equations and the formation of the special group of diagrams classified as disconnected: E_5^{Tds} , E_5^{Qds} , and E_5^{ds} , which is justified only from the CC point of view.

From the perturbation viewpoint a more natural classification would refer rather to the level of excitation at each intervertex level, which is also much closer to the CI classification. The classification of diagrams based on this criterion would look slightly different. Out of four interver-

TABLE III

GRAPHIC PRESENTATION OF THE ITERATIVE SCHEME OF THE CCSDTQ METHOD IN A FIFTH-ORDER ENERGY CALCULATION



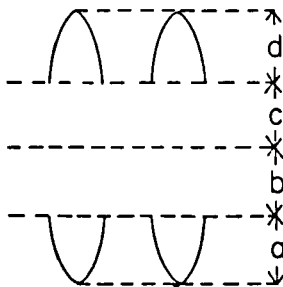


Fig. 19. General structure of the fifth-order diagrams. Intervertex levels a and d are always of double excitation type for an HF reference state.

tex levels in each of the diagrams in Fig. 19, only two are of importance, namely, b and c, since a and d are always of double excitation character for a HF reference. In analogy to the former notation we describe each diagram as $E^{(n_c n_b)}$, where n_c , n_b stand for symbols S, D, T, and Q corresponding to single, double, triple, and quadruple types of excitation. Thus, for instance, diagram Fig. 10a may be described as $E^{(SS)}$, Fig. 10b as $E^{(SD)}$, etc. It is straightforward to see that all diagrams belonging to the group E_5^{AB} are contained in the group $E_5^{(AB)}$. The latter, however, may contain also some terms absent in the former, namely, those classified in the group of disconnected diagrams, which now disappears, since in this classification it is irrelevant whether the diagram is of connected or disconnected origin. This is why the relevant columns in Table II, i.e., 9, 13, and 16, which refer to the disconnected diagrams bear double descriptions. Thus diagrams denoted as E_5^{Tds} (col. 9 of Table II) are now reassigned to the groups $E_5^{(TS)}$ and $E_5^{(TQ)}$, respectively, 3/12 and 6/24 diagrams. Diagrams E_5^{Qds} (col. 13) are reassigned to groups $E_5^{(QD)}$ and $E_5^{(QQ)}$, respectively, 8/28 and 16/56 graphs; and the last group of disconnected diagrams (col. 16) would belong now to the groups $E_5^{(TS)}$ and $E_5^{(TQ)}$, respectively, 1/4 and 2/8 diagrams.

Now the mutual Hermiticity of the corresponding diagrams is more transparent. In addition to the pairs $E_5^{SD} - E_5^{DS}$ and $E_5^{DT} - E_5^{TD}$, we have Hermitian correspondence within pairs $E_5^{(ST)} (= E_5^{ST}$ in col. 4 of Table II) and $E_5^{(TS)}$ (col. 9a) and $E_5^{(TS)}$ (col. 16a); $E_5^{(DQ)} (= E_5^{DQ}$, col. 8) and $E_5^{(QD)}$ (col. 13a); $E_5^{(TQ)} (= E_5^{TQ}$, col. 12) and $E_5^{(TQ)}$ (col. 9b); and $E_5^{(TQ)}$ (col. 16b) and $E_5^{(QT)} (= E_5^{QT}$, col. 14), so altogether 252 diagrams belonging to the groups $E_5^{(SD)}$, $E_5^{(ST)}$, $E_5^{(DT)}$, $E_5^{(DQ)}$, and $E_5^{(TQ)}$ have their Hermitian equivalents in the 252 diagrams, belonging to the analogous groups with interchanged superscripts, i.e., $E_5^{(DS)}$, $E_5^{(TS)}$, $E_5^{(TD)}$, $E_5^{(QD)}$, and $E_5^{(QT)}$. Assuming that we are dealing with real one-electron functions, these two groups of conjugate

diagrams have the same value, and this would result in reducing the total number of computationally different fifth-order antisymmetrized energy diagrams to $840 - 252 = 588$. In addition, within classes E^{SS} , E^{DD} , E^{TT} , and E^{QQ} , there occur pairs of hermitially equivalent diagrams, respectively, 1, 21, 65, and 38 pairs. This means that an additional 125 diagrams may be skipped, which further reduces the number of computationally distinct fifth-order diagrams to 463. This number includes 377 diagrams that possess a Hermitian equivalent and 86 that are symmetric with respect to the horizontal plane (by turning the latter upside down, the same diagram is obtained).

The other important simplification in the fifth-order diagrammatics is due to the already-mentioned factorization theorem. As was mentioned before, the number of the nonlinear terms (from the CC point of view) may be substantially reduced by combining the various time orders together, which results in a smaller number of diagrams to be considered, and a much simpler computational algebraic expression assigned to them due to the removal of some complex triple and quadruple excitation denominators. This refers to the diagrams classified as E_5^{Tds} , E_5^{Qds} , E_5^{ds} already described in previous sections, but also to the diagrams classified as E_5^{QT} and E_5^{QQ} given in Fig. 17a,b. All the diagrams presented in Fig. 17a can be paired in such a way that one of them can be obtained from the other by switching the two top interaction lines. This will result, as in the case of the nonlinear diagrams, in generating one factorized diagram instead of two regular ones. This leads to the reduction of the total number of diagrams by two and to something that is computationally much more important (n^6 instead of n^8) in eliminating quadruple excitation denominators.

The same treatment can be applied to the E_5^{QQ} group (Fig. 17b). In this case we have two quadruple denominators, and to eliminate them we have to switch both top and bottom pairs of interaction lines, which reduces by 4 the number of diagrams. By switching the bottom interaction we obtain in some cases the same diagrams as those obtained by switching the top interactions. Thus in this case we obtain also a reduction in the number of diagrams by two, while we have to attach to the fully factorized diagram a coefficient of $\frac{1}{2}$. The net total of computationally distinct fifth-order antisymmetrized directed line diagrams then becomes 328.

The question arises whether we need T_4 amplitudes in order to generate all fifth-order diagrams. The answer depends on the approach. If we solve the CCSDT equations and obtain converged results, then we have the full fourth-order energy, but not the fifth-order energy, since we miss 168 diagrams, denoted here as E_5^{QT} and E_5^{QQ} . We do include some other diagrams that are formally of quadruple excitation type that are termed as

E_5^{Qds} (or according to the other classification as $E_5^{(\text{QD})}$ and part of $E_5^{(\text{QQ})}$). These quadruples are of the same nature as those in fourth order; i.e., they are generated by the inclusion of T_2^2 into the CCD equation. Diagrams E_5^{QT} and E_5^{QQ} are of different character than E_4^{Q} , and if we pursue a pure CC calculational approach, they can be included only by solving the CCSDTQ equations.

On the other hand, it is possible to calculate these terms without employing the T_4 coefficient, but in order to do that we have to write some additional code beyond the CCSDT approach. Diagrams E_5^{QT} and E_5^{QQ} can be calculated, because of the above-mentioned factorization theorem, with the help of only T_2 and T_3 coefficients.

This problem may be approached in a more systematic manner. From the point of view of some intervertex level, the energy diagram may be considered as being of k -tuple character; i.e., there is a k -tuple excitation denominator required for that diagram. If the considered intervertex level divides an n th-order diagram into two parts of m th and $(n - m)$ th order, $m \leq (n - m)$, we can express it symbolically as

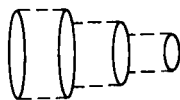
$$E_k^{(n)} = \dots + \langle \Psi_k^{(n-m)} | E_0 - H_0 | \Psi_k^{(m)} \rangle + \dots \quad (41)$$

Now, in order for the considered diagram to be factorizable from the point of view of the considered intervertex level, we only need at least one of the wave function components in Eq. (41) to be of disconnected character. If the component $\langle \Psi_k^{(n-m)} |$ is disconnected, the diagram is factorizable, but in order to generate it by a CC iteration, the k -tuple type of the CC equation must be considered. If $|\Psi_k^{(m)}\rangle$ is disconnected, the diagram is also factorizable but is generated by the lower-rank CC equation. If both components of the wave function in Eq. (41) are connected, the diagram is not factorizable and the k -tuple CC equation is required.

Thus in the case of fifth-order quadruples, according to this procedure, we obtain $\langle \Psi_4^{(2)} |$ and $|\Psi_4^{(3)}\rangle$, or vice versa, and in both cases $\Psi_4^{(2)}$ is of disconnected character, so all fifth-order quadruples are factorizable (with respect to the quadruple denominator).

The possibility of the factorization of all diagrams involving quadruple excitation denominators is essential since this permits the elimination of *all* quadruple excitation denominators from fifth-order energy diagrams. This reduces the computational dependence of such terms from n^9 (n is the number of basis functions) down to n^6 (n^7 when triple excitation denominators are present). [In all asymptotic dependences it should be recognized that the actual dependence is always far less since (1) the actual dependence is $n_{\text{occ}}^p n_{\text{virt}}^q$, not n^{p+q} ; and (2) space and spin symmetry greatly reduce the number of distinct terms. When we say n^{p+q} these additional simplifications are understood.]

There is still another class of diagrams involving quadruple denominators that appears in sixth order, which may be looked at as two diagrams from Fig. 16a put together as



These diagrams may be obtained, from the CC point of view, only by an inclusion of T_4 . However, they cannot be obtained without T_4 even if we would like to calculate them beyond the CC scheme since they are not factorizable.

We can apply the same procedure to the diagrams involving triple excitation denominators. Again we can distinguish three categories of these diagrams:

1. nonfactorizable—those in Fig. 14a–c—altogether 324 (antisymmetrized) diagrams and those in Fig. 11c—80 diagrams (computationally equal to those in Fig. 14a).
2. factorizable but generated by the T equation—diagrams in Figs. 10c—altogether 16 diagrams, and
3. factorizable and generated by CCSD—diagrams in Figs. 12 and 18—altogether 48 diagrams.

VII. Computational Strategy in a Fifth-Order MBPT Calculation

There are several different methods of calculating fifth-order diagrams. One of the most straightforward would be to collect all the different fifth-order diagrams, to factorize them if possible, and to compute them one by one, some of them requiring multiplication by two to account for their Hermitian conjugates. According to the discussion in the preceding section, taking into account all the possible interdiagrammatic relationships, we would wind up evaluating 328 directed antisymmetrized diagrams and the computational scheme would be rather time-consuming.

The other obvious strategy would be that based on the CC equations. The most straightforward one would rely on coding the full CCSDTQ equations and on performing the required number of iterations, according to Table III, in order to calculate $T_2^{(4)}$ and then to obtain the fifth-order energy. This method, although probably more efficient than the former one, would require a substantial amount of computer time because of the simultaneous iteration of four types of equations: the D equation (three

iterations), the S and T equations (two iterations), and the Q equation (one iteration) (cf. Table III), and some of them would have a very high basis set dependence (see the following discussion).

The efficient way of calculating the fifth-order energy terms would be by combining the CC scheme with Wigner's $2n + 1$ rule. The $2n + 1$ rule in MBPT calculations was effectively exploited in fourth-, fifth-, and higher-order calculations by Bartlett and co-workers.^{16,32,39} It is particularly suitable in fifth-order calculations. This method is effectively based on Eq. (24) according to which we can express the fifth-order energy as

$$E_5 = \langle \Psi^{(2)} | E_0 - H_0 | \Psi^{(3)} \rangle_L$$

and take only linked terms. Further, following our previous considerations, we can divide the fifth-order energy into four parts corresponding to $E_5^{(S)}$, $E_5^{(D)}$, $E_5^{(T)}$, and $E_5^{(Q)}$,

$$E_5 = \langle \Psi_S^{(2)} | E_0 - H_0 | \Psi_S^{(3)} \rangle + \langle \Psi_D^{(2)} | E_0 - H_0 | \Psi_D^{(3)} \rangle \\ + \langle \Psi_T^{(2)} | E_0 - H_0 | \Psi_T^{(3)} \rangle + \langle \Psi_Q^{(2)} | E_0 - H_0 | \Psi_Q^{(3)} \rangle_L \quad (42)$$

Thus, going term by term in Eq. (42) the contribution to $E_5^{(S)}$ can be obtained by simply multiplying $T_1^{(2)}$ corresponding to the diagram Fig. 8a by $T_1^{(3)}$ given by the diagrams in Fig. 9 and accounting for the excessive denominators according to the formula

$$E_5^{(S)} = \sum_{ai} t_i^{a(2)} t_i^{a(3)} D_i^a \quad (43)$$

The basis set dependence of the computations is determined by the step leading to the $t_i^{a(3)}$ factor. Depending on what type of $T_1^{(3)}$ is considered (cf. Section V,F,1), we will have an n^5 dependence for $T_1^{(3)}(S)$, n^6 for $T_1^{(3)}(D)$, and n^7 for $T_1^{(3)}(T)$.

In an analogous way we can calculate $E_5^{(D)}$ by taking second- (Fig. 8b) and third- (Fig. 7) order T_2 amplitudes; $E_5^{(T)}$ by using corresponding T_3 amplitudes; and $E_5^{(Q)}$, by using T_4 amplitudes. It should be pointed out that the simple formula of the type given in Eq. (43) holds only if we have antisymmetrized $t_{ij\dots}^{ab\dots}$ amplitudes, as discussed in Section IV,B.

The antisymmetrized form of the $T_k^{(n)}$ coefficient may be obtained by taking all possible combinations of labels with respect to all nonequivalent lines. This can be visualized with the following example.

In order to account for the terms denoted in Table II as E_5^{Tds} and E_5^{ds} we have to use the expression

$$E_5^{\text{Tds}} + E_5^{\text{ds}} = \frac{1}{36} \sum_{\substack{abc \\ ij k}} t_{ijk}^{abc(2)} t_{ijk}^{abc} (\text{ds})^{(3)} D_{ijk}^{abc} \quad (44)$$

where $t_{ijk}^{abc}(\text{ds})^{(3)}$ stands for the disconnected contribution to the third order, T_3 . Both $T_3^{(2)}$ and $T_3(\text{ds})^{(3)}$ must be in antisymmetrized form. The antisymmetrized form of $T_3^{(2)}$ may be obtained by switching labels among nonequivalent open lines in Fig. 8c [see Eq. (22) of Ref. 10a]. Similarly, the antisymmetrized form of $T_3(\text{ds})^{(3)}$ will be given as

$$\begin{aligned}
 i \quad j \quad k \\
 \swarrow \quad \downarrow \quad \searrow \\
 \text{a} \quad \text{b} \quad \text{c} \\
 \swarrow \quad \downarrow \quad \searrow \\
 \text{ds}
 \end{aligned}
 =
 \begin{aligned}
 & \begin{array}{c} i \quad j \quad k \\ \swarrow \quad \downarrow \quad \searrow \\ \text{a} \quad \text{b} \quad \text{c} \\ \swarrow \quad \downarrow \quad \searrow \\ \text{c} \end{array} - \begin{array}{c} i \quad j \quad k \\ \swarrow \quad \downarrow \quad \searrow \\ \text{c} \quad \text{b} \quad \text{a} \\ \swarrow \quad \downarrow \quad \searrow \\ \text{a} \end{array} - \begin{array}{c} i \quad j \quad k \\ \swarrow \quad \downarrow \quad \searrow \\ \text{a} \quad \text{c} \quad \text{b} \\ \swarrow \quad \downarrow \quad \searrow \\ \text{b} \end{array} \\
 & - \begin{array}{c} k \quad j \quad i \\ \swarrow \quad \downarrow \quad \searrow \\ \text{a} \quad \text{b} \quad \text{c} \\ \swarrow \quad \downarrow \quad \searrow \\ \text{c} \end{array} + \begin{array}{c} k \quad j \quad i \\ \swarrow \quad \downarrow \quad \searrow \\ \text{c} \quad \text{b} \quad \text{a} \\ \swarrow \quad \downarrow \quad \searrow \\ \text{a} \end{array} + \begin{array}{c} k \quad j \quad i \\ \swarrow \quad \downarrow \quad \searrow \\ \text{a} \quad \text{c} \quad \text{b} \\ \swarrow \quad \downarrow \quad \searrow \\ \text{b} \end{array} \\
 & - \begin{array}{c} i \quad k \quad j \\ \swarrow \quad \downarrow \quad \searrow \\ \text{a} \quad \text{b} \quad \text{c} \\ \swarrow \quad \downarrow \quad \searrow \\ \text{c} \end{array} + \begin{array}{c} i \quad k \quad j \\ \swarrow \quad \downarrow \quad \searrow \\ \text{c} \quad \text{b} \quad \text{a} \\ \swarrow \quad \downarrow \quad \searrow \\ \text{a} \end{array} + \begin{array}{c} i \quad k \quad j \\ \swarrow \quad \downarrow \quad \searrow \\ \text{a} \quad \text{c} \quad \text{b} \\ \swarrow \quad \downarrow \quad \searrow \\ \text{b} \end{array}
 \end{aligned}
 \quad (45)$$

Inserting the preceding form of $T_3^{(3)}$ and the form of $T_3^{(2)}$ given in Eq. (40) of Ref. 10a into Eq. (44), we obtain $E_3^{\text{Tds}} + E_3^{\text{ds}}$ contributions. We can skip the $\frac{1}{3!}$ factor in Eq. (44) by ordering the indices to $a > b > c$ and $i > j > k$, which is also desirable from a computational viewpoint.

Similar but not identical situations occur in the calculation of E_3^Q . We also have to antisymmetrize the $T_4^{(2)}$ and $T_4^{(3)}$ coefficient. However, in this case it may happen that both components are of disconnected type ($T_4^{(2)}$ is always disconnected; $T_4^{(3)}$ may be both connected and disconnected). This also creates by simple multiplication of $T_4^{(2)}$ and $T_4^{(3)}$ unlinked contributions that are nonphysical and must be skipped over [this is a reason why the last term in Eq. (42) bears the subscript L].

This may be illustrated diagrammatically as

$$\langle \Psi_Q^{(2)} | E_0 - H_0 | \Psi_Q^{(3)} (\text{disconnected}) \rangle = \left(\begin{array}{cc} \begin{array}{c} \text{Diagram (1)} \\ \text{Diagram (1)} \end{array} & \begin{array}{c} \text{Diagram (1)} \\ \text{Diagram (2)} \end{array} \end{array} \right) D_{ijkl}^{abcd} \quad (46)$$

where D_{ijkl}^{abcd} denotes a quadruple excitation type denominator and all possible full connections of the open lines in the upper part with those of the lower part are considered. This would lead to the 24/84 linked diagrams, presented in Fig. 15 and 6/18 unlinked ones. The latter are given in Fig. 20a. Since the diagrams in Fig. 20 differ from each other only in the time order of the interaction lines, they can be factorized as shown in Fig.

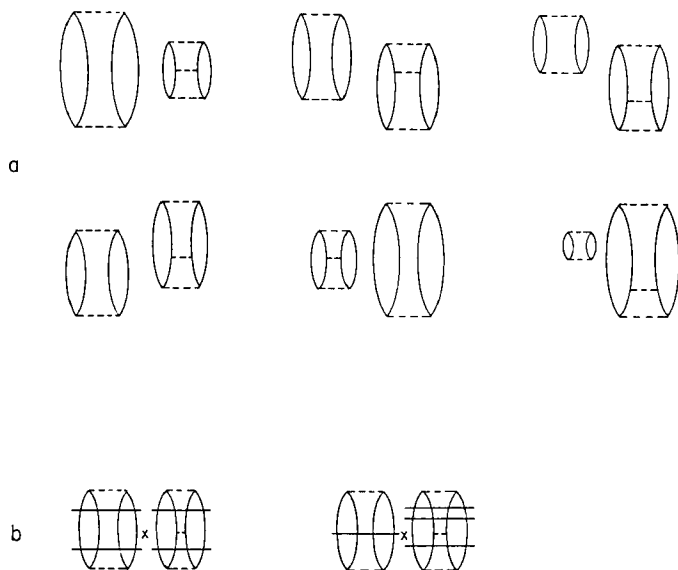


Fig. 20. (a) Unlinked diagrams in fifth-order MBPT; (b) illustration of factorization of unlinked diagrams.

20b, to the quantity

$$E_5^Q(\text{unlinked}) = \Delta_2 E_3 + \Delta_3 E_2 \quad (47)$$

where E_2 and E_3 are the second- and third-order energy, respectively, and Δ_2 and Δ_3 are a sort of amplitude overlap analogous to that occurring in fourth order:^{6,8}

$$\begin{aligned} \Delta_2 &= \frac{1}{4} \sum_{ijab} \frac{|\langle ab || ij \rangle|^2}{(D_{ij}^{ab})^2} \\ \Delta_3 &= \frac{1}{8} \sum_{abijkl} \frac{\langle ij || ab \rangle \langle kl || ij \rangle \langle ab || kl \rangle}{(D_{ij}^{ab})^2 D_{kl}^{ab}} \\ &\quad + \frac{1}{8} \sum_{abcdij} \frac{\langle ij || ab \rangle \langle ab || cd \rangle \langle cd || ij \rangle}{(D_{ij}^{ab})^2 D_{ij}^{cd}} \\ &\quad - \sum_{abcijk} \frac{\langle ij || ab \rangle \langle ak || cj \rangle \langle cd || ik \rangle}{(D_{ij}^{ab})^2 D_{ik}^{bc}} \end{aligned} \quad (48)$$

Thus, according to the preceding scheme, the formula for the calculation of the fifth-order quadruple contribution would be straightforward to implement: first by calculating $T_4^{(3)}$ according to the formula given in terms of diagrams in Fig. 16, and then by antisymmetrizing the $T_2^{(1)} \cdot T_2^{(2)}$ and $T_2^{(1)} \cdot T_2^{(1)}$ products, and finally by subtracting from the final energy value the unlinked quantity given by Eq. (47).

The preceding procedure for obtaining E_5 by combining the $2n + 1$ rule with the CC approach is convenient for implementation, but it is still inefficient with respect to the required computer time. This is due to the fact that E_5^Q requires time that depends on the basis set size as n^9 . In addition, many of the terms that are identical are calculated independently, which contributes also to the overall cost of computations.

TABLE IV
COMPONENTS OF E_5 SEPARATED FOR EFFICIENT COMPUTATIONS

E_5 com- ponent	Definition	Computational formula	Basis set dependence
S	$E_5^{SS} + E_5^{SD}$	$\sum_{ai} t_i^{a(2)} \cdot [t_i^a(S)^{(3)} + t_i^a(D)^{(3)}] D_i^a$	n^6
D_1	$E_5^{DS} + E_5^{DD} + E_5^{DQ}$	$\sum_{\substack{a>b \\ i>j}} t_{ij}^{ab(2)} \cdot [t_{ij}^{ab}(S)^{(3)} + t_{ij}^{ab}(D)^{(3)} + t_{ij}^{ab}(Q)^{(3)}] \cdot D_{ij}^{ab}$	n^6
D_2	E_5^{DT}	$\sum_{\substack{a>b \\ i>j}} t_{ij}^{ab(2)} \cdot t_{ij}^{ab}(T)^{(3)} \cdot D_{ij}^{ab}$	n^7
T_1	E_5^{TT}	$\sum_{\substack{a>b>c \\ i>j>k}} t_{ijk}^{abc(2)} \cdot t_{ijk}^{abc}(T)^{(3)} D_{ijk}^{abc}$	n^8
T_2	E_5^{TQ}	$\sum_{\substack{a>b>c \\ i>j>k}} t_{ijk}^{abc(2)} \cdot t_{ijk}^{abc}(Q)^{(3)} D_{ijk}^{abc}$	n^7
T_3	$E_5^{Tds} + E_5^{ds}$	$\sum_{\substack{a>b>c \\ i>j>k}} t_{ijk}^{abc(2)} t_{ijk}^{abc}(ds)^{(3)} D_{ijk}^{abc}$	n^6
Q_1	E_5^{Qds}	Formulas analogous to those used in the E_4^Q computations	n^6
Q_2	E_5^{QQ}	$\sum_{\substack{a>b>c>d \\ i>j>k>l}} t_{ijkl}^{abcd(2)} t_{ijkl}^{abcd}(Q)^{(3)} D_{ijkl}^{abcd}$	n^5, n^6
Diagram by diagram, see text			

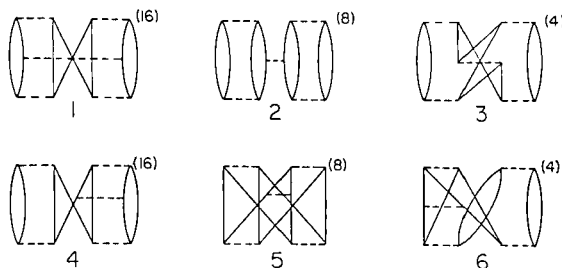


Fig. 21. Factorized fifth-order diagrams corresponding to the E_5^{QQ} term.

In order to avoid this difficulty we propose a more efficient approach to calculations. We separate out of the fifth-order energy several parts that are listed in column 1 of Table IV. They are defined in column 2 and calculated according to the formula given in column 3. The total fifth-order energy is then given as

$$E_5 = S + D_1 + 2D_2 + T_1 + 2T_2 + 2T_3 + Q_1 + Q_2$$

The last column of Table III gives an approximate estimate of the basis set dependence for the calculation of a particular term. We observe that most of the formulas given in Table IV rely on the $2n + 1$ rule. The bottleneck of these calculations seems to be the E_5^{TT} terms, which have an n^8 basis set dependence, as well as some terms in the E_5^{TT} expression.

To avoid the n^9 dependence of the E_5^{QQ} terms, we propose calculating this contribution by doing a diagram-by-diagram calculation. This is possible because of the fact that according to our assessments in Section VI, all the fifth-order quadruple contributions are factorizable. Figure 21 presents all 56 energy diagrams in arrowless factorized form. The overall number of diagrams is greatly reduced to 6 skeleton or 21 antisymmetrized factorized diagrams. All the E_5^{QQ} factorized diagrams may be decomposed into pieces in such a way that none of them requires higher than an n^6 basis set size dependence. See Appendix C.

VIII. Summary

The results discussed in the present paper show that the calculation of the fifth-order energy is feasible and when carefully implemented may be applied to moderate-sized systems. The number of terms that must be considered may be substantially reduced by taking into account the fact that many of the diagrams have identical values and many are amenable to factorization.

The problem arises primarily with one contribution: E_5^{TT} , which involves 164 diagrams out of 840. Those 164 terms show an n^8 basis set dependence that makes computations for large systems difficult. A question persists as to how large this contribution might be. However, it should be noted that although the fourth-order triple excitation diagrams are asymptotically n^7 (actually $n_{\text{occ}}^3 n_{\text{virt}}^4$), the CRAY implementation actually evaluates these terms faster than some of the n^6 (actually $n_{\text{occ}}^3 n_{\text{virt}}^3$) steps.⁴¹ Also, it is always possible to restrict the number of T_3 amplitudes to what is, it is hoped, a dominant subset. In addition, we may make other approximations that force denominator factorization as has been suggested^{34b} to diminish this asymptotic dependence, perhaps without introducing significant errors.

The analysis of the several different CC approaches in terms of the fifth-order energy contributions points out that within an n^6 dependent scheme, i.e., LCCD to CCSD in Table I, the CCSD is much preferred since it accounts for nearly one-third of all terms and avoids potential singularities in LCCD.⁴² It may also be observed that it pays off to include, even partially, the triple contribution, as was done in the CCSDT-1 method.¹⁰ In this model the number of terms is nearly doubled as compared to CCSD, and, of course, this method is correct through the fourth-order energy and the second-order wave function. Also, the connected T_3 contributions are numerically important.^{11,34}

We may conclude that the recommended CC approximation would be CCSDT, which accounts for 80% of the fifth-order terms, but the basis set dependence is still n^8 . The inclusion of T_4 in the coupled-cluster scheme would appear to cause a significant increase in computational time for what is normally considered to be a fairly small correction since $T_4 \ll \frac{1}{2} T_2^2$ for most nonmetallic cases. Of course, if a reference function is sufficiently poor, T_4 and even higher clusters could be important. However, as was shown in the preceding section, the missing, i.e., beyond CCSDT, fifth-order MBPT energy terms that arise from T_4 may be calculated by supplementing the CCSDT code with a few additional diagrams, the basis set dependence of which is n^6 or less, to introduce most of the correction due to T_4 .

Appendix A. Choice of Skeleton Diagrams and MBPT Diagram Rules

In this appendix we summarize the rules concerning the antisymmetrized skeleton diagrams. It was said in Section IV that in order to obtain a skeleton antisymmetrized diagram, we ignore the arrows. However, in order to do that we need first to have an antisymmetrized diagram in

correct form. Since any of the set of Goldstone diagrams that are obtained one from the other by switching pairs of incoming or outgoing lines can be chosen as an antisymmetrized one, we have several different antisymmetrized diagrams, all of them equivalent. Not all of them, however, can be used to create the skeleton diagram, since we can obtain the same antisymmetrized diagram more than once. This may be illustrated more clearly with the following example.

In the fourth-order energy expansion there are 12 diagrams that are classified as doubles. All of them can be restored by providing arrows to the four skeleton diagrams presented in Fig. 22. Diagrams a, b, c have two asymmetric loops, diagram d one. By an asymmetric loop we mean a loop that is connected with the rest of the diagram by three or more vertices. Thus, by providing arrows for each loop in a clockwise or counterclockwise manner, we obtain for skeleton diagrams a and b in Fig. 22 $3 + 3$ antisymmetrized diagrams; for skeleton diagram c, 4 antisymmetrized ones; and for the skeleton d, containing one asymmetric loop, 2 antisymmetrized diagrams. In diagrams a and b there is a vertical symmetry plane that reduces the number of antisymmetrized diagrams from 4 to 3. If we compare these diagrams with the full set of fourth-order diagrams, given, e.g., in Fig. 2 of Ref. 7, we see that skeleton a corresponds to the diagrams D5, D6 and D13; skeleton b to D7, D8, and D14; c to D9, D10, D11, and D12; and d to diagrams D15 and D16. It must be stressed that the form of skeleton diagram d in Fig. 22 is not accidental. If instead we used a skeleton diagram obtained by removing arrows from, e.g., diagram D15 or D16, then we would recover both missing doubles, i.e., D15 and D16, but in addition we would obtain also diagram D9 and D11, which are already generated by skeleton c. Thus in order to prevent doubling (tripling, etc.)

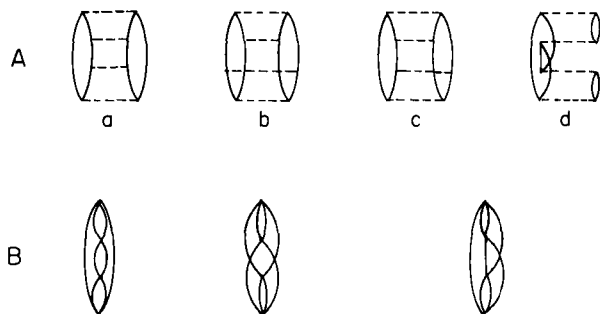


Fig. 22. Fourth-order skeleton (A) and Hugenholtz skeleton (B) diagrams of double excitation type. By providing arrows in all possible ways, all the fourth-order antisymmetrized and Hugenholtz doubles are restored.

of some diagrams when adding arrows we have to choose the form of the antisymmetrized diagram in a systematic manner.

As was mentioned in Section IV, it is still possible to reduce the number of graphs to be considered by using Hugenholtz diagrams.³⁸ In the case of fourth-order doubles we would have instead of four antisymmetrized skeleton diagrams, Fig. 22A, only three Hugenholtz skeleton diagrams, Fig. 22B. However, adding rows to the diagrams is not automatic, and besides, there is an ambiguity concerning the sign factor that should be assigned to the diagram, although a rule has been suggested for the sign.⁴³ The observation that adding arrows to the skeleton Hugenholtz diagram may cause some problems is illustrated by the example given in Fig. 23. Presented in this figure is one fifth-order Hugenholtz skeleton diagram (a) and three antisymmetrized skeleton diagrams that correspond to it (b). The arrows can be provided to the graph a in 24 ways, while there are 8 ways to add them to the b graphs. In both cases, the result is 24 antisymmetrized directed diagrams. There is only one such situation in fifth order. Note that providing arrows to each of the antisymmetrized skeletons is trivial, while in the case of the Hugenholtz graph it requires some effort.

When the antisymmetrized diagrams are restored in order to obtain the corresponding algebraic expression, we apply the rules, summarized in Section IV but now somewhat modified for MBPT diagrams instead of CC diagrams. We assign to each vertex an antisymmetrized integral, with the (left out, right out||left in, right in) convention. We determine the sign

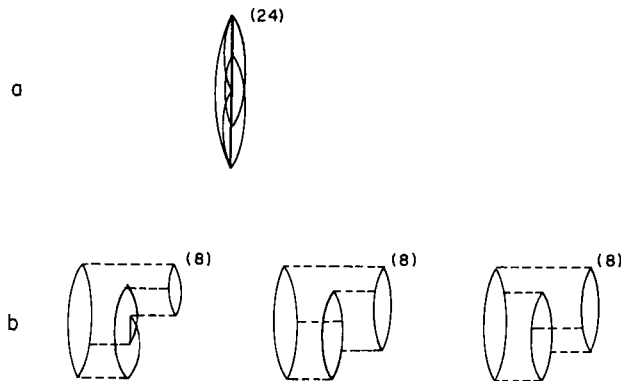


Fig. 23. Example of fifth-order skeleton Hugenholtz diagram (a) and (b) skeleton diagrams corresponding to it. Arrows can be added to (a) in 24 ways, to each diagram in (b) in 8 ways.

according to the loop and hole rule. For each diagram we add a factor of 2^{-N} , where N is the number of pairs of equivalent lines. Unlike the CC rules, to each intervertex level we assign a denominator factor according to the formula

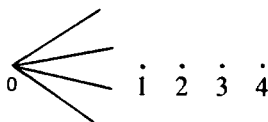
$$D_{ijkl\dots}^{abc\dots} = \varepsilon_i + \varepsilon_j + \varepsilon_k \cdots - \varepsilon_a - \varepsilon_b - \varepsilon_c \cdots$$

where indices i, j, k, \dots (a, b, c, \dots) refer to down (up)-going lines encountered at the considered intervertex level. All the up (down)-going lines are summed over virtual (occupied) orbital levels. Since the MBPT diagrams are closed, there is no permutation of external orbital labels.

Appendix B. Systematic Generation of MBPT Energy Diagrams

One way of generating MBPT diagrams is to iterate the CC equations as has been discussed. The other option would be to generate them directly at the given perturbation order without going through the lower-order terms. This approach has been analyzed in the papers of Paldus and Wong.⁴⁴ Here we give a very short scheme used to generate fifth-order Hugenholtz skeleton diagrams, from which all other types of diagrams may be obtained.

In the Hugenholtz approach each vertex is represented by a dot, with which four lines are attached (V is assumed to be only of two-body character). We can first attach the four lines with the topmost dot, which has number 0 and then consider all the possibilities of connecting those four lines with the remaining dots numbered 1–4:

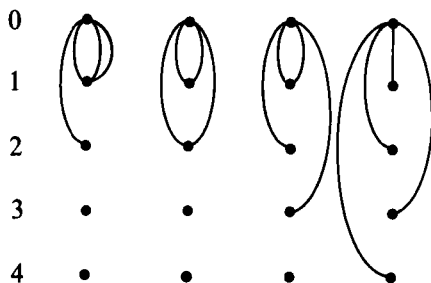


To make it more systematic we can consider partitions of the number 4, which are

$$\begin{aligned} &3, 1, 0, 0 \\ &2, 2, 0, 0 \\ &2, 1, 1, 0 \\ &1, 1, 1, 1 \end{aligned}$$

We understand each partition as a number of lines connected with first,

second, third, and fourth dots. This is demonstrated graphically as



For instance, partition 2, 1, 1, 0 corresponds to the graph in which two lines outgoing from the 0th dot are connected with the first dot, one line with the second and third, and none with the fourth.

It is obvious that in order to account for all the diagrams we have to consider all permutations within each partition. There are 12 distinct permutations in the partitions 3, 1, 0, 0 and 2, 1, 1, 0; 6 permutations in the partition 2, 2, 0, 0; and 1 in partition 1, 1, 1, 1. Our next step is to complete the preceding graphs to the full diagram in which to each dot four lines are attached. The graph corresponding to the partition 3, 1, 0, 0 can be completed in three ways; see Fig. 24a. This is valid for any permutation within this partition, since the permutation graphically corresponds to the different time ordering of respective indices. For instance, the exchange of the third and fourth interactions corresponds to the exchange of two zeros in the partition and hence does not lead to a new diagram. It holds also for the diagrams in Fig. 24a, since switching the two lowest interactions in the first diagram leads to the same diagram, the same operation for the second diagrams creates the third one, and vice versa. Any other switching of the interaction leads to a new diagram. Hence, for the partition 3, 1, 0, 0 we obtain $12 \times 3 = 48$ skeleton Hugenholtz diagrams. It is interesting that the diagrams presented in Fig. 24 contain important topological information. For example, for any diagram obtained from those in Fig. 24 by different time ordering, there is the same number of antisymmetrized and Goldstone diagrams. Thus, on the basis of skeleton diagrams presented in Fig. 24, we can calculate the total number of diagrams of the other types. The numbers in parentheses standing next to each diagram represent the number of antisymmetrized diagrams and the number of Goldstone diagrams. In the whole class of diagrams generated by the partition 3, 1, 0, 0, there are $12 \times 12 = 144$ antisymmetrized diagrams and $12 \times 112 = 1344$ Goldstone diagrams.

Similarly, the graph corresponding to the partition 2, 2, 0, 0 may be completed in five ways (Fig. 24b), and we see that exchange of the inter-

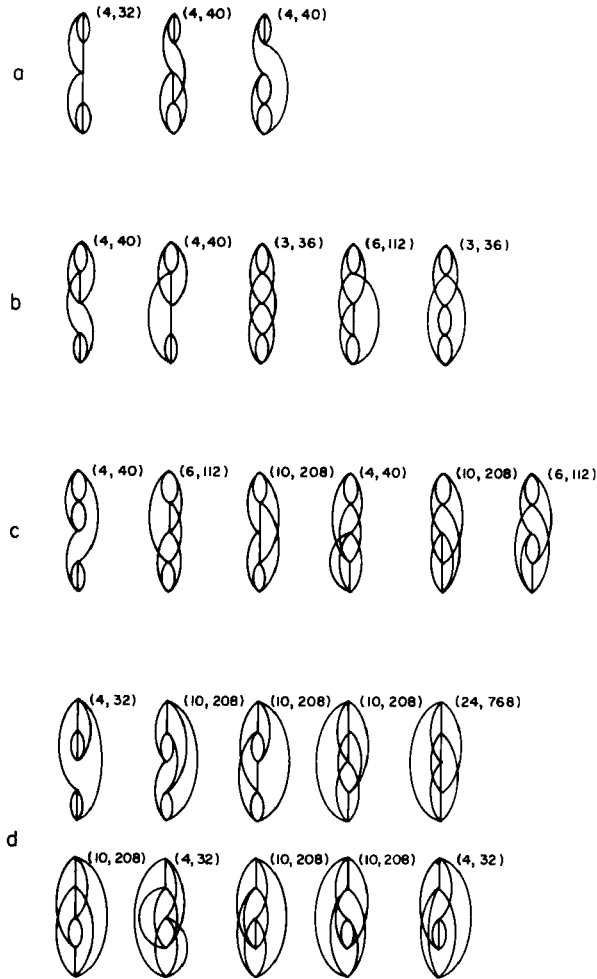


Fig. 24. Fifth-order skeleton Hugenholtz diagrams related to partitions: (a) 3, 1, 0, 0; (b) 2, 2, 0, 0; (c) 2, 1, 1, 0; and (d) 1, 1, 1, 1. Numbers in parentheses refer to the number of antisymmetrized and Goldstone diagrams corresponding to the Hugenholtz skeleton diagram. All remaining fifth-order graphs can be obtained by taking all distinct permutations of vertices 1, 2, 3, and 4. That is, 1, 3, 0, 0 is a new partition that would correspond to exchanging the first two vertices in the 3, 1, 0, 0 partition.

action dots 1 and 2 as well as 3 and 4 does not lead to a new diagram, whereas exchange of any other pair of dots does. Analogously, we can deduce the number of antisymmetrized and Goldstone diagrams to be equal to $6 \times 20 = 120$ and $6 \times 264 = 1584$, respectively.

For the partition 2, 1, 1, 0 (Fig. 24c), we have 6 skeleton Hugenholtz diagrams that, when all 12 permutations are taken, results in 72 graphs. This, in turn, corresponds to $12 \times 40 = 480$ and $12 \times 720 = 8640$ antisymmetrized and Goldstone diagrams, respectively.

The partition 1, 1, 1, 1 (Fig. 24d) is the most tedious to work out, and moreover, we do not gain anything by permuting dots since there is only a single permutation. It may be observed that switching any two dots (except for the topmost) does not lead to a new diagram. The number of antisymmetrized and Goldstone diagrams for this case is 96 and 2112, respectively.

The total number of antisymmetrized and Goldstone diagrams amounts to 840 and 13,680, respectively.

There is also a very simple relationship between the diagrams presented in Fig. 24 and the antisymmetrized skeleton diagrams used throughout this paper. To all those graphs in Fig. 24 that correspond to 3 or 4 antisymmetrized diagrams, 1 skeleton is related, while to those corresponding to 6 or 10 antisymmetrized diagrams, 2 skeleton diagrams are related. The fifth diagram in Fig. 24d, corresponding to 24 antisymmetrized diagrams, has 3 antisymmetrized skeleton equivalents.

Appendix C. Diagram Factorization and Basis Set Size Dependence in MBPT–CC Computations

According to the number of summations in the algebraic expression assigned to the MBPT diagram, the cost of computations should depend on the size of the basis set roughly as $\sim n^{2N}$, where n is the basis set size and N is the order of perturbation theory. Fortunately, for the orders higher than three this formula is no longer valid due to the possible factorizations. In addition to the factorization mentioned in Sections V to VII, which will be called here denominator factorization, we, for pedagogical reasons, introduce two other types of factorizations that we call horizontal and vertical factorization. Both types are implicit in the computer codes that have been written,^{6–10} but these simplifying schemes have not been systematically presented.

To illustrate the first type of factorization, i.e., horizontal, we pick at random a fifth-order diagram, which, after providing arrows and labels, is presented in Fig. 25 (leftmost). Since this is a fifth-order diagram, there are 10 lines and the same number of summation indices in the general algebraic formula. The factorization of the diagram is possible due to the fact that we can calculate independently some parts of the diagram. This

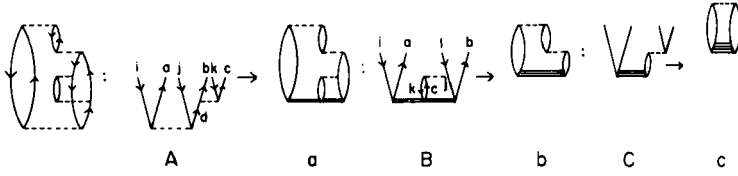


Fig. 25

is pictured in Fig. 25, in which currently calculated pieces of the diagram are denoted as A , B , C and corresponding “factorized” diagrams by the letters a , b , and c .

Thus, in the first step, we calculate that part that involves the two lowest interaction lines and is denoted as A . It contains one internal line and six external. Thus, we compute the quantity A_{ijk}^{abc} according to the formula

$$A_{ijk}^{abc} = \sum_d \frac{\langle bc || dk \rangle \langle ad || ij \rangle}{D_{ij}^{ad}}$$

and the sign is positive (three loops and three hole lines) and no equivalent lines. This has an n^7 basis size dependence. In this way we obtain diagram a , which involves one “dressed” interaction (the lowest one). The second step is to calculate diagram B according to the formula

$$B_{il}^{ab} = -\frac{1}{2} \sum_{j,c,k} \frac{\langle kj || cl \rangle A_{ikj}^{abc}}{D_{ijk}^{abc}}$$

where there is one set of equivalent lines and three loops and four hole lines. This is also of n^7 dependence. The new factorized diagram is presented as C in Fig. 25, which can be calculated directly according to the formula

$$C_{im}^{ae} = \sum_{b,l} \frac{\langle el || mb \rangle B_{il}^{ab}}{D_{il}^{ab}}$$

an n^6 step, and finally the entire diagram is

$$\sum_{i,m,a,e} \frac{\langle im || ae \rangle C_{im}^{ae}}{D_{im}^{ae}}$$

This kind of factorization can be performed for all diagrams from the fourth-order energy and up. It is obvious that these stepwise-type calculations, presented in Fig. 25 are, in fact, exercised in the coupled-cluster

scheme. The overall basis size dependence is determined by the slowest step, which is that involving the highest number of indices. By selectively saving some of these intermediate quantities and using repeatedly, contributions of large classes of similar diagrams can be efficiently evaluated.

The second type of factorization, the vertical one, is applicable only to those diagrams that are denominator factorizable. A set of diagrams that is denominator factorized is presented in Fig. 17. The essence of the vertical factorization lies in the fact that we can cut the diagram vertically into parts, which is possible only when each of the pieces has an independent denominator. This procedure is very convenient from the computational point of view since we can lower the n dependence for all diagrams in Fig. 17 to n^6 and lower. The details of factorization are presented in Fig. 26, in which at the leftmost side all E_s^{QQ} types of diagrams are presented. Then column F_1 presents the pieces of the original diagram that are calculated first. Almost all of them (with the exception of Fig. 26b, which is n^5 dependent) are of n^6 dependence since they involve summa-

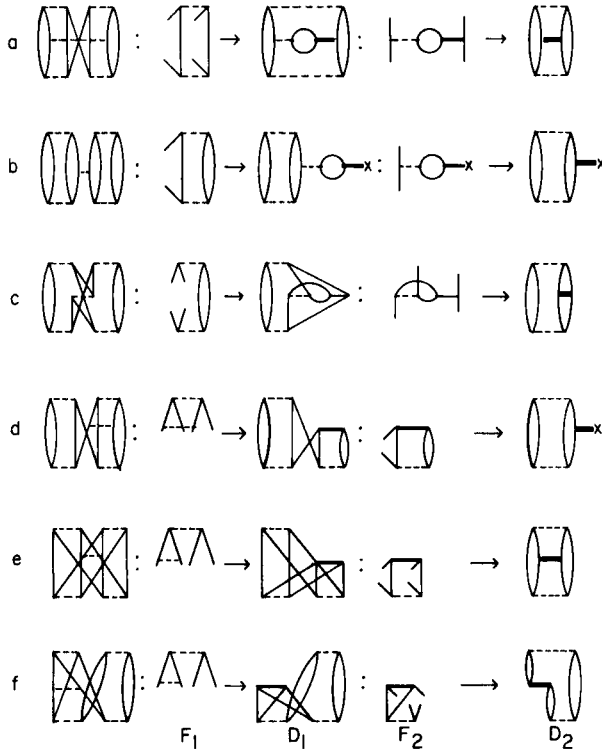


Fig. 26. Factorization of the E_s^{QQ} diagrams into independently computed fragments with n^6 and lower basis set size dependence.

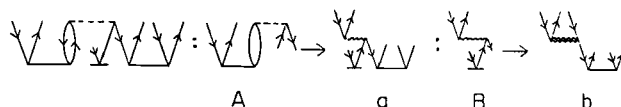


Fig. 27

tion over two internal lines and they are four index quantities (due to four external lines). In column D_1 the new, partly factorized diagram is presented with one dressed vertex. In the next step, parts F_2 are computed, which are also of n^6 character (except for b and d, which are n^4 and n^5 dependent, respectively) for the same reason as before. Column D_2 presents fully factorized diagrams that being of n^6 dependence (except b and d, which are n^5 dependent) are computed directly.

Finally, a similar vertical type of factorization is applicable to coupled-cluster diagrams, since they are, by definition, denominator factorized. Figure 27 presents an example of the CC diagrams and its decomposition, for computational efficiency, into independently calculated parts. The first part (A) is computed with an n^6 dependence. The second one (B) is of n^5 , and finally the fully factorized diagram b requires an n^7 basis set dependence.

REFERENCES

1. F. Coester, *Nucl. Phys.* **1**, 421 (1958); F. Coester and H. Kuemmel, *Nucl. Phys.* **17**, 477 (1960).
2. J. Cizek, *J. Chem. Phys.* **45**, 35 (1969); J. Cizek, *Adv. Chem. Phys.* **14**, 35 (1969); J. Paldus and J. Cizek, In "Energy, Structure and Reactivity" (D. W. Smith and W. B. McRae, eds.), Wiley, New York, 1973.
3. J. Hubbard, *Proc. R. Soc. London, Ser. A* **240**, 539 (1957); J. Hubbard, *Proc. Roy. Soc. London, Ser. A* **243**, 336 (1958).
4. O. Sinanoglu, *J. Chem. Phys.* **36**, 706 (1967); O. Sinanoglu, *Adv. Chem. Phys.* **6**, 315 (1964).
5. H. Primas, In "Modern Quantum Chemistry" (O. Sinanoglu, ed.), Vol. 2, p. 45. Academic Press, New York, 1965.
6. R. J. Bartlett and G. D. Purvis, III, *Int. J. Quantum Chem.* **14**, 561 (1978); *Phys. Scripta* **21**, 255 (1980).
7. R. J. Bartlett, *Ann. Rev. Phys. Chem.* **32**, 359 (1981).
8. R. J. Bartlett, I. Shavitt, and G. D. Purvis, *J. Chem. Phys.*, in press.
9. G. D. Purvis, III, and R. J. Bartlett, *J. Chem. Phys.* **76**, 1910 (1982); G. D. Purvis, R. Shepard, F. B. Brown, and R. J. Bartlett, *Int. J. Quantum Chem.* **23**, 835 (1983).
10. Y. S. Lee, S. A. Kucharski, and R. J. Bartlett, *J. Chem. Phys.* **81**, 5906 (1984); **82**, 5761 (1985); Y. S. Lee and R. J. Bartlett, *J. Chem. Phys.* **80**, 4371 (1984).
11. R. J. Bartlett, H. Sekino, and G. D. Purvis, III, *Chem. Phys. Lett.* **98**, 66 (1983); S. A. Kucharski, Y. S. Lee, G. D. Purvis, III, and R. J. Bartlett, *Phys. Rev.* **A29**, 1619 (1984).
12. J. A. Pople, R. Krishnan, H. B. Schlegel, and J. S. Binkley, *Int. J. Quantum Chem.* **14**, 545 (1978).

13. V. Kvasnicka, V. Laurinc, and S. Biskupic, *Mol. Phys.* **39**, 143 (1980).
14. R. J. Bartlett, C. E. Dykstra, and J. Paldus, In "Advanced Theories and Computational Approaches to the Electronic Structure of Molecules" (C. E. Dykstra, ed.), p. 127. Reidel, Dordrecht, 1984.
15. G. D. Purvis, III, and R. J. Bartlett, *J. Chem. Phys.* **75**, 1284 (1981).
16. W. D. Laidig, G. Fitzgerald, and R. J. Bartlett, *Chem. Phys. Lett.* **113**, 151 (1985).
17. R. J. Bartlett and G. D. Purvis, III, *Phys. Rev. A* **20**, 1313 (1981); G. D. Purvis, III, and R. J. Bartlett, *Phys. Rev. A* **20**, 1594 (1981).
18. G. H. F. Diercksen and A. J. Sadlej, *Mol. Phys.* **47**, 33 (1982); G. H. F. Diercksen and A. J. Sadlej, *Theor. Chim. Acta* **61**, 485 (1982).
19. G. H. F. Diercksen, V. Kellö and A. J. Sadlej, *J. Chem. Phys.* **79**, 2918 (1983).
20. P. J. Knowles, K. Somasundram, N. C. Handy, and K. Hirao, *Chem. Phys. Lett.* **113**, 8 (1985).
21. J. Paldus and J. Cizek, *Adv. Quantum Chem.* **9**, 105 (1975).
22. A. Messiah, "Quantum Mechanics." Wiley, New York (1965).
23. P. O. Löwdin, *J. Math. Phys.* **3**, 1171 (1962); P. O. Löwdin, *J. Math. Phys.* **3**, 969 (1962).
24. K. A. Brueckner, *Phys. Rev.* **100**, 36 (1955).
25. J. Goldstone, *Proc. R. Soc. London, Ser. A* **239**, 267 (1957).
26. N. H. March, W. H. Young, and S. Sampanthar, "The Many Body Problem in Quantum Mechanics." Cambridge Univ. Press, Cambridge, 1967; S. Raimes, "Many-Electron Theory." North-Holland, Amsterdam, 1972.
27. P. Carsky and M. Urban, "Lecture Notes in Chemistry," No. 16. Springer-Verlag, Berlin (1980).
28. H. P. Kelly, *Adv. Chem. Phys.* **14**, 129 (1969).
29. I. Hubac, M. Urban, and V. Kellö, *Chem. Phys. Lett.* **62**, 584 (1979); M. Urban, I. Hubac, V. Kellö, and J. Noga, *J. Chem. Phys.* **72**, 3378 (1980).
30. R. J. Bartlett and D. M. Silver, *Phys. Rev. A* **10**, 1927 (1974); R. J. Bartlett and D. M. Silver, *Chem. Phys. Lett.* **29**, 199 (1974); R. J. Bartlett and D. M. Silver, *J. Chem. Phys.* **62**, 3258 (1975); R. J. Bartlett and D. M. Silver, *J. Chem. Phys.* **64**, 4578 (1976).
31. R. J. Bartlett, S. Wilson, and D. M. Silver, *Int. J. Quantum Chem.* **12**, 737 (1977).
32. R. J. Bartlett and I. Shavitt, *Chem. Phys. Lett.* **50**, 190 (1977).
33. G. D. Purvis, and R. J. Bartlett, *J. Chem. Phys.* **68**, 2114 (1978).
34. M. J. Frisch, R. Krishnan, and J. A. Pople, *Chem. Phys. Lett.* **75**, 66 (1980); R. Krishnan, M. J. Frisch, and J. A. Pople, *J. Chem. Phys.* **72**, 4244 (1980).
35. P. O. Löwdin, *J. Chem. Phys.* **43**, 5175 (1965); P. O. Löwdin, *J. Math. Phys.* **6**, 1341 (1965).
36. R. J. Bartlett and D. M. Silver, *Int. J. Quantum Chem. Symp.* **9**, 183 (1975).
37. B. H. Brandow, *Adv. Quantum Chem.* **10**, 187 (1977).
38. N. M. Hugenholtz, *Physica* **23**, 481 (1957).
39. R. J. Bartlett and D. M. Silver, In "Quantum Science" (J. L. Calais, O. Goscinski, J. Linderberg, and Y. Öhrn, eds.), p. 393. Plenum, New York, 1976.
40. J. Paldus, "Diagrammatical Methods for Many-Fermion Systems." Lecture Notes, University of Nijmegen, 1981.
41. S. Binkley, private communication.
42. J. Paldus, P. E. S. Wormer, F. Visser, and A. van der Avoird, *J. Chem. Phys.* **76**, 2458 (1982).
43. A. Szabo and N. Ostlund, "Modern Quantum Chemistry." MacMillan, New York, 1982.
44. J. Paldus and P. Wong, *Comp. Phys. Com.* **6**, 1-7 (1973); J. Paldus and P. Wong, *Comp. Phys. Com.* **6**, 9-16 (1973).

A

- Adenine tautomers, 113
- Amide/imidate tautomers, 100
- Amino-imino tautomerism, 90, 113
- Anisotropy, in degenerate states
 - of hyperpolarizability, 28–68
 - of intermolecular interactions, 75–81, 141
 - collision-induced light absorption, 75–78
 - of polarizability, 28–68
- Atom-Atom potential, 136–137
 - expanded in symmetry-adapted functions, 141–144
- 1-Azacarbazole tautomers, 118
- 7-Azaindol tautomers, 118

B

- Birefringence
 - in external fields, 29–35
 - in inhomogeneous electric fields, 69–75
 - deformation contribution, 70–71
 - molecules with D_{3h} symmetry, 73–74
 - orientational contribution, 71–75
 - spherical-top molecules, 74–75
 - Langevin–Born mechanism, 28, 32
 - in spherical-top molecules, 28–45
 - Voigt mechanism, 28, 29, 32
- Born–Oppenheimer approximation, 135, 212, 283
- Brandow diagram, 225, 229

C

- CC, *see* Coupled-cluster theory
- CCD, *see* Coupled-cluster doubles model
- CCM, *see* Coupled-cluster singles, doubles, and triples model of electron correlation

- CCSD, *see* Coupled-cluster singles and doubles model
- CCSDT, *see* Coupled-cluster singles, doubles, and triples model of electron correlation
- 6-Chloro-2-hydroxypyridine tautomers, 106
- 6-Chloro-2-pyridone, *see* 6-Chloro-2-hydroxypyridine tautomers
- CI, *see* Configuration interactions
- Configuration interactions, 207, 209, 211, 221, 277, 281–282
- Cotton–Mouton effect, 28–45
 - in electronic states $G_{3/2}$, 42–45
- Coupled-cluster doubles model, 209–210
 - linearized, relationship to MBPT, 282, 308, 321–323
 - relationship to MBPT, 282, 321–323, 327
- Coupled-cluster singles and doubles model, 210–211
 - linearized, relationship to MBPT, 282, 321–323
 - relationship to MBPT, 282, 321–323
- Coupled-cluster singles, doubles, and triples model of electron correlation, 207–279
 - diagrams and rules, 223–234
 - antisymmetrized cluster operators, 225
 - Dirac spinor lines, 227
 - electron annihilation, 224
 - electron creation, 224
 - hole annihilation, 224
 - hole creation, 224
 - hole lines, 226
 - particle lines, 226
 - equations, 219–223, 264–276
 - key words, 210–211
 - matrix elements, 234–264
 - relationship to fifth-order MBPT, 282, 321–323, 326, 327
 - renormalization, 211–219

Coupled-cluster theory, 207–279, 281, *see also* specific coupled-cluster models
 diagrams, 298–306
 skeleton diagrams, 306
 T_2 coupled-cluster equation, 304
 T_3 coupled-cluster equation, 304
 equations, 306
 relationship to fifth-order many-body
 perturbation theory, 281–344
 synopsis, 289–292
 Coupled-pair many-electron theory, 209–
 211, 282
 CPMET, *see* Coupled-pair many-electron
 theory
 Crystal Hamiltonian, 135–159, 165–171
 anharmonic corrections, 153–159
 for oxygen, solid, 195–200
 Crystals, *see* Molecular crystals
 Cytosine tautomers, 100, 101

D

Degenerate diagram, 224
 Degenerate electronic states
 anisotropy, *see* Anisotropy, in degener-
 ate states
 of highly symmetric molecules, 5–28
 intermolecular torque, 78–81
 twofold dipolar type, 6–9
 Depolarization, of light
 free-rotating systems, 47–53
 in viscous medium, 53–59
 second harmonic, 55–57
 third harmonic, 57–59
 Dielectric losses, 23–28
 2,4-Dimethoxypyrimidine tautomers, 100
 1,3-Dimethyl-2-pyrimidinone tautomers,
 100
 Dipolarly unstable molecules, 9–12
 properties in viscous nonpolar medium,
 23–28
 four-minima systems, 26–28
 three-minima systems, 26
 two-minima systems, 25
 pure rotational absorption spectrum, 16
 Dipole moment
 Jahn–Teller effect, *see* Jahn–Teller
 effect, in dipole moments
 of symmetric molecular systems, 5–28

temperature dependence, 5–12
 dipolarly unstable molecules, 9–12
 twofold degenerate electronic states,
 6–9
 Double proton transfer, 117, 118, 124
 DPT, *see* Double proton transfer
 Dynamical models, for large-amplitude
 lattice vibrations, *see* Lattice vibra-
 tions, large-amplitude dynamical
 models
 Dynamics of molecular crystals, *see* Mo-
 lecular dynamics

E

Electron correlation, model description of,
 207–279
 Excitation operators, 207–209
 Exclusion principle violating diagrams, 286
 Extended coupled-pair many-electron
 theory, 210, 211

F

Fluorobenzene radical, 102
 5-Fluorouracil tautomers, 102
 Formamide tautomers, 89, 124
 Formamidic acid tautomers, 89, 124

G

Goldstone diagram, 224, 225, 229, 295–
 297, 335, 339, 340

H

Harmonic theory of lattice dynamics, *see*
 Lattice vibrations, harmonic theory
 Hartree–Fock approximation, 89–92, 100,
 133, 284, 291, 296–297, 307, 325
 HF, *see* Hartree–Fock approximation
 Hugenholtz diagram, 225
 skeleton diagrams, 297, 335–340
 Hydrogen, solid, 162
 Hydroxyazine tautomers, 106
 N-4-Hydroxycytosine tautomers, 100, 101
 2-Hydroxypyridine, *see* 2-Pyridone tauto-
 mers
 4-Hydroxypyridine, *see* 4-Pyridone tauto-
 mers

- 2-Hydroxy-4-pyridinone tautomers, 97
- 4-Hydroxy-2-pyridinone tautomers, 97
- Hyperpolarizability, anisotropy of, in degenerate states, 28–68
- Hyper-Rayleigh scattering, depolarization of light in, 45–59

I

- Intermolecular interactions, quadrupole moments, manifestations of, 68–81
- Intermolecular potential, 137–141
- Intermolecular vibrations, *see* Lattice vibrations
- Intramolecular vibrations, *see* Vibronic interactions

J

- Jahn–Teller effect
 - in dipole moments, 1–84
 - induction of pure rotational transitions, 18–23
 - in polarizability of molecules, 1–84

K

- Kerr effect, 28–45, 69
 - anomalous, 35–36
 - ground electronic terms, 36–41
 - temperature dependence, 35–41

L

- Lactim–lactam tautomers, 89, 93–96
 - Hartree–Fock approximation, 92
 - relative electronic energies, 94
 - thermodynamic quantities, 94
- Lattice vibrations, 132–206
 - coupled rotational–translational, 162–173
 - crystal Hamiltonian, *see* Crystal Hamiltonian
 - harmonic approximation, 150–154
 - harmonic theory, 149–162
 - in solid nitrogen, 178–181
 - large-amplitude
 - dynamical models, 162–175
 - in ordered phases, 181–186
 - linear molecules, theory, 175–178

- quasi-harmonic theory, 149–162
 - in solid nitrogen, 178–181
- rotational, 131–206
 - tetrahedral functions, 139, 147
- translational, 131–206
- LCCD, *see* Coupled-cluster doubles model, linearized
- LDT, *see* Linked diagram theorem
- Librons, 131–206
- Linked diagram theorem, 286, 287, 292
 - to reduce diagrammatic terms in MBPT, 294–295
 - time-dependent proof, 292

M

- Many-body perturbation theory, 281–344
 - choice of skeleton diagrams and rules, 334–337
 - coupled-cluster computations, diagram factorization and basis set size dependence, 340–343
- diagrams, 292–298
 - antisymmetrized skeleton energy diagrams, 307
 - generation by coupled-cluster iterations, 306–320
 - reduction of terms, 294–297
- fifth-order, relationship to coupled-cluster approaches, 281–344
 - summary, 333–334
- fifth-order energy diagrams, 311–320
 - computational components, 332
 - computational strategy, 328–333
 - connected triples, 316–318
 - disconnected contribution to, 319–320
 - from disconnected quadruples, 318–319
 - disconnected triples, 314–316
 - doubles, 313–314
 - factorized, 333
 - general structure, 325
 - iterative scheme, 324
 - quadruples, 319
 - singles, 312
 - summary analysis, 322
 - unlinked diagrams, 331
- fourth-order energy, 308–310
 - computational scheme, 310–311
 - from coupled-cluster doubles, 309–310

- from coupled-cluster quadruples, 310
 - from coupled-cluster singles, 308–309
 - from coupled-cluster triples, 310
 - second-order energy, 306–308
 - third-order energy, 308, 309
 - wave function diagram, 287
 - wave operator diagram, 291
- MBPT, *see* Many-body perturbation theory
- Mean field model, 165–170
 - for nitrogen, solid, 183–190
 - order parameter, temperature dependence, 185
 - orientational probability distribution, 184
 - translational and librational amplitudes, 183
 - for oxygen, solid, 198
 - stability conditions, 173–175
- 2-Methoxy-3-methyl-4-pyrimidine, 100
- 4-Methoxy-1-methyl-2-pyrimidinone, 100
- 2-Methoxypyridine tautomers, 121
- 1-Methyladenine tautomers, 113
- 3-Methylcytosine tautomers, 113
- N*-Methylformamide tautomers, 97
- Methylformimidate, *see N*-Methylformamide tautomers
- 1-Methyl-2-pyridinone, *see* 2-Methoxypyridine tautomers
- 5-Methyluracil, 102
- Molecular crystals
 - dynamics, *see* Molecular dynamics
 - Hamiltonian, *see* Crystal Hamiltonian
 - plastic, 150, 162, 186–191
 - vibrations, *see* Lattice vibrations
- Molecular dynamics, 131–206
 - classical, 163–165
 - for solid nitrogen, 181
- Monte Carlo method, 110, 136, 163–165
 - for solid nitrogen, 186
- Multipole moments, 1–84, 135
- Mutation theory, role of tautomers, 121–126

N

- Nitrogen, solid
 - crystal structure, 176–177
 - free energy, 190
 - molecular motions, 175–191
 - from harmonic and quasi-harmonic models, 178–181
 - large-amplitude, in ordered phases, 181–186
 - lattice frequencies, 178, 179
 - orientational probability distribution, 184, 189
- ## O
- OMTP, *see* Overlap multipole procedure
 - Order-disorder phase transition, 186–191
 - Overlap multipole procedure, 108, 110
 - 2-Oxo-6-methylpyridine, 89
 - 2-Oxopyridine 1-oxide tautomers, 121
 - 2-Oxopyridine tautomers, 89, 93–96, 100, 120–121
 - in excited state, stabilization by solvation, 120, 121
 - polyhydration energies, 112
 - relative electronic energies, 93–96
 - calculation steps, 95
 - vapor phase, 93
 - thermodynamic quantities, 93–95
 - vapor phase, 93
 - 3-Oxopyridine tautomers, 100
 - 4-Oxopyridine tautomers, 100
 - in excited state, solvation stabilization, 120, 121
 - polyhydration energy, 112
 - relative electronic energies, 94, 96
 - thermodynamic quantities, 94
 - 2-Oxopyrimidine tautomers
 - relative electronic energies, 94
 - thermodynamic quantities, 94
 - 4-Oxopyrimidine tautomers
 - relative electronic energies, 94
 - thermodynamic quantities, 94
 - Oxygen, solid
 - coupling between lattice vibrations and spin dynamics, 195–200
 - crystal Hamiltonian, 195–200
 - crystal structure, 192
 - dynamics and magnetism, 191–200
 - exchange coupling parameter, 198
 - exchange interaction energy, orientational dependence, 197
 - Heisenberg exchange coupling constant, orientational dependence, 197, 199, 200

quadrupole moment, 193
spin Hamiltonian, 194–200
spin wave calculations, 193–195

P

Perturbation theory, 153–159, 207, 230, 276
 many-body, *see* Many-body perturbation theory
Phonons, 131–206
Phototautomerism, in nucleic acid base pairs, 118
Polarizability, molecular
 anisotropy of, in degenerate states, 28–68
 Jahn–Teller effect, *see* Jahn–Teller effect
Polarization, atomic, 7, 8
Proton tunneling, 117, 118, 123
PT, *see* Perturbation theory
2,4-Pyridinediol, 97
 tautomeric energies, 98
2-Pyridone tautomers
 in solution, 108, 109
 in vapor, 97, 103
4-Pyridone tautomers
 in solution, 108, 109
 in vapor, 97

Q

Quasi-harmonic theory of lattice dynamics, *see* Lattice vibrations, quasi-harmonic theory

R

Raman scattering
 pure rotational, 50–53
 depolarization of light, 45–59
 vibronic–rotational transitions, selection rules, 48–50
Random phase approximation, 170–173, 185
 for nitrogen, solid, 182, 186, 187, 191
 for oxygen, solid, 198
Rayleigh scattering
 depolarization of light in, in viscous medium, 54–55

 optical active states, 66–68
 in symmetric molecular systems, 66–68
Rayleigh–Schrödinger theory, review, 283–289
Rotational absorption, pure
 dipolarly unstable systems, 13–18
 temperature dependence, 17
 tetrahedral spectrum, 16, 17
 spectra, 12–23
 Raman, 50–53
 transitions, 18–23
RPA, *see* Random phase approximation

S

Self-consistent phonon method, 157–162, 180, 185
Spherical-top molecules
 birefringence, 74–75
 gas, 28–45
 depolarization of light, 45–59
 pure rotational spectrum, 18–23
Spin–orbital interactions, induction of pure rotational transitions, 18–23
Symmetric molecular systems
 dipole moments, *see* Dipole moment, of symmetric molecular systems
 optical activity, temperature dependent, 59–68
 in anisotropic external fields, 63–66
 in external fields, 59–63
 quadrupole moments, 68–81
 measurement by birefringence, 69–75
 rotational absorption spectra, 12–23
Symmetry-adapted functions, 137–141, 167
 expansion of atom–atom potentials, 141–144
 to express intermolecular potential, 137–141

T

Tautomeric equilibria, 85–130
 in electronic ground state
 in solution, 104–114
 in vapor, 89–104
 in excited electronic state, 114–121
 effect of solvation, 120
 in nucleic acid bases, 121–126
 potential energy surface, 90–92, 115
 role in mutation theory, *see* Mutation theory, role of tautomers

TDH, *see* Random phase approximation

Tetrahedral rotation functions, 139,

147

Thermodynamic variation principle, 200–
203

Thione–thiol tautomerism, 90

Time-dependent Hartree approximation,

see Random-phase approximation

Tunneling, *see* Proton tunneling

Tunneling–rotational transitions, 15

U

Uracil tautomers, 89, 91, 94, 98, 102, 103

relative tautomeric energies, 99, 100

V

Vibronic interactions, 1–84, 132

ground states, 8

reduction factor, 8